

**Landscape Structure and Sustainability of Flood Regulating Service:  
Landscape and Hydrologic Modelling of the Ci Kapundung and Ci Sangkuy  
Upper Water Catchment Areas in the Bandung Basin**

**Medria Shekar Rani**

Submitted in partial fulfilment of the requirements for the degree of Doctor of Philosophy  
Department of Landscape Architecture



The  
University  
Of  
Sheffield.

September 2019

**Supervisors:**

Professor Eckart Lange, Department of Landscape Architecture, University of Sheffield

Dr. Ross Cameron, Department of Landscape Architecture, University of Sheffield

Professor Olaf Schroth, Department of Landscape, Weihenstephan-Triesdorf University  
of Applied Sciences



## ACKNOWLEDGEMENTS

I would like to express my sincere gratitude for my supervisors, Professor Eckart Lange, Dr. Ross Cameron, and Professor Olaf Schroth, for their endless supports and advices for my study. To my internal examiner Professor Nigel Dunnett (University of Sheffield) and my external examiner Professor Felix Kienast (ETH Zürich) for their review and feedback.

This research would not have been possible without the scholarship from The Directorate General of Resources for Science Technology and Higher Education, Ministry of Research Technology and Higher Education of Indonesia. I wish to thank the academic and administrative staff at the Department of Architecture, the Department of Landscape Architecture, and School of Architecture, Planning, and Policy Development (SAPPD), Institut Teknologi Bandung (ITB), Indonesia.

Staff members of the Department of Landscape Architecture University of Sheffield for their support, and the permission from the department to use their equipment during the field surveys in Indonesia.

DHI (Danish Hydraulic Institute) who provided a student license to use MIKE Powered by DHI Software during my study. BKSDA (Nature Conservation Agency, Indonesia), THR Ir. H. Djuanda, PTPN and PSDA (Water Resource Management in West Java province) staff for providing the spatial data and the access to collect the data inside the protected areas and plantation area.

Dr. Manoj Menon (University of Sheffield), Dr. Sumit Sinha (University of Leeds), Dr. Georges Kesserwani (University of Sheffield), Dr. Arnaud Duranel (Université Jean Monnet, France), Daniel Schläpfer, Dr.sc.nat., Prof. (ReSe Applications LLC, Switzerland), Dr. Courage Kamusoko (Asia Air Survey Co., Ltd, Japan), and Roni Farfian for their feedback to my research. Djuandi (Herbarium curator, SITH ITB, Indonesia) for his help with plant identification in the forests, and Fadillah Ayu for her help to collect the data.

To my Mom, Dad, Mba Nes, Mas Rian, and Linang, who have given the greatest support in the last four years. Khaerani, Mba Widi, Sofia, Yttria, Mba Yunita, and Mba Ari, for the chats and discussions. To the Indonesian society in Sheffield and the Indonesian embassy. To all my friends in the Department of Landscape Architecture and the Department of Architecture at the University of Sheffield; Luxi, Aimee, Sholeh, Pai, Azlina, Sarah, Eun Yeong, Veronica, Camilla, Hannah, Linyan, Mahsa, Lauriane, Fadilah, Emad, Khalid, Youmei, Frankie, Jinvo, Mingyu, Junyi, Yuanyuan, Olivia, and Faith.

## ABSTRACT

It is widely acknowledged that the alteration of landscape structure affects the provision of ecosystem services. Many studies have been conducted to simulate land cover changes based on scenarios and to assess the impact of changes in the environment using modelling. However, the assessments of how land cover changes influence streamflow regimes are still lacking. **This research aims to investigate potential landscape structure scenarios of Ci Kapundung and Ci Sangkuy upper water catchment areas.** The two watersheds are located in Bandung Basin, Java Island, Indonesia. This thesis addresses the ongoing needs of comparative studies on landscape planning to support ecosystem services using sites with different biophysical environment.

**An integrated Cellular Automata-Markov (CA-Markov) model** was used in this research to simulate the land cover change and to project the future land cover compositions and distributions based on four scenarios (e.g. Status Quo, existing policy-based scenario, ecological design-based scenario, and Backcasting scenario). The model used land cover maps, which have been developed from the multi-resolution of satellite imagery. Although CA-Markov models have been broadly used to simulate urban growth, the applications to model forest cover are still rare. **Moving average analysis** was conducted to assess the impact of land cover change to flood regulation. The CA-Markov model was coupled with the **MIKE SHE hydrologic model** to assess the flow metric responses across the four future development scenarios and to investigate the types of vegetation that can improve flood regulation.

In this research, potential approaches in the land cover map development, the land change modelling, and the hydrologic modelling have been evaluated through iterative processes. The outcomes from the three iterations of the map development process show that **the backdating and updating procedure can mitigate the data gaps in satellite imagery** caused by continuous cloud coverage. It is argued that different methods chosen and assumptions made during the process affect the map accuracies. The results of the land change modelling suggest that **‘the likelihood of land cover change’ is the most influential driver of land cover alteration in the study areas.** The problems of mixed pixels in the satellite imagery are prominent, contributing to uncertainty in land change modelling.

The results from the land cover change and moving average analyses indicate that **the increasing trend of annual Ci Kapundung River discharge (2001-2017)** was more influenced by the land cover change rather than the precipitation trend. On the other hand, **the declining trend of Ci Sangkuy River discharge (2001-2017)** was caused by the increasing percentage of forest cover and the decreasing precipitation rates in 16 years.

The results from iterative MIKE SHE modelling demonstrate how **the compositions and distributions of land cover in the two study areas affect the river discharges and overland flow**. Scenario 4 (Backcasting scenario) in the first case study area has the lowest peak discharge among all scenarios in spite of higher accumulated surface runoff than scenario 1 (Status Quo) and scenario 3 (ecological design-based scenario). On the other hand, scenario 2 in the second case study area generates the least volume of surface runoff and accumulated overland outflow compared with other scenarios. It is argued that this result is due to the higher percentage of areas covered with conifers and mixed vegetation on clayey soil.

The results from the vegetation analysis using 64 hypothetical catchments confirm that **runoff generation process is not only affected by the plant characteristics (e.g. canopy interception) but also by the rainfall trend, slope gradients and soil types**. In general, overland outflow from the catchments with clay soil is higher than the outflow from other scenarios with different soil. It is also found that the catchments covered by conifers on four soil types generate the lowest volume of overland flow under low-intensity rainfall. The simulated overland flow is slightly lower than the outflow from the catchments with mixed vegetation. This analysis also has shown that conifers on clay, silty loam, and loam, and mixed vegetation on sandy loam, generate the lowest volume of runoff on both slope gradients under a continuous heavy rainfall (100 mm/day).

This study offers **plausible approaches to integrate hybrid data sources in the land change and hydrologic models**, by mitigating the data gaps in satellite imagery and the limited spatial data, which is required by the two models. The research discusses how models provide opportunities for researchers and practitioners to assess the effects of landscape planning in a water catchment area to flooding.

# TABLE OF CONTENTS

ACKNOWLEDGEMENTS .....	i
ABSTRACT .....	ii
LIST OF FIGURES .....	ix
LIST OF TABLES .....	xvii
LIST OF EQUATIONS .....	xxi
<b>Chapter 1 Introduction .....</b>	<b>1</b>
1.1 Research background	1
1.2 Scope of the thesis	4
1.3 Research questions	6
1.4 Thesis structure	7
<b>Chapter 2 Literature review .....</b>	<b>11</b>
2.1 Flood regulating service of water catchment areas	11
2.1.1 Ecological integrity in a river ecosystem	11
2.1.2 Vegetation to improve flood regulation	12
2.2 Land cover map development using remote sensing	13
2.2.1 Land cover identification	14
2.2.2 Satellite image preprocessing	16
2.2.3 Cloud, shadow, and water masking	19
2.2.4 Image classification and accuracy assessment	20
2.2.5 Uncertainty factors in a land cover mapping process	22
2.3 The development of scenarios and land change models	23
2.3.1 Scenario definition and types of scenario	23
2.3.2 Pareto-frontier	24
2.3.3 The development of land change models	25
2.3.4 Uncertainty factors in land change modelling	28
2.4 Flood risk assessment and the development of hydrologic models	28
2.4.1 Flood risk assessment	29
2.4.2 The development of hydrologic models and model categorisation	31
2.4.3 MIKE SHE hydrologic model	33
2.4.4 Uncertainty factors in hydrologic modelling	37

2.5 Conclusion to the literature review	38
<b>Chapter 3 Case study areas .....</b>	<b>39</b>
3.1 Bandung Basin	39
3.1.1 Bandung Basin development	40
3.1.2 Environmental conditions of Bandung Basin	41
3.1.3 Land cover change in Bandung Basin over a period of time	50
3.1.4 The history of flood events in the basin and the river improvement project	51
3.1.5 Current spatial planning policies for municipalities in Bandung Basin	55
3.1.6 Protected areas in Bandung Basin	56
3.2 Case study areas as indicators of water catchments to cause flooding in Bandung Basin	57
3.3 Ci Kapundung upper water catchment area	60
3.2.1 Land cover of Ci Kapundung upper water catchment area	62
3.2.2 River networks in the Ci Kapundung upper water catchment area	63
3.4 Ci Sangkuy upper water catchment area	63
3.3.1 Land cover of Ci Sangkuy upper water catchment area	64
3.3.2 River networks in the Ci Sangkuy upper water catchment area	65
3.5 Summary of Chapter 3	67
<b>Chapter 4 Methodology .....</b>	<b>68</b>
4.1 The development of land cover maps (research phase 1)	68
4.1.1 Data collection for the development of land cover maps	69
4.1.2 Field surveys	73
4.1.3 Catchment delineation process	81
4.1.4 Satellite image preprocessing	82
4.1.5 Masking process in SPOT and Landsat imagery	87
4.1.6 Image classification and accuracy assessment	92
4.2 Scenario development and land change modelling (research phase 2)	96
4.2.1 Data collection for the land change simulations	96
4.2.2 Scenario development	97
4.2.3 Land change simulations	101

4.3	The impact of land cover change to flood regulation and the assessment of flood risk (research phase 3)	105
4.3.1	Moving average analysis	106
4.3.2	Flood frequency estimation	106
4.3.3	Flood discharge estimation	107
4.3.4	Effective rainfall to cause flooding in the Bandung Basin	110
4.4	Hydrologic modelling (research phase 3)	112
4.4.1	Data collection for the hydrologic modelling	113
4.4.2	MIKE SHE modelling parameter estimation	114
4.4.3	Initial parameters of the MIKE SHE models	122
4.4.4	Calibration and validation procedures	133
4.4.5	Landscape structure scenarios to support flood regulation	134
4.4.6	The capacity of vegetation to reducing surface runoff	137
4.5	Decision tree diagrams and boundaries of research	139
4.6	Summary of Chapter 4	141
<b>Chapter 5 Results.....</b>		<b>142</b>
5.1	Land cover maps of the case study areas	142
5.1.1	Results from the image classification process of the first case study area	142
5.1.2	Results from the image classification for the second case study area	148
5.2	The impact of land cover change in the two case study areas on flood regulation in Bandung Basin	151
5.2.1	Land cover change assessments	152
5.2.2	Flood frequency analysis	154
5.2.3	Flood discharge analysis	155
5.2.4	Effective rainfall analysis	156
5.2.5	The impact of land cover change to river discharges	160
5.3	Landscape structure scenarios for the two case study areas to support flood regulation	164
5.3.1	Constraints on future land development	165
5.3.2	The first iteration of land change simulation (LCM 1)	170
5.3.3	The second iteration of land change simulation (LCM 2)	173
5.3.4	The first iteration of hydrologic modelling (MIKE SHE 1)	186



5.3.5 The second iteration of hydrologic modelling (MIKE SHE 2)	187
5.4 Types of vegetation to improve flood regulation	193
5.4.1 Vegetation analysis in MIKE SHE 1	193
5.4.2 Vegetation analysis in MIKE SHE 2	194
5.5 Summary of Chapter 5	196
<b>Chapter 6 Discussion.....</b>	<b>197</b>
6.1 Accuracy of land cover maps, land change, and hydrologic models	197
6.1.1 Challenges in developing highly accurate land cover maps	197
6.1.2 Improving classification accuracy and consistency of multi-temporal land cover maps	201
6.1.3 Uncertainty factors in the land change analysis	204
6.1.4 Approaches for improving land change simulations	207
6.1.5 Factors influencing the uncertainty in hydrologic models	208
6.1.6 Improvement of the hydrologic model performance	210
6.2 Land cover alteration and flood regulating service	212
6.2.1 Rainfall variability	212
6.2.2 Impact of land cover alteration on flood regulation in Bandung Basin	215
6.3 Effective scenarios of landscape structure to support flood regulation	216
6.3.1 Driving forces and the rates of land cover changes	216
6.3.2 The comparison of results from MIKE SHE 2	217
6.3.3 Optimization of land cover distributions	224
6.4 Characteristics of plants to improve flood regulation	228
6.4.1 Evapotranspiration	228
6.4.2 Canopy interception	230
6.4.3 Implication of the findings to the proposed landscape planning for the two case study areas	232
6.5 Summary of Chapter 6	233
<b>Chapter 7 Planning recommendation.....</b>	<b>234</b>
7.1 Land change modelling of Backcasting scenario (LCM 3)	234
7.1.1 Landscape planning for the Ci Kapundung upper water catchment area	234
7.1.2 Landscape planning for the Ci Sangkuy upper water catchment area	237

7.2	Implication of landscape planning to flood regulation (MIKE SHE 3)	240
7.2.1	Simulated river discharges and water balance in the Ci Kapundung upper water catchment area (MIKE SHE 3)	240
7.2.2	Simulated river discharges and water balance in the Ci Sangkuy upper water catchment area (MIKE SHE 3)	241
7.3	Summary of Chapter 7	243
<b>Chapter 8 Conclusions and outlook .....</b>		<b>244</b>
8.1	Research novelty	244
8.2	Main empirical findings	245
8.3	Main methodological findings	247
8.4	Research outlook	247
<b>References.....</b>		<b>249</b>
<b>Appendix.....</b>		<b>263</b>
A.	Calibrated parameters for MIKE SHE 2 models	263
B.	Land cover maps for the Ci Kapundung and Ci Sangkuy watersheds (first iteration)	265
C.	The flood discharge ( $Q_{bkf}$ ) of Ci Tarum River	267
D.	Baseflow of Ci Kapundung and Ci Sangkuy Rivers	270
E.	Vegetation analysis	273
F.	Additional water balance analysis	277

## LIST OF FIGURES

Figure 1-1 Bandung Basin in the West Java province. ....	2
Figure 1-2 Scope of the thesis .....	4
Figure 1-3 The assessment of landscape structure in this research .....	5
Figure 1-4 Gaps in knowledge addressed in this thesis.....	7
Figure 1-5 Thesis structure .....	8
Figure 1-6 Structure for Chapter 4 Methodology .....	9
Figure 2-1 Spectral reflectance of vegetation, soils, and water bodies .....	14
Figure 2-2 Superimposing a geometrically correct image on a distorted image .....	16
Figure 2-3 The six types of scenario .....	23
Figure 2-4 The timeline of land change model development and integration .....	26
Figure 2-5 A watershed which is viewed as a hydrologic system.....	31
Figure 2-6 (a-b) Aerial rainfall calculation by Thiessen and isohyetal methods.....	31
Figure 2-7 MIKE SHE model structure .....	34
Figure 2-8 Crop coefficient curve.....	35
Figure 2-9 The primary sources of uncertainty in flood risk mapping .....	38
Figure 3-1 (a-d) Bandung Basin area delineation according to the four arguments .....	39
Figure 3-2 The climatic regions in Indonesia .....	43
Figure 3-3 Annual precipitation rates in Bandung Basin.....	43
Figure 3-4 Topography of Bandung Basin .....	44
Figure 3-5 Soil map of Bandung Basin .....	45
Figure 3-6 Landslide risk maps for (a) Bandung regency; (b) West Bandung regency; (c) Bandung city; (d) The location of each case study area in the three municipalities .....	46
Figure 3-7 The watersheds in Bandung Basin .....	47
Figure 3-8 Ci Tarum water catchment area.....	47
Figure 3-9 Geomorphological structures of Bandung Basin .....	48
Figure 3-10 The earthquake hazard map for Bandung Basin.....	49
Figure 3-11 The aquifer in Bandung Basin .....	50
Figure 3-12 Land cover in Bandung Basin (1983-2002) .....	50
Figure 3-13 Total flooded areas in Bandung and recorded Ci Tarum River flows (1990-2002) .....	51
Figure 3-14 The location of nine tributaries for the river improvement project in the Bandung Basin .....	52
Figure 3-15 (a-e) The inundated areas during major flood events in the Bandung Basin in 1986, 2005, 2006, 2007, and 2010 respectively .....	54
Figure 3-16 Spatial plans for (a) Bandung regency; (b) West Bandung regency; (c) Bandung city; (d) The location of each case study area in the three municipalities .....	55

Figure 3-17 Spatial plan for Bandung Basin .....	56
Figure 3-18 Runoff coefficients for the watersheds in Bandung Basin (2008-2016).....	59
Figure 3-19 Linear trend of runoff coefficients in the Ci Kapundung upper water catchment area (2008-2016).....	60
Figure 3-20 Map of Ci Kapundung upper water catchment area .....	61
Figure 3-21 Annual precipitation in Ci Kapundung upper water catchment area (2004-2017) and the location of five meteorological stations in the area .....	61
Figure 3-22 Six land covers in the Ci Kapundung upper water catchment area; (a) developed area; (b) agricultural area; (c) mixed woodland; (d) conifers; (e) broad-leaved woodland; (f) water body.....	62
Figure 3-23 (a) Upper Ci Kapundung river networks; (b) Water supply and demand of the Ci Kapundung River (in m <sup>3</sup> /s).....	63
Figure 3-24 Ci Sangkuy upper water catchment area .....	64
Figure 3-25 Annual precipitation in Ci Sangkuy upper water catchment area (2004-2017) and the location of four meteorological stations in the area.....	64
Figure 3-26 Seven land covers in the Ci Sangkuy upper water catchment area; (a) developed area; (b) agricultural area; (c) plantation; (d) mixed woodland; (e) conifers; (f) broad- leaved woodland; (g) water body.....	65
Figure 3-27 (a) River networks in the Ci Sangkuy upper water catchment; (b) Water supply from tributaries and demand of the Ci Sangkuy River (in m <sup>3</sup> /s and L/s).....	66
Figure 4-1 The iterative process of developing land cover maps in this study .....	68
Figure 4-2 Different reflectance value in the NIR band between three vegetation classes.....	70
Figure 4-3 Infrared images developed from the raw satellite data of Ci Kapundung watershed; (a) the 2013 image; (b) the 2015 image; (c-d) the 2017 images.....	71
Figure 4-4 Infrared images developed from the raw satellite data of Ci Sangkuy watershed; (a) the 2013 image; (b) the 2015 image; (c) the 2017 image (.....	72
Figure 4-5 (a-b) The 2000 infrared images of Ci Kapundung and Ci Sangkuy watersheds .....	72
Figure 4-6 (a) Limited access inside the Cikole forest in the Ci Kapundung upper water catchment area; (b) Small pathway on a steep slope in the Ci Sangkuy upper water catchment area .....	74
Figure 4-7 (a-b) Developed area in the Ci Kapundung upper water catchment area; (c-d) Developed areas in the Ci Sangkuy upper water catchment area.....	75
Figure 4-8 (a-b) Cultivated land in the first case study area; (c-d) Bare land and cultivated land at the beginning of growth cycle in the second case study area.....	76
Figure 4-9 Tea plantations in the Ci Sangkuy upper water catchment area .....	76
Figure 4-10 (a-b) Conifers in the Ir. H. Djuanda protected area in the Ci Kapundung upper water catchment area; (c-d) Conifers in the Ci Sangkuy upper water catchment area.....	77

Figure 4-11 (a-b) Broad-leaved trees in the arboretum of Ir. H. Djuanda protected area ;(c-d) <i>Agathis damara</i> in the Cikole research forest; (e-f) Broad-leaved trees along the streets; (g-h) Broad-leaved plants in the riparian of the Ci Kapundung watershed .	78
Figure 4-12 (a) Cultivated forests near the Mt. Tilu protected area in the second case study area; (b) <i>Melaleuca leucadendra</i> trees along the streets and are scattered in the second case study area; (c-f) Broad-leaved plant trees near the tea plantations .....	79
Figure 4-13 Mixed woodland in the Mt. Tilu protected area (Source: Author’s documentation and a pan-sharpened infrared image of SPOT 6 from © AIRBUS DS 2015) .....	80
Figure 4-14 (a-b) A reservoir inside the Ir. H. Djuanda protected area in the first case study area; (c-d) Cileunca Lake in the second case study area .....	81
Figure 4-15 (a) An example of works defining flow direction in the first case study area; (b) the basin delineation process .....	82
Figure 4-16 (a) An example of works defining streams in the first case study area; (b) the area of Ci Kapundung upper catchment.....	82
Figure 4-17 (a-b) Slope and aspect images from DEM with a 30-m resolution of the first case study area .....	85
Figure 4-18 (a-b) Slope and aspect images from DEM with a 30-m resolution of the second case study area .....	85
Figure 4-19 Samples of the linear regression of $\cos i$ and reflectance for Band 2 (Blue), Band 3 (Green), Band 4 (Red), and Band 4 (NIR) of Landsat images of the first case study area retrieved on 28 June 2015.....	86
Figure 4-20 Samples of the linear regression of $\cos i$ and reflectance for Band 2 (Blue), Band 3 (Green), Band 4 (Red), and Band 4 (NIR) of Landsat images of the second case study area retrieved on 12 June 2015.....	87
Figure 4-21 Masking and the image classification process for an individual map .....	88
Figure 4-22 Cloud, cloud shadow and water masking process .....	89
Figure 4-23 (a) The SPOT infrared imagery of the first case study area (20 September 2015); (b) Samples of cloud and cloud shadow masks indicated by the black and grey polygons respectively.....	89
Figure 4-24 (a) The infrared imagery of the second case study area (20 September 2015); (b) Samples of water mask indicated by the blue polygons .....	90
Figure 4-25 (a) The Landsat infrared imagery of the first case study area (19 December 2000); (b) Cloud and cloud shadow masking indicated by black and grey polygons respectively.....	91
Figure 4-26 (a-b) The 2000 and 2017 infrared imagery of the second case study areas overlaid by the delineation of water bodies in 2015 .....	92
Figure 4-27 Sample of segments developed in the infrared imagery of the first case study area .....	93
Figure 4-28 The updating and backdating process in this study.....	94

Figure 4-29 The iterative process of land change simulations in this study .....	96
Figure 4-30 Scenario development in this research.....	98
Figure 4-31 An artificial neural network structure with multiple output neurons .....	103
Figure 4-32 Land change simulation process .....	104
Figure 4-33 Diagram of the workflow to estimate flood discharge.....	108
Figure 4-34 The iterative process of hydrologic simulations in this study.....	112
Figure 4-35 The availability of precipitation data.....	113
Figure 4-36 Linear regression of LAI and age of Pine trees in the Perhutani forest in the Ci Kapundung watershed.....	119
Figure 4-37 The soil map of (a) Ci Kapundung and (b) Ci Sangkuy upper water catchment areas overlaid with the boundary of case study areas.....	120
Figure 4-38 (a-b) The topography of Ci Kapundung and Ci Sangkuy watersheds.....	123
Figure 4-39 (a-b) The spatial distribution of rainfall in the Ci Kapundung and the Ci Sangkuy watersheds.....	124
Figure 4-40 Logarithmic regression of $ET_0$ (mm/day) and $Q$ mm/day) for the Ci Kapundung upper water catchment area .....	125
Figure 4-41 Estimated reference evapotranspiration in the Ci Kapundung upper water catchment area (1/1/2008 - 31/12/2015).....	125
Figure 4-42 Inverse regression of $ET_0$ (mm/day) and $Q$ mm/day) for the Ci Sangkuy upper water catchment area .....	125
Figure 4-43 Estimated reference evapotranspiration in the Ci Sangkuy upper water catchment area (1/1/2008 - 31/12/2015).....	126
Figure 4-44 The distribution of new land cover classes with a similar range of LAI in the Ci Kapundung watershed in 2015.....	127
Figure 4-45 The distribution of new land cover classes with a similar range of LAI in the Ci Sangkuy watershed in 2015.....	128
Figure 4-46 New soil maps of the Ci Kapundung and Ci Sangkuy upper water catchment areas .....	131
Figure 4-47 A grid system used in MIKE SHE model.....	134
Figure 4-48 The implementation of Pareto-frontier analysis in the study .....	135
Figure 4-49 Distribution of land cover classes in the Ci Kapundung upper water catchment area .....	136
Figure 4-50 Distribution of land cover classes in the Ci Sangkuy upper water catchment area .....	136
Figure 4-51 Sixteen combinations of soil and land cover types the first case study area .....	138
Figure 4-52 Sixty-four combinations of precipitation, slope, soil and land cover classes in the first case study area .....	138
Figure 4-53 Decision tree diagram for the first phase of research.....	139

Figure 4-54 Decision tree diagram for the second phase of research to answer research question 2 .....	140
Figure 4-55 Decision tree diagram for the third phase of research to answer research question 2 .....	140
Figure 4-56 Decision tree diagram for the third phase of research to answer research question 3 .....	141
Figure 5-1 (a) The uncorrected map; (b) The corrected land cover map for the Ci Kapundung upper water catchment area in 2015 .....	142
Figure 5-2 (a-c) The results from the second iteration of image classification for the Ci Kapundung upper water catchment area in 2013, 2015, and 2017 respectively using SPOT imagery .....	144
Figure 5-3 (a-c) The results from the third iteration of image classification for the Ci Kapundung upper water catchment area in c.2000, 2015 and 2017 respectively using SPOT and Landsat imagery.....	147
Figure 5-4 The uncorrected map; (b) The corrected land cover map for the Ci Sangkuy upper water catchment area in 2015 .....	149
Figure 5-5 (a-c) The results from the second iteration of image classification for the Ci Sangkuy upper water catchment area in c.2000, 2015 and 2017 respectively using SPOT and Landsat imagery.....	150
Figure 5-6 (a) Gains and losses of six land cover types in the first case study area between 2013 and 2015 (km <sup>2</sup> ); (b) the contribution of all land cover types to the increasing developed areas in 2015 .....	152
Figure 5-7 (a) Gains and losses of six land cover types in the first case study area between 2000 and 2015 (km <sup>2</sup> ); (b) the contribution of all land cover types to the increasing developed areas in 2015 .....	153
Figure 5-8 Change map of the first case study area (2000-2015) .....	153
Figure 5-9 Gain and losses of six land cover types in the second case study area between 2000 and 2015 (km <sup>2</sup> ); (b) the contribution of all land cover types to the increasing developed areas in 2015 .....	154
Figure 5-10 Change map of the second case study area (2000-2015) .....	154
Figure 5-11 Flow duration curve for the Ci Tarum River (2008-2015).....	158
Figure 5-12 The regression diagrams showing the correlation between peak direct runoff and rainfall events in Bandung Basin (2008-2015).....	159
Figure 5-13 The 5-year Moving Average of Ci Tarum annual river discharge .....	160
Figure 5-14 The 5-year Moving Average of annual river discharge in the Ci Kapundung upper water catchment area.....	161
Figure 5-15 The composition of land cover in the Ci Kapundung upper water catchment area .....	161

Figure 5-16 The 5-year Moving Average of precipitation rates from; (a) Thiessen-weighted polygons; (b) Kayu Ambon station; (c) Dago Pakar station; (d) Cipeusing station; (e) Margahayu station; and (f) Cibiru station .....	162
Figure 5-17 The 5-year Moving Average of annual river discharge in the Ci Sangkuy upper water catchment area .....	163
Figure 5-18 The composition of land cover in the Ci Sangkuy upper water catchment area .	163
Figure 5-19 The 5-year Moving Average of precipitation rates from; (a) Thiessen-weighted polygons; (b) Cileunca; (c) Ciherang; (d) Cisondari; (e) Cibeureum .....	164
Figure 5-20 (a-e). Constraints maps which delineate areas restricted to the further development of settlements and agriculture in scenario 1, 2, and 3 in the Ci Kapundung watershed .....	168
Figure 5-21 (a-e). Constraints maps which delineate areas restricted to the new development of settlements and agriculture in scenario 1, 2, and 3 in the Ci Sangkuy watershed	169
Figure 5-22 Four drivers of land change in the first case study area: (a) existing disturbance; (b) existing road networks; (c) river networks; (b) the likelihood of area to change....	170
Figure 5-23 (a-c) Initial simulation results for the 2030 land cover of Ci Kapundung upper water catchment area based on scenario 1, 2, and 3 .....	172
Figure 5-24 Driver variables in the land change modelling for the first case study area; (a) likelihood to change; (b) distance from disturbance; (c) population density; (d) elevation; (e) slopes; (f) distance from streams .....	174
Figure 5-25 (a) Potential transition map in 2017; (b) Projected 2017 land cover map based on the Status Quo scenario.....	176
Figure 5-26 (a-d) The projected 2030 land cover maps of the first case study area based on scenario 1, 2, 3, and 4 .....	179
Figure 5-27 Driver variables in the land change modelling for the second case study area; (a) likelihood to change; (b) distance from disturbance; (c) population density; (d) elevation; (e) slopes; (f) distance from streams .....	181
Figure 5-28 (a) Potential transition map in 2017; (b) Projected 2017 land cover map based on the Status Quo scenario.....	183
Figure 5-29 (a-d) The projected 2030 land cover maps of the second case study area based on scenario 1, 2, and 3 .....	185
Figure 5-30 The location of three observation points in the Ci Kapundung upper water catchment area in MIKE SHE 1 model.....	187
Figure 5-31 Simulated discharges (2008-2015) in the Ci Kapundung upper water catchment area (uncalibrated model) .....	188
Figure 5-32 Simulated discharges (2008-2015) in the Ci Sangkuy upper water catchment area (uncalibrated model) .....	188
Figure 5-33 Simulated discharges (2008-2015) in the Ci Kapundung upper water catchment area (calibrated model).....	189



Figure 5-34 Simulated discharges (2008-2015) in the Ci Sangkuy upper water catchment area (calibrated model).....	189
Figure 5-35 Projected discharges in the Ci Kapundung upper water catchment area .....	190
Figure 5-36 Projected discharges in the Ci Sangkuy upper water catchment area .....	190
Figure 5-37 Accumulated overland boundary outflow of Ci Kapundung upper water catchment area with 16 combinations of different land cover and soil types (2008-2015) (mm) .....	194
Figure 5-38 Accumulated overland boundary outflow of a hypothetical catchment with 32 combinations of different land cover, soil types, and slope gradients under low rainfall event (2008-2015) (5 mm/day) .....	195
Figure 5-39 Accumulated overland boundary outflow of a hypothetical catchment with 32 combinations of different land cover, soil types, and slope gradients under high rainfall event (2008-2015) (100 mm/day).....	196
Figure 6-1. (a) Infrared image of the forest in Ci Kapundung watershed; (b) Distribution of error surrounding clouds (orange circle) .....	199
Figure 6-2. White pixels identified as developed areas in the 2015 Landsat imagery of the first case study area .....	200
Figure 6-3 The annual trend of Ci Tarum River discharges and the precipitation in Bandung Basin .....	213
Figure 6-4. Annual precipitation rates recorded by nine weather stations in the two case study areas and the indication of strong La Nina and very strong El Nino events .....	214
Figure 6-5 The proposed Design discharges for Ci Tarum and its tributaries in 2007 .....	219
Figure 6-6 Land cover compositions of Ci Kapundung upper water catchment area on flat-moderate and steep slopes.....	221
Figure 6-7 Land cover compositions of Ci Sangkuy upper water catchment area on flat-moderate and steep slopes.....	222
Figure 6-8 Soil compositions in the Ci Kapundung upper water catchment area on flat-moderate and steep slopes.....	222
Figure 6-9 Soil compositions in the Ci Sangkuy upper water catchment area on flat-moderate and steep slopes.....	222
Figure 6-10 Rainfall and the physical attributes influencing the flood regulation in the Ci Kapundung upper water catchment area .....	225
Figure 6-11 Total areas on flat-moderate slopes and are covered by vegetation in the Ci Kapundung upper water catchment area .....	225
Figure 6-12 Scenario projection of overland flow in the Ci Kapundung upper water catchment area .....	226
Figure 6-13 Rainfall and the physical attributes influencing the flood regulation in the Ci Sangkuy upper water catchment area .....	227

Figure 6-14 Total areas on flat-moderate slopes and are covered by vegetation in the Ci Sangkuy upper water catchment area .....	227
Figure 6-15 Scenario projection of overland flow in the Ci Sangkuy upper water catchment area .....	228
Figure 7-1 Constraints maps which delineate: (a-b) areas restricted to the new development of settlements and agriculture; (c-d) outside the area to be planted with conifers and mixed vegetation .....	235
Figure 7-2 The projected 2030 land cover map of the first case study area based on scenario 4 .....	236
Figure 7-3 Constraints maps which delineate areas restricted to the new development of settlements and agriculture (a-b) and areas to be planted with broad-leaved trees and conifers (c-d) in scenario 4 .....	238
Figure 7-4 The projected 2030 land cover map of the second case study area based on scenario 4.....	239
Figure 7-5 Simulated discharges (2008-2015) in the Ci Kapundung upper water catchment area .....	241
Figure 7-6 Simulated discharges (2008-2015) in the Ci Sangkuy upper water catchment area (scenario 4).....	242
Figure C-1 (a-b). Section A-A' of Ci Tarum River (662.039 – 664.00 m asl) .....	267
Figure C-2 (a-b). Section B-B' of Ci Tarum River (661.00 – 662.7827 m asl) .....	268
Figure D-1 Flow duration curve for the Ci Kapundung River (2008-2015).....	277
Figure D-2 Flow duration curve for the Ci Sangkuy River (2008-2015).....	278
Figure E-1 Simulated overland outflow from Ci Kapundung catchment covered by broad-leaved vegetation with soil A, B, C, and D .....	280

## LIST OF TABLES

Table 3-1 Runoff coefficients of all water catchments in Bandung Basin in 1983, 1993, and 2002 .....	51
Table 3-2 Estimated baseflow of eight rivers in the Bandung Basin .....	58
Table 3-3 Estimated runoff coefficients for the eight watersheds in the Bandung Basin (2008-2016) .....	59
Table 3-4 Annual rainfall rates in Ci Kapundung upper catchment and the downstream .....	60
Table 4-1 The existing spatial plans for Bandung City, Bandung regency, and West Bandung Regency .....	99
Table 4-2 West Java Province population growth projection (2010-2035) .....	100
Table 4-3 Population in the four districts in the watersheds (2015 and 2017) .....	101
Table 4-4 Transition probability matrix .....	102
Table 4-5 Allometric equations to estimate biomass and LAI from various plant species .....	116
Table 4-6 Estimated mean value of LAI of plant species in the case study areas .....	117
Table 4-7 The composition of each soil type in the Ci Kapundung upper water catchment area .....	120
Table 4-8 The composition of each soil type in the Ci Sangkuy upper water catchment area .....	121
Table 4-9 The list of estimated LAI values for reclassified land cover types .....	126
Table 4-10 Crop coefficient (Kc) and root depth of all land cover types in the two case study areas .....	129
Table 4-11 Manning's N and M values of land cover used in the MIKE SHE model .....	129
Table 4-12 Soil reclassification in the Ci Kapundung upper water catchment area .....	130
Table 4-13 Soil reclassification in the Ci Sangkuy upper water catchment area .....	130
Table 4-14 Soil parameters for the Ci Kapundung hydrology model .....	131
Table 4-15 Soil parameters for the Ci Sangkuy hydrology model .....	132
Table 4-16 Geological layer parameters for the Ci Kapundung hydrology model .....	133
Table 4-17 Geological layer parameters for the Ci Sangkuy hydrology model .....	133
Table 5-1 Confusion matrix for the 2013 land cover map of the Ci Kapundung watershed (second iteration) .....	145
Table 5-2 Confusion matrix for the 2015 land cover map of the Ci Kapundung watershed (second iteration) .....	145
Table 5-3 Confusion matrix for the 2017 land cover map of the Ci Kapundung watershed (second iteration) .....	145
Table 5-4 Confusion matrix for the 2015 land cover map of the Ci Kapundung watershed (third iteration) .....	148
Table 5-5 Confusion matrix for the 2017 land cover map of the Ci Kapundung watershed (third iteration) .....	148
Table 5-6 Confusion matrix for the 2015 land cover map of the Ci Sangkuy watershed .....	151

Table 5-7 Confusion matrix for the 2017 land cover map of the Ci Sangkuy watershed.....	151
Table 5-8 The predicted return periods and discharges of Ci Tarum River .....	155
Table 5-9 Samples of the Ci Tarum streamflow data and the rank within the period of 2008-2015.....	157
Table 5-10 Existing and projected population in Bandung city, Bandung regency, and West Bandung regency.....	165
Table 5-11 The estimated population in five districts in the two case study areas (2015 and 2030) .....	165
Table 5-12 Land cover composition in the Ci Kapundung upper water catchment area for each scenario.....	173
Table 5-13 Driver variables of land change in the first case study area .....	175
Table 5-14 Transition probability matrix to simulate the 2017 land cover map of the first study area .....	175
Table 5-15 Model accuracy retrieved from the validation process.....	176
Table 5-16 Transition probability matrix to simulate the 2030 land cover map of the first study area .....	177
Table 5-17 Land cover composition in the Ci Kapundung upper water catchment area for each scenario.....	179
Table 5-18 Driver variables of land change in the second case study area.....	181
Table 5-19 Transition probability matrix to simulate the 2017 land cover map of the second study area .....	182
Table 5-20 Model accuracy retrieved from the validation process.....	182
Table 5-21 Transition probability matrix to simulate the 2030 land cover map of the second study area .....	184
Table 5-22. Land cover compositions in the Ci Sangkuy upper water catchment area for each scenario.....	186
Table 5-23. The estimated depth of overland flow (mm) from the first iteration of hydrologic simulations of the Ci Kapundung upper water catchment area.....	187
Table 5-24 The highest observed and simulated discharges in the Ci Kapundung and Ci Sangkuy upper water catchment areas in each scenario.....	191
Table 5-25 Accumulated water balance of Ci Kapundung upper water catchment area (2008-2015) (mm).....	191
Table 5-26 Accumulated water balance of Ci Sangkuy upper water catchment area (2008-2015) (mm).....	192
Table 5-27 Accumulated water balance of Ci Kapundung upper water catchment area with a uniform land cover type (2008-2015) (mm).....	192
Table 5-28 Accumulated water balance of Ci Sangkuy upper water catchment area with a uniform land cover type (2008-2015) (mm).....	193

Table 5-29 The depth of overland flow (mm) estimated from the 2030 land cover map of Ci Kapundung watershed with a single type of vegetation (MIKE SHE 1) .....	193
Table 6-1. The overall accuracies of individual land cover maps generated from SPOT 6 imagery .....	203
Table 7-1 The altered Markov matrix to simulate the 2030 land cover map of the first study area .....	236
Table 7-2 Land cover composition in the Ci Kapundung upper water catchment area in scenario 4 compared to the other scenarios .....	237
Table 7-3 The altered Markov matrix to simulate the 2030 land cover map of the second study area .....	239
Table 7-4 Land cover composition in the Ci Sangkuy upper water catchment area in scenario 4 compared to the other scenarios.....	240
Table 7-5 Simulated water balance of Ci Kapundung upper water catchment area (2008-2015) (mm) .....	241
Table 7-6 Simulated water balance of Ci Sangkuy upper water catchment area (2008-2015) (mm).....	243
Table A-1 Calibrated parameters for Ci Kapundung model.....	261
Table A-2 Calibrated parameters for Ci Sangkuy model.....	262
Table B-1 Confusion matrix for the 2015 uncorrected land cover map of the Ci Kapundung watershed (first iteration).....	263
Table B-2 Confusion matrix for the 2015 corrected land cover map of the Ci Kapundung watershed (first iteration).....	264
Table B-3 Confusion matrix for the 2015 uncorrected land cover map of the South Ci Sangkuy watershed (first iteration) .....	264
Table B-4 Confusion matrix for the 2015 corrected land cover map of the Ci South Sangkuy watershed (first iteration) .....	264
Table D-1 Samples of the Ci Kapundung streamflow data and the rank within the period of 2008-2015.....	268
Table D-2 Samples of the Ci Sangkuy streamflow data and the rank within the period of 2008-2015.....	269
Table E-1 Initial results from water balance analysis for the Ci Kapundung upper water catchment area (mm) (2008-2015).....	271
Table E-2 Final results from the water balance analysis for the Ci Kapundung upper water catchment area (mm) (2008-2015) .....	272
Table F-1 Accumulated water balance of Ci Kapundung upper water catchment area with a uniform land cover type (2008-2015) (mm) .....	275
Table F-2 Accumulated water balance of Ci Sangkuy upper water catchment area with a uniform land cover type (2008-2015) (mm) .....	275



## LIST OF EQUATIONS

Equation 2-1.....	30
Equation 3-1.....	58
Equation 3-2.....	58
Equation 3-3.....	58
Equation 4-1.....	83
Equation 4-2.....	83
Equation 4-3.....	83
Equation 4-4.....	84
Equation 4-5.....	84
Equation 4-6.....	101
Equation 4-7.....	106
Equation 4-8.....	106
Equation 4-9.....	107
Equation 4-10.....	107
Equation 4-11.....	108
Equation 4-12.....	109
Equation 4-13.....	110
Equation 4-14.....	111
Equation 4-15.....	112
Equation 4-16.....	115





# Chapter 1 Introduction

The concept of ecosystem services has become a research focus that is related to biodiversity and an environmental context, as well as ecological processes and human activities (Bennett et al., 2015; Chaudhary et al., 2015; Abson et al., 2014). According to the Millennium Ecosystem Assessment (2005), the term 'ecosystem services' is defined as "the benefits ecosystem provide to human wellbeing" (p.V), and is divided into four categories (e.g. supporting, provisioning, regulating, and cultural services). This research is focused on the flood regulation service provided by watershed ecosystems. According to Stürck et al. (2014), 'flood regulation' refers to the ecosystem service to reduce flood risk prompted by rainfall events with a high precipitation level.

It is argued that landscape structure affects the provision of ecosystem services. Landscape structure and ecological processes generate a capacity for ecosystems to provide services (Kangas et al., 2018). Landscape structure, which is described as "the spatial relationships among distinctive ecosystems or element present" (Forman & Godron, 1986 p.11), can be altered by natural processes and human activities (Sohel, Mukul, & Burkhard, 2015; Forman, 1995). Extensive agriculture practices in newly cleared forests and the massive development of new settlements in riparian areas are some examples of anthropogenic activities which change the landscape structure and have become a threat to the sustainability of ecosystem services. However, it cannot be denied that high demand for new settlement areas and agricultural land farms has been a prevalent issue for a local government land-use planning.

This research aims to investigate potential landscape structure scenarios of two upper water catchment areas<sup>1</sup> in Bandung Basin, Indonesia. The objectives of this study are to simulate land cover changes using a land change model, to assess the changes on flood regulation using a hydrologic model, and to determine the types of vegetation that can improve flood regulation in each upper water catchment area.

## 1.1 Research background

Bandung Basin is a lacustrine plain in the Ci Tarum watershed in West Java Province. Among all provinces in Indonesia, West Java is considered to be the most susceptible province to drought and flood events during El Nino and La Nina respectively (the Directorate of Plant Protection 2000 *cited in* Boer et al., 2012). The Bandung Basin covers an area of 338,394 hectares and is surrounded by mountains and hills where nine protected areas are located (Figure 1-1).

---

<sup>1</sup> Chow, Maidment, & Mays (1988) define the term catchment or watershed as "the area of land draining into a stream at a given location".

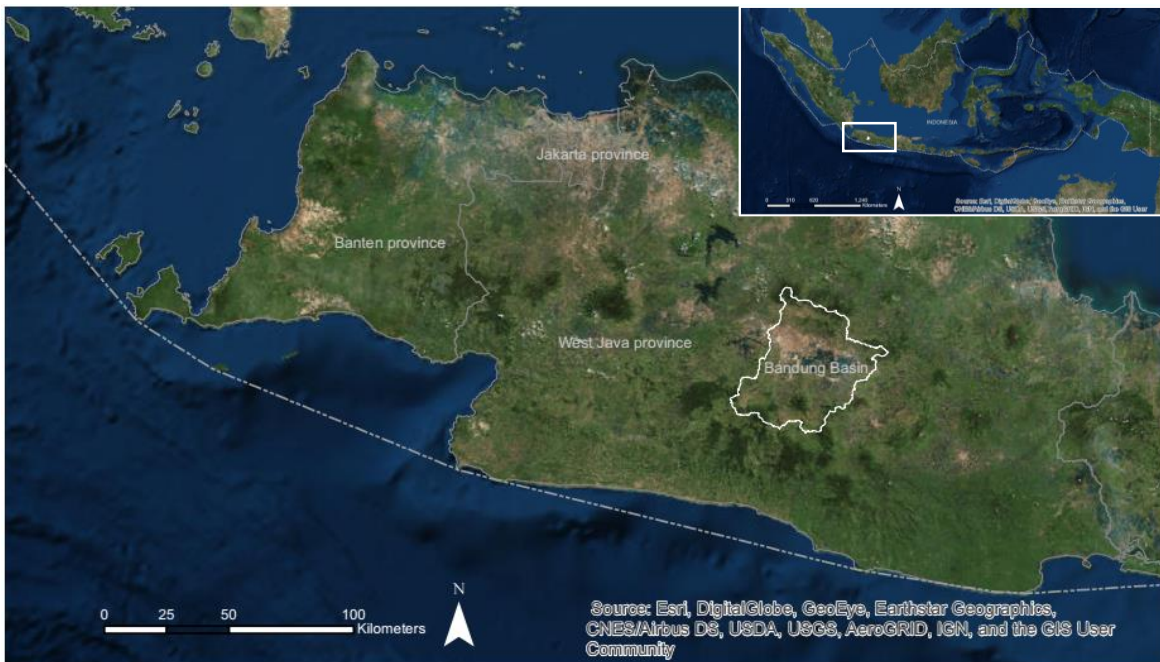


Figure 1-1 Bandung Basin in the West Java province. Inset map shows the location of West Java in Indonesia (Indonesia and province maps from BIG (*Badan Informasi Geospasial*/ Indonesia Geospatial Agency), the Ministry of Home Affairs, Ministry of Foreign Affairs, Ministry of Defence, Ministry of Maritime Affairs and Fisheries, DITOP TNI-AD, DISSURPOTRUD TNI-AU, and DISHIDROS TNI-AL. Source of background image: Esri, DigitalGlobe, GeoEye, Earthstar Geographics, CNES/Airbus DS, USDA, USGS, AeroGRID, IGN, and the GIS User Community)

Floods which occur in the Bandung Basin are affected by the regulating services degradation of the water catchment areas and heavy sedimentation in its main rivers. Natural landscape fragmentation in the water catchment areas derives from the high demand for new settlement and agricultural land farms which prompts the degradation of ecosystem services to accelerate. According to Haryanto et al. (2007), runoff coefficients for all water catchment areas in Bandung Basin were increased over the period 1983-2002 and contributed to the occurrence of floods. The floods were affected by the land-use changes in the basin from permeable to impervious surfaces; the forest area was reduced by 21.89% while the urban area increased by 6.36% during the same period.

The occurrence of flood events in Bandung Basin has been recorded since the beginning of the 20<sup>th</sup> century. Newspaper archives (e.g. *Bataviaasch Nieuwsblad*, *Het Nieuws van den dag*, *Arnhemsche Courant*, *Provinciale Overijsselsche en Zwolsche Courant*, *De vrije pers*, *Java-bode*, *Pikiran Rakyat*, and *Kompas*) from 1916 to 2015 described flood events in various parts of Bandung city and Bandung regency caused by the overflowing of the Ci Kapundung, Ci Tarik, and Ci Tarum Rivers. In addition, a report from BNPB (*Badan Nasional Penanggulangan Bencana*/ Indonesian National Board for Disaster Management) showed that at least 13 flood events occurred in Bandung Basin in 2014-2015.

A river improvement project has been proposed and implemented in the Bandung Basin by JICA (Japan International Cooperation Agency) to increase the flow capacity of Ci Tarum River in 1987-2010. After the first two stages of the project (1987-2007), the inundated areas during

the major floods were reported as decreasing, compared with the flooded areas in 1986. According to the data from JICA (2010), the total flooded area in 1986 was 71 km<sup>2</sup>, whereas the inundated areas in 2005, 2006, and 2007 decreased to 22.1 km<sup>2</sup>, 25.2 km<sup>2</sup>, and 32.6 km<sup>2</sup> respectively. However, although a river improvement project has been conducted, the floods still occur in the area due to the heavy sedimentation and extreme runoff from the upper catchment areas in the basin (JICA, 2010). Therefore, the proposed scenarios of landscape structure, which can contribute to minimising the runoff to the main rivers in the basin, are required.

This study assesses landscape structure and the provision of flood regulation from two case studies in the Bandung Basin. The two case studies are located in the Ci Kapundung and the Ci Sangkuy upper water catchment areas. The watersheds encompass areas of 102.86 sq km and 204.99 sq km and are situated in the northern and southern parts of the basin respectively. Ci Kapundung is the fastest degrading catchment area, and it has the highest runoff coefficient among all the catchment areas in the Bandung Basin in 1983-2002 (Haryanto, Herwanto, & Kendarto, 2007). On the other hand, Ci Sangkuy River has high fluctuation in terms of the maximum and minimum discharge, high rates of erosion (182 ton/Ha/year) and sedimentation in Saguling reservoir (3.02 – 4.32 mil m<sup>3</sup>/year) (Sarminingsih 2007 *cited in* Subarna 2015).

Both case study areas have different landscape scales and depict distinctive environmental settings. The southern part of the Ci Kapundung upper water catchment area is located in Bandung city. New settlements and tourism facilities were mostly built in the central part of the watershed in recent years, whereas the eastern part of the area is conserved as a protected area (i.e. *Taman Hutan Raya*<sup>2</sup> Ir. H. Djuanda). On the other hand, Ci Sangkuy watershed is located in a rural area. The landscapes are predominantly covered by agricultural areas, settlements, and forests. There is also a protected area (i.e. *Cagar Alam*<sup>3</sup> Tilu Mt.) in this upper water catchment area, which is located in the western part of the area.

Previous studies have been conducted to assess the impact of land-use changes on the runoff generation process in different catchment areas in Indonesia. These studies analysed the influences of land-use changes on the magnitude of the river and the runoff in the Way Kuala Garuntang water catchment area, Bandar Lampung (Yuniarti, 2013), and the Kali Gata water catchment area, Surakarta (Sudarto, 2009), as well as in Jakarta (Wiryawan, 2017). Other studies were conducted in the upper Ci Tarum watershed (Lasco & Boer 2006; Djuwansah 2009; Mulyadi 2010; Adrionita 2011; Tommi 2011; Wahdani 2011; Hidayat et al. 2013), the Ciwidey watershed (Putri, 2016), the Ci Sangkuy watershed (Subarna, 2015), the upper Citanduy watershed (Karim, 2014), the Bandung Regency (Warmerdam, 2014), and the Cipopokol water catchment area, the Bogor Regency (Arini et al., 2007) using hydrologic models to predict the

---

<sup>2</sup> The term *Taman Hutan Raya* is equal to category V of protected area (Protected Landscape/Seascape), according to IUCN (International Union for Conservation of Nature)

<sup>3</sup> The term *Cagar Alam* is equal to category Ia of protected areas which have the highest protection among all types of protected area.

watershed hydrological conditions. However, these studies did not specify particular types of vegetation which could reduce the runoff, or their potential composition and spatial distribution in each case study. Therefore, the study of vegetation characteristics in Indonesia, which could benefit flood regulation on a watershed scale, is still needed. In particular, there is a need to assess the impact of land-use changes on the hydrological process (DeFries & Eshleman, 2004 cited in Amatya et al., 2013).

## 1.2 Scope of the thesis

This research project was conducted within the context of landscape ecology and ecosystem services discourse (Figure 1-2). Within the broader study of landscape ecology, this thesis focuses on the assessment of landscape structure and change (Forman & Godron, 1986). Whereas in the concept of ecosystem services, this study specifically analyses the provision of flood regulation, as part of regulating services in water catchment areas.

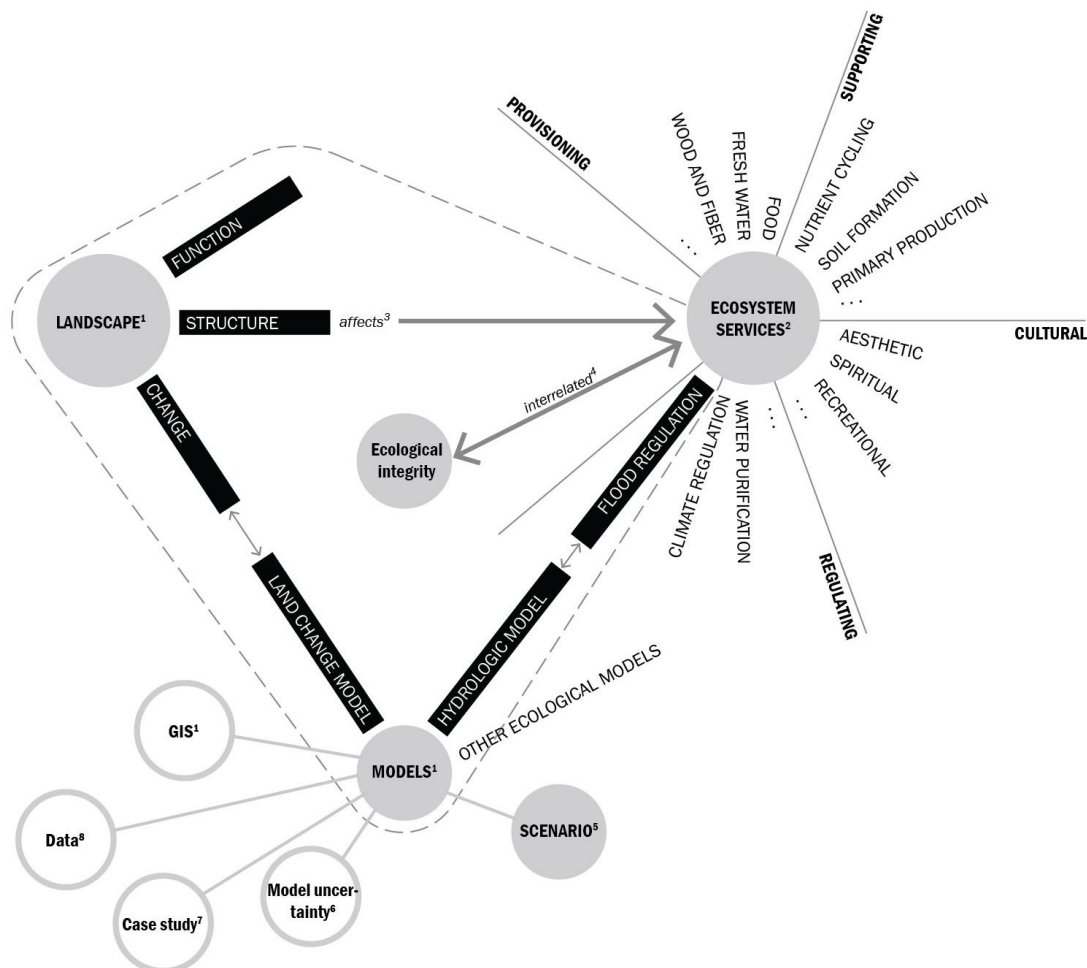


Figure 1-2 Scope of the thesis (the diagram was created based on literature review: <sup>1</sup>Forman (1986); <sup>2</sup>Millenium Ecosystem Assessment (2005); <sup>3</sup>Forman (1995); <sup>4</sup>La Notte et al. (2017); <sup>5</sup>Peterson et al. (2003); <sup>6</sup>Refsgaard & Storm (1996), Verburg et al. (2013), Vliet et al. (2016); <sup>7</sup>Turner (2013); <sup>8</sup>Brown et al. (2014))

Land change and hydrologic models were used to explore potential future landscape structure scenarios which aim to maintain the sustainability of flood regulation. Scenarios are described as “hypothetical results of events which are designed to highlight the consequences of certain decisions” (Rotmans et al. 2000 cited in Rosenberg et al. 2014 p.2). The assessment of factors which influence the sustainability of ecosystem services is expected to contribute to landscape ecology discourse, as suggested by Turner et al. (2013). In this context, the sustainability concept refers to the state of ecological integrity and the availability of resources to meet basic human needs (Forman, 1995).

The term landscape structure can also be defined as a landscape pattern, which is determined by various factors, including the arrangement and distribution of landscape elements (Walz, 2011). In this research project, the physical surface materials (land cover) were identified and mapped as a spatial unit using remote sensing, GIS (Geographic Information Systems), and auxiliary data (Figure 1-3).

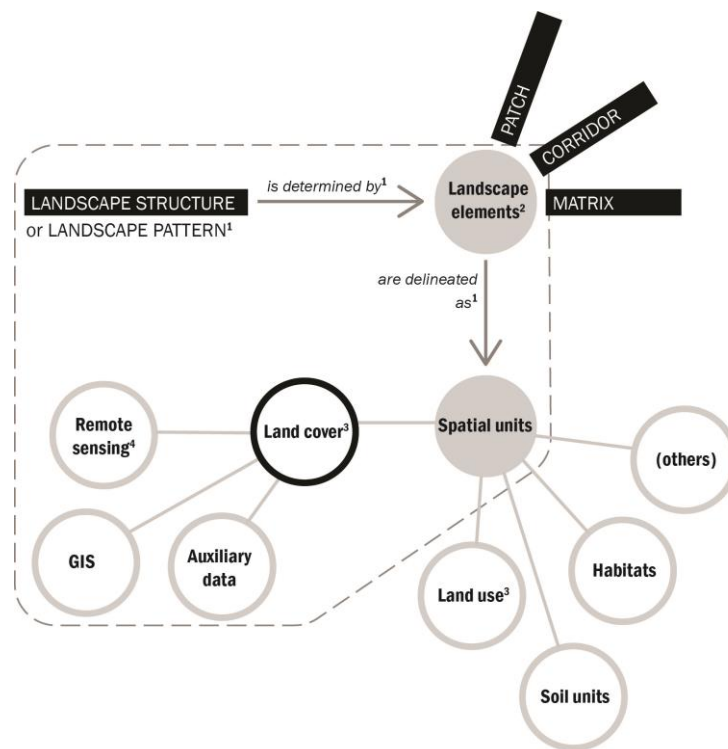


Figure 1-3 The assessment of landscape structure in this research (Sources: <sup>1</sup>Walz (2011); <sup>2</sup>Forman (1986); <sup>3</sup>Fisher, Comber, & Wadsworth (2005); <sup>4</sup>Lillesand, Kiefer, & Chipman (2008))

### 1.3 Research questions

This research was conducted in response to the following questions:

- (1) **How does the land cover alteration in the Ci Kapundung and Ci Sangkuy upper water catchment areas affect flood regulation in the Bandung Basin?**

Ci Kapundung and Ci Sangkuy upper water catchment areas have different biophysical characteristics and scales. The biophysical characteristics include the land cover composition and distribution in the catchments, geomorphology, hydrology, and the geology of the sites. The first research question specifically assesses the effects of land cover alteration in both case study areas on flood regulation in Bandung Basin.

- (2) **What are the most effective scenarios of landscape structure for the two upper water catchment areas which can benefit flood regulation?**

This research assesses the potential scenarios of landscape structure (i.e. land cover composition and spatial distribution, given the particular types of soil, the geomorphology and geology of the case study areas, and the river networks). Assumptions and uncertainties in the development of land change scenarios, land change simulations, and the parameters for hydrologic simulations are addressed in this thesis.

- (3) **Which types of vegetation can improve flood regulation in each upper water catchment area?**

Hydrologic simulations were performed using scenarios of landscape structure with different types of vegetation. Vegetation with different parameters, such as the Leaf Area Index (LAI) and root depth, were assigned, and the results from hydrologic model provide an insight into how particular types of vegetation can contribute significantly to minimalising surface runoff in the upper catchment areas.

This thesis contributes to filling the gap of the study found in the literature review (Figure 1-4). This study used an integrated Cellular Automata (CA) and Markov (CA-Markov) model to simulate the future land change in the two case study areas. **Despite wide applications of the modelling to predict urban growth in various studies, the application of CA-Markov to model forest cover is understudied** (Ghosh et al., 2017). Approximately 48% and 43% of total areas of Ci Kapundung and Ci Sangkuy upper water catchment areas, respectively, are still covered by forests in 2015<sup>4</sup>. Therefore, this study attempted to examine the forest cover change along with the urban growth in both areas using the CA-Markov model (Gap 1).

---

<sup>4</sup> The land cover compositions were retrieved from land cover maps (2015) developed from SPOT 6 satellite imagery.

Hydrology modelling was employed in this study as part of the method to address the second and third research questions by predicting streamflow in each development scenario. It is argued that **only a few studies reviewed the capacities of different development scenarios to support the streamflow regimes** (Wu et al., 2015) (Gap 2). Land change and the runoff generation process in catchments in Indonesia have been assessed in at least fifteen studies, listed in the first sub-chapter. However, **types of vegetation found to be influencing surface runoff have not yet been explored** (Gap 3). This research also responded to a call for **a study to assess how the provision of ecosystem services might change with different landscape characteristic and scale** (Jones et al., 2013) (Gap 4).

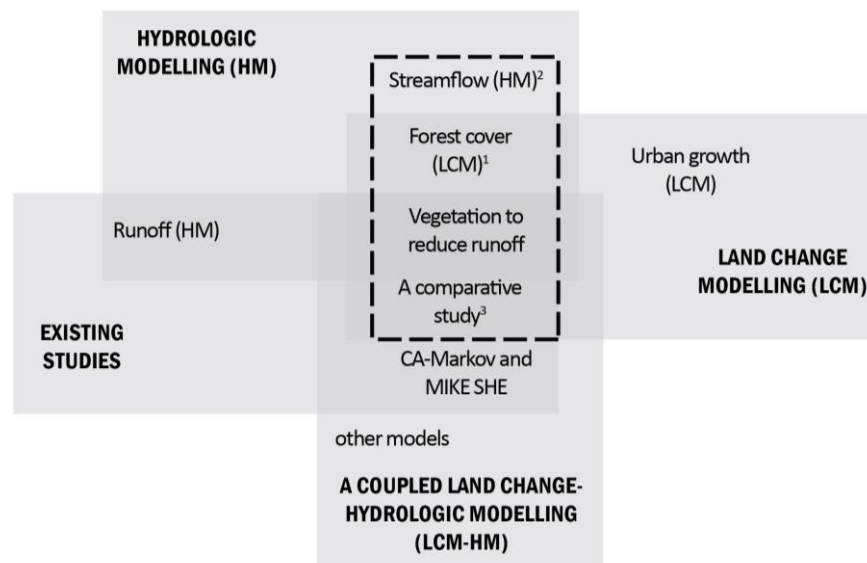


Figure 1-4 Gaps in knowledge addressed in this thesis (the diagram was created based on literature review: <sup>1</sup>Ghosh et al. (2017); <sup>2</sup>Wu et al. (2015); <sup>3</sup>Jones et al. (2012))

## 1.4 Thesis structure

The thesis was conducted in **three phases of study**: developing the land cover maps of Ci Kapundung and Ci Sangkuy upper water catchment areas, simulating the future landscape structure of the case study areas based on development scenarios, and conducting flood risk analysis and hydrologic modelling. This thesis consists of seven chapters, which describe the PhD project to assess the three research questions (Figure 1-5).

### (1) Chapter 1 Introduction

The first chapter of this thesis gives the background for conducting the PhD study, the research questions, and the thesis structure.

(2) Chapter 2 Literature review

The second chapter presents an overview of flood regulating service, the development of land cover maps using remote sensing, the description of scenarios and land change models, and the review of hydrologic models.

				<b>Chapter 1 - Introduction</b>
				1.1 Research Background
				<i>Problem statements:</i> <b>Ci Kapundung</b> is the fastest degrading watershed among all catchments in Bandung Basin, and <b>Ci Sangkuy</b> River has high fluctuation of maximum and minimum discharges, indicating a degradation of flood regulation in the catchments. <b>A combination between CA-Markov to model land change, and MIKE SHE to project future flow regimes in catchments</b> was used in this research. The applications of this integrated model in previous studies are rare, and none of the projects have been conducted using a case study in Indonesia before.
				1.2 Scope of the thesis
				1.3 Research questions:
				<b>Research Question (1)</b> How does the land cover alteration in the Ci Kapundung and Ci Sangkuy upper water catchment areas affect flood regulation in the Bandung Basin?
				<b>Research Question (2)</b> What are the most effective scenarios of landscape structure for the two upper water catchment areas which can benefit flood regulation?
				<b>Research Question (3)</b> Which types of vegetation can improve flood regulation in each upper water catchment area?
				1.4 Thesis structure
				<b>Chapter 2 - Literature review</b>
				2.1 Flood regulating service of water catchment area
				2.2 Land cover map development using remote sensing
				2.3 The development scenarios and land change models
				2.4 Flood risk assessment and the development of hydrologic models
				2.5 Conclusion to the literature review
				<b>Chapter 3 - Case study areas</b>
				3.1 Bandung Basin
				3.2 Case study areas as indicators of water catchments to cause flooding in Bandung Basin
				3.3 Ci Kapundung upper water catchment area
				3.4 Ci Sangkuy upper water catchment area
				3.5 Summary of Chapter 3
				<b>Chapter 4 - Methodology</b>
				4.1 The development of land cover maps (research phase 1)
				4.2 Scenario development and land change modelling (research phase 2)
				4.3 The assessment of flood risk and the impact of land cover change to support flood regulation (research phase 3)
				4.4 Hydrologic modelling (research phase 3)
				4.5 Decision tree diagrams and boundaries of research
				4.6 Summary of Chapter 4
				<b>Chapter 5 - Results</b>
				5.1 Land cover maps of the case study areas ( <b>phase 1</b> )
				5.2 The impact of land cover change in the two case study area on flood regulation in Bandung Basin ( <b>phase 2 and 3</b> )
				5.3 Landscape structure scenarios for the two case study areas to support flood regulation ( <b>phase 3</b> )
				5.4 Types of vegetation to improve flood regulation ( <b>phase 3</b> )
				5.5 Summary of Chapter 5
				<b>Chapter 6 - Discussion</b>
				6.1 The accuracy of land cover maps, land change and hydrologic models ( <b>phase 1 and 2</b> )
				6.2 Land cover alteration and the flood regulating service ( <b>phase 3</b> )
				6.3 The effective scenarios of landscape structure to support flood regulation ( <b>phase 2 and 3</b> )
				6.4 Characteristics of plants to improve flood regulation ( <b>phase 3</b> )
				6.5 Summary of Chapter 6
				<b>Chapter 7 - Planning recommendation</b>
				7.1 Land change modelling of Backcasting scenario (LCM 3)
				7.2 Implication of landscape planning to flood regulation (MIKE SHE 3)
				7.3 Summary of Chapter 7
				<b>Chapter 8 - Conclusions and outlook</b>
				8.1 Research novelty
				8.2 Main empirical findings
				8.3 Main methodological findings
				8.4 Research outlook

- : Chapters and subchapters related to data preparation
- : Chapters and subchapters related to research question 1
- : Chapters and subchapters related to research question 2
- : Chapters and subchapters related to research question 3

Figure 1-5 Thesis structure



This chapter also summarises the challenges in map developing process and model uncertainty from the literature. Conclusions to the literature review are given at the end of the chapter to provide a background of land change and hydrologic models selected.

### (3) Chapter 3 Study areas

The third chapter of this thesis introduces the context and environmental conditions of Bandung Basin and the case study areas; the Ci Kapundung and the Ci Sangkuy upper water catchment areas.

### (4) Chapter 4 Methodology

The fourth chapter presents the processes to develop land cover maps and scenarios, the selected methods to address the three research questions, the decision tree diagrams, and the boundaries in the research. Figure 1-6 shows the workflow in each phase of research as an iterative process, and the decision trees to address the three research questions.

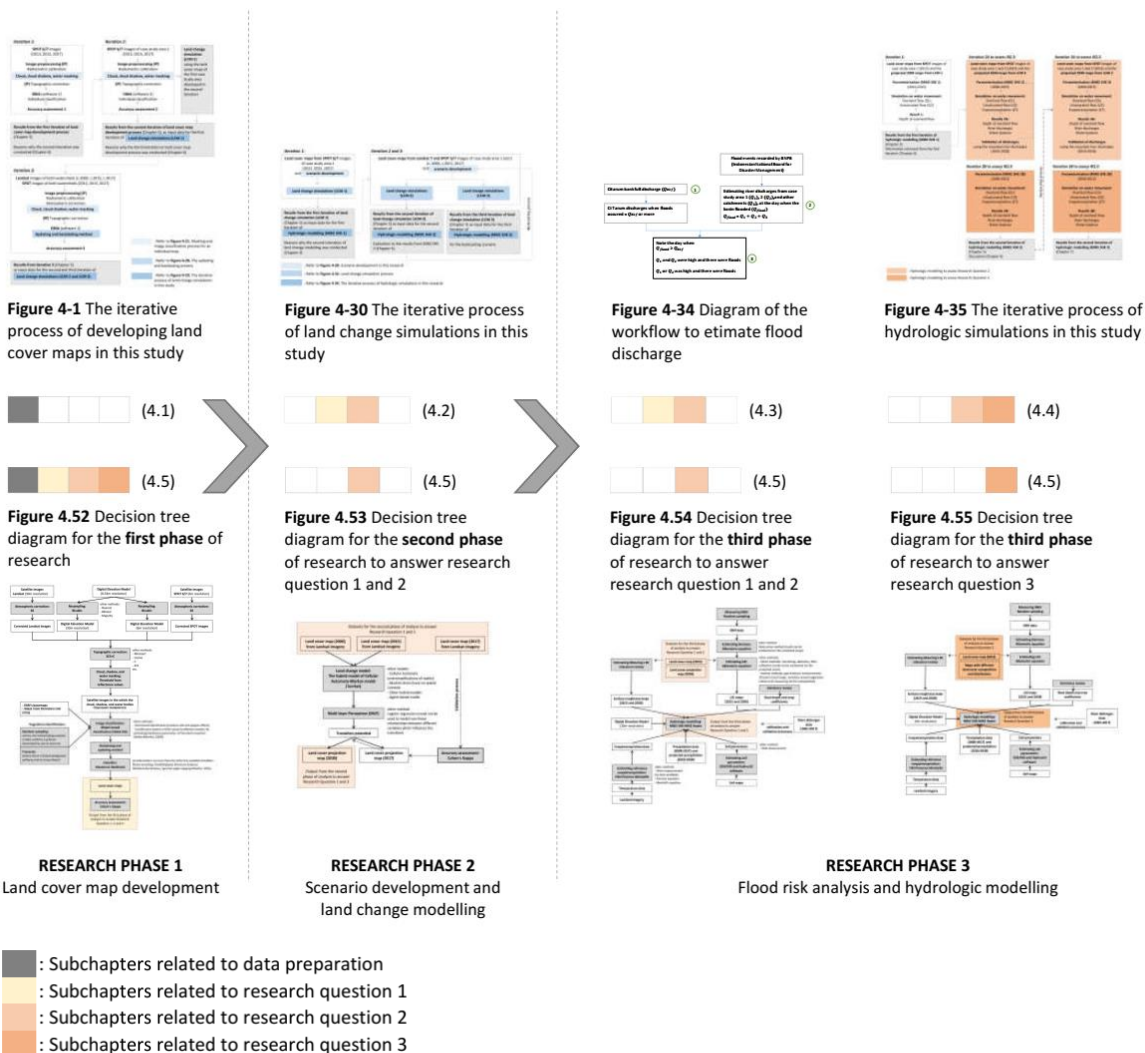


Figure 1-6 Structure for Chapter 4 Methodology

#### (5) Chapter 5 Results

The fifth chapter provides the results from land cover map development (research phase 1), and the outcomes from land change and hydrologic modelling to address the three research questions (research phase 2 and 3 respectively).

#### (6) Chapter 6 Discussion

The sixth chapter discusses the principal factors that influence the accuracy of land cover maps, including land cover change and hydrologic simulations. This covers the arguments regarding the outcomes from each research phase. The chapter also outlines the factors which influence the changes in flow regimes in the catchments. The following part presents reviews of future landscape structure scenarios in each case study area which can benefit flood regulation. The types of vegetation, which could be used to improve flood regulation, are discussed in the last section of this chapter.

#### (7) Chapter 7 Planning recommendation

The results from the final iteration of land change and hydrologic modelling are presented and discussed in this chapter.

#### (8) Chapter 8 Conclusions and outlook

The eighth chapter restates the novelty of the research and concludes the thesis with empirical findings from the research. The conclusions include the answers to the research questions, the contribution from research, the limitations and boundaries of the research, including suggestions for potential future studies on landscape structure and flood risk.

## Chapter 2 Literature review

Chapter 2 covers the review of literature on flood regulating services of water catchment areas, the development of land cover maps and scenarios, and the land change and hydrological modelling. Examples of previous research projects that have applied similar methods and the gaps of research are also provided in this chapter.

### 2.1 Flood regulating service of water catchment areas

Regulating services is one of four categories in ecosystem services (Millennium Ecosystem Assessment, 2005). The services are provided from the interactions between biotic and abiotic elements in the ecosystems (La Notte et al., 2017). It is argued that ecosystem services are interrelated with the concepts in ecological theory, such as ecological integrity and complexity (Kremen, 2005 *cited in* La Notte et al., 2017). One of the regulating services that becomes the focus of this research is the flood regulating service.

#### 2.1.1 Ecological integrity in a river ecosystem

Ecological integrity is a critical factor to sustain the regulating services in a river ecosystem. The ecological integrity is regulated by flow regimes, which refer to the patterns of river flow variation and are influenced by river size, climate, geology, topography, and vegetation (Poff et al., 1997). Poff et al. (1997) describe the five components of flow regimes with the following definitions. The magnitude of flow refers to the volume of water per unit time ( $m^3/s$  or  $ft^3/s$ ), which is affected by climate and the size of a watershed. Frequency is defined with the number of occurrence of flows exceeding a particular magnitude, while duration is described as a period when a specific flow condition occurs. The timing of flows is associated with the regularity of occurred flow discharges. The rate of change shows how quickly a flow changes from one magnitude to another.

Various elements, such as climate, geology, topography, soils, and vegetation, affect the amount of inflow water and the runoff pathway to the river (Poff et al., 1997). Land cover and land-use changes influence the rates of surface runoff in a watershed (Sajikumar & Remya, 2015), thus increasing the stream flashiness (Poff et al., 1997), and could potentially contribute to flooding (Schüler, 2007 *cited in* Hümann et al. 2011).

It is argued that modelling is needed to assess the flood regulating services provided by ecosystems functioning (Liquete et al. 2016 *cited in* La Notte et al. 2017). An identified landscape structure could be a basis for producing a scenario-based future landscape development. Turner et al. (2013) state that further studies are needed to examine possible scenarios of landscape development, and factors that influence the ecosystem services sustainability.

### 2.1.2 Vegetation to improve flood regulation

This research assesses different types of vegetation to improve flood regulation in case studies. Different types of vegetation have different rates of rainfall interception. Rainfall interception is argued to be a significant factor in the water balance of catchments (Liu et al., 2014). Merriam (1960) describes interception as a process involving a canopy to catch the rainfall, which is distributed to the ground, evaporated to the atmosphere, or absorbed into the plant. The evaporated rainfall or the absorbed water from this process is defined as interception loss (Merriam, 1960).

A study of rainfall interception in two types of forest in Eastern Tibet, China, shows that conifers have more interception loss than mixed forest due to the evapotranspiration of small water droplets from the coniferous leaves (Liu et al., 2014). A study was also conducted by Zabrett and Sraj (2015), assessing the rainfall interception of coniferous and deciduous trees in Slovenia. The result suggests that conifers intercept more rainfall than deciduous tree canopies.

There are three groups of factors influencing the rainfall interception; the tree characteristics, the meteorological factors and the rainfall factors (Xiao et al., 2000). The tree characteristics include the species, shape, and surface roughness of the tree. The meteorological factors comprise of wind speed, wind direction, solar radiation, and air temperature. The last factor is specifically related to the intensity, magnitude, and duration of rainfall. The rainfall interception rates also vary with geographical location (Venkatraman & Ashwath, 2016).

The characteristics of leaves are related to the Leaf Area Index (LAI). John Monteith & Unsworth (1973) defined the LAI as the area of one-sided leaves per unit of ground area. The definition can be applied for broad flat leaves. However, a different definition is needed to describe LAI for non-flat leaves (Chen & Black, 1992). Chen and Black (1992) later defined the LAI for non-flat leaves as “the total intercepting area per unit ground surface” (p.421). LAI is believed to affect rainfall interception (Herbert & Fownet 1999 *cited in* Konôpka et al. 2016). The leaf shape is one of the factors which influence the canopy water storage capacity and the estimation of interception loss (Chen & Li, 2016). A study on LAI of a subtropical broad-leaved forest in Taiwan conducted by Chen and Li (2016) showed that LAI has a positive correlation with the mean storage capacity. The outcome is in line with results retrieved by Zheng et al. (2018), who concluded that plants with higher LAI have higher percentages of interception loss.

There are different methods for LAI estimations; the direct methods and indirect methods (Bréda, 2003). The direct techniques include harvesting, allometry and litter collection. The collected litter is dried and weighted to estimate the dry mass of litter, which will be converted into LAI by multiplying the value with SLA (specific area index). Litter collection traps were used in many studies to measure LAI (e.g. Cotter, 2017; Isihara, 2011).

On the other hand, indirect methods consist of the transmission of radiation measurements and gap-fraction methods (Bréda, 2003). The gap-fraction measures have been applied in various

studies using canopy analysers, such as LAI-2000 (Chen & Li, 2016; Mason et al., 2012), or hemispherical image analysis (Basuki, 2015; Park & Cameron, 2008). However, it is argued that the indirect methods do not estimate the actual LAI, because the measurements also include not only the leaves but also other canopy elements, such as branches and stems (Bréda, 2003).

The development of technology in remote sensing has prompted the use of remotely sensed vegetation indices to estimate LAI. The LAI value can be obtained from one of the spectral vegetation indices (i.e. NDVI/ normalised difference vegetation index<sup>5</sup>) (Gigante et al., 2009). However, the LAI measurements of plants with complex canopies (i.e. forest with a high value of LAI) using vegetation indices still do not provide suitable results (Bréda, 2003).

Another LAI estimation method is the measurement using a 3D point cloud image (Hosoi & Omasa, 2009). In their study, Hosoi and Omasa (2009) used a portable LiDAR (light detection and ranging) scanner to obtain contact frequencies of laser beams on leaves and to estimate LAD (Leaf Area Density). The LAI, then, was calculated based on the LAD data.

In this research, the LAI values of different plants were estimated using allometric equations from previous studies, which were conducted on the same plant species or forest types in Indonesia and other tropical countries. One limitation identified from this method is that the LAI value resulted from the equations cannot be transferred to different areas (Deblonde, Penner, & Royer, 1994). This method is applied based on the premise that LAI correlates with the tree biomass, as suggested by Albaugh et al. (1998). Diameter at breast height (DBH) of the tree samples is measured, in which the results are used to estimate biomass<sup>6</sup> for each tree using a specific allometric equation. According to Siregar & Heriyanto (2010), DBH is known as one of the factors which affect biomass<sup>7</sup>. Then, using different equations, LAI values were calculated based on the biomass data.

## 2.2 Land cover map development using remote sensing

According to Fisher et al. (2005), land cover is defined as “the physical material at the surface of the Earth” (p.2). Land cover is one of the spatial units used to delineate landscape elements (e.g. patches, corridors, and matrices), in which their size, shape, arrangement and distribution determine the pattern of landscape (i.e. landscape structure) (Walz, 2011). Examples of the land cover are grasses, asphalt, trees, and water bodies. The term land cover is different from land-use. Land-use is a term to describe how people use the land (e.g. sports grounds and residential land). Land cover is identified by direct observation, while land-use can be classified

---

<sup>5</sup> NDVI is one of the widely used vegetation indices to measure vegetation biomass within a pixel. The NDVI value is the ratio of NIR-R (subtraction of the values in NIR band with the Red band) and NIR+R (added values of NIR and Red bands) (Champbell & Wynne, 2011).

<sup>6</sup> Biomass can be defined as “the total weight or mass of living organisms in an area” (Forman & Godron, 1986). Biomass can be calculated using direct methods, such as harvesting and weighting fresh and dried tree components, and indirect methods, such as using LiDAR (Beets et al., 2011).

<sup>7</sup> Other factors include tree height, stand density, and soil fertility.

based on the activities that occur on the land (Fisher, Comber, & Wadsworth, 2005). This subsection covers the process of land cover identification and the procedures to develop land cover maps (e.g. image preprocessing, masking, and image classification) using remote sensing.

### 2.2.1 Land cover identification

The application of remote sensing for mapping land cover has enabled many studies on monitoring the availability of ecosystem services (de Araujo Barbosa, Atkinson, & Dearing, 2015). According to Lillesand, Kiefer & Chipman (2008 p.1-2), remote sensing is a technique to collect environmental data from a distance using sensors. The sensors detect electromagnetic energy from the Earth surface, which reflects and emits the radiation (Lillesand, Kiefer, & Chipman, 2008 p.1-2). Reflectance is the brightness of a surface and is affected by the wavelength of incident radiation and the surface materials (Chambbell & Wynne 2011 p.52; Zhu 2016;). As shown in Figure 2-1, vegetation, soils, and water bodies have distinct characteristics of spectral reflectance.

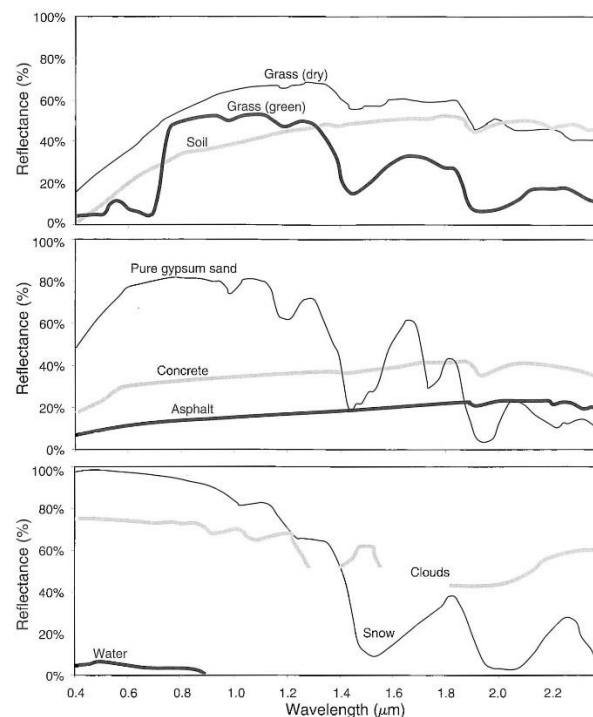


Figure 2-1 Spectral reflectance of vegetation, soils, and water bodies (Source: Lillesand, Kiefer & Chipman, 2008)

Chlorophyll absorbs radiation in blue and red bands for photosynthesis. Thus more green light is reflected, causing the living vegetation to appear as green to human eyes (Chambbell & Wynne, 2011). Most of the infrared radiation is either reflected by surfaces or transmitted. Therefore, in the infrared images, vegetation would appear very bright, compared to clear water. Thus the images are often used to distinguish land cover classes (Zhu, 2016; Chambbell & Wynne, 2011).

Dimopoulous, et al. (2014), classified sensors into four types: sensors with very high spatial resolution<sup>8</sup> (e.g. IKONOS, QuickBird, GeoEye, WorldView-2), sensors with medium-to-high spatial/ temporal resolution (e.g. Landsat, IRS, SPOT), sensors with coarse spatial resolution and very high temporal resolution (e.g. MODIS, AVHRR), hyperspectral sensors (e.g. HyMAP, CASI, Hyperion), Laser Scanning (LiDAR), and active microwave sensors. Spatial resolution is the size of a pixel in the imagery (Zhu, 2016). On the other hand, temporal resolution is related to the ability of remote sensing to record sequences of images (Champbell & Wynne 2011, p.286).

Consistent historical time series data has been provided by remote sensing using satellite imagery since 1960 (Herold, Goldstein, & Clarke, 2003). Land cover maps can be generated from remotely sensed data using remote sensing and geographic information systems (GIS) (Keshtkar & Voigt, 2016).

It is argued that the image resolutions influence the level of detail and accuracy of generated land cover maps (Toure et al., 2018). Townsend et al. (2009) suggest that coarse-scale imagery, such as Landsat with 30 metres of resolution, can be used to identify landscape pattern at a broad scale. Images retrieved from hyperspectral sensors, on the other hand, are not suitable for mapping large areas. SPOT imagery with medium spatial resolutions is appropriate for developing land cover maps of moderately sized areas. In a forest image with a resolution of 6 metres, a local variance can be detected easier than in the imagery with higher spatial resolution, where each pixel might represent both trees and their surroundings area (Woodcock & Strahler, 1987).

According to Helmer et al. (2012), despite the rapid development of remote sensing to map vegetation in various landscapes in the world, there are potential problems when mapping land cover in tropical areas. First, most of the images covering tropical forests have clouds as a data gap. Second, similar features of some types of vegetation viewed from the satellite imagery are prone to be misinterpreted at first glance. Third, a gap-filling process produces residual errors which make an overlap to different forest types. Fourth, there is limited reference data as training samples for image classification. Therefore, the data gap should be filled in with other image data from different dates and combined with data retrieved from field works (Helmer et al., 2012).

One method to fill the data gap during the image classification process is the backdating and updating method (Linke et al., 2009). A land change analysis is incorporated in the procedure by projecting a base map backwards and forwards. Therefore, only the area showing the land cover change in the previous or later imagery is classified, thus increasing the efficiency of the analysis. The backdating and updating method can be used to develop maps with multi-spatial

---

<sup>8</sup> Champbell & Wyne (2011 p.285) define the resolution as the remote sensing capacity to capture images and to show their spatial, spectral, and radiometric information.

resolution data. The method is particularly useful when there is limited access to get a high resolution of imagery at the start of the commercial satellite era (circa 2000) (Toure et al., 2018).

### 2.2.2 Satellite image preprocessing

Image preprocessing is required during the analysis of remote sensing data because the raw data may be distorted due to sensor-Earth geometry variations, or has deficiencies (Zhu, 2016). In the context of remote sensing data analysis, the term preprocessing refers to the operations which are required before conducting the principal analysis (Chambbell & Wynne 2011, p.305).

The two types of image preprocessing are geometric and radiometric calibration (Zhu 2016, p.245). Zhu (2016) describe the geometric calibration as a process to project the distorted coordinates of an image to correct coordinates (Figure 2-2). On the other hand, radiometric calibration is conducted to correct the brightness values which might be altered due to sensor malfunctions and atmospheric scattering (Zhu, 2016; Chambbell & Wynne, 2011).

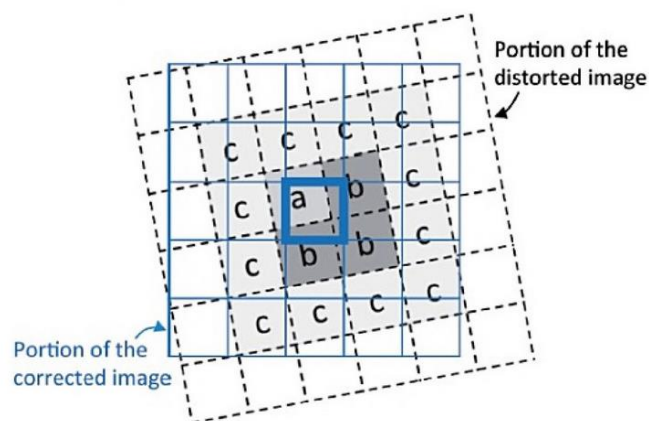


Figure 2-2 Superimposing a geometrically correct image on a distorted image (Source: Zhu 2016)

Pixel values, which appear as digital numbers (DNs) in the satellite images, do not represent the brightness of the actual object. Using the DN, the brightness of an image cannot be examined over time, or compared with different scenes. The DN, therefore, should be converted into the radiance to get the objects' original brightness (Chambbell & Wynne, 2011 p.311).

In remote sensing analysis (e.g. the assessment of vegetation index), the biophysical information of objects can be acquired from reflectance values or properties of objects which are observed by a sensor. A radiance-to-reflectance conversion should be conducted during the radiometric correction process to get the objects' reflectance values (Zhu, 2016).

The radiometric correction also includes the applications of a sun elevation correction and an Earth-Sun distance correction. The first correction accounts for the variation of solar elevation angle during different times, which can affect the object illumination. One way to conduct the



sun elevation correction is to calculate the solar zenith, which is  $90^\circ$  minus the solar elevation angle. The Earth-Sun distance correction, on the other hand, normalises the length alteration between the Earth and the Sun. Both of the correction processes do not account for the atmospheric and topographic corrections in the image data (Lillesand, Kiefer, & Chipman, 2008).

Two corrections in the image preprocessing are described as follows.

(1) Atmospheric correction

There is a high possibility that the brightness values recorded by sensors do not represent the objects' reflectance values due to atmospheric scattering. The term scattering refers to the transmission process of electromagnetic energy by particles in the atmosphere. Three types of scattering include the Rayleigh scattering, Mie scattering, and the nonselective scattering. The Rayleigh scattering occurs in a perfectly clean atmosphere, where there are atmospheric particles with a microscopic diameter (e.g. dust or atmospheric gasses such as nitrogen and oxygen). Mie scattering is influenced by the occurrence of large atmospheric particles (e.g. pollen, smoke, and water droplets), in which the diameter of particles is nearly equal to the wavelength of scattered radiation. Nonselective scattering can be observed in the imagery as haze, which is caused by particles larger than the scattered radiation, such as airborne dust (Chapman & Wynne, 2011 p.39-41). Atmospheric correction is required when working with multitemporal or multisensor data (Lu & Weng, 2007). However, the procedure is not essential for an individual image (Song 2001 *cited in* Lu & Weng 2007).

There are three broad categories of atmospheric correction; the correction using radiative transfer code (RTC) models, image-based atmospheric correction, and the dark object subtraction (DOS) method (Chapman & Wynne, 2011, p. 306). Chapman & Wynne (2011) defines the first models as a tool to demonstrate the physical performance of solar radiation passing through the atmosphere. Advantages of using the models include the high accuracy and broad scope of application, whereas the disadvantages found during data acquisition required by the models consist of the difficulty to retrieve in situ atmospheric data at the same time with the acquired satellite images.

The image-based atmospheric correction involves the assessment of brightness values due to atmospheric effects in the multispectral imagery, based on the image itself. The dark object subtraction (DOS) is recognised as the simplest method to conduct the atmospheric correction (Chavez 1975 *cited in* Chapman & Wynne 2011, p.308). The method is applied by identifying objects in the imagery with known brightness (i.e. dark object with brightness at or near zero, for example, clear water). It is often found that in the imagery, these objects have a larger value due to the atmospheric scattering. Therefore, the atmospheric correction using the DOS method is applied by subtracting the brightness values of all pixels in each band.

Four examples of the advanced models for atmospheric corrections are the modified DOS methods, MODTRAN (MODerate resolution atmospheric TRANsmission), ATCOR, and 6S (Second Simulation of the Satellite Signal in the Solar Spectrum) (Chapman & Wynne, 2011, p. 308-311). Notable modified DOS methods were proposed by Gilabert et al. (1994), Teillet and Fedosejevs (1995), and Song et al. (2001). The MODTRAN (MODerate resolution atmospheric TRANsmission) model was invented by the U.S. Air Force and the Spectral Science Corporation, to calculate the atmospheric transmission under different atmospheric conditions. The third model, ATCOR, was developed by the German Aerospace Center (DLR) to implement the correction for various sensors.

Among all radiative transfer models, 6S is the most widely applied in the preprocessing of satellite imagery (Chapman & Wynne 2011). The 6S model was developed by Vermote et al. (1997) to simulate the observed signal from both Lambertian and BRDF (bidirectional reflectance distribution function) conditions. It incorporates the three processes which affect the electromagnetic radiation (i.e. absorption, scattering, and emission) into the correction process.

## (2) Topographic correction

Land cover is prone to be misinterpreted due to a topographic effect, which alters the radiance values recorded by the satellite sensors (Ediriweera et al., 2013). The problem is prominent, especially when conducting a land cover classification in rugged terrain landscapes, such as mountainous areas (Veraverbeke et al. 2010 *cited in* Vanonckelen et al. 2013). Veraverbeke et al. (2010) further stated that different illumination on the slopes causes distinct reflectance values for similar land cover, affecting the accuracy of land cover maps.

Different topographic correction methods have been widely used in various studies. Sola et al. (2016) argued that the correction performance is affected by the illumination conditions that are shown on the imagery. The correction methods include C-Correction and Statistical-Empirical (Teillet, Guindon, & Goodenough, 1982), a modified sun-canopy-sensor/SCS+C (Soenen, Peddle, & Coburn, 2005), and pixel-based Minnaert (Lu et al. 2008, *cited in* Vanonckelen et al. 2013). The performances of these four methods to correct the SPOT5 images of a case study area in a mountain range in Spain were evaluated by using multi-criteria analysis (Sola, González-Audícana, & Álvarez-Mozos, 2016). The study also includes six other topographic correction methods, such as Smoothed C-Correction, Minnaert, Enhanced Minnaert, Modified Minnaert, Two-stage normalisation, and Slope-Matching. The study concludes that C-Correction, Statistical-Empirical, and SCS+S methods could reduce the topographic effects compared with the other methods.

In particular, SCS+C is arguably an effective topographic correction method for satellite imagery in forested areas and on steep slopes (Soenen, Peddle, & Coburn, 2005). The model normalises the sun-canopy-sensor (SCS) and adds a semiempirical moderator (C) proposed by Teillet, Guindon, & Goodenough (1982). Therefore, SCS+C is used as the selected topographic correction method in this research.

### 2.2.3 Cloud, shadow, and water masking

All radiation reflected from the Earth's surface can be blocked by clouds, causing no at-surface reflectance from objects beneath the clouds could be retrieved by the satellite sensors (Lu 2007 *cited in* Liu et al. 2011). Different methods were developed to detect clouds, shadows, and water bodies in satellite imagery. Cloud masking plugins for open-source image processing software packages, such as QGIS and SAGA (System for Automated Geoscientific Analyses) GIS, are available especially for the types of satellite imagery which are widely used (e.g. Landsat, Sentinel, and MODIS). The plugins use the assigned parameters of filters and the thresholds for specific bands. Examples of masking methods in the open-source GIS software packages are described as follows.

Cloud masking can be performed in SAGA GIS using Automated Cloud-Cover Assessment (ACCA) for Landsat 7 Enhanced Thematic Mapper Plus (ETM+) imagery based on the method from Irish (2000). The weaknesses of ACCA include the missing thin cirrus clouds over water (Irish et al., 2006). The CloudMasking plugin in QGIS provides a different procedure of cloud masking using five cloud filters (i.e. Fmask, Blue Band, Cloud QA, Aerosol, and Pixel QA), which can be chosen depending on the type of Landsat imagery.

Thermal band<sup>9</sup> in satellite imagery is commonly used to detect clouds, whereas SWIR (Shortwave Infrared) band can be used to differentiate clouds from open areas. However, cloud detection using these two bands could not be performed in satellite imagery with a limited number of spectral bands, such as SPOT images. In the absence of the thermal and SWIR bands in SPOT imagery, the cloud masking can be conducted using the reflectance and geometric approach (Candra, Kustiyo, & Ismaya, 2014).

A study on cloud masking conducted by Candra, Kustiyo, & Ismaya (2014) shows that the reflectance and geometric approach can be used to detect medium and small clouds on SPOT 6 data. A high percentage of accuracy (>97%) was retrieved when detecting clouds and shadows in the imagery. A verification based on location is performed when particular small-size objects (less than 500 pixels) are surrounded by large-size pixels identified as clouds or shadows. Verifications based on distance and total area use specific thresholds of pixels, to reassign the

---

<sup>9</sup> Thermal bands in Landsat imagery show land surface temperature at 100-meter resolution, which is resampled into 30-meter. Pixels with dark colour represent areas with cool temperatures, whereas bright colour pixels depict hot temperature (USGS n.d.).

'uncertain clouds' as 'clouds' class and the 'uncertain shadows' as 'shadows' class (Candra, Kustiyo, & Ismaya, 2014).

#### 2.2.4 Image classification and accuracy assessment

Lu & Weng (2007) summarise the essential measures of image classification. The measures include the selection of remotely sensed data, training samples, data preprocessing, feature extraction, a suitable classification procedure, post-classification processing, and an accuracy assessment.

In the digital image classification process, pixels are assigned to classes (Chambbell & Wynne 2011). Chambbell and Wynne (2011) categorise the classification processes into several types (e.g. unsupervised classification, supervised classification, fuzzy clustering, Artificial Neural Networks (ANNs), and object-based classification). The unsupervised classification requires no prior knowledge of the case study. Classes are automatically created during the classification process.

Supervised classification uses samples of pixels with identified land cover, which are located within training areas, to classify other pixels with no land cover data. Training data can be retrieved from the plots distributed across the study area in which their locations have been recorded using GPS (Global Positioning System). Errors in the classification process can be easily detected by the examination of training areas. However, when the training areas are manually selected, the spectral data of pixels in different classes are not often clearly distinctive (Chambbell & Wynne, 2011).

The most common classifier in the supervised classification process is the maximum likelihood classifier (Lu & Weng, 2007). The maximum likelihood classifier uses a probability model to define the decision regions. The classifier computes the probability of an unknown pixel to be a part of a particular class, and based on the results, the classifier assigns the pixel to the class that has the highest probability (Zhu, 2016).

The supervised and unsupervised classification methods to categorise different types of vegetation have been applied in various studies. Two examples of the works were conducted in semiarid Mediterranean saline wetlands (Martínez-López et al., 2014), and in the tropical forest of the Western Ghats of India (Nagendra & Gadgil 1999, *cited in* Nagendra 2001).

Fuzzy clustering uses a different classification logic where a specific pixel may not be assigned to a single class. The value for one class varies from 0 for a non-member to 1.0 for a member of the class, and the intermediate values indicate the partial membership in one or more classes (Chambbell & Wynne, 2011).

Artificial Neural Networks (ANNs) simulate the process of a human brain to learn through the establishment of pathways between input data and output data. In the image classification process, ANNs use the remote sensing data in different bands, which are acquired from several dates, as the input data. The output layer from the process is the land cover classes. ANNs develop one or more hidden layers with specific weight for each layer for classifying unknown spectral values (Chapman & Wynne, 2011)

Object-based image analysis (OBIA) uses both spectral and spatial patterns of objects in the image for the classification process (Lillesand, Kiefer, & Chipman, 2008). Firstly, discrete objects are developed during the segmentation process, which is influenced by the scale of objects. Secondly, objects are classified based on their characteristics (i.e. spectral properties, texture, and shape), and the connectivity and proximity to objects.

In contrast with the OBIA, pixel-based image classification distinguishes different land cover classes only based on the spectral characteristics (Casals-Carrasco et al. 2000 *cited in* Gao & Mas 2008). 'Salt and pepper' effects are generated when using the traditional pixel-based classifiers (Lu & Weng, 2007). Pixels do not represent the actual geographical objects, and the current pixel-based image analysis does not count into the spatial photo-interpretive elements, such as texture, context, and shape. Furthermore, the complex variables within the imagery with high spatial resolution affect the performance of the classification process, resulting in lower classification accuracy (Hay & Castilla, 2006).

It is argued that the results from OBIA have higher accuracy than that of pixel-based image classification, especially in imagery with high resolution (Gao & Mas, 2008). An experiment conducted by Gao & Mas (2008) showed that OBIA using SPOT 5 imagery produced higher accuracy than that obtained by pixel-based maximum likelihood and nearest neighbour classifiers. Another example of OBIA application is a study conducted by Moreira & Valeriano (2014) who evaluated the classification accuracy on a Landsat 5 TM image after performing topographic corrections.

A classification error matrix, or a confusion matrix, is widely used for estimating the accuracy of image classification (Foody, 2002). It is only suitable for 'hard' classification (Lu & Weng, 2007). The matrices compare the reference data (ground truth) and the results of an automated classification (Lillesand, Kiefer, & Chipman, 2008). An error matrix describes not only the overall accuracy but also the accuracy of an individual class (Congalton, 1991).

After the error matrix has been generated, other accuracy assessment elements can be derived, such as overall accuracy and Kappa coefficient (Lu & Weng, 2007), as well as the producer's and user's accuracies (Story & Congalton 1986 *cited in* Congalton 1991). The "producer's accuracy" shows how accurate one particular area can be classified, while the "user's accuracy" provides information on how one classified pixel represents the class on the ground (Story & Congalton 1986 *cited in* Congalton 1991).

Specific thresholds for the minimum percentage of a class to be allocated correctly were proposed by Thomlinson et al. (1999), who appointed a target of 85% for an overall accuracy with no class to have accuracy lower than 70% (Foody, 2002). Another approach for the accuracy assessment is to have more than one measure in the image accuracy assessment process (Muller et al. 1998 *cited in* Foody, 2002).

#### 2.2.5 Uncertainty factors in a land cover mapping process

Uncertainty in the context of land cover map development from remotely sensed imagery could be defined as a “quantitative statement about the probability of error” (Dungan 2002, p.26). A map is considered as a model or generalisation which contains errors, and there is a possibility that the land cover might have been classified correctly by chance (Foody 2002). Therefore, it is essential to identify the processes in remote sensing, which cause uncertainty (Woodcock 2002, p.22).

Accumulated uncertainties are often retrieved from the development process of GIS data from raw remotely sensed images (Gahegan & Ehlers 2000 *cited in* Zhang & Goodchild, 2002). Statistical methods and tools are used to assess the error that causes uncertainty, despite the doubt of how effective they are (Zhang & Goodchild, 2002).

There is no single measure of classification accuracy derived from a confusion matrix (Lark 1995 & Stehman 1997a *cited in* Foody 2002). Although a Kappa coefficient is considered as a standard measure to assess the image accuracy, some problems arise when using the Kappa coefficient (Foody, 1992). Therefore, it is essential to adopt more than one measure in the accuracy assessment, as well as to describe the classification accuracy using a confusion matrix (Foody, 2002).

The uncertainty in the accuracy assessment also stems from many factors, such as sampling design, preprocessing of satellite imagery, the accuracy of reference data, the spatial distribution of error, and the occurrence of mixed pixels (Foody, 2002). The contribution of each factor to the inaccuracy of a map is described as follows. Problems in the sampling process include the insufficient number of sampling points, which leads to classes could not be represented in the accuracy assessment, budget constraint, and accessibility to reach the site, especially when using a simple random sampling. An issue in the preprocessing of satellite images is the mislocation of pixels caused by various issues, including the properties of sensors and ground, and the methods used in the image preprocessing. The ground or reference data is prone to inaccuracy because it also contains errors in the development process. When the data is used for validating maps, there is uncertainty in the accuracy assessment result. A confusion matrix could not provide information regarding the location where the error occurs on the map. A mixed pixel contains two or more classes, which are often misclassified when using a standard (hard) classifier. Tools, such as uncertainty analysis and sensitivity analysis, have been

developed to assess the uncertainty in maps generated from remotely sensed images (Crosetto, Moreno Ruiz, & Crippa, 2001).

## 2.3 The development of scenarios and land change models

This sub-chapter provides a description and types of scenario, the overview of Pareto-frontier to optimise the scenario development, the types of land change models, and the uncertainty in land change modelling.

### 2.3.1 Scenario definition and types of scenario

Scenarios are defined as “archetypal descriptions of alternative images of the future, created from mental maps or models that reflect different perspectives on past, present and future developments” (Rotmans, 1998). Scenarios are developed to provide an understanding of drivers of change and propose alternatives of action (Peterson, Cumming, & Carpenter, 2003). Scenarios of alternative developments are used to test options of landscape structure using models, based on selected assumptions for future land-use (Hulse et al., 2009).

Börjeson et al. (2006) propose nine typologies of scenario which were developed based on the principal questions researchers would like to know about the future; “*What will happen?*”, “*What can happen?*”, and “*How can a specific target be reached?*”. The questions are responded to by specific categories of scenario, which are described by Börjeson et al. (2006) as follow. Predictive scenarios respond to the question of “*What will happen?*”, based on two distinct conditions which may apply. Forecast scenarios are related to the condition of what will happen if the most likely development occurs, whereas what-if scenarios take into account the conditions of some particular events when predicting the future (Figure 2-3).

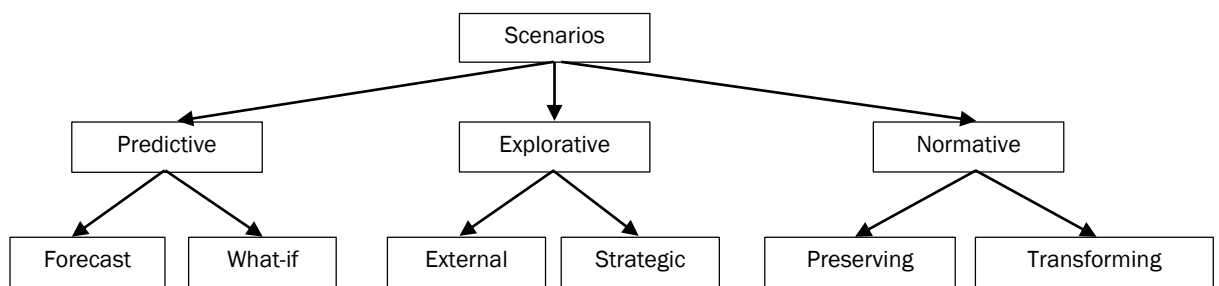


Figure 2-3 The six types of scenario (the diagram was redrawn from Börjeson et al. 2006)

The explorative scenarios are divided into two groups: the external scenarios and the strategic scenarios. The external scenarios are used to assess the factors which could not be controlled by the relevant actors, by providing a framework for developing and evaluating policies and strategies. The strategic scenarios are developed to provide possible consequences from

specific strategic decisions. Target variables are described, and the different policies are evaluated, including their impacts on the target variables (Börjeson et al., 2006).

The normative scenarios use normative starting points and take into consideration the future conditions and the way they could be realised. Two types of scenario in this category are the preserving scenarios and the transforming scenarios. Preserving scenarios seek the most efficient method to achieve a specific target, usually by utilising some optimising modelling. In regional planning, for example, the preserving scenarios are often used to define the most efficient way to reach one or several environmental targets. Transforming scenarios, on the other hand, aim to reach a high-level target, which would not be achieved if the current development continues (Höjer 2000 *cited in* Börjeson et al. 2006). Backcasting is one example of transforming scenarios which provide new paths for the development to occur (Höjer & Matson 2000 *cited in* Börjeson et al. 2006).

Backcasting is defined as “developing and assessing the relative feasibility of alternative futures” (Robinson 1980 *cited in* Voorn et al. 2012). In the backcasting scenarios, specific goals and constraints are stated, the policy measures are defined, and the implications of the scenarios are assessed (Robinson, 1982). The backcasting approach has been applied in various studies. The first example is the development of transition pathways of scenario to sustain the future ecosystem services provision in Switzerland (Brunner, Huber, & Grêt-Regamey, 2016). The second case is the assessment of climate strategies in the coastal region in South Africa using backcasting scenarios (van der Voorn, Pahl-Wostl, & Quist, 2012). The last example is the integration of the agent-based model with the backcasting approach to propose sustainable land-use planning in Austria (Haslauer, Biberacher, & Blaschke, 2016). Backcasting approaches can also be integrated with participatory methods to explore alternative futures using 3D visualisation tools criteria and indicators, as shown in a study conducted by Robinson et al. (2011) in Canada.

### 2.3.2 Pareto-frontier

Scenarios have been frequently used in many studies in assessing plausible futures, including the integration of the models with optimisation algorithms, which examine ecosystem functions and possible management options. The examination of possible scenarios can be performed by implementing Pareto-frontier or Pareto optimality (Seppelt, Lautenbach, & Volk, 2013).

Pareto-frontier has been used in many studies to project optimal land-use allocation. Gong et al. (2012) examined the land-use optimisation, which could provide both economic and ecological benefits in the urban fringe in Guangzhou, China. In this study, a performance evaluation of a land-use allocation model was conducted using Pareto-frontier by comparing the possible tradeoffs, which could be acquired by the land-use allocation.



Another study of land-use optimisation was conducted using a model which combined multiple zoning objectives with land-use constraints in Loess Plateau (Xia et al., 2014). Five scenarios were developed, and Pareto-frontier was used to search the optimal solution for the land-use allocation. The concept of Pareto-frontier was also applied by Verstegen et al. (2017) to redesign the land-use policies in the Business-as-Usual scenario after the impact of this scenario to ethanol production in a region in Brazil had been evaluated.

### 2.3.3 The development of land change models

Turner et al. (2001 p.47) defined a model as “an abstract representation of a system or process”. Models represent real-world systems which are responsive to the simulations of system changes (Clarke, 2014). Models are used to investigate particular issues on landscape structure and dynamics in a large and complex landscape in ecology studies. Models are also often employed to explore conditions which cannot be implemented in the field (e.g. severe disturbances, forest fire, and spatial arrangement of animals) (Turner et al. 2001). One example of models is land change modelling (Turner, 1989).

In response to the needs of sustainable land-use development, land change models have been developed to assess the factors influencing the land change, to simulate the future development scenarios, and to analyse the effects of changes (Verburg et al., 2004). Six categories of land change modelling approaches proposed by Brown et al. (2014) include the machine-learning and statistical, cellular, sector-based economic, spatially disaggregated economic, agent-based, and hybrid approaches. Two other distinguished models are Markov chains and system dynamic models. The integration of different models (i.e. hybrid models) is proposed to simulate the complexity of land change (Dang & Kawasaki, 2016). The timeline for the hybrid model development is shown in Figure 2-4.

Among the six categories of land change models mentioned by Brown et al. (2014), two modelling approaches are recognised for their performance and accuracy for simulating regional systems (i.e. cellular automata (CA) models and agent-based models (ABM)). Initial conditions and calibration procedures are required by the models. CA are often chosen to model land change with identified states of cells on a geographic grid and a known transition probability (Clarke, 2014).

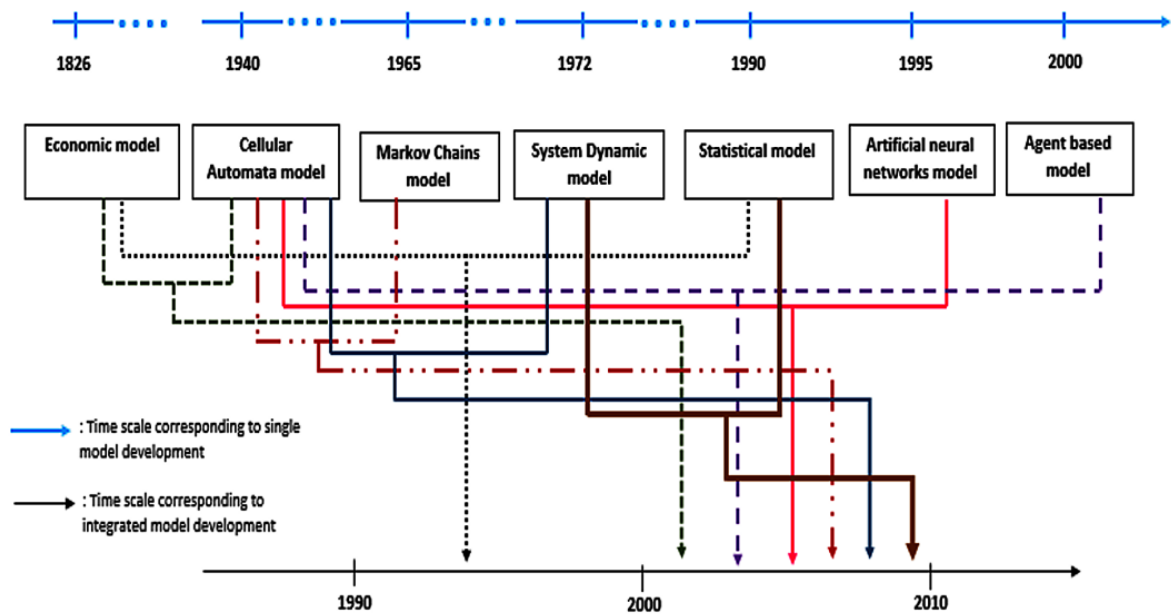


Figure 2-4 The timeline of land change model development and integration (Source: Dang & Kawasaki 2016)

CA are defined as “discrete spatiotemporal dynamic systems based on local rules” (Miller, 2009). The model was developed by S. Ulan and J. von Neumann in the late 1940s (Santé et al 2010), and it was first introduced in the geographical modelling by Tobler (1979) (White & Engelen 2000). CA models are known for their simplicity and the way they employ local interaction among cells to simulate extraordinarily complex behaviour (Batty 2000 *cited in* Clarke 2014). Spatially distributed process simulations, such as spread and dispersal, can be best simulated using CA, especially when the geometry, scale, and basic system behaviour are known (Clarke, 2014). CA use transitions rules to define the state of a cell at time  $t + \Delta t$  based on the states of neighbour cells at time  $t$  (Miller, 2009). Historic LULC (land-use/land cover) maps, which could be derived from satellite data, as well as other data such as topography, road networks, and zones with limited development, are required as the input datasets for CA models (Clarke, 2014). CA models have been used to simulate land cover changes in many case studies (e.g. Feng & Liu 2016; Jafari 2016; Liu & Feng 2016).

On the other hand, ABM models mimic the actual object or people, in which the independent agents interact with each other and the surroundings (Steinitz, 2012). The models simulate the impact of one agent or a behaviour type on the system, without no prior precedent and past data (Clarke, 2014). The term ‘agent’ in ABM refers to a particular independent unit which has a set of goals to fulfil (Miller, 2009). The remaining challenge of ABM is to look into sets of rules to represent human beliefs and desires (Bithell et al. 2008 *cited in* Clarke 2014). The applications of ABM models in land change studies include the scenario modelling of the Willamette river basin development in Oregon (Hulse et al., 2009), and the impact assessment on urban expansion into farmlands and forests (Guzy et al., 2008). One example of ABM models is the Envision model, which was developed by Oregon State University. The application of this model

has been tested in many studies (e.g. Waldick et al., 2015; Wu et al., 2015; Bolte & Vache, 2012; Munguia et al., 2009).

Compared to ABM, CA models have a better performance in the simulations of ecological and biogeophysical phenomena (Parker et al., 2003). However, they are limited to simulating land changes when human decisions are integrated into the models (Ghosh et al., 2017).

Four other categories of land change models, which are also proposed by Brown et al. (2014) (e.g. machine-learning and statistical, sector-based economic, spatially disaggregated economic, and hybrid approaches) are described as follows. The machine-learning and statistical model requires the past land-use changes data to calibrate parametric and non-parametric relationships between factors which initiate the changes, and spatially and temporally related predictors. The sector-based economic approach focuses on the supply and demand for land by economic sectors. The spatially disaggregate economic model aims to assess the relationships which influence the spatial equilibrium in land systems. The last category, the hybrid approach, combines different models into one modelling framework.

Uncertainty in real-world systems manifests a challenge when using traditional methods (e.g. CA and Markov model) to model the land change (Ghosh et al., 2017). Brown et al. (2014) argue that hybrid models offer an opportunity to modellers to select the modelling procedure from each model based on practical needs. In this research, the integration between CA and Markov models with multi-layer perceptron (MLP) is used to simulate the land change in the two case study areas based on developed scenarios. The coupled CA-Markov model is the most acknowledged model for simulating trends and growth patterns, and the integration of the two models can eliminate the shortcoming of each model (Hamdy et al., 2016). Two examples of studies using the hybrid models of CA and Markov include the land-use scenario simulation in Ethiopia (Gidey et al., 2017), and the forest cover changes model of Bannerghatta National Park in India (Adhikari & Southworth, 2012).

The Markov model simulates land change based on historical trends (Brown et al., 2014), without considering the spatial patterns of land cover (Ghosh et al., 2017). A transition matrix computed in a Markov model shows the transition probabilities of one land cover type to change to another (Brown et al., 2014). The model assumes the transition is stationary within the simulation period, although a land change in the real-system is a non-stationary process (Baker, 1989). Changes in the endogenous variables (e.g. natural processes and age of a particular landscape structure), and the exogenous variables (e.g. socioeconomic factors and climatic conditions) in the landscapes affect the transition probabilities among land cover types (Boerner et al., 1996).

Although the CA-Markov models have been extensively used to predict urban growth, the applications to model forest cover change have rarely been explored (Ghosh et al., 2017). The models have at least two limitations: the assumption of factors which cause the land-use

changes will remain the same in the future, and the missing variables of human decision which are not integrated into the models (Ghosh et al., 2017).

The coupled CA-Markov model has been used to assess land change in various case study areas, including in Indonesia (e.g. Kusratmoko, Albertus, & Supriatna, 2017; Mujiono et al., 2017; Marko, Zulkarnain, & Kusratmoko, 2016a; Yulianto et al., 2016; Akbar AS et al., 2015; Nurmiaty, Baja, & Arif, 2014; Susilo, 2011; Wassahua, 2010; Wen, 2008; Mulianta & Hariadi, 2004). However, none of the research has been conducted in the Ci Kapundung and Ci Sangkuy upper catchments.

### 2.3.4 Uncertainty factors in land change modelling

Land change models are influenced by human preferences, in which the cognitive process of all actors cannot be assessed (van Vliet et al., 2016). Random variations in a model could produce a different outcome in each simulation (Brown et al. 2005 *cited in* van Vliet et al., 2016). van Vliet et al. (2016) summarise the sources of uncertainty in land change modelling from various studies. The sources include the physical and socioeconomic factors, the equifinality in open systems, the uncertainty in observations, and the nonstationary of land change processes. The risk of uncertainty is higher in the modelling where the simulation period is longer than the calibration and validation periods (Chaudhuri & Clarke 2014 *cited in* van Vliet et al., 2016).

According to Rykiel (1996), calibration can be defined as a process to increase model accuracy by estimating and modifying the model parameters. The procedure is often used to assess unknown parameter values in the model. Validation shows the model ability to provide a high accuracy of prediction, which is assessed by comparing the simulation output with observation data.

Other sources of uncertainty in land change modelling stem from the uncertainty in input data and model parameters (Brown et al., 2014; Verburg, Tabeau, & Hatna, 2013). An assessment of land change using maps as input data, which were developed from different dates, might produce sliver patches or objects due to the misalignments between maps. This problem can distort the rate of land cover change and/or alter the direction of change (Linke et al., 2009). Verburg et al. (2013) suggested that better observation data and model parameterisation can reduce model uncertainty. Plotting the uncertainties at a macro level in spatial patterns of land change provides an insight into how uncertainty can affect the model input.

## 2.4 Flood risk assessment and the development of hydrologic models

This subchapter provides a literature review on the flood risk assessment, the development of hydrologic models and the description of the selected model used in this research. Uncertainty elements in hydrologic modelling are presented in the last part of this subchapter.

### 2.4.1 Flood risk assessment

Apel et al. (2008) define flood risk as “the exceedance probability of events of a given magnitude and a given loss” (p. 149). The flood risk assessments consist of a hazard assessment (i.e. the analysis on the extent and magnitude of massive floods), and a vulnerability assessment which focuses on the effects of flooding on particular objects, such as building, infrastructure, or people. The uncertainty in the flood risk assessment is related to the flood frequencies analysis (Apel et al. 2008). In this section, the descriptions of flood frequency, flood discharge, and effective rainfall analyses as part of the flood risk assessment are presented.

#### (1) Flood frequency analysis

A flood frequency analysis can be conducted using probability distributions. The outputs from this analysis are often used for assessing flood control structures, delineating flood plain, and analysing the effects of land change on a flood plain (Chow, Maidment, & Mays, 1988). One of the applications of flood frequency analysis is the assessment of a discharge return period.

Chow, Maidment, & Mays (1988) summarised seven types of probability distributions for fitting hydrologic data. They are Normal, Lognormal, Exponential, Gamma, Pearson Type III, Log Pearson Type III, and the Extreme Value Type I distributions. Among seven probability distributions, Pearson Type III and Log Pearson Type III were listed as the common procedures to assess flood peak.

#### (2) Flood discharge analysis

There are at least three models which can be used to estimate the flood discharge; Manning equation, Kinematic wave parameter, and SCS curve number (Roy & Mistri, 2013). Manning equation is commonly applied to estimate discharges for a specified depth of flow, based on the roughness of bed channel (Chow, Maidment, & Mays, 1988 p.428). Manning’s n number varies between 0 and 1, with typical values of the coefficient for surfaces covered with concrete and dense trees are 0.012 and 0.1, respectively (Chow 1956 cited in Chow, Maidment, & Mays, 1988). Kinematic wave model shows the flow distribution as a function of distance (x) and time (t), with no acceleration in flow rate (Chow, Maidment, & Mays, 1988 p.282 & 287). SCS was developed by the Soil Conservation Service (1972) to calculate abstractions and excesses from storm rainfall. Curve number (CN) has been generated from plotting the total rainfall and rainfall excess from many water catchments, in which the numbers are ranging from 0 to 100 (Chow, Maidment, & Mays, 1988 p. 147-149).

Roy & Mistri (2013) suggest that Manning’s equation is considered to be an accurate and reliable method to estimate river discharge when there is limited data availability. The equation is used to compute water velocity, which takes into account the river hydraulic radius, or the proportion of channel cross-sectional area and wetted perimeter, the slope of water surface,

and the Manning resistance coefficients. Bankfull discharges, then, can be estimated by multiplying the bankfull width and depth, and velocity when the river is at full capacity (Dunne & Leopold, 1978).

### (3) Effective rainfall contributing to flooding

The volume of floods can be estimated by calculating the direct runoff in a watershed caused by effective rainfall (Viessman et al., 1977 cited in Dasanto, et al., 2014). An example of effective rainfall estimation has been conducted by Dasanto et al. (2014) using a case study in Ci Tarum watershed (i.e. Bandung Basin). This study is part of research assessing the flood-prone area in the basin under historical and future rainfall scenarios. Historical rainfall data from 2000-2011, Ci Tarum river daily discharge data from 2000-2009, and information on flood events in the Bandung Basin (2000-2010) were collected to conduct the study. The result showed that the duration of effective rainfall, which has high possibility to cause flooding in the Bandung Basin, was the rainfall accumulation for four days before the peak of direct runoff (DROp) occurred in each flood event (with  $R^2 = 0.625$ ).

The assessment of effective rainfall requires the estimated rainfall rates at the day when the highest direct runoff (DROp) occurred during the flood events and the accumulated areal rainfall (Dasanto et al., 2014). Chow (1964) proposed the continuity equation to model a hydrologic system (Equation 2-1). In this system, a watershed is viewed as a model where precipitation is the input, whereas streamflow from a specific watershed within the model is the output (Figure 2-5).

$$\frac{dS}{dt} = I(t) - Q(t) \quad \text{Equation 2-1}$$

where  $dS/dt$ ,  $I(t)$ , and  $Q(t)$  denote the time rate of change of storage, the water input and output to the river, respectively.

Areal rainfall can be estimated using at least four different methods; the arithmetic-mean method, Thiessen method, the isohyetal method, and the reciprocal-distance-squared method (Chow, 1964 p.78). The arithmetic-mean method is used by calculating the rainfall rates from all gauges divided by the number of weather stations in a watershed. This method works the best when the distribution of all gauges is uniform and no extreme discrepancies of the mean values recorded by individual gage. The Thiessen method refers to the process to define the area of precipitation over a catchment with a non-uniform distribution of rain gauges (Fetter, 1988). Thiessen polygons are created over a catchment in which the polygon boundaries are perpendicular to the lines joining every two gauges (Figure 2-6a). The isohyetal method includes the development of isohyets, in which the rainfall data recorded by gauges are used and interpolated (Figure 2-6b) (Chow, 1964 p.79). The last method, the reciprocal-distance-squared

method, involves the calculation of rainfall at an ungauged point in the process (Wei & McGuinness, 1973 cited in Chow, 1964 p.79).

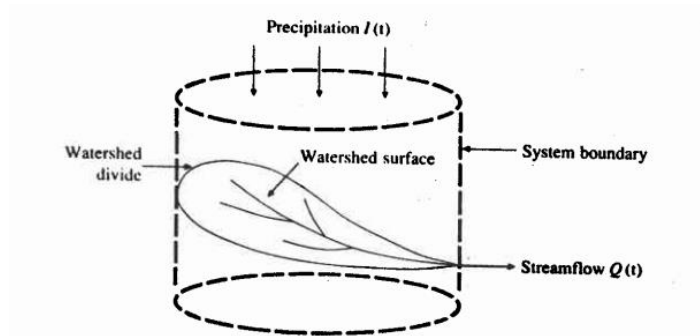


Figure 2-5 A watershed which is viewed as a hydrologic system (Source: Chow, 1964)

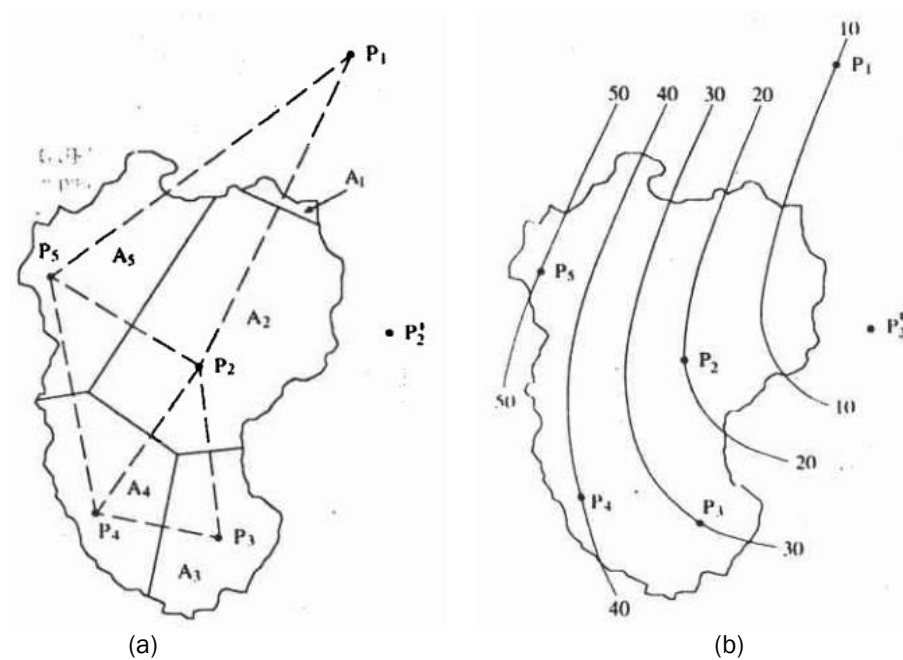


Figure 2-6 (a-b) Aerial rainfall calculation by Thiessen and isohyetal methods (Source: Chow, 1964)

#### 2.4.2 The development of hydrologic models and model categorisation

Various kinds of models are utilised to assess the potential effects of landscape structure changes on ecosystem services, including the hydrologic models, graph theory, circuit theory, landscape genetics, and meta-analysis (Stürck, Poortinga, & Verburg, 2014; Jones et al., 2013). Particularly, there is a need to study the impact of land-use changes on the hydrological process (DeFries & Eshleman, 2004 cited in Amatya, et al., 2015).

Several studies using hydrologic models have been conducted to assess the hydrological impacts of future possible land-use change scenarios. Beckers, Smerdon & Wilson (2009) reviewed 25 hydrologic models for predicting the impact of forest management and climate change on hydrologic metrics. The models are categorised based on five criteria:

- (1) Model functionality; the ability to simulate a specific hydrologic process based on the availability of data, the model discretisation (e.g. lumped models, semi-distributed

models, and distributed models), and the time step to perform the simulation. The model discretisation is described as follows (Kampf & Burges 2007 *cited in* Beckers et al. 2009). Lumped models do not include the spatial distribution of parameters (e.g. vegetation and soils) in a site. In the semi-distributed models, a watershed is divided into several units, which have similarities in their hydrologic properties, such as terrain, land cover, and/or soil types. The distributed models require the watershed to be equally divided into a specific size of grid cells, and the spatial distribution of parameters is taken into account in the model.

- (2) Model complexity (e.g. the requirement of data, resources, and time to simulate a hydrologic model). Low-complexity models are usually utilized for a screening-level study, which requires low-level data input (e.g. monthly temperature and precipitation data) and produces limited accuracy output. Medium-complexity and high-complexity models have higher requirements for data input.
- (3) Model applicability to simulate hydrological processes in particular climatic and physiographic settings (e.g. terrain setting, watershed sizes, and a specific hydrologic process modelling).
- (4) Model ability to provide outputs (e.g. full hydrograph, peak flow, low flow, evapotranspiration, water balance, soil moisture, infiltration, water table, overland flow, subsurface hillslope runoff, groundwater, road flow, and watershed runoff).
- (5) Model adaptability to represent the future watershed conditions (e.g. forest growth, landscape structure changes, climate prediction).

Based on the criteria above, the MIKE SHE model is selected in this study. MIKE SHE is a distributed model and requires high requirements for data input (Beckers, Smerdon, & Wilson, 2009). This research assesses potential scenarios for future land cover composition and distribution in water catchment areas, in which the spatial distribution of hydrologic properties should be considered as the main factor influencing the modelling output. MIKE SHE model has been extensively used in several studies in water catchment areas and can assess the most important hydrological processes (Ma et al., 2016). These include the runoff generation process and river flow, which are required in this research. There is a large user community around the world who use the model, including in the United Kingdom.

Previous studies using the MIKE SHE model include the simulation of water levels in a riparian wetland based on climate models in Berkshire, United Kingdom (House, Thompson, & Acreman, 2016), and the assessment of hydrological responses to changes in a lowland wet grassland, in southeast England (Thompson et al., 2004). Various studies have also been done in other countries in Europe (Moussoulis, Zacharias, & Nikolaidis, 2016; Refsgaard et al., 2016; Dimitriou et al., 2009), Asia (Gorantiwar et al., 2015; Keilholz, Disse, & Halik, 2015; Zhang et al., 2008), and America (Dai et al., 2010; Larsen, et al., 2016) using the MIKE SHE model. In



Indonesia, hydrological modelling using MIKE SHE has been conducted in various studies, including the assessment of flood risk in Jakarta (Wiryawan, 2017).

The development of hydrologic models has prompted the emerging study on assessing the impact of climate change and/or future land cover scenarios. However, most flood risk analyses focused on assessing either climate change or land cover, rather than the combination of both factors (Chang & Franczyk, 2008). Chang and Franczyk (2008) suggest that the uncertainty from unknown future precipitation trends and hydrological model parameters for future land cover will remain in the modelling process. Despite their difficulty to predict the future rainfall trend at a local scale, most studies rely on the general circulation models (GCMs) to simulate precipitation rate, which can lead to misleading results.

In this research, a coupled Cellular Automata (CA) and Markov modelling is integrated with the application of MIKE SHE to project the future landscape structure in the two case study areas and to evaluate the impact of land cover changes on river flow regimes. Although many studies have used CA and hydrological models to assess flood risk in watersheds, the application of an integrated CA-Markov with MIKE SHE model is rare in the environmental studies (e.g. Wijesekara 2013 and Farjad et al. 2017), and none of the studies were conducted in Indonesia.

#### 2.4.3 MIKE SHE hydrologic model

MIKE SHE is a physically-based hydrologic model, which was developed by the Danish Hydraulic Institute (DHI). MIKE SHE works based on the hydrological cycle (Figure 2-7). In the cycle, a proportion of the rainfall is intercepted by tree canopies or infiltrates to the soil and groundwater, which discharges to rivers as baseflow. When the soil is saturated, water runs off directly to rivers, which flows to the oceans. Water evaporates from the oceans, rivers, lakes, or other water surfaces, and from the soil and is transpired by plants. In the atmosphere, the water vapour condenses and falls down as rainwater. MIKE SHE can model the water movement in the hydrological cycle, including the evapotranspiration process, unsaturated flow, overland flow, channel/ river flow, and saturated flow (Danish Hydraulic Institute 2017b).

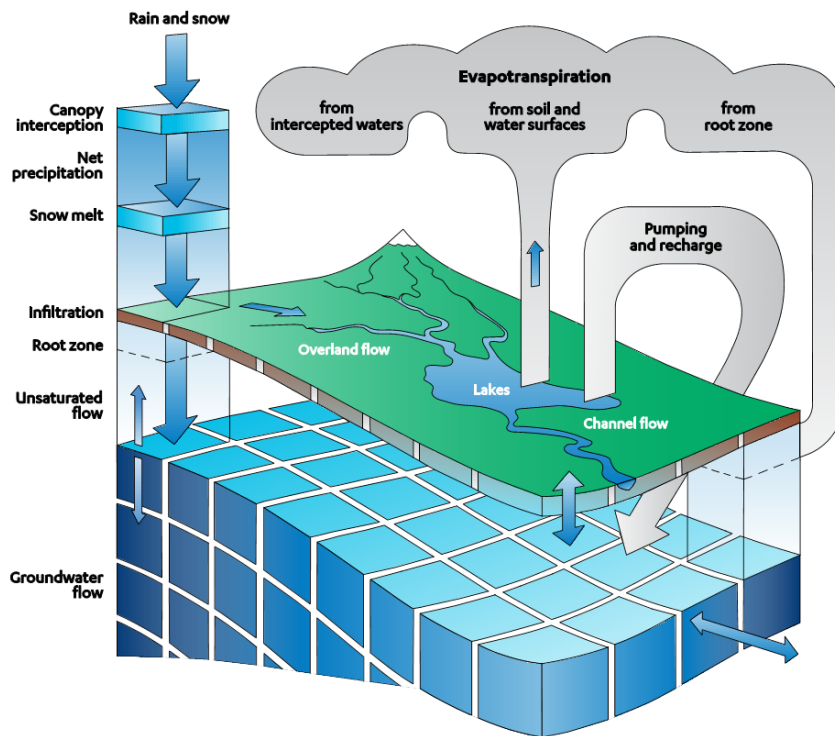


Figure 2-7 MIKE SHE model structure (Source: Danish Hydraulic Institute 2017b)

### (1) Evapotranspiration ( $ET$ )

The modelling of evapotranspiration in MIKE SHE includes the rainfall interception process by the canopy, surface water runoff and water absorption by the soil surface, water evapotranspiration from the upper part of the root zone or uptake by plant roots, and the water infiltration to the saturated zone<sup>10</sup>. MIKE SHE calculates the crop evapotranspiration ( $ET_{crop}$ ) based on reference evapotranspiration and crop coefficient (Danish Hydraulic Institute, 2017b).

Reference evapotranspiration ( $ET_0$ ) refers to the rate of evapotranspiration from a reference surface with an unlimited amount of water (Allen et al., 1998). The reference surface is described by FAO (Food and Agriculture Organization of the United Nations) as a hypothetical surface, which is equal to a surface of green grass on the ground with sufficient water. There are at least three methods to estimate the  $ET_0$ ; the Penman equation, Monteith equation, and the FAO Penman-Monteith equation.

Crop coefficient ( $K_c$ ) is determined by dividing the actual/crop evapotranspiration ( $ET_{crop}$ ) with the reference evapotranspiration ( $ET_0$ ). While  $ET_0$  values denote the climatic conditions in a particular area,  $K_c$  only depends on the crop or plant characteristics. Thus the coefficient is transferable between different locations and climate. The values of  $K_c$  vary in different stages of plant growth, which are depicted in the crop coefficient curve (Figure 2-8) (Allen et al., 1998).

<sup>10</sup> In the saturated zone, water is extracted directly by roots near the water table, or indirectly by the movement of water to the unsaturated zone to replace water uptake by plant roots

The evapotranspiration process is mainly modelled using the equation from Kristensen and Jensen (1975). The Kristensen and Jensen method assumes that the actual evapotranspiration will not exceed the reference evapotranspiration (i.e. evapotranspiration rate of a surface with an unlimited amount of water). The actual evapotranspiration is affected by water scarcity in the root zone, and the plant density (LAI/Leaf Area Index) (Danish Hydraulic Institute, 2017b).

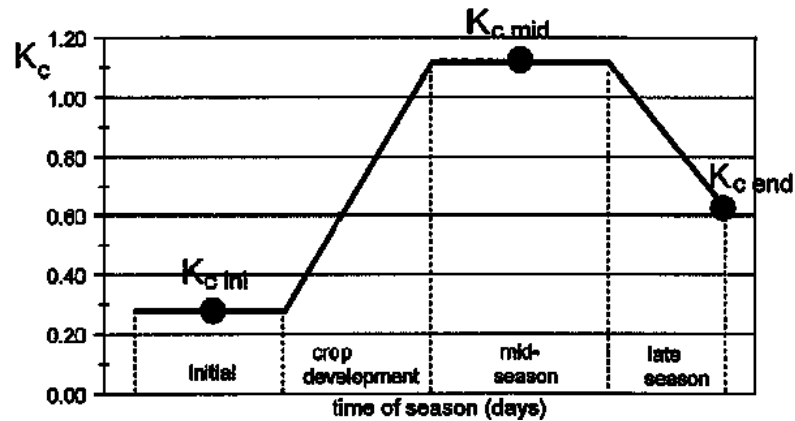


Figure 2-8 Crop coefficient curve (Source: R.G. Allen *et al.*, 1998)

A simplified ET model in the ET/UZ two-layer water balance method is provided in MIKE SHE as an alternative to the Kristensen and Jensen method. The ET/UZ two-layer method uses a formula from Yan and Smith (1994) to simulate the evapotranspiration process and the water movement to the saturated zone (Danish Hydraulic Institute, 2017b). The two-layer method is also part of one method to simulate unsaturated flow in MIKE SHE.

## (2) Unsaturated flow (UZ)

In the unsaturated zone, water flows from the soil surface to the water table, before it infiltrates to the saturated zone as groundwater, or absorbed by the plant roots. The vertical flow in the unsaturated zone is calculated using the Richard Equation, Gravity Flow, or the Two-Layer Water Balance methods. The first option offers the most accurate calculation for a dynamic unsaturated flow, but it is the most computationally intensive among all methods. Water flows from the soil to the upper layer of saturated zone where water could also flow from this zone to the soil. The second option is suitable to estimate groundwater recharge based on precipitation and evapotranspiration. The vertical gradient is assumed to be uniform, and capillary forces are ignored. The last method is suitable for an unsaturated flow calculation where the water table is shallow, and groundwater recharge is mainly influenced by water uptake by plants in the root zone.

### (3) Overland flow

Overland flow occurs when soil is saturated; thus, water from rainfall ponds on the ground surface and flows downhill towards the river network. The flow direction and volume are affected by the topography, flow resistance, and the evapotranspiration and infiltration process along the path. The overland flow can be estimated in MIKE SHE using the finite difference method. Two numerical solvers provided in this method are successive over-relaxation and explicit numerical solutions. The two solvers use the Diffusive Wave Approximation to the St Venant Equations (Danish Hydraulic Institute, 2017b).

Surface roughness (the Strickler roughness coefficient) and slope gradients affect the overland flow. The surface roughness of each land cover type is the first parameter of overland flow and is derived from Manning's equation (Danish Hydraulic Institute, 2017b). The calculation assesses the velocity of open channel flow based on the roughness coefficient  $n$  (Chow, Maidment, & Mays, 1988). The second parameter of overland flow is detention storage. The storage determines the amount of water flowing from one cell to its adjacent cell. The last parameter is the initial and boundary condition (Danish Hydraulic Institute, 2017b).

### (4) River flow

River flow can be simulated in MIKE SHE by linking the model to MIKE 11 or MIKE Hydro via river links. The links are located on the edges between grid cells in MIKE SHE. MIKE Hydro is the Graphical User Interface framework which was developed by DHI to model water resources in a basin and river networks (Danish Hydraulic Institute, 2017c). In particular, MIKE Hydro requires various datasets, such as the parameters for river hydrodynamics and the rainfall-runoff model.

### (5) Saturated flow

In MIKE SHE, the saturated flow modelling is integrated with other hydrologic components (e.g. evapotranspiration, overland flow, river flow, and unsaturated flow). Two available methods to calculate the saturated flow in MIKE SHE are the 3D finite difference method and the linear reservoir method. The finite difference method provides the flexibility of flow to shift between unconfined and confined conditions of a heterogeneous aquifer. The linear reservoir method, on the other hand, is often selected when available data is limited to model a complex hydrological response at the catchment scale (Danish Hydraulic Institute, 2017a).

In physical-based models, such as MIKE SHE, a calibration is required to find an optimal set of parameter values which can accurately simulate the hydrological metrics (Sooroshian & Gupta 1995 *cited in* Sahoo et al. 2006). A validation process is also needed to see the capability of a

calibrated model to make accurate predictions for the selected hydrological metric in a period other than the calibration period (Refsgaard, 1997). Results from the calibration and validation processes can be evaluated using visual graphical techniques and statistical measures (e.g. root mean square error (RMSE), correlation coefficient (R), and mean error (ME)) (Sahoo, Ray, & de Carlo, 2006).

#### 2.4.4 Uncertainty factors in hydrologic modelling

In hydrological modelling, all spatial and temporal variants of flows and state variables are not possible to be measured, and there would be errors in the measurements. Therefore, the output from modelling contains uncertainty because models use data with sampling errors. Thus, it is argued that the model uncertainty should be assessed when the outcome might affect the decision-making for flood mitigation (Beven et al. 2014). It should be noted that a hydrologic modelling program is not a complete product. It is always improved by the feedback from users (Floyd 1987 cited in Refsgaard & Storm, 1996).

Various studies have been done to identify the sources of uncertainty in hydrology modelling. According to Refsgaard & Storm (1996), the sources include errors in the input data (e.g. precipitation rates, temperature) and recorded data (e.g. river discharges), errors caused by non-parameter values, and errors caused by an incomplete or biased model structure (Refsgaard & Storm, 1996). Merz & Thielen (2005) argued that there are two types of uncertainty: the natural and epistemic uncertainties. Natural uncertainty occurs because of the different variables in the stochastic processes. On the other hand, the epistemic uncertainty is caused by the lack of understanding of the modelling process. In particular, Beven et al. (2015) pointed out the sources of uncertainty in flood inundation mapping, which include aleatory and epistemic uncertainties.

Figure 2-9 illustrates an example of the source-pathway-receptor framework of the primary sources of uncertainty for mapping flood inundation (Beven et al., 2015). The sources of uncertainty at the beginning of studies may include the decisions whether the design flood magnitude and the impact of climate change and land change should be incorporated in the process. It is also important to identify several factors, such as the uncertainty elements along the flood inundation mapping process, the uncertainty features on receptors, the implementation of uncertainty analysis, and the observation conditions.

Multiple viewpoints, including various methods and assumptions, should be considered in the flood mapping, and the output from uncertainty analysis should be communicated. Some communication methods include scenario modelling, an assessment to determine limitations in the model, and a comparative analysis of the outputs (Teng et al. 2017). The assessment of model uncertainty is also essential to interpret the output from model validation tests. Different methods of validation will give different uncertainty levels (Refsgaard, 1997).

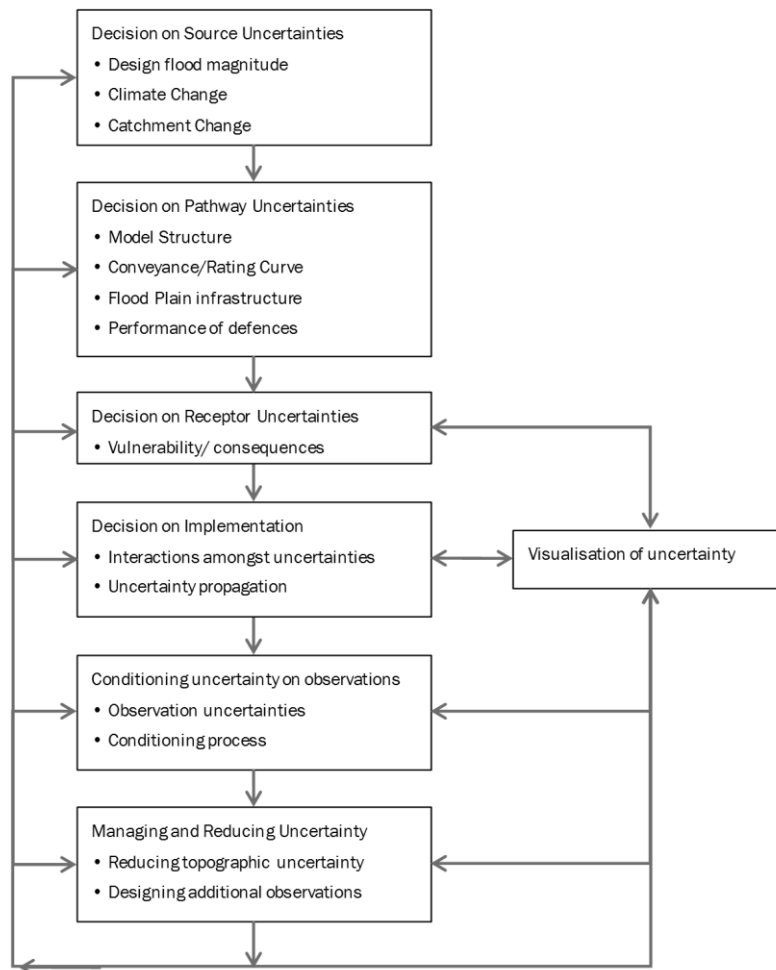


Figure 2-9 The primary sources of uncertainty in flood risk mapping (the diagram was redrawn from Beven et al. 2014 cited in Beven et al. 2014)

## 2.5 Conclusion to the literature review

In this research, land cover maps of the two upper water catchment areas and the land change scenarios were developed following the selected methods from the literature. Based on the model ability to simulate the future land cover scenarios, a combined CA-Markov is selected as the land change model in this research. Although the hybrid model has been widely used in the land change modelling, the applications for simulating forest cover change have rarely been explored (Ghosh et al., 2017). The CA-Markov model has also been applied in many case studies in Indonesia. However, none of the studies have been conducted in Ci Kapundung and Ci Sangkuy upper water catchments, in which parts of the two case study areas are covered by forest plantations and natural forests.

Criteria to select a hydrologic model to assess the hydrological impacts on land change have also been mentioned in this chapter, and MIKE SHE was chosen in this study. Despite the extensive applications of CA and hydrologic models to assess land change and flood risk in watersheds, a combination of CA-Markov to model the land cover change, and MIKE SHE to project future flow regimes is rare, and none of the projects were conducted in Indonesia.

## Chapter 3 Case study areas

This chapter provides an overview of Bandung Basin and the two case study areas; the Ci Kapundung and Ci Sangkuy upper water catchment areas. The two catchments were selected as the case study areas because they have contrasting biophysical settings and scales, and demonstrate as useful indicators of flood risk in the Bandung Basin. Bandung Basin and its catchment areas were delineated from the digital elevation model (DEM) from BIG (*Badan Informasi Geografi/ Indonesian Geospatial Agency*), using a hydrology toolbox in ArcGIS.

### 3.1 Bandung Basin

There are four ways in which the perimeter of Bandung Basin can be defined (Figure 3-1) (Brahmantyo 2004). The first perception sees the Bandung Basin as a plateau. The area of the basin covers the large plain which is located in the southern Bandung city.

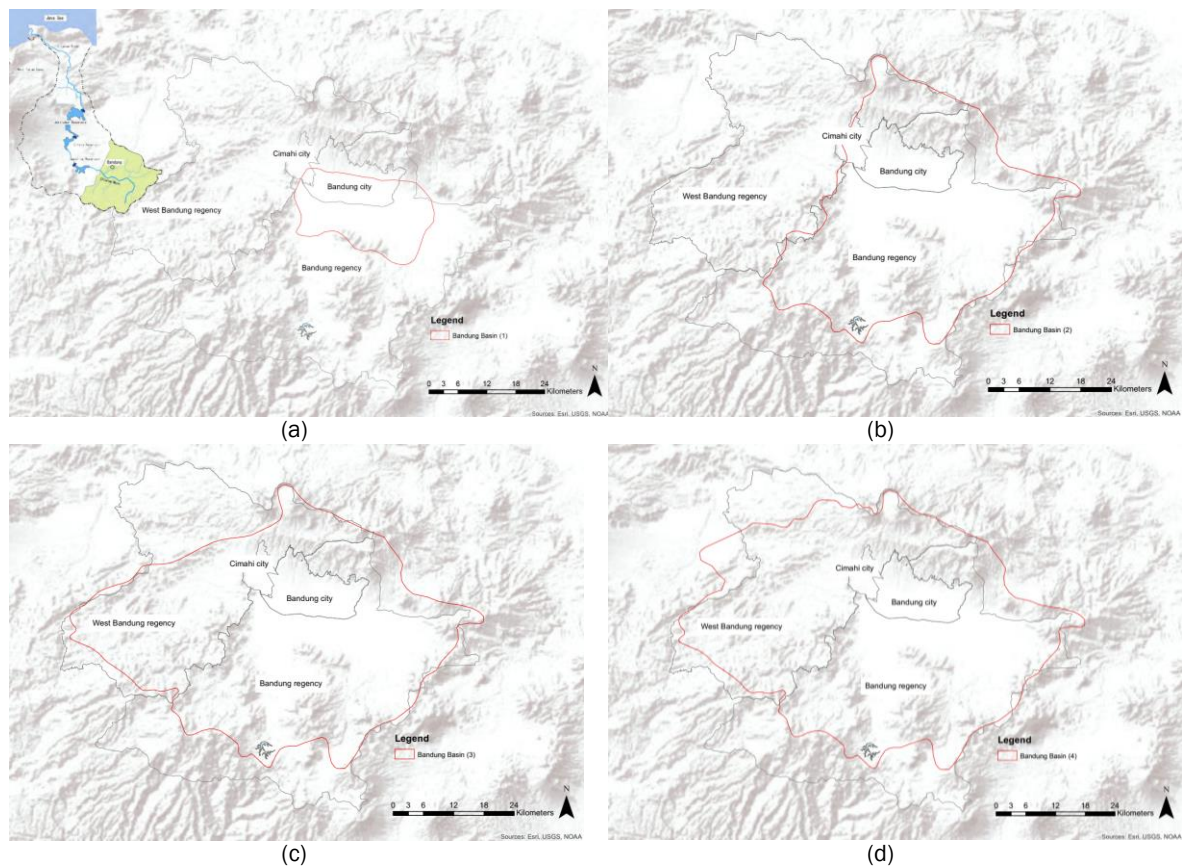


Figure 3-1 (a-d) Bandung Basin area delineation according to the four arguments (the delineation was drawn based on the original images from Brahmantyo, 2004). Source of background image: Esri, USGS, NOAA. Source of inset map: A modified map from JICA 2010)

The second viewpoint proposes the area of Ci Tarum upper water catchment as a part of the basin. It encompasses the hills and peaks of Mt. Tangkuban Perahu, Mt. Burangrang, Mt. Bukittunggul, and Mt. Manglayang in the north, Mt. Bukitjarian, Mt. Dusung, and Mt. Geulis in

the east, and Mt. Mandalawangi, Mt. Malabar, Mt. Patuha, and Mt. Tilu in the south, as well as the Selacau and Lagadar hills in the western part of the basin.

The third perception includes the Saguling reservoir as a part of the Bandung Basin. This delineation is based on the geological history of Bandung Basin. In this viewpoint, Sanghyang Tikoro<sup>11</sup>, a place which was once assumed to be the area where the outflow of ancient Bandung Lake was located, is included in its delineation. The last definition includes the whole area of West Bandung regency as part of Bandung Basin. This research uses the second perspective to define the area of Bandung Basin. In this viewpoint, the area is seen as a basin with lacustrine sediments surrounded by volcanos (Brahmantyo 2004).

An overview of the Bandung Basin development, the environmental conditions, the land cover changes over a period of time, the history of flood events, the current spatial planning policies, and the regulations of different protected areas in Indonesia are presented as follows.

### 3.1.1 Bandung Basin development

Early documentation of the environment of Bandung Basin was done by Franz Wilhelm Junghuhn in 1857, who wrote books depicting Java's mountain characteristics, including Preanger (the mountainous area in West Java, Indonesia) (Setiawan & Sabana, 2015). In other publications in 1845 and 1850-1854, Junghuhn also provided detailed descriptions of the natural vegetation in Java, and how those pristine conditions were destroyed by the increasing demand for agriculture (van Steenis & Schippers-Lammerste, 1965). Other documentation, written by L. van der Pijl in 1933, was about the undisturbed condition of limestone forest in Padalarang, which is located in the northern part of Bandung Basin (Whitten, Afiff, & Soeriaatmadja, 1996).

The distribution of rainfall throughout the year and altitude have created a condition which characterised flora in Java (van Steenis & Schippers-Lammerste, 1965). According to Whitten, Afiff, & Soeriaatmadja (1996), the natural vegetation of Java can be classified into six types: evergreen rain forests, semi-evergreen rain forests, moist deciduous forests, dry deciduous forests, aseasonal montane forests, and seasonal montane forests<sup>12</sup>. In addition, there are five types of forest which occupy small areas; mangrove forest, swamp forest, lower montane forest,

---

<sup>11</sup> Sanghyang Tikoro is located near the water body which is known as Saguling reservoir at the present time.

<sup>12</sup> Whitten et al. (1996) describe the difference between the evergreen rain forests and the semi-evergreen rain forests is that the latter can be found in the area with two to four dry months each year and almost half of the tree species are deciduous. Moist deciduous forests in Java are located in the region with four to six dry months and the annual rainfall of 1,500-4,000 mm. Whereas rainfall in the dry deciduous forests is less than 1,500 mm/year with more than six dry months. Fewer species are found in the deciduous forests than in the rain forests. The types of vegetation on mountain slopes differ with the increasing altitude.

Whitten et al. (1996) summarise the characteristics of plants in different forests on mountains based on the works from Raunkier (1934) and Webb (1959). More trees with canopy height or more than 25 metres and emergent with height up to 67 metres are found in the lowland forests. Shorter trees and less massive plant communities are more common with the increasing altitude. Tree buttresses are usually absent and creepers are very rare in the upper montane forests (1,800 - 3,000 m asl). However, epiphytes (e.g. moss, lichen) are usually abundant in this forest.



upper montane forest, subalpine vegetation, dry evergreen forest, lowland forest and thron forest.

Another vegetation classification was proposed by van Steenis in 1950. The proposed categories include the submerged littoral vegetation, mangrove, beach formations, barringtonia formation, dunes, lowland swamp forests, hydrophytic vegetation, rheophytic vegetation, mixed lowland and hill rain-forest on dry land, montane everwet rain-forest, mountain swamps and lakes, subalpine vegetation, and monsoon forest (van Steenis & Schippers-Lammerste, 1965).

Coffee was first cultivated in Preanger in 1707, and plantations were mainly located on the lower slope of mountainous areas, particularly in the areas where primary forests were cleared (Knaap 1986 cited in Zakaria 2012). Among the regencies in Preanger, Bandung was the top coffee production area in 1832-1864 because of its suitability for growing coffee (Zakaria 2012). On the other hand, the construction of *Grote Postweg* (Great Post Road) across Java in the early 19<sup>th</sup> century initiated the development of towns in the island (Siregar, 1990). Siregar (1990) further described that during this time, there were scattered settlements in the Bandung Basin. The opening of the railway in 1884 connecting Bandung to Batavia (former name of Jakarta) has accelerated economic growth in the region. In 1906, Bandung received its municipality status along with the other ten cities/towns in Java and other islands. Initially covering an area of 900 Ha, Bandung area had increased to 2,130 Ha in 1911.

A study of the Bandung expansion plan (*Uitsbreidingsplan Bandoeng-Noord*) was proposed by the Department of Public Works in Bandung and the AIA Architecture Bureau of Batavia in 1917. The plan focused on the development of the north-east and north-west side of Bandung following the concept of 'garden-city'. It has transformed the town structure into a radio-concentric pattern, although the design was only partially implemented (Siregar, 1990).

Further development in southern Bandung was initiated by the kampong improvement project in 1925. The city densification continued after the independence of Indonesia. The first masterplan of Bandung city was developed in 1965, including for the satellite towns (e.g. Lembang and Cimahi in northern Bandung, and Ujung Berung and Dayeuh Kolot in southern Bandung). New dispersed settlements were started to be built in the regencies surrounding Bandung city in the early 1980s. At the same time, densification phenomena inside the city could be seen, particularly in the southern and north-western side of the city (Siregar, 1990).

### 3.1.2 Environmental conditions of Bandung Basin

In this section, six aspects of the environmental conditions of the Bandung Basin are explored. The aspects are the climate, topography, soil, hydrology, geology, and hydrogeology aspects, which characterise the landscapes of the basin. All the figures on Bandung Basin in this section

were retrieved from five different departments and research projects<sup>13</sup>, which show two different perimeters of the basin. However, the analysis part of this research uses only one version of basin delineation (i.e. the basin as Ci Tarum upper water catchment area). The delineations are shown in red in all basin maps in the following sections.

### (1) Climate

Many studies have suggested that rainfall patterns in Indonesia are generally affected by different climate drivers, such as the El Nino-Southern Oscillation (ENSO), the Indian Ocean Dipole (IOD), and monsoon (e.g. Qalbi, Faqih, & Hidayat, 2017; Aldrian & Dwi Susanto, 2003). ENSO is affected by the sea surface temperature anomalies (SSTA) in the Pacific Ocean, whereas IOD is a climate mode of SSTA variability in the Indian Ocean (Webster et al. 1999 & Saji et al. 1999 cited in Stuecker et al., 2017). The monsoon wind is generated by the different physical air properties between the ocean and continent and is affected by solar radiation (Tjasyono H. K. et al., 2008).

Indonesia can be divided into three climatic regions based on the characteristics of rainfall variability and the correlation between rainfall and the occurrence of ENSO and the monsoon (Figure 3-2) (Aldrian & Susanto, 2003). Region A, where the Bandung Basin is located, is influenced by two monsoons; the wet northwest and the dry southeast, which occur from November to March and May to September respectively. Region B is located in northwest Indonesia and experiences two peaks in rainfall with the highest precipitation rates every year from October to November and March to May. Region C covers the eastern part of the country, with one peak rainfall event in June-July.

The impact of climate change on rainfall patterns in four stations in Indonesia (1876–1996) were assessed using the moving average analysis (Lasco & Boer, 2006). The four stations are located in Jakarta, Kupang, Ambon, and Maulaboh, representing the regions with three different rainfall patterns in Indonesia; monsoon, equatorial, and local. The results show that the rainfall patterns in Jakarta and Kupang<sup>14</sup> affected by monsoon had decreased before the pre-industrial era (1900s-1920s). The rainfall intensity then gradually increased from the 1940s. The rainfall pattern in Ambon<sup>15</sup> is the local type, which indicates an opposite pattern from the monsoonal type. Maulaboh<sup>16</sup> is located in a region with the equatorial rainfall type. This rainfall pattern had gradually decreased until the early 1940s before it increased steeply in the following few years, and then decreased steadily from the early 1950s.

---

<sup>13</sup> The five departments and research projects are Bakosurtanal, UNPAD and Indonesia Power, Soil and Agroclimate Centre (1993), Brahmantyo (2005), Nurliana & Widodo (2009), Haryanto (2007), and JICA (2010)

<sup>14</sup> Jakarta and Kupang are located in Java and the East Nusa Tenggara islands respectively, in the southern part of Indonesia

<sup>15</sup> Ambon is the capital city of Maluku province, which is located in the eastern part of Indonesia

<sup>16</sup> Maulaboh is a city in Aceh province, which is located in the northwest part of Indonesia

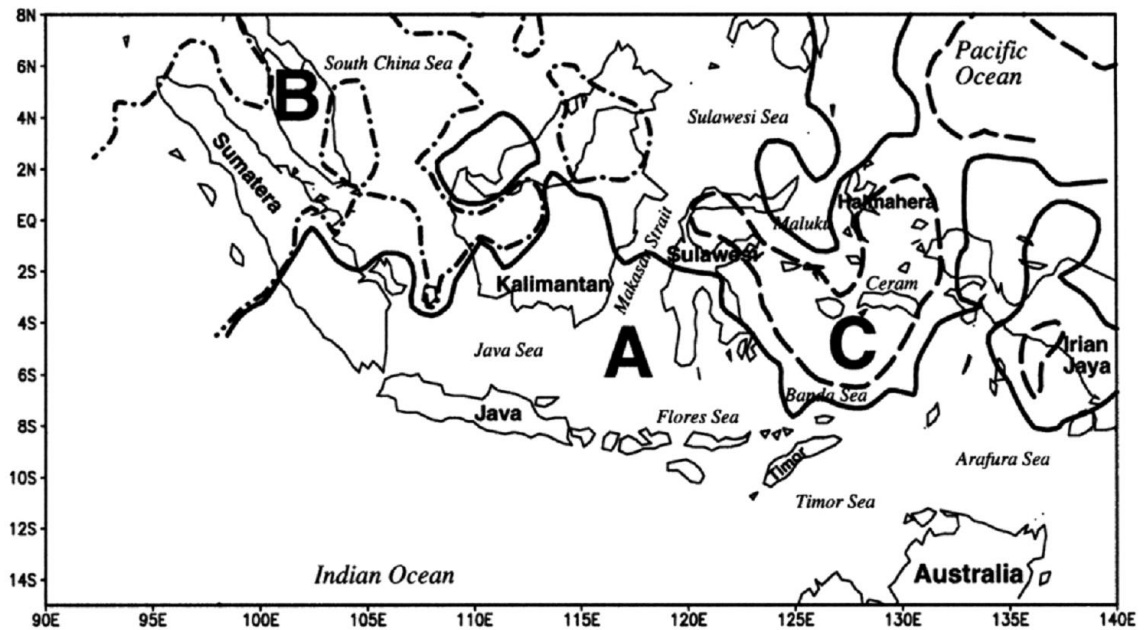


Figure 3-2 The climatic regions in Indonesia (Source: Aldrian & Dwi Susanto 2003)

The Bandung Basin climate is not only affected by the monsoon circulation, but also the topography of West Java province and the elevation of the basin (Brahmantyo 2005). A study was conducted to assess the influence of ENSO on the rainfall patterns in seven cities in Indonesia, including Bandung city, using precipitation data from 1970-1997 (Lasco & Boer, 2006). The analysis shows that the chance of rainfall anomalies occurring in Bandung City during La Nina events, which is indicated by strong positive SOI (Southern Oscillation Index (SOI), is more than 40%. However, the impact of ENSO on the local climate in Bandung might be less due to its location in the valley of Bandung Basin, compared with other cities.

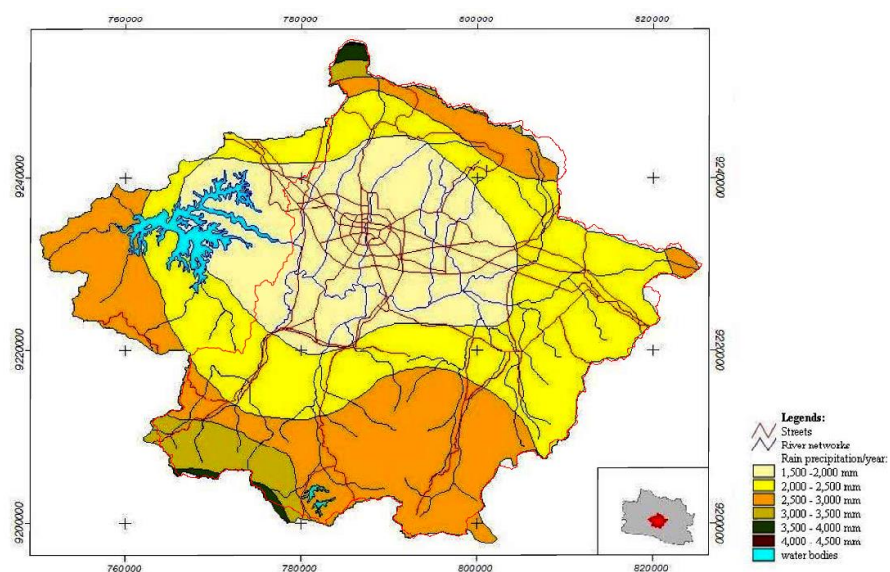


Figure 3-3 Annual precipitation rates in Bandung Basin (The map was redrawn from Bakosurtanal, UNPAD and Indonesia Power. The delineation of the Bandung Basin is shown in red)

The annual precipitation rates per year in Bandung Basin, which vary with elevation, are shown in Figure 3-3 (Bakosurtanal, UNPAD, and Indonesia Power). BMKG (the Indonesian Agency for Meteorology, Climatology and Geophysics) forecasts changes in the rainfall patterns in Indonesia caused by climate change. More intense rainfall with precipitation rates over 50 mm/day is predicted to occur in Bandung Basin in the future, while the trends of wet spells will also increase (BMKG, 2017).

## (2) Topography

A topography map of Bandung Basin was created from DEM (Digital Elevation Model), and is illustrated in Figure 3-4. The map shows that the basin was surrounded by highlands with steep slopes on the northern, eastern, and southern parts of the region. The highest and lowest altitudes in the basin are 2,595 metres and 638 metres respectively. Lembang fault is located in the Ci Kapundung catchment in the northern part of Bandung Basin. The fault breaks at the centre of the upper catchment where the Ci Kapundung River flows.

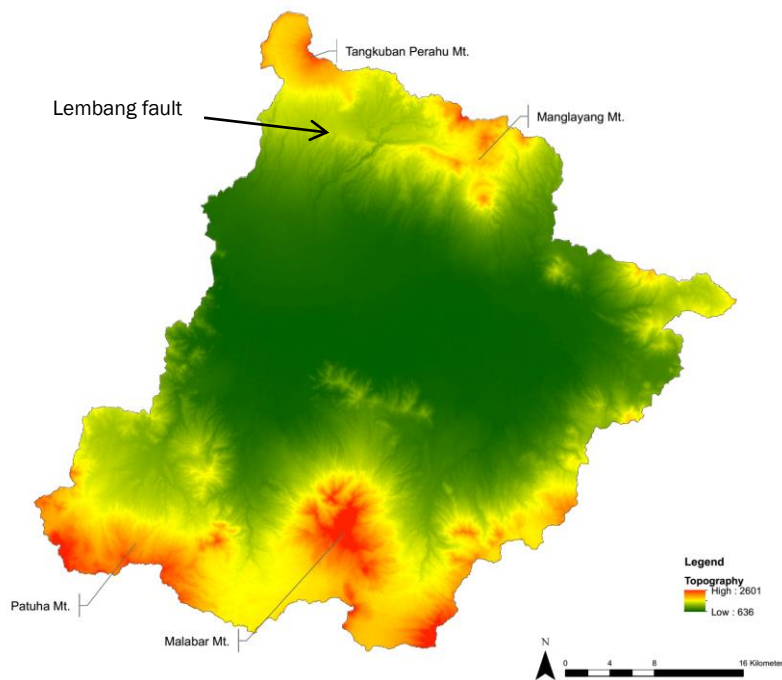


Figure 3-4 Topography of Bandung Basin (Source: a surface analysis using DEM from BIG (*Badan Informasi Geografi/Indonesian Geospatial Agency*))

## (3) Soil

The Soil and Agroclimate Research Centre (1993) identified the composition of clay, sand, and silt of soil types in Bandung Basin and the northwest side of the basin, excluding the area of Bandung city. The soil has been classified into 6 orders, which comprise of 8 suborders, 19 great groups, and 40 subgroups, based on Soil Taxonomy (Soil Survey Staff, 1999). The region was

divided into 78 zones based on the landform, soil compositions, and lithology. The soil map shows that the dominant soil types in the basin are Typic Tropaquepts and Aeric Tropaquepts, which were generated from lacustrine sediments. The soil is mostly located at the centre of the basin (Figure 3-5).

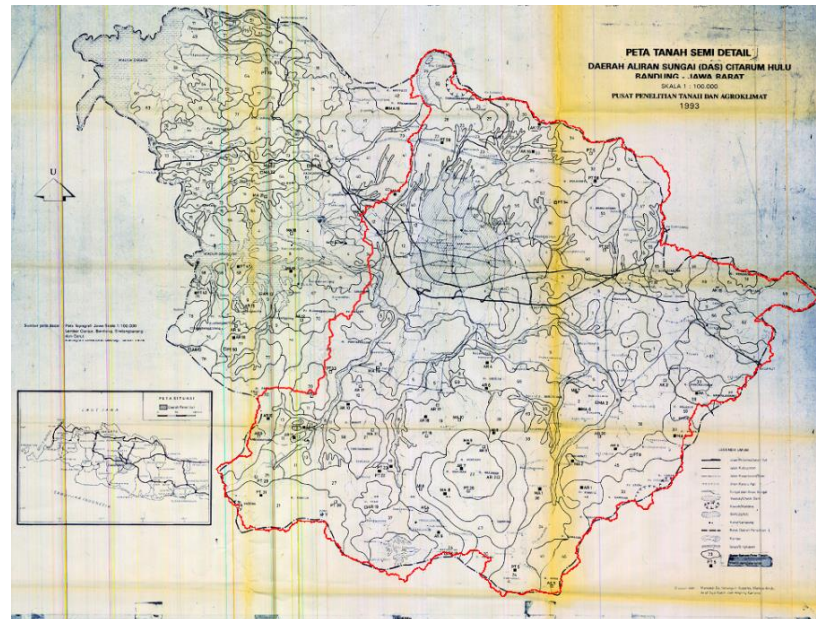


Figure 3-5 Soil map of Bandung Basin (Source: Soil and Agroclimate Research Centre 1993)

The landslide risk maps of Bandung City, Bandung Regency, and West Bandung Regency, where the two case study areas were located, were retrieved from the Center for Vulcanology and Geological Hazard Mitigation, Ministry of Energy and Mineral Resources (Figure 3-6). Each municipality is divided into four zones based on the level of landslide risk. The characteristics of the four zones are described as follows.

The first zone has very low susceptibility to landslides. The zone is mainly located in areas with a gradient of slopes less than 15% and is not formed by landslide deposits, filling material or plastic and swelling clay. The second zone has low susceptibility to landslides. There are traces of the occurrence of small landslides, especially near the rivers or gullies with gentle to steep slopes. The steep slope areas are mostly composed of rock with a thin layer of soil and are covered with dense vegetation. The third zone has a moderate susceptibility to landslides. This zone includes the areas along rivers, scarps, roadcuts, and disturbed slopes. The recurrence of landslides might be induced by high precipitation rates and erosion. The fourth zone has a high susceptibility to landslides. Landslides occur in the areas with moderate to very steep slopes, depending on the physical and engineering properties of rocks, as well as the soil formed from the weathering process.

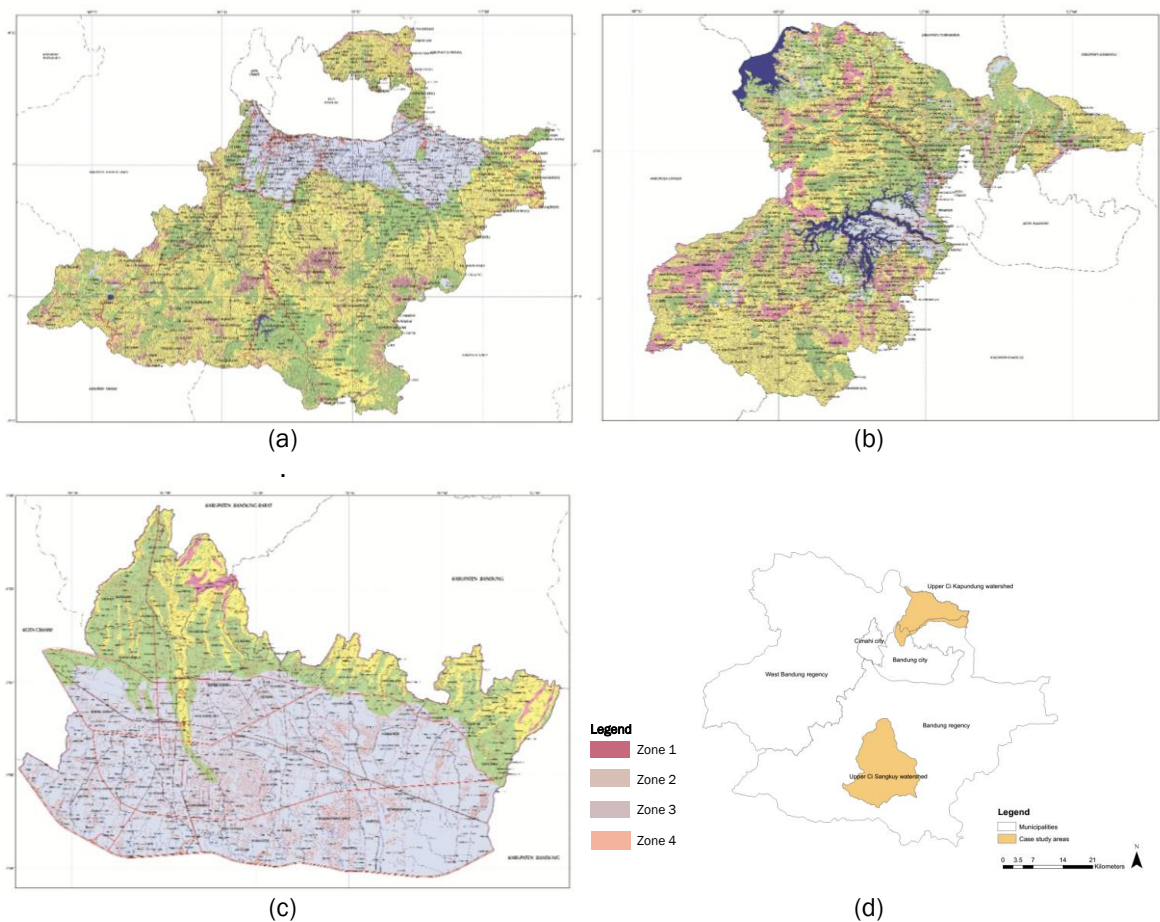


Figure 3-6 Landslide risk maps for (a) Bandung regency; (b) West Bandung regency; (c) Bandung city; (d) The location of each case study area in the three municipalities (Source: The Center for Vulcanology and Geological Hazard Mitigation, Ministry of Energy and Mineral Resources)

#### (4) Hydrology

Thirteen water catchment areas in Bandung Basin were delineated based on the DEM using a hydrology toolbox in ArcGIS. The thirteen watersheds are the Ci Widey, Ci Tepus, Upper Ci Tarum, Ci Tarik, Ci Sangkuy, Ci Pamokolan, Ci Mahi, Ci Keruh, Ci Kapundung, Ci Durian, Ci Cadas, Ci Bolerang, and Ci Beureum watersheds (Figure 3-7). All river networks from these watersheds flow to the Ci Tarum River, at the centre of the basin. Water from rivers in the Bandung Basin is extracted for drinking water, irrigation, industry, and electricity. There are three hydroelectric power plants in the Ci Kapundung and Ci Sangkuy watersheds (i.e. Bengkok, Lamajan, and Plengan hydroelectric power plants).

The impact of ENSO on the Ci Tarum River discharge in the Bandung Basin was assessed using long-term historical data (Lasco & Boer, 2006). The result suggests that the river flow increased by 0.37 m<sup>3</sup>/s and 0.24 m<sup>3</sup>/s for every 10-unit increase in SOI (Southern Oscillation Index) in May-July and August-October, respectively.

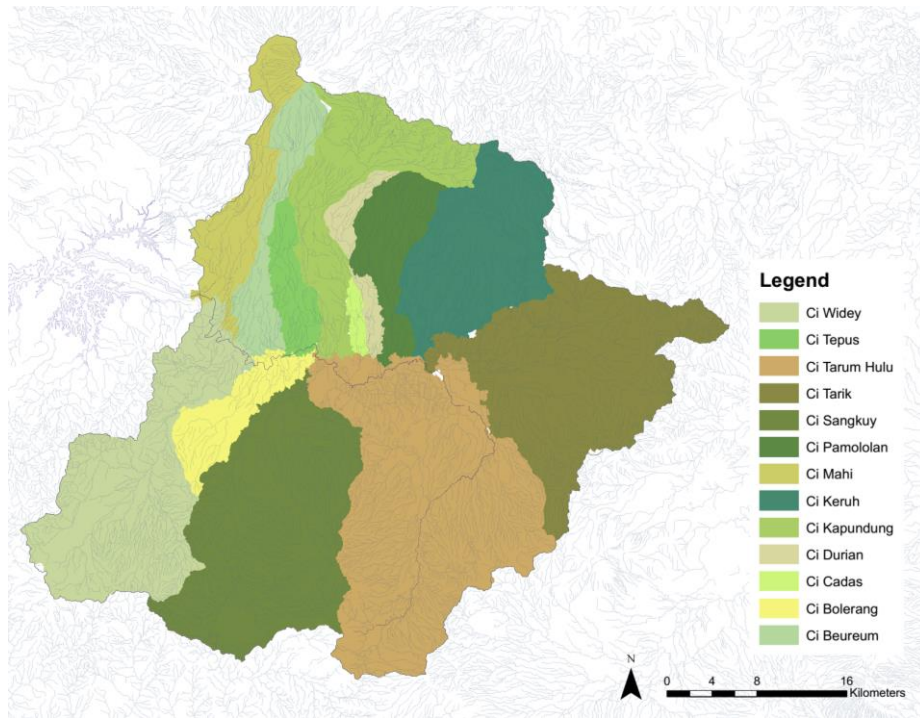


Figure 3-7 The watersheds in Bandung Basin (Source: catchment delineation analysis in ArcGIS using DEM. The overlaid river network image from Indonesian Geospatial Portal)

At a bigger scale, Bandung Basin can be seen as the upper catchment of Ci Tarum River (Figure 3-8). The river runs outside the basin to the Java Sea on the northern part of Java Island. Three reservoirs were built alongside the river, Jatiluhur, Cirata, and Saguling reservoirs, in which the inflow to the dams are affected by the ENSO. During El Nino events, the inflow could decrease up to 40% of the regular inflow to the three dams (Lasco & Boer, 2006).

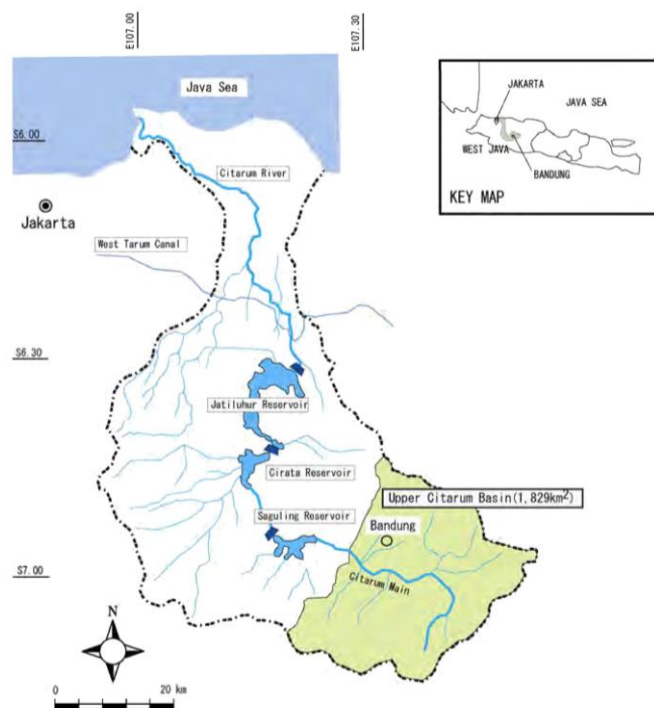


Figure 3-8 Ci Tarum water catchment area (A modified map from JICA 2010)

## (5) Geology

The geologic structure of Bandung Basin is characterised by the volcanic and tectonic activities during the Oligo-Miosen until early-middle Quaternary (approximately 30 million to 18 million years ago). The geomorphological structure of Bandung Basin consists of volcanic mountains and hills, alluvial fan and lacustrine plain, and anticline (Figure 3-9) (Brahmantyo, 2005). The volcanoes and hills are located in the northern, eastern, and southern parts of the basin. River networks on the hills of old volcanoes are characterised by the rough texture of the river bed. Approximately 85% of springs are located on the hills of Bandung Basin.

The alluvial fan and lacustrine plain are located at the centre part of Bandung Basin. The alluvial fan was developed when sediments from volcanoes flowed into the rivers on the mountains and were deposited when they reached the lacustrine plain. The lowest part of the plain is located in the elevation of 650 metres above sea level. The delineation of this lacustrine plain is the contour line of 700 metres above sea level. This alluvial plain is a floodplain area of the Ci Tarum River, which flows slowly in the relatively flat terrain with a slope of 2%. An intrusive rock as a natural dam in Selacau and Lagadar hills in the western part of the basin also affects the flow of Ci Tarum River (Brahmantyo 2005).

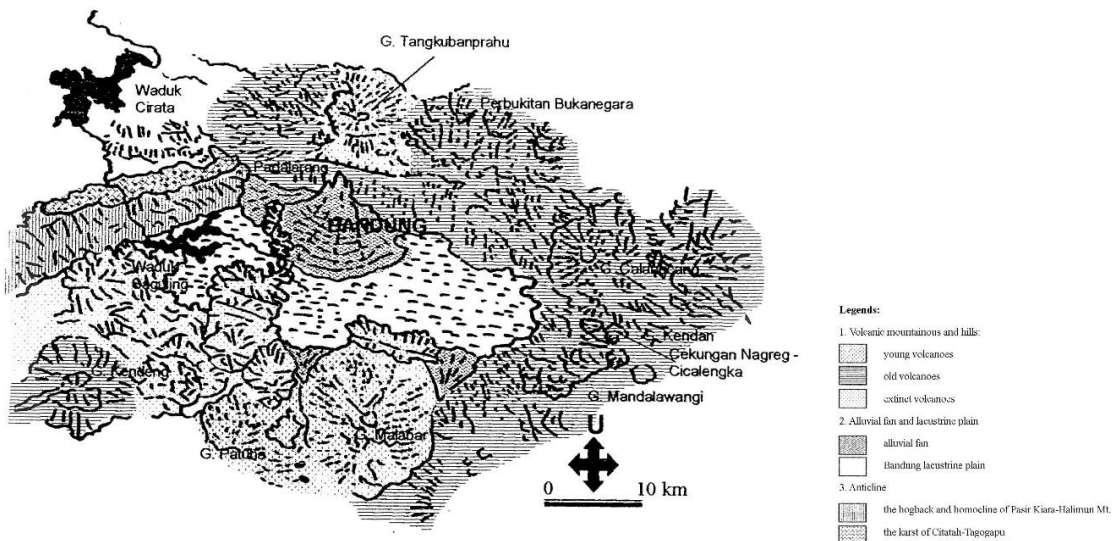


Figure 3-9 Geomorphological structures of Bandung Basin (Source: Brahmantyo 2005)

The anticline is spread out in the north-west part of the basin. The geology of the area can be classified into two parts; the hogback and homocline of Pasir Kiara-Halimun Mt. and the karst of Citatah-Tagogapu. Many cascades and waterfalls are found in the hogback and homocline. This area is assumed to be the location of the outflow which led to the creation of the ancient Bandung Lake 16,000 years ago.



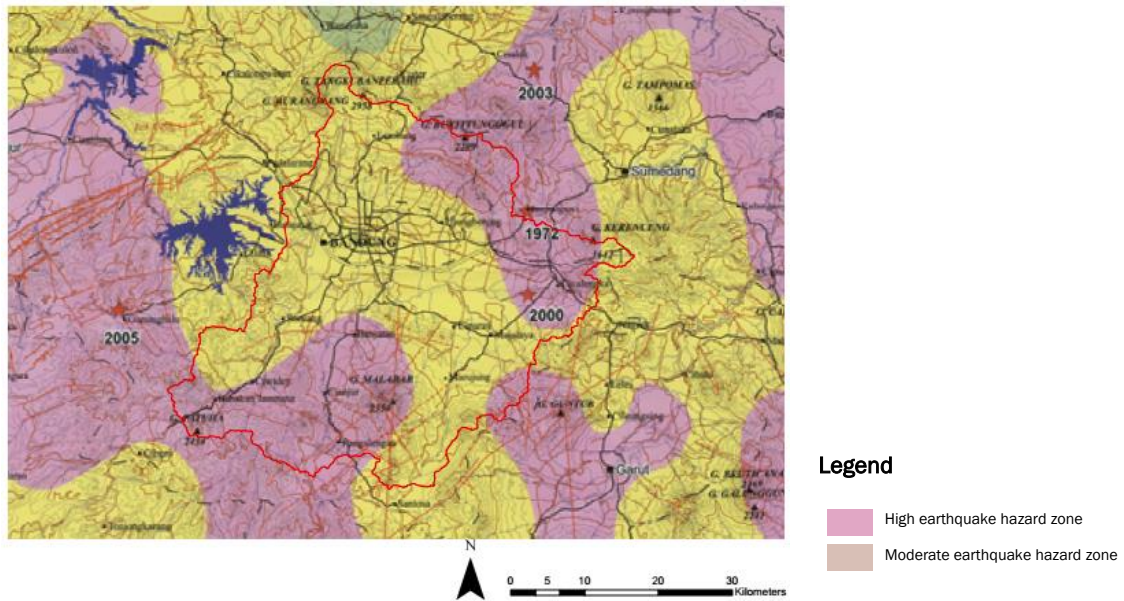


Figure 3-10 The earthquake hazard map for Bandung Basin (A modified map from The Center for Vulcanology and Geological Hazard Mitigation, Ministry of Energy and Mineral Resources 2008)

According to the earthquake hazard map of Bandung Basin (2008) (Figure 3-10), the basin is located in the high and moderate hazard zones. The first zone is prone to earthquakes with an intensity of VII-VIII MII (Modified Mercalli Intensity) scale, ground fissures, liquefaction, and landslides on the steep slope areas. The area is located near the hypocentre at shallow depths, which is composed of Quaternary deposits, such as alluvium and young volcanic sediments. The second zone has a moderate risk of earthquakes with an intensity of VI MMI scale. Ground fissures, liquefaction, and landslides might occur on a smaller scale. The area is mostly composed of Tertiary and Quarternary deposits. The hypocentre in this zone is located 35-90 km below ground level.

#### (6) Hydrogeology

There are two types of aquifers in Bandung Basin which have different lithology, conductivity, and transmissivity (i.e. the aquifer in the centre part of the basin and the aquifer in the northern, southern, and eastern parts of the basin). The first aquifer was developed from young and old volcano deposits, as well as from lake deposits. The lake deposits are located on top of the young volcano deposits (Cibeureum formation) (Figure 3-11). The second aquifer was composed by the deposits from young volcanoes (Cikidang and Cibeureum formations) and Tangkubanperahu Mt. (Cikapundung formation) in the north, deposits from Malabar Mt. and Wayang Mt. in the south, and the deposits from Mandalawangī Mt. in the east (Nurliana & Widodo, 2009).

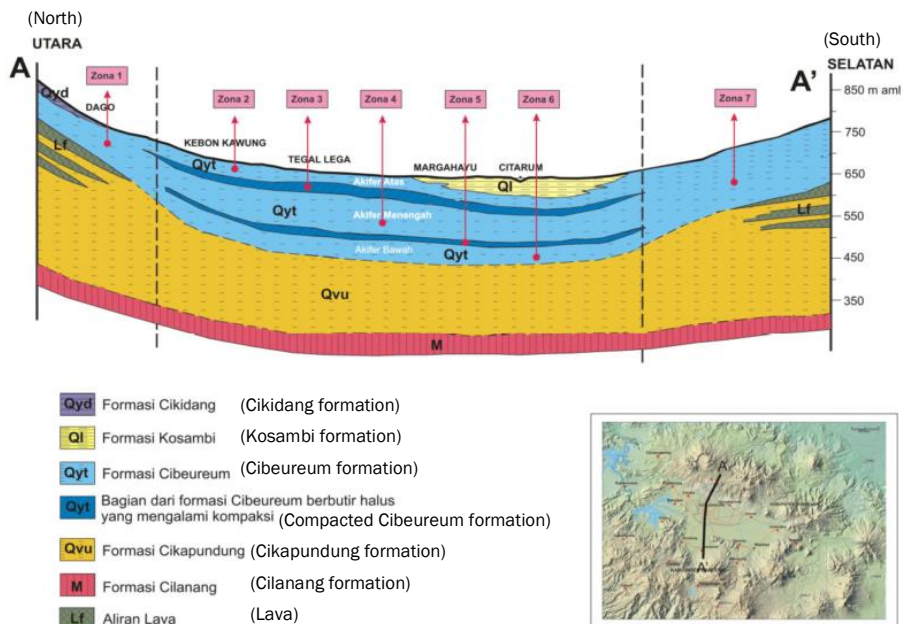


Figure 3-11 The aquifer in Bandung Basin (the image was modified to include an English translation. The original image was retrieved from Nurliana & Widodo (2009), who developed the aquifer model based on Priowirjanto (1985), IWACO & WASECO (1990), and Department of Mines and Energy, West Java province and LPPM-ITB (2002 & 2006))

### 3.1.3 Land cover change in Bandung Basin over a period of time

The assessment of a land cover changes in Bandung Basin, including the area where the Saguling reservoir is located (Figure 3-12), shows that there was an increase of the runoff coefficient in all catchments within the period of 1983-2002 (Haryanto, Herwanto, & Kendarto, 2007). The analysis was conducted using the table of runoff coefficients for different types of land cover from Chow et al. (1988). Higher runoff coefficients show a lower ability of the surface to absorb runoff water. The result of the assessment is presented in Table 3-1.

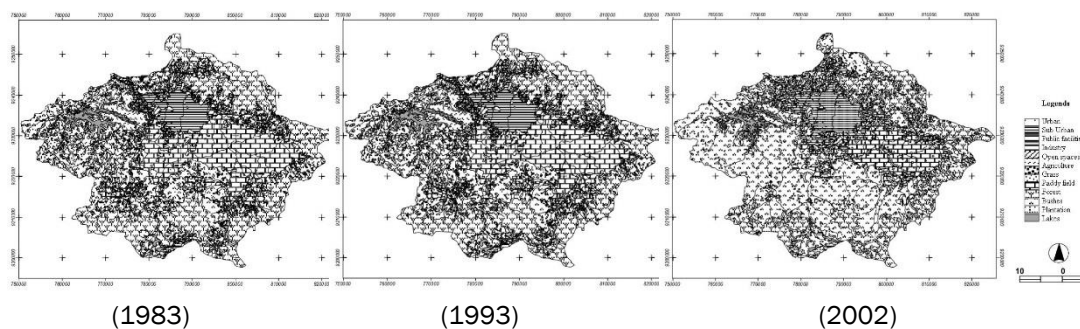


Figure 3-12 Land cover in Bandung Basin (1983-2002) (Source: BPLHD West Java Province cited in Haryanto, 2007)

Table 3-1 Runoff coefficients of all water catchments in Bandung Basin in 1983, 1993, and 2002  
(Source: Haryanto et al. 2007)

Catchments	Runoff coefficient		
	1983	1993	2002
Ci Kapundung	0.18	0.26	0.37
Ci Keruh	0.01	0.09	0.15
Ci Tarik	0.05	0.08	0.13
Ci Sarea	0.06	0.08	0.09
Ci Sangkuy	0.06	0.08	0.12
Ci Widey	0.06	0.08	0.11

### 3.1.4 The history of flood events in the basin and the river improvement project

Intense and prolonged rainfall and saturated soil to increase the rates of overland flow have caused the overflowing of major rivers in Bandung Basin. Figure 3-13 shows the total flood areas in the basin within the period of 1990-2002. The analysis from Lasco & Boer (2006) reveals that there was a chance of approximately 75% of floods occurring in the basin with flows of more than 200 m/s<sup>3</sup>, while massive floods were likely to happen when the flows are more than 250 m/s<sup>3</sup>.

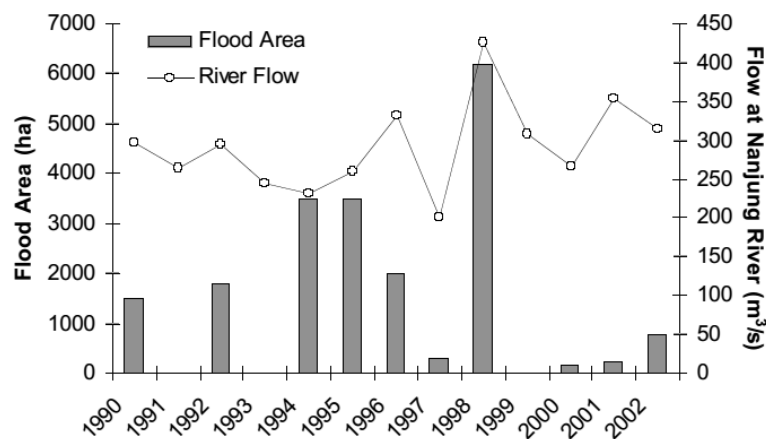


Figure 3-13 Total flooded areas in Bandung and recorded Ci Tarum River flows (1990-2002) (Source: Lasco & Boer, 2006)

To minimise flood damage in the basin, JICA (Japan International Cooperation Agency) proposed a series of flood mitigation plans from the 1980s. The Master Plan for flood control in nine tributaries (i.e. Ci Tarum upstream, Citarik upstream, Cimande, Cikijing, Cikeruh, Cibeusi, Ci Sangkuy upstream, Citagulung, and Ciputat) was generated in 1987-1988 (Figure 3-14), which was followed by the Feasibility Study, Detailed Design (D/D), and construction work within the period of 1992-2007 (JICA, 2010). The 2007 Detailed Design (D/D) comprises an improvement plan for the nine tributaries. The D/D includes the estimated design discharge, design river alignment, profile, and cross-sections. The river improvement project made a contribution to the decrease in the area affected by major floods in 1986-2007.

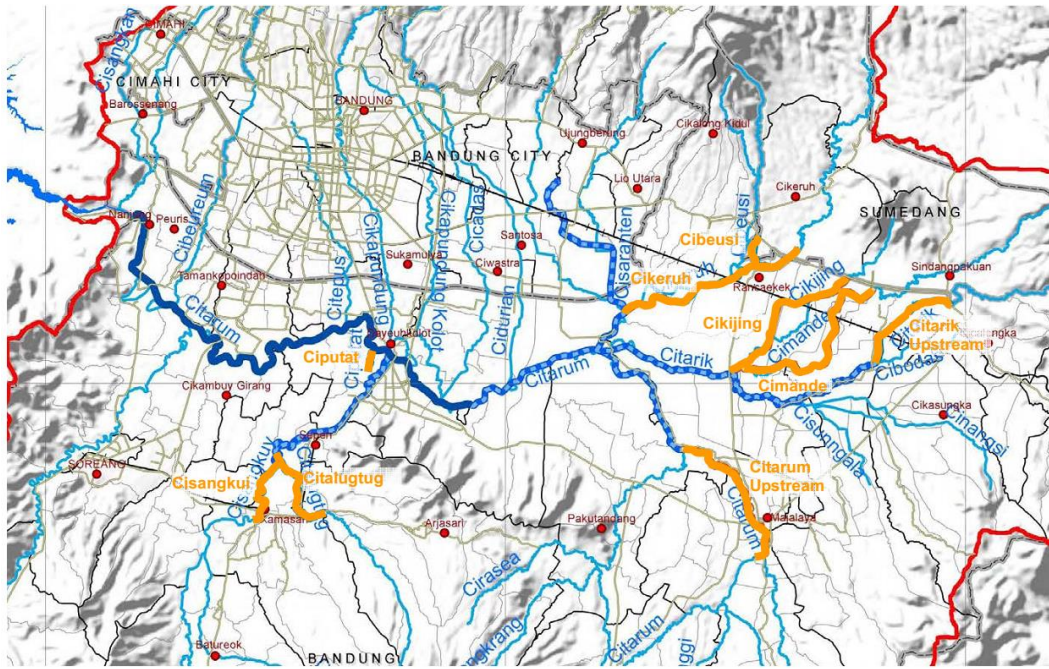
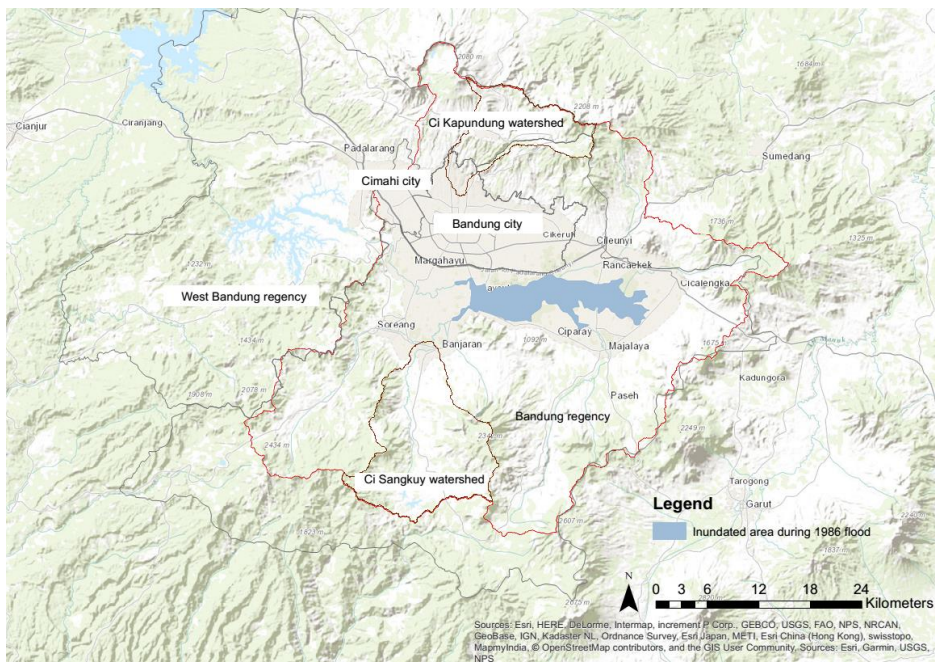
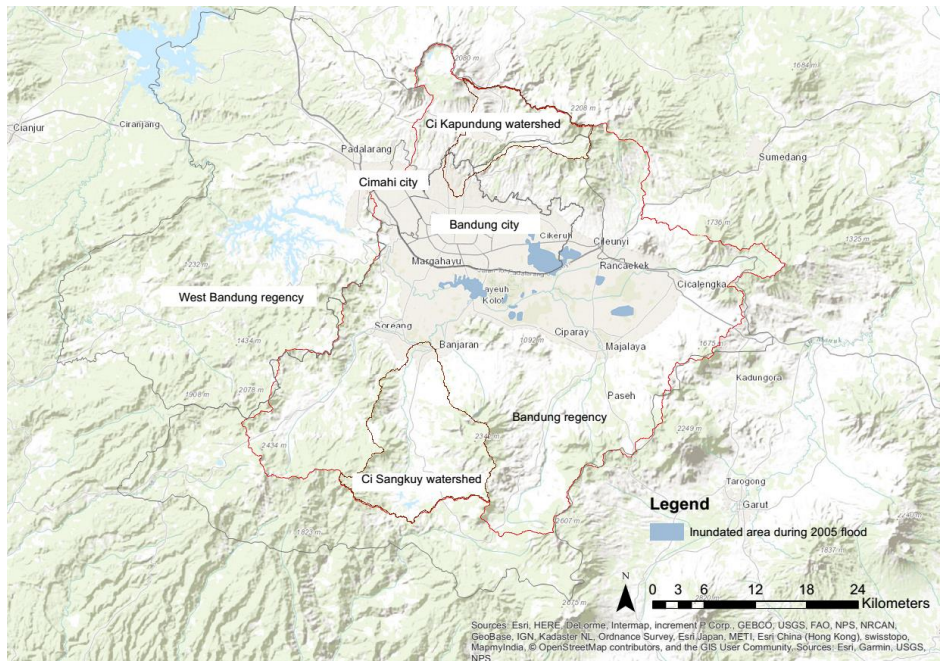


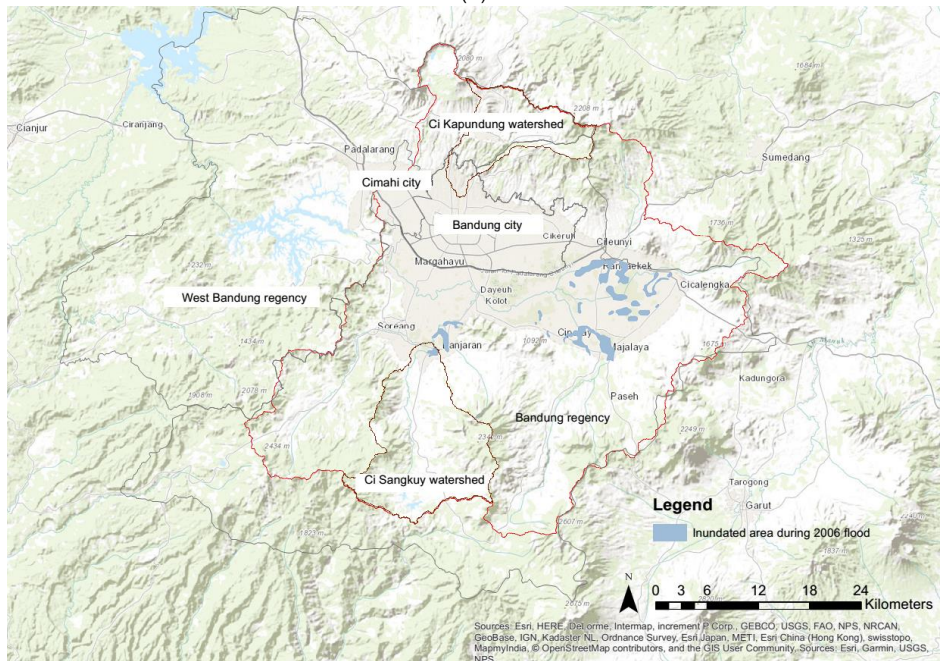
Figure 3-14 The location of nine tributaries for the river improvement project in the Bandung Basin (Source: JICA, 2010)



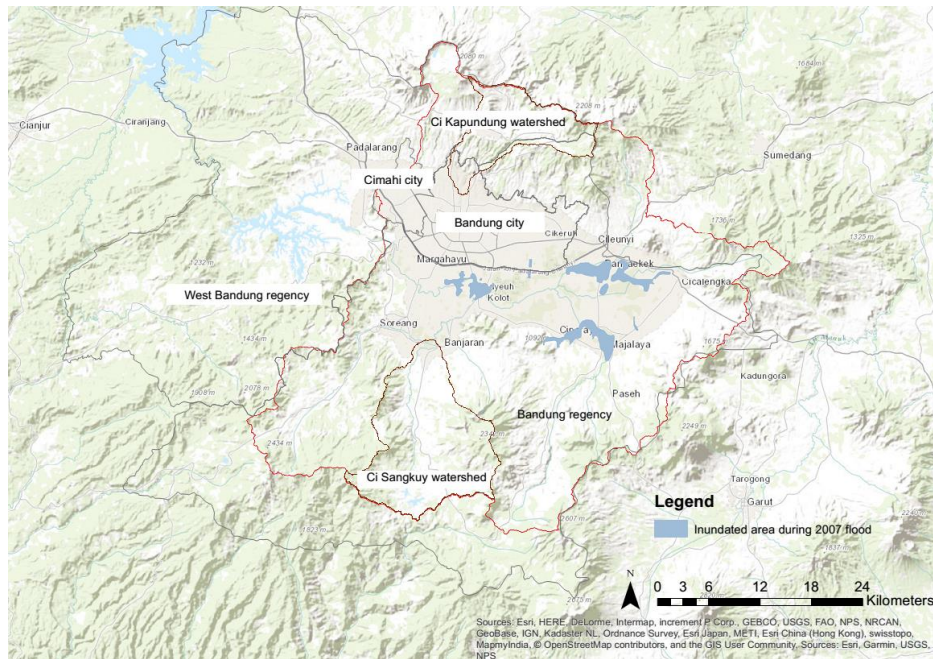
(a)



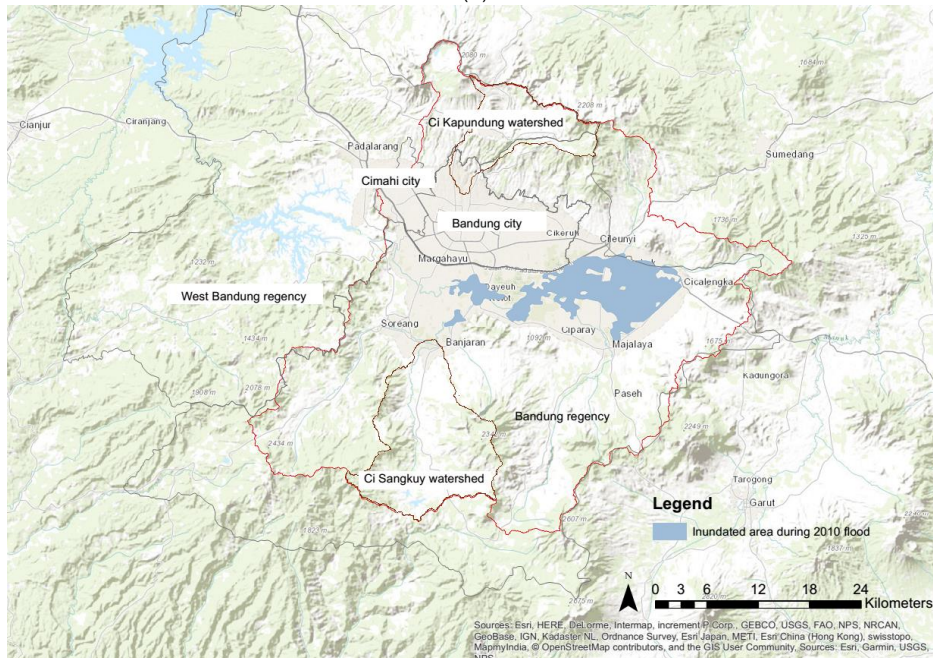
(b)



(c)



(d)



(e)

Figure 3-15 (a-e) The inundated areas during major flood events in the Bandung Basin in 1986, 2005, 2006, 2007, and 2010 respectively (the figures were redrawn from original images from JICA 2010; Source of background image: Esri, Garmin, HERE, DeLorme, Intermap, increment P Corp., GEBCO, USGS, FAO, NPS, NRCAN, GeoBase, IGN, Kadaster NL, Ordnance Survey, Esri Japan, METI, Esri China (Hong Kong), swisstopo, MapmyIndia, © OpenStreetMap contributors, and the GIS User Community. Sources: Esri, Garmin, USGS, NPS

Figure 3-15a shows the inundated area in Bandung Basin during a flood event in 1986 before the river improvement project was conducted. The total inundated area in the basin during the 1986 flood was 71 km<sup>2</sup>, as recorded by JICA. Higher precipitation caused by a strong La Nina event in 1998 (Null, 2018) resulted in the increased areas of flooding in the basin (Figure 3-13). The flooded areas during 2005, 2006, and 2007 flood events were gradually shrinking, compared with conditions in 1986 (Figure 3-15b-d). However, the lack of sufficient mitigation measures and heavy sedimentation from the upstream areas in the Bandung Basin prompted

recurrent floods in the area because of the decreasing flow capacity of Ci Tarum River (JICA, 2010).

### 3.1.5 Current spatial planning policies for municipalities in Bandung Basin

Every city and regency in Indonesia has a spatial plan (RTRW), which is developed from the plans at national and province levels. Based on the RTRW, municipalities develop more detailed spatial plans (RDTR). RTRW provides policies for spatial planning, land-use, and establishment of strategic areas, as well as strategies to control land utilisation. The land-use policies regulate the development of settlements, agriculture, public facilities and infrastructure in the area, including the protection of specific sites, such as the conservation areas, and areas prone to landslides, earthquakes, and volcanic activities. In this research, the two case studies are located in three municipalities in Bandung Basin (i.e. Bandung City, Bandung Regency, and West Bandung Regency). Each of these municipalities has a different spatial policy. Figure 3-16 shows the spatial plan for Bandung city and the two regencies.

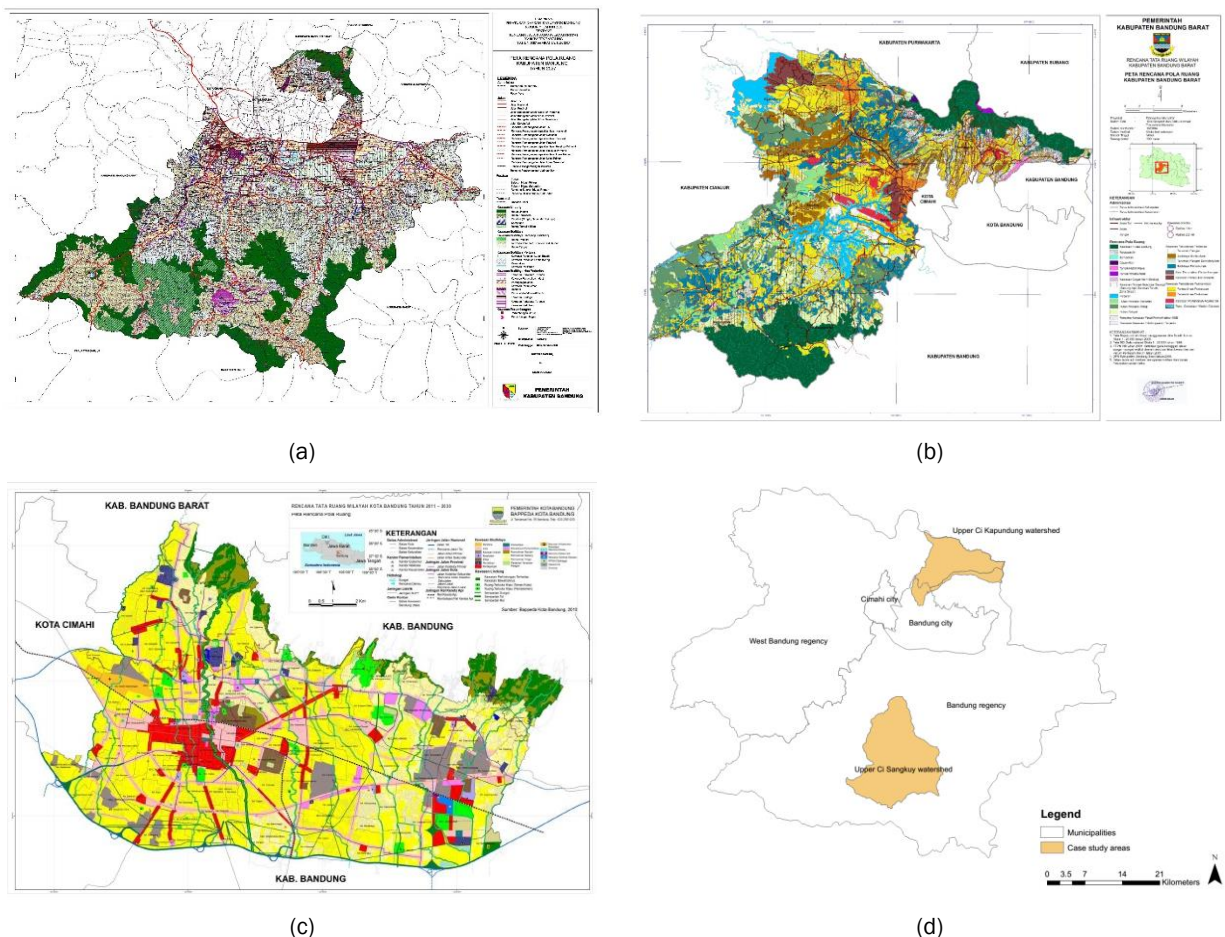


Figure 3-16 Spatial plans for (a) Bandung regency; (b) West Bandung regency; (c) Bandung city; (d) The location of each case study area in the three municipalities (Sources: Bandung regency, 2008; West Bandung regency, 2009; Bandung city, 2011)

In 2018, the government of Indonesia released a presidential regulation for Bandung Basin<sup>17</sup> spatial policy. The regulation proposes the spatial arrangements for seven different types of conservation areas (e.g. protected forests, recharge areas, areas providing protection to specific landscape features, protected areas, areas with specific geological features, cultural heritage sites, and other conservation areas), and the built-up areas. The original spatial plan is divided into 46 maps in an A4-size. Figure 3-17 shows the maps which have been georeferenced, and the area of Bandung Basin delineated from the DEM.

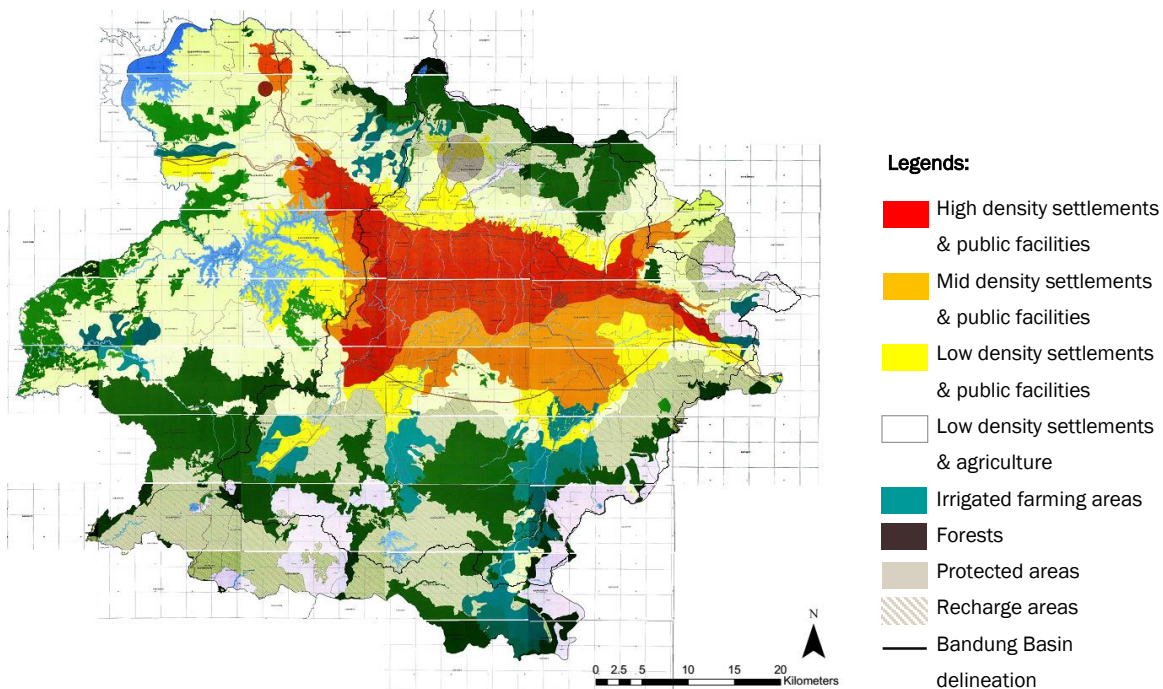


Figure 3-17 Spatial plan for Bandung Basin (Georeferenced maps of Bandung Basin spatial plan from the Indonesian presidential regulation no 45/2018. Boundary line in black is the basin delineation used in this research)

### 3.1.6 Protected areas in Bandung Basin

There are nine protected areas which are located in the mountainous areas surrounding the Bandung Basin; *Cagar Alam* (CA) Burangrang Mt (2,700 Ha), CA Tangkuban Perahu Mt. (1,290 Ha), *Taman Wisata Alam* (TWA) Tangkuban Perahu Mt. (370 Ha), and *Taman Hutan Raya* (THR) Ir. H. Djuanda (526.98 Ha) in the northern part of the basin, CA Kawah Kamojang (7,763.19 Ha), TWA Kawah Kamojang (535 Ha), CA Papandayan Mt. (6,807 Ha), TWA Papandayan Mt. (225 Ha) and CA Tilu Mt. (7,478.86 Ha), in the southern part of the basin. These protected areas were established with distinct purposes and management objectives, and demonstrate typical problems found in tropical forest protected areas in an urbanised region.

According to the Indonesian Law of Natural Resources and Ecosystem Conservation (1990) and the Indonesian Law of Forest (1999), *Cagar Alam* (CA) is a protected area where typical plants,

<sup>17</sup> In this regulation, the term of Bandung Basin refers to a region covering the whole area of Bandung city, Bandung regency, West Bandung regency, Cimahi city, and some parts of Sumedang regency.



wildlife, and the ecosystem are required to be conserved. *Taman Wisata Alam* (TWA) is a protected area which is dedicated mainly for nature-based tourism and recreation activities. *Taman Hutan Raya* (THR) is a protected area to display a collection of both indigenous and exotic plants and wildlife, which is dedicated to research, education, and tourism activities.

Based on the IUCN (International Union for Conservation of Nature) protected areas categories system, the term CA depicts the IUCN category Ia. This category refers to the protected areas that are established to protect biodiversity and geological/geomorphological features, where human activities in the areas are controlled to preserve nature. The term TWA is equal to the category VI of the protected area. In this category, most parts of the area are in a natural condition where the public can access for recreational purposes while conserving the natural resources. THR is equal to category V (Protected Landscape/Seascape). Protected areas in this category conserve the sustainability of ecological, biological, cultural and scenic value of an area where people and nature have interacted over time.

### **3.2 Case study areas as indicators of water catchments to cause flooding in Bandung Basin**

A preliminary study has been conducted to select two watersheds in Bandung Basin as the case study areas in this research. One of the criteria is the possibilities of the watersheds to cause flooding in Bandung Basin. The analysis was performed by assessing the runoff coefficients of all watersheds in Bandung Basin within the period of 2008-2016. A similar analysis has been done in the Bandung Basin using land cover data in 1983, 1993, and 2002, and the list of runoff coefficient for different land cover from Chow, Maidment, & Mays (1988) (Haryanto, Herwanto, & Kendarto, 2007). In this research, the assessment of runoff coefficients was conducted using the rainfall data and the estimated volume of direct runoff (2008-2016).

A runoff coefficient (C) denotes the proportion of runoff to rainfall over a period (Chow, Maidment, & Mays, 1988). It is common to use storm rainfall and the runoff data to assess the runoff coefficient. However, the coefficients can also be derived from monthly or annual rainfall and streamflow data. Direct runoff is generated by rainfall, which is not absorbed into the soil and is affected by the land cover and soil types. A watershed with high rates of change in runoff coefficients has a high proportion of permeable areas which have been converted to impervious surfaces. Thus there is a chance of the catchment to generate a high volume of direct runoff, especially during an intense and long-duration rainfall event.

Runoff coefficients can be estimated using Equation 3-1 (Chow, Maidment, & Mays, 1988). The original units of rainfall and river discharge retrieved from the weather stations and river gauges respectively are in metric. Therefore, the analysis was conducted using the same unit system.

$$C = \frac{r_d}{\sum_{m=1}^M R_m} \quad \text{Equation 3-1}$$

where

- C : runoff coefficient (dimensionless)  
 $\sum_{m=1}^M R_m$  : total rainfall (in)  
 $r_d$  : the corresponding depth of runoff (in)

In this study, the Thiessen-weighted averages of the daily rainfall data from rainfall gauges in all water catchment areas in Bandung Basin were computed. Then, the total annual rainfall in each watershed in 2008, 2010, 2013, and 2016, was calculated. The depth of runoff ( $r_d$ ) was estimated using Equation 3-2. The volume of direct runoff ( $V_d$ ) is the accumulated direct runoff ( $Q_n$ ) within a period of time ( $\Delta_t$ ) (Equation 3-3), which was calculated by subtracting the observed streamflow with the baseflow. Streamflow and rainfall datasets were derived from 10 river gauges and 13 weather stations respectively in eight watersheds in 2008-2016. The eight watersheds are Ci Kapundung, Ci Sangkuy, Ci Beureum, Ci Keruh, Ci Mahi, Ci Tarik, Ci Widey, and Upper Ci Tarum watersheds. Due to limited streamflow data, five other catchments in the basin were excluded from the analysis.

$$r_d = \frac{V_d}{\text{watershed area}} \quad \text{Equation 3-2}$$

$$V_d = \sum_{n=1}^{365} Q_n \Delta_t \quad \text{Equation 3-3}$$

Baseflow for rivers in the basin was estimated based on the river discharges data (2008-2016) of each river, following the method from Oregon State University, which is explained in chapter 4. The results are presented in Table 3-2.

Table 3-2 Estimated baseflow of eight rivers in the Bandung Basin

Rivers	River gauges	Estimated baseflow (m <sup>3</sup> /s)
Ci Kapundung	Pasir Luyu	0.64
Ci Sangkuy	Pataruman	3.06
Ci Beureum	Cihideung	0.25
Ci Keruh	Cikuda	0.22
Ci Mahi	Cicangkuang	0.42
Ci Tarik	B Cangkuang	0.46
Ci Widey	Cigenteng	6.47
Upper Ci Tarum	Majalaya	2.03

The estimated runoff coefficients of the eight watersheds in 2008, 2010, 2013, and 2016 are shown in

Table 3-3 and Figure 3-18. The result shows that runoff coefficients in the Ci Sangkuy water catchment area have the highest rate of change within the period of 2008-2016, compared with the other seven catchment areas in Bandung Basin. A further assessment has been performed to analyse the runoff coefficient in the Ci Kapundung upper water catchment area, although the regression line of coefficient in the whole catchment area shows the decreasing linear trend. Ci Kapundung had the fastest rate of land cover change in the basin in 1983-2002 (Haryanto, Herwanto, & Kendarto, 2007)<sup>18</sup>. Therefore, the analysis was done to discover how rapid land cover changes in the upper catchment has influenced the increasing volume of surface runoff, given the rainfall variability in the upstream.

Table 3-3 Estimated runoff coefficients for the eight watersheds in the Bandung Basin (2008-2016)

Watersheds	Runoff Coefficient			
	2008	2010	2013	2016
Ci Kapundung	0.1639	0.0437	0.0313	0.0095
Ci Sangkuy	0.1360	0.6419	0.8365	0.6139
Ci Beureum	0.0061	0.0238	0.0454	0.0656
Ci Keruh	0.0392	0.1160	0.0895	0.0634
Ci Mahi	0.0403	0.0175	0.0547	0.0775
Ci Tarik	0.0738	0.0297	0.0246	0.0398
Ci Widey	0.4473	0.3405	0.6275	n/a
Upper Ci Tarum	0.2429	0.1702	0.2641	0.2870

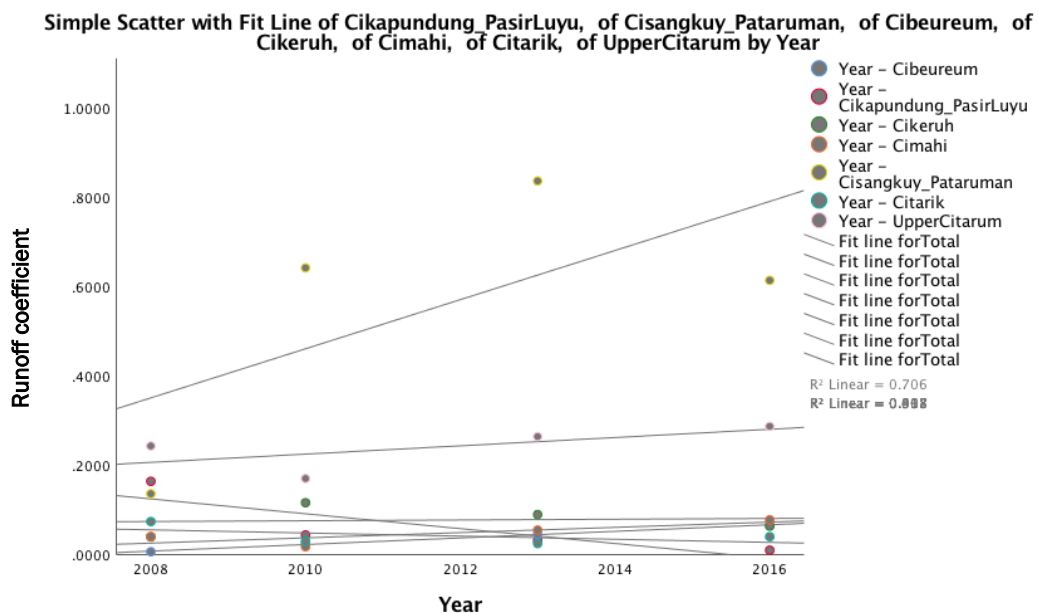


Figure 3-18 Runoff coefficients for the watersheds in Bandung Basin (2008-2016)

<sup>18</sup> Haryanto et al. (2007) divided the Bandung Basin into six main catchments area in their study (i.e. Ci Kapundung, Ci Keruh, Ci Sarea, Ci Sangkuy, Ci Tarik, and Ci Widey catchments. Other watersheds, which are identified in this PhD research (i.e. Ci Mahi, Ci Beureum, Ci Tepus, Ci Cadas, Ci Durian, and Ci Pamokolan) were classified as part of Ci Kapundung watershed, whereas the Ci Bolerang was recognised as part of Ci Sangkuy watershed.

The linear trend of runoff coefficients in the Ci Kapundung upper water catchment area (2008-2016) with an  $R^2$  value of 0.917 is illustrated in Figure 3-19. The outcome suggests that runoff coefficient had increased within the period of eight years, indicating rapid land cover changes in the area. This result might also be affected by the high precipitation in the catchment. As seen from Table 3-4, Thiessen-weighted average daily rainfall in the upstream and downstream of Ci Kapundung catchment (2008-2016) indicates that Ci Kapundung catchment in the upstream received higher precipitation than the downstream in 2008, 2009, 2011, 2002 and 2006.

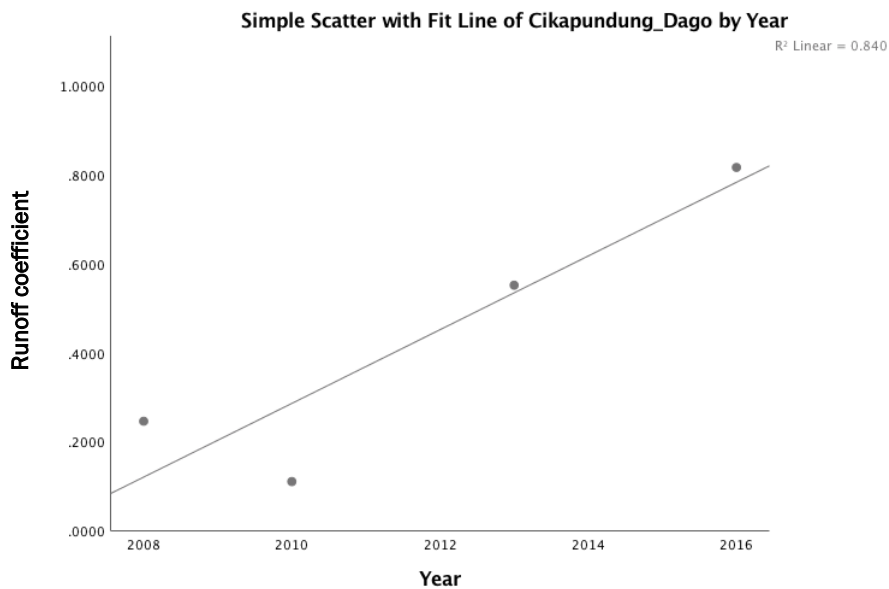


Figure 3-19 Linear trend of runoff coefficients in the Ci Kapundung upper water catchment area (2008-2016)

Table 3-4 Annual rainfall rates in Ci Kapundung upper catchment and the downstream (Source: analysis on rainfall data from PSDA)

Year	Annual rainfall rates	
	Ci Kapundung upper catchment (mm)	Downstream (mm)
2008	2,840.01	1,679.02
2009	2,889.20	1,729.47
2010	3,172.46	3,556.43
2011	1,988.29	1,394.72
2012	2,305.41	1,697.58
2013	2,251.79	2,541.68
2014	1,954.84	2,100.24
2015	1,777.25	2,214.28
2016	2,625.77	2,581.01

### 3.3 Ci Kapundung upper water catchment area

The upper catchment covers an area of 102.86 sq km and consists of rugged terrain with elevation varying between 760 and 2,206 metres above sea level and the maximum slope of

62°. The watershed is located at the latitude coordinates of 6°45'50"S – 6°53'20"S and the longitude coordinates of 107°35'27"E – 107°44'57"E (Figure 3-20).

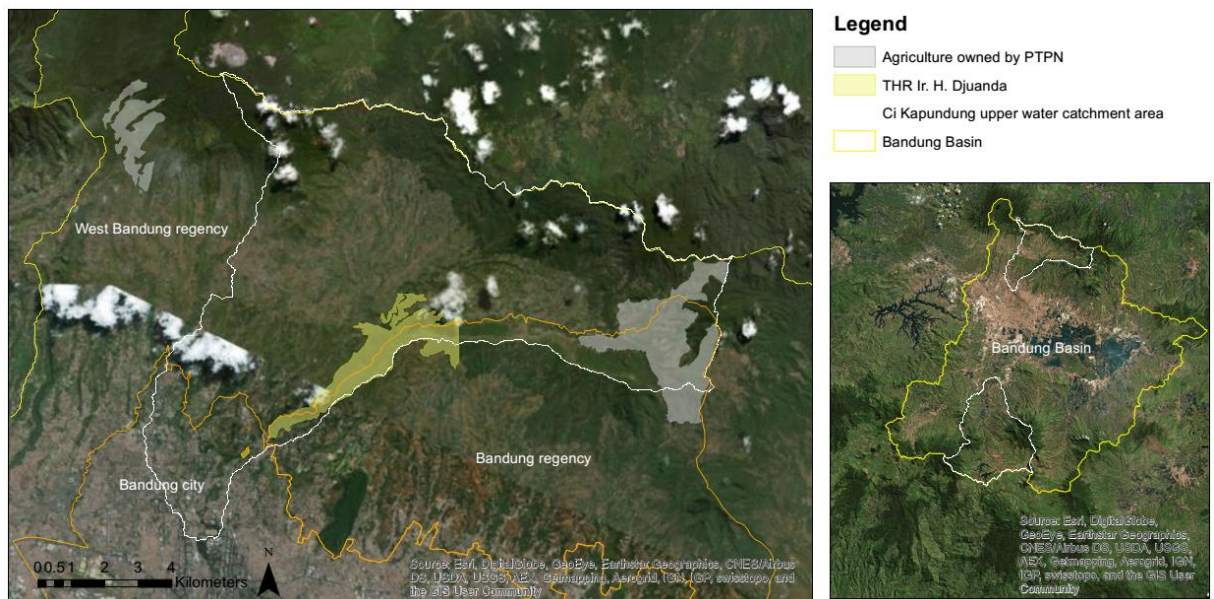


Figure 3-20 Map of Ci Kapundung upper water catchment area (Source: Protected area management 2008; PTPN 2016; Background image from Esri, DigitalGlobe, GeoEye, Earthstar Geographics, CNES/Airbus DS, USDA, USGS, AEX, Getmapping, Aerogrid, IGN, IGP, and the GIS User Community)

Precipitation in Ci Kapundung upper catchment area is recorded by five weather stations, which are located in and around the case study area (i.e. Kayu Ambon, Dago Pakar, Cipeusing, Margahayu, and Cibiru). Figure 3-21 shows the fluctuation annual precipitation rates recorded by the five meteorological stations (gaps in the graph lines indicate no complete data taken in a year). The average daily temperature in Bandung city in 1990-2015 is 23.3°C (BMKG 2015).

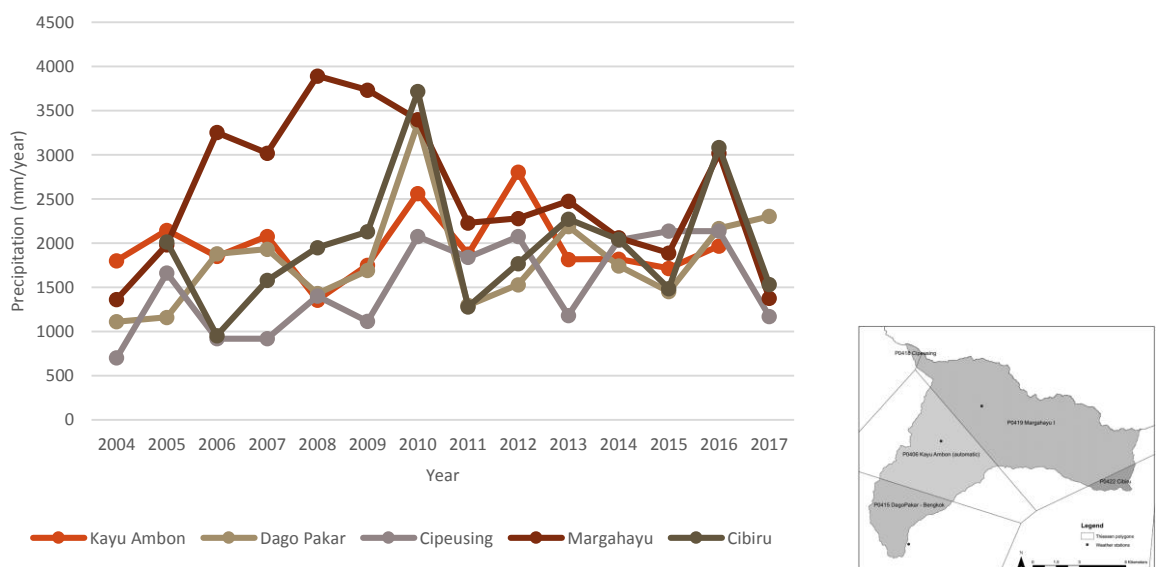


Figure 3-21 Annual precipitation in Ci Kapundung upper water catchment area (2004-2017) and the location of five meteorological stations in the area (Source: Author's analysis of precipitation data from PSDA 2017)

### 3.2.1 Land cover of Ci Kapundung upper water catchment area

Landscapes in the area are dominated by forests, agriculture, and developed areas. State-owned forests are located in the northern part of the area, which comprises of conifers, broad-leaved trees (e.g. *Agathis borneensis*, *Eucalyptus*, *Cinnamomum*), and mixed vegetation. Bamboo, Caliantra, and low shrubs are often found in the riparian areas of Ci Kapundung watershed. Agricultural areas are mostly located in undulated terrains. Settlements were built as the expansion of urban development of Bandung city in the south and West Bandung Regency in the western part of the area (Figure 3-22).

In the 1950s, conifers were planted in the eastern part of the catchment area, which was later managed as Ir. H. Djuanda protected area since 1985. The protected area is categorised as *Taman Hutan Raya* (THR), which has a lower protection level compared to other protected areas in Indonesia, thus is prone to landscape changes. The area was part of the Pulosari protected forest in 1922 before it was established as a botanical garden in 1965, a nature-based tourism area in 1980, and as the first protected area in Indonesia in 1985. THR Ir. H. Djuanda comprises an area of 526.98 Ha which is located at the latitude coordinates of 6°49'22"S – 6°52'0"S and the longitude coordinates of 107°32'2"E–107°40'33"E, and in the elevation of 770-1,350 m asl. The dominant vegetation in the protected area includes Pine (*Pinus merkusii*), Caliantra (*Calliandra calothyrsus*), Mahogany (*Switenia sp.*), Bamboo (*Bambusa sp.*), Kiriyyuh (*Euphatorium sp.*), and *Ficus sp.*



Figure 3-22 Six land covers in the Ci Kapundung upper water catchment area; (a) developed area; (b) agricultural area; (c) mixed woodland; (d) conifers; (e) broad-leaved woodland; (f) water body (Source: Author's documentation)

### 3.2.2 River networks in the Ci Kapundung upper water catchment area

The river networks in the Ci Kapundung upper water catchment area form a dendritic river system (Figure 3-23a). The river water outtake scheme (Figure 3-23b) shows that water from the Ci Kapundung River has been extracted for various purposes such as drinking water, irrigations, and water supply to Dago Pakar and Bengkulu hydroelectric power plants. It is estimated that the water outtake from the river is approximately 0.492 m<sup>3</sup>/s. There are three stream gauges which are located in the watershed to record the river discharges (i.e. the Cigulung, Maribaya, and Gandok). This research used the river discharge record from the Gandok gauge for the hydrologic simulations.

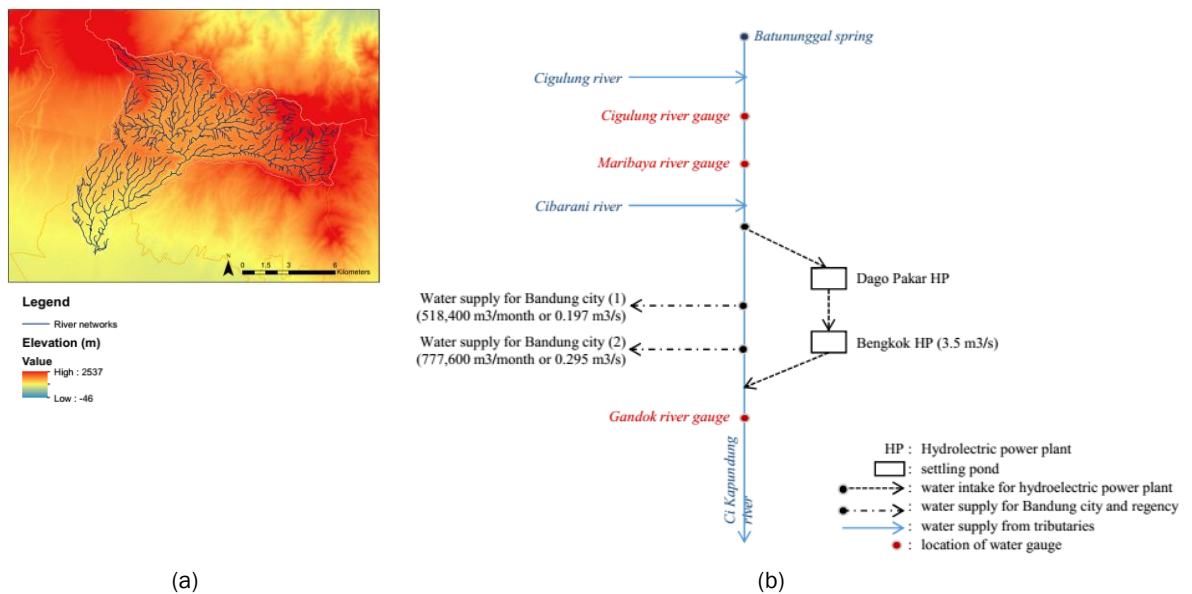


Figure 3-23 (a) Upper Ci Kapundung river networks; (b) Water supply and demand of the Ci Kapundung River (in m<sup>3</sup>/s) (background image a: DEM (30,9 metre); image b is redrawn from the original diagram provided by PSDA, 2016)

### 3.4 Ci Sangkuy upper water catchment area

The second case study is an area of 204.99 sq km, which is located in the elevation between 661 and 2,337 metres above sea level with a maximum slope of 54°. Coordinates of the watershed's boundary are 7°2'29"S–7°13'53"S and 107°28'56"E–107°38'47"E (Figure 3-244).

Four weather stations are located in and around the Ci Sangkuy upper catchment area (i.e. Ciherang, Cisondari, Cileunca, and Cibeureum). The annual precipitation rates for the case study area (2004-2017) recorded by the four weather stations are presented in Figure 3-25 (gaps in the graph lines indicate no complete data taken in a year).

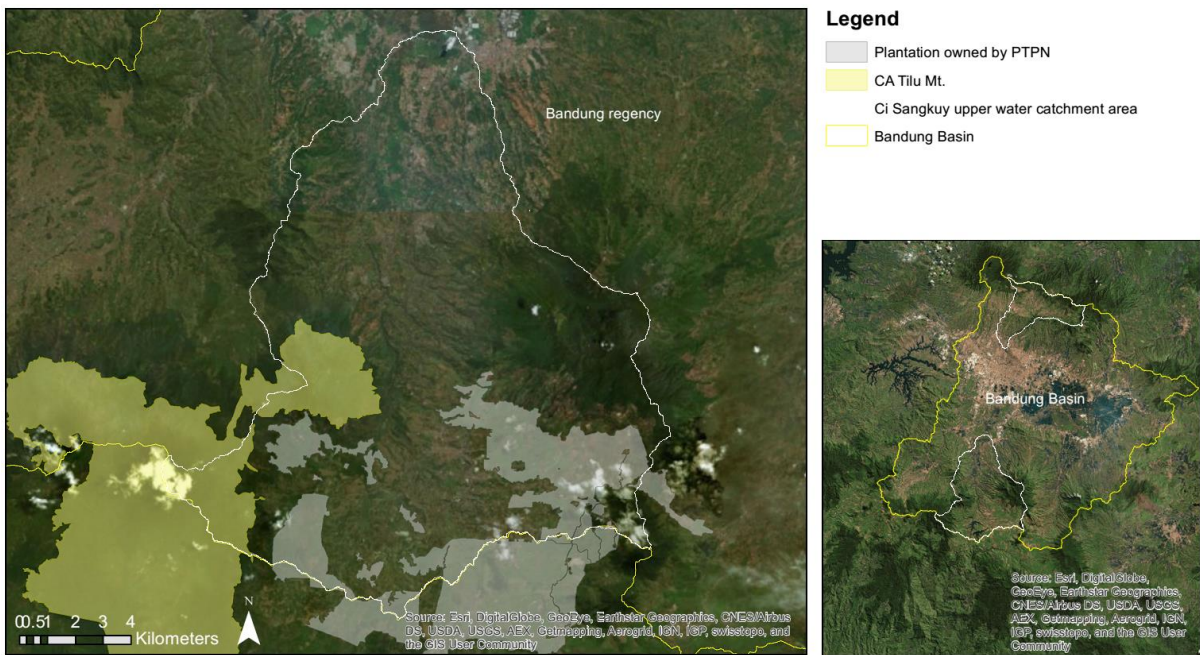


Figure 3-24 Ci Sangkuy upper water catchment area (Source: BKSDA, 2016; PTPN 2016; Background image from Esri, DigitalGlobe, GeoEye, Earthstar Geographics, CNES/Airbus DS, USDA, USGS, AEX, Getmapping, Aerogrid, IGN, IGP, swisstopo, and the GIS User Community)

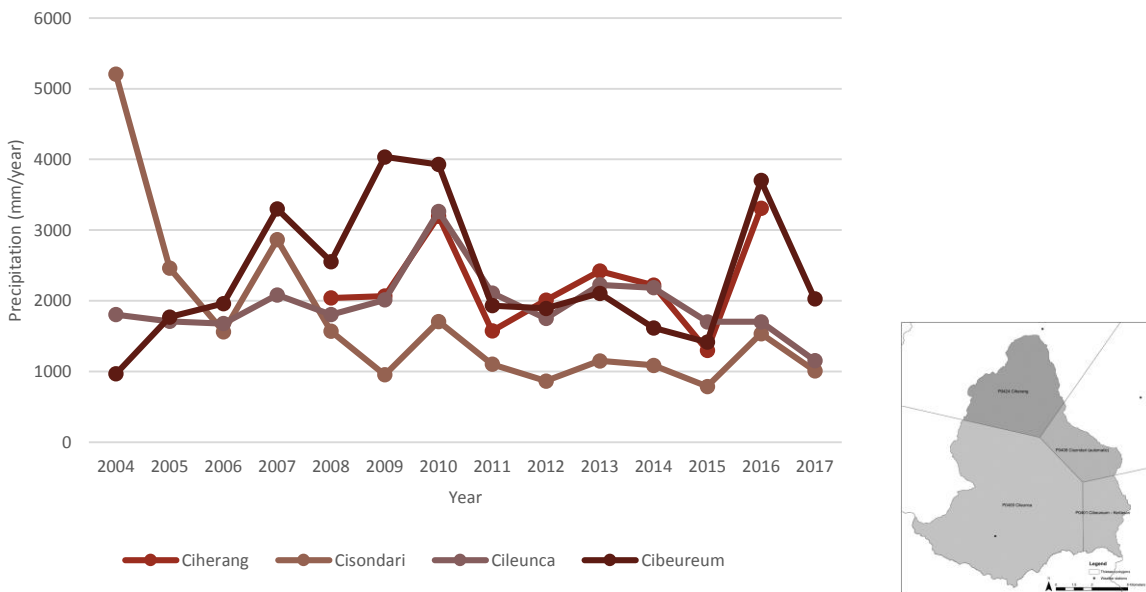


Figure 3-25 Annual precipitation in Ci Sangkuy upper water catchment area (2004-2017) and the location of four meteorological stations in the area (Source: Author's analysis of precipitation data from PSDA 2017)

### 3.3.1 Land cover of Ci Sangkuy upper water catchment area

Forests, agriculture, and tea plantations are the predominant landscapes in the area (Figure 3-26). Developed areas are mainly located along the main roads in relatively flat terrains. Productive forests in the western and eastern parts of the area are managed by a state-owned forest enterprise. Conifers and broad-leaved trees, such as *Altingia excelsa* and *Eucalyptus*, are



the dominant plant species in the forests. Meanwhile, mixed vegetation are found in the forests and within the Tilu Mt. protected area.

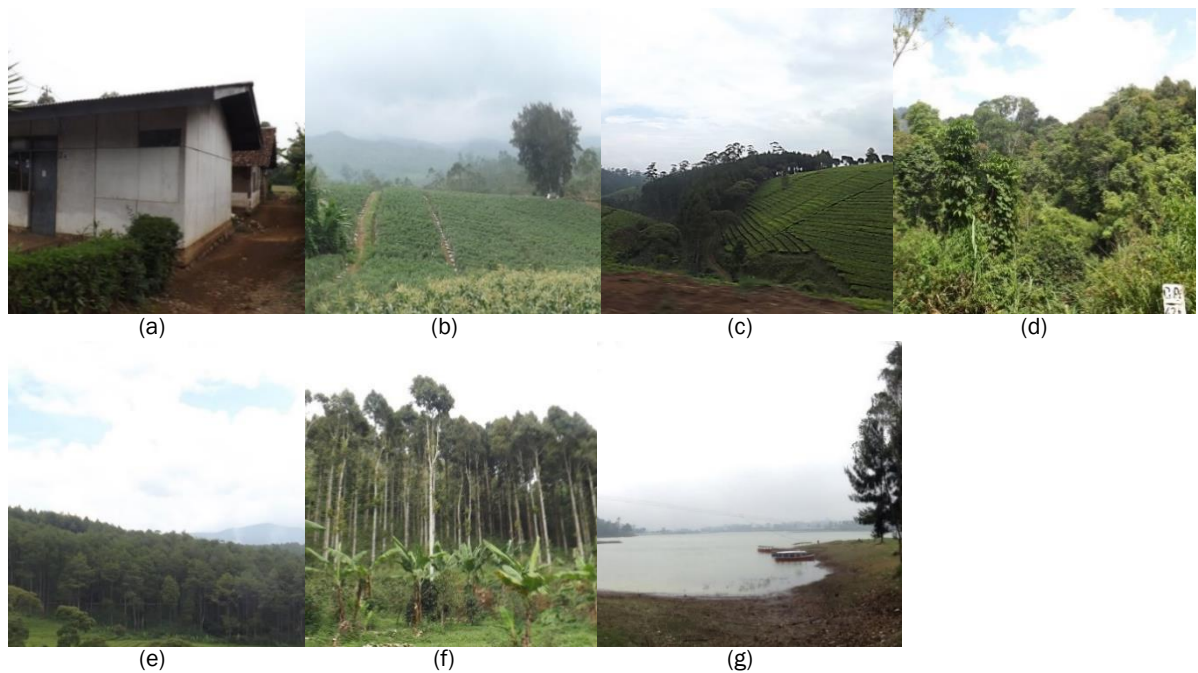


Figure 3-26 Seven land covers in the Ci Sangkuy upper water catchment area; (a) developed area; (b) agricultural area; (c) plantation; (d) mixed woodland; (e) conifers; (f) broad-leaved woodland; (g) water body (Source: Author's documentation)

Tilu Mt. protected area is categorised as *Cagar Alam*, in which the use of the area is strictly controlled and limited for conservation purposes. The *Cagar Alam* comprises an area of approximately 8,000 Ha and is managed by BKSDA/Nature Conservation Agency, under the Ministry of Environment and Forestry of Indonesia since 1978. The area is located at the latitude coordinates of 7°2'17"S–7°16'5"S and the longitude coordinates of 107°27'E–107°32'E, and in the elevation between 1,030 and 2,140 m asl. The ecosystem in the area is a highland rainforest, and the dominant tree species are Saninen (*Castanopsis argentea*), Rasamala (*Altingia excels*), Kiputri (*Podocarpus nerifolius*), Pasang (*Quercus lineata*), Puspa (*Schima walichii*), Kondang (*Ficus variegata*), and Tunggeureuk (*Castanopsis tunggurut*).

The tea plantations are managed by PTPN (state-owned agriculture enterprise in Indonesia) and some private companies. Distinct reflectance values of the tea plantation areas prompted them to be categorised as one land cover type separated from forests or agriculture areas.

### 3.3.2 River networks in the Ci Sangkuy upper water catchment area

A dendritic river system defines the river network in the Ci Sangkuy watershed (Figure 3-27a). Water from the two lakes in the area (i.e. Cipanunjang and Cileunca Lakes) runs into Ci Sangkuy River and provides water supply for the Plengan, Lamajan, and Cikalong hydroelectric power

plants (Figure 3-27b). Water from the hydropower turbines flows back to the Ci Sangkuy River. Two river gauges are located in the watershed to record the Ci Sangkuy river discharges. The discharge data used in the hydrologic simulation in this research was taken from the Kamasan river gauge, which is located at the northern part of the case study area. The water extractions include a supply for irrigation and drinking water in the Ci Sangkuy watershed. Estimated water extraction from the river is approximately 34,665 L/s or 34.66 m<sup>3</sup>/s.

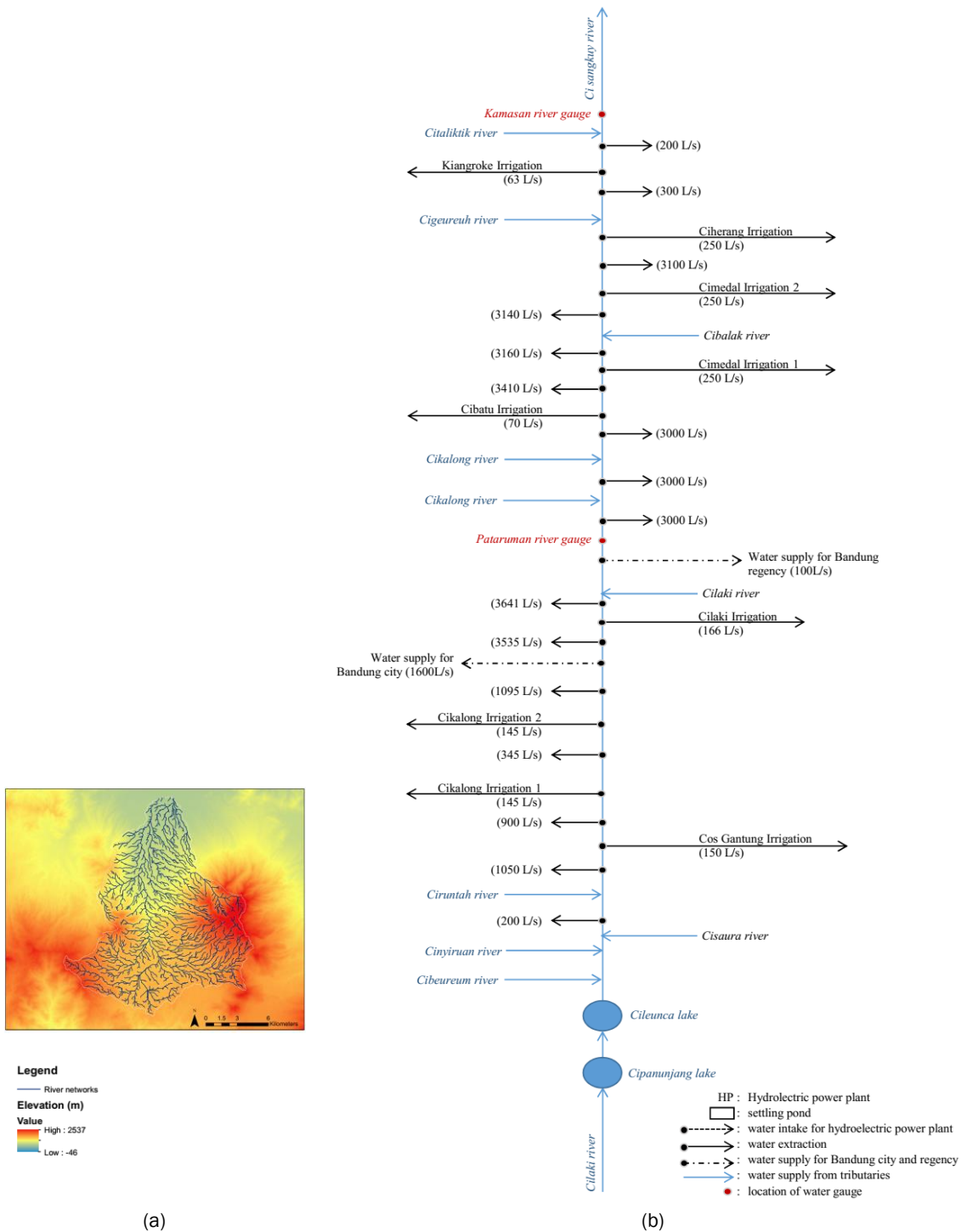


Figure 3-27 (a) River networks in the Ci Sangkuy upper water catchment; (b) Water supply from tributaries and demand of the Ci Sangkuy River (in m<sup>3</sup>/s and L/s) (background image a: DEM (30,9 metre); image b is redrawn from the original diagram provided by PSDA, 2016)

### 3.5 Summary of Chapter 3

- (1) Two case study areas were used in this research to compare the provision of flood regulating service in different catchments with distinct biophysical conditions and characteristics. The southern part of Ci Kapundung upper water catchment area is located in Bandung city, whereas the whole part of Ci Sangkuy watershed is located in a regency, in which the landscapes are predominantly covered by agriculture and forests. The two watersheds have protected areas with different levels of protection.
- (2) The first case study area was selected based on a study conducted by Haryanto, Herwanto, & Kendarto (2007), who concluded that the Ci Kapundung had the fastest rate of land cover change compared with the other catchments in Bandung Basin in 1983-2002. Although the runoff coefficient for the catchment showed a decreasing trend in 2008-2016, the upper catchment has an increasing trend.
- (3) The second case study area was selected because Ci Sangkuy River has high fluctuation in terms of the maximum and minimum discharge, high rates of erosion, and sedimentation in Saguling reservoir (Sarminingsih 2007 *cited in* Subarna, 2015). The catchment had an increasing trend of runoff coefficient in 2008-2015.

# Chapter 4 Methodology

This chapter presents the procedures of the land cover map development process and the methods to assess the three research questions in an iterative process. The methods include the use of land change and hydrologic modelling to project the future land cover maps and to assess the impact of land cover change to flood regulation. Decision tree diagrams and the limitations and boundaries of the research are given at the end of this chapter.

## 4.1 The development of land cover maps (research phase 1)

In this research, the development of land cover maps of Ci Kapundung and Ci Sangkuy upper water catchment areas was done in three iterative processes (Figure 4-1).

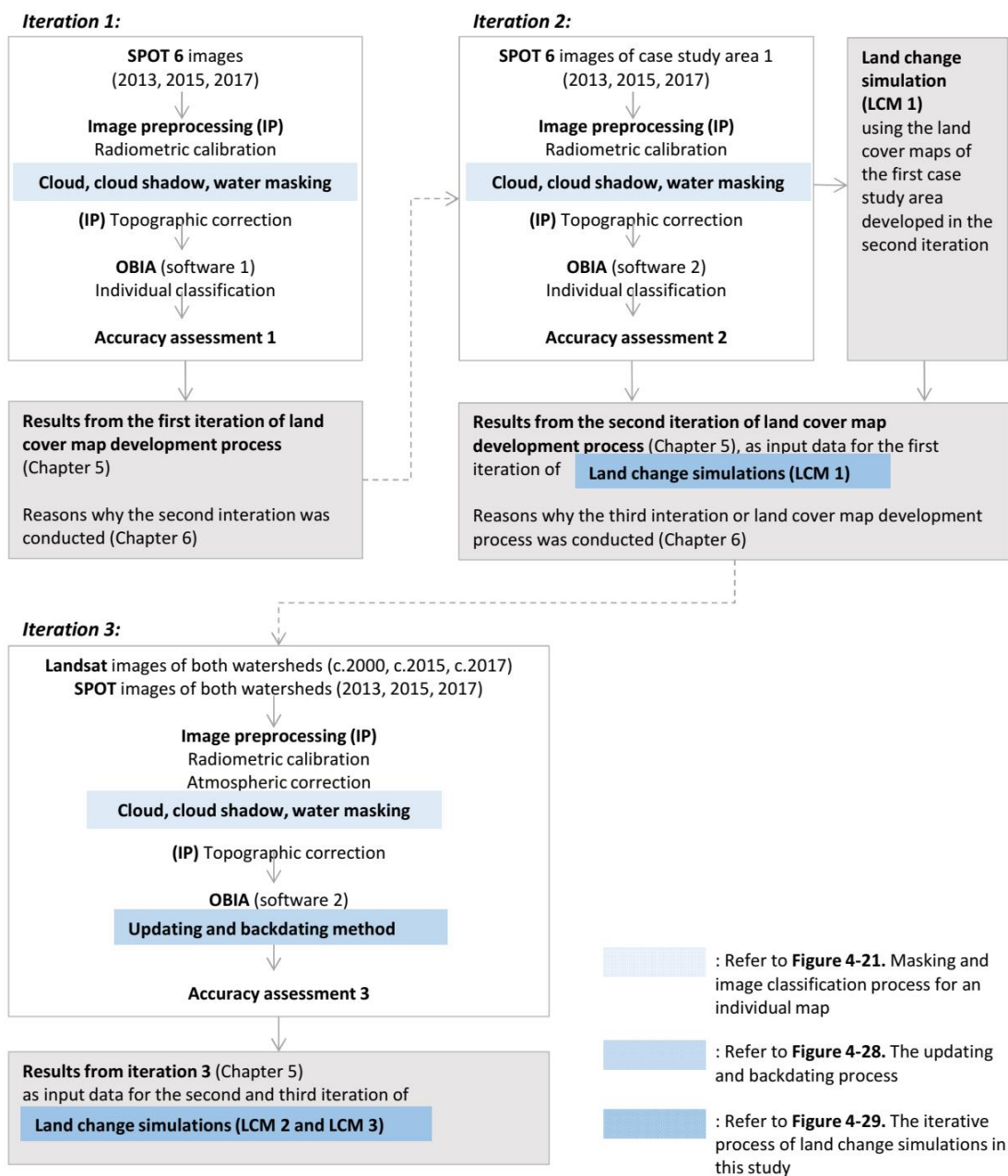


Figure 4-1 The iterative process of developing land cover maps in this study

The first two iterations were conducted to select appropriate approaches to generate land cover maps using SPOT imagery. Atmospheric correction was not applied to the satellite imagery. Based on the results from these processes, the final iteration of land cover map development was conducted using SPOT and Landsat images. Both atmospheric and topographic correction procedures were performed before the object-based image classification was conducted. This sub-chapter presents the process to develop land cover maps, which consists of data collection, image preprocessing, masking processes, atmospheric and topographic corrections of the images, and the object-based image classification.

#### 4.1.1 Data collection for the development of land cover maps

The land cover maps of Ci Kapundung and Ci Sangkuy upper water catchment areas were developed using SPOT 6 and Landsat 7 satellite images, based on field surveys, visual interpretation of satellite imagery with higher resolutions, and the updating-backdating method (Linke et al. 2009).

SPOT (Satellite Pour L'Observation de la Terre) 6 is a commercial satellite from Airbus Defence & Space, which was launched on 9 September 2012. The SPOT imagery consists of four spectral bands with the resolution of 6 metres, and one panchromatic band with a resolution of 1.5 metres. The four spectral bands are a blue band (450 – 525 nm), a green band (530 – 590 nm), a red band (625 – 695 nm), and a near-infrared band (760 – 890 nm). SPOT 6 images were used to develop land cover maps in the case study areas because local variance can be observed in forest images at a 6-m resolution. In the imagery with higher resolution, pixels show a mix of trees and background (Woodcock & Strahler 1987). In this study, SPOT 6 imagery from 2013, 2015, and 2017 was used for the development of land cover maps. Although there are SPOT 5 images taken before 2012, no completed imagery was available for the first case study area.

On the other hand, Landsat imagery with a 30-m resolution was used to generate land cover maps on a broad scale. Landsat 7 is a satellite from the National Aeronautics and Space Administration (NASA), which was launched on 15 April 1999. Landsat 7 imagery has seven spectral bands (30-metre resolution), and one panchromatic band (15-metre). In this study, four spectral bands of Landsat 7 was used to develop infrared images for the image classification process. The four bands of Landsat 7 are band 1 or blue (450 – 520 nm), band 2 or green (520 – 600 nm), band 3 or red (630 – 690 nm), and band 4 or near-infrared (770 – 900 nm).

Each band of satellite imagery is an individual greyscale image with a number of pixels which have different brightness values called digital numbers (DNs). In the image analysis and interpretation processes, the bands are combined as colour composites. A composite with natural colour can be developed using the visible blue, green, and red bands. A false colour or

infrared image, on the other hand, is composed by blending the green, red, and near-infrared (NIR).

Infrared imagery is used to develop the land cover maps because plants can be clearly differentiated in the NIR band (Figure 4-2) (Champbell & Wynne, 2011). Deciduous (broad-leaved) and coniferous (needle-shaped leaves) trees have different spectral reflectance in the NIR band, and not many differences in the reflectance values in other bands (Lillesand, Kiefer & Chipman, 2008, p.15). Conifers, which have cone-like crowns and needle-shaped leaves, absorb more NIR wave than deciduous trees do (Ranson & Williams 1992 cited in Walker & Kenkel 2000). So, little NIR radiation is reflected.

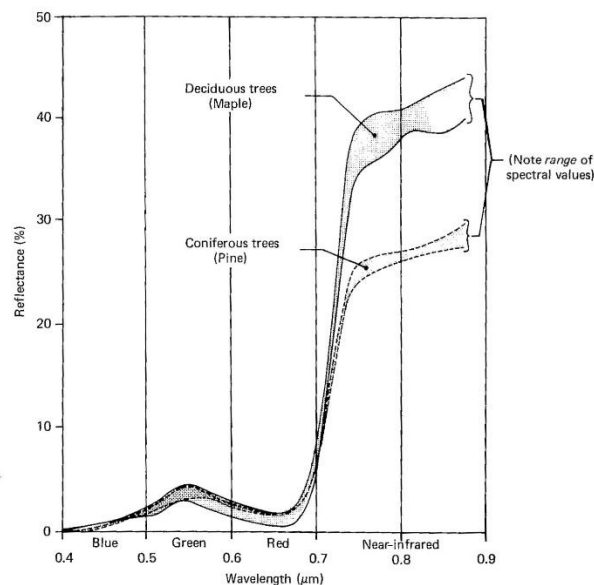


Figure 4-2 Different reflectance value in the NIR band between three vegetation classes (Source: Lillesand, Kiefer & Chipman, 2008)

The SPOT 6 satellite images were purchased from Airbus Defence and Space. The 2013 and 2015 images were taken on 10 June 2013 and 20 September 2015, with solar elevation angles of  $59.37^\circ$  and  $47.64^\circ$  respectively (Figure 4-3 and Figure 4-4). Due to the unavailability of the complete data from Airbus and the severe cloud cover over the area, two images were used to develop the land cover map in 2017 for the first case study area. The two images were retrieved on 22 July and 3 August 2017 with solar elevation angles of  $45.66^\circ$ , and  $48.66^\circ$  respectively). The 2017 images for the second case study area were taken on 1 July 2017, with a solar elevation angle of  $46.50^\circ$ . The geometric calibration was done previously by Airbus.

The Landsat imagery was retrieved from the USGS EROS website (<https://earthexplorer.usgs.gov/>). Earth Resources Observation and Science (EROS) Center manages the Landsat satellite program with NASA and provides a collection of satellite imagery around the world. Images used in this study were taken on 19 December and 3 December 2000 for developing the land cover maps of the Ci Kapundung and Ci Sangkuy watersheds respectively (Figure 4-5). The images were acquired by the Enhanced Thematic Mapper Plus (ETM+), the sensor of Landsat 7 satellite.

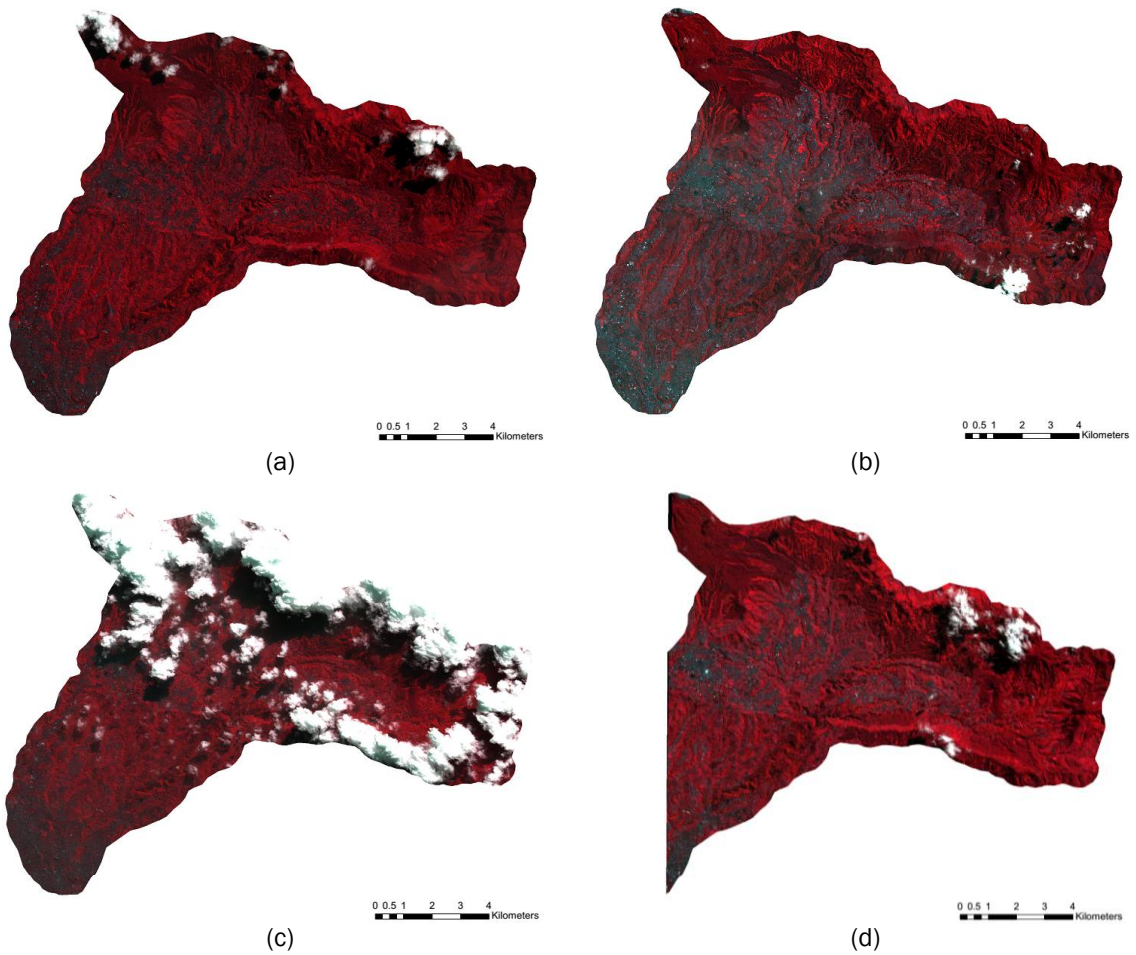
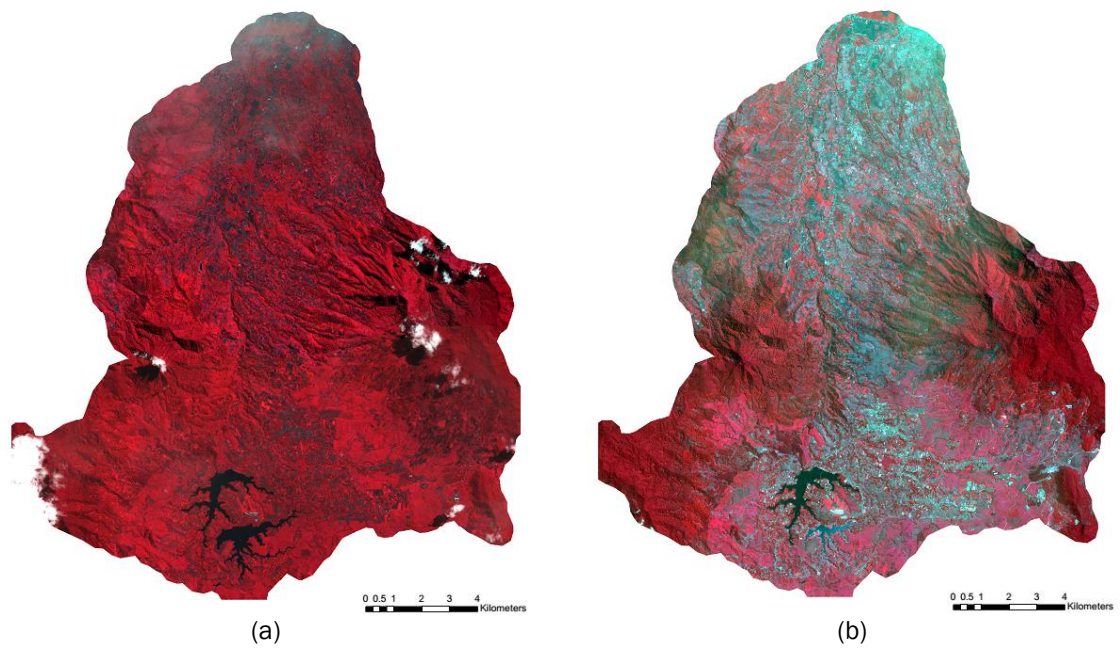


Figure 4-3 Infrared images developed from the raw satellite data of Ci Kapundung watershed; (a) the 2013 image; (b) the 2015 image; (c-d) the 2017 images (Analysis from SPOT 6 images © AIRBUS DS (2013, 2015, 2017))



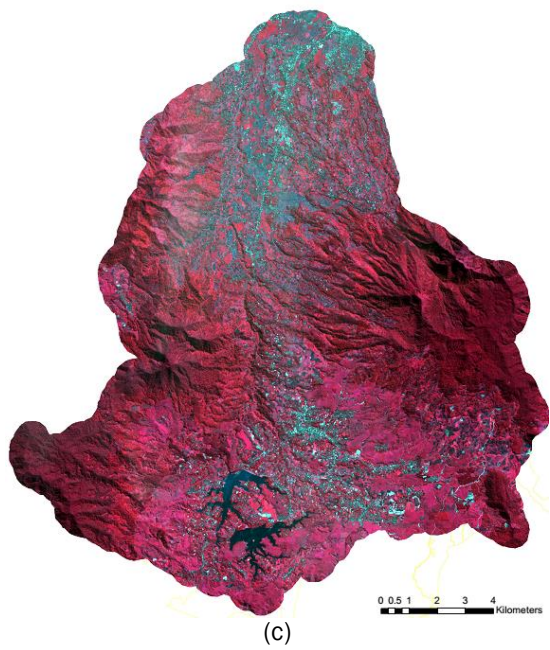


Figure 4-4 Infrared images developed from the raw satellite data of Ci Sangkuy watershed; (a) the 2013 image; (b) the 2015 image; (c) the 2017 image (Analysis from SPOT 6 images © AIRBUS DS (2013, 2015, 2017))

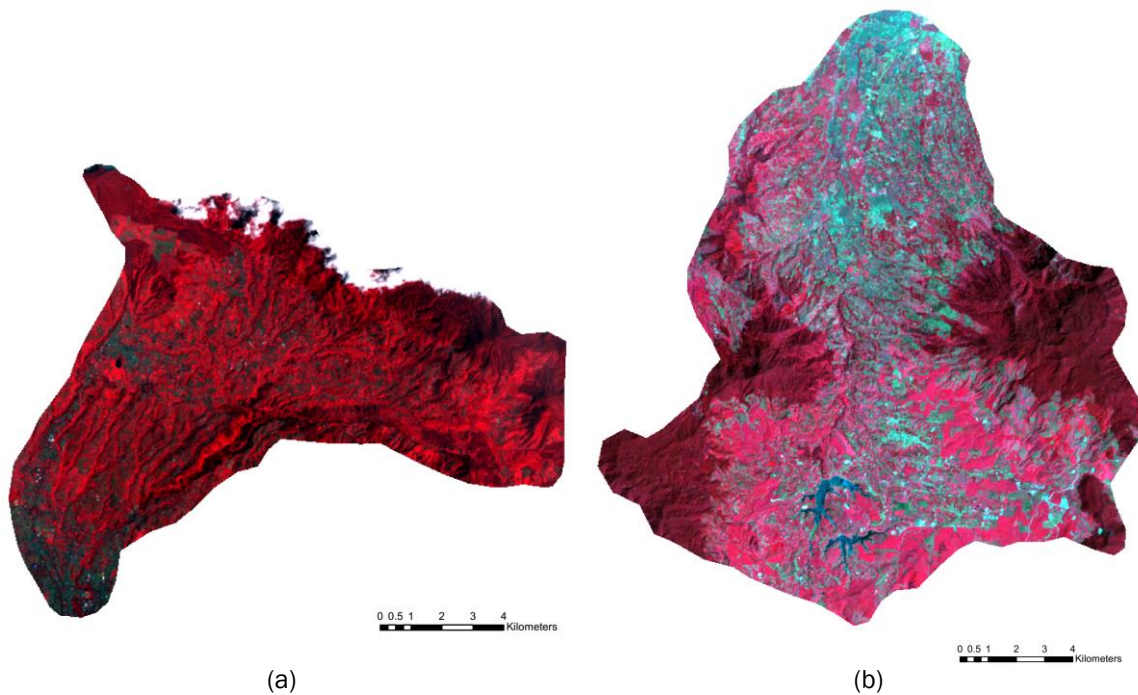


Figure 4-5 (a-b) The 2000 infrared images of Ci Kapundung and Ci Sangkuy watersheds (Source: USGS EROS)

Forest maps from Perhutani (a state-owned forest enterprise in Indonesia) and tea plantation maps from PTPN (an agriculture enterprise in Indonesia), were used during the identification of land cover types in the two sites. Data from OpenStreetMap is used to map the street networks. OpenStreetMap is an open-sourced medium for contributors to generate accurate street maps using areal imagery and GPS devices (Haklay & Weber 2008).



The digital elevation model (DEM) was retrieved from BIG (*Badan Informasi Geografi/ Indonesian Geospatial Agency*) with a spatial resolution of 0.27-arcsecond or 8.34 metre (<http://tides.big.go.id/DEMNAS/>). The DEM raster was resampled into a pixel size of 6 metres and 30 metres to match the resolution of SPOT and Landsat datasets respectively. Cubic convolution was used as the preferred resampling method for DEM because it can produce the smoothest output images among other three available techniques in ArcGIS (i.e. nearest, bilinear, and majority), while keep preserving DEM accuracy and terrain characteristics (USGS n.d.). The DEM data was required in the topographic correction process of satellite images, as well as in the catchment area delineation process.

#### 4.1.2 Field surveys

Field surveys were conducted on July-mid September 2016 and August-September 2017 to identify the land cover types and to record the physical properties of main trees in the case study areas. The methods, the list of recorded data and identified land cover types are described as follows.

##### (1) Methods

The identification of land cover types in the Ci Kapundung and Ci Sangkuy upper water catchment areas was conducted during the field surveys. Maps of the two case study areas from BIG (*Badan Informasi Geospasial/ Geospatial Information Agency*) with a scale of 1:25,000 were used for orientation during field surveys. The maps provide on-site information, such as contour lines, the location of road networks, buildings, water bodies, vegetated areas, and village boundary lines.

There were 203 points assigned in both upper water catchment areas during the field surveys, in which the locations of the points were recorded through transect walks. The method is selected because there is limited access, mainly in the forests and steep slope areas (Figure 4-6 ). Maps from Perhutani and PTPN were georeferenced and overlaid with Esri's base maps. Then, samples were assigned on each land cover type based on the slope condition and site accessibility. During the field surveys, the dominant tree species along the transect pathways were identified. Tree trunks' diameter at breast height (DBH) of the trees in the sample plots were also recorded.



Figure 4-6 (a) Limited access inside the Cikole forest in the Ci Kapundung upper water catchment area; (b) Small pathway on a steep slope in the Ci Sangkuy upper water catchment area (Source: Author's documentation)

## (2) List of recorded data

The datasets which were acquired during the field surveys, included:

- a. The coordinates of trees and sample points on different land cover types, which were recorded using GPS (Global Positioning System). The location of all samples was mapped using ArcGIS.
- b. The photos of trees and landscapes.
- c. Tree trunks' diameter at breast height (DBH).

## (3) Land cover classes

The land cover of the area was classified into seven broad classes based on the site surveys, and the forest and plantation maps. Pixels representing the land cover classes in the satellite images have a specific range of reflectance values. Therefore, each land cover type has a distinct colour in the infrared image. The seven land cover classes are:

- a. Developed areas, which are mainly located at a relatively flat landscape, comprise of settlements, industry area, streets, and other impervious areas (Figure 4-7a). These objects appear in pixels with light blue or white colour in the infrared image (Figure 4-7b).

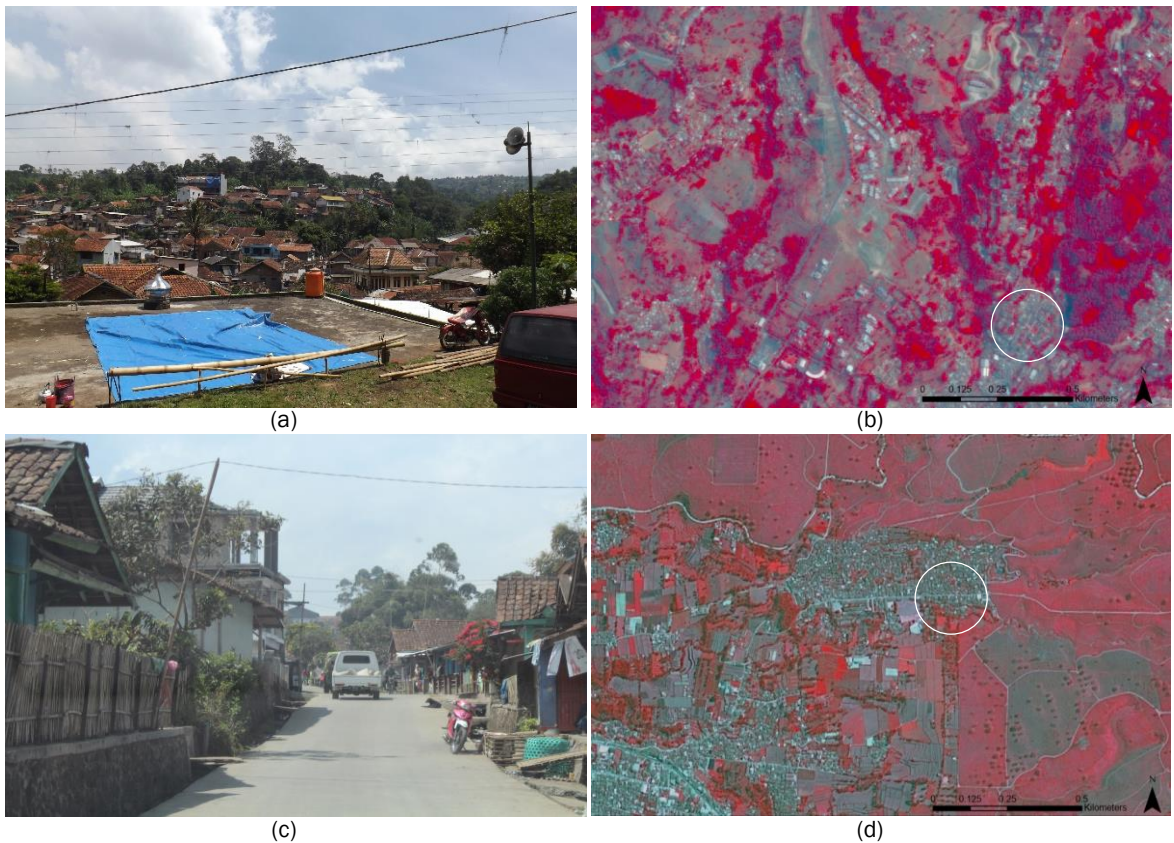


Figure 4-7 (a-b) Developed area in the Ci Kapundung upper water catchment area; (c-d) Developed areas in the Ci Sangkuy upper water catchment area (Source: Author's documentation and the pan-sharpened infrared images of SPOT 6 from © AIRBUS DS 2015)

- b. Bare land and cultivated land, which are located in rural areas in the two upper catchment areas, including the steep slopes. The second land cover type appears in two different colours in the infrared imagery (Figure 4-8a-d). Objects with a bright red colour represent grasses and agricultural plants in their full growth cycle, whereas the objects with grey colour are bare land.





Figure 4-8 (a-b) Cultivated land in the first case study area; (c-d) Bare land and cultivated land at the beginning of growth cycle in the second case study area (Source: Author's documentation and the pan-sharpened infrared images of SPOT 6 from © AIRBUS DS 2015)

- c. Tea plantations, which are located in the Ci Sangkuy upper water catchment area. The areas are shown as bright-pink objects in the infrared image of SPOT 6 (Figure 4-9a and b). A map from the PTPN was also used along with the results from the field surveys to identify the tea plantation in the case study area.

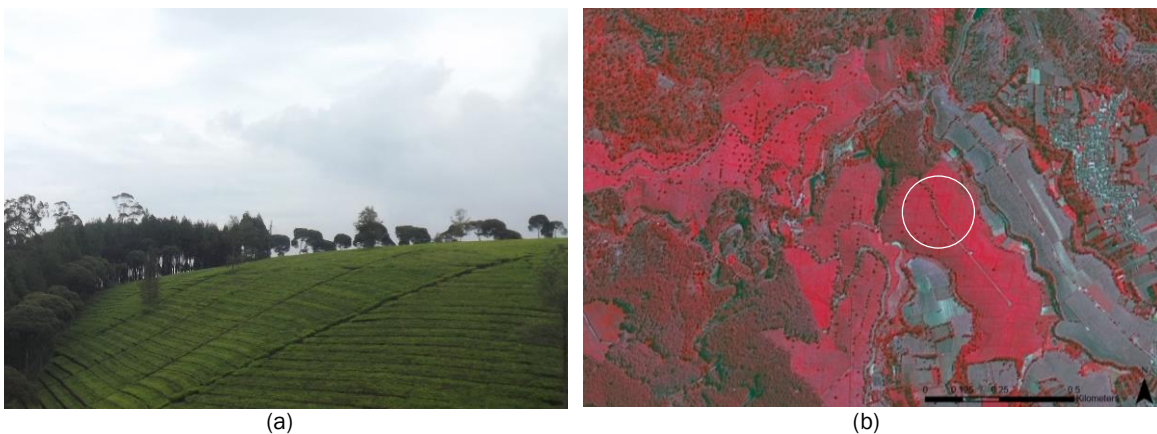


Figure 4-9 Tea plantations in the Ci Sangkuy upper water catchment area (Source: Author's documentation and a pan-sharpened infrared image of SPOT 6 from © AIRBUS DS 2015)

- d. Conifers, refer to the plants with needle-shapes leaves. According to the forest maps from Perhutani, conifers in the Ir. H. Djuanda protected area was planted in the 1960s, while conifers in Perhutani forests in the northern part of Ci Kapundung upper water catchment area were planted in 1962-2008. Conifers planted in the second case study area were mostly planted in 1995. Coffee plantations were often found under the canopy of conifer forest in the second case study area. Seedlings and ground cover as understory were identified in both sites.

In the infrared imagery, conifers show different shades of grey and red colours, depending on the age of plants (Figure 4-10). Figure 4-10a and b show the identification of conifers in the Ir. H. Djuanda protected area using the infrared image of the first case study area, in contrast with the Caliandra (i.e. the broad-leaved plants which are mostly found in the steep

slopes near the river in the protected area). Conifers appear as objects with dark grey colours, while *Caliandra* is represented in the image as objects with bright red colour.

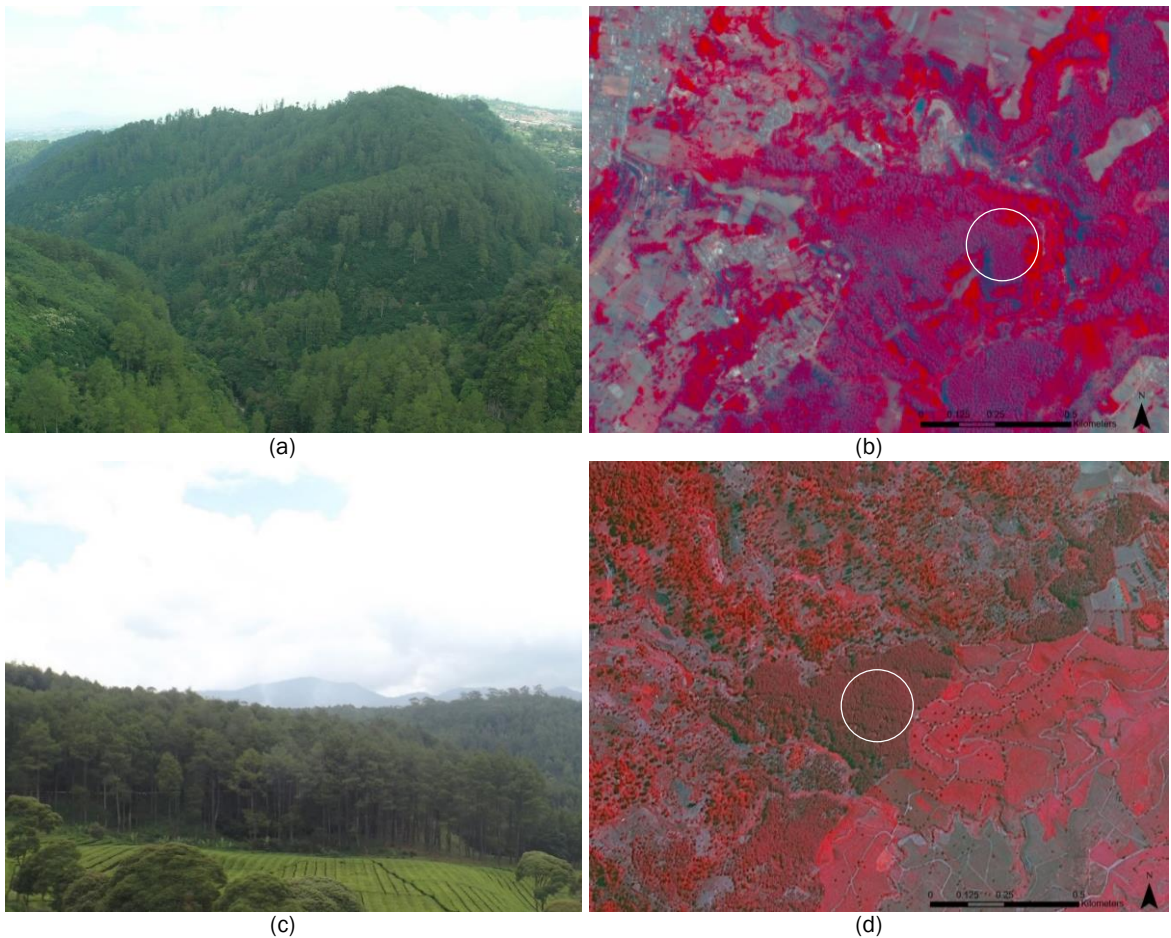


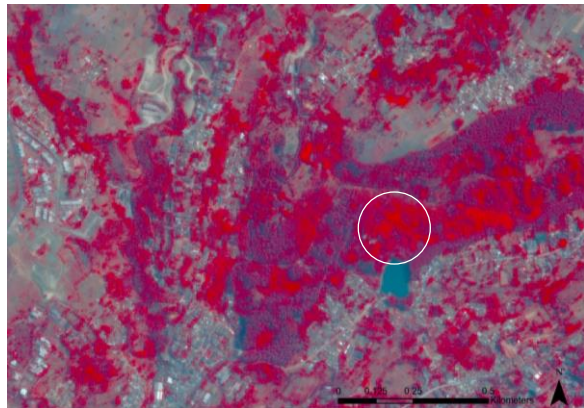
Figure 4-10 (a-b) Conifers in the Ir. H. Djuanda protected area in the Ci Kapundung upper water catchment area; (c-d) Conifers in the Ci Sangkuy upper water catchment area; (Source: Author's documentation and the pan-sharpened infrared images of SPOT 6 from © AIRBUS DS 2015)

On the other hand, conifers in the second case study area are shown as dark red pixels (Figure 4-10c and d). The pixels have different reflectance values compared with those representing the tea plantations and other land cover types (e.g. developed areas and bare land).

- e. Broad-leaved plants. The land cover type is mostly found in the arboretum of Ir. H. Djuanda protected area (e.g. *Khaya anthotheca*, *Pterigota hoesfieldii*, and *Meopsis eminii*), the Cikole research forest (e.g. *Agathis damara*), and along the streets and rivers (e.g. *Swietenia macrophylla* and *Bambusa sp.*) in the first case study area (Figure 4-11).



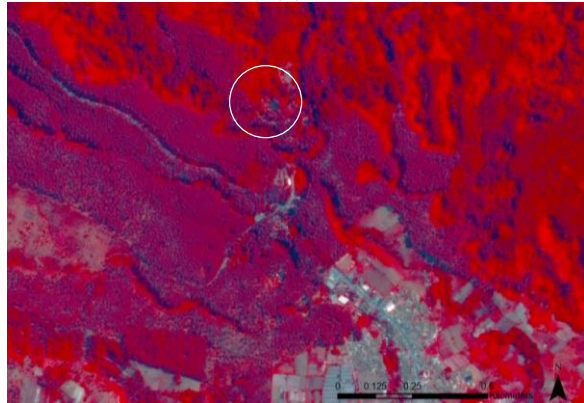
(a)



(b)



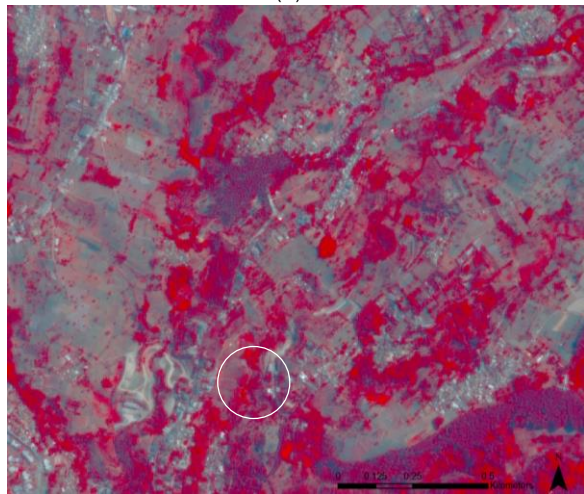
(c)



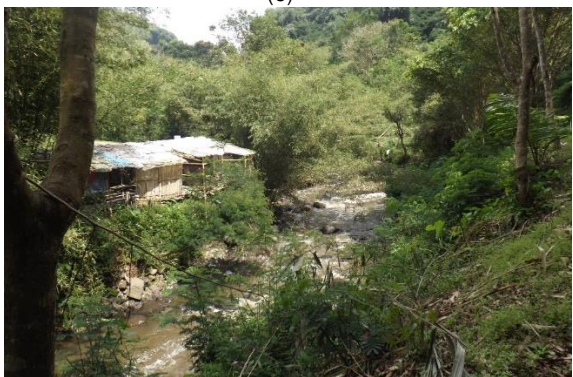
(d)



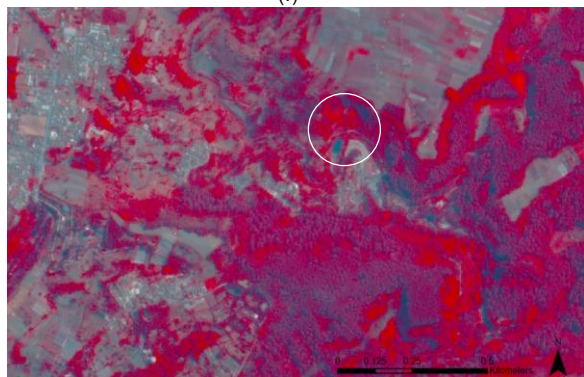
(e)



(f)



(g)



(h)

Figure 4-11 (a-b) Broad-leaved trees in the arboretum of Ir. H. Djuanda protected area ;(c-d) *Agathis damara* in the Cikole research forest; (e-f) Broad-leaved trees along the streets; (g-h) Broad-leaved plants in the riparian of the Ci Kapundung watershed (Source: Author's documentation and the pan-sharpened infrared images of SPOT 6 from © AIRBUS DS 2015)

In the second case study area, broad-leaved trees can be identified in the cultivated forests, along the streets, near the Ciluenca Lake and the tea plantations. Two-layer broad-leaved trees are common in the watershed consist of tall trees (e.g. *Melaleuca leucadendra* and *Agathis damara*) and plantations, such as coffee (Figure 4-12 a-b). *Melaleuca leucadendra* (cajeput tree or weeping paperbark) is also one of the dominant tree species, which is found along the streets and is scattered in the Ci Sangkuy watershed (Figure 4-12 c-f).



Figure 4-12 (a) Cultivated forests near the Mt. Tilu protected area in the second case study area; (b) *Melaleuca leucadendra* trees along the streets and are scattered in the second case study area; (c-f) Broad-leaved plant trees near the tea plantations (Source: Author's documentation and the pan-sharpened infrared images of SPOT 6 from © AIRBUS DS 2015)

g. Mixed vegetation, which consists of both conifers and broad-leaved trees in one specific area. Mixed trees are mainly found in the forests owned by Perhutani and natural forests, such as inside the Tilu Mt. protected area (Figure 4-13). Due to steep slopes and high difficulty to access the forests, the identification of mixed plants was conducted using the maps from Perhutani and the results from site surveys in the forest periphery.



Figure 4-13 Mixed woodland in the Mt. Tilu protected area (Source: Author's documentation and a pan-sharpened infrared image of SPOT 6 from © AIRBUS DS 2015)

h. Water bodies, which consist of ponds and natural lakes in the case study areas. One pond used as a recreational facility is located at the western part of Ci Kapundung watershed, and a small reservoir for a hydroelectric dam is situated inside the Ir. H. Djuanda protected area (Figure 4-14 a and b). The water bodies in the second case study area, on the other hand, consist of two lakes which are located in the southern part of the watershed. These lakes are used by PLN (the government owned-corporation dealing with the generation and distribution of electricity in Indonesia) and for recreational activities (Figure 4-14 c and d).







Figure 4-14 (a-b) A reservoir inside the Ir. H. Djuanda protected area in the first case study area; (c-d) Cileunca Lake in the second case study area (Source: Author's documentation and the pan-sharpened infrared images of SPOT 6 from © AIRBUS DS 2015)

In the areas covered with conifers and broad-leaved trees, only plants with the highest canopies can be identified from the satellite images. However, it should be noted that different land cover types may exist under the plant canopies. For examples, there are pathways made from bricks under the canopies of conifers and broad-leaved trees in the protected areas, and bare land under the dense canopies.

#### 4.1.3 Catchment delineation process

The delineation of case study areas, as well as the whole area of Bandung Basin was conducted using the Hydrology toolset in ArcGIS, based on a DEM with 6m resolution. At the beginning of the process, the Fills tool was used to correct the errors on DEM due to the image resolution or the rounding of elevations to integer values (ESRI, 2016). The tool can fill a sink or remove a peak on a DEM, based on the elevation of the surrounding surface. After the DEM had been corrected, a raster of flow direction was created according to the conditions of eight neighbouring cells. Then, using the output from flow direction analysis, the delineation of watersheds was created by finding pixels which belong to the similar watershed. Figure 4-15 a and b present a sample of works to define the flow of direction of each cell in the first case study area, and the watershed delineation process, respectively.

Streams in both case study areas were identified using the Flow Accumulation toolbox, based on the output from the flow direction analysis. The area of Ci Kapundung and Ci Sangkuy upper catchments, then, were defined based on the results from the watershed delineation procedure and the location of streams (Figure 4-16). The same procedures were taken to delineate the other catchments in Bandung Basin.

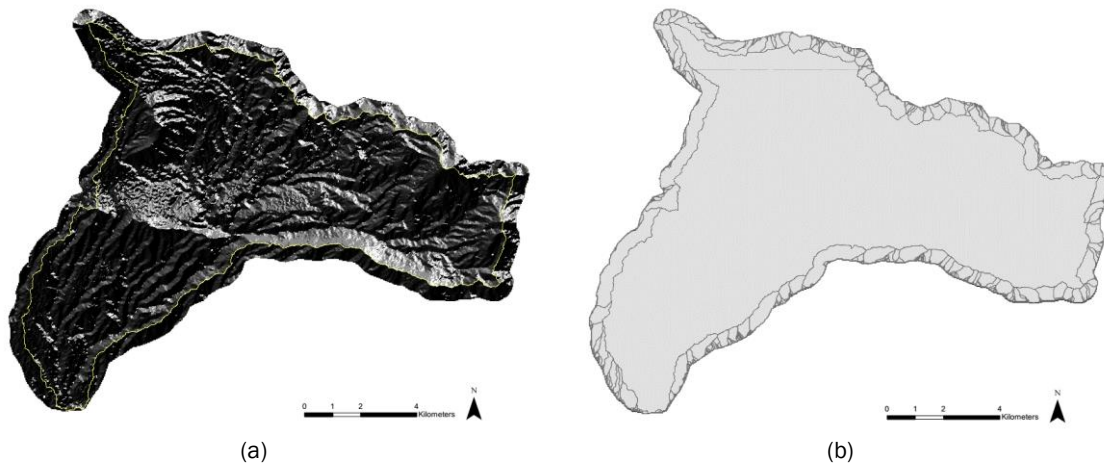


Figure 4-15 (a) An example of works defining flow direction in the first case study area; (b) the basin delineation process (Source: an analysis using the Hydrology toolset in ArcGIS)

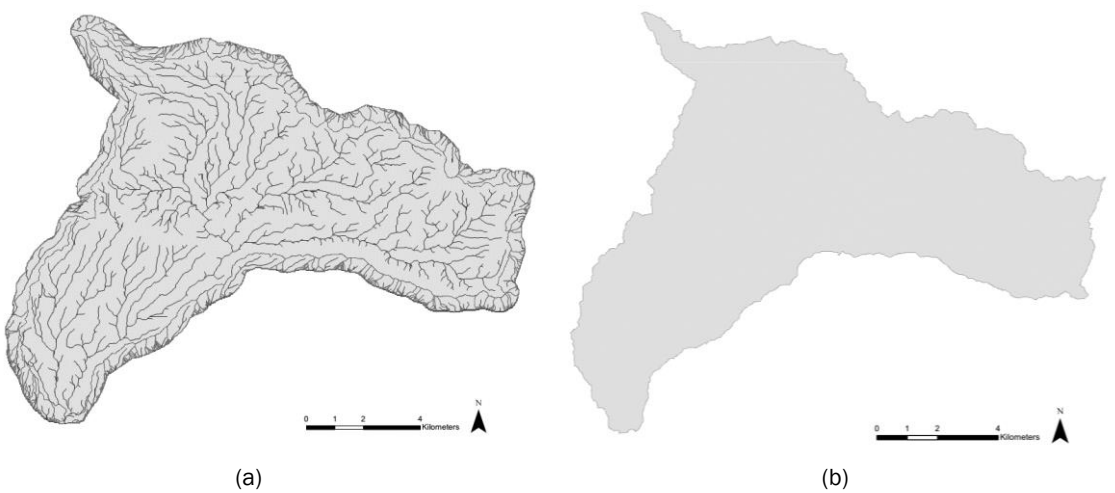


Figure 4-16 (a) An example of works defining streams in the first case study area; (b) the area of Ci Kapundung upper catchment (Source: an analysis using the Hydrology toolset in ArcGIS)

#### 4.1.4 Satellite image preprocessing

The SPOT and Landsat satellite images have a different coordinate system from the system used in this study. Therefore, the properties of all images were checked at the beginning of image preprocessing, and their spatial data were projected to WGS (World Geodetic System) 1984 UTM Zone 48S. Methods to conduct the radiometric correction, which consists of radiometric calibration, atmospheric correction, and topographic correction, are presented as follows.

##### (1) Radiometric calibration

During the radiometric calibration, the digital number ( $DN_{\lambda}$ ) for a specific band  $\lambda$  of the SPOT satellite images were calibrated to at-satellite radiance ( $L_{s,\lambda}$ ). The at-satellite radiance ( $L_{s,\lambda}$ ) is the value which is directly measured by sensor, and can be estimated using Equation 4-1. Information on gain and offset can be retrieved from the satellite metadata for each band. The

radiance values, then, were converted to at-surface reflectance ( $\rho_{T,\lambda}$ ), or the actual value of an object, using Equation 4-2 (Chander, Markham, & Helder, 2009).

$$L_{s,\lambda} = DN_{\lambda}/gain + offset \quad \text{Equation 4-1}$$

$$\rho_{T,\lambda} = \frac{\pi L_{s,\lambda} d^2}{ESUN_{\lambda} \cos \theta_s} \quad \text{Equation 4-2}$$

where

$\pi$  : constant value equal to 3.14159 [unitless]

$d$  : Earth-sun distance for the day of image acquisition [astronomical units]

$ESUN_{\lambda}$  : Solar irradiance at the top of the atmosphere [W/(m<sup>2</sup> μm)]

$\theta_s$  : the solar illumination (zenith) angle [radians which is converted from degrees]

The values of gain, offset, and solar irradiance for each band can be retrieved from the image metadata. The solar illumination (zenith) angle ( $\theta_s$ ), which is described as the angle between the Sun and the vertical line from an object, can be calculated using the information on sun elevation angle provided in the metadata ( $\theta_s = 90 - \text{sun elevation}$ ). The zenith angle is converted from degrees to radians using multiplication of  $\pi/180$  before it can be used to estimate the irradiance on an object (E).

The Earth-Sun distance (d) was estimated based on the date when the images were taken. Based on the tabulated data of d in astronomical units throughout the year in Chander et al. (2009), the Earth-Sun distance for the 2013 and 2015 images are 1.00430 and 1.01664 astronomical units respectively, whereas the distance for the 2017 images taken on day 203, 215, and 182 of Julian date calendar are 1.01601, 1.01471, and 1.01667 respectively.

The conversion of Digital Number (DN) to Radiance in the Landsat imagery was conducted following the method from USGS (<https://landsat.usgs.gov/>), using Equation 4-3.

$$L_{\lambda} = M_L \times Q_{cal} + A_L \quad \text{Equation 4-3}$$

where  $M_L$  and  $A_L$  are a multiplicative and an additive rescaling factors from Landsat metadata for a specific band L.  $Q_{cal}$  is the Digital Number (DN). The Landsat images with radiance value, then, were used in the atmospheric correction process.

## (2) Atmospheric correction

In this study, atmospheric correction (AC) was conducted in the last iteration of the map development process because multi-resolution satellite images were used in the procedure (Lu & Weng, 2007). AC was applied using the *i.atcorr* module in GRASS GIS (Geographical Resources Analysis Support System) 7.4.2, through QGIS 3.4.3, and GRASS 7.0.5 in QGIS 2.18.2. The module performs atmospheric correction using the 6S (Second Simulation of the

Satellite Signal in the Solar Spectrum) algorithm. In this study, 6S is used as the selected atmospheric correction method because the model is widely used among other radiative transfer models (Chambell & Wynne 2011 p. 311).

The required input data for conducting the 6S atmospheric correction include four elements. The elements are the geometrical condition (i.e. the name of satellite, coordinates of the case study area, date and hour when the imagery was taken), the atmospheric model (e.g. tropical, mid-latitude summer, midlatitude winter, etc), the aerosol model (e.g. continental model, maritime model, urban model, etc), the aerosol concentration model, the target and sensor altitude, and the sensor band. The output from *i.atcorr* is a raster map with reflectance values, which were rescaled to a range of 0-1. This raster map, then, was used as one of the input datasets for the topographic correction process.

### (3) Topographic correction

A modified sun-canopy-sensor (SCS+C) as a topographic correction procedure (Soenen, Peddle, & Coburn, 2005) was applied to the SPOT and Landsat satellite images of Ci Kapundung and Ci Sangkuy upper water catchment areas, to improve the image classification accuracy. Pixels representing clouds and cloud shadows were excluded in the topographic correction process. Spatial models were generated in ArcGIS based on the SCS+S equation from Soenen et al. (2005) to develop the corrected images. SCS+C was performed using imagery with reflectance values after the atmospheric correction had been applied before (Equation 4-4). The correction procedure requires the value of the cosine of the incidence angle ( $i$ ), which is estimated using Equation 4-5 (Teillet et al. 1982).

$$\rho_{H,\lambda} = \rho_{T,\lambda} \frac{\cos \theta_t \cos \theta_s + C_\lambda}{\cos i + C_\lambda} \quad \text{Equation 4-4}$$

with

$$\cos i = \cos \theta_s \cos \theta_t + \sin \theta_s \sin \theta_t \cos(\phi_s - \phi_t)$$

Equation 4-5

where

$\rho_{H,\lambda}$  : at-surface reflectance (the actual object's reflectance value)

$i$  : Solar incident angle

$\theta_t$  : Slope angle

$\theta_s$  : Solar zenith angle ( $90^\circ$  - sun elevation angle)

$\phi_s$  : Solar azimuth angle

$\phi_t$  : Aspect angle

$C_\lambda$  : Empirical parameters

Solar zenith and azimuth angle for Landsat 7 and SPOT 6 images was retrieved from the image metadata. The values of solar zenith should be converted from degrees into radians (Zenith\_rad). The azimuth angle was changed into a mathematical unit (Azimuth\_math) before it was converted into radians (Azimuth\_rad).

A slope image depicts the rate of change of one cell to its neighbours, while an aspect image shows the slope direction (Burrough & McDonell 1998). Slope and aspect images of the two case study areas were derived from DEM as the input dataset for conducting the topographic corrections. Slope and aspect images derived from DEM with the 30-m resolution are presented in Figure 4-17 and Figure 4-18. Colours in the slope and aspect images represent different slope degrees and the direction of downslopes respectively.

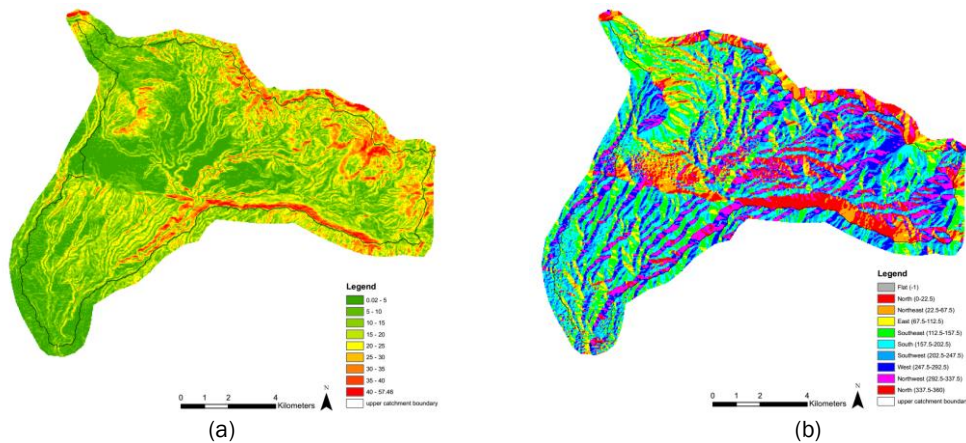


Figure 4-17 (a-b) Slope and aspect images from DEM with a 30-m resolution of the first case study area (Source: Analysis using ArcGIS)

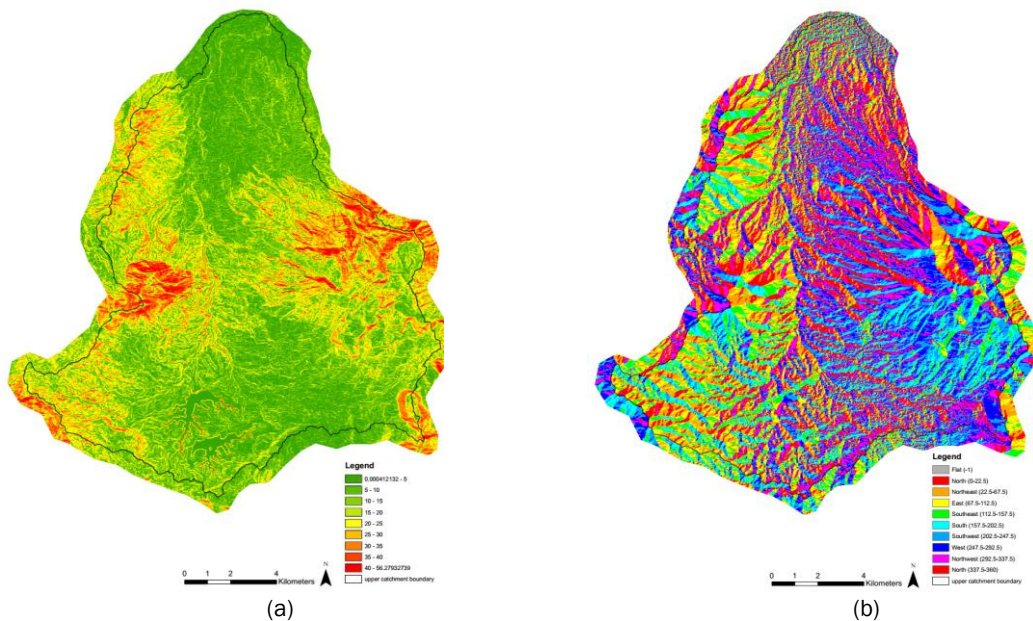


Figure 4-18 (a-b) Slope and aspect images from DEM with a 30-m resolution of the second case study area (Source: Analysis using ArcGIS)

$C_\lambda$  is an empirical parameter of  $c=a/b$ , where  $c$  is a function of the regression slope ( $b$ ) and intercept ( $a$ ).  $C_\lambda$  was assessed by calculating the slope and coefficient of the linear regression between  $\cos i$  and reflectance value ( $\rho_{T,\lambda}$ ) of each band. In this study, the SPSS statistic software was used to compute the linear regression. 6,500 and 13,000 random sample points were assigned on each band in both types of satellite imagery of the first and the second case study areas respectively with different terrain and illumination condition, to derive  $\cos i$  values. Due to the constant cloud coverages in the watersheds, the locations of sample points were different for each set of satellite images. No sample point was assigned on areas where clouds and cloud shadows are located in the images.

Following the formula to develop the linear regression (Reflectance =  $m \cos i + b$ ), the slope and intercept values for each band in all Landsat and SPOT imagery of the first and second case study areas were defined based on the regression analysis of  $\cos i$  and reflectance of Blue, Green, Red, and NIR bands for each scene. Figure 4-19 and Figure 4-20 show the samples of linear regression to retrieve the slope ( $b$ ) and intercept ( $m$ ) values from the 2015 Landsat imagery, and the slope and aspect maps.

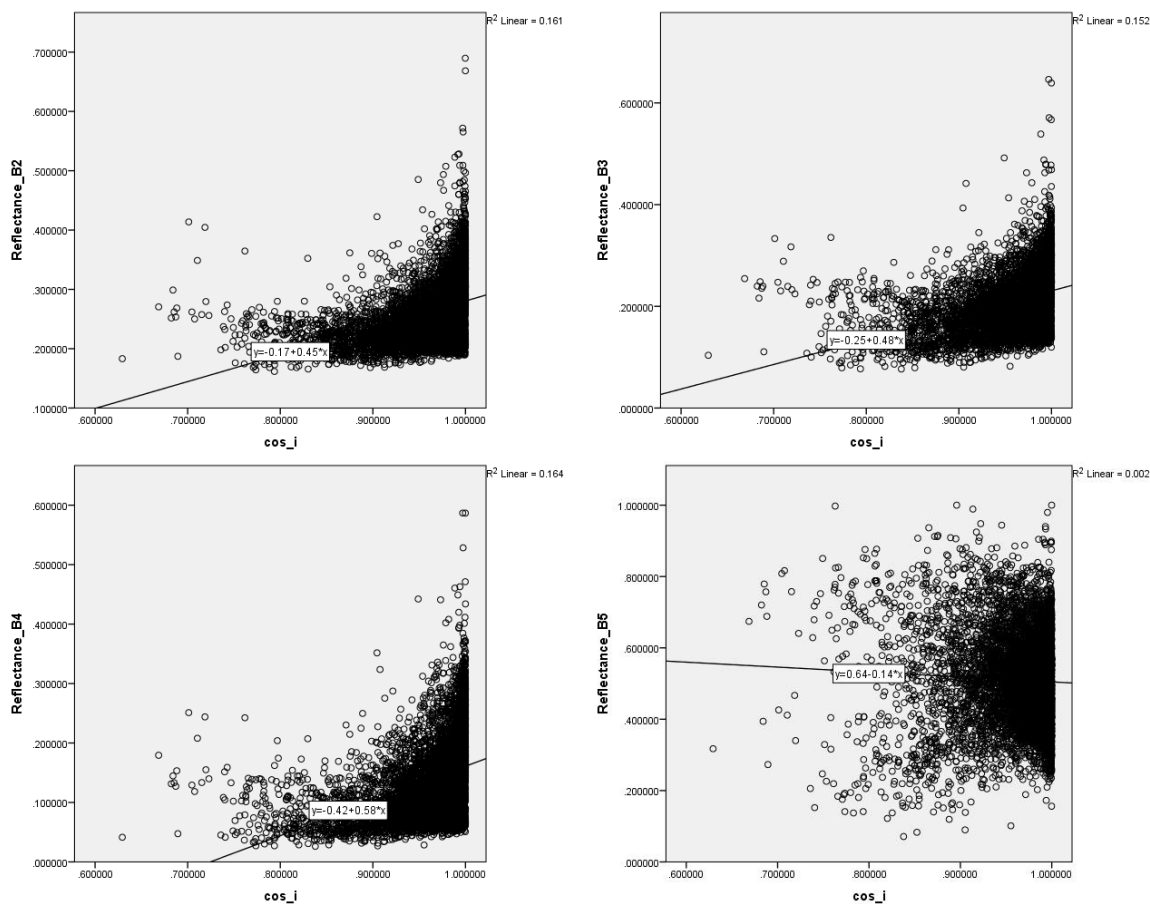


Figure 4-19 Samples of the linear regression of  $\cos i$  and reflectance for Band 2 (Blue), Band 3 (Green), Band 4 (Red), and Band 4 (NIR) of Landsat images of the first case study area retrieved on 28 June 2015 (Source: Analysis from SPSS)

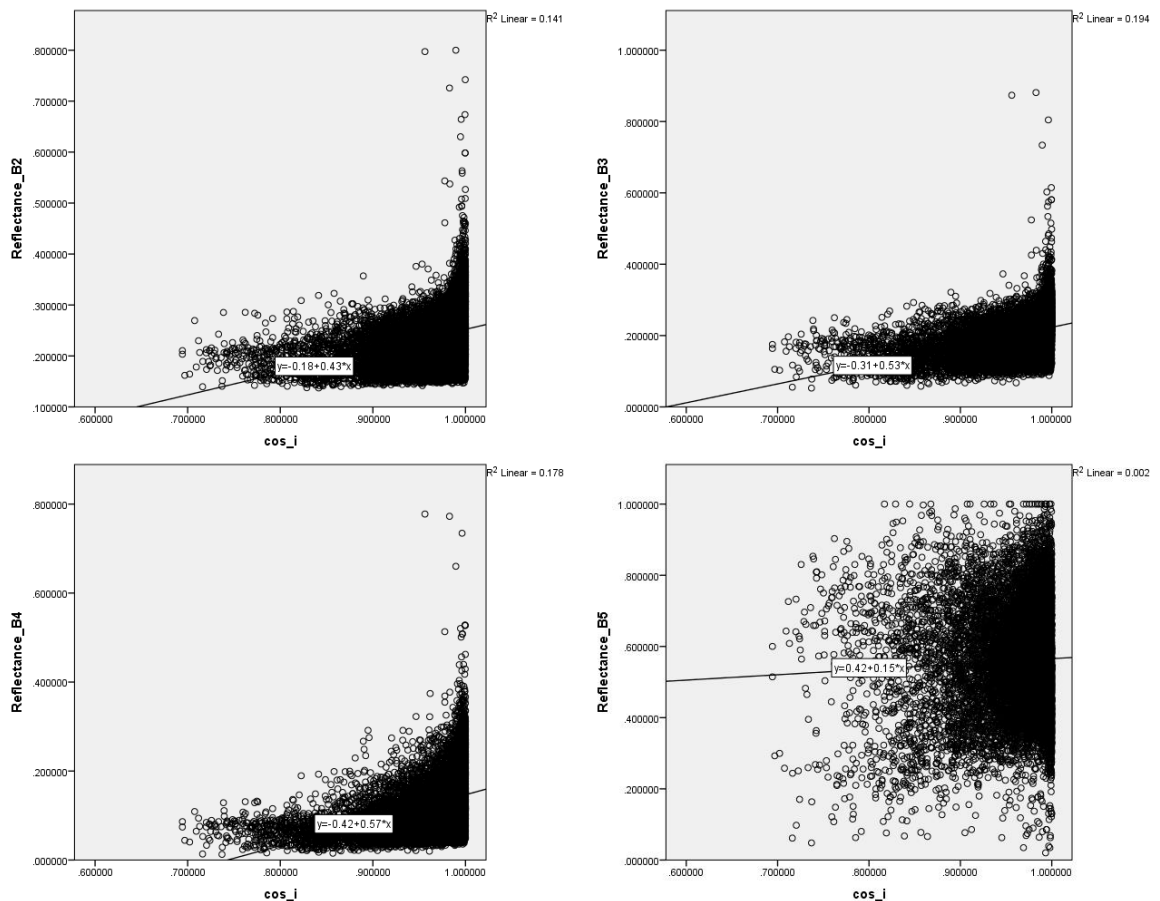


Figure 4-20 Samples of the linear regression of  $\cos_i$  and reflectance for Band 2 (Blue), Band 3 (Green), Band 4 (Red), and Band 4 (NIR) of Landsat images of the second case study area retrieved on 12 June 2015 (Source: Analysis from SPSS)

After the C coefficients had been estimated ( $C=b/m$ ), the C values were used to perform the SCS+C topographic correction. ModelBuilder in ArcGIS was used to develop the corrected image based on Equation 4-4 and Equation 4-5. Raster calculator was incorporated in the model to calculate the  $\cos_i$  and to compute the topographic correction.

#### 4.1.5 Masking process in SPOT and Landsat imagery

In this study, masking was conducted to identify pixels which should be excluded in the image classification process, to classify water bodies, and to differentiate the land cover of small objects with the adjacent land cover. Cloud coverages in the imagery cause the reflectance values of land cover types could not be retrieved by satellite sensors (Lu 2007 cited in Liu et al. 2011). Whereas reflectance values of pixels covered with cloud shadows are altered. Thus they could not be included in the image classification process.

The diagram of the masking process is shown in Figure 4-21. Cloud, cloud shadow and water masking processes were conducted using two different methods for SPOT and Landsat imagery (Masking A). However, the process for each scene can be done simultaneously (i.e. every masking process can generate masks for clouds, cloud shadows, and water bodies). Pixels located inside the water masks were automatically classified as water bodies. The area of the

water body is changing depending on seasons. There is usually less water in the lakes during the dry season. Thus there would be more open areas surrounding the water. Therefore, it is assumed that the area of water bodies would not change during the land change simulation period.

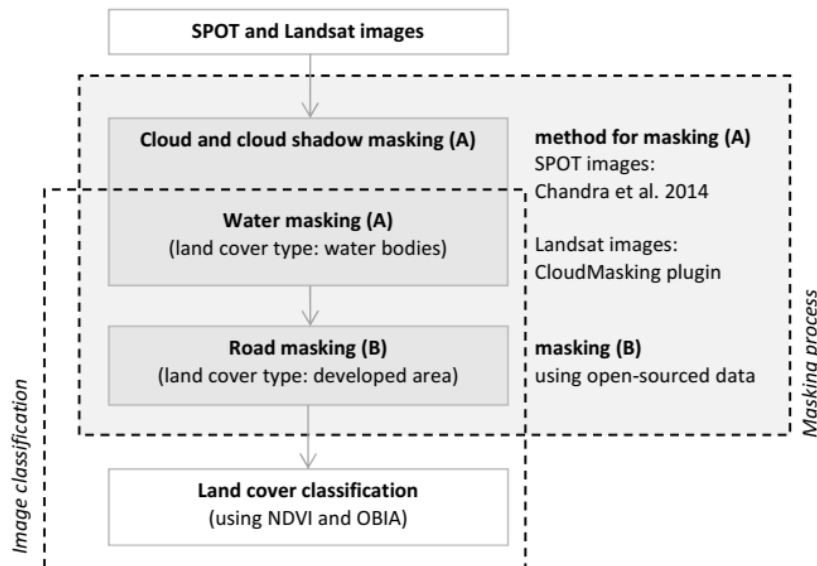


Figure 4-21 Masking and the image classification process for an individual map

During the road masking process (Masking B), pixels showing the road networks in the raster images were defined using the information from OpenStreetMap. The road width is determined based on the policies from the Ministry of Public Works, Indonesia, for each road class. The width for the arterial, collector and local roads are 11 metres, 9 metres, and 6.5 metres respectively. The detailed descriptions of cloud, cloud shadow, and water masking procedures in SPOT and Landsat imagery are presented as follows.

(1) Cloud, cloud shadow, and water masking process in SPOT imagery

During the image acquisition, not all parts of the case study areas are free from clouds and cloud shadows. According to the SPOT image metadata, the percentages of cloud coverage for the first case study area<sup>19</sup> are 7.13% and 1.12% in 2013 and 2015 respectively (Figure 28a and 28b), and 64.45% and 3.17% in 2017 for the images of the whole watershed and eastern part of the watershed respectively (Figure 28c and 28d). Approximately 5.51% of the total second case study area is covered with clouds in the 2013 image, whereas the 2015 and 2017 images are free from clouds during the image acquisition.

Cloud, cloud shadow and water body masking processes for the SPOT images were conducted in the imagery with reflectance value, following the masking method from Candra et al. (2014),

<sup>19</sup> The SPOT 6 satellite images provided by Airbus also include the surrounding areas of the Ci Kapundung and Ci Sangkuy upper catchments, approximately 30% of the total area of the watersheds. The cloud coverage was estimated by Airbus based on the delineation of case study areas and their surroundings. Therefore, the percentages of cloud coverage presented here may not represent actual coverage in the two watersheds, as the clouds may cover parts of the surrounding watersheds.



as shown in Figure 4-22. In the process, specific thresholds for the near-infrared (NIR) and blue bands were used to identify the cloud objects. Shadows and water bodies were also identified using the same method based on the reflectance values of NIR and green bands.

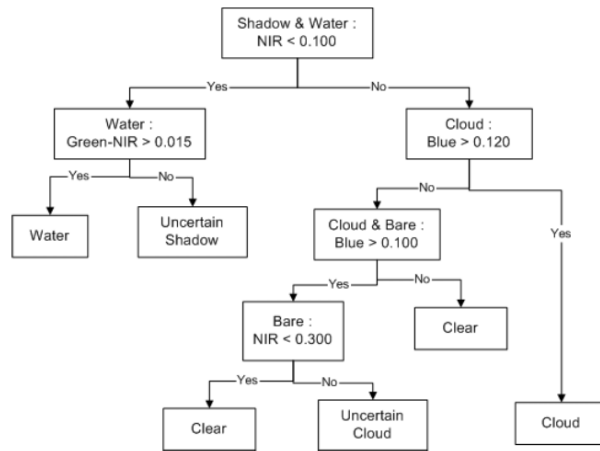


Figure 4-22 Cloud, cloud shadow and water masking process (Source: Candra et al. 2014)

The reflectance approach often produces results with salt-and-pepper effects. In this case, the filter minority method was applied to mitigate the problem. Small-size pixels, which were automatically defined as clouds and shadows, are erased and reassigned as the same class as the pixels surrounding them. Small objects categorised as clouds and cloud shadows were reclassified as the same land cover types as the surrounding pixels. An example of results from the cloud and cloud shadow masking for the Ci Kapundung upper water catchment area using the 2015 SPOT imagery is shown in Figure 4-23. The output for water masking for the Ci Sangkuy upper water catchment area using the 2015 SPOT imagery is illustrated in Figure 4-24.

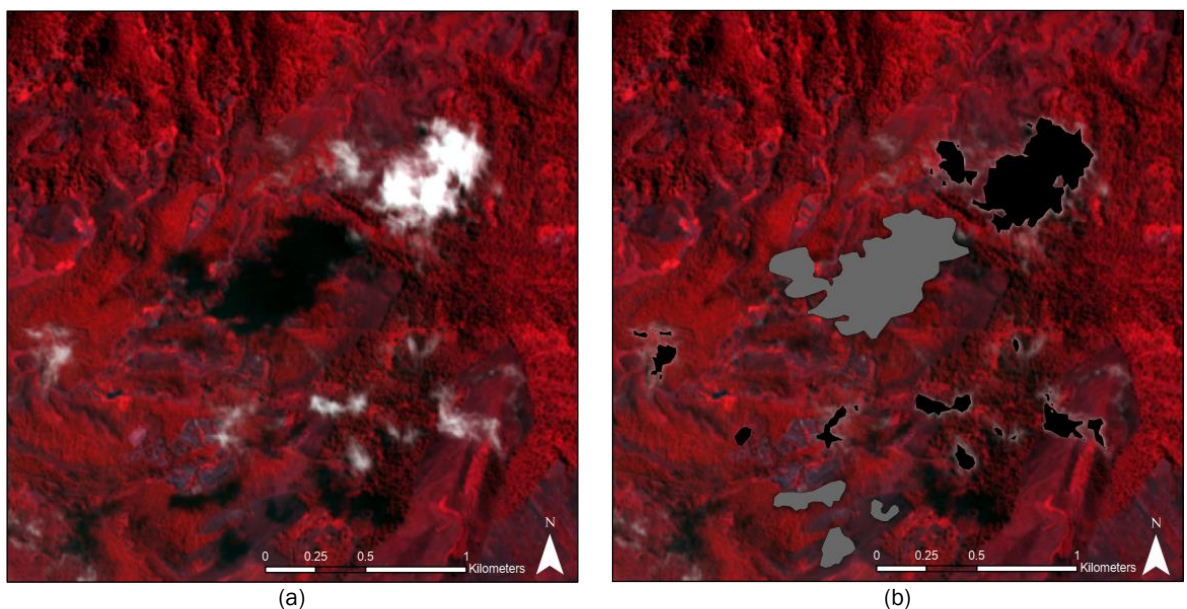


Figure 4-23 (a) The SPOT infrared imagery of the first case study area (20 September 2015); (b) Samples of cloud and cloud shadow masks indicated by the black and grey polygons respectively (Source: © AIRBUS DS 2015 and image masking analysis)

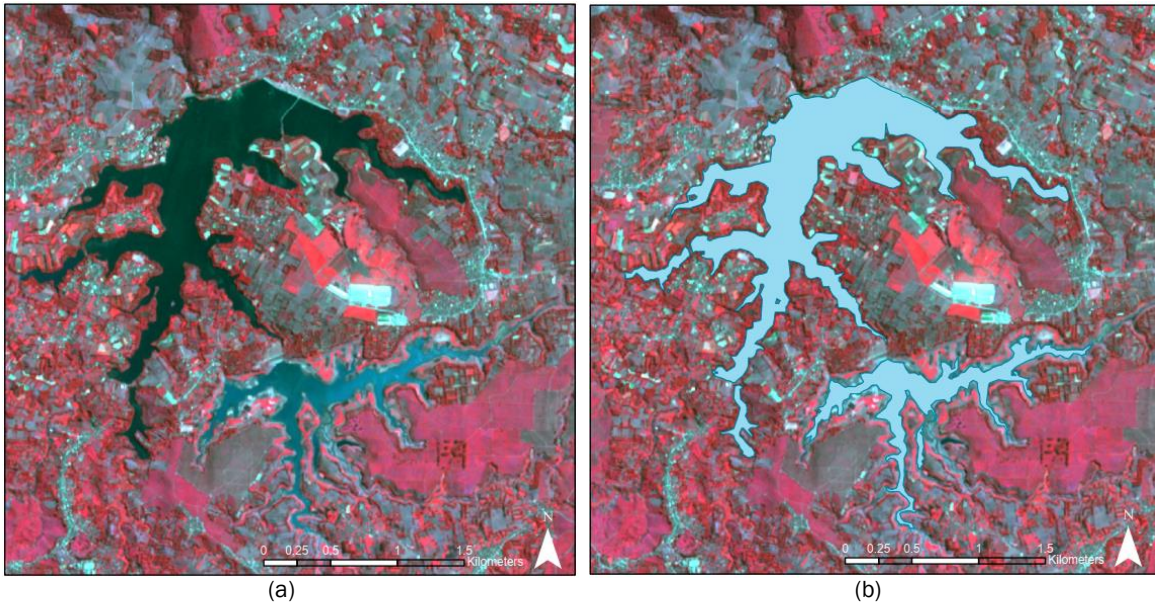


Figure 4-24 (a) The infrared imagery of the second case study area (20 September 2015); (b) Samples of water mask indicated by the blue polygons (Source: © AIRBUS DS and image masking 2015)

## (2) Cloud, cloud shadow, and water masking process in Landsat imagery

The masking of clouds, shadows, and water bodies in the Landsat images was performed using CloudMasking, a QGIS plugin for detecting and masking clouds, cloud shadow, cirrus, aerosols, ice/snow and water.

In this study, Fmask was used as the filter method to identify clouds, cloud shadows, and water bodies in the Landsat 7 and 8 images. This method was chosen because it had an average accuracy of 96.4% when it was tested in a globally distributed set of reference data in tropical countries (Zhu & Woodcoc 2011). Input datasets for this procedure are the Landsat Top of Atmosphere (TOA) reflectance and brightness temperature. The required datasets for masking include the Landsat metadata files and the parameters for the filters, such as cloud and shadow buffers, cloud probability threshold, and cirrus probability ratio.

According to the Landsat metadata, the percentages of cloud coverage for the scene taken on 3 December 2000 is 27%. Clouds and cloud shadows in the imagery of Ci Kapundung watershed are located in the northern part of the site (Figure 4-25a). On the other hand, the imagery of the second site taken on 19 December 2000 is almost cloud-free. Figure 4-25b shows the output from the cloud and cloud shadow masking process for the first case study area. A new TIFF raster showing clouds, cloud shadows, and water bodies with a value of 2 (black colour), 3 (grey colour), and 5 (white colour) respectively was generated in the process. Other pixels in the raster (i.e. where there is no cloud, cloud shadow, and water present in the imagery) were classified with the value of 255.

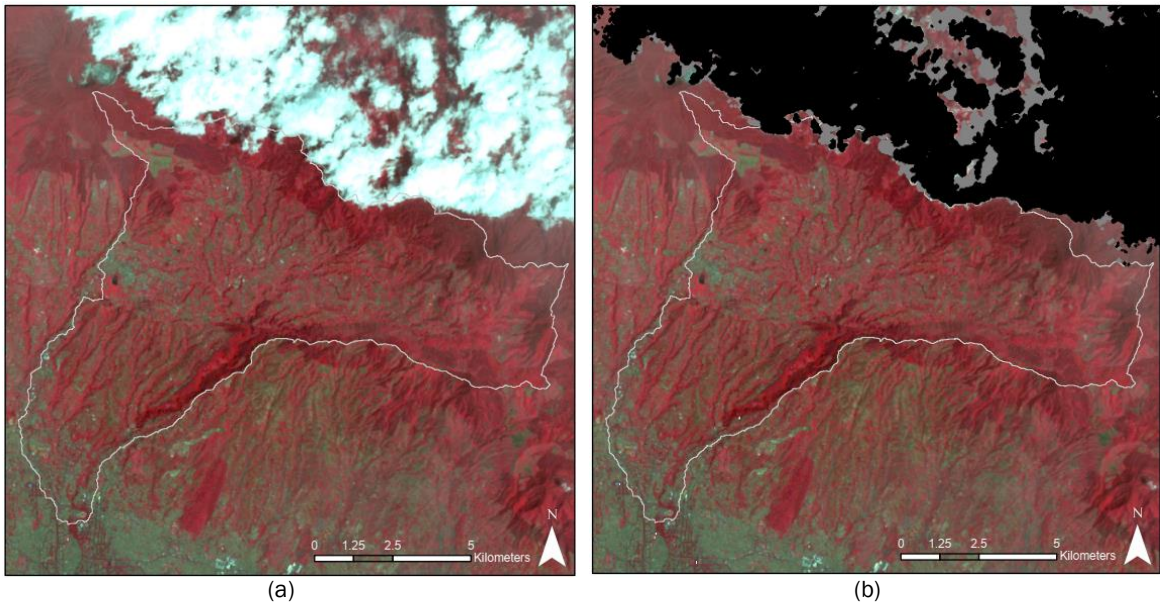


Figure 4-25 (a) The Landsat infrared imagery of the first case study area (19 December 2000); (b) Cloud and cloud shadow masking indicated by black and grey polygons respectively (Source: Landsat imagery from USGS 2000 and image masking analysis)

### (3) The fluctuating water level in the Ci Sangkuy upper water catchment area

The fluctuating water level in lakes in the second case study area can be seen in the Landsat imagery on 3 December 2000, and the SPOT images on 20 September 2015 and 1 July 2017. Figure 4-26 illustrates the delineation of lakes in 2015 which is overlaid on the 2000 and 2017 images. In this study, it is assumed that there were no significant changes in the area of water bodies in both case study areas within the simulation period (2000-2015), although in reality, the water levels would vary depending on the seasons. The 2000 and 2015 images were taken when the water receded. Thus the areas identified as water bodies were smaller and the bare land surrounding the lakes were more prominent than those in the 2017 imagery. Water bodies were excluded in the land change simulations; there is no change from and into water bodies simulated in the CA-Markov modelling.

The final delineation of water bodies in 2000 and 2015 was generated using water masks in the 2015 images. An exception was made when developing the 2017 map from SPOT imagery. Water bodies in this map were delineated based on the actual condition in 2017 since this map was only used in the validation process of land change modelling, and not in the simulations<sup>20</sup>.

<sup>20</sup> This study use the integrated Cellular Automata and Markov model which works based the information on the previous states of pixels to project the future land change. Therefore, it would not be relevant if the water bodies are included in the land change simulations, because the area of the lakes is changed depending on the seasons (the change is non-stationary, thus it cannot be simulated using the CA-Markov model).

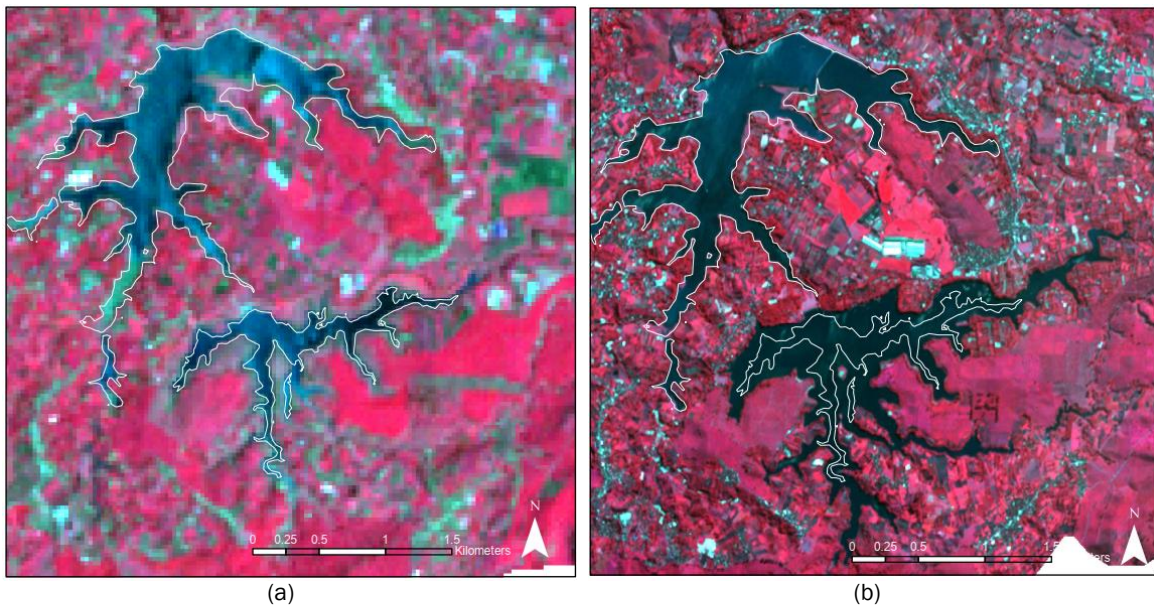


Figure 4-26 (a-b) The 2000 and 2017 infrared imagery of the second case study areas overlaid by the delineation of water bodies in 2015 (Source of background images: Landsat imagery from USGS (2000) and SPOT imagery from AIRBUS DS (2017))

#### 4.1.6 Image classification and accuracy assessment

The first iteration of the map development process was conducted using the uncorrected images and corrected images<sup>21</sup> of the first case study area, and the southern part of the second case study area using the object-based image classification in ArcGIS (Rani et al., 2017). The classifications were only performed using SPOT imagery retrieved in 2015 without applying the updating and backdating method. Radiometric calibration and SCS+C topographic correction were applied on all bands of infrared images. No atmospheric correction was applied in the satellite imagery.

The results showed that the classification accuracy could be improved by applying the topographic correction without atmospheric correction was conducted before (the interpretation of this initial assessment are presented in Chapter 6). Based on the results from the accuracy assessment of the land cover maps, the second iteration of the land cover development process was conducted using different software to ascertain if there is an improvement of the accuracy.

The subsequent object-based classifications were conducted in SAGA (System for Automated Geoscientific Analyses) using segmented satellite images (iteration 2 in Figure 4-1). Segmented images were developed from the SPOT infrared images (i.e. composite imagery using green, red and NIR bands), in which the preprocessing and the masking procedures had been conducted before. Samples were assigned for all land cover types in each segmented imagery.

<sup>21</sup> The uncorrected and corrected images in this context refer to the raw image and the image after topographic correction had been applied to respectively.

The second iteration of the classification process was done only using the SPOT images of Ci Kapundung upper water catchment area, which were retrieved in 2013, 2015, and 2017. Small road lines could not be distinguished from the surrounding land cover types in the segmentation process, for example, bare land and broad-leaved trees, due to the short width of the road and the spatial resolution of SPOT 6 imagery (i.e. 6 metres). Therefore, the street networks had been masked out before the classification process for SPOT 6 imagery was conducted (Figure 4-27).

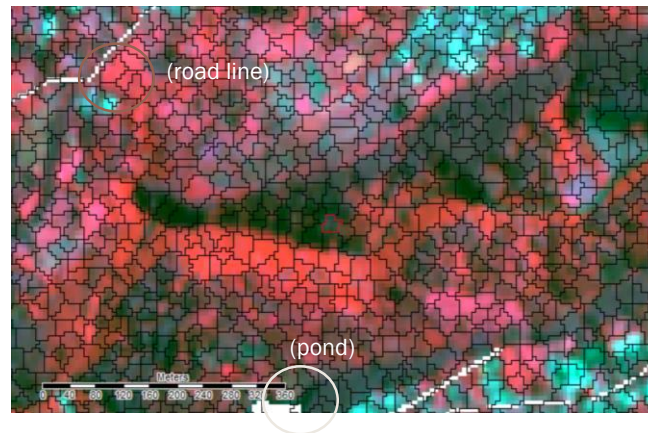


Figure 4-27 Sample of segments developed in the infrared imagery of the first case study area (Analysis using satellite images from © AIRBUS DS (2015) and road networks data from © OpenStreetMap)

Training samples were assigned to each land cover type. Maximum likelihood was chosen as the classifier in the classification process because of its robustness compared to the other classifiers (Lu & Weng, 2007). In the absence of information on the land cover beneath the clouds and land cover covered with shadows, the land cover data from previous years and the maps from Perhutani were used to define the land cover in the areas with no pixel/data.

The results from the second iteration of classification were used as the input data for the initial analysis of land change (LCM 1). The 2013, 2015, and 2017 images were developed individually, affecting the results from the first iteration of land change simulations. The outputs from the classification and land change simulation are presented in Chapter 5 and are discussed in Chapter 6. Based on the results, the third iteration of the image classification process was conducted using Landsat and SPOT imagery of the two case study areas.

In the third iteration, the updating and backdating method (Linke et al. 2008) was used to achieve better classification and land change modelling accuracies than those in the previous iterations (Figure 4-28). The backdating and updating method required a series of assumptions along the process, which were addressed in this study. The first assumption is that the 2015 maps developed from SPOT images can be used as base maps, because they have the complete information on land cover, compared with the 2013 and 2017 satellite images. The second assumption was adopted from Toure et al. (2018) who assessed the method to increase land cover maps from multi-temporal satellite imagery, assuming that the unbuilt areas in later years were also not built in the previous years.

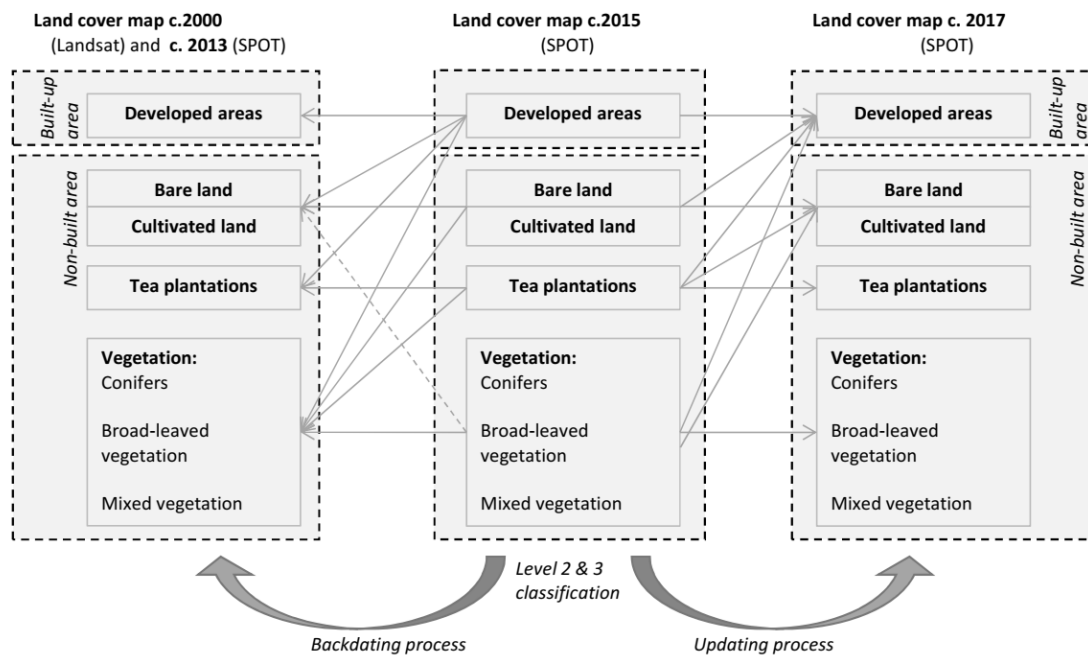


Figure 4-28 The updating and backdating process in this study

SPOT satellite images taken in 2013 and 2015 were used to develop the 2015 land cover maps after atmospheric and topographic corrections had been conducted. Unbuilt areas in 2015 were identified as unbuilt in 2013. If there are areas covered with clouds and shadow clouds<sup>22</sup> in the 2015 imagery, then, the missing information regarding the land cover will be retrieved from the 2013 satellite images. It was assumed that unbuilt areas and vegetation would remain the same from 2013 through 2015. Therefore, the development of 2013 land cover maps was focused on the classification of unbuilt areas.

Based on the classification results from previous iterations and visual validation using high resolution of ESRI's base maps, there are no buildings and impervious land in the areas where the clouds and cloud shadows in the 2015 imagery are located. Therefore, to increase the computation speed, pixels identified as built-up areas in 2015 are excluded in the object-based classification (OBIA) process. It should be noted that these pixels are both developed and undeveloped areas in 2013. Not all buildings identified in 2015 were already built in 2013. Thus there is still a possibility that these pixels can be classified as undeveloped/ unbuilt in 2013. However, since they are located outside the cloud and cloud shadow masks in the 2015 imagery, then, it is assumed that the results of OBIA which were used to develop the 2015 maps would not be affected.

No information on the land cover can be retrieved in the areas with constant cloud and cloud shadow coverages in 2013, 2015, and 2017 in the SPOT images. Therefore, the forest map from Perhutani was used to identify the forest cover in c.2015.

<sup>22</sup> Areas covered with clouds and cloud shadows are mainly located in the forests and are resulted the developed maps to have voids or no data.

Landsat images (2000) of the two case study areas were taken regularly by the ETM (Enhanced Thematic Mapper) satellite. However, most of the images have cloud coverages, which limit the options to choose the suitable imagery for the classification process. The information of land cover in circa 2015 (c.2015) retrieved from SPOT imagery was used to develop the 2000 maps using the backdating method (Figure 4-28). Firstly, the unbuilt area in c.2015 was assigned as unbuilt in 2000. The remaining unbuilt area in 2000 was defined from NDVI analysis on the Landsat imagery. The analysis was conducted to separate the non-vegetation class (e.g. developed areas and bare land), and vegetation classes. Secondly, OBIA was performed to identify two land cover types in the first case study area (e.g. bare land and cultivated land, and vegetation), and three land cover types in the second case study area (e.g. bare land and cultivated land, tea plantations, and vegetation). At this stage, the three types of trees cannot be differentiated. Therefore, the information regarding the trees was retrieved from 2015 land cover maps. No street map in 2000 can be retrieved from the OpenStreetMap. Thus no existing street network could be shown in the developed maps.

The accuracy of land cover maps was calculated using the point-based accuracy assessment, with the consideration that there is another method of assessment which could be used and is more appropriate for assessing the accuracy of land cover maps developed using OBIA (i.e. area-based assessment) (Lei Ma et al. 2017). In this study, the accuracy assessment was conducted using the 'Compute Confusion Matrix' option of the Segmentation and Classification toolbox in ArcGIS. Five hundred accuracy assessment points were assigned in each map, and the 'stratified random' option was selected as the sampling scheme. In this scheme, the assessment points are distributed randomly within a class, and the number of points is proportional to its relative area (ESRI 2016).

Confusion matrices were constructed to assess the image accuracy. Historical maps in Google Earth and maps from Perhutani and PTPN were used to calculate the accuracy in the c.2000 maps. Whereas land cover identification during field surveys, maps from Perhutani and PTPN, as well as the high resolution of ESRI's base maps, which were visually interpreted, were used to estimate the c.2015 and c.2017 image accuracies. The latter method was chosen because visitation to a large number of sites in the case study areas is not feasible due to the steep slopes and no accessibility in most parts of the areas.

The data considered as ground truth is submitted and compared with the land cover data from the classified maps. The confusion matrix, then, was computed in each map to derive a kappa index<sup>23</sup> of agreement between the classified land cover types and the ground truth.

---

<sup>23</sup> Kappa statistic is often used to assess the percentage of predicted land cover types compared with the ground truth data (Visser and de Nijs 2006 *cited in* Fu et al. 2018)

## 4.2 Scenario development and land change modelling (research phase 2)

The future composition and distribution of land cover in each case study area were simulated under different scenarios. The process was conducted in three iterations (Figure 4-29). After the land cover maps of the first case study area had been developed in the second iteration of the map development process, the output was used in the initial land change simulation (LCM1). Based on the results from LCM 1, the second iteration of land change modelling was conducted using maps from Landsat and SPOT imagery (LCM 2). The output from hydrologic modelling (MIKE SHE 2) provided feedback for the last iteration of land change modelling (LCM 3).

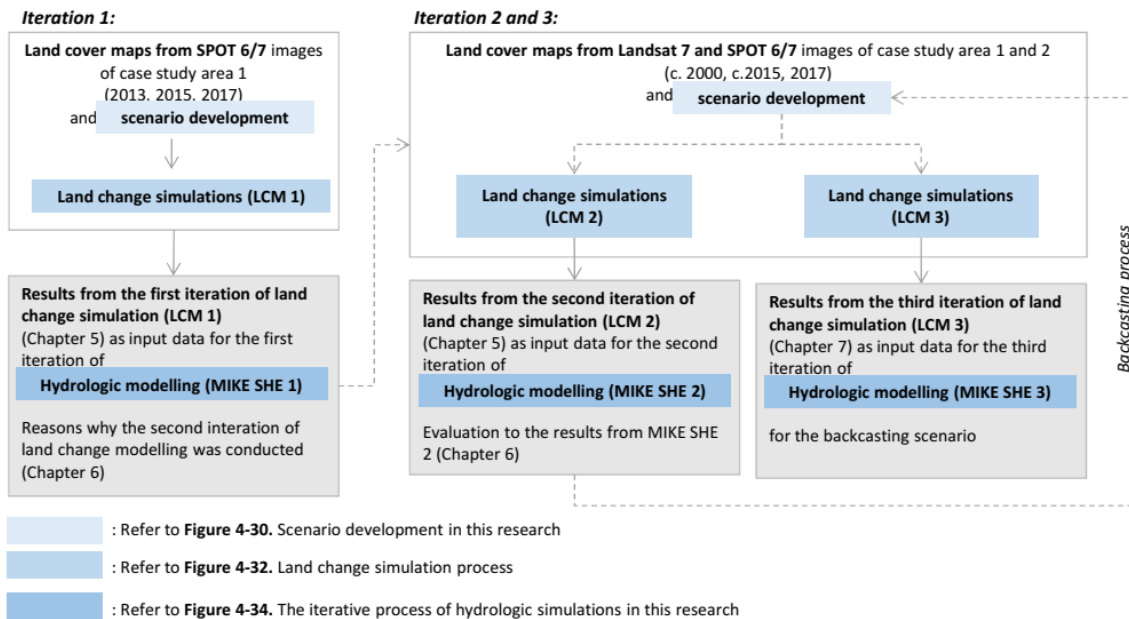


Figure 4-29 The iterative process of land change simulations in this study

### 4.2.1 Data collection for the land change simulations

The datasets for the land change simulation were collected from government offices in Indonesia, and from the spatial analyses using GIS. The following list is the datasets required for the land change simulations:

- (1) The existing land cover maps developed from SPOT 6 and Landsat imagery.
- (2) Elevation and slope maps created from the DEM using ArcGIS.
- (3) Landslide hazard maps for Bandung City, Bandung Regency, and West Bandung Regency collected from the Ministry of Energy and Mineral Resources, Indonesia.
- (4) The spatial data of river networks in each water catchment area developed from DEM using the hydrology toolbox of ArcGIS.
- (5) The existing development policies and the spatial plan for Bandung City, Bandung Regency, and West Bandung Regency as an input dataset to make possible scenarios for future development in the two sites. The policies consist of guidelines (e.g. land



slope, accessibility and location to the area prone to hazard) for each land-use development.

- (6) Spatial data (e.g. coordinates of enclave and park boundaries) and the existing management policies for Ir. H. Djuanda and Tilu Mt. protected areas retrieved from each management office.
- (7) The forest and tea plantation maps from Perhutani and PTPN, respectively.
- (8) Road network from OpenStreetMap.
- (9) Population density map in 2015 from WorldPop (2018).

#### 4.2.2 Scenario development

The development of scenarios in this study is related to the second research question: “what are the most effective scenarios of landscape structure for the two upper water catchment areas which can benefit flood regulation in Bandung Basin?” and the third research question: “which types of vegetation can improve flood regulation in each upper water catchment area?”. The potential optimum solutions were assessed using the initial Pareto-frontier analysis to answer the two research questions. First, the desired vision for the future development of case study areas was defined. Then, scenarios were developed, and the future land cover for each scenario was simulated using Land Change Model (LCM).

##### (1) Scenarios for the land change model

Three scenarios were developed in the first iteration of land change modelling (LCM 1) to project the future land cover maps in 2030. The three scenarios are the Status Quo scenario, existing policy-based scenario, and the ecological design-based scenario (Figure 4-30). The capacity of each scenario to reduce surface runoff in the watersheds was simulated in the hydrologic modelling. Based on the outcomes from hydrologic modelling, a backcasting scenario was developed from the third scenario. In this study, the year of 2015 is selected as the benchmark for the land change and hydrologic simulations, whereas 2030 is chosen as the end of simulation period following the end of existing spatial policies, which were implemented in one of the scenarios (i.e. the existing policy-based scenario).

The type of Status Quo scenario is predictive (forecast), which is created based on the development trend in the area. There are spatial policies which have not been implemented yet in the area. Thus the current trend does not comply with the existing spatial policies. Future demand for the new settlements and agriculture in 2030 was estimated based on the current development trend in each municipality. The information regarding the development trends was retrieved from BPS (*Badan Pusat Statistik*/ The Indonesian Central Bureau of Statistics). In the first scenario, there is no specific allocation for all land cover types and no restriction to develop riparian and lake buffer.

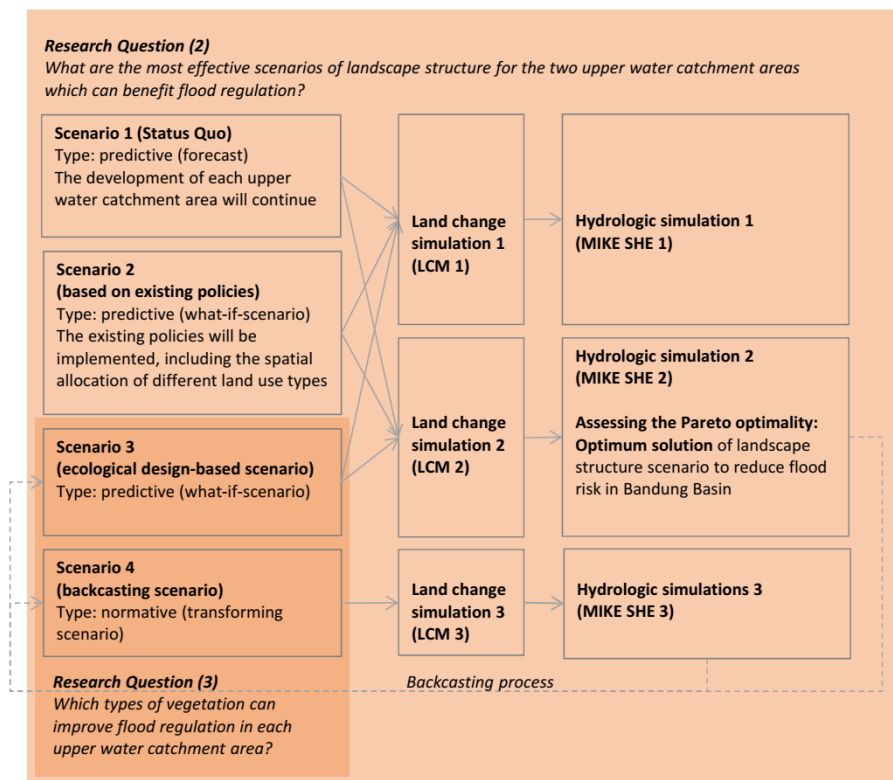


Figure 4-30 Scenario development in this research

The second scenario is a predictive (what-if scenario) scenario, which was developed based on the current spatial planning policies in the respective municipalities. In this scenario, spatial constraints will be developed based on existing spatial policies. The development of a scenario for the Ci Kapundung watershed incorporates the spatial plans for Bandung City (2015-2035), Bandung Regency (2007-2027), and West Bandung Regency (2009-2029), while the scenario for the Ci Sangkuy watershed includes the existing spatial plans for Bandung Regency (2007-2027). In this research, the newly published Bandung Basin spatial planning policy was not used in the development of the second scenario because it comprises a plan for a large-scale region. Therefore, there is no detailed spatial plan for each case study area.

The existing spatial policies include the land-use zoning and the guidelines for developing new settlements and agriculture based on the slope condition, distance from main roads, rivers and lakes, as well as the development restriction of particular areas, such as protected areas, disaster-prone areas, and forests. The policies for both watersheds are summarised in Table 4-1.

Table 4-1 The existing spatial plans for Bandung City, Bandung regency, and West Bandung Regency (Sources: the existing spatial planning of Bandung city (2011-2031), Bandung Regency (2007-2027), and West Bandung Regency (2009-2029))

Policies	Municipalities		
	Bandung City	Bandung Regency	West Bandung Regency
<b>New housing</b>	Built in the areas with a slope less than 15%, more vertical housing, should not be built in the areas dedicated as cultural heritage sites and conservation areas. Regulation for specific Building Coverage Ratio (BCR), Floor Area Ratio (FAR) and green area ratio.	Built in the areas with a slope less than 15%, is not located at the disaster-prone area and area with high permeability soil and good accessibility. Non-landed houses near the district centre, and low-density housing in rural areas	Regulation for settlements in the northern part of Bandung city (e.g. low-density buildings, specific engineering methods with can conserve the hydrological processes, specific Building Coverage Ratio (BCR))
<b>Agricultural areas</b>	Land intensification	Development criteria based on different types of agricultural practices (e.g. irrigated farming, dryland farming, perennial plantation)	Areas with different range of slope are allocated for specific types of agricultural practices
<b>Conservation areas</b>	Include the recharge areas (e.g. slope less than 15%, soil with percolation more than 1m/day), areas which protect specific landscape features (e.g. river buffers, open spaces along the railways, areas surrounding springs), green open space, cultural heritage sites, and disaster-prone areas. Prohibited for land-use in which the activities occurred would disrupt the conservation, are allowed for infrastructure development with maximum BCR of 2%	Include the areas which provide protection to other areas and specific landscape features (e.g. forests conservations, areas with slope of 40% or more, permeable areas, river buffers, areas surrounding lakes and springs), protected areas, disaster-prone areas (e.g. areas with soil movement, 200 metres from an active fault, volcanic eruption zone) and the cultural heritage sites	Include the forest conservation areas, areas which protect other areas and specific landscape features (e.g. river buffers, areas surrounding lakes and springs), protected areas, disaster-prone areas, and areas with specific geological features
<b>River and lake buffer</b>	Designated width of lake and river buffer	Designated width of lake and river buffer	Designated width of lake and river buffer

The third scenario was developed using the ecological design principles, including the protection to riparian, forests, and protected areas. The river and lake buffer was proposed to protect the

river ecosystem and reduce runoff flowing into the river. No further development in areas with high-permeability soils to maximize the capacity of catchment to absorb runoff. All criteria for the three scenarios were used to develop constraint maps required by the land change model. The maps show the restricted areas for new development in the two upper water catchment areas in the future.

The fourth scenario is the backcasting scenario, which was generated to address the Pareto optimality (i.e. reducing flood risk in Bandung Basin). Evaluation pathways were conducted as part of the backcasting modelling. If the results from flood risk simulation could not meet the desired vision of the area, new constraint maps for the two case study areas would be proposed. This would generate new simulated maps with different land cover distributions. Then, the hydrology simulation would be conducted again.

(2) Allocated areas for future development in the case study areas

The allocated areas for new settlements and agriculture in each case study area in 2030 were estimated based on the projection of population growth rates in West Java Province (Table 4-2). The estimation assumes that the rates can represent the population growth in the three municipalities. Based on the projection of population growth rates, the number of population in 2030 in each municipality was predicted.

Table 4-2 West Java Province population growth projection (2010-2035) (Source: BPS)

Year	Population growth rates
2010-2015	1.56
2015-2020	1.34
2020-2025	1.12
2025-2030	0.90
2030-2035	0.69

Most areas in the Ci Kapundung watershed are located at three different districts (i.e. the Cidadap in Bandung City, Cimenyan district in Bandung Regency, and the Lembang district in West Bandung Regency), whereas Ci Sangkuy watershed is situated at two districts in the Bandung Regency (i.e. the Pangalengan and Cimaung districts). According to BPS (*Badan Pusat Statistik/ the Indonesian Central Agency of Statistics*), the number of population in the Bandung City, Bandung Regency, and West Bandung Regency in 2015 is 2,481,469, 3,534,111, and 1,636,316 respectively. The proportion of the population in the districts inside the watersheds compared to other districts in a municipality was calculated to represent the projected population in each watershed (Table 4-3).

Table 4-3 Population in the four districts in the watersheds (2015 and 2017) (Source: BPS)

Watersheds	Districts	Population in the districts (2015)	Population in the districts (2017)
Ci Kapundung	Cidadap (BC)	58,426	58,700
Ci Kapundung	Sukasari (BC)	82,012	82,600
Ci Kapundung	Coblong (BC)	132,002	133,100
Ci Kapundung	Cimencyan (BR)	115,475	119,360
Ci Kapundung	Cilengkrang (BR)	52,359	54,076
Ci Kapundung	Lembang (WBR)	187,815	196,690
Ci Sangkuy	Pangalengan (BR)	148,353	152,735
Ci Sangkuy	Banjaran (BR)	124,233	128,691
Ci Sangkuy	Kertasari (BR)	69,793	71,755
Ci Sangkuy	Pacet (BR)	109,084	112,197
Ci Sangkuy	Pasir Jambu (BR)	85,294	87,932

Notes: BC (Bandung City), BR (Bandung Regency), WBR (West Bandung Regency)

After the future population in each municipality had been estimated, the projected population in the seven districts (i.e. Cidadap, Sukasari, Coblong, Cimencyan, Cilengkrang, Lembang, Pangalengan, and Cimaung) in 2030 was calculated. This estimation was used to validate the outputs from land change modelling.

#### 4.2.3 Land change simulations

##### (1) Land Change Modeler (LCM) module of Terrset

In this study, the land change simulation was conducted using Land Change Modeler (LCM) from Terrset. LCM is one of the modules in the software, which was developed by Clark University in Worcester MA, USA. LCM applies a combined cellular automata and Markov model (CA-Markov), and a multilayer perceptron (MLP) neural network to run the simulation. Cellular Automata (CA) simulate the future land change based on the previous state of each cell as well as the phase of its adjacent neighbours, following a particular rule. A standard form of Cellular Automata is presented as (Equation 4-6):

$$S^{t+1} = f(S^t, N) \quad \text{Equation 4-6}$$

where S is possible states of the Cellular Automata model at the time t, N is the values of neighbouring cells, f is a transition function that determines the changes from time t to t+1 (Li & Yeh, 2000). Markov analysis calculates the transition probabilities of each land cover type (Table 4-4). P<sub>ij</sub> (i rows and j columns) denotes the probability of one land cover type (S) to change into another (Clark, 1965).

Table 4-4 Transition probability matrix (Source: Clark, 1965)

$$P = \begin{matrix} & \begin{matrix} S_1 & S_2 & S_3 & \dots & S_n \end{matrix} \\ \begin{matrix} S_1 \\ S_2 \\ S_3 \\ \vdots \\ S_n \end{matrix} & \left[ \begin{array}{ccccc} p^{11} & p^{12} & p^{13} & \dots & p^{1n} \\ p^{21} & p^{22} & p^{23} & \dots & p^{2n} \\ p^{31} & p^{32} & p^{33} & \dots & p^{3n} \\ \vdots & \vdots & \vdots & \vdots & \vdots \\ p^{n1} & p^{n2} & p^{n3} & \dots & p^{nn} \end{array} \right] \end{matrix}$$

The CA-Markov model in LCM generates probability maps used to simulate future land-use/land cover (Adhikari & Southworth, 2012; Eastman, 2006). LCM module from Terrset is selected in this research because the model construction is easier than other CA-Markov models, such as the CA\_Markov in Terrset, CLUE, and DINAMICA (Mas et al., 2014).

The MLP neural network is able to simulate the non-linear relationships between different variables which influence the transition, such as the land cover change related to the proximity to urban centre or roads. Furthermore, it can also model several or all transitions at once by making a group of transitions with the same explanatory variable (Eastman, 2016). Pixels assigned as water bodies were excluded in the land change simulation process with an assumption that the pixels will not change into different land cover throughout the simulation period.

MLP is one of the common models of Artificial Neural Network which is used in machine learning (Gallant, 1993). Machine learning algorithms mimic biological learning systems using artificial intelligence tools. The algorithm develops a relationship between the land-use patterns and the explanatory variables in an iterative process by adjusting the model parameters (Baker, 1989). MLP neural network consists of three layers; the input layer, the hidden layer, and the output layer (Figure 4-31). The input layer has nodes which represent the site attributes (i.e. variables that cause the land change). The hidden layer is located between the input layer and the output layer. The number of nodes in the hidden layer can be estimated using Kolmogorov's theorem (Hecht-Nielsen, 1987). The theorem suggests that the number of nodes in the middle layer is  $2n+1$ , where  $n$  is the number of input nodes. A higher number of hidden nodes can increase the MLP accuracy. However, it also increases the training time without achieving a significant improvement in accuracy (Wang, 1994). Wang (1994) later demonstrated how an MLP network with  $2n/3$  hidden nodes could obtain almost the same accuracy level but with less training time. Therefore, the number of hidden nodes for the MLP neural networks in this research was determined using the latter method.

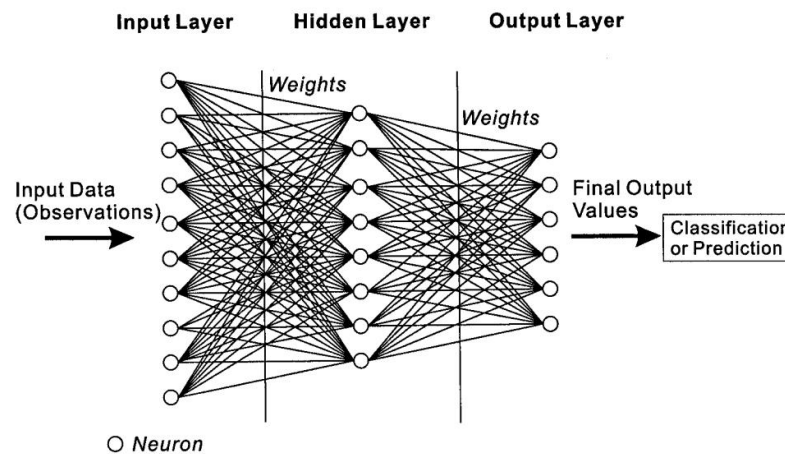


Figure 4-31 An artificial neural network structure with multiple output neurons (Source: Li & Yeh 2002)

The explanatory variables in the transitions include static and dynamic variables. Static components are the basic suitability factors for the transitions and unchanging over time, whereas the dynamic components are time-dependent variables that will be recalculated over time (Eastman, 2016). Anthropogenic disturbances to the areas are affected by several variables, such as the distance from roads, urban centres, areas prior to disturbance, elevation, and slope. The development of new settlements tends to occur near roadways, urban centres, and areas which have been disturbed before. Elevation and slope data could be used to allocate suitable land for settlements and agriculture.

Maps showing the driver variables which influence the land change were developed in the land change modelling, and the explanatory power of each variable was evaluated using Cramer's V test. The results from Cramer's V test show how good the potential explanatory value of the variable is. Variables with Cramer's values of 0.4 or higher are considered as good, whereas values of about 0.15 or higher are useful variables. Based on the test, the driver variables with high Cramer's value were selected to be included in the modelling process. The types of variable, then, were specified in the transition sub-model structure as static or dynamic components. Variables are considered as static if they are unchanging during a period. On the other hand, the dynamic components are changing over time (e.g. the development of roads) (Eastman, 2006).

LCM uses a list of constraints and incentives to assess the impacts of specific policies on land change. A constraint map for each transition provides a guide in the change prediction process by multiplying the transition potentials by the values in the incentives or constraints maps. Value of 0 on the map represents an absolute constraint to the changes, whereas the value of 1 shows no impact. Values between 0 and 1 are seen as disincentives, and values above 1 are incentives to changes (Eastman, 2016).

An example of LCM is the simulation of urban growth in the Greater Cairo, Egypt (Megahed et al., 2015). In this study, three land cover maps (1984, 2003, and 2014) were developed from satellite images, and the land cover transitions to urban were simulated to predict the future scenarios for the year 2025. The research on land cover change simulation was also conducted

by Rodríguez Eraso et al. (2013), who assessed land changes between 1985 and 2008 in the Colombian Andes. LCM was also used to assess the drivers of the deforestation in Ecuador (Rajan, 2007), and to predict the future growth of Muzaffarpur city in India (Mishra, Rai, & Mohan, 2014).

(2) Land change simulations of the two case study areas

In this study, the land change simulations were conducted using the four scenarios where different constraints maps were applied (Figure 4-32). The MLP process produces maps of transitions from one land cover type to another to model the future land cover composition and distribution. The simulation results, then, show the model accuracy.

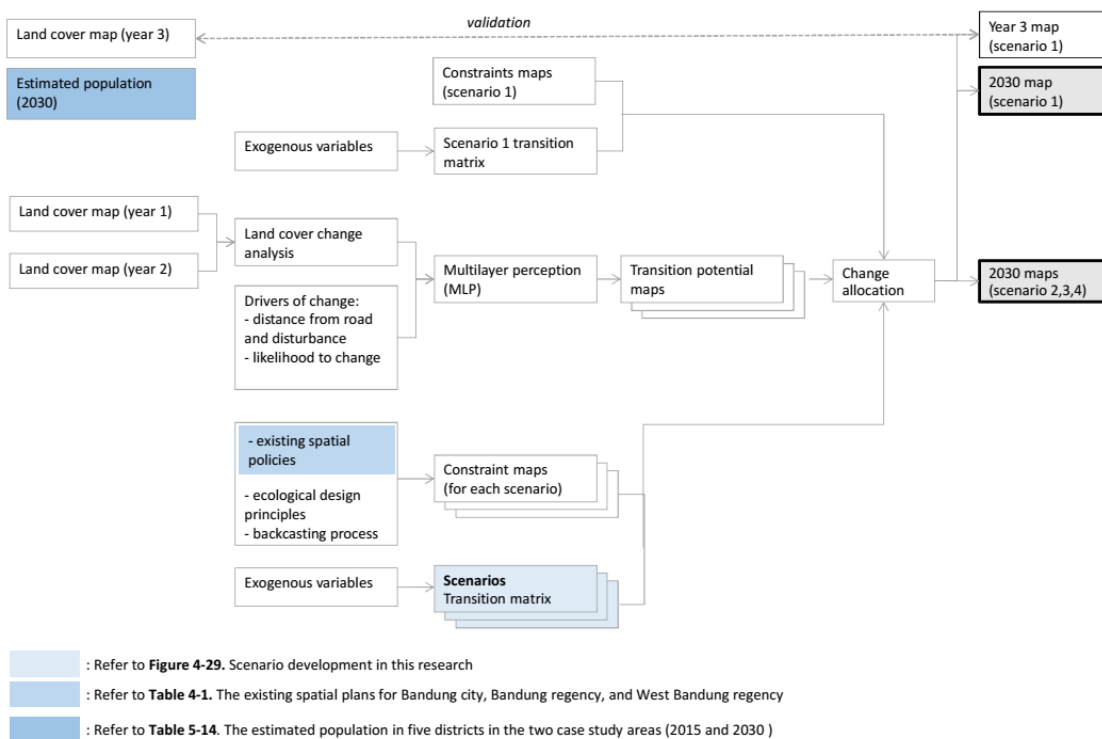


Figure 4-32 Land change simulation process

An initial simulation (LCM 1) was performed based on the land cover maps in 2013, 2015, and 2017, which were developed from SPOT 6 imagery. In this simulation, the 2017 land cover map in the first scenario (Status Quo) was first simulated using the 2013 and 2015 land cover maps, in which the result was validated using the actual 2017 map. Four land change drivers (e.g. distance from disturbance, distance from existing roads, distance from existing streams, and likelihood to change) were included at the beginning of the simulation process.

A map showing the distance from disturbance was computed in Terrset by extracting the existing developed areas in the earlier map (i.e. 2013 land cover map), removing extraneous pixels, and calculating the distance from the developed areas. Distance from existing roads and streams maps were generated using a road network map from OpenStreetMap and the stream networks



developed in ArcGIS respectively. The 'likelihood to change' driver was mapped based on the information on the land change in 2013-2015. Based on the Cramer's V test, the 'distance from existing streams' variable was excluded in the final LCM 1 simulation.

The second simulations (LCM 2) were conducted using the land cover maps in c.2000, c.2015, and c.2017 generated from SPOT 6 and Landsat 7 imagery. Six land change driver variables were used in the modelling and are divided into two groups. The first group is the demographic-economic drivers (e.g. likelihood to change, distance from disturbance, and population density). The second group is the environmental drivers (e.g. elevation, slopes, and distance from streams).

Maps showing the likelihood to change, the distance from disturbance and streams used in LCM 2 were generated the same way as the driver maps used in LCM 1. The only difference in the process is the base maps utilised in LCM 2; the 2000 and 2015 maps resulted from the final iteration of map generation process were used instead of the base maps used in LCM 1. The population density map was retrieved from WorldPop (2018). The original map has 100-m resolution, and each pixel in the map shows the number of population estimated by the United Nations. The map had been resampled into 6 metres before it was used in the modelling. The elevation and slope maps were developed from the DEM in ArcGIS.

During the simulation process, the c.2000 and c.2015 maps were used as the input dataset for the LCM model to project the 2017 and 2030 land cover maps. The accuracy of the projected 2017 land cover map was calculated using Kappa statistics.

### **4.3 The impact of land cover change to flood regulation and the assessment of flood risk (research phase 3)**

The impact of land cover change in the two case study areas to flood regulation was assessed using the Moving average (MA) analysis. The output from the MA analysis was interpreted to address **the first research question assessing how land cover alteration in the two case study areas affects flood regulation in the Bandung Basin.**

A flood risk assessment was conducted to analyse the characteristics of floods occurred in Bandung Basin. The assessment includes the analysis of flood frequency, flood discharge, and the effective rainfall that cause flooding. The river discharges of Ci Kapundung and Ci Sangkuy rivers, which have high possibility to cause floods in the basin, were also estimated to provide a benchmark to define the minimum volume of river discharges the catchments would have in the future development scenarios to cause the floods. The benchmark was used **to evaluate the results from MIKE SHE hydrologic modelling, addressing the second research question.**

### 4.3.1 Moving average analysis

A 5-year moving average (MA) analysis was performed to model the trends of Ci Tarum, Ci Kapundung, and Ci Sangkuy annual river discharges and annual precipitation in each case study area. The outputs from the MA analysis were used to assess how historical land cover change in both case study areas influenced the flood regulation. The analysis was also conducted to ascertain whether the precipitation rates also affected flood regulation.

Moving averages can be used to identify patterns in data in which the actual trend is covered by noise (Montgomery et al. 1990). The simple moving average used in this study computes the average of the most recent  $N$  observations (Equation 4-7).

$$M_T = \frac{x_T + x_{T-1} + x_{T-2} + \dots + x_{T-N+1}}{N} \quad \text{Equation 4-7}$$

where  $M_T$  is the simple moving average,  $N$  is the period of the moving average,  $x$  is the data at a specific time  $T$ .

The moving average analyses of discharges, rainfall, baseflow, and runoff coefficient were conducted to assess the change of hydrological regime in the Ci Kapundung water catchment area<sup>24</sup> (1978-2012) by Pradiko et al. (2015). The change of the hydrological regime was evaluated by analysing the relationship between the trend of river discharges with the rainfall and land conversion (runoff coefficient). The study used the 5-year moving average because the land cover changes can be seen clearly after five years (Ridwan 2001 cited in Pradiko et al. 2015).

### 4.3.2 Flood frequency estimation

The probability analysis of floods in the Bandung basin was conducted using the Log-Pearson Type III distribution, following the method which is described by the Oregon State University (<http://streamflow.engr.oregonstate.edu/analysis/floodfreq/index.htm>). The type of distribution was chosen because it was used in many studies for fitting a curve to data and mainly produces good results for flood peak data (Chow et al., 1988). The equation for calculating the Log-Pearson Type III distribution is

$$\log x = \overline{\log x} + K\sigma_{\log x} \quad \text{Equation 4-8}$$

where

$x$  : flood discharge of a specific return period

$\overline{\log x}$  : mean of the  $\log x$  value

$K$  : a frequency factor

$\sigma$  : the standard deviation of the  $\log x$  values

---

<sup>24</sup> The site used in the research conducted by Pradiko et al. (2015) comprises of the whole Ci Kapundung watershed, which is larger than the first study site used in this PhD research.

The values of frequency factors ( $K$ ) vary depending on the skewness coefficient ( $C_s$ ) and flood return period, and the values can be seen from the table of frequency factor for the Log-Pearson Type III (Chow et al. 1988). Skew coefficient ( $C_s$ ) can be calculated using Equation 4-9, while the standard deviation of the log  $x$  values ( $\sigma$ ) is estimate using Equation 4-10.

$$C_s = \frac{n \sum (\log x - \overline{\log x})^3}{(n-1)(n-2)(\sigma_{\log x})^3} \quad \text{Equation 4-9}$$

$$\sigma_{\log x} = \sqrt{\frac{\sum (\log x - \overline{\log x})^2}{n-1}} \quad \text{Equation 4-10}$$

where  $n$  is the number of entries, and  $x$  is the flood discharge.

Based on the availability of data, the flood frequency analysis was conducted using the maximum average daily discharges of Ci Tarum River throughout 1974-1988 and 1990-2016 (there is no data for the water year 1989). The data was collected from PSDA (*Pusat Sumber Daya Air/ Water Resource Management* in West Java Province). The flood frequency of Ci Tarum River, then, was computed based on the following steps.

Firstly, the maximum daily discharges of the river ( $Q$ ) for each water year were ranked and converted from  $m^3/s$  to  $ft^3/s$ . Secondly, skew coefficient and standard deviation were calculated using Equation 4-9 and Equation 4-10 respectively, based on the maximum daily discharge on each water year (in this study, there are 42 water years). Thirdly, the  $k$  values for the 2, 5, 10, 25, 50, 100, and 200 flood recurrence interval were estimated based on the skew coefficients. Finally, the discharge in each recurrence interval was calculated, and a graph of the flood return period was generated.

#### 4.3.3 Flood discharge estimation

This research focuses on the assessment of landscape changes in the Ci Kapundung and Ci Sangkuy upper water catchment areas, and the impact of the changes on the Ci Kapundung and Ci Sangkuy river discharges. The flood risk is examined by assessing the river discharges of both rivers which can affect the occurrence of flood in the basin. However, the fluctuation of Ci Tarum river discharge is affected not only by the two rivers but also by the discharges of rivers from other catchments in the basin. Therefore, it is also important to include the river discharges from other catchments in the analysis. The workflow of this assessment can be seen in Figure 4-33.

Firstly, the bankfull discharge of Ci Tarum River was calculated to estimate the flood discharge. Floods will occur if the river discharge at one particular time ( $t$ ) is higher than the bankfull

discharge ( $Q_{bkf}$ ). The estimation of Ci Tarum bankfull/ flood discharge is presented in the first section of this subchapter.

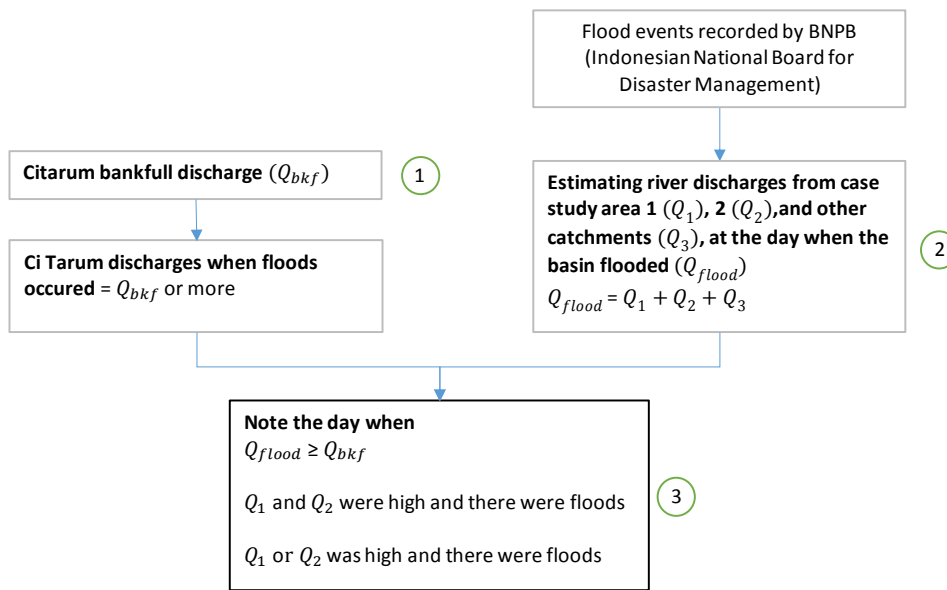


Figure 4-33 Diagram of the workflow to estimate flood discharge

Secondly, the flood event data from BNPB (Indonesian National Board for Disaster Management) was used to define the river discharges from all catchments in the basin which might affect the occurrence of floods in the region. Due to the limited river discharge data from the Ci Sangkuy upper water catchment area, the analysis was conducted using the data from 2008-2016. The calculation of river discharges from the Ci Kapundung watershed ( $Q_1$ ), Ci Sangkuy watershed ( $Q_2$ ), and other catchments ( $Q_3$ ) at the day when the basin was flooded, is described in section 2. Lastly, the discharges of Ci Kapundung and Ci Sangkuy rivers during flood events in the basin (2008-2016) were identified.

#### (1) Estimating the bankfull/ flood discharge of Ci Tarum River

In this study, the Manning's equation is selected as a method to predict the bankfull discharge of the Ci Tarum River because the method is considered to be more accurate and reliable than two other methods (i.e. Kinematic wave and SCS curve number) according to Roy & Mistri (2013). The Manning equation from Chow et al. (1988) was used to estimate the velocity of Ci Tarum River flow (Equation 4-11). Then, bankfull discharge is estimated using Equation 4-12 (Dunne & Leopold, 1978).

$$u = \frac{1.49 R^{2/3} S^{1/2}}{n} \quad \text{Equation 4-11}$$

where

$u$  : water velocity [ft/sec]

- $R$  : hydraulic radius, the ratio of the cross-sectional area of flowing water to the wetted perimeter,  $A/wp$
- $S$  : the slope of the water surface
- $n$  : the Manning resistance coefficient [ $ft^{1/6}$ ] (refer to Chow (1964) p.35 to get the coefficients for different channel surfaces)

$$Q_{bkf} = w_{bkf} \times u_{bkf} \times d_{bkf} \quad \text{Equation 4-12}$$

where

- $Q_{bkf}$  : discharge at bankfull or when a channel is at capacity [cfs]
- $w_{bkf}$  : bankfull width [ft]
- $u_{bkf}$  : velocity [ft/sec]
- $d_{bkf}$  : bankfull depth [ft]

A cross-sectional area ( $A$ ) of the river was calculated, and the wetted perimeter for the cross-section ( $wp$ ) was estimated based on the DEM (Digital Elevation Model) with 6 metres of resolution. Secondly, the hydraulic radius ( $R$ ) can be estimated by dividing  $A$  with  $wp$ . Using the Manning equation, water velocity when the river is at full capacity was calculated ( $u_{bkf}$ ). In this study, the slope of water surface ( $S$ ) was retrieved from literature (Brahmantyo 2005). Manning resistance coefficients were derived from the table of Manning's  $n$  values from Chow et al. (1988). After the water velocity ( $u_{bkf}$ ) was computed, then, the bankfull discharge of the Ci Tarum River ( $Q_{bkf}$ ) in each river section was estimated, based on the bankfull width ( $w_{bkf}$ ) and bankfull depth ( $d_{bkf}$ ).

## (2) River discharges from the catchments during flood events

River discharges from the Ci Kapundung and Ci Sangkuy upper water catchment areas during flood events in the Bandung Basin (2008-2015) were examined to get the estimated flood discharges from both watersheds. The estimated river discharges, then, were used as the thresholds for determining whether the land change in particular future development scenarios in each case study area contribute to the flooding in the basin. For example, if the projected river magnitudes in the two case study areas are above the thresholds, then, there is a high possibility that the discharges from the two watersheds cause the flooding in the basin.

The data of historical flood events in the basin was retrieved from BNPB (Indonesian National Board for Disaster Management). The analysis was conducted by determining the river discharges from the Ci Kapundung and Ci Sangkuy upper water catchment areas (i.e.  $Q_1$  and  $Q_2$  respectively), and from other catchments in the basin ( $Q_3$ ), during the flood events.  $Q_3$  was

estimated by subtracting the Ci Tarum discharges when the basin was flooded ( $Q_{\text{flood}}$ ) with  $Q_1$  and  $Q_2$ . The river discharges data was retrieved from PSDA. The recorded data from Dago Bengkok and Kamasan gauges was used to assess the river discharges of Ci Kapundung and Ci Sangkuy rivers respectively. The data from the Nanjung gauge was analysed to determine the Ci Tarum flood discharges during the flood events in the basin.

#### 4.3.4 Effective rainfall to cause flooding in the Bandung Basin

The assessment of the correlation between direct runoff (DRO) and rainfall events in Bandung Basin was conducted to determine the effective rainfall which causes the floods, following the same method used by Dasanto et al. (2014). In this assessment, the direct runoff was identified by subtracting the Ci Tarum river discharges with the baseflow.

The next analysis processes include the estimation of the rainfall magnitude at the day of peak direct runoff (DROp) during the flood events, the calculation on rainfall accumulation, and the development of regression models between the DROp and the rainfall accumulation. The information on flood events in the basin was retrieved from the BNPB, Bandung Regency official website<sup>25</sup>, and the online local newspapers during the data collection process.

##### (1) Calculating the Ci Tarum baseflow

The Ci Tarum baseflow is estimated following the guidelines to analyse the streamflow duration from Oregon State University. The total number of time step intervals (day) was computed using the river magnitude data of Ci Tarum River (1 January 2001 – 31 December 2016). Then, the discharge data was ranked by magnitude, and the per cent of the time that each discharge is equalled or exceeded was calculated using Equation 4-13.

$$P = 100 * [M/(n + 1)] \quad \text{Equation 4-13}$$

where

P : the probability that specific river flow will be equalled or exceeded [%]

M : the rank on the list

n : the number of events for one period

Samples of the Ci Tarum streamflow data within the period of 2001-2016 and the rank of river magnitude were used to estimate the river baseflow. According to Dasanto et al. (2014), baseflow can be estimated using the flow duration curve by defining the river discharge, which has a probability value of 90%.

---

<sup>25</sup> Floods in the Bandung Basin were mostly occurred in the centre part of the region, which is located in the Bandung regency. The municipality website ([www.bandungkab.go.id](http://www.bandungkab.go.id)) provides the latest and archived news related to many aspects including the disaster management in the area.

## (2) Determining the rainfall magnitude at the day of peak direct runoff (DROp) in the Bandung Basin

In this study, the rainfall magnitude on each day from 1 January 2008 to 31 December 2016 was calculated as the sum of Thiessen-weighted average rainfall for all weather stations in the basin, following the method described by Chow (1964). The rainfall datasets from 13 weather stations were used in this analysis. Each station has different availability of recorded rainfall data. However, the completed datasets were available from 2008 onwards. Therefore, the analysis could only be conducted using the rainfall data from 2008-2016.

The direct runoff (DRO) of all catchments in the basin was calculated using the continuity equation (Chow, 1964). In a watershed system, DRO can be viewed as the water storage which varies over time (i.e.  $dS/dt$ ). DRO can be computed by subtracting the rainfall, as the input to the system, with river magnitude, as the output from the watershed system. The information on flood events in the basin was used to identify the day when the highest direct runoff (DROp) occurs, and to determine the precipitation rate that day.

## (3) Estimating rainfall accumulation

The rainfall accumulation was calculated during the peak of direct runoff (DROp) in each flood event in Bandung Basin ( $R_0$ ) within the period of 1 January 2008 – 31 December 2016, until six consecutive days before the highest DROp in one flood event occurred, using Equation 4-14.  $R_1$  until  $R_6$  are the accumulated rainfall total during 1 day to 6 days before DROp respectively.

$$R_0 = R_t$$

$$R_1 = R_t + R_{t-1}$$

$$R_2 = R_t + R_{t-1} + R_{t-2}$$

$$R_3 = R_t + R_{t-1} + R_{t-2} + R_{t-3}$$

$$R_4 = R_t + R_{t-1} + R_{t-2} + R_{t-3} + R_{t-4}$$

$$R_5 = R_t + R_{t-1} + R_{t-2} + R_{t-3} + R_{t-4} + R_{t-5}$$

$$R_6 = R_t + R_{t-1} + R_{t-2} + R_{t-3} + R_{t-4} + R_{t-5} + R_{t-6}$$

Equation 4-14

## (4) Developing regression models

After the accumulated rainfall during DROp ( $R_0$ ), as well as the sum of rainfall rates during 1 day to 6 days before DROp occurred (i.e.  $R_0$ ,  $R_1$ ,  $R_2$ ,  $R_3$ ,  $R_4$ ,  $R_5$ , and  $R_6$ ) had been calculated, a regression model was developed (Equation 4-15). The regression model is adopted from Dasanto et al. (2014) to illustrate the correlation between direct runoff (DRO) and the rainfall rates.

$$DRO_i = b_0 + b_i R_{hi}$$

Equation 4-15

where  $DRO_i$  is the peak of direct runoff during flood events  $i$ ,  $b_0$  and  $b_i$  are the constants, and  $R_{hi}$  denotes the accumulated rainfall rates in  $h$  days during flood events  $i$  in the basin.

#### 4.4 Hydrologic modelling (research phase 3)

MIKE SHE model was used to simulate the future flow regimes (i.e. the patterns of river flow variation) of the two case study areas under different development scenarios and to assess the types of vegetation that can improve the flood regulation (Figure 4-34). **The two modelling objectives address the second and third research questions.**

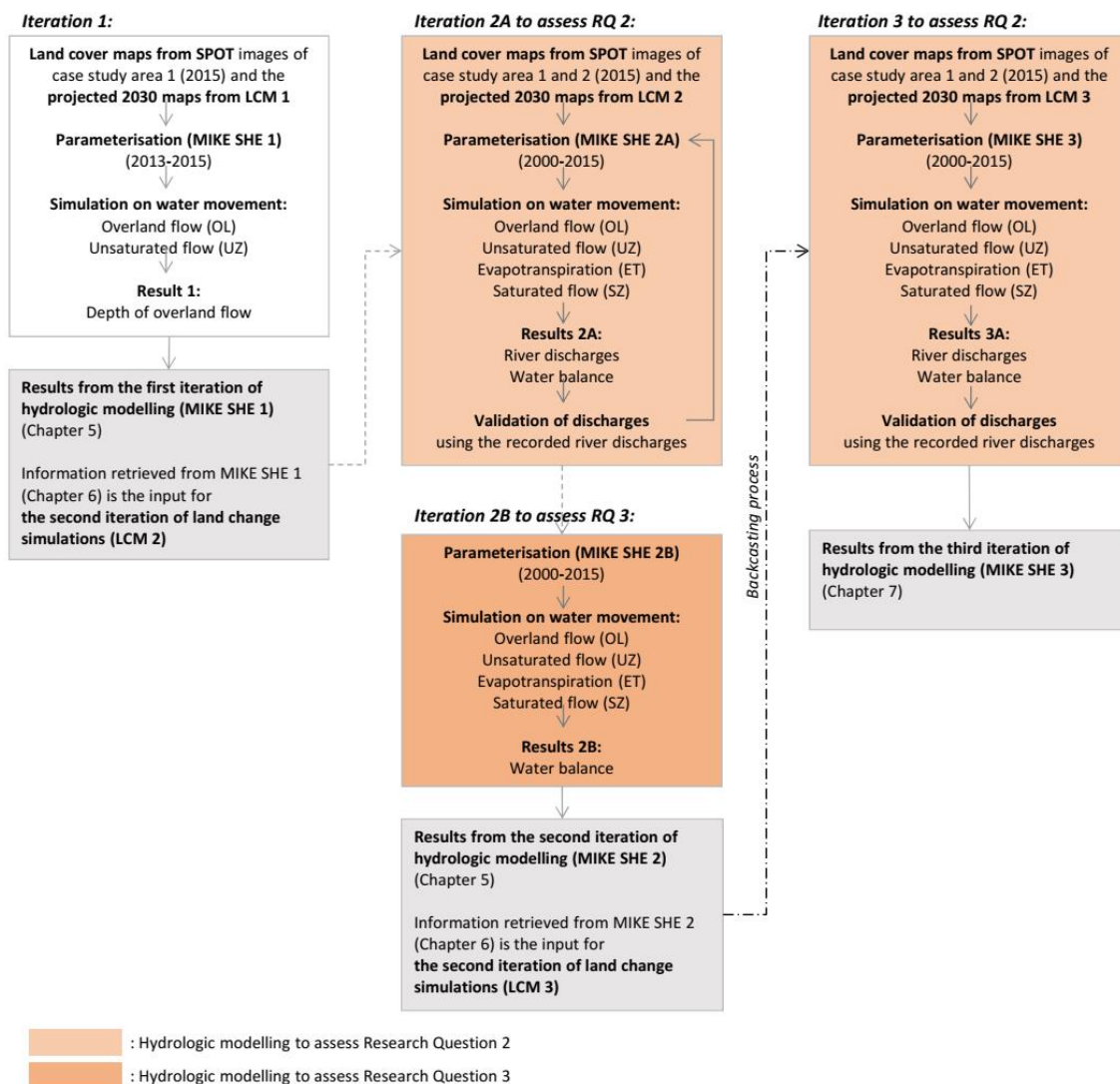


Figure 4-34 The iterative process of hydrologic simulations in this study

At the beginning of hydrologic modelling, the outputs from the first iteration of land change modelling (LCM 1) (i.e. projected 2030 land cover maps) were used to develop base maps for the first MIKE SHE model (MIKE SHE 1). In this process, overland flow (OL), unsaturated flow (UZ), and uniform value of evapotranspiration (ET) were included in the water movement



simulations. Saturated flow (SZ) was excluded in the simulations. The outcome of this process is the depth of overland flow (i.e. an initial phase of runoff). The result provides an indication during the parameterisation in the second iteration of hydrologic modelling (MIKE SHE 2).

In MIKE SHE 2, the river discharges were estimated from the simulated P Flux and Q Flux<sup>26</sup>. The water balance on each site was also projected in addition to the river discharges. The 2015 land cover maps from the last iteration of the map development process and the 2030 maps from the three scenarios in LCM 2 were used as base maps in the MIKE SHE 2 model. The model outputs (i.e. simulated discharges and water balance) were evaluated to determine the benchmark to develop the backcasting scenario (LCM 3).

The last hydrologic modelling (MIKE SHE 3) was conducted using the backcasting scenario. In MIKE SHE 3, river discharges and water balance analysis was also conducted to evaluate the landscape structure scenario to support flood regulation.

#### 4.4.1 Data collection for the hydrologic modelling

The following list shows the datasets required by the MIKE SHE model:

- (1) Historical rainfall data from nine weather stations in Ci Kapundung and Ci Sangkuy upper water catchment areas collected from PSDA (Water Resource Management in West Java Province). The data availability varies for each station (Figure 4-35). Therefore, only rainfall data from 2008-2015 was used in the modelling.

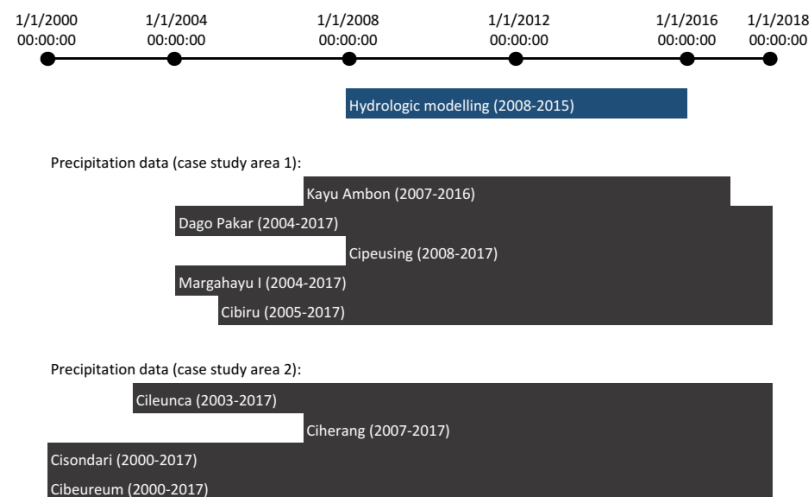


Figure 4-35 The availability of precipitation data

- (2) The temperature and wind speed data of Bandung City to estimate the reference evapotranspiration. The data was retrieved from BMKG (the Indonesian Agency for Meteorology, Climatology and Geophysics) and BPS (The Indonesian Central Bureau of Statistics).

<sup>26</sup> P Flux and Q Flux (m<sup>3</sup>/s/m) represents the flux density in x-direction and y-direction respectively. Q (discharge) to the x or y direction can be estimated by multiplying the flux with the model resolution.

- (3) The land cover maps of Ci Kapundung and Ci Sangkuy upper water catchment areas from 2015 and the simulated 2030 land cover maps.
- (4) Leaf Area Index (LAI) of each land cover class. The LAI was estimated using the allometric equations from various studies based on the estimated biomass of each sample tree. Allometric equations show the relationships of specific properties of plants, such as biomass and LAI, with another property, and are presented in logarithm forms. This method is used in this research because it is not destructive. Therefore, it is suitable to be conducted in the case study areas, especially when estimating LAI values of trees inside the two protected areas and the forests, where harvesting trees are prohibited by law. The allometric equations for estimating the biomass and LAI were derived from references (e.g. Siregar 2007, Malhado et al. 2009, Ahmad et al. 2014, Das 2014), in which the case study areas are located in West Java Province, Indonesia or other regions in the tropics.
- (5) The root depth and crop coefficients of various plants (Allen et al., 1998; Djaenuddin et al., 1994).
- (6) Manning's M values of different land cover types retrieved from the literature review (e.g. Kouwen & Fathi-Moghadam 2000; Kalyanapu et al. 2009; Rossman & Huber 2016).
- (7) River magnitude data of Ci Kapundung and Ci Sangkuy Rivers (2008-2015) retrieved from PSDA to calibrate and validate the hydrologic model.
- (8) Digital elevation model (DEM) from BIG (Indonesian Geospatial Agency) with a spatial resolution of 0.27-arcsecond or 8.34 metres. The DEM was developed by BIG from IFSAR (5-metre resolution), TERRASAR-X (5-metre resolution), and ALOS PALSAR (11.25-metre resolution) data with added mass point data from stereo-plotting. In this study, the DEM coordinate system was projected from the original system EGM2008 to WGS\_1984\_UTM\_Zone\_48S.
- (9) The delineation of water catchments in Bandung Basin generated from DEM with a spatial resolution of 6 metres using the hydrology toolbox of ArcGIS.
- (10) The soil distribution map of Bandung Basin and the soil properties data (e.g. the composition of clay, silt, and sand) retrieved from the Indonesian Soil and Agroclimate Research Centre (1993).
- (11) Parameters for geological layers from literature (e.g. Darul et al., 2016; Nurliana & Widodo, 2009; Maria, 2008; Morris & Johnson, 1967).

#### 4.4.2 MIKE SHE modelling parameter estimation

Model parameters which could not be acquired from the field surveys, government offices, and literature, were estimated in this research. The estimation of the parameters is presented below.

## (1) Evapotranspiration

The FAO (Food and Agriculture Organisation of the United Nations) Penman-Monteith method was used to calculate reference evapotranspiration ( $ET_0$ )<sup>27</sup> for the case studies (Equation 4-16). This approach is chosen because the method is widely used (Danish Hydraulic Institute, 2017b) and is suitable to be used in data-short situations (Allen et al., 1998). The Penman-Monteith method estimates the evapotranspiration from an open water surface using climatological data such as solar radiation, air temperature, humidity, and wind speed.

$$ET_0 = \frac{0.408\Delta(R_n - G) + \gamma \frac{900}{T + 273} U_2 (e_s - e_a)}{\Delta + \gamma(1 + 0.34u_2)} \quad \text{Equation 4-16}$$

Where

- $ET_0$  : reference evapotranspiration [mm day<sup>-1</sup>]
- $R_n$  : net radiation at the crop surface [MJ m<sup>-2</sup>day<sup>-1</sup>]
- $G$  : soil heat flux density [MJ m<sup>-2</sup>day<sup>-1</sup>]
- $T$  : mean daily air temperature at 2 m height [°C]
- $U_2$  : wind speed at 2 m height [m s<sup>-1</sup>]
- $e_s$  : saturation vapour pressure [kPa]
- $e_a$  : actual vapour pressure [kPa]
- $e_s - e_a$  : saturation vapour pressure deficit [kPa]
- $\Delta$  : slope of saturation vapour pressure curve at air temperature T [kPa°C<sup>-1</sup>]

R.G. Allen *et al.* (1998) describe the required climatological datasets for estimating the evapotranspiration using the above equation as follows. The net radiation ( $R_n$ ) is the balance between the absorbed, reflected, and emitted energy by the Earth's surfaces. The soil heat flux ( $G$ ) is the energy for heating the soil.

The actual vapour pressure ( $e_a$ ) refers to “the vapour pressure exerted by the water in the air”. The saturation vapour pressure deficit ( $e_s - e_a$ ) describes the air actual evaporative capacity. The value of vapour pressure is commonly derived from dewpoint temperature (the temperature which can make the air saturated). If no humidity data was recorded, the actual vapour pressure ( $e_a$ ) can be derived by assuming the dewpoint temperature is near the daily minimum temperature  $T_{\min}$ . The equation requires the data of saturation vapour pressure at the air temperature T ( $e^0$ ). The value of  $e_a$  can also be derived from the table of saturation vapour pressure for different temperatures (T) in the guideline for computing crop evapotranspiration

---

<sup>27</sup> Reference evapotranspiration ( $ET_0$ ) is defined as the highest value of evapotranspiration derived from a fully watered grass surface (Danish Hydraulic Institute, 2017b p.38)

(Allen et al., 1998). The guideline book also provides the estimation of the slope of the vapour pressure curve (D) for different temperatures (T).

There is no temperature data available for the Ci Kapundung and Ci Sangkuy upper water catchment areas. Therefore, the daily maximum and minimum temperature data of Bandung City (1 January 2002-6 September 2015 or 4712 days) was used to estimate  $ET_0$  (mm/day) in each case study area. However, there are missing temperature data in 2013-2015. Therefore, the assessment was conducted using the data from 4,502 days. The weather station that records the temperature in Bandung city is located at approximately 700 m asl. Daily wind speed data was estimated from the mean monthly data retrieved from BPS (*Badan Pusat Statistik/* The Indonesian Central Bureau of Statistics), assuming that the wind speed was similar every day in a month. The highest and lowest daily temperature in Bandung City had been corrected to represent the temperature of each case study area using the Earth Atmosphere model from NASA (2015). For elevation less than 11,000 m asl (Troposphere), the air temperature can be estimated as  $T = 15.04 - 0.00649 h$ , where T is the temperature ( $^{\circ}\text{C}$ ) and h is altitude (m) (National Aeronautics and Space Administration (NASA), 2015).

Regression analyses were performed using the computed  $ET_0$  and river discharges. The output from regression analyses can be used to estimate the missing  $ET_0$  data based on the recorded river discharges. The river discharge unit was converted from  $\text{m}^3/\text{s}$  to mm/day.

## (2) Leaf Area Index (LAI)

In this study, the biomass of the dominant trees in the two case study areas (e.g. *Pinus merkusii*, *Switenia mahogany*, *Eucalyptus urophylla*) was estimated from the tree trunks' diameter at breast height (DBH) using allometric equations. Based on the biomass, the LAI was predicted using the other allometric equations, which show the relationships between biomass and LAI of various vegetation. All the allometric equations were derived from studies on biomass and LAI of the conifers, broad-leaved plants, and mixed plants in Indonesia and other countries (Table 4-5).

Table 4-5 Allometric equations to estimate biomass and LAI from various plant species

Plant species	Location	Allometric Equations	References
<i>Pinus merkusii</i>	North Sumatera, Indonesia	Biomass = $0,2451(\text{DBH})^{2,2757}$ (suitable for DBH<45 cm)	(Ahmad et al., 2014)
<i>Pinus merkusii</i>	West Java, Indonesia	Biomass = $0,1031(\text{DBH})^{2,4587}$ (suitable for DBH 45-120 cm)	(Siregar, 2007)
<i>Pinus taeda</i> L.	North Carolina	Biomass = $2.33+(7.26*\text{LAI})$	(Albaugh et al., 1998)

Plant species	Location	Allometric Equations	References
<i>Switenia mahogany</i>	Bangladesh	SLA = LA/drymass (cm <sup>2</sup> /g) Biomass = 0.052574*DBH <sup>2.25004</sup> LAI = Biomass*SLA	(Das, 2014)
<i>Eucalyptus urophylla</i>	North eastern Brazil	Foliage Biomass = 0.0034*(DBH) <sup>2.5722</sup>	(Stape, Binkley, & Ryan, 2004)
<i>Eucalyptus urophylla</i> <i>Eucalyptus grandis</i>	South China	Biomass = -1.0081(LAI) <sup>2</sup> - 2.948(LAI) + 4.5839 or LAI = 2.948 + ((2.948) <sup>2-4</sup> *- 1.0081*(4.5839-Biomass)) <sup>0.5</sup>	(Wen et al., 2009)
Secondary forest ( <i>Acacia mangium</i> with understory plants)	West Java, Indonesia	Biomass = 0.1969V <sup>2.0611</sup>	(Siregar & Heriyanto, 2010)
Secondary forest	Amazon forest, Brazil	SLA = 8.16 m <sup>2</sup> /kg or 81.6 cm <sup>2</sup> /g LAI = Biomass*SLA	(Malhado et al., 2009)
Grass (barley)	Spain	LAI = 0.0299 x Ground cover (%) (if ground cover (%) ≤ 97)	(Ramirez-Garcia, Almendros, & Quemada, 2012)

The LAI for mixed plants, tea plantations, grass and agricultural plants were derived from the literature review. The LAI value for developed areas and water bodies is 0 because there is no vegetation in the two land cover classes. The LAI of 6.2 is assigned for mixed plants, following the study conducted by (Dietz et al. 2006), who estimated the LAI of natural forest in Central Sulawesi, Indonesia using hemispherical photos. LAI for tea plantations (*Camellia sinensis*) is between 5 to 6 (Tanton, 1979).

The LAI values of the three types of forests (i.e. conifers, broad-leaved plants, and mixed forests) were estimated, assuming that the LAI of all trees within the same age group and species is relatively similar (Table 4-6). The information on the age of trees was retrieved from Perhutani.

Table 4-6 Estimated mean value of LAI of plant species in the case study areas

Group	Plant species	Site	Age	Mean value of LAI
A	<i>Pinus merkusii</i>	The southern part of Ir. H. Djuanda protected area	n/a	9.56
B	<i>Pinus merkusii</i>	The northern part of Ir. H. Djuanda protected area	n/a	10.62
C	<i>Pinus merkusii</i>	North Bandung city	n/a	9.39
D1	<i>Pinus merkusii</i>	Perhutani forest (site 1)	16 years	6.55

Group	Plant species	Site	Age	Mean value of LAI
D2	<i>Pinus merkusii</i>	Perhutani forest (site 2)	46 years	15.63
D3	<i>Pinus merkusii</i>	Perhutani forest (site 3)	50 years	13.29
D4	<i>Pinus merkusii</i>	Perhutani forest (site 4)	51 years	16.86
D5	<i>Pinus merkusii</i>	Perhutani forest in the Ci Kapundung watershed outside areas in the Perhutani forest with Pines age of 16, 46, 50, and 51	9-55 years	Estimated from the regression eq. (Figure 4-36)
E	Eucalyptus	Perhutani forest (site 5)	n/a	7.63
F	Broad-leaved trees	Ir. H. Djuanda protected area	n/a	3.62
G	Mahogany	North Bandung city	n/a	3.78
H	<i>Pinus merkusii</i>	Forest (site 6)	n/a	10.89
I	<i>Pinus merkusii</i>	Outside forest (site 7)	n/a	8.76
J	Eucalyptus	Forest (site 8)	n/a	8.45
K	Broad-leaved trees	Ci Sangkuy watershed	n/a	4.79
M	<i>Camellia sinensis</i>	Ci Sangkuy watershed	n/a	5
L	Mixed plants	All sites	n/a	6.2
N	Grass	All sites	n/a	2.09

Pine trees (*Pinus merkusii*) in the Perhutani forest in the northern part of Ci Kapundung upper water catchment area were planted in 1951-2008. Thus the trees have a different range of DBH, biomass, and LAI value. Due to the technical difficulty to access all parts of the forest, only sixteen samples were taken from four age groups (i.e. conifers which were planted in 1966, 1967, 1971, and 2001). Therefore, the LAI for pine trees from other age groups in the Perhutani forest was estimated from a linear regression. Figure 4-36 shows the relationship between estimated the LAI and the age of Pine trees in the Perhutani forest in the Ci Kapundung watershed. The straight line indicates the regression equation of  $Y = 2.5 + 0.26 \cdot X$ , where Y is the LAI and X is the age of trees.

The DBH of eleven tree samples of Eucalyptus in the Perhutani forest (site 5) was measured to estimate the LAI. Twenty samples of Pine trees and broad-leaved trees were assigned in the Ir. H. Djuanda protected area, whereas twenty-three samples were taken in the North Bandung City outside the protected area.

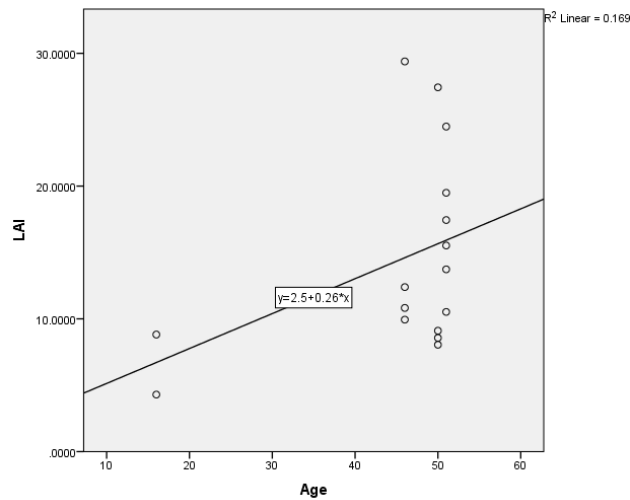


Figure 4-36 Linear regression of LAI and age of Pine trees in the Perhutani forest in the Ci Kapundung watershed

The DBH data of eight samples of Pine trees and eleven samples of Eucalyptus and other broad-leaved trees were collected in the Perhutani forest (site 6, 7, and 8) in the Ci Sangkuy upper water catchment area. Due to the difficulty to access the site, samples taken could not represent plants in all age groups. After the LAI of all plants had been estimated, the mean value of LAI was calculated.

### (3) Soil parameters

The soil map was retrieved from the Soil and Agroclimate Research Centre (1993). The research centre divided the area of Bandung Basin and the northwest side of the basin into 78 zones based on the landform and characteristics of soil in each zone. The soil taxonomy and the content of sand, silt, and clay were identified according to the Soil Taxonomy (Soil Survey Staff, 1999). The soil maps for the two watersheds are shown in Figure 4-37 (a-b). Since Bandung city was not part of the research area conducted by the research centre, the area is not included on the map (Figure 4-37a). Therefore, a geological map of Bandung Basin with a scale of 1:100.000 from the Directorate of Environmental Geology (1993) was referred to derive the soil data for Bandung City.

The soil types of the two watersheds are presented in Table 4-7 and Table 4-8. In this study, the soil compositions for dominant soil type in each zone (marked with the letter D) are derived from Soil and Agroclimate Research Centre 1993), and various studies in Bandung Basin (Adrionita, 2011), Bandung city (Rahmaniar & Kamil, 2015), and North Bandung (e.g. Djaenudin 2004; Ichwan 2009).

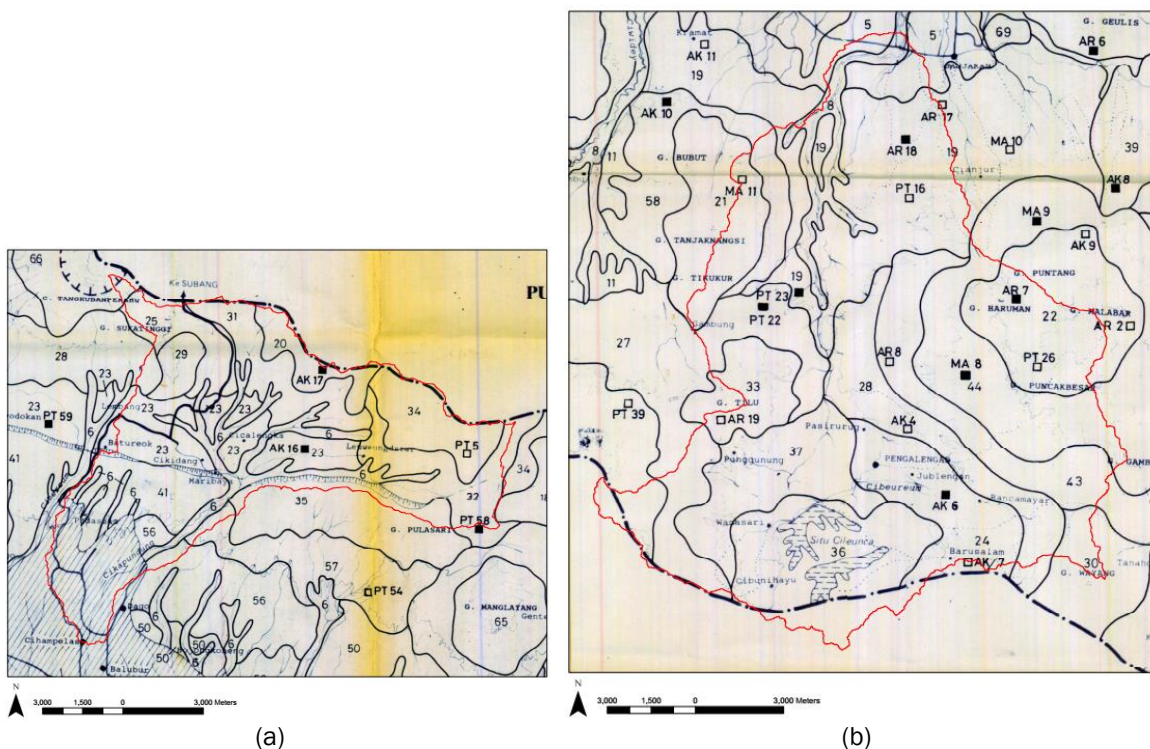


Figure 4-37 The soil map of (a) Ci Kapundung and (b) Ci Sangkuy upper water catchment areas overlaid with the boundary of case study areas (Source of soil map: Soil and Agroclimate Research Centre 1993)

Table 4-7 The composition of each soil type in the Ci Kapundung upper water catchment area (Sources: Soil and Agroclimate Research Centre 1993; Djaenudin 2004; Ichwan 2009; Adrionita 2011; Rahmaniar & Kamil 2015)

Zone	Soil sub-groups	Sand	Silt	Clay	References
6	Aquic Eutropepts (D) Aeric Tropaquepts	22.25%	31.50%	46.25%	(Adrionita, 2011)
20	Typic Humitropepts	78.25%	5.50%	16.25%	(Soil and Agroclimate Research Centre 1993)
23	Thapic Hapludands (D) Typic Melanudands	65.86%	23.57%	10.57%	(Soil and Agroclimate Research Centre 1993)
25	Eutric Hapludands	22.50%	68.50%	9.00%	(Ichwan, 2009)
31	Typic Hapludands (D) Eutric Hapludands	32.00%	48.14%	19.86%	(Djaenudin, 2004)
41	Cumulic Haplodolls (D) Andic Eutropepts	19.10%	28.62%	52.28%	(Adrionita, 2011)
56	Typic Hapludalfs	14.00%	28.30%	57.70%	(Adrionita, 2011)
0	Soil from Cikidang f.	14.00%	67.00%	19.00%	(Rahmaniar & Kamil, 2015)



Table 4-8 The composition of each soil type in the Ci Sangkuy upper water catchment area (Sources: Soil and Agroclimate Research Centre 1993; Singh & Kundu 2010; Adrionita 2011)

Zone	Soil sub-groups	Sand	Silt	Clay	References
5	Typic Tropaquepts (D) Vertic Tropaquepts Vertic Eutropepts	8.03%	43.20%	48.77%	(Singh & Kundu, 2010)
8	Typic Eutropepts (D) Typic Tropaquepts Fluventic Dystropepts	19.50%	31.00%	49.50%	(Adrionita, 2011)
19	Typic Humitropepts (D) Aquic Eutropepts Typic Eutropepts	15.57%	31.34%	53.00%	(Soil & Agroclimate Research Centre, 1993)
21	Typic Humitropepts (D) Typic Eutropepts	39.93%	33.67%	27.00%	(Soil & Agroclimate Research Centre, 1993)
22	Oxic Humitropepts (D) Typic Eutropepts	19.00%	24.60%	56.40%	(Soil & Agroclimate Research Centre, 1993)
24	Thapic Hapludands (D) Eutric Hapludands	28.55%	37.30%	34.15%	(Soil & Agroclimate Research Centre, 1993)
27	Eutric Hapludands (D) Typic Kandiodalfs	10.80%	29.60%	59.60%	(Soil & Agroclimate Research Centre, 1993)
28	Eutric Hapludands	10.80%	29.60%	59.60%	(Soil & Agroclimate Research Centre, 1993)
30	Eutric Hapludands	10.80%	29.60%	59.60%	(Soil & Agroclimate Research Centre, 1993)
33	Typic Hapludands (D) Eutric Hapludands	37.71%	39.00%	23.29%	(Soil & Agroclimate Research Centre, 1993)
36	Typic Melanudands (D) Eutric Hapludands	89.00%	9.00%	2.00%	(Adrionita, 2011)
37	Typic Melanudands (D) Eutric Hapludands	89.00%	9.00%	2.00%	(Adrionita, 2011)
43	Typic Hapludolls (D) Typic Eutropepts	25.25%	25.25%	49.50%	(Adrionita, 2011)
44	Typic Hapludolls (D) Andic Hapludolls Oxic Dystropepts	14.42%	28.21%	57.38%	(Soil & Agroclimate Research Centre, 1993)
58	Typic Hapludalfs (D) Typic Eutropepts	7.80%	21.80%	70.40%	(Soil & Agroclimate Research Centre, 1993)

The soil properties for the MIKE SHE model are described as follows (Danish Hydraulic Institute, 2017a). Soil water content at saturation is the maximum volume of water in the soil. Water content at field capacity can be reached during a dry period. Water content at the wilting point

is the minimum volume of water that plants can extract from the soil. Saturated hydraulic conductivity refers to the soil infiltration rate.

In this study, the soil parameters were estimated based on the soil composition data using Hydrus-1D software. Hydrus-1D was used in many soil and hydrology studies to derive soil moisture and to model water flow and solute transport in the soil and groundwater (Tárník & Igaz, 2017).

#### 4.4.3 Initial parameters of the MIKE SHE models

Parameterisation of the hydrologic model was conducted at the beginning of the modelling process to determine preliminary values for each input data. The initial parameterisation for hydrologic modelling is presented as follows.

##### (1) Model grid size and simulation specification

An initial simulation for the first case study area (MIKE SHE 1) was performed based on the data from 1 January 2013 00:00:00 to 1 January 2016 00:00:00 (1095 days) (Figure 4-34). This simulation provides an indication of how the model works and an examination of potential errors in the simulation. The errors might be caused by inputting different data types and units in the file properties or defining wrong computational control parameters.

Model grid size in MIKE SHE 1 is 6 metres, following the resolution of land cover maps used in the model. The run times required by the model is more than 8 hours (with an Intel Core i5-4210U 1.70GHz 2.40GHz processor). Therefore, the modelling was conducted only to assess the depth of overland flow at the day with the highest daily precipitation rate in 2013-2015. A seven-day long simulation was performed instead of conducting the initial three-year-long modelling. Three observation points were assigned in the model. The three points are located in the area with different land cover, soil types, and slope gradients (Rani, Lange, Cameron, et al., 2019).

MIKE SHE 2 modelling was run for the calibration from 1 January 2008 00:00:00 to 1 January 2012 00:00:00 and the validation from 1 January 2012 00:00:00 to 1 January 2016 00:00:00. The base maps were changed into the projected 2030 land cover maps generated from the last iteration of land change modelling of the case study areas (LCM 2). Model grid size for MIKE SHE 2 and 3 is 120m to decrease the computational time.

Time steps and the computational control parameters of overland flow (OL) and unsaturated flow (UZ) were defined at the beginning of the simulation. The time step for MIKE SHE modelling is 24 hours. The maximum allowed OL and UZ time steps are 24 hours for both layers. Overland flow (OL) is solved using Successive Overrelaxation (SOR) because the method is faster than the

other method (i.e. Explicit Numerical Solution), which requires smaller time steps (Danish Hydraulic Institute, 2017b).

The overland and saturated flow were computed using the Finite Difference method. The 2-Layer water balance was first selected as the method to simulate the unsaturated flow in MIKE SHE 1 and at the beginning of MIKE SHE 2. Examination of the MIKE SHE results suggested that Richards equation performed better than the 2-Layer water balance method. Thus, the method was used to compute the unsaturated flow in the final hydrologic simulations.

## (2) Topography

The Digital Elevation Model (DEM) with a resolution of 6 metres was used in the MIKE SHE model. There are 2,876,014 and 5,691,053 points derived from the DEM of Ci Kapundung and Ci Sangkuy watersheds respectively and interpolated in the MIKE SHE to create the ground surface of the case study areas (Figure 4-38). The grid size for each map in the model, then, was adjusted to define the model resolution.

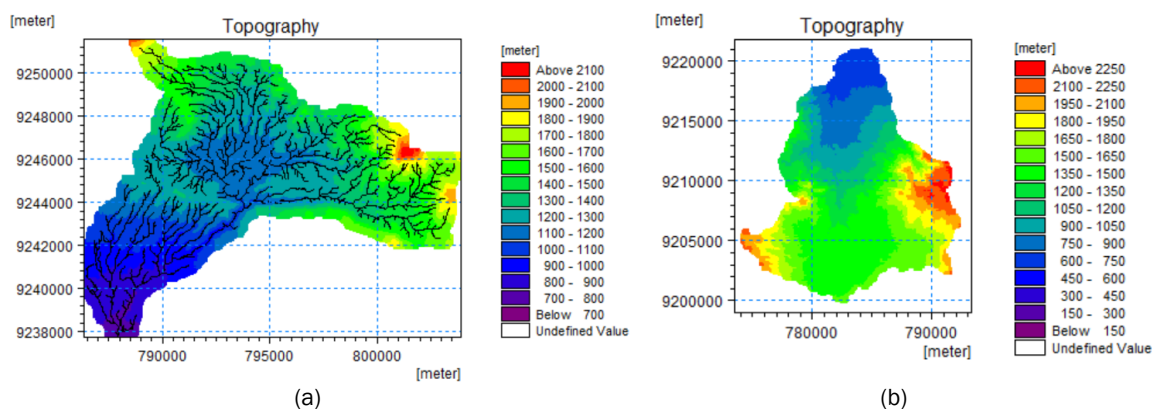


Figure 4-38 (a-b) The topography of Ci Kapundung and Ci Sangkuy watersheds

## (3) Precipitation

MIKE SHE model requires the climatic data either is recorded as the precipitation data [mm/hour] (i.e. accumulated rainfall water divided by length of the observation period), or the rainfall data [mm] (i.e. accumulated rainfall water). Thiessen polygons were created to map the spatial distribution of rainfall data in the two case study areas based on the location of weather stations in and around the areas (Figure 4-39 a and b).

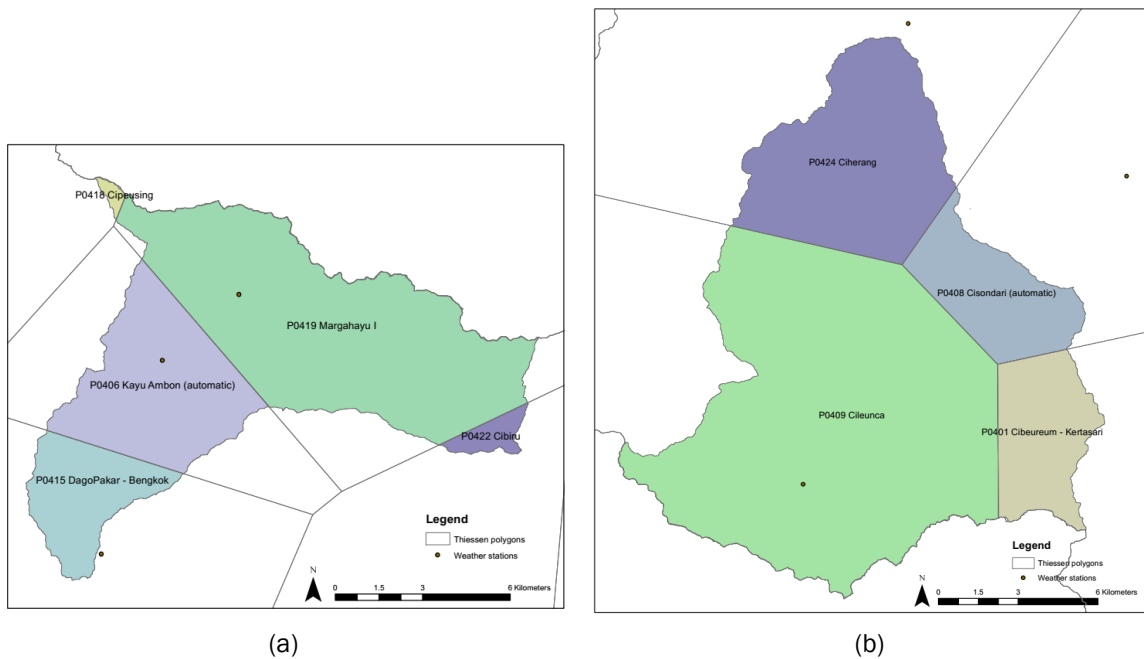


Figure 4-39 (a-b) The spatial distribution of rainfall in the Ci Kapundung and the Ci Sangkuy watersheds (the dots representing the location of rain gauges in each case study area)

#### (4) Reference evapotranspiration

In MIKE SHE, the reference evapotranspiration ( $ET_0$ ) is multiplied by crop coefficient to retrieve the crop reference evapotranspiration (Danish Hydraulic Institute, 2017a). Logarithmic and inverse regression analyses were performed to identify the trend of  $ET_0$  in the two upper catchment areas.

The computed regression equation for the first case study area is  $Y = 6.568 - 0.694 \cdot \ln(X)$  with R square of 0.155. Whereas the regression equation for estimating  $ET_0$  for the second case study area is  $Y = 5.581 + (0.535/X)$  with R square of 0.116. X is discharges/ Q (mm/day) and Y is estimated  $ET_0$  (mm/day) (Figure 4-40 and Figure 4-42). The estimated  $ET_0$  in the Ci Kapundung and Ci Sangkuy upper water catchment areas (1/1/2008 – 31/12/2015) are presented in Figure 4-41 and Figure 4-43, respectively. Grey lines represent the calculated ETO based on the Penman-Monteith equation, whereas the black lines represent the estimated ETO from the missing temperature data.

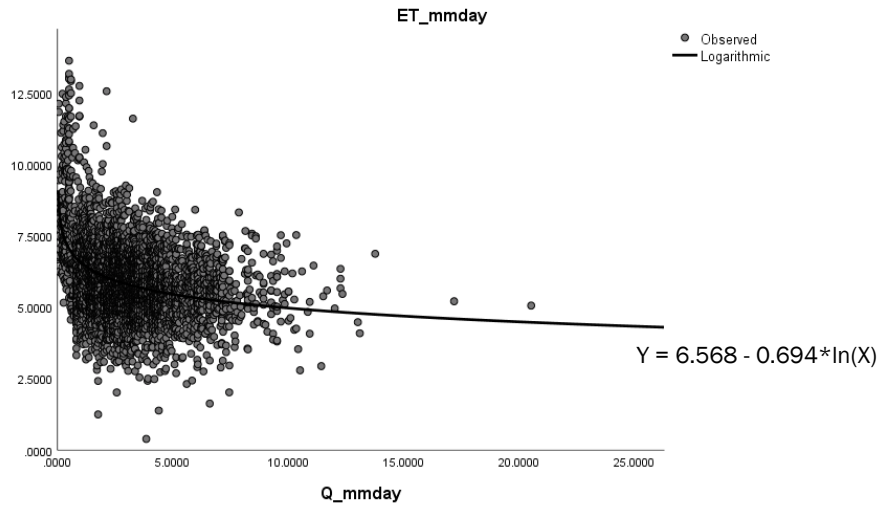


Figure 4-40 Logarithmic regression of  $ET_0$  (mm/day) and Q mm/day) for the Ci Kapunding upper water catchment area

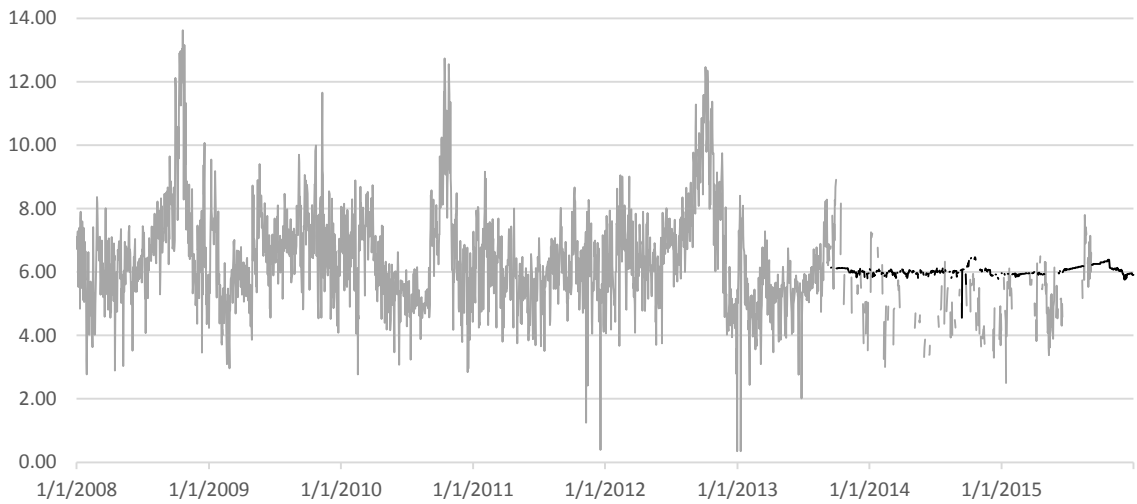


Figure 4-41 Estimated reference evapotranspiration in the Ci Kapunding upper water catchment area (1/1/2008 - 31/12/2015)

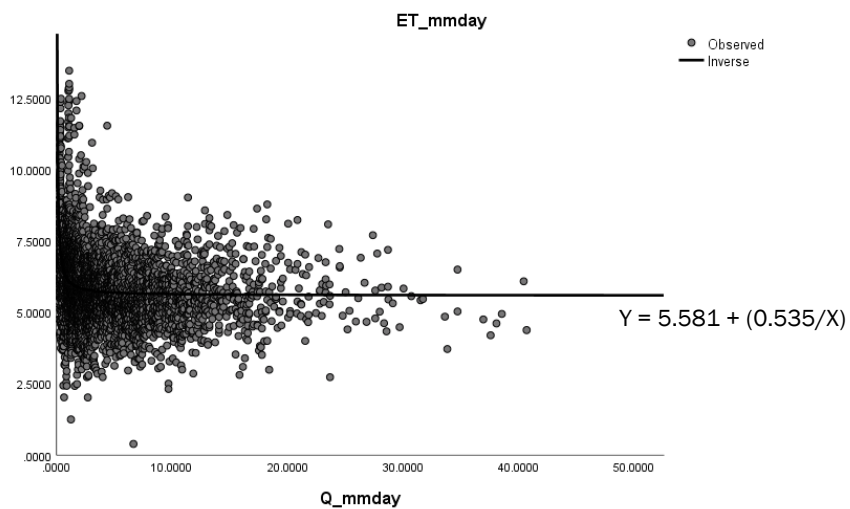


Figure 4-42 Inverse regression of  $ET_0$  (mm/day) and Q mm/day) for the Ci Sangkuy upper water catchment area

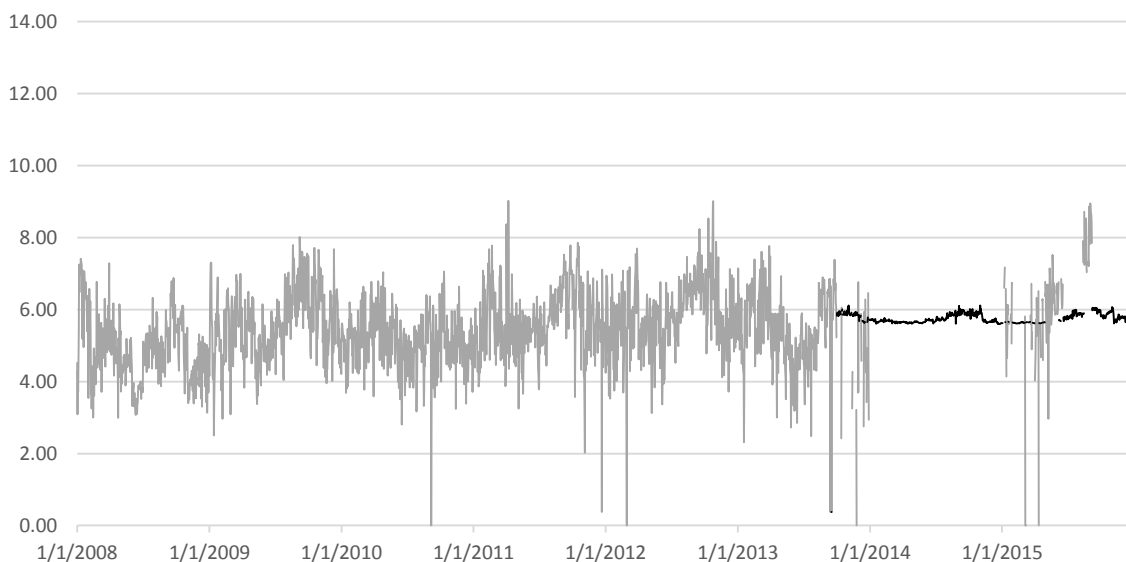


Figure 4-43 Estimated reference evapotranspiration in the Ci Sangkuy upper water catchment area (1/1/2008 - 31/12/2015)

(5) Leaf Area Index (LAI)

Table 4-9 presents the estimated LAI for all land cover types in the Ci Kapundung and Ci Sangkuy watersheds. There are eleven groups of land cover in the first case study area, five groups in the second case study area, and four groups in both case study areas. LAI values were assigned in the 2015 and 2030 land cover maps. The distribution of the new land cover classes with a similar range of LAI in both case study areas in 2015 can be seen in Figure 4-44 and Figure 4-45.

Table 4-9 The list of estimated LAI values for reclassified land cover types

Location	Vegetation	Group	Age	Mean value of LAI
Perhutani forest and Ir.H.Djuanda protected area in the Ci Kapundung watershed	Conifer ( <i>Pinus merkusii</i> )	1	≤16 years	5.83
		2	17-26 years	8.09
		3	27-36 years	10.88
		4	≥37 years	14.98
Outside Perhutani forest and Ir.H.Djuanda protected area	Conifer ( <i>Pinus merkusii</i> )	5	n/a	6.23
Perhutani forest in the Ci Kapundung watershed	Broad-leaved trees (e.g. <i>Eucalyptus sp.</i> , <i>Schima wallichii</i> )	6	n/a	7.63
Ir.H.Djuanda protected area	Broad-leaved trees (e.g. Mahagony, <i>Artocarpus</i> )	7	n/a	3.7

Location	Vegetation	Group	Age	Mean value of LAI
and north Bandung City	<i>elasticus, Pterygota horsfieldii</i>			
Perhutani forest in the Ci Sangkuy watershed	Conifer ( <i>Pinus merkusii</i> )	8	n/a	10.89
Outside forest in the Ci Sangkuy watershed	Conifer ( <i>Pinus merkusii</i> )	9	n/a	8.76
Perhutani forest in Ci Sangkuy watershed	Broad-leaved trees	10	n/a	8.45
Outside forest in Ci Sangkuy watershed	Broad-leaved trees	11	n/a	4.79
Tea plantation	<i>Camellia sinensis</i>	12	n/a	5
All watersheds	Mixed trees	13	n/a	6.2
	Bare land and cultivated land	14	n/a	2.09
	Developed areas	15	n/a	0
	Water bodies	16	n/a	0

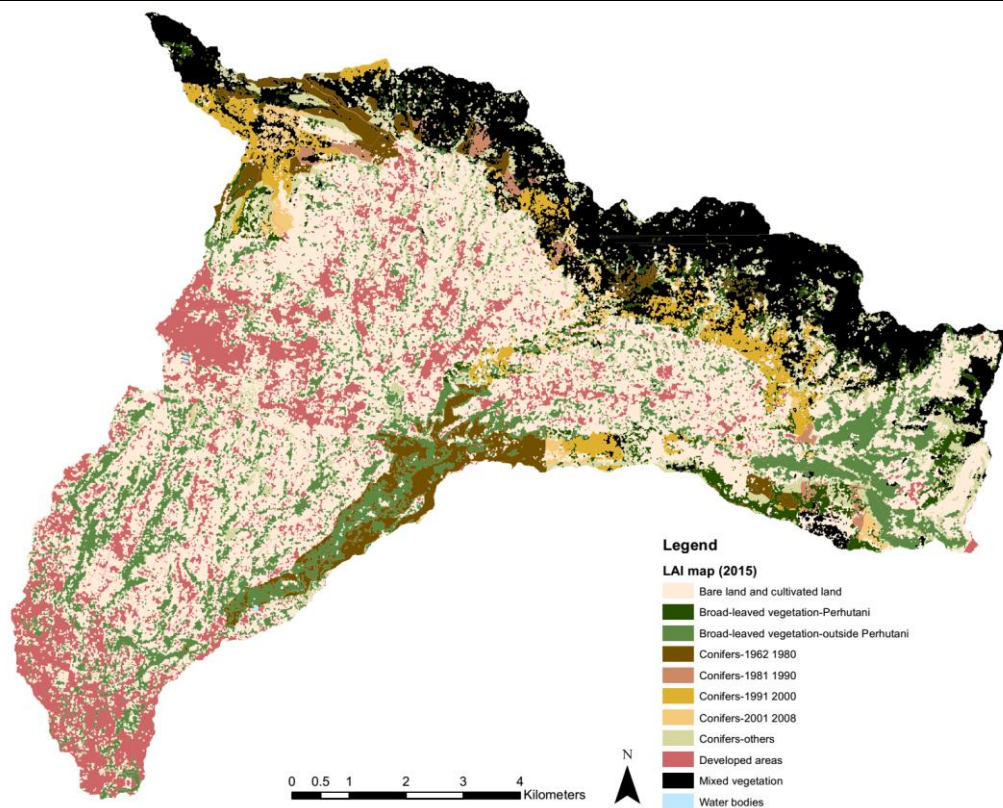


Figure 4-44 The distribution of new land cover classes with a similar range of LAI in the Ci Kapundung watershed in 2015

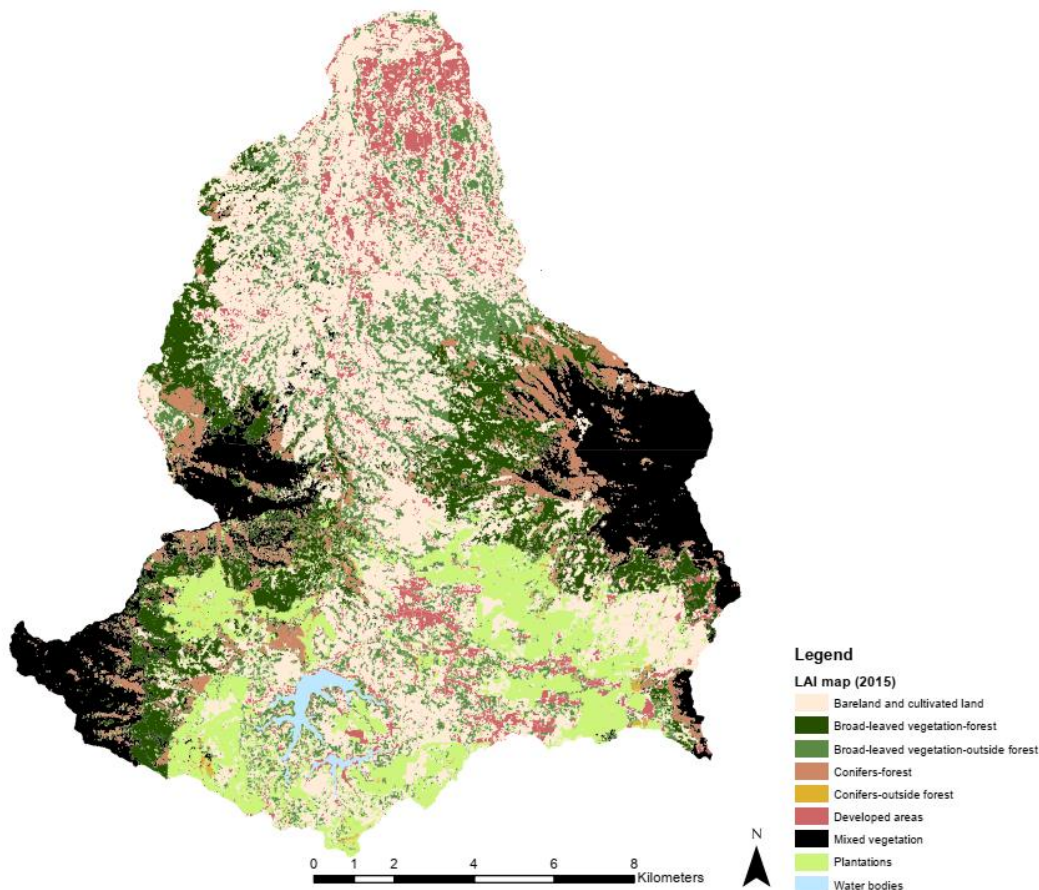


Figure 4-45 The distribution of new land cover classes with a similar range of LAI in the Ci Sangkuy watershed in 2015

#### (6) Crop coefficient ( $K_c$ ) and root depth

Crop coefficient ( $K_c$ ) is used in MIKE SHE to adjust the reference evapotranspiration ( $E_{To}$ ) for different types of vegetation. The data of  $K_c$  values of various vegetation during the three growth stages and water bodies was retrieved from literature (Allen et al., 1998). For agricultural plants, the values of  $K_c$  vary in the initial, mid-season, and late-season stages. At the beginning of MIKE SHE 2, it was assumed that the  $K_c$  for bareland and cultivated plants is equal to grass. After evaluating the results from the iterative simulations,  $K_c$  values which vary in during the growing season were assigned in the final MIKE SHE 2 model. The  $K_c$  value of 0 is assigned for developed areas, assuming there is no vegetation, or only small parts of the pixel of 6 metres showing developed areas in the SPOT 6 satellite images, is covered by vegetation.

The root depth of different vegetation in the case study areas was determined based on the data of potential soil depth of agricultural areas to plant crops and trees, such as rice paddy, tea, conifers, and fruit trees (Djaenudin, et al., 2011). The parameters of crop coefficient and root depth assigned in the MIKE SHE models are presented in Table 4-10.



Table 4-10 Crop coefficient (Kc) and root depth of all land cover types in the two case study areas

Land cover	Kc	Root depth (mm)
Developed areas	0	0
Bare land and cultivated land	0.90	800
Tea plantations	1.00	100
Conifers in all age groups	1.00	1000-1200
Broad-leaved vegetation	0.90	1000-1200
Mixed vegetation	1.00	1000-1200
Water bodies	0	0

#### (7) Overland flow

In this research, the finite difference method is chosen in the MIKE SHE model to simulate the overland flow because it is the most common method used in the modelling (Danish Hydraulic Institute, 2017b). Manning's M number of each land cover type is required (Table 4-11) to estimate the overland flow. The numbers are equivalent to the Stickler roughness coefficient ranging between 10 (for thickly vegetated channels) and 100 (smooth channels). Manning's M value of 18 is assigned for tea plantations, assuming that the land cover map has similar characteristic of surface roughness as agriculture. A uniform value of 0 metres is assigned as the initial water depth (the depth of water on the ground at the beginning of simulation).

Table 4-11 Manning's N and M values of land cover used in the MIKE SHE model

Land cover	N	M	References
Developed areas	0.011	<b>90</b>	(Engman 1986 cited in Rossman & Huber 2016)
Bare land and cultivated land	0.055	<b>18</b>	(Yen 2001 cited in Rossman & Huber 2016)
Tea plantations		<b>18</b>	
Mixed vegetation	0.40	<b>2.5</b>	(Kalyanapu, Burian, & McPherson, 2009)
Conifers	0.1	<b>10</b>	(Kouwen & Fathi-Moghadam, 2000)
Broad-leaved vegetation	0.32	<b>3</b>	(Yen, 2001 cited in Rossman & Huber 2016)
Water Bodies		<b>99</b>	

#### (8) Unsaturated zone

The 2-Layer water balance method was selected to calculate the water flow in the unsaturated zone in MIKE SHE 1 and at the beginning of MIKE SHE 2 simulations. Then, the Richards equation was used in the final MIKE SHE modelling. The soil types and distributions in each case study area were identified from the soil map retrieved from the Indonesian Soil and Agrilclimate Research Centre (soil map in Chapter 3). The soil parameters required in the unsaturated flow simulation were estimated based on the compositions of clay, silt, and sand of each soil type.

Due to a large number of soil categories in the case study areas, the soil was reclassified based on the content of sand-silt-clay, because soil with relatively the same composition has the same soil properties. The soil compositions of the new soil categories were calculated from the mean values of sand-silt-clay composition of each soil category. Table 4-12 and Table 4-13 show the

soil reclassification in the Ci Kapundung and Ci Sangkuy upper water catchment areas, respectively. The distribution of reclassified soil types in both watersheds can be seen in Figure 4-46.

Table 4-12 Soil reclassification in the Ci Kapundung upper water catchment area

No	Dominant soil sub-groups	New soil category	Sand	Silt	Clay
A1	Aquic Eutropepts	Soil A	18.53%	29.47%	52.07%
A2	Cumulic Hapludolls				
A3	Typic HapludalFs				
B1	Eutric Hapludands	Soil B	18.25%	67.75%	14.00%
B2	Soil from Cikidang f.				
C1	Typic Humitropepts	Soil C	72.05%	14.53%	13.41%
C2	Thapic Hapludands				
D	Typic Hapludands	Soil D	32.00%	48.14%	19.86%

Table 4-13 Soil reclassification in the Ci Sangkuy upper water catchment area

No	Dominant soil sub-groups	New soil category	Sand	Silt	Clay
E1	Typic Eutropepts	Soil E	13.59%	28.23%	58.18%
E2	Typic Humitropepts				
E3	Oxic Humitropepts				
E4	Eutric Hapludands				
E5	Eutric Hapludands				
E6	Eutric Hapludands				
E7	Typic Hapludolls				
E8	Typic HapludalFs				
F1	Typic Hapludolls	Soil F	25.25%	25.25%	49.50%
G1	Typic Melanudands	Soil G	62.01%	20.40%	17.59%
G2	Typic Melanudands				
G3	Typic Tropaquepts				
H1	Typic Humitropepts	Soil H	35.20%	36.66%	28.15%
H2	Thapic Hapludands				
H3	Typic Hapludands				

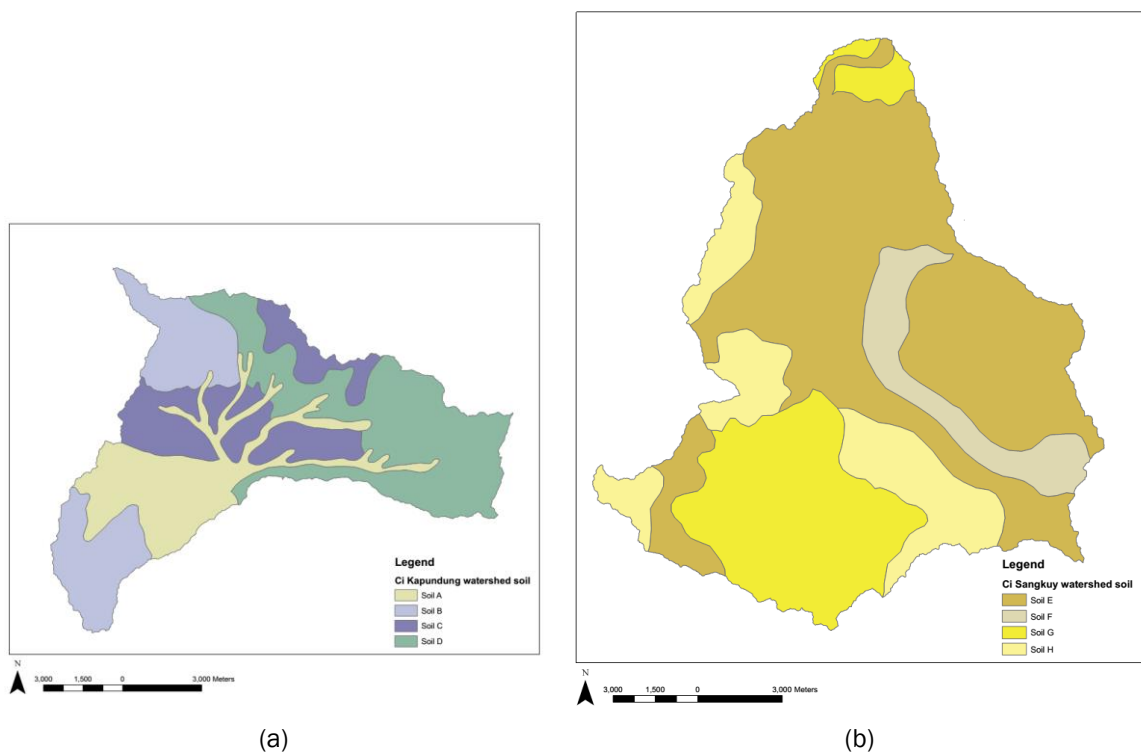


Figure 4-46 New soil maps of the Ci Kapundung and Ci Sangkuy upper water catchment areas

Eight soil categories identified in the Ci Kapundung upper water catchment area were reclassified into four new soil categories (Table 4-14). In the first case study, four soil categories with the dominant soil sub-groups of Aquic Eutropepts, Cumulic Haplodolls, and Typic Hapludalfs are classified as one group (Soil A) because they have a relatively high percentage of clay (52.07%), compared with other soil categories. Eutric Hapludands and soil from Cikidang formation are grouped as soil category B because they are mainly composed of silt (67.75%). The other soil categories, Typic Humitropepts and Thapic Hapludands have a high composition of sand (72.05%) (Soil C). The last soil type (Soil D), Typic Hapludands has relatively balance compositions of sand and silt. Thus it is not regrouped with the other soil types.

Table 4-14 Soil parameters for the Ci Kapundung hydrology model

	Residual moisture content (Qr)	Saturated moisture content (Qs)	Alpha	n	Saturated hydraulic conductivity (Ks)(cm/s)	Saturated hydraulic conductivity (Ks)(m/s)	Water content at field capacity	Water content at wilting point
Soil A	0.0965	0.4835	0.0173	1.2663	17.61	2.038194e-6	0.403626	0.183273
Soil B	0.0613	0.4390	0.0045	1.6918	23.24	2.689815e-6	0.405052	0.0810226
Soil C	0.0496	0.3805	0.0332	1.4226	40.41	4.677083e-6	0.239252	0.0730275
Soil D	0.0645	0.4146	0.0064	1.5748	16.07	1.859954e-6	0.366793	0.0890997

In the Ci Sangkuy upper water catchment area, there are thirteen different soil categories, which can be reclassified into four soil categories (Table 4-15). Soil E is the new soil type, which is formed from six different soil categories in the area with high percentages of clay (58.18%). Eutric Hapludands is mentioned twice in the table because it is the dominant soil sub-group in the soil category number 27, while it is the only content in the soil category number 28. Soil F consists of only one soil category which has the same percentage of sand and silt. Soil G, which was formed by three soil categories, has a high composition of sand (62.01%). The last soil category (Soil H) is composed of three soil categories, in which the compositions of sand, silt, and clay are relatively similar.

Table 4-15 Soil parameters for the Ci Sangkuy hydrology model

	Residual moisture content (Qr)	Saturated moisture content (Qs)	Alpha	n	Saturated hydraulic conductivity (Ks)(cm/s)	Saturated hydraulic conductivity (Ks)(m/s)	Water content at field capacity	Water content at wilting point
Soil E	0.0997	0.4977	0.0182	1.2403	23.09	2.672454e-6	0.419324	0.201712
Soil F	0.093	0.4668	0.0189	1.2578	14.26	1.650463e-6	0.387004	0.178929
Soil G	0.0554	0.3855	0.0272	1.3669	23.13	2.677083e-6	0.270557	0.0910445
Soil H	0.0758	0.4259	0.0115	1.4409	7.430	8.59954e-7	0.349974	0.111068

The residual moisture content (Qr), saturated moisture content (Qs), alpha, n, and the hydraulic conductivity (Ks)<sup>28</sup> were estimated based on the soil composition, using Hydrus 1D. The estimated values were submitted to the MIKE Zero UZ soil properties model to retrieve the other required soil parameters for the MIKE SHE model (e.g. water content at field capacity and water content at the wilting point<sup>29</sup>). The uniform soil depth of 150 m was assigned in the model for computing the unsaturated flow using Richards equation.

#### (9) Saturated zone

The 3D finite difference method was used to model the water movement in the saturated zone in the two case study areas. The required datasets required in the 3D finite difference method include the hydrogeologic parameters of the lower level, horizontal and vertical hydraulic conductivity, specific yield, and specific storage. In general, there are three geological layers in

<sup>28</sup> Residual moisture content (Qr), saturated moisture content (Qs), and hydraulic conductivity (Ks) are defined as follows (Danish Hydraulic Institute, 2017a). Qr is the minimum amount of water in the soil at high absorption conditions. Qs is the maximum amount of water in the soil. Ks is maximum soil infiltration rate.

<sup>29</sup> Water content at field capacity is measured in a soil that is completely drained. Water content at wilting point can be the amount of water when plants cannot absorb the water and starting to wilt.

the two case study areas identified from the study conducted by Nurliana & Widodo (2009) (refer to Figure 3-11). The three layers are Cibereum formation (Aquifer), Cikapundung formation, and Cilanang Formation. Only the first two layers that were included in the MIKE SHE modelling, due to the incomplete geological dataset for the Cilanang Formation. The initial parameters assigned in the model is presented in Table 4-16.

Table 4-16 Geological layer parameters for the Ci Kapundung hydrology model

Parameters	Geological layers		References
	Cibereum formation	CiKapundung formation	
Lower level	100 m	400 m	(Nurliana & Widodo, 2009)
Horizontal hydraulic conductivity	1e-6 m/s	4e-6 m/s	(Darul et al., 2016; Maria, 2008)
Vertical hydraulic conductivity	1e-6 m/s	4e-6 m/s	
Specific yield	0.02	0.21	(Maria, 2008; Morris & Johnson, 1967)
Specific storage	0.02	0.21	

Table 4-17 Geological layer parameters for the Ci Sangkuy hydrology model

Parameters	Geological layers		References
	Cibereum formation	CiKapundung formation	
Lower level	150 m	450 m	(Nurliana & Widodo, 2009)
Horizontal hydraulic conductivity	1e-6 m/s	4e-6 m/s	(Darul et al., 2016; Maria, 2008)
Vertical hydraulic conductivity	1e-6 m/s	4e-6 m/s	
Specific yield	0.02	0.21	(Maria, 2008; Morris & Johnson, 1967)
Specific storage	0.02	0.21	(Maria, 2008; Morris & Johnson, 1967)

#### 4.4.4 Calibration and validation procedures

Three calibration procedures in hydrological modelling are trial-and-error with manual parameter adjustment, automatic with numerical parameter optimisation, and a combination of trial-and-error and automatic methods. The first method is widely applied in hydrologic modelling, and it is beneficial for complicated models. The second method requires a numerical algorithm to assess the maximum and minimum variables of a particular parameter. The third method employs the trial-and-error method to find a range of initial parameter values, which are then, adjusted using automatic optimisation (Refsgaard & Storm, 1996).

The trial-and-error method was used to calibrate the hydrologic models in this research. Initial parameters were applied in the uncalibrated model. Then, alterations on the parameters were

done during the calibration process. In a validation process, the calibrated model was tested using a different set of data used in the calibration stage.

The calibration process was performed using the observed and predicted river discharges ( $\text{m}^3/\text{s}$ ). The P Flux and Q Flux values (i.e. fluxes at the x- and y-directions) at the area where the water gauges are located on both sites were simulated. Discharges at four cells were calculated following the method described in the MIKE SHE model manual (Figure 4-47). The discharge from one cell can be calculated as the sum of discharges across the four boundaries of the cell ( $\Sigma Q = Q_N + Q_S + Q_E + Q_W$ ) (Danish Hydraulic Institute, 2017b).

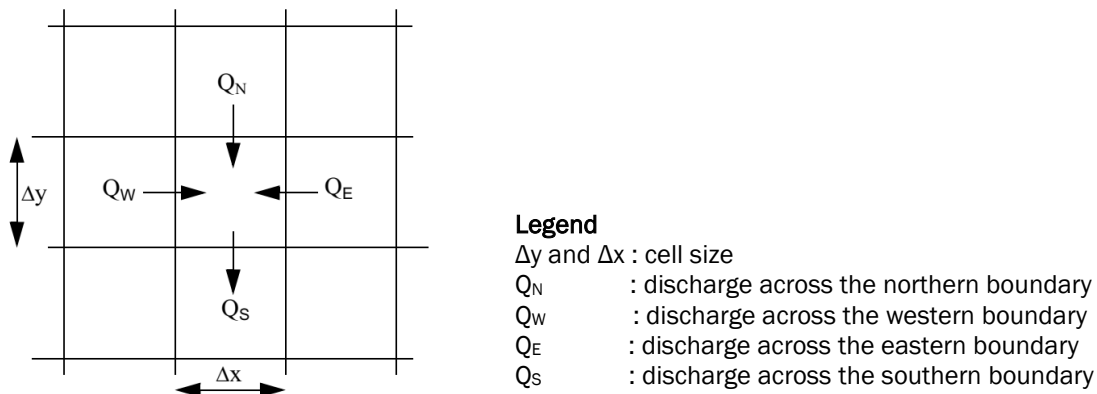


Figure 4-47 A grid system used in MIKE SHE model (Source: Danish Hydraulic Institute, 2017b)

MIKE software provides the calculation to assess the model performance. The analyses include Mean Error (ME), Mean Absolute Error (MAE), Root Mean Square Error (RMSE), and Index of Agreement. The final simulations to assess the impact of land cover alteration to flood regulation in each watershed were conducted using the calibrated model. More than 20 simulations have been conducted to calibrate each MIKE SHE model. The calibrated parameters for Ci Kapundung and Ci Sangkuy models are presented in Appendix A.

#### 4.4.5 Landscape structure scenarios to support flood regulation

Iterative hydrologic simulations were conducted to assess landscape structure scenarios that can support the flood regulation in each case study area (the second research question). MIKE SHE 1 and 2 were performed with specific constraints to assess the research question, and are described as follows.

##### (1) MIKE SHE 1 modelling

MIKE SHE 1 was conducted on the first case study area using the 2015 and the 2030 land cover maps (the Status Quo and Ecological design-based scenarios in LCM 1) to assess the depth of overland flow. It should be noted that there is no actual depth of overland flow recorded at the

site. Thus, no calibration and validation process has been done in the first iteration of hydrologic simulations. The results, therefore, were interpreted only based on the available data or parameters assigned.

(2) MIKE SHE 2 modelling and the initial phase of Pareto-frontier analysis

**Q Flux and P Flux were simulated in MIKE SHE 2 modelling to estimate the river discharges in each case study area.** The existing 2015 land cover maps generated from the last iteration of the land cover map development process and the three scenarios of 2030 land cover maps from LCM 2 were used in this process. In addition to the river discharge simulations, **water balance analysis was also performed under all scenarios.** One of the outputs from water balance simulations is the estimated overland outflow.

**The influence of precipitation rates and the three physical attributes of landscape (e.g. land cover, slopes and soil types) to flood regulation was further analysed.** The assessment involved parameterisation in MIKE SHE 2 model and the water balance analysis. The output from this process was used as the criteria to develop the backcasting scenario in LCM 3. The method to conduct the analysis is presented in the next part of this subchapter (4.4.6).

**A Pareto-frontier concept was used to assess the capacity of all landscape structure scenarios for reducing runoff in the two case study areas** (Figure 4-48). The criteria of two impact indicators were determined at the beginning of the initial Pareto-frontier analysis. The first indicator is the overland (OL) outflow estimated from the water balance analysis (y-axis). Lower overland outflow surface storage means that the site has a lower volume of runoff flowing outside the catchment. The second indicator is the composition of an area that falls within a specific category<sup>30</sup>, which arguably can reduce overland outflow effectively (x-axis).

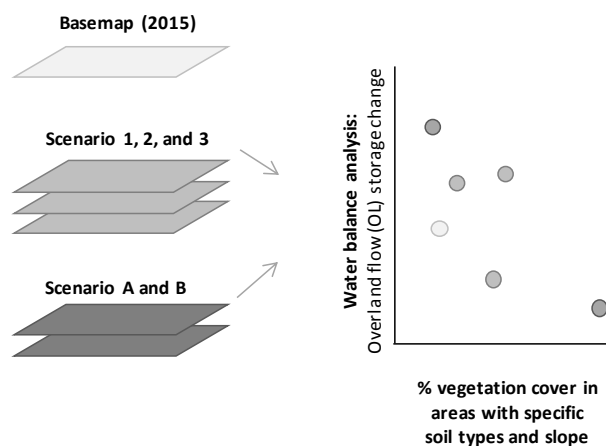


Figure 4-48 The implementation of Pareto-frontier analysis in the study

<sup>30</sup> This category was determined based on the results from the vegetation and soil analysis on the two case study areas (refer to 4.4.6 for the detailed methods to conduct the analysis and 6.3 for the results from the analysis).

Two more scenarios with extreme land cover conditions were used as benchmarks for the Pareto-frontier assessment. All parts of case study areas are covered by bare land and cultivated land in Scenario A, and conifers in Scenario B, except for the water bodies (Figure 4-49 and Figure 4-50). Other model parameters, such as precipitation, evapotranspiration, and soil types, were not altered during this process.

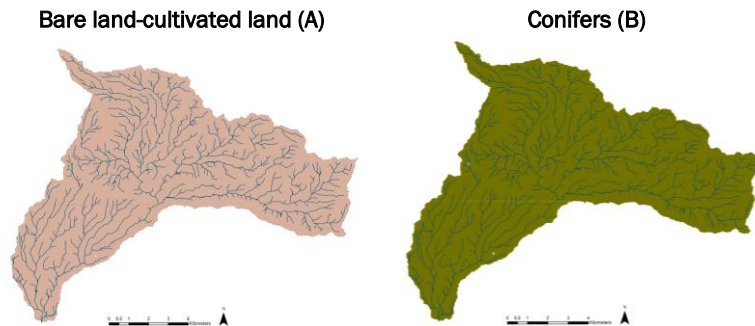


Figure 4-49 Distribution of land cover classes in the Ci Kapundung upper water catchment area

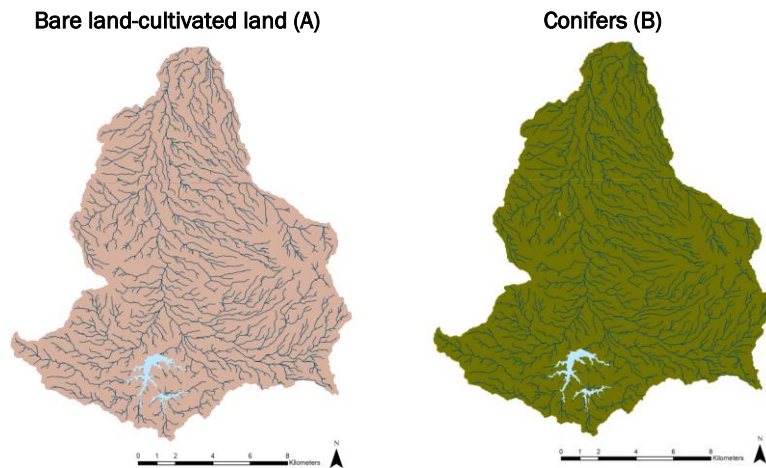


Figure 4-50 Distribution of land cover classes in the Ci Sangkuy upper water catchment area

**Water balance analysis for the two case study areas was performed under Scenario A and B.** The values of OL outflow estimated from the water balance analysis were mapped in a graph to assess the capacity of each scenario to support flood regulation in the catchments. It should be noted that the Pareto-frontier assessment in this study was only limited to comparing the results from MIKE SHE 2, and to ascertain how close or far the modelling outputs are from the desired outcome. In this case, the desired outcome is to retrieve a possible option for landscape planning that can support flood regulation. In this study, there is no assessment using optimization algorithms or models which are often used by studies related to Pareto optimality (e.g. Seppelt, Lautenbach and Volk, 2013; Xia *et al.*, 2014).



### (3) MIKE SHE 3 modelling

The outcomes from MIKE SHE 2 modelling (e.g. simulated river discharges and water balance) were used to develop the Backcasting scenario of the two case study areas in the third land change simulations (LCM 3). In MIKE SHE 3, Q Flux and P Flux were also simulated to calculate the river discharges. Water balance analysis was performed based on the backcasting scenarios of the two watersheds to evaluate the proposed landscape planning.

#### 4.4.6 The capacity of vegetation to reducing surface runoff

The capacity of different vegetation types to reducing surface runoff in the case study areas was tested to address the third research question.

##### (1) MIKE SHE 1 modelling

In MIKE SHE 1, the depth of overland flow at three sample points in the first case study area was simulated using the 2030 land cover map developed from the ecological design-based scenario generated in LCM 1. The three points are located in the area with the same precipitation trend but in the different type of soil and land cover. The types of vegetation in the 2030 land cover maps used in the modelling were altered. Thus, each land cover map only has a single vegetation type. The compositions and distributions of other land cover classes remained the same.

##### (2) MIKE SHE 2 modelling

Two assessments were conducted **to test the vegetation capacity to reduce runoff on slopes with different gradients in high and low precipitation rates**. The output was used to generate **guidelines to develop the backcasting scenario** (e.g. where to plant specific types of vegetation on the two sites). In the first assessment, there are sixteen scenarios with the combinations of four land cover (e.g. broad-leaved vegetation, conifers, mixed vegetation, and cultivated land) and four soil types in the first case study area (Figure 4-51). One soil type and one land cover type were assigned in each scenario. The modelling was conducted based on existing precipitation rates from five weather stations (2008-2015), the initial *ET<sub>o</sub>* and the initial soil parameters. The 2-Layer water balance was used as the selected method to compute the unsaturated flow. A water balance analysis was performed to estimate the accumulated overland boundary outflow from each scenario.

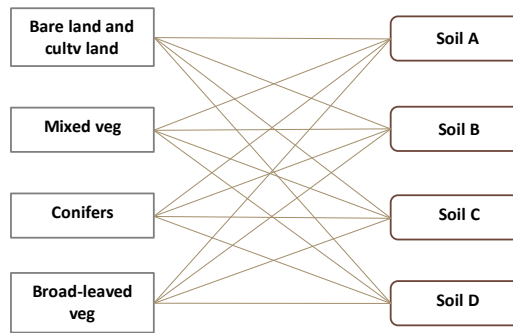
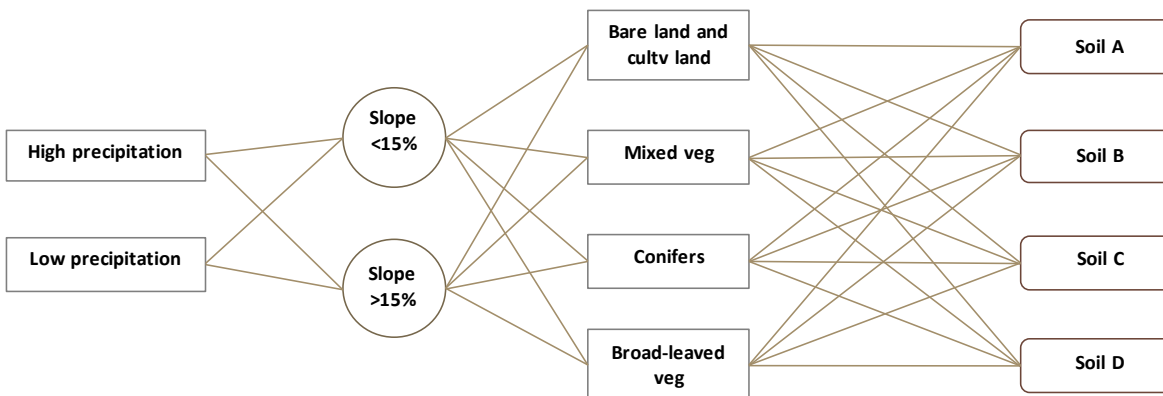


Figure 4-51 Sixteen combinations of soil and land cover types the first case study area

Based on the outcomes from the first assessment, the second analysis was performed by adding two more variables (e.g. precipitation and slope gradients) into the process (Figure 4-52). There are two categories of precipitation rates tested in this analysis; low precipitation (5 mm/day) and high precipitation (100 mm/day). New topography maps showing two slope gradient classes were added; flat-moderate slopes (0-15%) and moderate to steep (>15%). These maps were generated by dividing the existing DEM of the area into the two gradient classes. Since the first case study area are dominated by areas with steep slopes (67.1%), only approximately half of the area was included in the process (0% slope gradient was assigned in the other parts of the area). Thus, the two new topography maps cover almost 33% area with two slope conditions and around 67% of the flat area. The second analysis used the Richards equation method and the calibrated parameters (Appendix A).



Ci Kapundung upper water catchment area

Figure 4-52 Sixty-four combinations of precipitation, slope, soil and land cover classes in the first case study area

It is assumed that the results from this analysis can also be used to evaluate the MIKE SHE results from the second case study area since there are no actual parameters assigned in the model except for the soil. Soil A in the first catchment has a high composition of clay, which is similar to Soil E and F in the second catchment. Soil C and F are sandy loam, whereas Soil D and H are loam (refer to Table 4-12 and Table 4-13).

## 4.5 Decision tree diagrams and boundaries of research

In this research, series of the decision to choose particular methods in each research phase (i.e. development of land cover maps, land change simulations, and hydrological simulations) were made to answer the three research questions. Figure 4-53 - Figure 4-56 show the decision tree diagrams of the study used in the final iteration of analysis. The selected methods can be seen in the grey boxes.

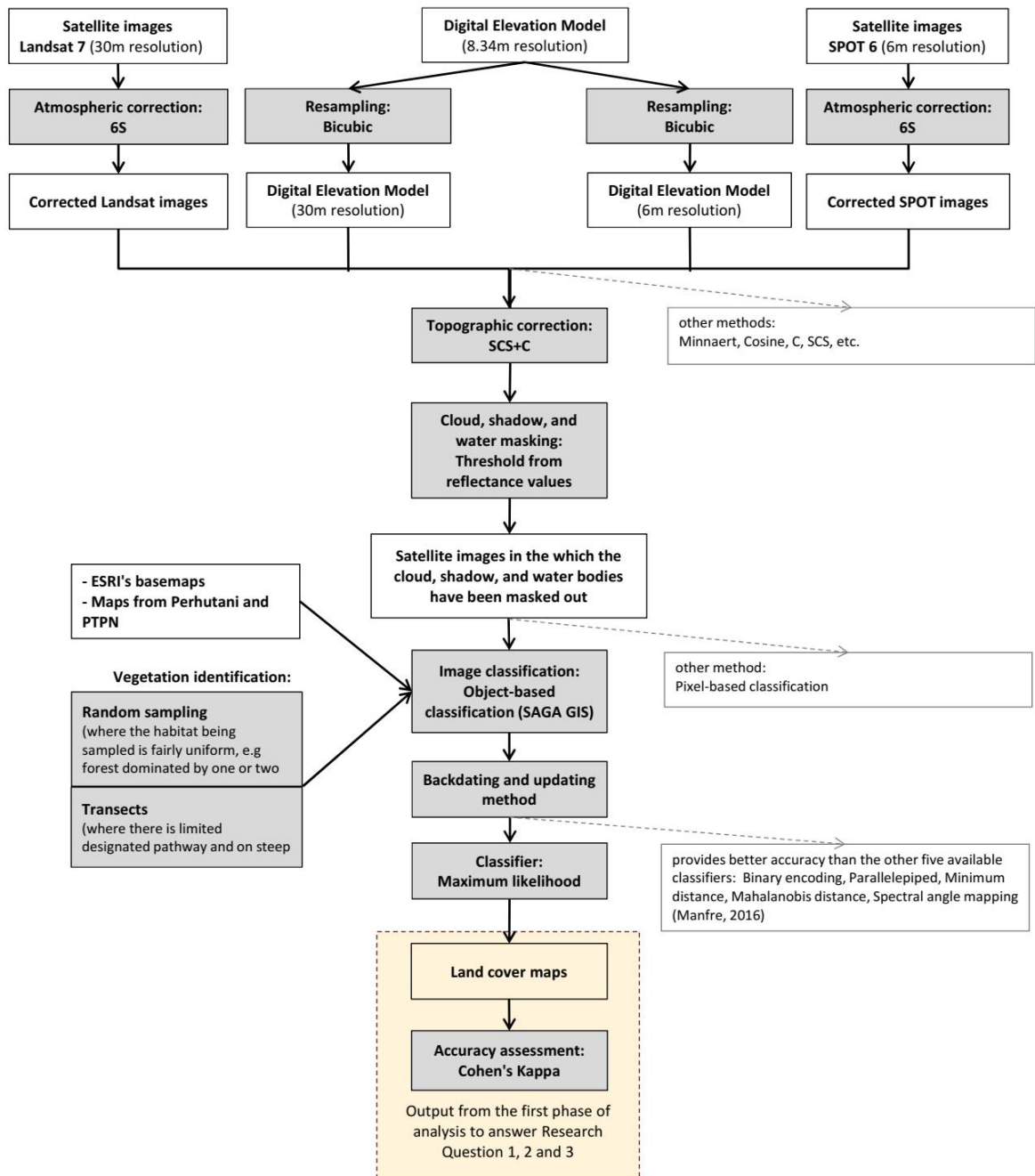


Figure 4-53 Decision tree diagram for the first phase of research

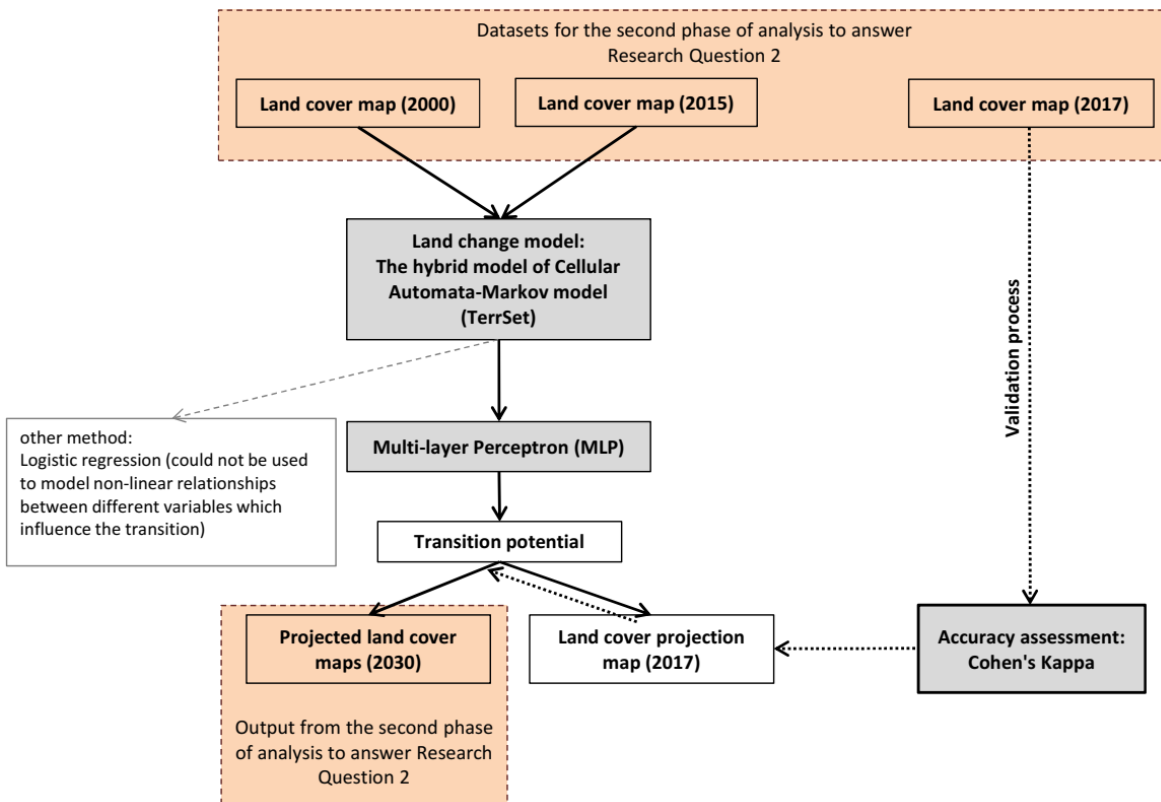


Figure 4-54 Decision tree diagram for the second phase of research to answer research question 2

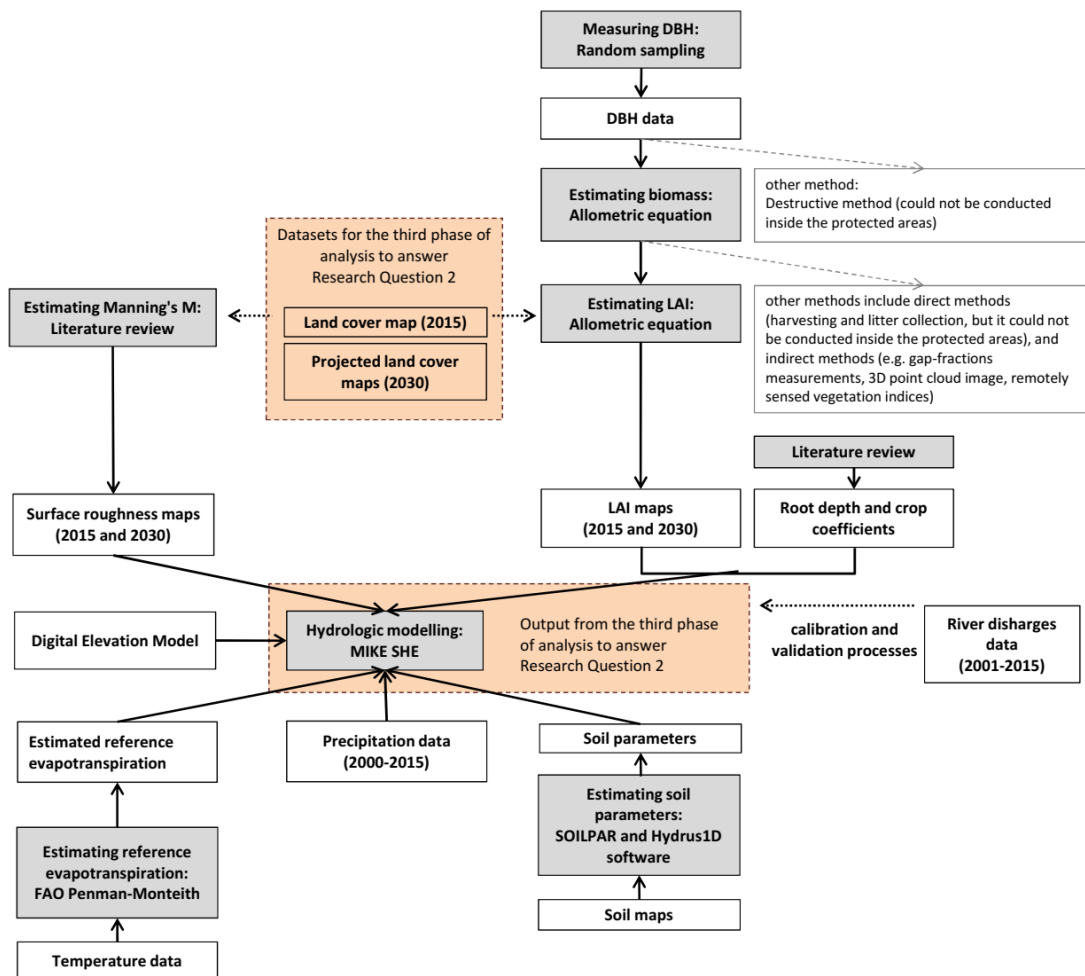


Figure 4-55 Decision tree diagram for the third phase of research to answer research question 2

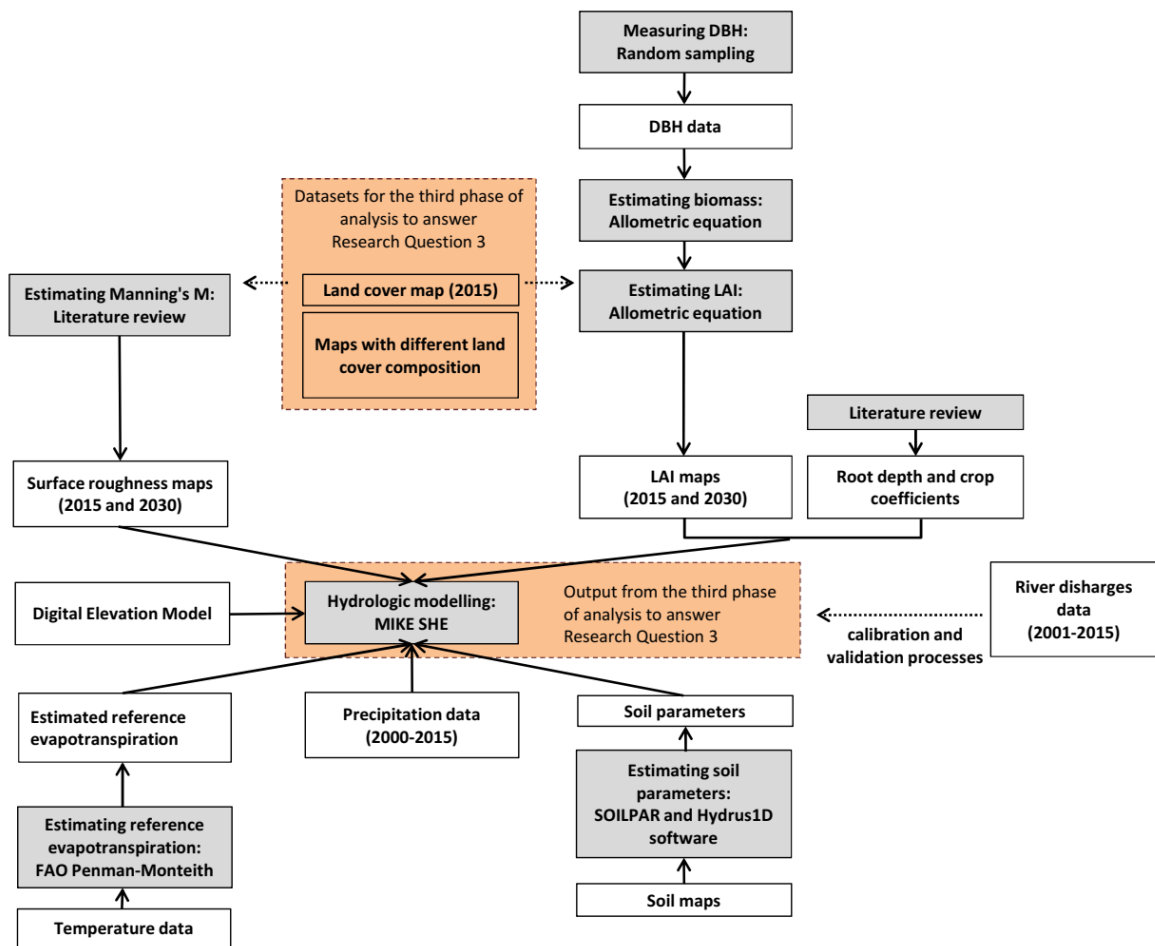


Figure 4-56 Decision tree diagram for the third phase of research to answer research question 3

## 4.6 Summary of Chapter 4

- (1) The final land cover maps for the two case study areas in 2000, 2015, and 2017 were generated from Landsat 7 and SPOT 6 satellite imagery, after 6S and SCS+C as correction methods had been applied, and the backdating and updating method (Linke et al., 2009) had been implemented. The development of land cover maps was conducted using the object-based image classification.
- (2) Moving average analysis was used to assess the impact on land cover change in the two sites (2000-2017) to flood regulation.
- (3) The CA-Markov-MLP model was coupled with MIKE SHE model to simulate the river discharges and water balance based on three future development scenarios. The application of CA-Markov to model forest cover is understudied (Ghosh et al., 2017). The capacity of vegetation to reducing runoff was analysed using the 64 hypothetical catchments.

## Chapter 5 Results

This chapter presents the outcomes from the development of land cover maps of the Ci Kapundung and Ci Sangkuy upper water catchment areas and the results from the land change and hydrologic modelling (scenario 1, 2, and 3). Results from the modelling are presented based on the way they were interpreted to answer the three research questions.

### 5.1 Land cover maps of the case study areas

The land cover maps of Ci Kapundung and Ci Sangkuy upper water catchment areas were developed using the object-based image classification. The classification accuracies were assessed, in which the results are shown in the confusion matrices. All developed land cover maps and the accuracies of image classification are presented in the following subchapters.

#### 5.1.1 Results from the image classification process of the first case study area

The object-based image classification for the first case study area was conducted three times (Figure 4-1). In the first iteration, the uncorrected and corrected land cover maps were developed using the SPOT 6 imagery taken in 2015 (Rani et al., 2017). The generated land cover maps are presented in Figure 5-1. The overall accuracies for the uncorrected and corrected maps are 74.25% and 77% respectively. The detailed confusion matrices computed for assessing the accuracy are given in Appendix B. Based on the results from this process, the second iterative process of land cover map development was conducted using SAGA GIS.

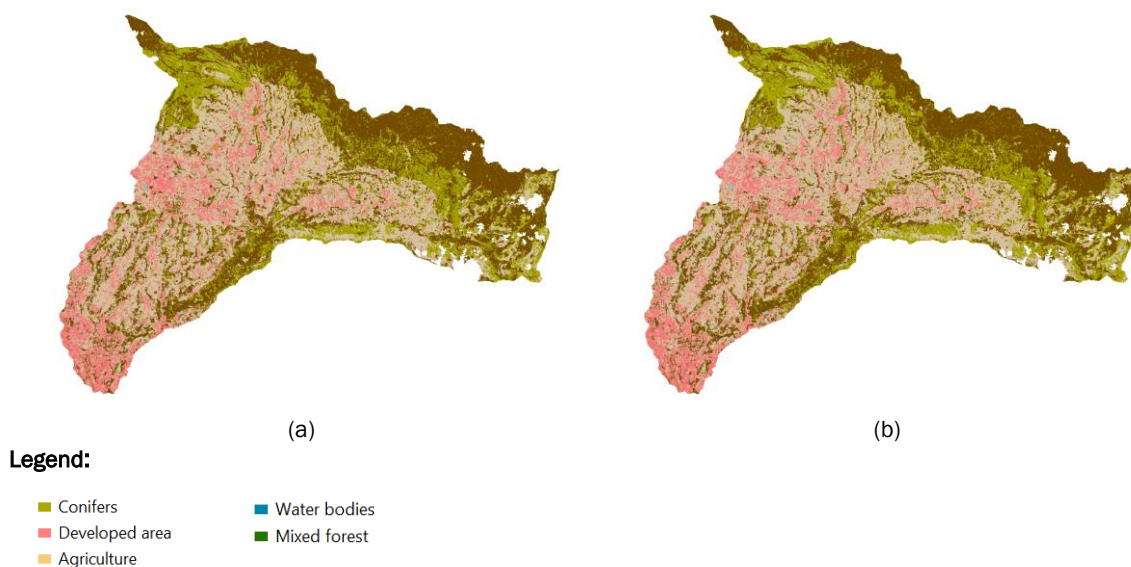
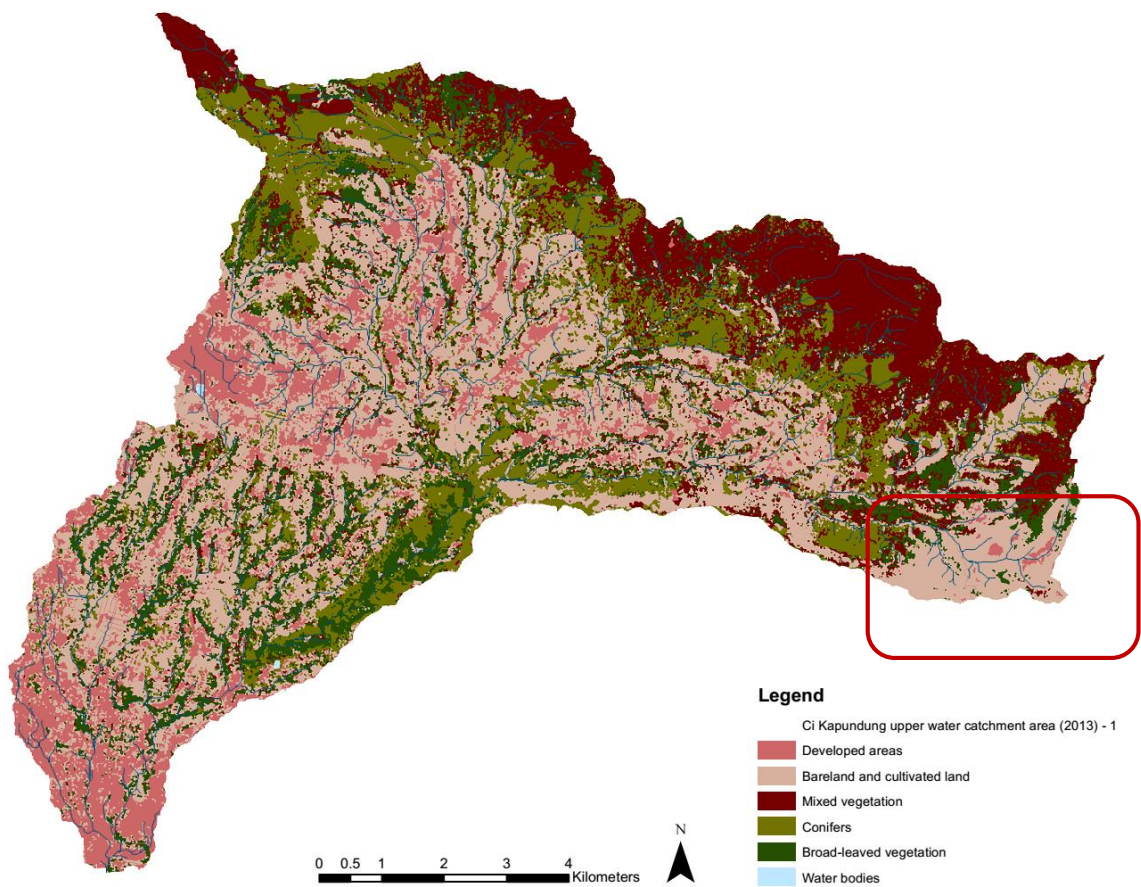


Figure 5-1 (a) The uncorrected map; (b) The corrected land cover map for the Ci Kapundung upper water catchment area in 2015 (Source: Rani et al., 2017)

In the second iteration, the 2013, 2015, and 2017 land cover maps were developed as individual maps. Although information for missing data due to the cloud coverages could be retrieved from other imagery or the auxiliary data, mixed pixels located near the clouds and/or cloud shadows were still misclassified (Figure 5-2a-c). Visible misclassified pixels can be clearly seen in the eastern part of the site in the 2013 land cover map (red box in Figure 5-2a). This part of the site was covered by a thin layer of cloud. The reflectance values were altered, thus the pixels were mostly classified as bare land.

The accuracies of image classification were assessed after the pixels containing information on water bodies, road networks, and pixels that are covered by clouds and cloud shadows were excluded. The confusion matrices for the 2013, 2015, and 2017 land cover maps of the first case study area, which were developed in the first iteration of land cover classification, are presented in Table 5-1, Table 5-2, and Table 5-3.

The overall accuracies for the 2013, 2015, and 2017 land cover maps are 78.64%, 87.40%, and 86.40% respectively. The land cover 'developed areas' has higher producer's accuracies (92.31% - 97.22%) and bare land and cultivated land has higher user's accuracies (96.75% - 97.54%), compared with other land cover types in all maps. The three vegetation types have lower producer's and user's accuracies (51.85% - 86.59%), in comparison to developed areas and bare land and cultivated land (Table 5-1 - Table 5-3).



(a)

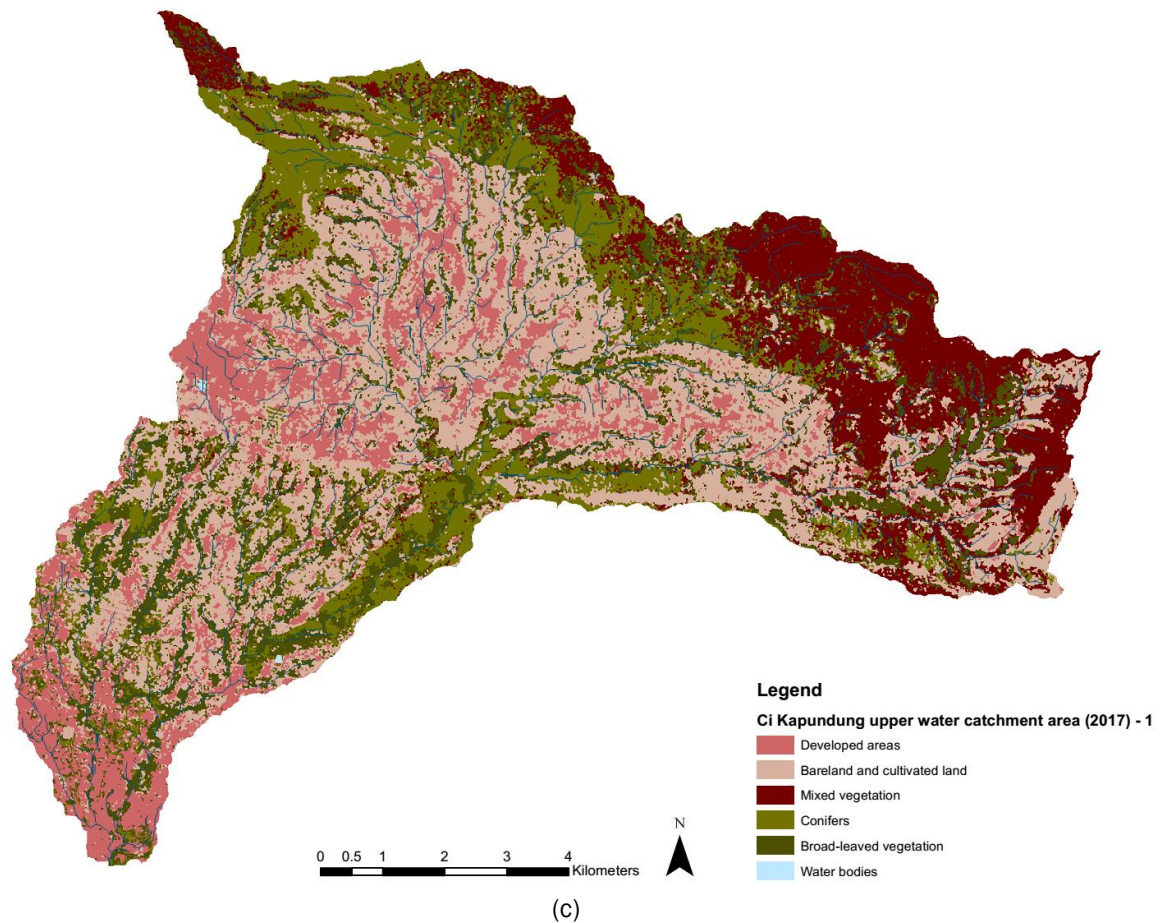
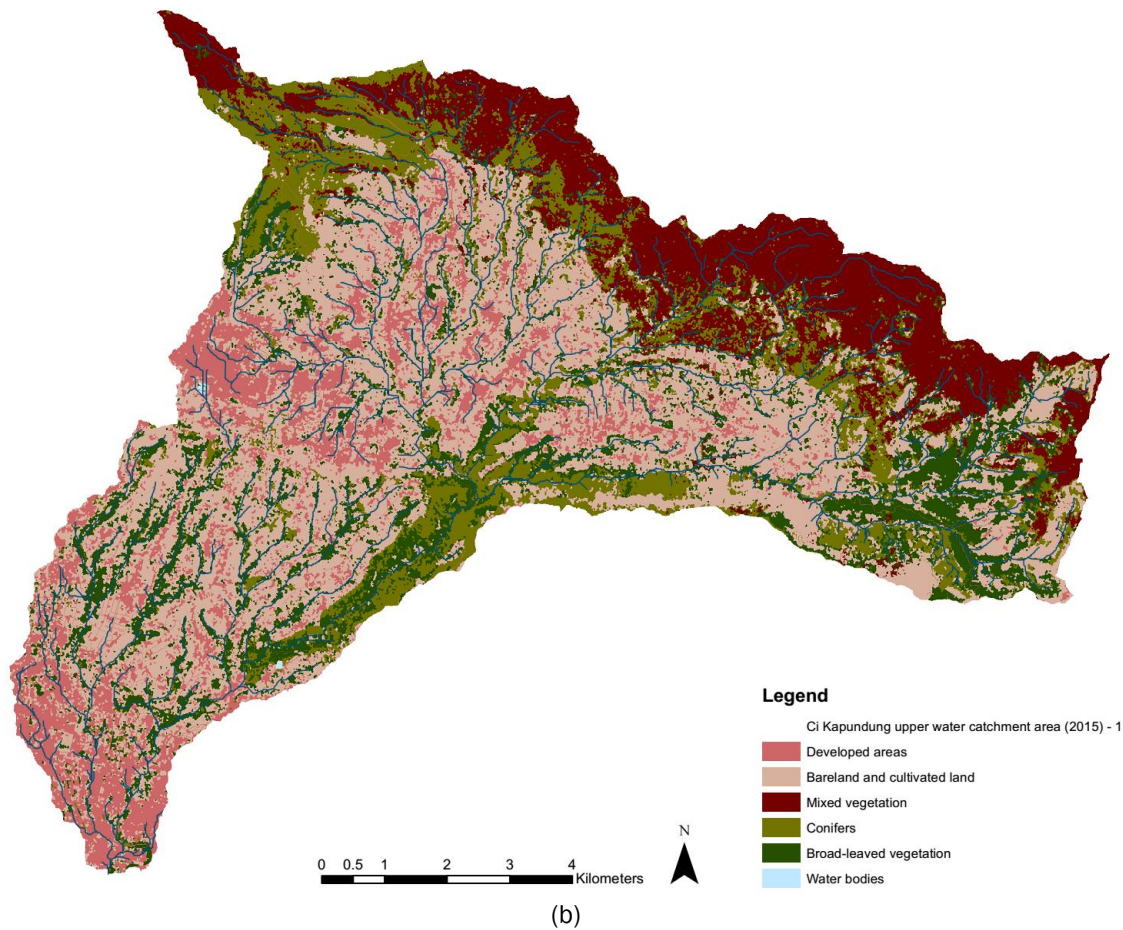


Figure 5-2 (a-c) The results from the second iteration of image classification for the Ci Kapundung upper water catchment area in 2013, 2015, and 2017 respectively using SPOT imagery



Table 5-1 Confusion matrix for the 2013 land cover map of the Ci Kapundung watershed (second iteration)

Classified image	Reference dataset						User Acc. (%)
	Dev.	Bare land cultivated land	Mixed vegetation	Conifers	Broad-leaved vegetation	Total	
Developed areas	50	8	0	0	1	59	84.75
Bare land & cultv. land	2	195	1	1	2	201	97.01
Mixed vegetation	0	6	42	24	9	81	51.85
Conifers	0	19	6	55	10	90	61.11
Broad-leaved veg.	0	5	6	7	52	70	74.29
Total	52	233	55	87	74	501	0.00
Producer Accuracy (%)	96.15	83.69	76.36	63.22	70.27	0.00	78.64
<b>Overall Accuracy: 78.64%</b>							
Kappa statistic: 0.71							

Table 5-2 Confusion matrix for the 2015 land cover map of the Ci Kapundung watershed (second iteration)

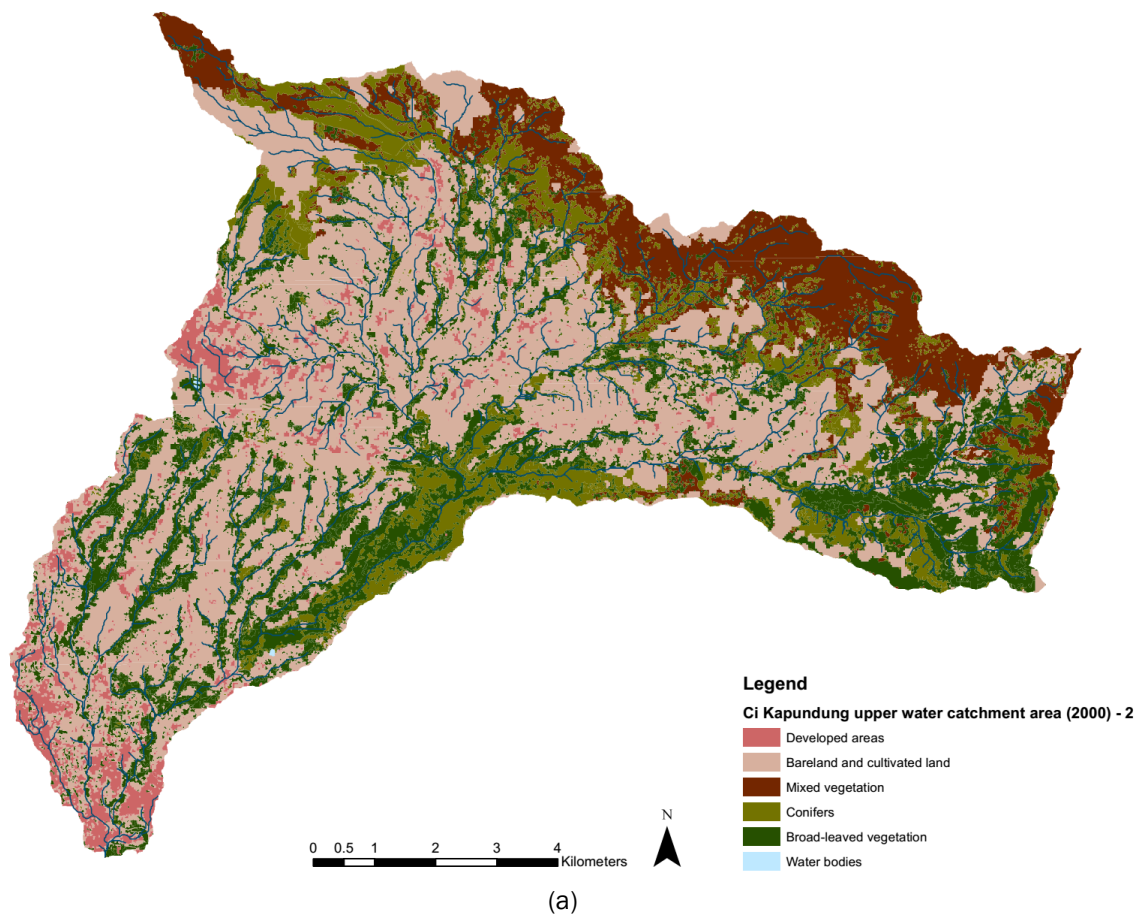
Classified image	Reference dataset						User Acc. (%)
	Dev.	Bare land cultivated land	Mixed vegetation	Conifers	Broad-leaved vegetation	Total	
Developed areas	48	13	0	0	0	61	78.69
Bare land & cultv. land	4	198	0	0	1	203	97.54
Mixed vegetation	0	0	71	9	2	82	86.59
Conifers	0	6	6	66	4	82	80.49
Broad-leaved veg.	0	6	8	4	54	72	75.00
Total	52	223	85	79	61	500	0.00
Producer Accuracy (%)	92.31	88.79	83.53	83.54	88.52	0.00	87.40
<b>Overall Accuracy: 87.4%</b>							
Kappa statistic: 0.83							

Table 5-3 Confusion matrix for the 2017 land cover map of the Ci Kapundung watershed (second iteration)

Classified image	Reference dataset						User Acc. (%)
	Dev.	Bare land cultivated land	Mixed vegetation	Conifers	Broad-leaved vegetation	Total	
Developed areas	70	7	0	0	0	77	90.91
Bare land & cultv. land	2	179	2	0	2	185	96.75
Mixed vegetation	0	0	40	16	8	64	62.50
Conifers	0	2	6	74	7	89	83.14
Broad-leaved veg.	0	5	9	2	69	85	81.17
Total	72	193	57	92	86	500	0.00
Producer Accuracy (%)	97.22	92.74	70.17	80.43	80.23	0.00	86.40
<b>Overall Accuracy: 86.4%</b>							
Kappa statistic: 0.82							

The 2013 and 2015 land cover maps generated from the second iteration of the map development process were used in the first land change modelling (LCM1). Based on the land change modelling outputs<sup>31</sup>, the third iteration of image classification was conducted. The updating and backdating method (Linke et al., 2009) was implemented to develop the 2000, 2015 and 2017 land cover maps (Figure 5-3a-c).

The accuracy assessment matrices for the land cover maps, which were developed in the second iterative image classification, are shown in Table 5-4 and Table 5-5<sup>32</sup>. The results show that the overall accuracies for the 2015 and 2017 maps are 87.42%, and 81% respectively. Developed areas, bare land and cultivated land, and broad-leaved vegetation have the producer's accuracies of more than 90% in the 2015 land cover map. Another essential point to make is the high user's accuracy of bare land and cultivated land in the 2015 land cover map (98.39%). Conifers and mixed vegetation have lower producer's accuracies in the 2017 land cover map, compared with the 2015 map. The 'bare land and cultivated land' class has the highest user's accuracy among other land cover types (92.93%).



<sup>31</sup> Results from the first iteration of land change modelling (LCM1) are presented in the third part of Subchapter 5.3  
<sup>32</sup> The number of sample is proportional to its relative area. Thus, the number for a particular class in two 2015 and 2017 images, which were developed in the second and third iteration, can be different depending on the size of the land cover class in each image.

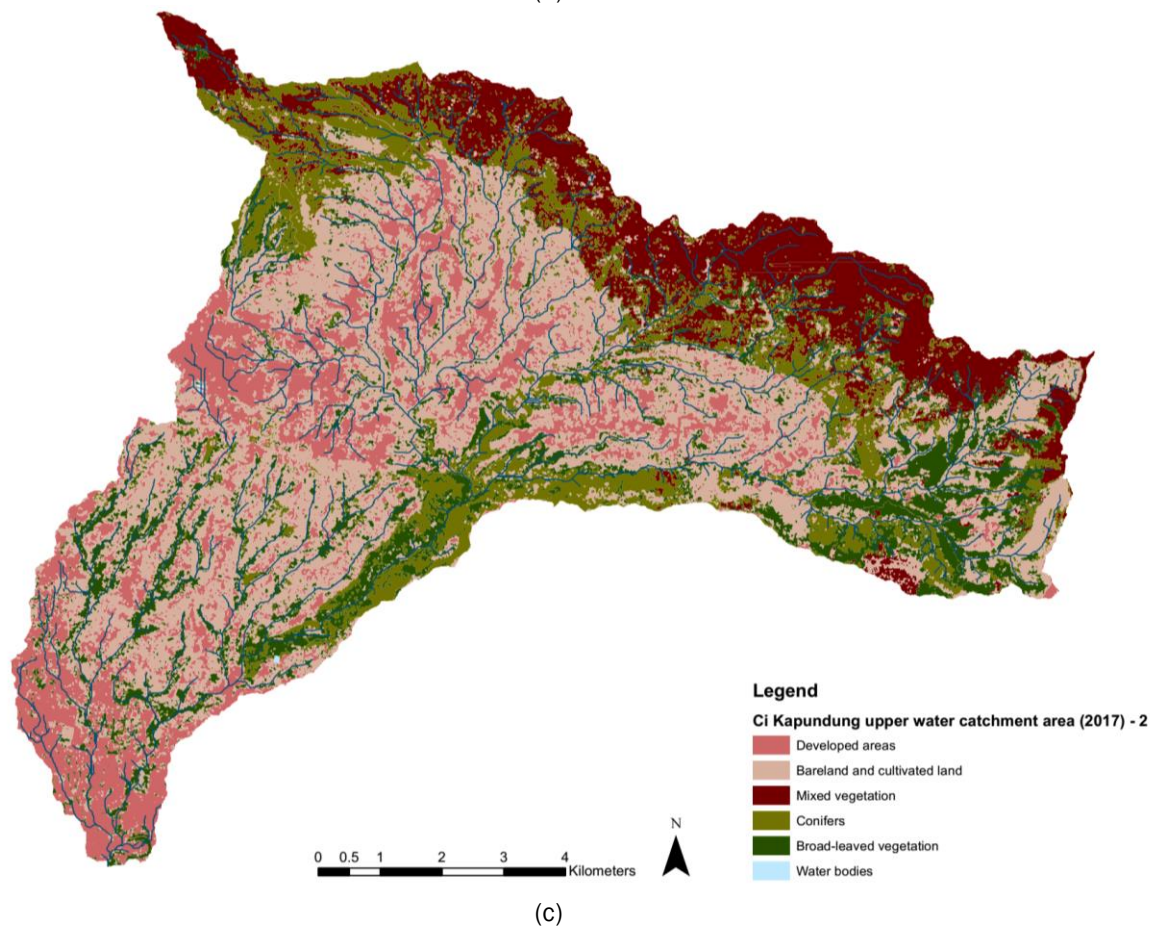
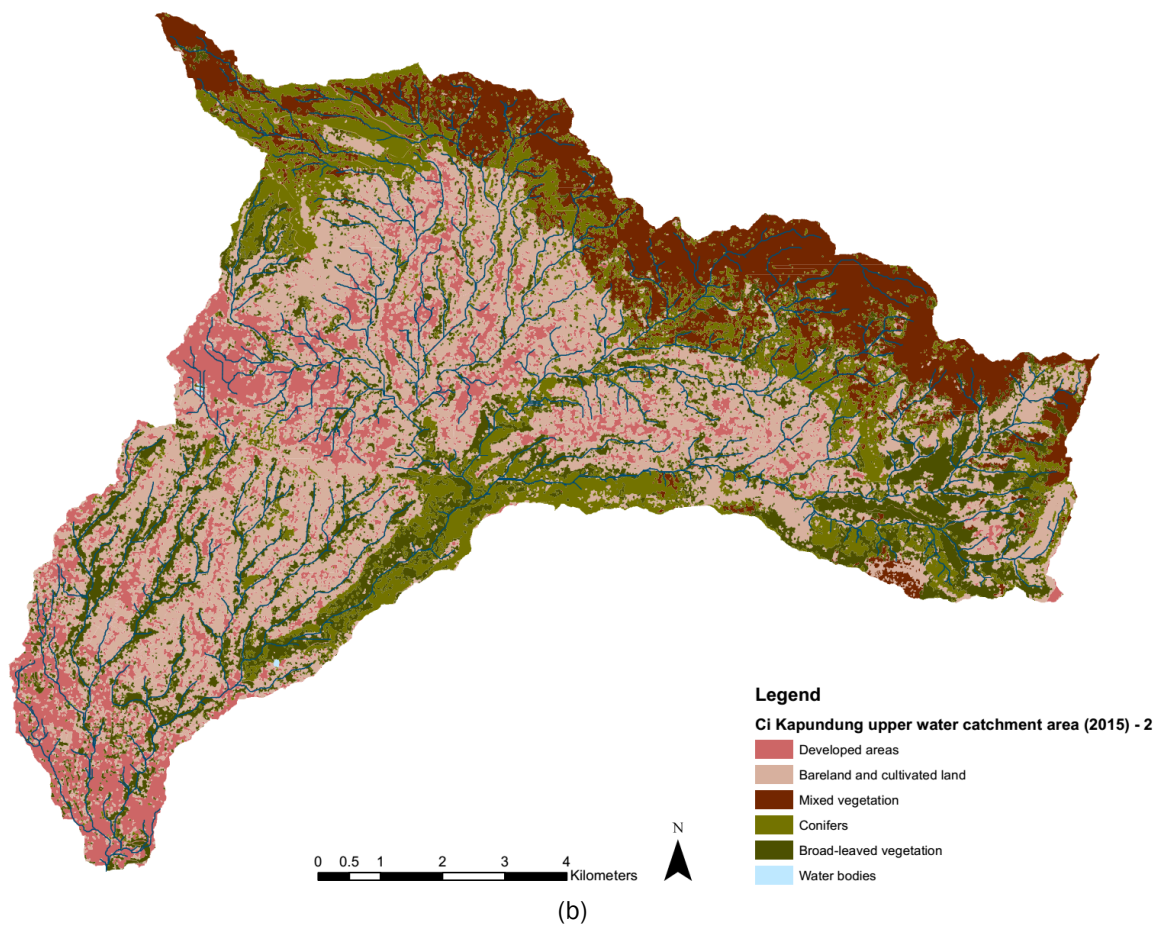


Figure 5-3 (a-c) The results from the third iteration of image classification for the Ci Kapung upper water catchment area in c.2000, 2015 and 2017 respectively using SPOT and Landsat imagery

Table 5-4 Confusion matrix for the 2015 land cover map of the Ci Kapundung watershed (third iteration)

Classified image	Reference dataset						User Acc. (%)
	Dev.	Bare land cultivated land	Mixed vegetation	Conifers	Broad-leaved vegetation	Total	
Developed areas	55	16	0	0	0	71	77.46
Bare land and cult land	3	183	0	0	0	186	98.39
Mixed vegetation	0	0	67	7	1	75	89.33
Conifers	1	0	14	62	6	83	74.70
Broad-leaved vegetation	0	0	11	4	71	86	82.56
Total	59	199	92	73	78	501	0.00
Producer Accuracy (%)	93.22	91.96	72.83	84.93	91.03	0.00	87.42
<b>Overall Accuracy: 87.42%</b>							
Kappa statistic: 0.83							

Table 5-5 Confusion matrix for the 2017 land cover map of the Ci Kapundung watershed (third iteration)

Classified image	Reference dataset						User Acc. (%)
	Dev.	Bare land cultivated land	Mixed vegetation	Conifers	Broad-leaved vegetation	Total	
Developed areas	74	24	0	0	1	99	74.75
Bare land and cult land	5	171	2	3	3	184	92.93
Mixed vegetation	0	0	55	19	1	75	73.33
Conifers	0	1	12	56	5	74	75.67
Broad-leaved vegetation	0	0	9	10	49	68	72.06
Total	79	196	78	88	59	500	0.00
Producer Accuracy (%)	93.67	87.24	70.51	63.64	83.05	0	81.00
<b>Overall Accuracy: 81.00%</b>							
Kappa statistic: 0.7496							

### 5.1.2 Results from the image classification for the second case study area

The first iteration of map development process for the second case study area was conducted to map the land cover in the southern part of the watershed. Similar methods conducted in the first iteration of Ci Kapundung watershed map development process had been performed before the object-based image classification was conducted. The uncorrected and corrected land cover map (2015) are presented in Figure 5-4. The overall accuracy for uncorrected and corrected images are 80.44% and 87.58% respectively. The confusion matrices to compute the accuracy are given in Appendix B.

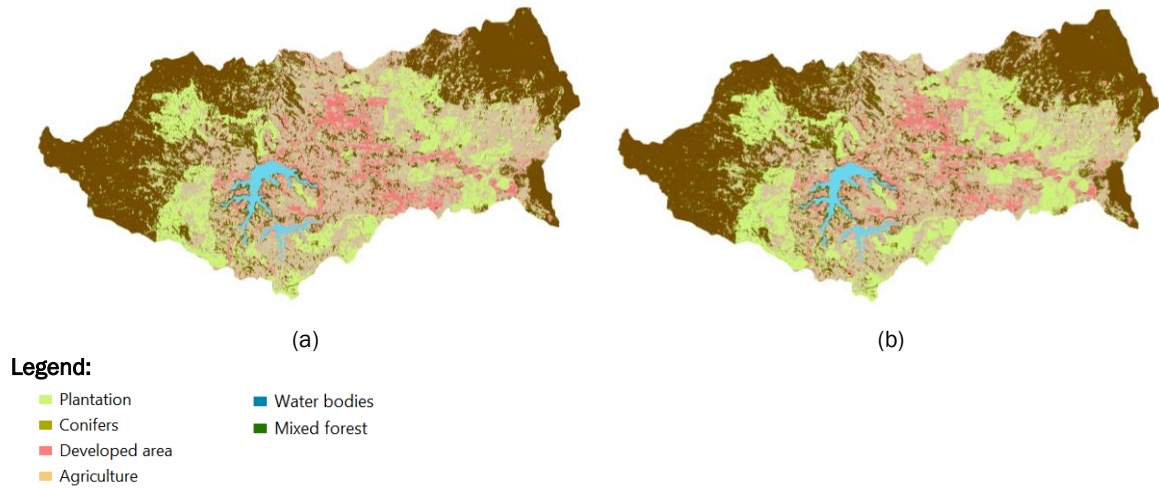
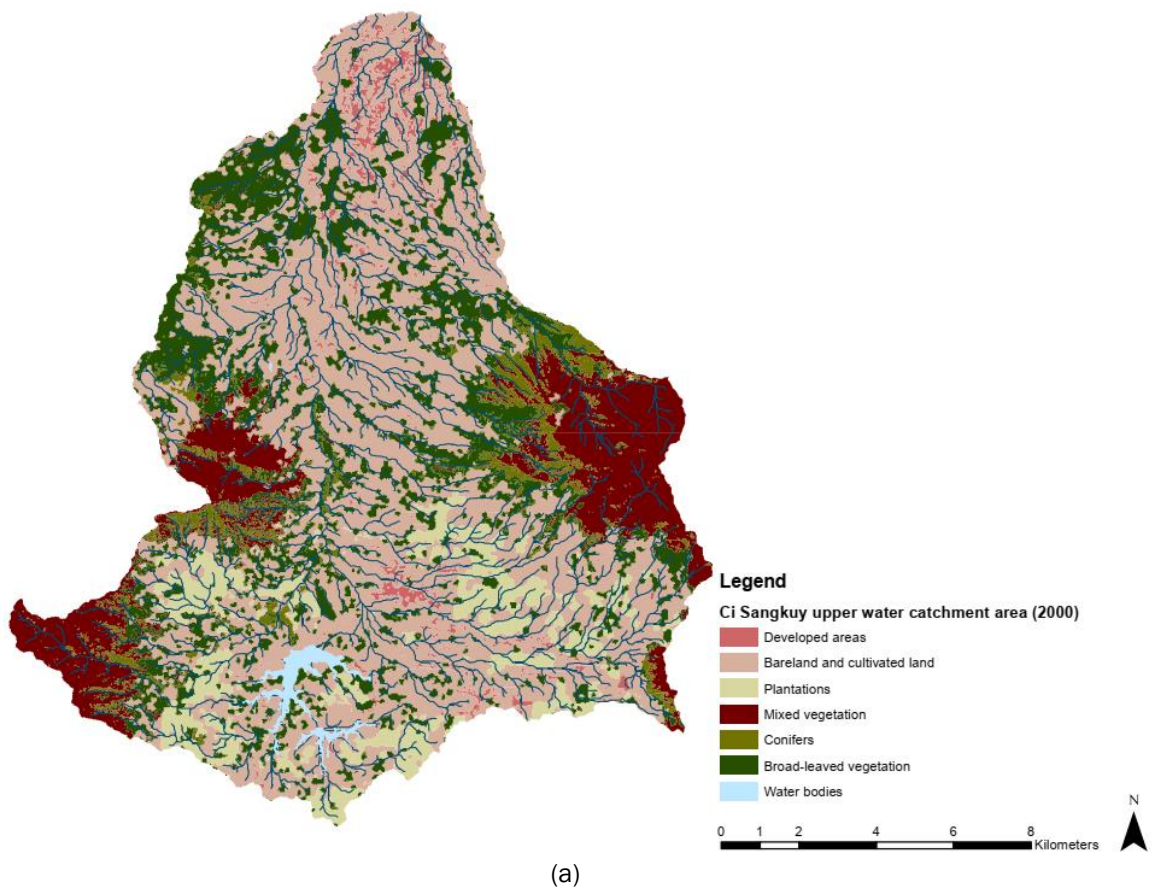
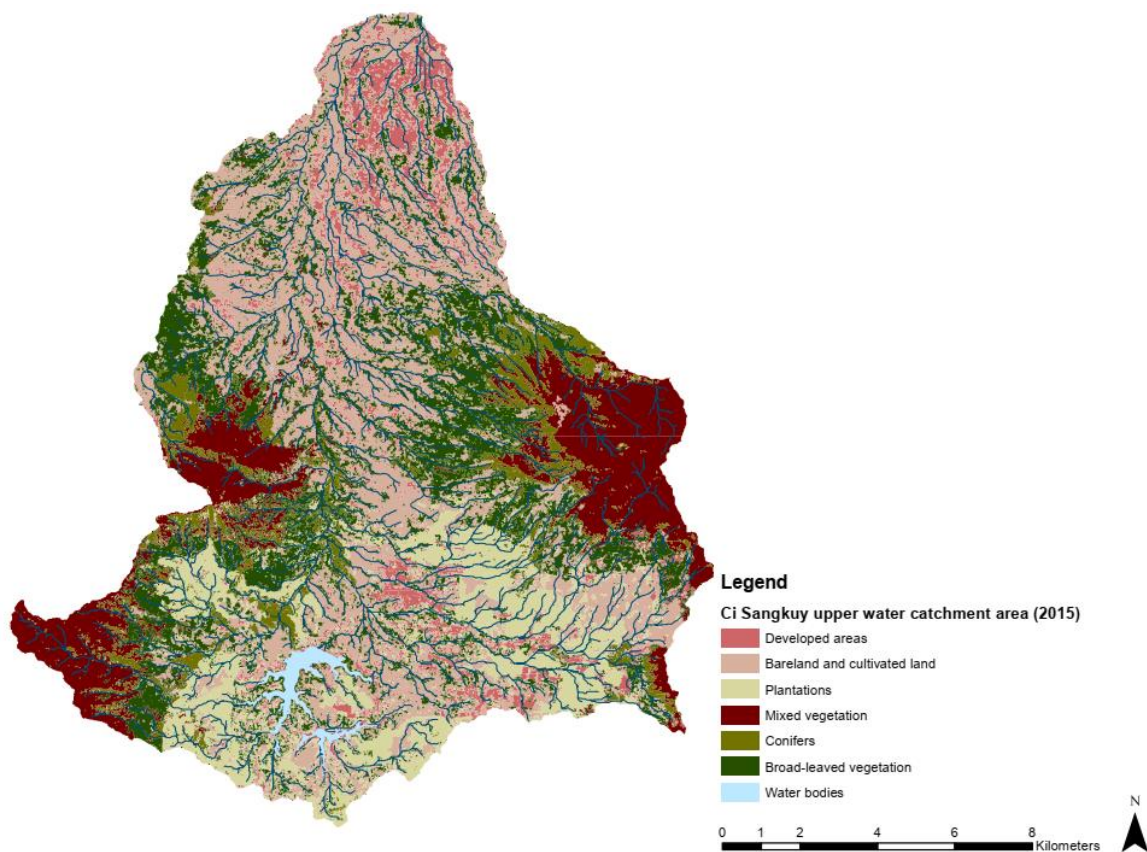


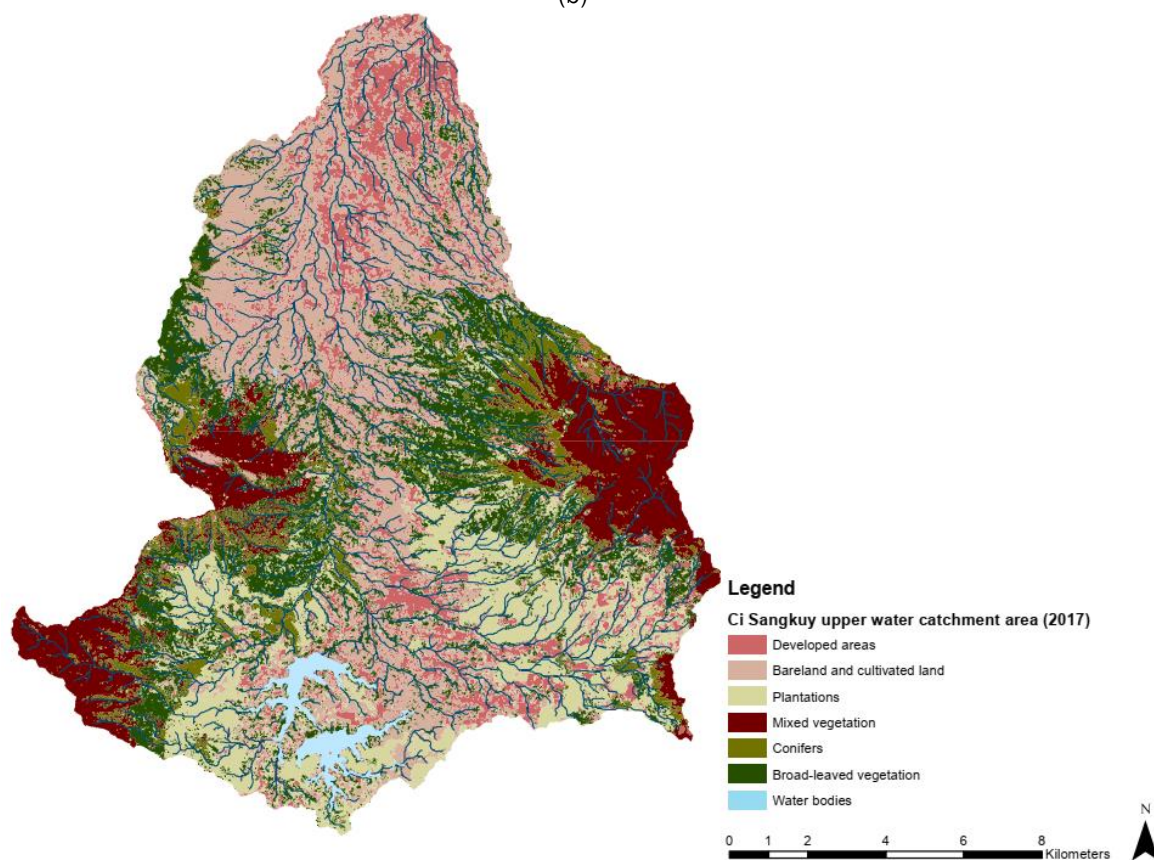
Figure 5-4 The uncorrected map; (b) The corrected land cover map for the Ci Sangkuy upper water catchment area in 2015 (Source: Rani et al., 2017)

The updating and backdating method (Linke et al., 2009) was also used in the second iterative process to develop land cover maps of the second case study area (Figure 5-5). The accuracies of land cover maps (2015 and 2017) for the second case study area are presented in Table 5-6 and Table 5-7.





(b)



(c)

Figure 5-5 (a-c) The results from the second iteration of image classification for the Ci Sangkuy upper water catchment area in c.2000, 2015 and 2017 respectively using SPOT and Landsat imagery

The overall accuracies for the 2015 and 2017 land cover maps of the Ci Sangkuy upper watershed are 74.80% and 75.40% respectively. 'Plantations' is the class which has the highest producer accuracy among all land cover classes according to the confusion matrices of all maps of the two case study areas. Bare land and cultivated land and mixed vegetation are two land cover types that have the highest user accuracies among all classes. Conifers class has the lowest user accuracy, which may be caused by the relatively similar range of reflectance values of other forest types (i.e. mixed and broad-leaved woodlands).

Table 5-6 Confusion matrix for the 2015 land cover map of the Ci Sangkuy watershed

Classified image	Reference dataset							User Acc. (%)
	Dev.	Bare-cultv land	Plantations	Mixed veg.	Conifers	Broad-leaved veg.	Total	
Developed areas	24	21	0	0	0	0	45	0.5333
Bare land & cultv. land	11	153	0	2	1	2	169	0.9053
Plantations	0	15	48	1	1	1	66	0.7273
Mixed vegetation	0	1	0	68	1	4	74	0.9189
Conifers	0	0	0	24	10	1	35	0.2857
Broad-leaved vegetation	0	3	0	32	5	71	111	0.6396
Total	35	193	48	127	18	79	500	0
Producer Accuracy (%)	0.6857	0.7927	1	0.5354	0.5556	0.8987	0	0.748
<b>Overall Accuracy: 74.80%</b>								
Kappa statistic: 0.675								

Table 5-7 Confusion matrix for the 2017 land cover map of the Ci Sangkuy watershed

Classified image	Reference dataset							User Acc. (%)
	Dev.	Bare-cultv land	Plantations	Mixed veg.	Conifers	Broad-leaved veg.	Total	
Developed areas	35	46	0	1	0	0	82	0.4268
Bare land & cultv. land	0	134	4	2	0	2	142	0.9437
Plantations	0	16	56	1	0	1	74	0.7567
Mixed vegetation	0	0	0	68	0	3	71	0.9577
Conifers	0	0	0	20	10	1	31	0.3226
Broad-leaved vegetation	0	1	0	21	4	74	100	0.7400
Total	35	197	60	113	14	81	500	0
Producer Accuracy (%)	1	0.6802	0.9333	0.6018	0.7143	0.9136	0	0.754
<b>Overall Accuracy: 75.40%</b>								
Kappa statistic: 0.689								

## 5.2 The impact of land cover change in the two case study areas on flood regulation in Bandung Basin

The alteration of land cover and flood regulation in the two case study areas have been examined to answer the first research question: "How does the land cover alteration in Ci Kapundung and Ci Sangkuy upper water catchment areas affect flood regulation in Bandung

Basin?”. This subchapter provides an insight into how the land cover has changed in the case study areas. The characteristics of floods and the effective rainfall to cause floods in the Bandung Basin are also presented to describe the existing condition of flood regulation in the region. Land cover alteration in each watershed has been assessed to determine whether the land change was the only influential factor to the occurrence of flood in the basin, or if there is another factor (e.g. rainfall trend).

### 5.2.1 Land cover change assessments

The land change of Ci Kapundung upper water catchment area from 2013-2015 was assessed in the first iteration of land change modelling (LCM 1). Based on the results, the second iteration of modelling for the two sites was conducted using the 2000 and 2015 land cover maps (LCM 2).

#### (1) Land cover change in the Ci Kapundung upper water catchment area

The result from LCM 1 for the first case study area (2013-2015) is presented in Figure 5-6. It can be seen that the land cover that changed the most is bare land and cultivated land. The coverage of developed areas increased from 12.66% in 2013 to 13.48% in 2015. Bare land and cultivated land also had a bigger area from approximately 37.61% to 40.09% within the same period of simulation.

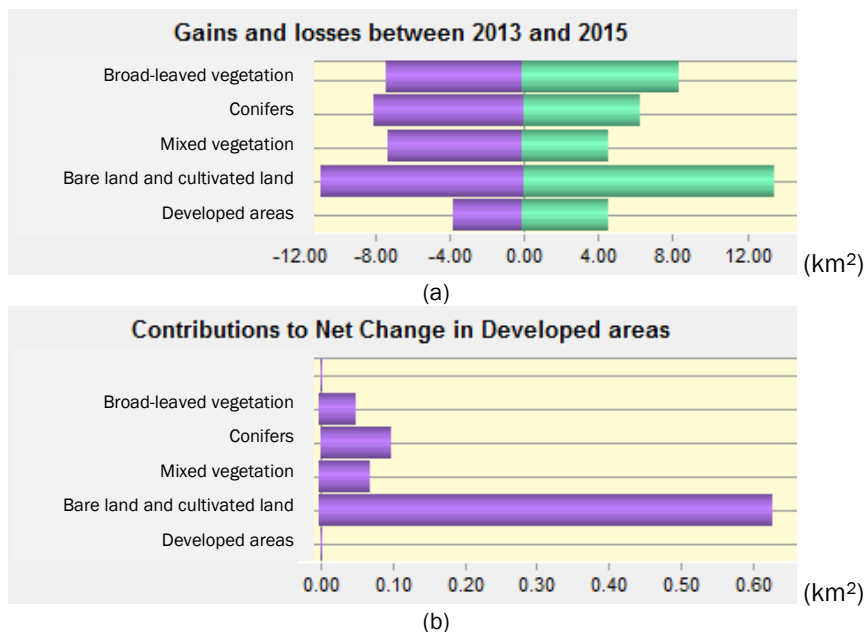


Figure 5-6 (a) Gains and losses of six land cover types in the first case study area between 2013 and 2015 (km<sup>2</sup>); (b) the contribution of all land cover types to the increasing developed areas in 2015 (Source: Analysis using the LCM module of Terrset)

In LCM 2, the land cover alteration of the first case study area within the period of 2000-2015 was assessed (Figure 5-7). There was increasing coverage of developed areas from 4.93% in 2000 to 14.90% in 2015. The composition of bare land and cultivated land in 2015 has also



risen from 31.66% to 36.82%. Higher coverages of conifers were identified in 2015 with 16.30% compared with the condition in 2000 (i.e. 14.42%). In contrary, the compositions of broad-leaved vegetation and mixed vegetation decreased within the same period. A visualisation of six land cover transitions from 2000 to 2015 in the case study area is presented in Figure 5-8.

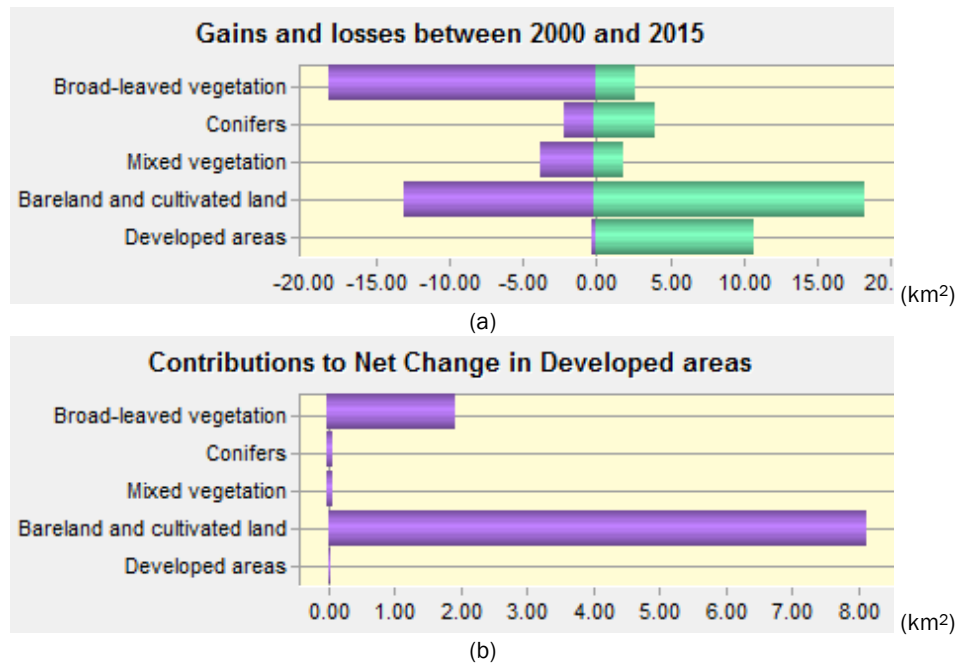


Figure 5-7 (a) Gains and losses of six land cover types in the first case study area between 2000 and 2015 (km<sup>2</sup>); (b) the contribution of all land cover types to the increasing developed areas in 2015 (Source: Analysis using the LCM module of Terrset)

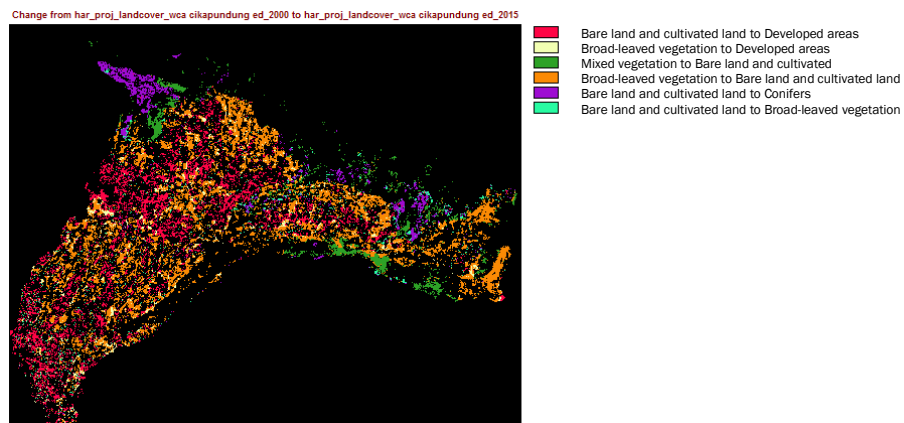


Figure 5-8 Change map of the first case study area (2000-2015)

## (2) Land cover change in the Ci Sangkuy upper water catchment area

The analysis of land cover change in the second case study area has been conducted using the land cover maps in 2000 and 2015. The results indicate that the coverage of developed areas increased from 3.40% in 2000 to 8.97% in 2015. Bare land and cultivated land had the highest rate of loss among all land cover types, and it contributed the most to the increasing percentage of developed areas in 2015 (Figure 5-9). Although the coverage of broad-leaved vegetation

decreased by approximately 20 km<sup>2</sup> due to the land change to developed areas and plantations outside the forests, the coverage increased particularly inside the forest (Figure 5-5). A land change map showing nine land cover transitions on the site is illustrated in Figure 5-10.

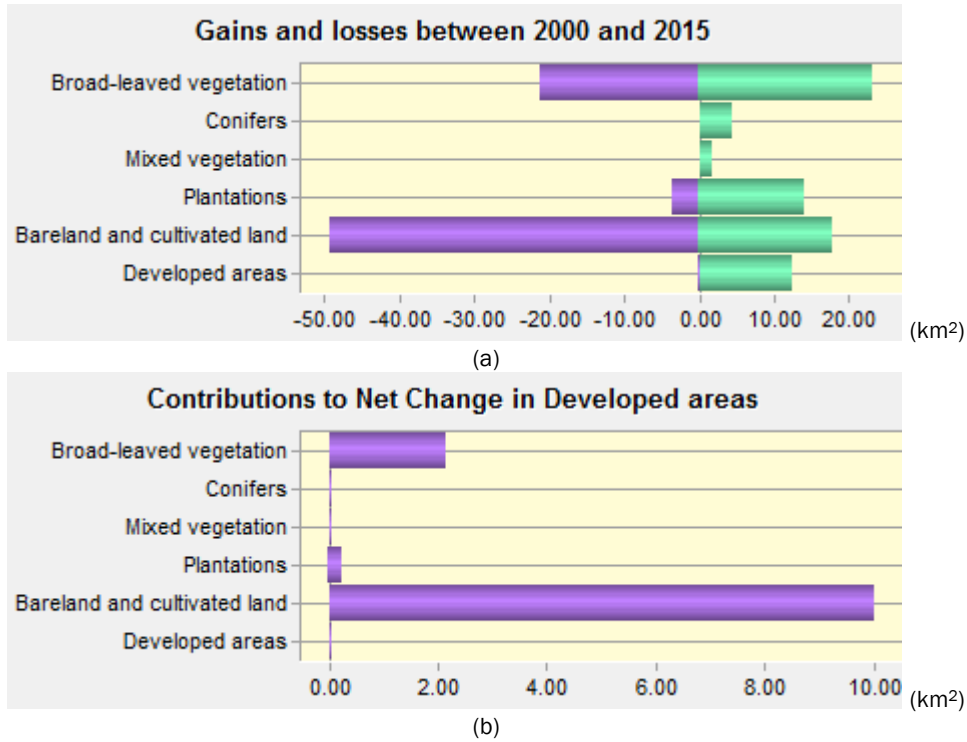


Figure 5-9 Gain and losses of six land cover types in the second case study area between 2000 and 2015 (km<sup>2</sup>); (b) the contribution of all land cover types to the increasing developed areas in 2015 (Source: Analysis using the LCM module of Terrset)

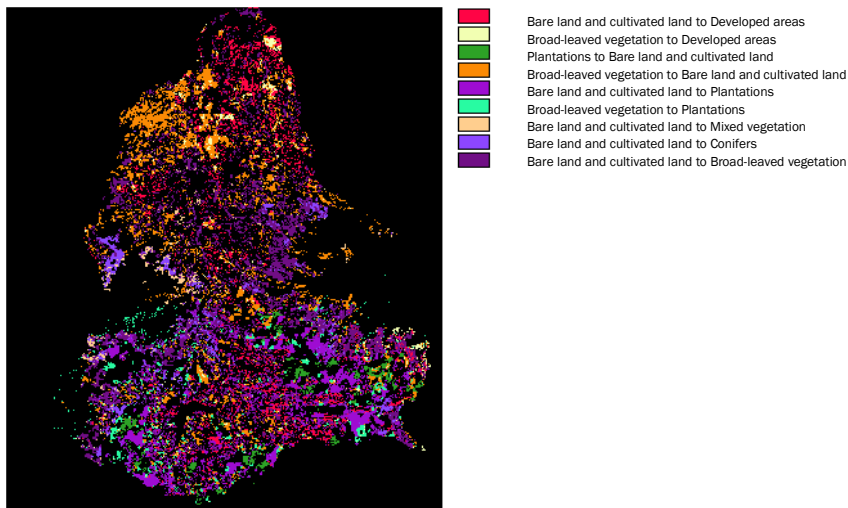


Figure 5-10 Change map of the second case study area (2000-2015)

### 5.2.2 Flood frequency analysis

In this study, the flood frequency of Ci Tarum River was assessed to analyse the possible flood discharges and return periods, which may occur in the Bandung Basin in the future. The

assessment was conducted using Log-Pearson Type III analysis based on the daily average maximum Ci Tarum river discharge data (1974-2016).

The result of flood frequency analysis can be seen in Table 5-8 and Figure 5-10. During the analysis process, the unit for discharge was converted to cfs (cubic feet per second). The unit, then, was converted back to m<sup>3</sup>/s. Floods with river discharges of approximately 292.34 m<sup>3</sup>/s and 374.81 m<sup>3</sup>/s have return periods of two and five years respectively. A discharge of 429.25 m<sup>3</sup>/s has a possibility not to be equalled or exceeded in nine years out of ten. Floods with a return period of 25 and 50 years are projected to occur with river discharges of 498.16 m<sup>3</sup>/s and 549.56 m<sup>3</sup>/s respectively, while the discharge of 601.39 m<sup>3</sup>/s is indicated as one per cent high flood or the hundred-year flood. It should be noted that the calculation of flood frequency in this study was conducted only based on the Ci Tarum River discharges from 1974 to 2016 using the Log-Pearson Type III analysis. Different time length used in the estimation or method might affect the outcomes (e.g. JICA (2010)).

Table 5-8. The predicted return periods and discharges of Ci Tarum River

Return Period (Tr)	Q (cfs)	Q (m <sup>3</sup> /s)
2	10,323.92	292.34
5	13,236.35	374.81
10	15,158.97	429.25
25	17,592.35	498.16
50	19,407.43	549.56
100	21,237.85	601.39
200	23,094.15	653.95

### 5.2.3 Flood discharge analysis

The flood discharges of Ci Kapundung and Ci Sangkuy Rivers were estimated to determine the river discharge of each river, which has a high possibility to affect the occurrence of floods in the Bandung Basin in the future. During the analysis, the bankfull/ flood discharge of Ci Tarum River, as well as the discharges from the two case study areas at the day when floods occurred in the basin (2008-2015) were assessed.

Two cross-sections of the Ci Tarum River have been generated using DEM, and the cross-sectional area (A) of the river was calculated. Hydraulic radius (R) was calculated based on the cross-sectional area (A) and wetted perimeter (wp). The slope of the river bed (S) for the Ci Tarum River is approximately 0.02 (Brahmantyo, 2005). The Manning resistance coefficient (n) for winding natural streams with rocky beds and rivers with variable sections and some vegetation along banks is 0.040-0.050 (Chow, Maidment, & Mays, 1988). In this study, the n value used in this analysis is 0.050. The bankfull width ( $w_{bkf}$ ) and the bankfull depth ( $d_{bkf}$ ) were estimated according to the cross-sections.

The cross-sections of the Ci Tarum River and the detailed estimation of flood discharge at bankfull ( $Q_{bki}$ ) are provided in Appendix C. From the two samples of bankfull discharge estimations, the initial value for the flood discharge for the Ci Tarum River is approximately 187.4 m<sup>3</sup>/sec – 195.4 m<sup>3</sup>/sec.

The analysis of river discharges from the Ci Kapundung and Ci Sangkuy upper water catchment areas (i.e. Q1 and Q2 respectively), and from other catchments in the Bandung Basin (Q3) during the flood events in the Bandung Basin (2008-2015) has been conducted. The highest Ci Tarum River discharge during the flood events was 544.9 m<sup>3</sup>/s on 20 March 2010. On this day, the daily discharge of Ci Sangkuy River that flowed outside the upper catchment (Q2) was 96 m<sup>3</sup>/s, the highest discharge during all flood events in 2008-2015. The Ci Kapundung river discharge on the same day (Q1) was recorded at 4.08 m<sup>3</sup>/s. River discharge from other catchments in the basin (Q3) was 444.82 m<sup>3</sup>/s.

During the flood event on 9 December 2015, Ci Kapundung has the highest river discharge at 14.3 m<sup>3</sup>/s. On the same day, the daily Ci Sangkuy river discharge was 6.07 m<sup>3</sup>/s. However, the basin was still flooded with the Ci Tarum river discharge recorded at 200.8 m<sup>3</sup>/s.

In this study, the thresholds of flood discharges from the two case study areas that were used to assess the results from the MIKE SHE model have been defined. The estimated daily river discharges for the Ci Kapundung River and the Ci Sangkuy River flowing from the upper catchments are 14.3 m<sup>3</sup>/s and 96 m<sup>3</sup>/s respectively. It is assumed that the daily river discharges from other catchments in the basin will not exceed 173.1 m<sup>3</sup>/s and 91.4 m<sup>3</sup>/s when simulating the river discharge from the first and the second case study area, respectively.

#### 5.2.4 Effective rainfall analysis

##### (1) Calculating the Ci Tarum baseflow

The Ci Tarum baseflow has been estimated following the guidelines to assess the stream flow duration from the Oregon State University, which has been previously described in Subchapter 4.3. Based on the samples of the Ci Tarum streamflow data within the period of 2008-2015 (Table 5-9), the streamflow was ranked according to the probability to exceed a certain percentage, and the Ci Tarum baseflow was estimated. Table 5-9 and the flow duration curve (Figure 5-11) show that from the assessment on flow duration of Ci Tarum river discharge (2008-2015), the baseflow for the river is 12.3 m<sup>3</sup>/s.

Table 5-9. Samples of the Ci Tarum streamflow data and the rank within the period of 2008-2015; Source for the streamflow data: PSDA (Pusat Sumber Daya Air/ Water Resource Management in West Java province).

Date	Streamflow (m <sup>3</sup> /s)	Rank	Percent Exceeded
20/03/2010	544.9	1	0.034211427
21/03/2010	542.5	2	0.068422853
24/03/2010	542.5	3	0.10263428
09/12/2010	542.5	4	0.136845706
04/12/2010	537.8	5	0.171057133
10/12/2010	537.8	6	0.20526856
19/02/2010	530.9	7	0.239479986
11/12/2010	530.8	8	0.273691413
22/03/2010	519.2	9	0.30790284
08/12/2010	516.9	10	0.342114266
...	...	...	...
27/09/2014	12.3	2629	89.94184057
18/10/2014	12.3	2630	89.976052
23/10/2014	12.3	2631	90.01026343
10/09/2015	12.3	2632	90.04447485
28/10/2015	12.3	2633	90.07868628
...	...	...	...
21/09/2008	7.54	2913	99.65788573
24/07/2008	7.36	2914	99.69209716
26/07/2008	7.36	2915	99.72630859
29/07/2008	7.19	2916	99.76052001
22/09/2008	7.19	2917	99.79473144
23/09/2008	7.19	2918	99.82894287
02/11/2013	7.15	2919	99.86315429
27/07/2008	7.01	2920	99.89736572
17/10/2011	6.79	2921	99.93157715
31/05/2013	0.22	2922	99.96578857
MAX VALUE	<b>544.9</b>	<b>2922</b>	<b>100</b>
MIN VALUE	<b>0.22</b>		<b>0</b>
COUNT	<b>3288</b>		

Note: the highlighted row shows the estimated river discharge that is equal to baseflow due to the occurrence of 90% of the time (2008-2015).

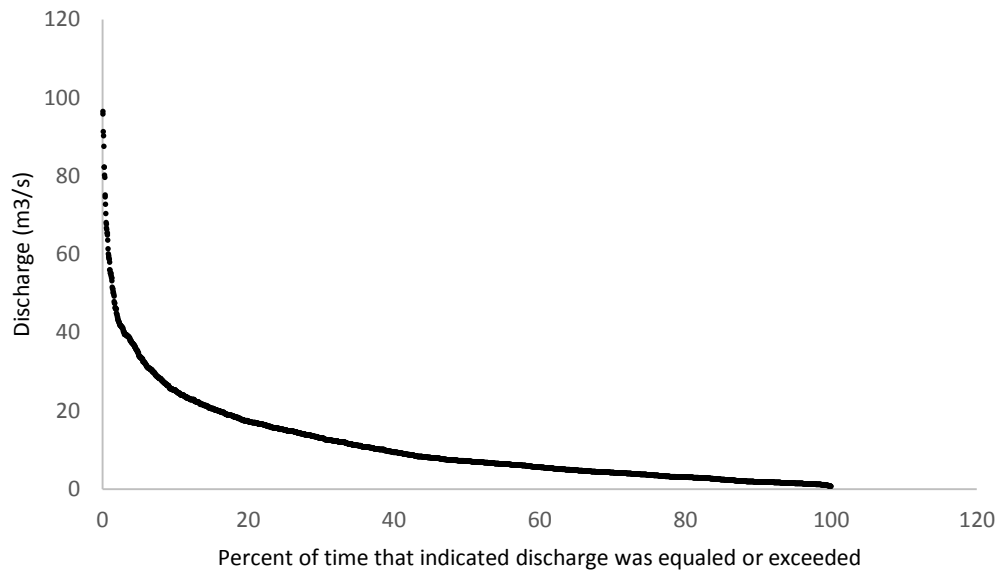
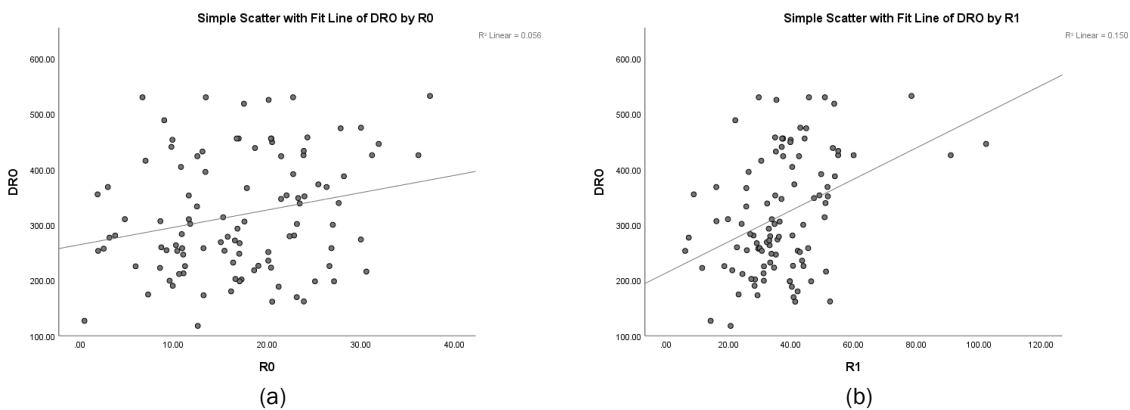


Figure 5-11 Flow duration curve for the Ci Tarum River (2008-2015)

Following the diagram of workflow to estimate the Ci Kapundung and Ci Sangkuy flood discharge (Subchapter 4.3), the direct runoff to the Ci Tarum River, which has high possibility to cause floods in the Bandung Basin can be estimated based on the calculations of the Ci Tarum bankfull discharge ( $Q_{bkf}$ ) and the Ci Tarum baseflow. According to the previous calculations, the Ci Tarum bankfull discharge ( $Q_{bkf}$ ) is approximately  $187.4 \text{ m}^3/\text{sec} - 195.4 \text{ m}^3/\text{sec}$ , whereas the Ci Tarum baseflow is  $12.3 \text{ m}^3/\text{s}$ . Therefore, the overland flow to the Ci Tarum River that has an effect on the occurrence of floods in the Bandung Basin ( $OF_{bkf}$ ) is estimated at  $175.1 \text{ m}^3/\text{sec} - 183.1 \text{ m}^3/\text{sec}$ .

The regression models have been generated to show the relation between direct runoff (DRO) and the rainfall events in the Bandung basin during the day the flood events occurred in the basin ( $R_0$ ), until 6 consecutive days before the events ( $R_6$ ), within the period of 1 January 2008 – 31 December 2015. The correlation diagrams can be seen in Figure 5-12.



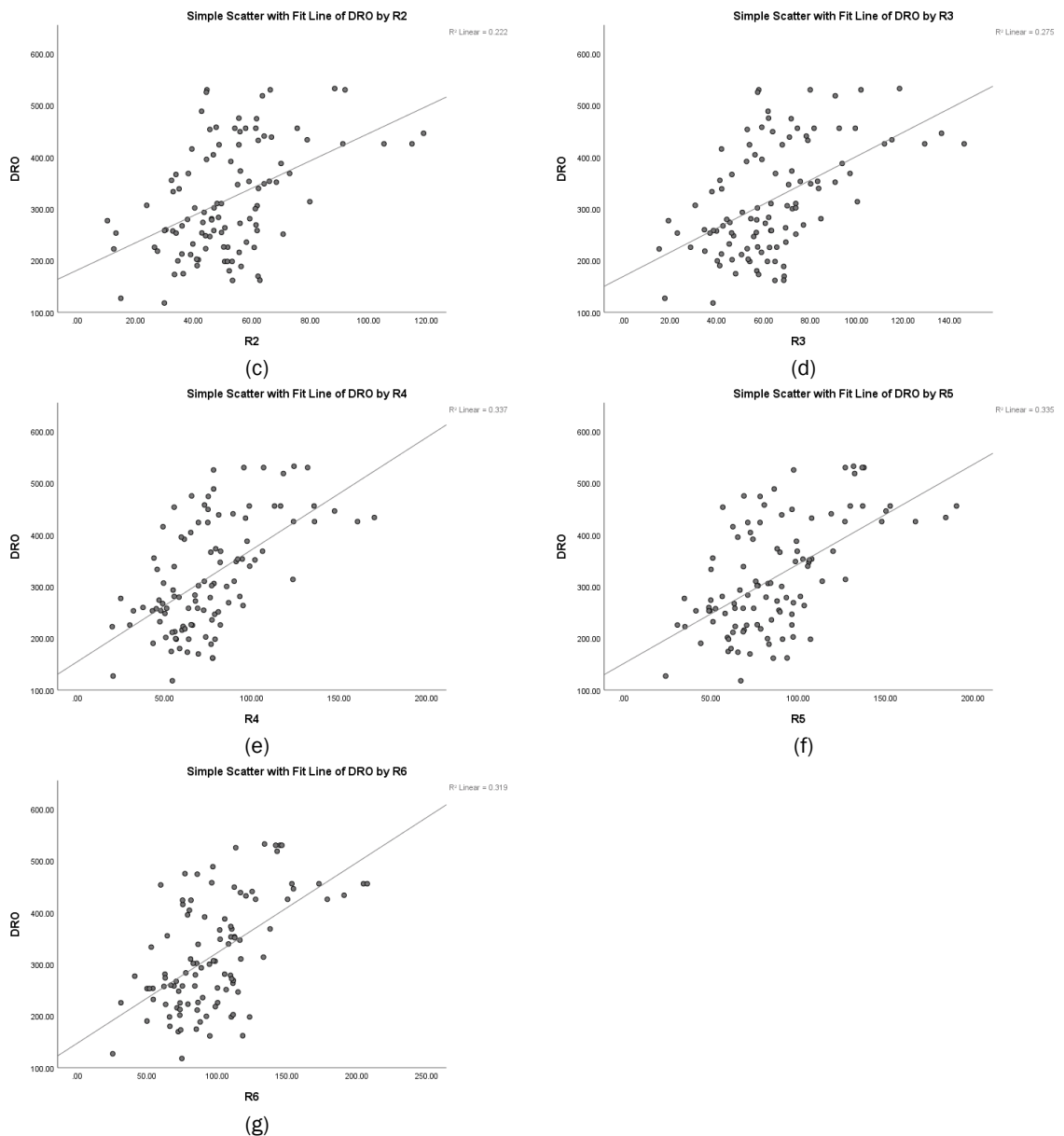


Figure 5-12 The regression diagrams showing the correlation between peak direct runoff and rainfall events in Bandung Basin (2008-2015)

Based on the analysis, the regression model of DROp and R4 has the highest value of R-squared. The R-squared is used to assess the data fitness to the regression line as well as to measure the accuracy of the models. As seen in the diagrams, the value of R<sup>2</sup> increased from 0.059 during the rainfall day (R<sub>0</sub>) to 0.337 after the fourth consecutive days (R<sub>4</sub>), before it decreased on the fifth and sixth day (R<sub>5</sub> and R<sub>6</sub>). It can be concluded that the effective rainfall, which has a high possibility to cause flooding in the Bandung Basin, is the accumulated rainfall total from the fourth day before the flood events occurred.

### 5.2.5 The impact of land cover change to river discharges

The moving average (MA) analysis has been conducted to assess the trend of Ci Tarum, Ci Kapundung, and Ci Sangkuy river discharges. The pattern of increasing coverages of impervious surface in both case study areas has also been plotted to evaluate the effects of the land cover change to the river discharge. The precipitation trend has been estimated using the MA analysis to ascertain if this factor also contributes to the trend of annual river discharge in the two watersheds.

#### (1) The trend of Ci Tarum River discharges (2001-2017)

A 5-year Moving Average (MA) analysis was performed to assess the trend of Ci Tarum River discharges. Rivers from all thirteen catchments in the Bandung Basin are flowing to the Ci Tarum River. Thus, the assessment of Ci Tarum River discharge trend provides an insight into the condition of flood regulation in the basin (2001-2017). The output from MA analysis shows that the rate of discharge trend is likely to increase ( $y = 2.3665x - 4673.9$ ). The highest annual discharge was recorded at 237.95 m<sup>3</sup>/s in 2010. The annual discharge reached another peak in 2016 (122.89 m<sup>3</sup>/s) before it dropped to 78.13 m<sup>3</sup>/s in the following year (Figure 5-13).

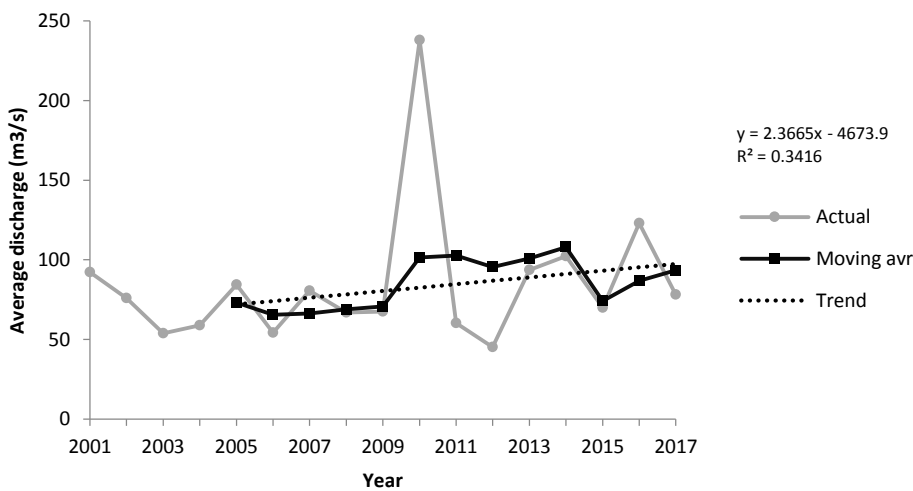


Figure 5-13 The 5-year Moving Average of Ci Tarum annual river discharge

#### (2) Land cover change and the impact on the trend of Ci Kapundung River discharges

The result from the 5-year Moving Average analysis (Figure 5-14) suggested that there was an increasing trend of annual river discharge in the Ci Kapundung upper water catchment area within the period of 2001-2017 ( $y = 0.2107x + 419.27$ ). Based on the land cover maps in 2000, 2015, and 2017, it can be seen that the composition of developed areas has increased (Figure 5-15).



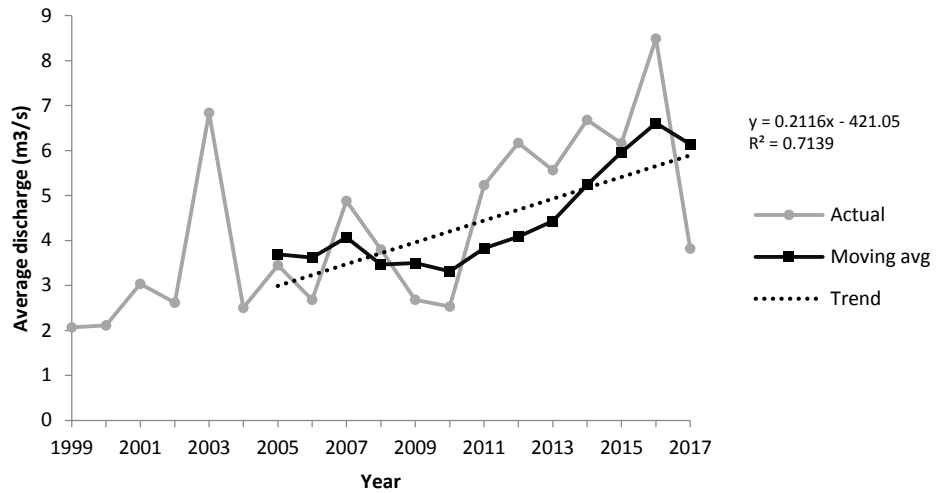


Figure 5-14 The 5-year Moving Average of annual river discharge in the Ci Kapundung upper water catchment area

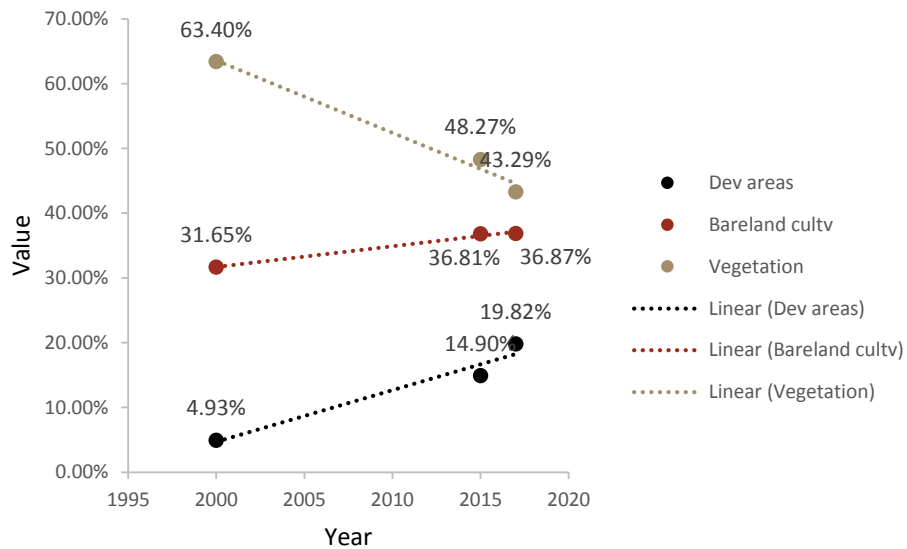


Figure 5-15 The composition of land cover in the Ci Kapundung upper water catchment area

The average annual precipitation rates were likely to increase in most parts of the site except for the area in which the precipitation rates were recorded by Margahayu station (Figure 5-16). However, the linear regression analysis of the MA for Thiessen-weighted average rainfall shows a decreasing trend ( $y = -0.0592x + 6.8075$ ).

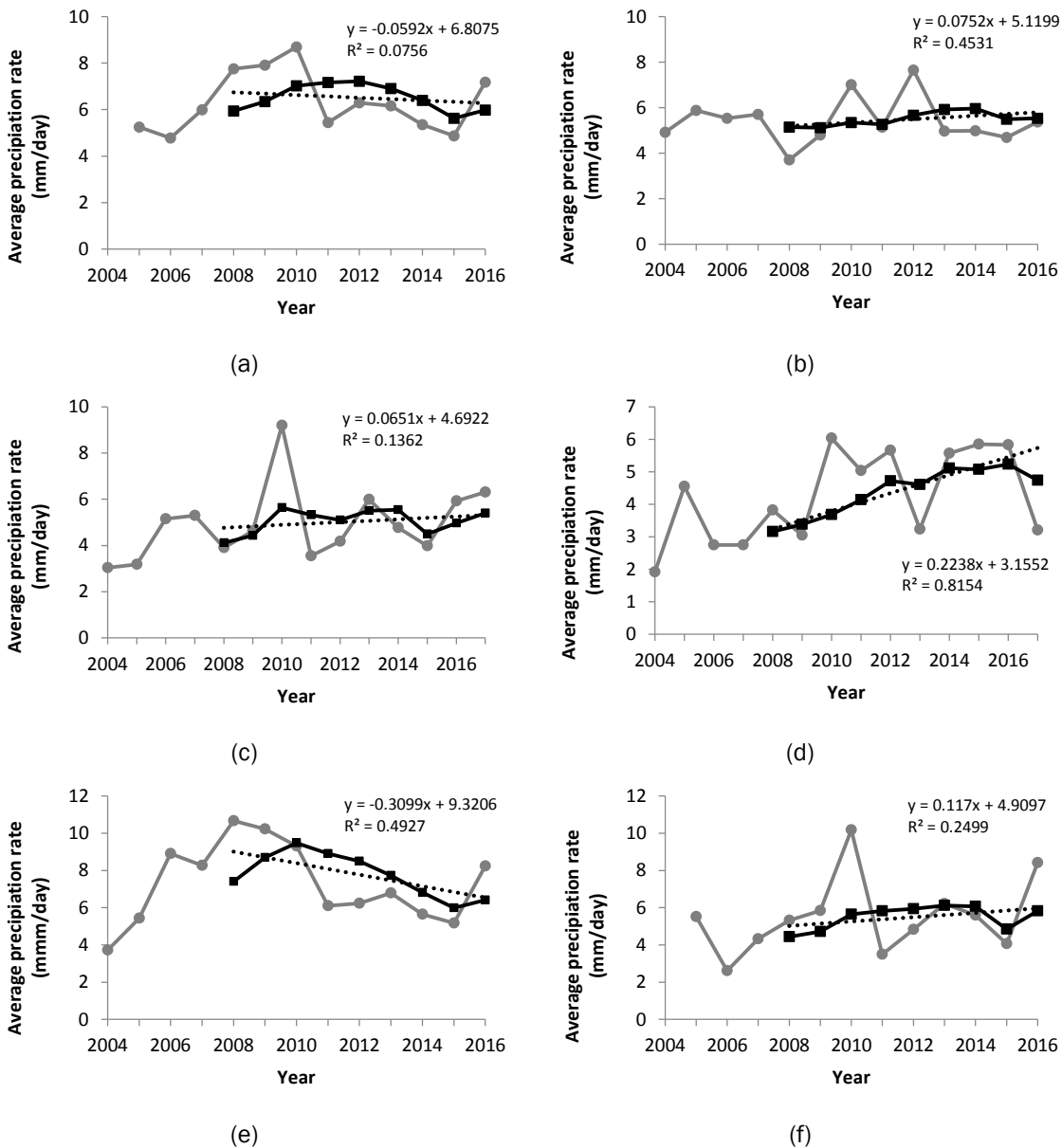


Figure 5-16 The 5-year Moving Average of precipitation rates from; (a) Thiessen-weighted polygons; (b) Kayu Ambon station; (c) Dago Pakar station; (d) Cipeusing station; (e) Margahayu station; and (f) Cibiru station

### (3) Land cover change and the impact on the trend of Ci Sangkuy River discharges

Figure 5-17 presents the results from the MA analysis to assess the trend of Ci Sangkuy river discharge (2001-2017), indicating the decreasing trend of river discharges ( $y = -0.3329x + 680.4$ ). Similar to the first case study area, the compositions of built-up areas and vegetation cover on the second case study area shows an increasing trend, whereas the coverages of plantations, bare land and cultivated land decreased (Figure 5-18).

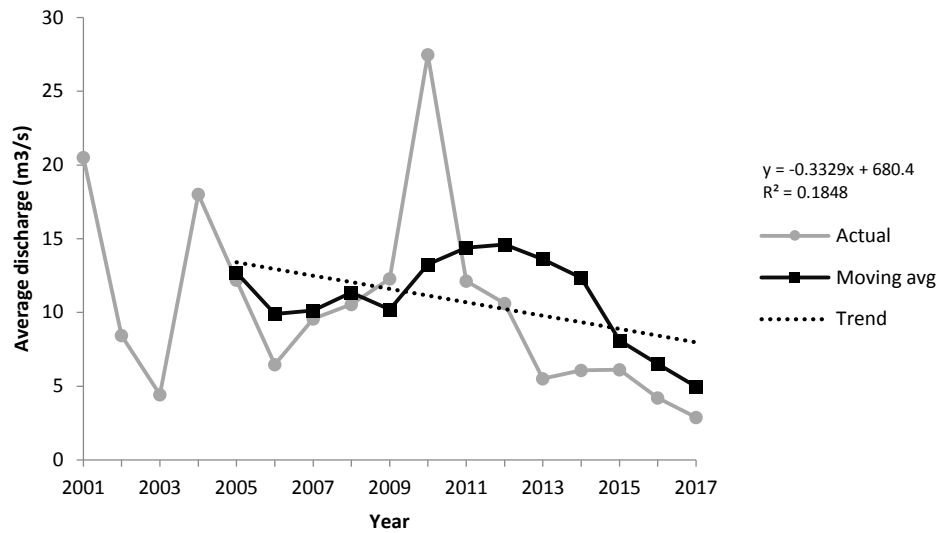


Figure 5-17 The 5-year Moving Average of annual river discharge in the Ci Sangkuy upper water catchment area

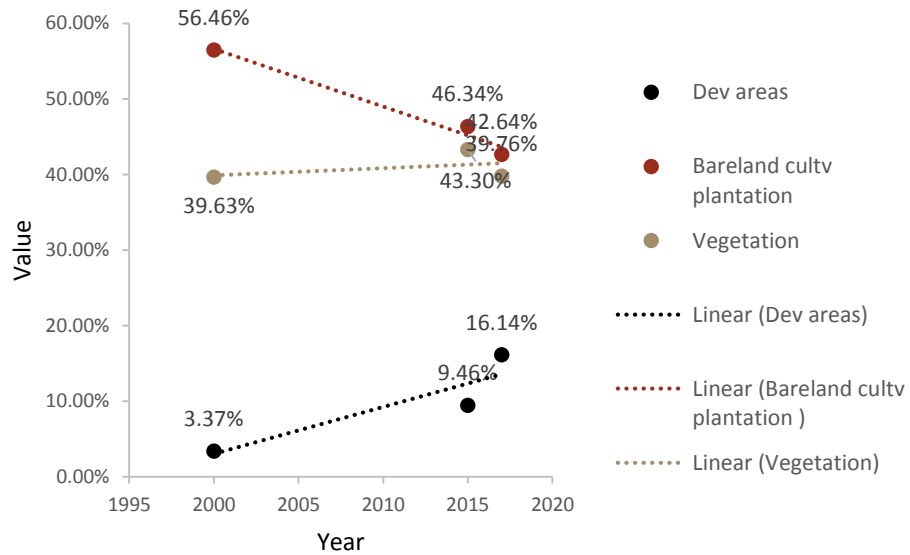


Figure 5-18 The composition of land cover in the Ci Sangkuy upper water catchment area

Further analysis to the precipitation trend on the site reveals that the Thiessen-weighted average rainfall and the precipitation rates as recorded by the four weather stations (e.g. Cileunca, Ciherang, Cisondari, and Cibeureum) have decreased (Figure 5-19). The regression line of precipitation rates as recorded by the Cisondari station has the steepest slope among all weather stations (-0.5723), indicating how significant the decreasing trend was.

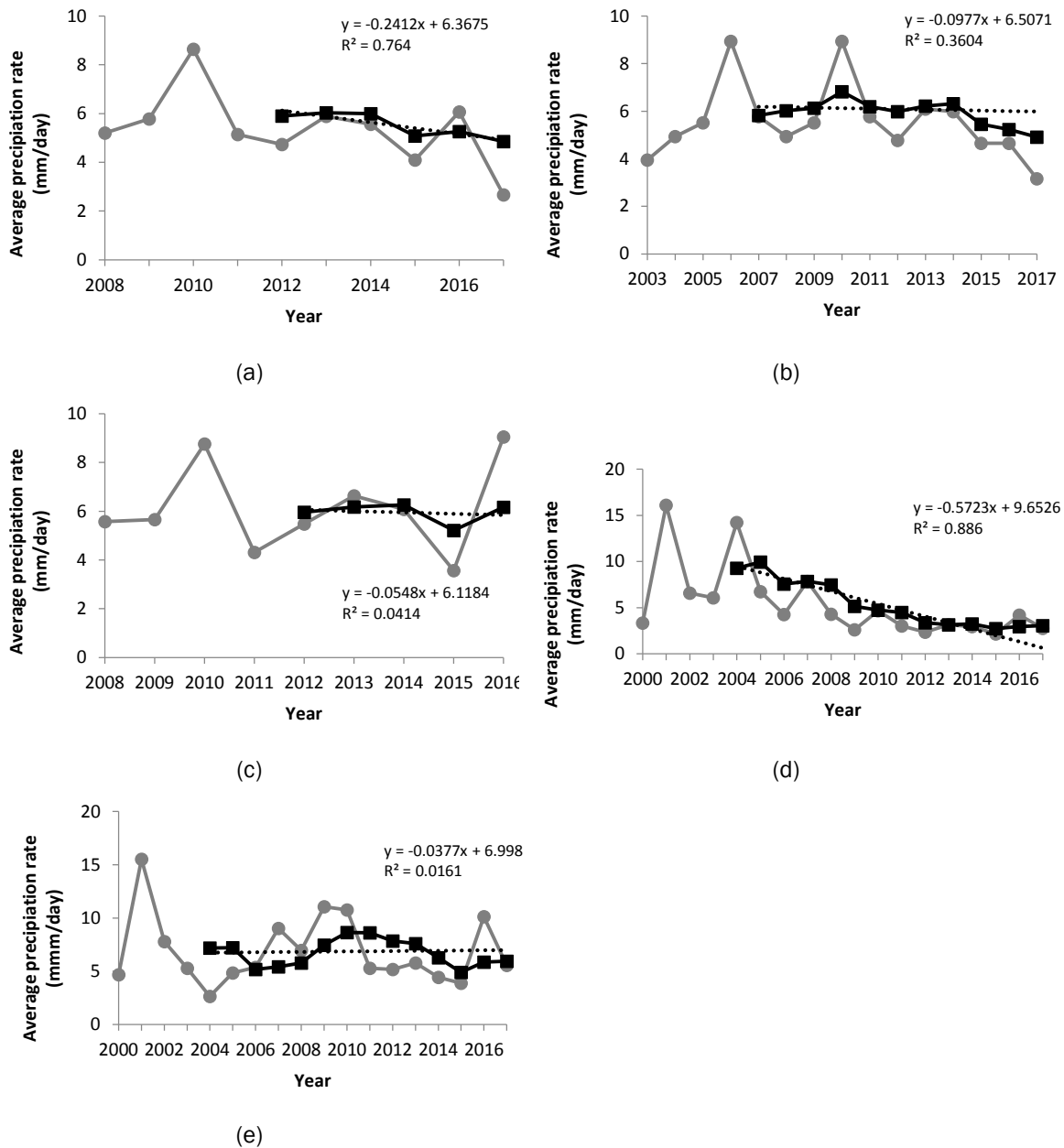


Figure 5-19 The 5-year Moving Average of precipitation rates from; (a) Thiessen-weighted polygons; (b) Cileunca; (c) Ciherang; (d) Cisondari; (e) Cibereum

### 5.3 Landscape structure scenarios for the two case study areas to support flood regulation

The development scenarios of the two case study areas have been generated and simulated in the land change modeler (LCM) module of Terrset. The outputs from land change modelling were used as part of the input datasets for MIKE SHE modelling. This subchapter presents results from the assessment related to the second research question: “What are the most effective scenarios of landscape structure for the two upper water catchment areas which can benefit flood regulation?”. This subchapter begins with the general description of constraints on future

land development in the two case study areas. Then, the results for two iterative land change modelling and hydrologic modelling are given.

### 5.3.1 Constraints on future land development

Constraints on future land development in the two case study areas are related to land availability and the allocated areas to build new settlements and to develop agricultural areas. Constraints maps were used in the land change modelling to allocate new development that will occur. The estimated population in the case study areas was used to check the outputs from LCM, whether the simulated land cover composition can provide the required land to build in the future.

#### (1) Estimated population in the two case study areas

Allocated areas for new settlements and agriculture was estimated based on the projected population in each case study area in 2030. Based on the projected population growth rates in West Java (2015-2035) developed by BPS (2015), the population in Bandung city, Bandung regency, and West Bandung Regency in 2030 was estimated (Table 5-10). This estimation, as well as the population data in the eleven districts in the case study areas, were used to predict the estimated population in the case study area (Table 5-11).

Table 5-10. Existing and projected population in Bandung city, Bandung regency, and West Bandung regency

Municipalities	Year	Population	Population increase (2015-2030)
Bandung city	2015	2,481,469	84,303
	2030	2,565,772	
Bandung regency	2015	3,534,111	120,064
	2030	3,654,175	
West Bandung regency	2015	1,636,316	55,590
	2030	1,691,906	

Table 5-11 The estimated population in five districts in the two case study areas (2015 and 2030)

Districts and the area of districts (km <sup>2</sup> )	District areas within the watersheds and the percentages of area relative to the districts (a)	Population in the district (2015) (b) and the percentages of area relative to the municipalities	Estimated population in each district (2015) within the watershed (a*b)	Estimated population in each district (2017) within the watershed	Population increase in each district within the watersheds (2015-2030)
Cidadap in Bandung city - case1 (6.11 km <sup>2</sup> )	6.11 km <sup>2</sup> (100%)	58,426 (2.35%)	58,426	58,700	1,984
Sukasari in Bandung city -	1.01 km <sup>2</sup> (23.48%)	82,012 (3.30%)	19,256	19,394	654

Districts and the area of districts (km <sup>2</sup> )	District areas within the watersheds and the percentages of area relative to the districts (a)	Population in the district (2015) (b) and the percentages of area relative to the municipalities	Estimated population in each district (2015) within the watershed (a*b)	Estimated population in each district (2017) within the watershed	Population increase in each district within the watersheds (2015-2030)
case1 (4.30 km <sup>2</sup> )					
Coblong in Bandung city-case1 (7.35 km <sup>2</sup> )	1.77 km <sup>2</sup> (24.08%)	133,002 (5.36%)	32,026	32,050	1,088
Cimenyang in Bandung regency-case1 (53.08 km <sup>2</sup> )	8.10 km <sup>2</sup> (15.26%)	115,475 (3.27%)	17,621	18,214	598
Cilengkrang in Bandung regency-case1 (30.12 km <sup>2</sup> )	5.25 km <sup>2</sup> (17.43%)	52,359 (1.48%)	9,126	9,425	310
Lembang in West Bandung regency - case 1 (95.56 km <sup>2</sup> )	79.82 km <sup>2</sup> (83.53%)	187,815 (11.48%)	156,881	164,295	5,329
Pangalengan in Bandung regency-case2 (195.41 km <sup>2</sup> )	152.40 km <sup>2</sup> (77.99%)	148,353 (4.20%)	115,700	119,118	3,930
Banjaran in Bandung regency-case2 (42.92 km <sup>2</sup> )	36.35 km <sup>2</sup> (84.69%)	124,233 (3.52%)	45,581	47,216	1,548
Kertasari in Bandung regency-case2 (152.07 km <sup>2</sup> )	3.38 km <sup>2</sup> (1.56%)	69,793 (1.97%)	1,088	1,119	36
Pacet in Bandung regency-case2 (91.94 km <sup>2</sup> )	2.34 km <sup>2</sup> (2.54%)	109,084 (3.09%)	2,770	2,849	94
Pasir Jambu in Bandung regency-case2 (239.58 km <sup>2</sup> )	10.57 km <sup>2</sup> (0.04%)	85,294 (2.41%)	34	35	1

Based on the calculation of population in each district within the watersheds (Table 5-11), the estimated number of inhabitants in 2015 in Ci Kapundung and Ci Sangkuy upper water catchment areas are 293,336 and 165,173 respectively. In 2017, these number increase to 302,078 and 170,337 for the first and the second case study area, respectively. It is expected that the population in urban and rural areas will increase by 3,726 and 6,237 people,

respectively, in the first case study area in 2030. On the other hand, the population increase of 5,609 people in the second case study area will live in the rural area in 2030.

The population data in 2015 and 2017 from Bandung city, Bandung regency, and West Bandung regency was used as a benchmark to project the number of people living in the watersheds in 2030 and to estimate the required land for new development in 2017 and 2030. According to the results from the second iteration of land cover map development, the estimated developed areas in Ci Kapundung and Ci Sangkuy upper water catchment areas in 2015 are 15.42 km<sup>2</sup> (14.90% of total area) and 19.38 km<sup>2</sup> (9.46% of total area) respectively.

It can be estimated that the required area per-person is approximately 52.57 m<sup>2</sup> and 117.36 m<sup>2</sup> in the first case study area and the second case study area respectively (including the housing, public facilities and infrastructure). Based on the estimated number of people living in 2017, the percentages of built-up areas in the first and the second case study areas are 15.34% and 9.75% respectively, assuming that the required area per-person in 2017 is similar to the area required in 2015. These numbers were used to validate the outcomes from land cover map development and land change modelling (see Subchapters 5.1, 5.3.2, and 5.3.3).

## (2) Constraint maps for each development scenario

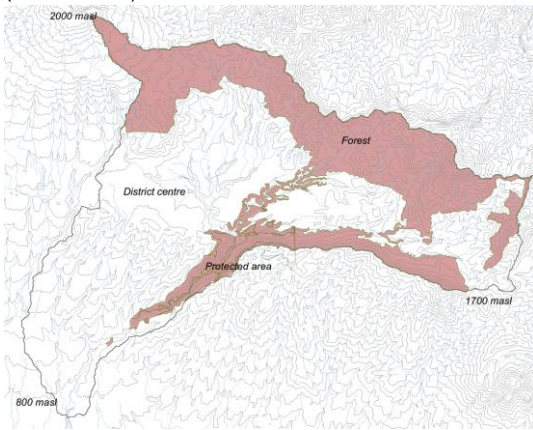
The first scenario is intended to project the future based on the current development trends in the case study areas. In the first iteration of land change modelling (LCM1), no constraint map was included in the simulation process for the first scenario (Status Quo). Based on the simulation results<sup>33</sup>, one constraint map was assigned on the first scenario in the second iterative modelling process (LCM2). The map shows the restriction to develop inside the protected area and forests (Figure 5-20a).

Constraints maps in scenario 2 (existing policy-based scenario) and scenario 3 (ecological design-based scenario) were developed based on a set of maps related to particular policies (Figure 5-20b-e). Two constraints maps showing the areas restricted to the new development of settlements and agriculture areas have been created for each scenario. The results from the land change modelling for the third scenario have been tested in the hydrologic model (MIKE SHE 1), to assess the impact of the land change in this scenario to the runoff generation in the two case study areas (the result is presented in Subchapter 5.3.4).

---


<sup>33</sup> The result is presented in the next part of this subchapter. The reasons why constraint maps were proposed in the second iterative modelling is discussed in Chapter 6.

(scenario 1)

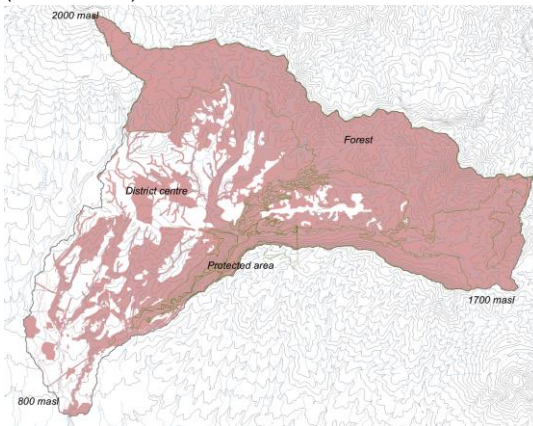


(a)

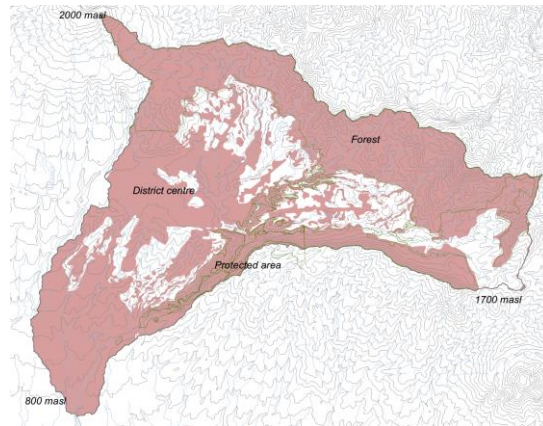
**Legend:**

 : Area restricted to further development

(scenario 2)

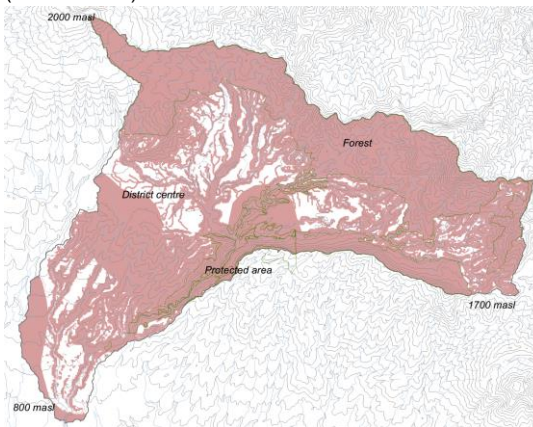


(b)

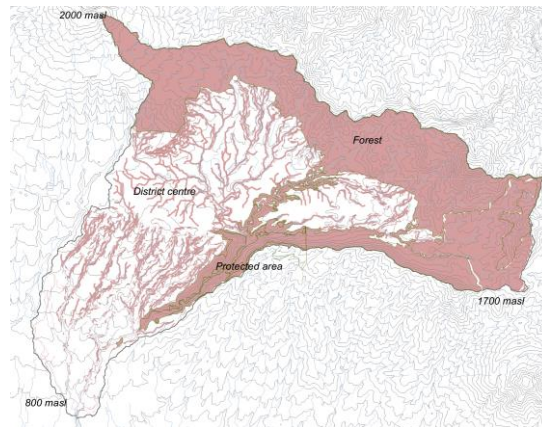


(c)

(scenario 3)



(d)



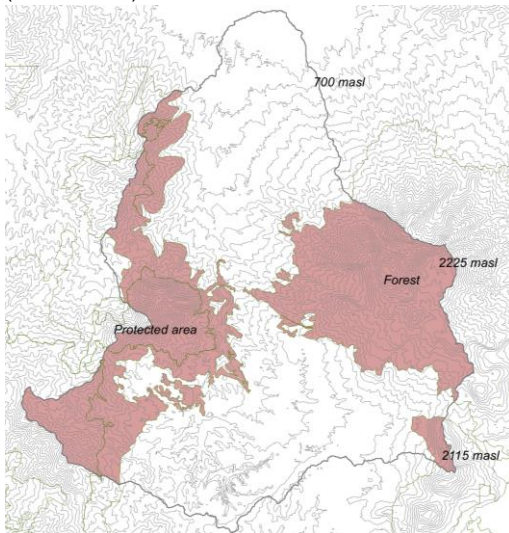
(e)

Figure 5-20 (a-e). Constraints maps which delineate areas restricted to the further development of settlements and agriculture in scenario 1, 2, and 3 in the Ci Kapundung watershed

There are also three scenarios developed for the land change modelling of the second case study area. In the first scenario, one constraint map was applied in the model. The map indicates areas inside the forests and protected area that is restricted to be built up. The second and third scenarios were developed based on the existing spatial policies and ecological design principles, respectively. Constraint maps for the three development scenarios of the second case study area are presented in Figure 5-21.




(scenario 1)

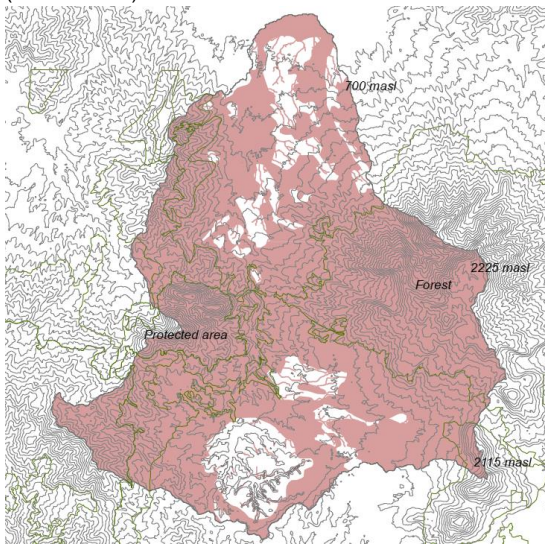


(a)

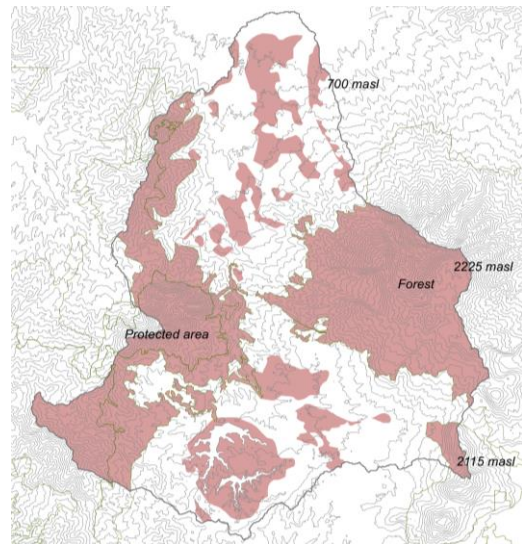
**Legend:**

 : Area restricted to further development

(scenario 2)

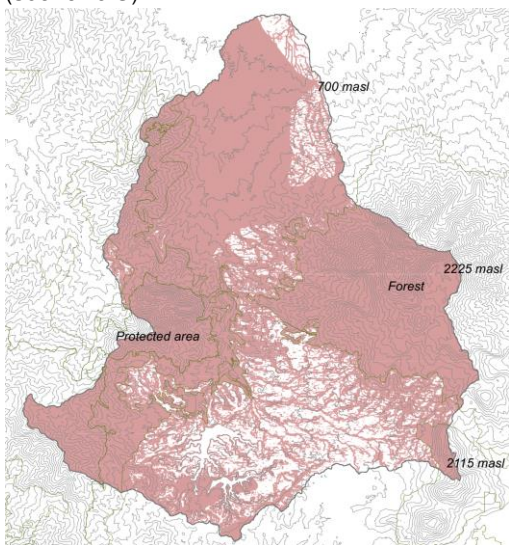


(b)

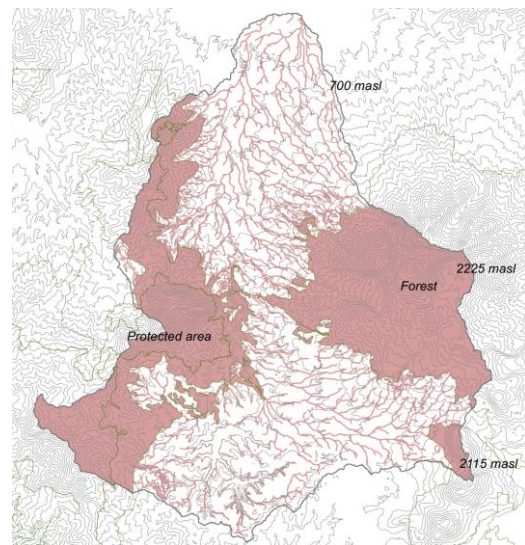


(c)

(scenario 3)



(d)



(e)

Figure 5-21 (a-e). Constraints maps which delineate areas restricted to the new development of settlements and agriculture in scenario 1, 2, and 3 in the Ci Sangkuy watershed

### 5.3.2 The first iteration of land change simulation (LCM 1)

In the first iteration of land change modelling of the first case study area, four variables causing the land change have been assessed using MLP to show the potential explanatory power of each variable. The outputs were indicated in an overall Cramer's V. The four drivers are the distance from existing disturbance, road and river networks, and the likelihood of change (Figure 5-22). Thirteen simulations have been conducted to test the variables. The model accuracy for the first simulation is 49.27%, with the third variable (i.e. river network) to have the least influence to the modelling. It is suggested that the model accuracy should be roughly 50%, and the model should be rerun when the accuracy is lower than 50% (Eastman, 2016). Therefore, subsequent simulations were conducted to achieve an accuracy of more than 50%.

The output from the second simulation also indicated that the 'distance from the river network' variable has the least influence on the model. Therefore, starting from the third simulation, this variable was excluded in the simulation. The result from the 13<sup>th</sup> MLP process shows that there was an increase in the modelling accuracy to 52.86%. Likelihood of change became the variable that has the most influence on the land change in 2013-2015.

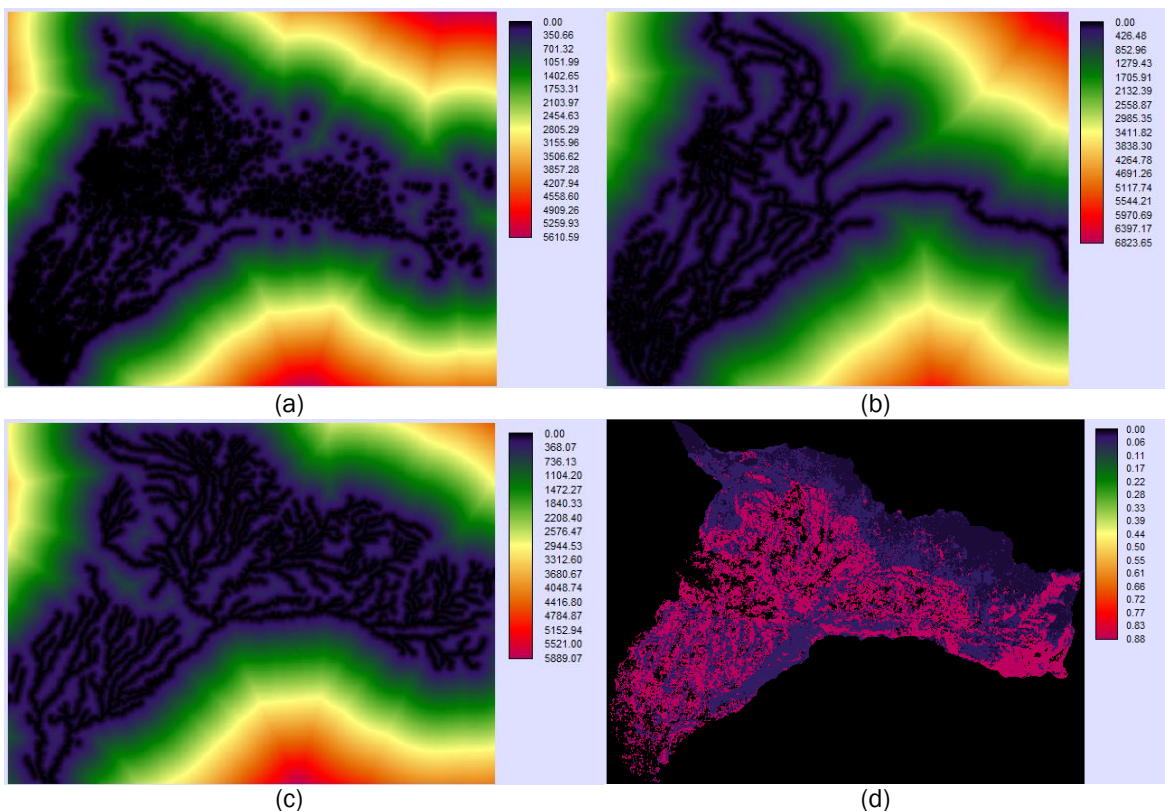
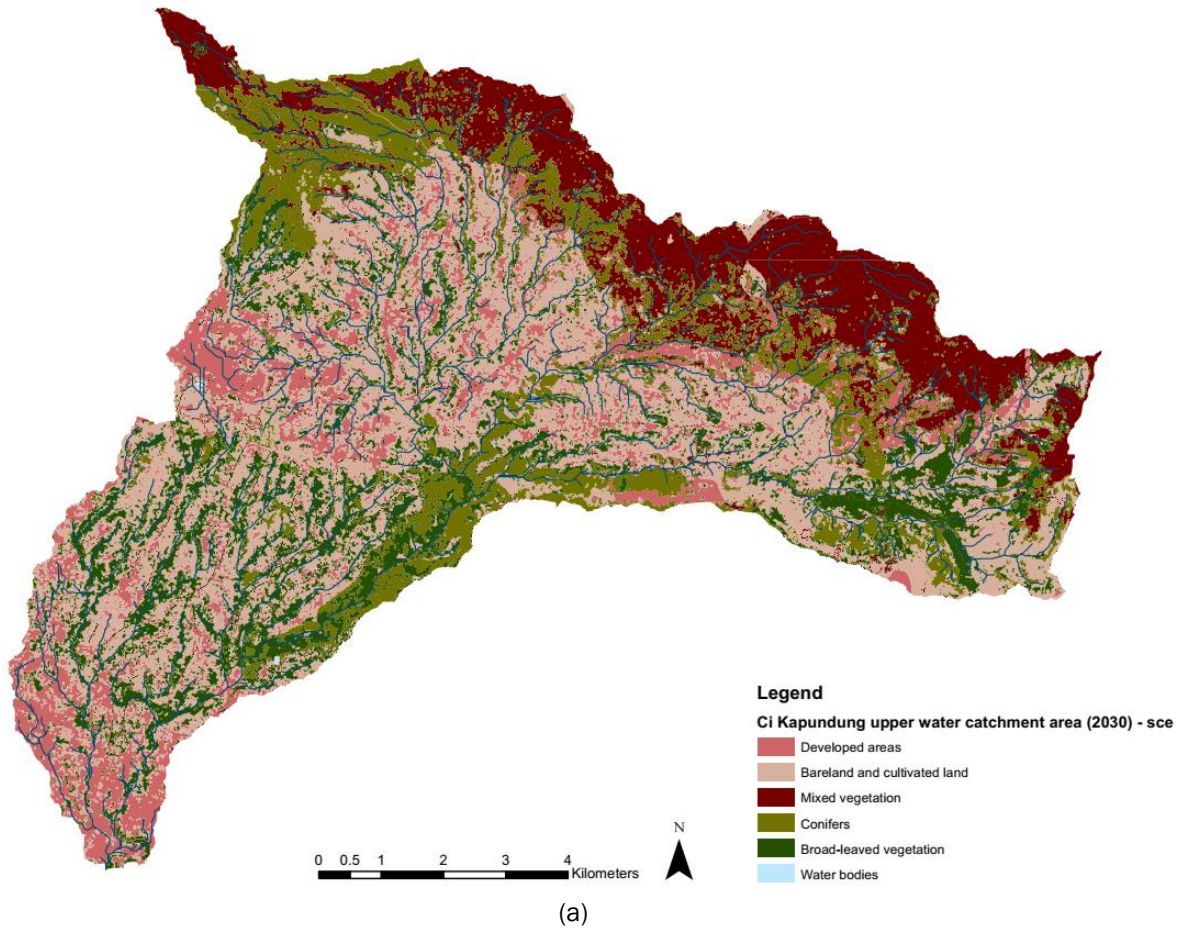


Figure 5-22 Four drivers of land change in the first case study area: (a) existing disturbance; (b) existing road networks; (c) river networks; (d) the likelihood of area to change

The 2017 land cover map has been simulated under the Status Quo scenario using the transition probability maps and the Markov matrix (2015-2017) in which the weighting factors have been applied before. The allocations for developed areas, bare land and cultivated land, mixed vegetation, conifers, and broad-leaved vegetation are 17.59%, 33.95%, 16.01%, 16.01%,

and 16.44% respectively. Model validation has been performed to assess model accuracy. There are 500 accuracy assessment points assigned to the predicted and actual land cover maps (2017). The validation result shows image accuracy of 60.52%.

Weighting factors have also been applied in the Markov matrix to generate transition probability (2015-2030) based on different spatial policies in each scenario. The results from land change simulations of the first case study area using three scenarios (e.g. Status Quo, existing policy-based scenario, and Ecological Design scenario) can be seen in Figure 5-23(a-c).



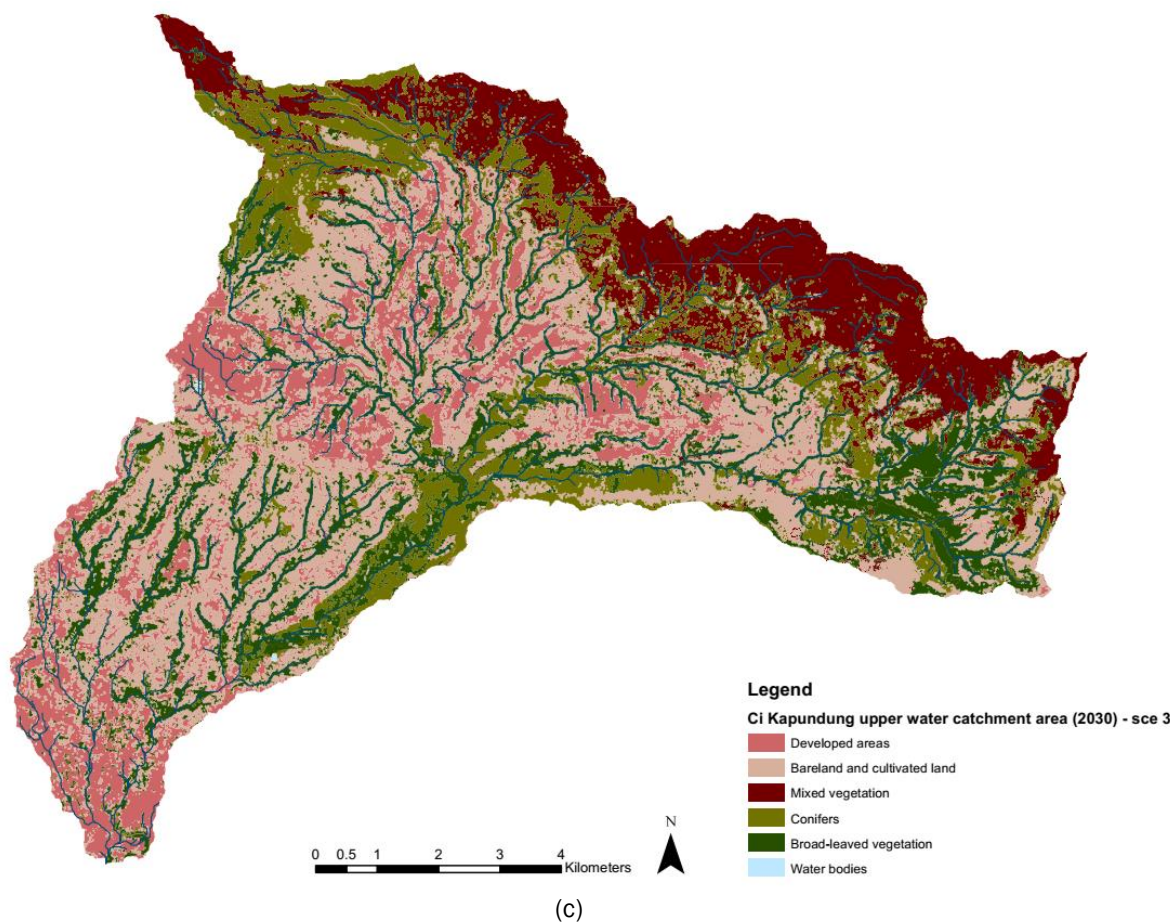
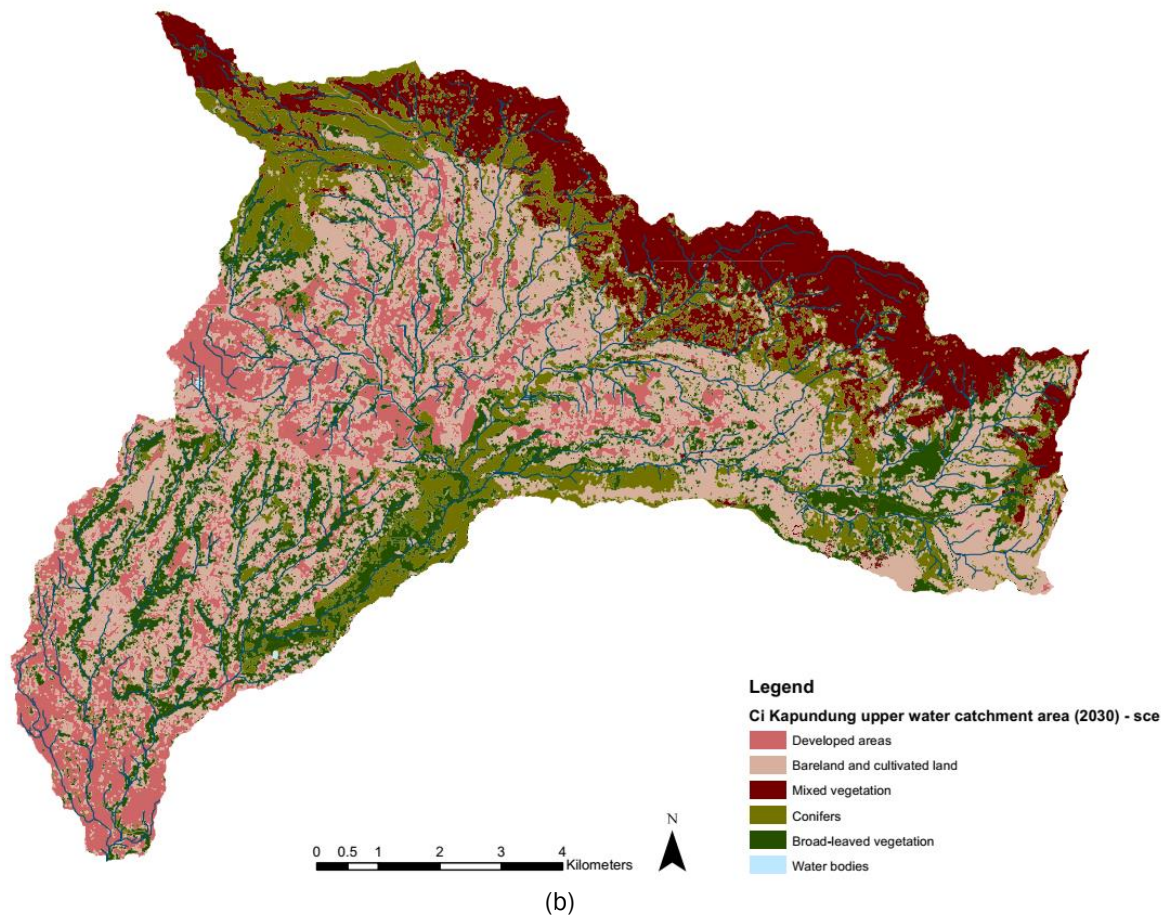


Figure 5-23 (a-c) Initial simulation results for the 2030 land cover of Ci Kapundung upper water catchment area based on scenario 1, 2, and 3 (Source: Modified images from Rani *et al.*, 2018)

In the first scenario (Status Quo) (Figure 5-23a), disperse settlements are projected to occur in the watershed, including the area with steep slopes and inside the river buffers. The agriculture practices still exist inside the forests. In the second scenario (the existing spatial policies-based scenario), the new settlements will be allocated according to the existing spatial policies from each municipality. The development of new settlements is projected to occur in steep slopes in the western part of the area because there are no restrictions in the existing spatial policies to build in such area. In the last scenario, no development will occur inside the forest, protected area, and the river buffer, as shown in the constraints map.

There is no difference in the compositions of land cover in scenario 1 and 2 (Table 5-12). Weighting factors added to the transition probability matrix in scenario 3 has resulted to the different percentages of land cover compositions, particularly for bare land and cultivated land (31.40%) and broad-leaved vegetation (18.74%).

Table 5-12 Land cover composition in the Ci Kapundung upper water catchment area for each scenario

Land cover types	Predicted land cover composition in 2030		
	Scenario 1	Scenario 2	Scenario 3
Developed areas	17.58%	17.58%	17.58%
Bare land and cultivated land	33.94%	33.94%	31.40%
Mixed vegetation	16.01%	16.01%	16.25%
Conifers	16.01%	16.01%	16.01%
Broad-leaved vegetation	16.44%	16.44%	18.74%
Water bodies	0.02%	0.02%	0.02%

### 5.3.3 The second iteration of land change simulation (LCM 2)

Based on the outputs from the first iteration of land change simulation, the final 2030 land cover maps of the two case study areas have been modelled in the second iteration of land change modelling. The c.2000 and 2015 land cover maps were used in the modelling.

#### (1) Land change simulation of the Ci Kapundung upper water catchment area

Another series of MLP processes have been conducted in the second iteration of land change modelling for the first case study area. In these processes, more drivers were included (Figure 5-24). The drivers were divided into two groups; the demographic-economic drivers (e.g. likelihood to change, distance from disturbance, and population density), and environmental drivers (e.g. elevation, slopes, and distance from streams). In general, all three demographic-economic drivers have higher values of Cramer's V values compared with the environmental drivers. Likelihood to change has the highest value (0.5675) among all variables, indicating the most influential driver for land change in the area. Distance from disturbance and population density (2015) are the second and third most significant drivers with the overall Cramer's V of 0.4120 and 0.3869, respectively. Elevation, slopes, and distance from streams have the overall

Cramer's values of 0.3463, 0.2396 and 0.0663, respectively (Rani, Lange, Schroth, et al., 2019).

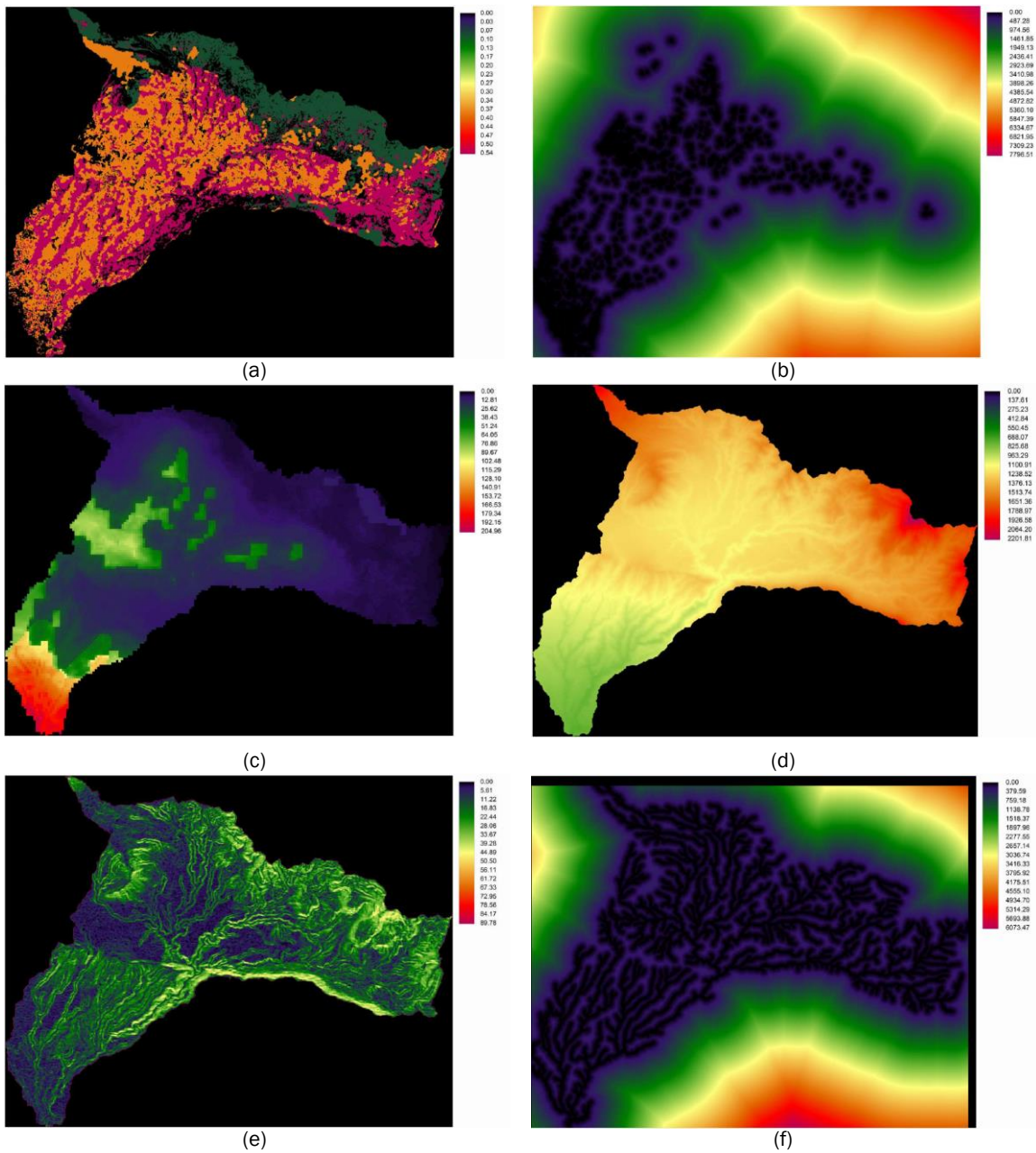


Figure 5-24 Driver variables in the land change modelling for the first case study area; (a) likelihood to change; (b) distance from disturbance; (c) population density; (d) elevation; (e) slopes; (f) distance from streams (Rani, Lange, Schroth, et al., 2019)

Table 5-13 Driver variables of land change in the first case study area (Rani, Lange, Schroth, et al., 2019)

	<b>Types of driver</b>	<b>Cramer's V</b>
<b>Demographic-economic drivers:</b>	Likelihood to change (LC)	0.5675
	Distance from disturbance (DD)	0.4120
	Population density (2015) (PD)	0.3869
<b>Environmental drivers:</b>	Elevation (EL)	0.3463
	Slopes (SL)	0.2396
	Distance from streams (DS)	0.0663

An iterative MLP process and the projection of 2017 land cover maps have been conducted using different groups of driver variables; all drivers, the demographic-economic drivers, and the environmental drivers. The results show that the MLP accuracy of 55.70% was achieved when all drivers were included in the iteration process. Lower accuracy was retrieved by the model if other groups of variables were used. The 2017 land cover maps of the first case study area were projected based on the land cover changes in 2000-2015 and the transition potential maps resulted from the MLP process under the Status Quo scenario.

The transition probability matrix (2000-2015) to model the land cover map in 2017 is presented in Table 5-14. The probability of land cover change from bare land and cultivated land to developed areas in 2015-2017 is 0.0872. It is expected that broad-leaved vegetation will be converted as bare land by 0.2512. There are still possibilities of change for one type of forest to another.

The actual 2017 land cover map, then, was used to validate the projected 2017 maps. The model accuracies were estimated using confusion matrices. There are 500 points assigned randomly in the imagery to compute the model accuracy. From Table 5-15, it can be seen that the model accuracy of 81.76% was achieved when only three demographic-economic drivers were included in the MLP process. This number is higher than the model accuracies when other combinations of driver variables were incorporated into the model.

Table 5-14 Transition probability matrix to simulate the 2017 land cover map of the first study area (Rani, Lange, Schroth, et al., 2019)

	<b>Developed areas</b>	<b>Bare land cultiv. land</b>	<b>Mixed veg.</b>	<b>Conifers</b>	<b>Broad-leaved veg.</b>
<b>Developed areas</b>	0.9841	0.0138	0.0000	0.0000	0.0021
<b>Bare land and cultiv. land</b>	0.0872	0.8509	0.0137	0.0237	0.0246
<b>Mixed veg.</b>	0.0000	0.0380	0.9558	0.0028	0.0034
<b>Conifers</b>	0.0000	0.0000	0.0059	0.9734	0.0207
<b>Broad-leaved veg.</b>	0.0000	0.2512	0.0000	0.0000	0.7488

Table 5-15 Model accuracy retrieved from the validation process (Rani, Lange, Schroth, et al., 2019)

Drivers	Model accuracy from validation
All drivers	81.36%
LC, DD, PD, EL	79.35%
3 demographic-economic drivers	81.76%
3 environmental drivers	81.36%

The potential transition and the projected 2017 maps simulated using three demographic-economic drivers are shown in Figure 5-25(a-b). The potential transition map shows the magnitude or possibility of land change. Area restricted to new development is shown in black (e.g. forests and protected area). Whereas the probabilities of land cover change in other areas are shown in the gradation of blue to red with red indicates a higher possibility of an area to change in 2017. The land cover compositions for the developed areas, bare land and cultivated land, mixed vegetation, conifers, and broad-leaved vegetation in the simulated 2017 map are 18.09%, 36.65%, 14.62%, 17.14%, and 13.49% respectively. Pixels identified as water bodies (0.02%) were excluded in the modelling, thus no change in the composition for this particular land cover.

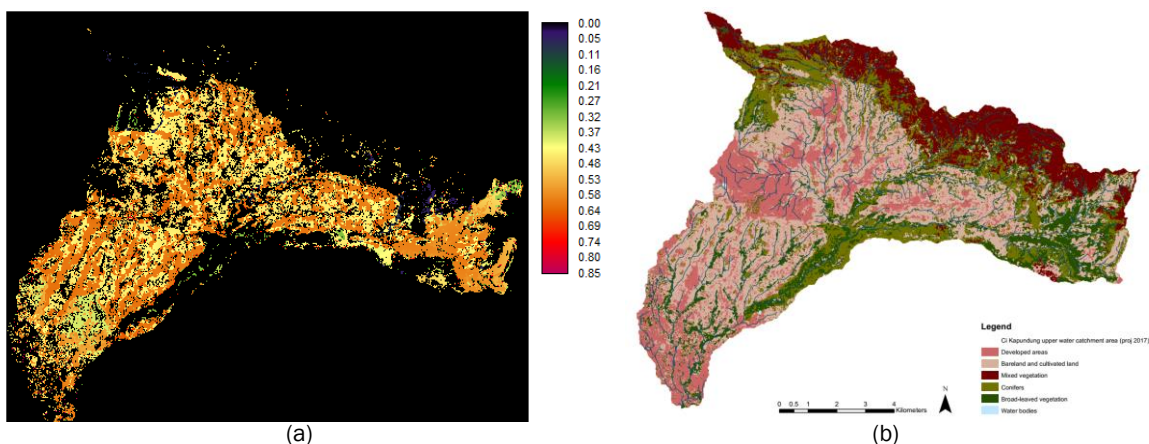


Figure 5-25 (a) Potential transition map in 2017; (b) Projected 2017 land cover map based on the Status Quo scenario (modified images from Rani, Lange, Schroth, et al., 2019)

Model validation was conducted again by comparing the coverages of the developed areas in the 2017 map generated from the satellite imagery, the output 2017 map from LCM, and the estimation based on the increasing population in the watersheds (2015-2017). The output map from LCM used in the validation is the map generated using the three drivers under the Status Quo scenario. The estimated increasing population has been given in the previous subchapter (5.3.1). Based on the 2017 land cover map, 19.82% of the total area is classified as the developed areas. However, only 18.09% of the total area was projected to be built in the watershed in 2017. A lower percentage of developed areas is estimated based on the number



of population (15.34%). Thus, it can be seen that there are discrepancies of the estimated composition of developed areas with the predicted maps.

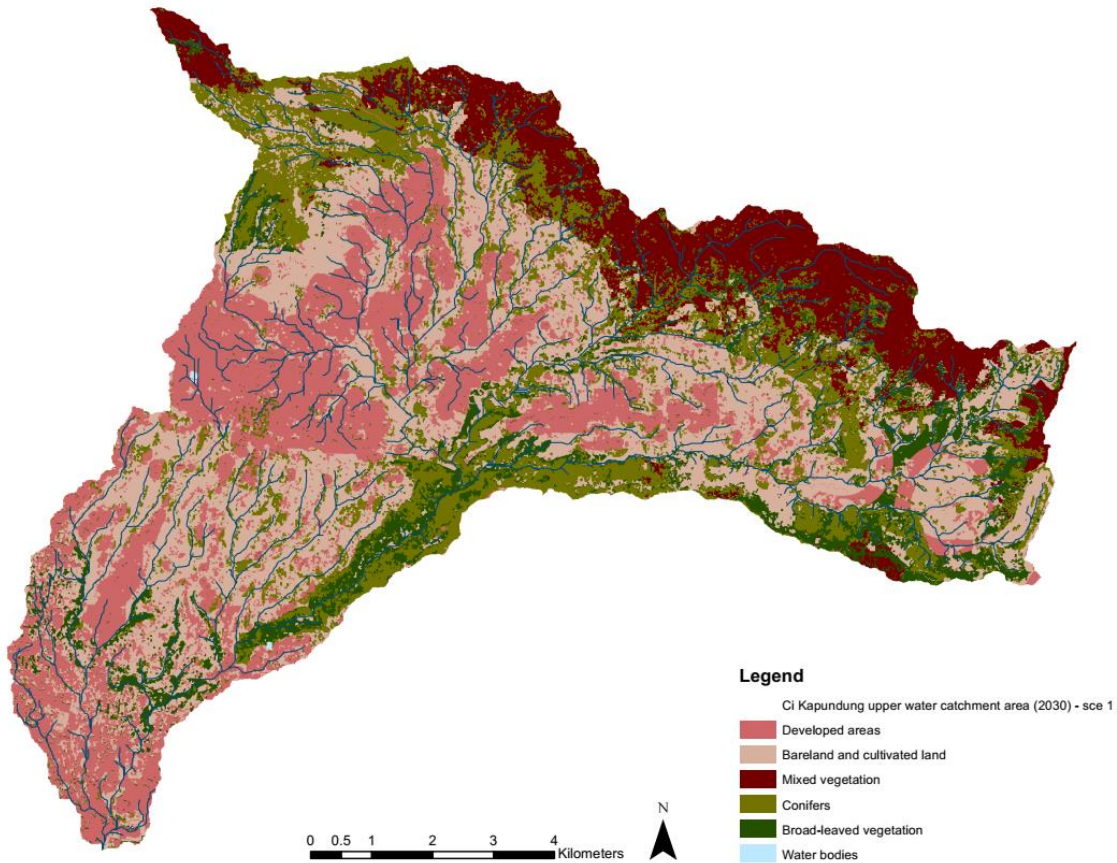
The 2030 land cover maps were modelled based on the three development scenarios and the transition probability matrix (Table 5-16). There is a possibility of 0.2572 that bare land and cultivated land will be converted to built-up areas in 2030. Another land cover alteration is also expected to occur on the site. Areas covered by broad-leaved vegetation outside the forests will be altered as newly cultivated land with the probability of 0.4482 (Table 5-16).

Table 5-16 Transition probability matrix to simulate the 2030 land cover map of the first study area

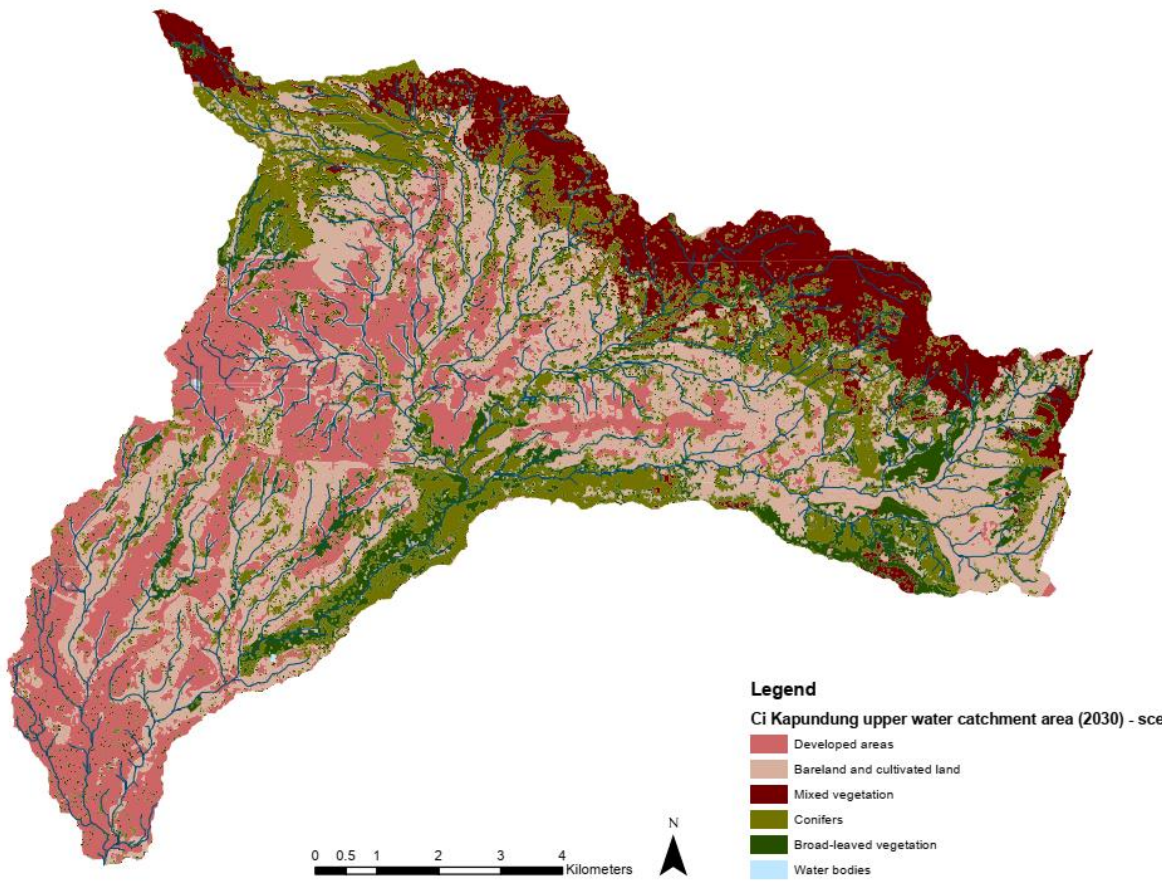
	<b>Developed areas</b>	<b>Bare land cultiv. land</b>	<b>Mixed veg.</b>	<b>Conifers</b>	<b>Broad-leaved veg.</b>
<b>Developed areas</b>	0.9325	0.0561	0.0000	0.0023	0.0090
<b>Bare land and cultiv. land</b>	0.2572	0.6013	0.0353	0.0663	0.0399
<b>Mixed veg.</b>	0.0061	0.1481	0.7824	0.0425	0.0208
<b>Conifers</b>	0.0070	0.0475	0.0365	0.8493	0.0596
<b>Broad-leaved veg.</b>	0.0607	0.4482	0.0070	0.0370	0.4471

The results from the land change simulation of the first case study area (2030) are presented in Figure 5-26 (a-d). Scenario 1, 2, and 3 were developed based on the same principles as the three scenarios used in the first iterative land change modelling. Based on the interpretation of results from hydrologic modelling, the fourth scenario was generated, as part of the backcasting process in this research (refer to Subchapter 6.3).

It is expected that the new development of settlements and other built-up areas in all future scenarios will occur near the existing developed areas. Different constraint maps applied in each scenario affect the distribution of land cover. For example, new settlements are built scattered on the site in the first scenario because the restriction to develop inside the forest and protected area is the only development constraints applied. Therefore, it is expected that the new development also occurs in the area with steep slopes near the streams. The spatial policies of each municipality have been applied in the second scenario. In the third scenario, new buildings are more concentrated in relatively flat terrain away from the streams.



(a)



(b)

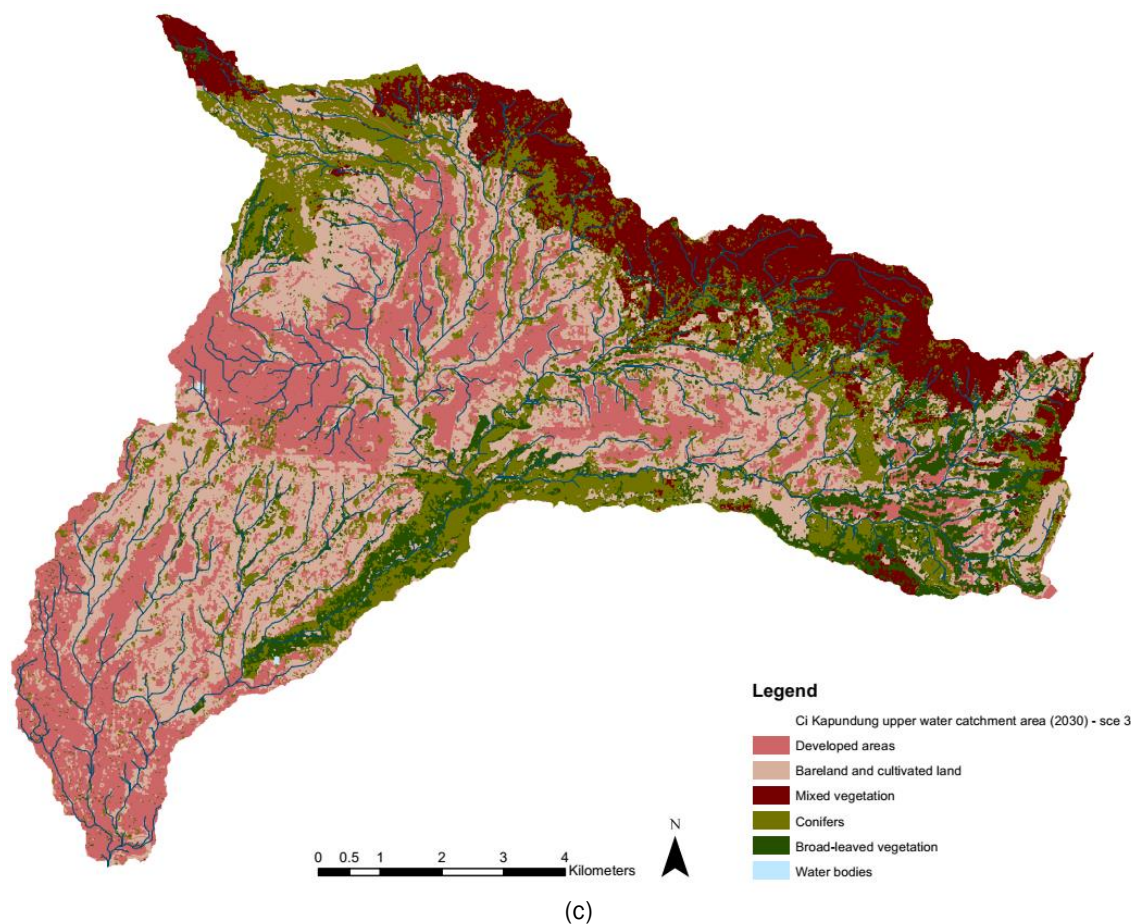


Figure 5-26 (a-d) The projected 2030 land cover maps of the first case study area based on scenario 1, 2, 3, and 4

The land cover compositions in 2030 are presented in Table 5-17. There is no difference with the percentage of for land cover types in each development scenario.

Table 5-17 Land cover composition in the Ci Kapundung upper water catchment area for each scenario

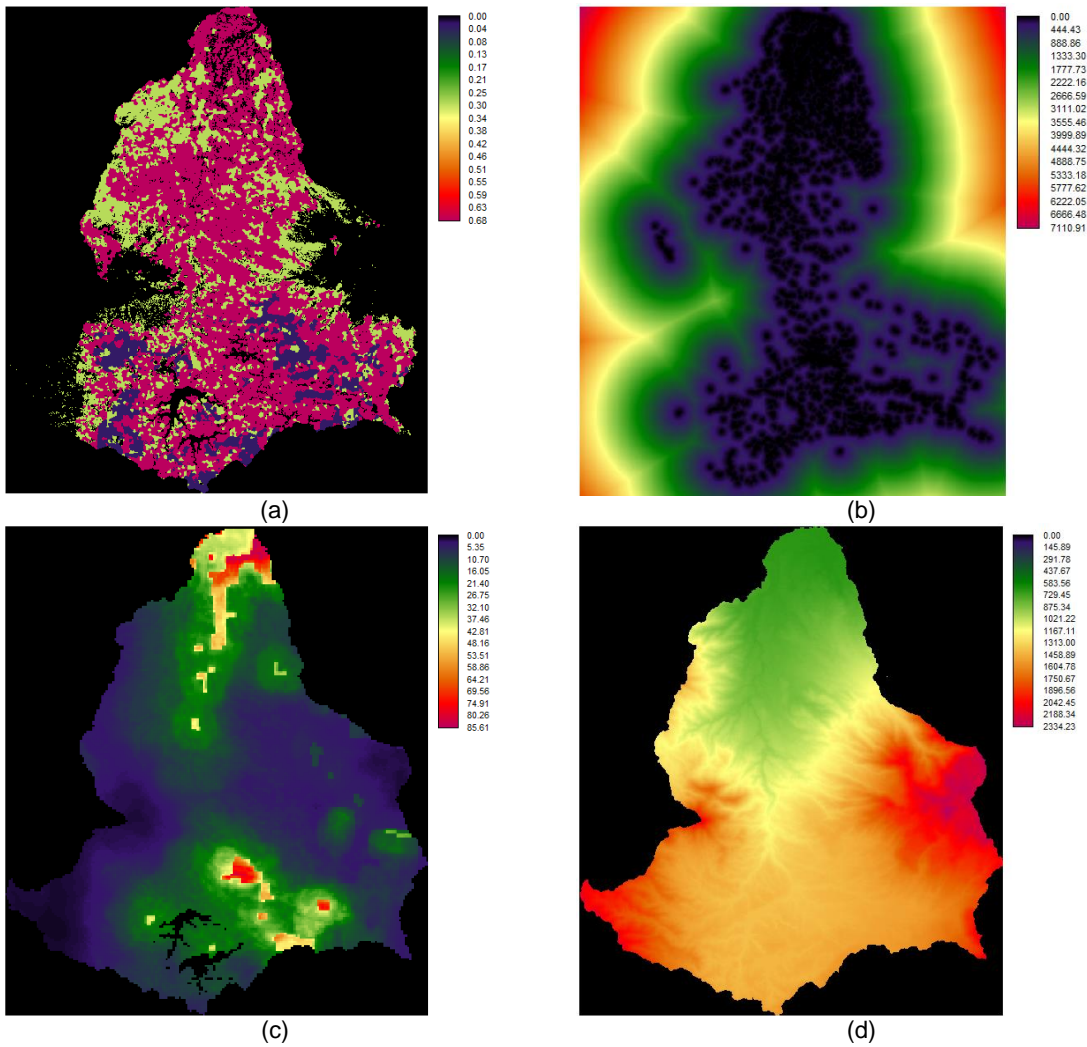
Land cover types	Predicted land cover composition in 2030		
	Scenario 1	Scenario 2	Scenario 3
Developed areas	25.38%	25.38%	25.38%
Bare land and cultivated land	33.23%	33.23%	33.23%
Mixed vegetation	12.94%	12.94%	12.94%
Conifers	18.71%	18.70%	18.70%
Broad-leaved vegetation	9.72%	9.72%	9.72%
Water bodies	0.02%	0.02%	0.02%

## (2) Land change simulation of the Ci Sangkuy upper water catchment area

After the land changes of the two case study areas from 2013-2015 had been assessed and the constraints maps for scenario 1, 2, and 3 had been created, the number of land cover transitions were specified in the development of transition potential maps. The six types of driver

variable as used in the LCM model of the first case study area were also evaluated in the land change modelling of the second case study area (Figure 5-27).

The potential explanatory power of each driver is summarised in Table 5-18. The 'likelihood to change' driver has the highest Cramer's V value among all drivers (0.4680). The elevation driver has the second-highest rate of value (0.4046) and is the highest in the environmental drivers. The distance from streams driver has the least influence on the land change on the site (0.0909).



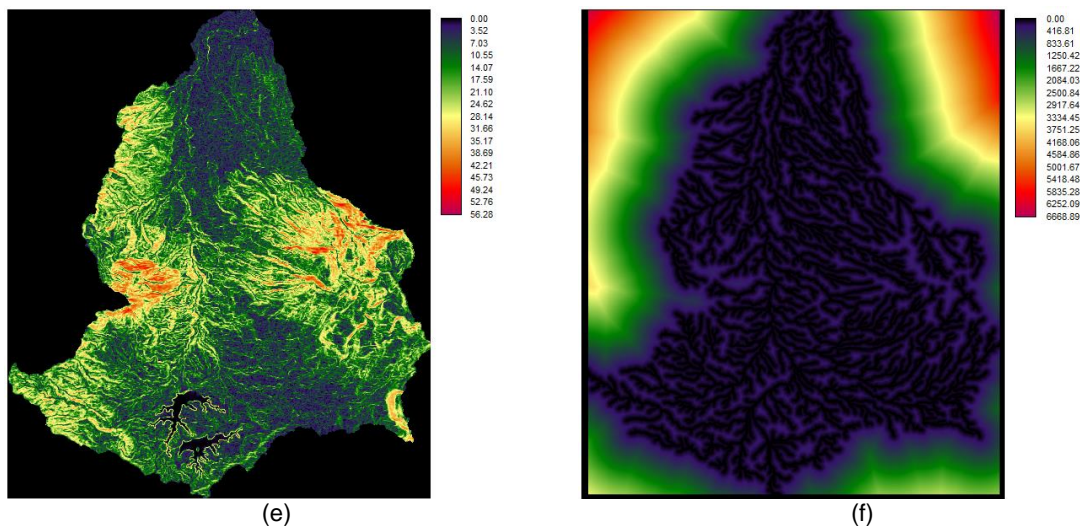


Figure 5-27 Driver variables in the land change modelling for the second case study area; (a) likelihood to change; (b) distance from disturbance; (c) population density; (d) elevation; (e) slopes; (f) distance from streams

Table 5-18 Driver variables of land change in the second case study area

	Types of driver	Cramer's V
<b>Demographic-economic drivers:</b>	Likelihood to change (LC)	0.4680
	Distance from disturbance (DD)	0.3636
	Population density (2015) (PD)	0.3397
<b>Environmental drivers:</b>	Elevation (EL)	0.4046
	Slopes (SL)	0.2490
	Distance from streams (DS)	0.0909

Different combinations of driver variables were used to model the transition probability in an iterative MLP process. An accuracy of 44.77% was retrieved from the MLP process when all six driver variables were incorporated in the modelling. Lower MLP accuracies were estimated when only three demographic-economic variables were included (27.25%), and when only three environmental variables were used (16.91%). The 2017 land cover maps were modelled using transition probability maps generated from different groups of driver variables under the Status Quo scenario. The results, then, were validated using the 2017 land cover map generated from satellite imagery.

LCM modelled the transition probability matrix (2000-2015) to project the 2017 land cover map. The matrix indicates that bare land and cultivated land is the only land cover that would change into developed areas with a probability of 0.0336. Approximately 27% of areas with broad-leaved trees are expected to alter into bare land and cultivated land in 2017 (Table 5-19). Possibility of one type of forest to change into another is described in the following chapter.

Table 5-19 Transition probability matrix to simulate the 2017 land cover map of the second study area

	Developed areas	Bare land cultiv. land	Plantations	Mixed veg.	Conifers	Broad-leaved veg.
Developed areas	0.9999	0.0001	0.0000	0.0000	0.0000	0.0000
Bare land and cultiv.	0.0336	0.7024	0.0430	0.0068	0.0168	0.1974
Plantations	0.0000	0.0567	0.9430	0.0001	0.0002	0.0000
Mixed veg.	0.0000	0.0000	0.0000	1.0000	0.0000	0.0000
Conifers	0.0000	0.0000	0.0000	0.0000	1.0000	0.0000
Broad-leaved veg.	0.0000	0.2774	0.0090	0.0000	0.0000	0.7136

All 2017 maps simulated from LCM using three combinations of driver variables (e.g. all drivers, three demographic-economic drivers, and three environmental drivers) were validated using the actual 2017 land cover map. A total of 500 points were also assigned in the maps to estimate the model accuracy. As seen from Table 5-20, the highest accuracy was retrieved when only three demographic-economic drivers were included in the MLP process (70.80%). Therefore, the following simulations were conducted based on the outcome from the MLP using the three land change drivers.

Table 5-20 Model accuracy retrieved from the validation process

Drivers	Model accuracy from validation
All drivers	68.00%
3 demographic-economic drivers	70.80%
3 environmental drivers	66.00%

The potential transition map in 2017 and the predicted map simulated using the three demographic-economic driver variables under the Status Quo scenario are illustrated in Figure 5-28. Areas near the existing disturbance have high potential to change in 2017, as indicated by the red and orange pixels in the potential transition map. The simulation outcomes show that the compositions of developed areas, bare land and cultivated land, plantations, mixed vegetation, conifers, and broad-leaved vegetation in the simulated 2017 map are 10.57%, 30.22%, 13.88% 14.82%, 7.46%, and 22.14%. There is no change in the coverage of water bodies (0.90%) because the pixels have been excluded before the land change simulations were conducted<sup>34</sup>.

<sup>34</sup> The output from land cover map development process from satellite imagery suggest that the area of lakes in the Ci Sangkuy upper water catchment in 2017 (1.46%) is larger than the area in the 2015 map (0.90%). LCM used the c.2000 and c.2015 maps to project the future land cover compositions and distributions in 2017 and 2030. Pixels identified as water bodies were excluded in the simulations. Therefore, the coverage of water bodies in the output from LCM (i.e. simulated 2017 and 2030 maps) is similar to the composition in the 2000 and 2015 base maps (i.e. 0.90% of total area).

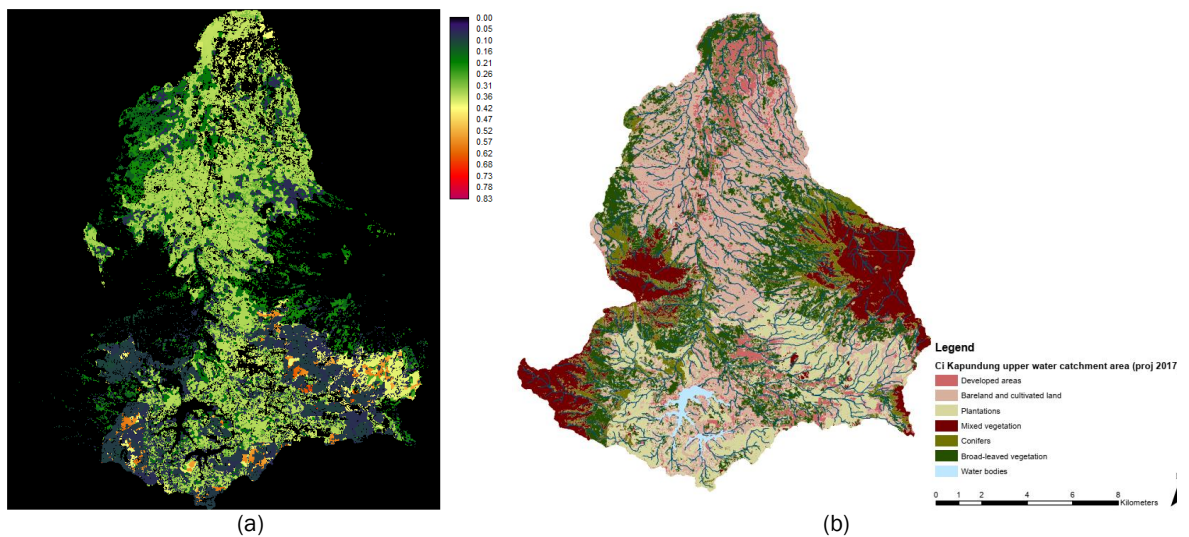


Figure 5-28 (a) Potential transition map in 2017; (b) Projected 2017 land cover map based on the Status Quo scenario

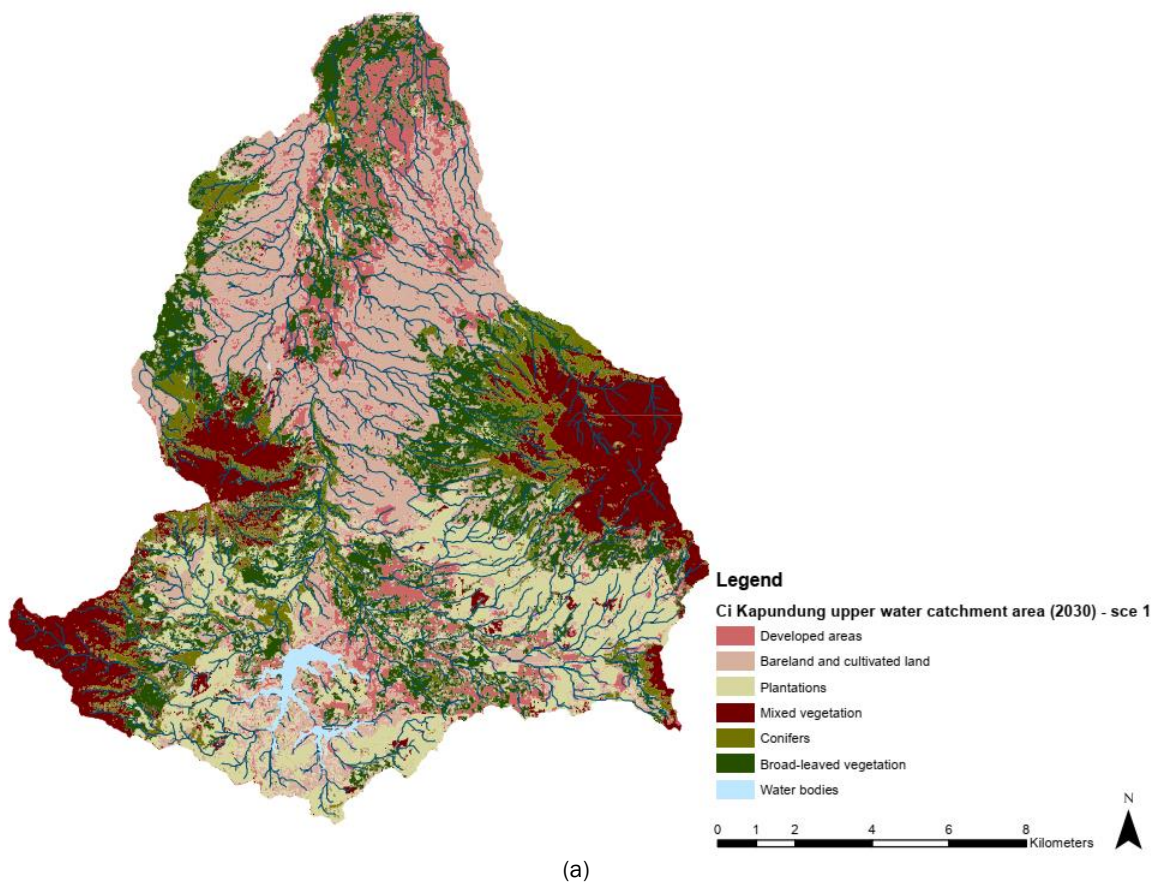
The compositions of developed areas in the 2017 map generated from the satellite imagery and in the simulated 2017 map were compared as part of model validation. This process was also performed by using the estimated increasing number of people living in the watersheds in 2015-2017 (refer to section 5.3.1). The coverage of developed areas in the 2017 map is 16.14% of the total area. The simulated map shows that the coverage of this land cover class is lower (10.57%). Based on the estimated population number on the site, only 9.75% of the region is built.

The actual 2030 land cover change was simulated based on the transition probability matrix (Table 5-21) and the transition maps generated from the MLP process using the three demographic-economic driver variables. It is expected that bare land and cultivated land is altered into developed areas with the probability of 0.1005. Bare land is also changed into other land cover classes, such as plantations and the three types of vegetation. Within the same period, the likelihood of areas covered by broad-leaved vegetation to change into bare land and cultivated land is 36.37%. There is a chance that bare land could change into plantation areas and vice versa in fifteen years. A possible explanation for this is given in Chapter 6.

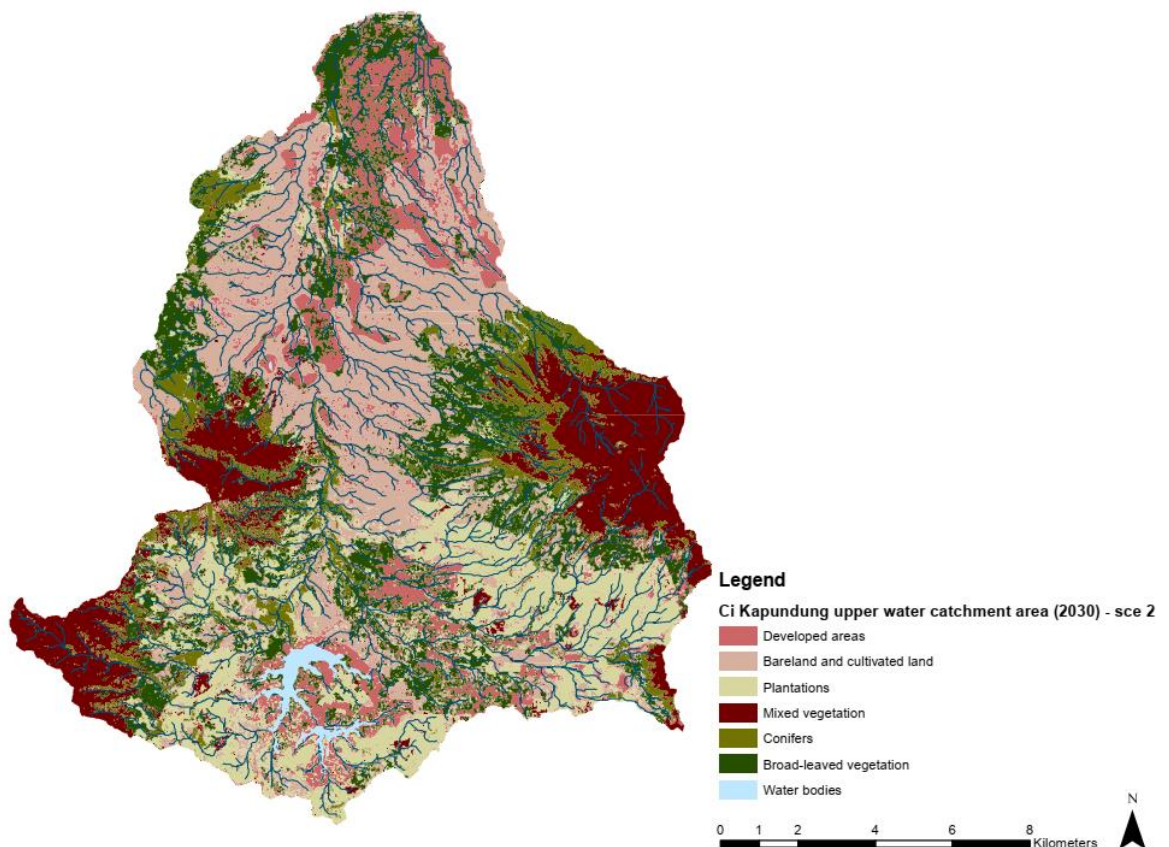
A similar approach to scenario development applied in land change simulations of the first case study area was used in this process. The results from land change modelling in the second case study area under three development scenarios are shown in Figure 5-29. The compositions of seven land cover types in each scenario in 2030 are presented in Table 5-22.

Table 5-21 Transition probability matrix to simulate the 2030 land cover map of the second study area

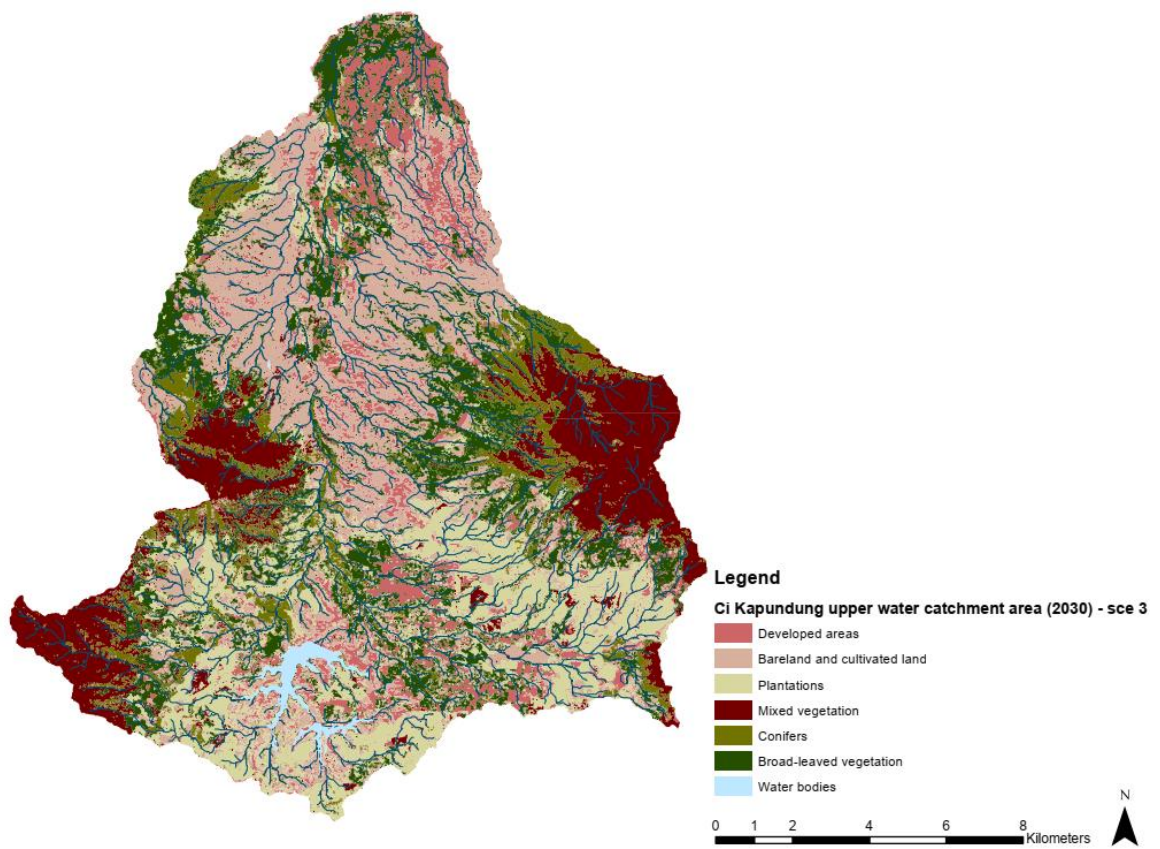
	Developed areas	Bare land cultiv. land	Plantations	Mixed veg.	Conifers	Broad-leaved veg.
Developed areas	0.9996	0.0004	0.0000	0.0000	0.0000	0.0000
Bare land and cultiv.	0.1005	0.5056	0.1070	0.0163	0.0405	0.2301
Plantations	0.0158	0.1583	0.7679	0.0083	0.0194	0.0303
Mixed veg.	0.0000	0.0000	0.0000	1.0000	0.0000	0.0000
Conifers	0.0000	0.0000	0.0000	0.0000	1.0000	0.0000
Broad-leaved veg.	0.0504	0.3637	0.0848	0.0000	0.0000	0.5011







(b)



(c)

Figure 5-29 (a-d) The projected 2030 land cover maps of the second case study area based on scenario 1, 2, and 3

Table 5-22. Land cover compositions in the Ci Sangkuy upper water catchment area for each scenario

Land cover types	Predicted land cover composition in 2030		
	Scenario 1	Scenario 2	Scenario 3
Developed areas	13.91%	13.91%	13.91%
Bare land and cultivated land	26.85%	26.85%	26.85%
Plantations	16.35%	16.35%	16.35%
Mixed vegetation	15.14%	15.14%	15.14%
Conifers	8.26%	8.26%	8.26%
Broad-leaved vegetation	18.60%	18.60%	18.60%
Water bodies	0.90%	0.90%	0.90%

It can be seen from the table that the compositions of all land cover types are similar in the three scenarios. However, the distribution of land cover is different. In general, the new development of settlements and infrastructure are concentrated near the existing disturbance on the north. In the first scenario, a scattered settlement pattern is expected to occur in the region, including areas near the streams. It is expected that more built-up areas occur surrounding the lakes in the second scenario, following the constraint maps developed using the existing spatial policies. However, the new settlements are also built on steep slopes area (5.17% of total area). In the third scenario, the new development is more dispersed in the centre of the watershed, and there is less percentage of the area will be built on steep terrain (4.13% of total area).

#### 5.3.4 The first iteration of hydrologic modelling (MIKE SHE 1)

MIKE SHE 1 was conducted to assess the depth of overland flow (m) and the capacity of different types of vegetation to reduce surface runoff in the first case study area using the 2015 and 2030 base maps (Rani et al. 2019). Three observation points were assigned to record the depth of overland flow on the day with the highest precipitation in 2013-2015 (Figure 5-30). Point 1 and 3 are located at the riparian with different types of plant, whereas Point 2 is located at the cultivated land near the riparian area. Saturated flow was excluded in the MIKE SHE simulations. Therefore, the results should be interpreted only based on the datasets used in the simulations (e.g. DEM, precipitation rate (2013-2015), reference evapotranspiration, projected 2030 land cover map, LAI, Manning's M numbers, and soil map and properties).

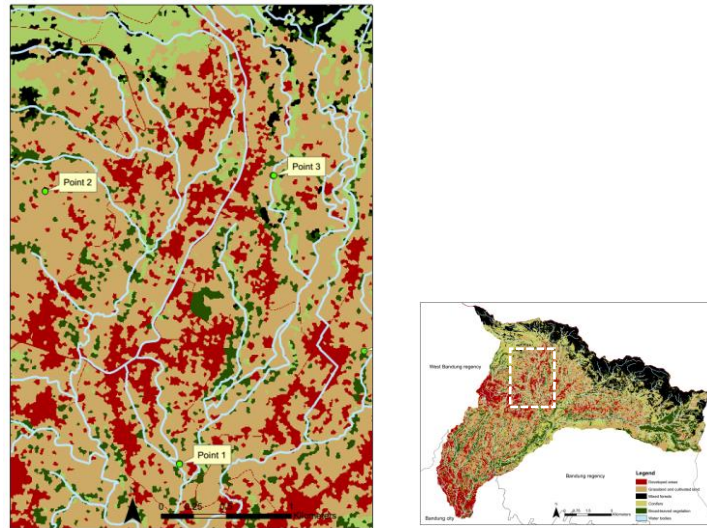


Figure 5-30 The location of three observation points in the Ci Kapundung upper water catchment area in MIKE SHE 1 model (Source: Rani et al. 2019)

The results from the first simulation of MIKE SHE 1 are presented in Table 5-23. It can be seen that the depth of overland flow in 2015 is relatively similar to the flow in 2030 in the Status Quo and the ecological design-based scenarios. The highest depth of overland flow in 2015 and in the two scenarios was recorded at Point 3. This point is located in the area dominated by clay soil (52.07%) and on the area with steeper slope (12.65°) compared with the other two points.

Table 5-23 The estimated depth of overland flow (mm) from the first iteration of hydrologic simulations of the Ci Kapundung upper water catchment area (Source: Rani et al. 2019)

Land cover maps	Depth of overland flow (mm)		
	Point 1	Point 2	Point 3
Existing 2015 land cover map	14.584	11.764	17.863
Projected 2030 map (Status Quo)	14.576	11.511	16.463
Projected 2030 map (Ecological Design)	11.697	12.244	17.146
<b>Dominant soil types:</b>	clay	silt	clay
<b>Slope gradient:</b>	4.76°	10.68°	12.65°

### 5.3.5 The second iteration of hydrologic modelling (MIKE SHE 2)

The second iterative hydrologic modelling (MIKE SHE 2) was performed to estimate the river discharges and the water balance.

#### (1) Model calibration and validation

MIKE SHE was used to simulating the P Flux and Q Flux at the observation points using the uncalibrated 120m models of Ci Kapundung and Ci Sangkuy watersheds. The initial model parameters described in the previous chapter were assigned in the MIKE SHE model. The

simulated P Flux and Q Flux had been multiplied by the model resolutions, and the base flow<sup>35</sup> had been added before the values were used in the model performance analysis. The uncalibrated Ci Kapundung and Ci Sangkuy models are presented in Figure 5-31 and Figure 5-32, respectively.

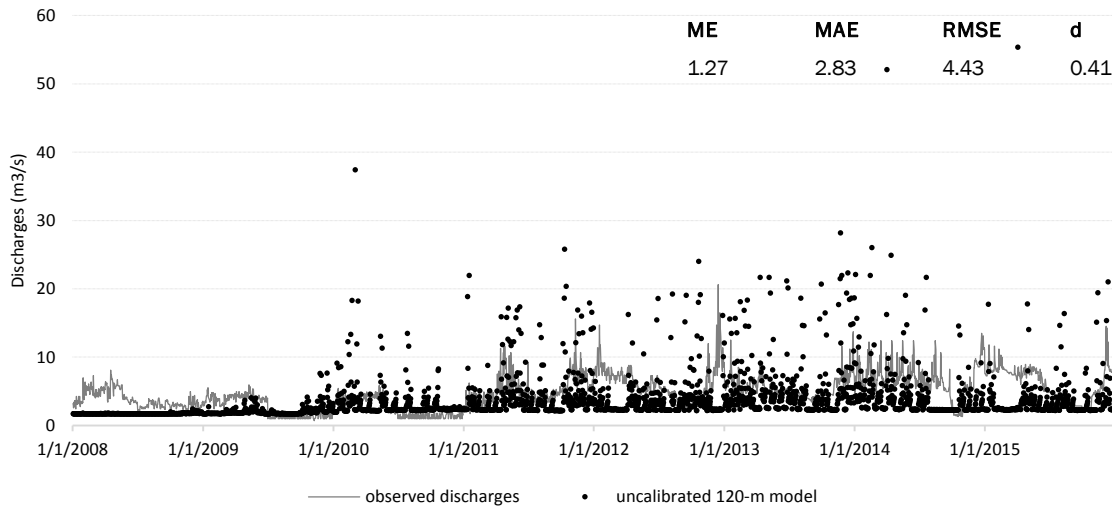


Figure 5-31 Simulated discharges (2008-2015) in the Ci Kapundung upper water catchment area (uncalibrated model)

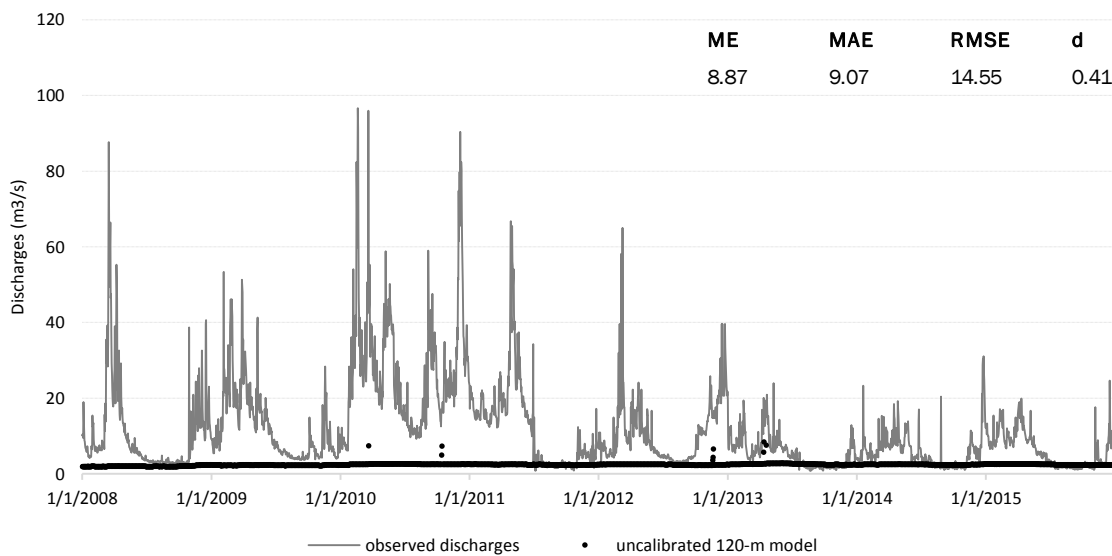


Figure 5-32 Simulated discharges (2008-2015) in the Ci Sangkuy upper water catchment area (uncalibrated model)

Model parameters (e.g. precipitation correction, canopy interception, and ET surface depth) were adjusted during the calibration process using the trial-and-error method. After the models had been calibrated (1/1/2008 00:00 – 01/01/2012 00:00), model validation (01/01/2012

<sup>35</sup> The estimation of baseflow of Ci Kapundung and Ci Sangkuy Rivers (2008-2015) can be seen in Appendix D.

00:00 – 01/01/2016 00:00) was performed. The model calibration and validation for the two case study areas can be seen in Figure 5-33 and Figure 5-34. The calibrated and validated models, then, were used to project the river discharges in the three scenarios.

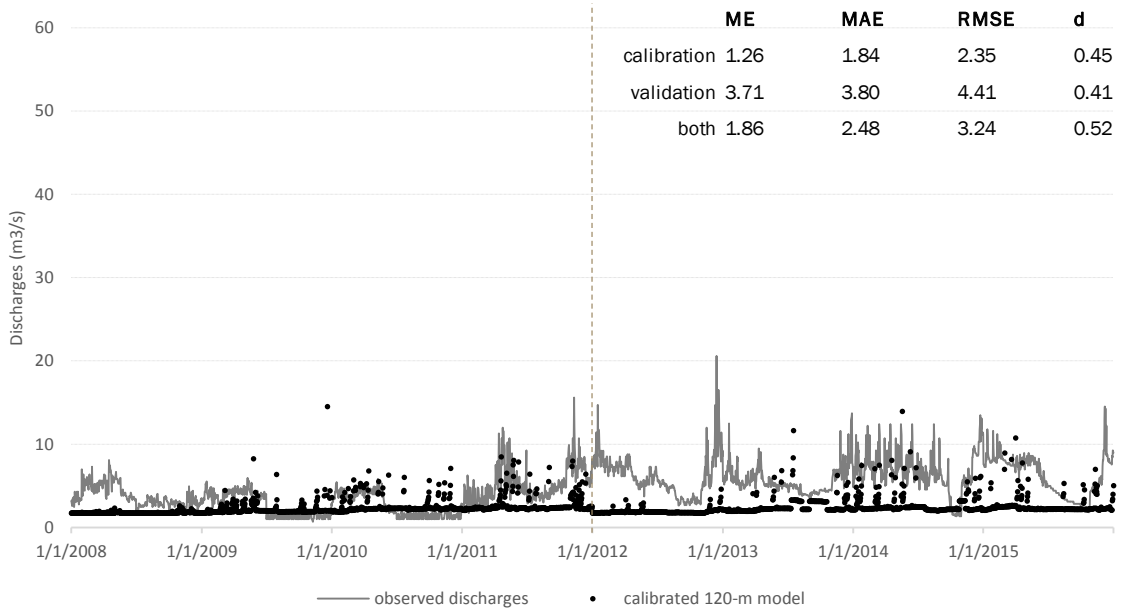


Figure 5-33 Simulated discharges (2008-2015) in the Ci Kapundung upper water catchment area (calibrated model)

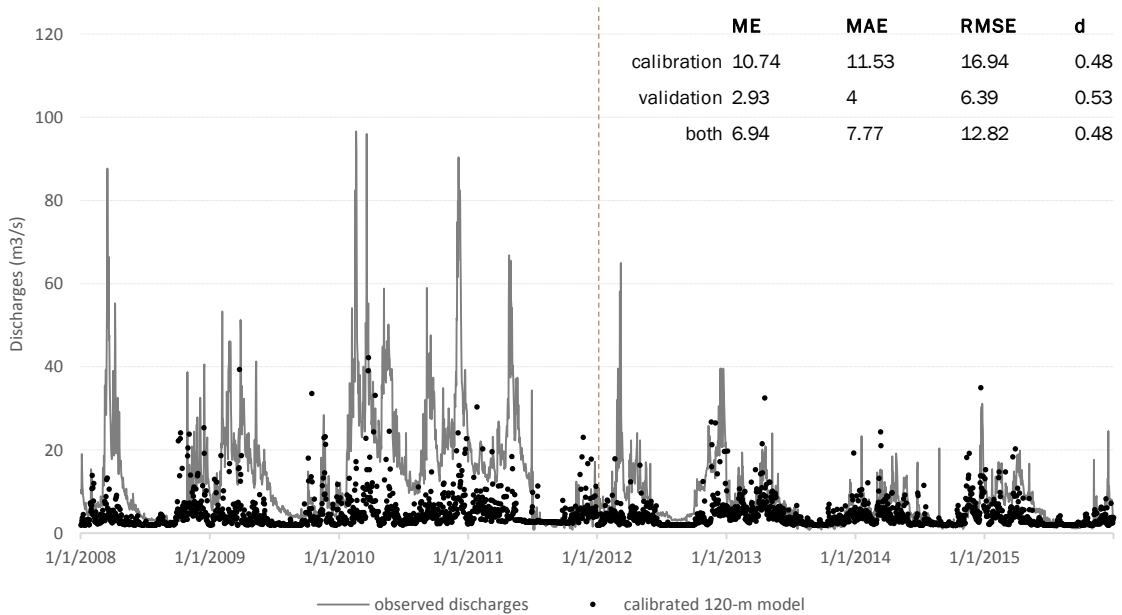


Figure 5-34 Simulated discharges (2008-2015) in the Ci Sangkuy upper water catchment area (calibrated model)

(2) Projected discharges in the three future development scenarios

The projected Ci Kapundung and Ci Sangkuy River discharges in the three scenarios are illustrated in Figure 5-35 and Figure 5-36, respectively.

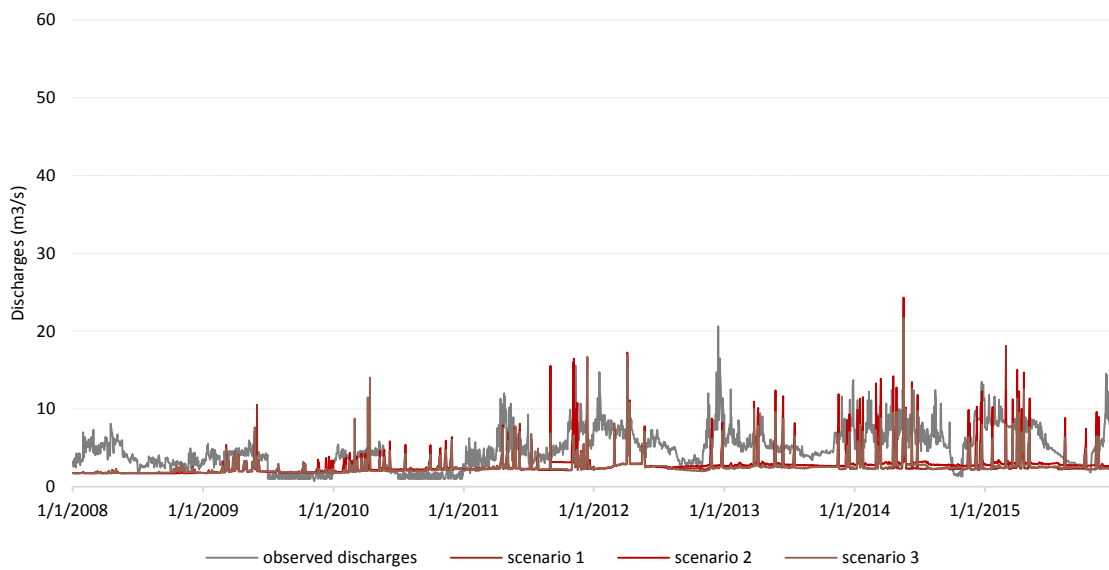


Figure 5-35 Projected discharges in the Ci Kapundung upper water catchment area

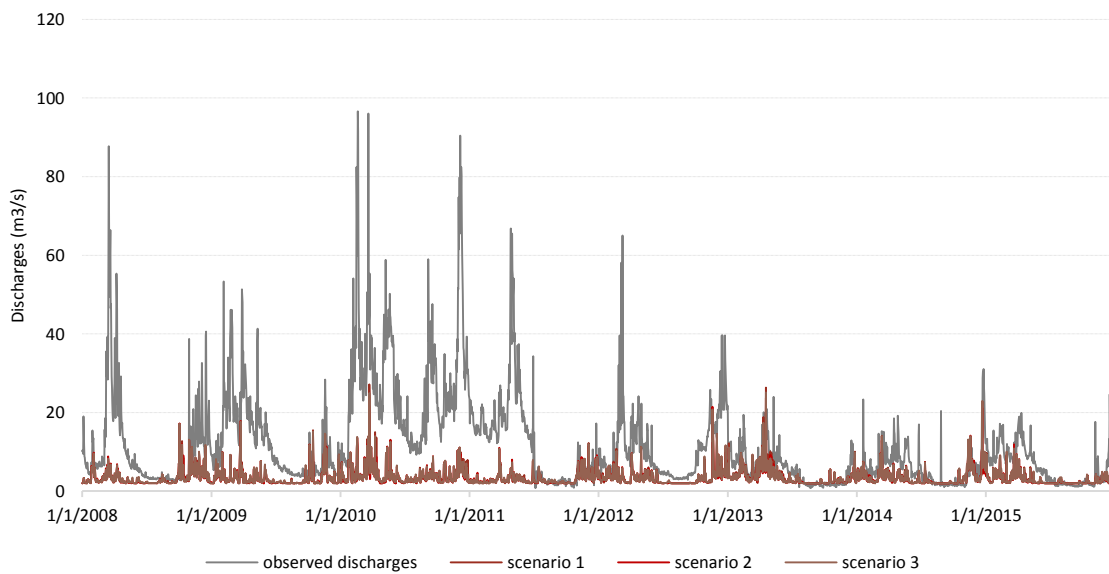


Figure 5-36 Projected discharges in the Ci Sangkuy upper water catchment area

The highest volume of discharges from the two rivers in the three scenarios was defined from the simulated discharges (Table 5-24). The results were evaluated against the observed discharges (2008-2015) to determine one of the benchmarks for the development of scenario 4 (i.e. backcasting scenario)<sup>36</sup>. The thresholds of flood discharges for the two rivers defined in

<sup>36</sup> The development of scenario 4 is presented in Chapter 7. Another benchmark for scenario 4 is the outcome from the water balance analysis as part of the initial phase of Pareto-frontier assessment.

the Subchapter 5.2 were used as part of the criteria to assess the capacity of each scenario to reduce peak discharges in each watershed.

The estimation of flood discharges in both rivers is presented in the third section of Subchapter 5.2. It is assumed that the discharges from other catchments in the Bandung Basin on the same day will not exceed 173.1 m<sup>3</sup>/s and 91.4 m<sup>3</sup>/s when conducting the simulations for the first and the second case study area, respectively.

Table 5-24 The highest observed and simulated discharges in the Ci Kapundung and Ci Sangkuy upper water catchment areas in each scenario

Scenario	Discharges	
	Ci Kapundung River	Ci Sangkuy River
Simulated existing condition	35.42 m <sup>3</sup> /s	42.26 m <sup>3</sup> /s
Scenario 1 (Status Quo)	18.08 m <sup>3</sup> /s	27 14 m <sup>3</sup> /s
Scenario 2 (Existing policy)	24.32 m <sup>3</sup> /s	23 71 m <sup>3</sup> /s
Scenario 3 (Ecological Design)	21.69 m <sup>3</sup> /s	25.13 m <sup>3</sup> /s
<b>The highest observed discharges:</b>	20.6 m <sup>3</sup> /s (14/12/2012)	96.6 m <sup>3</sup> /s (28/02/2010)
<b>Estimated flood discharges:</b>	14.3 m <sup>3</sup> /s	96 m <sup>3</sup> /s

### (3) Water balance

Water balance from the existing conditions (2008-2015) and the three future scenarios of the two case study areas has been estimated (Table 5-25 and Table 5-26). The results suggest that all scenarios have lower surface runoff compared with the existing condition. Scenario 1 has the highest rate of evapotranspiration (10,913.80 mm), and scenario 3 has the lowest overland (OL) boundary outflow (2,415.17 mm) among all future scenarios in the Ci Kapundung upper catchment area.

Table 5-25 Accumulated water balance of Ci Kapundung upper water catchment area (2008-2015) (mm)

	Basemap	Scenario 1	Scenario 2	Scenario 3
Precipitation	-31,791.50	-31,791.50	-31,791.50	-31,791.50
Canopy storage ch	0.18	0.17	0.17	0.18
Evapotranspiration	10,909.70	10,913.80	10,801.90	10,772.80
OL storage change	954.52	838.69	882.10	803.19
OL boundary outflow	4,624.89	2,590.24	3,173.42	2,415.17
Subsurface storage ch	120.88	119.58	120.11	119.14
Total error	-15,181.40	-17,329.10	-16,813.90	-17,681.10

Similar to the first case study area, the simulated overland outflow from scenario 1, 2, and 3 is lower than the flow from the existing condition. The highest rate of evapotranspiration was retrieved from scenario 2 (11,778.20 mm). The high number of evapotranspiration has a correlation with the lowest overland outflow from scenario 2 (64,554.60 mm), in comparison with scenario 1 (70,933.10 mm) and scenario 3 (69,187.20 mm).

Table 5-26 Accumulated water balance of Ci Sangkuy upper water catchment area (2008-2015) (mm)

	<b>Basemap</b>	<b>Scenario 1</b>	<b>Scenario 2</b>	<b>Scenario 3</b>
Precipitation	-240,866.00	-240,866.00	-240,866.00	-240,866.00
Canopy storage ch	2.45	2.55	2.85	2.52
Evapotranspiration	10,967.70	11,130.30	11,778.20	11,097.80
OL storage change	2,299.51	1,898.55	3,311.83	1,838.20
OL boundary outflow	134,450.00	70,933.10	64,554.60	69,187.20
Subsurface storage ch	20.18	19.66	21.12	19.56
Total error	-93,126.50	-156,882.00	-161,197.00	-158,721.00

Water balance analysis was also conducted using the maps with uniform land cover (e.g. bare land and cultivated land and conifers) for the initial phase of Pareto-frontier analysis (Table 5-27 and Table 5-28). Ci Kapundung upper catchment with conifers as the land cover type area generates less runoff volume (4,616.01 mm) compared with bare land and cultivated land (6,444.69 mm). Conifers in the Ci Sangkuy upper water catchment area also have a lower volume of overland outflow (713,180.00 mm) than that of bare land and cultivated land (831,341.00 mm).

Table 5-27 Accumulated water balance of Ci Kapundung upper water catchment area with a uniform land cover type (2008-2015) (mm)

	<b>Bare land-cultivated land</b>	<b>Conifers</b>
Precipitation	-31,791.50	-31,791.50
Canopy storage ch	0.00	2.65
Evapotranspiration	8,850.32	13,264.50
OL storage change	1,220.49	1,041.51
OL boundary outflow	6,444.69	4,616.01
Subsurface storage change	123.95	120.34
Total error	-15,152.20	-12,746.60



Table 5-28 Accumulated water balance of Ci Sangkuy upper water catchment area with a uniform land cover type (2008-2015) (mm)

	Bare land-cultivated land	Conifers
Precipitation	-240,866.00	-240,866.00
Canopy storage ch	0.0008	8.27
Evapotranspiration	9,492.48	13,195.40
OL storage change	17,510.80	14,320.70
OL boundary outflow	831,341.00	713,180.00
Subsurface storage change	33.93	38.69
Total error	614,322.00	503,068.00

## 5.4 Types of vegetation to improve flood regulation

The capacity of vegetation to reduce surface runoff was assessed in the first and second iteration of hydrologic simulations to address the third research question: “Which types of vegetation can improve flood regulation in each upper water catchment area?”. The results from MIKE SHE 1 and 2 to assess the vegetation capacity to reducing runoff are presented as follows.

### 5.4.1 Vegetation analysis in MIKE SHE 1

In MIKE SHE 1, the third research question was addressed by simulating the depth of overland flow (mm) using the altered 2030 land cover map of Ci Kapundung watershed. The map was developed from the ecological design-based scenario (scenario 3 in LCM 1). There is only one type of vegetation in each map. The three observation points assigned in the previous MIKE SHE 1 simulations (Figure 5-30) were used again to record the depth of overland flow (Table 5-29).

The result suggests that runoff at the second point has the lowest level compared with the other two points despite the different type of vegetation assigned on the maps. The depth of overland flow on the map with conifers as the single vegetation are 7.574 mm and 8.356 mm recorded at the first and third points respectively. These values are lower than the runoff recorded at the same points when broad-leaved or mixed vegetation was assigned on the maps (Rani, Lange, Cameron, et al., 2019).

Table 5-29 The depth of overland flow (mm) estimated from the 2030 land cover map of Ci Kapundung watershed with a single type of vegetation (MIKE SHE 1) (Source: Rani et al. 2019)

Vegetation	Depth of overland flow (mm)		
	Point 1	Point 2	Point 3
Conifers	7.574	5.103	8.356
Broad-leaved vegetation	7.949	5.044	8.364
Mixed vegetation	7.949	5.044	8.364
<b>Dominant soil types:</b>	clay	silt	clay
<b>Slope gradient:</b>	4.76°	10.68°	12.65°

### 5.4.2 Vegetation analysis in MIKE SHE 2

Iterative MIKE SHE simulations and water balance analyses have also been performed to assess the capacity of vegetation on different soil types to reduce runoff. Figure 5-37 summarises the total overland boundary outflow in the first case study areas, as the output from the first assessment of vegetation analysis. The detailed results from the initial water balance analysis of the first case study area are given in Appendix E.

The outcome from the first analysis suggests that scenarios with cultivated plants in the four soil types generate the least total outflow (379.22 – 864.18 mm). Areas with broad-leaved vegetation and soil C has the highest total outflow (13,015.20 mm) in the catchment compared with the other fifteen scenarios. The possible reasons for this unexpected outcome are further discussed in the preceding chapter. Based on this result, the second vegetation analysis was performed.

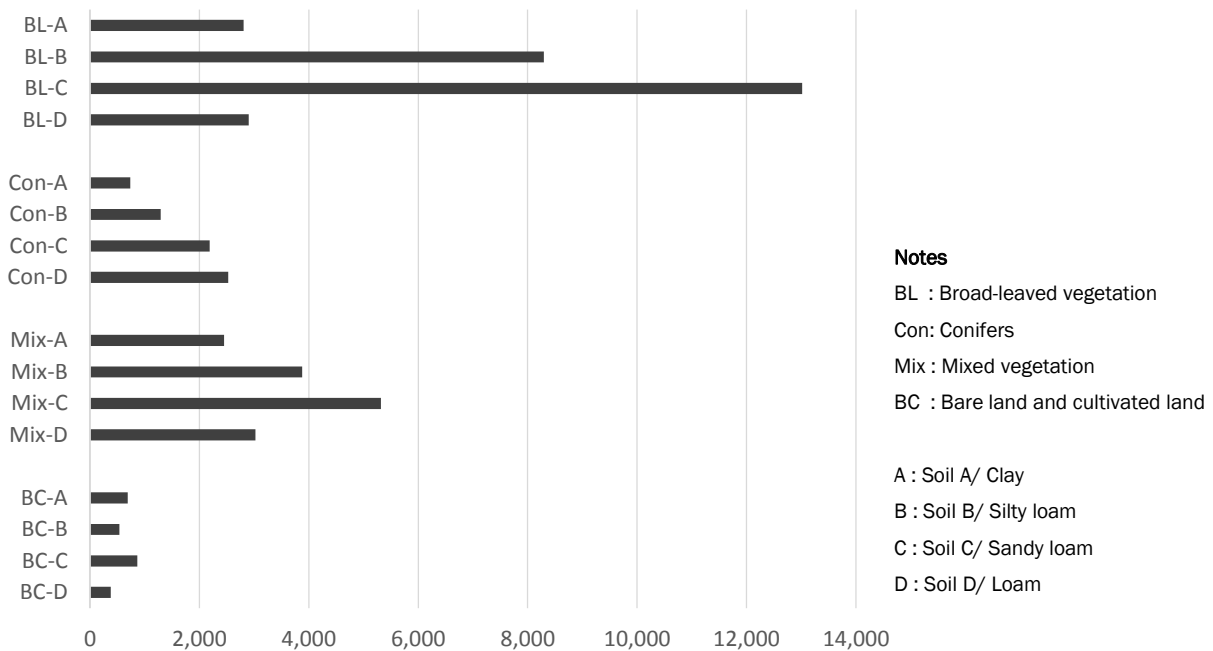


Figure 5-37 Accumulated overland boundary outflow of Ci Kapundung upper water catchment area with 16 combinations of different land cover and soil types (2008-2015) (mm)

The second vegetation analysis using a hypothetical catchment was then conducted based on the evaluation to the result from the previous analysis. The analysis included an additional two variables that arguably affect the runoff generation process (e.g. precipitation rates and slope gradients), in addition to land cover and soil types. The simulated overland outflow under low and high precipitation rates are presented in Figure 5-38 and Figure 5-39, respectively.

It is apparent from the two graphs that overland outflow from the forested catchments on moderate and steep slopes is almost similar under the low rainfall but varies under higher

rainfall (refer to Appendix E). Overland flow values from the catchment covered by conifers on all four soil types are the lowest among all scenarios under low rainfall (5,699.80 – 5,733.35 mm). These values are slightly lower than the overland flow in the four mixed vegetation scenarios (5,707.39 – 5,741.17 mm).

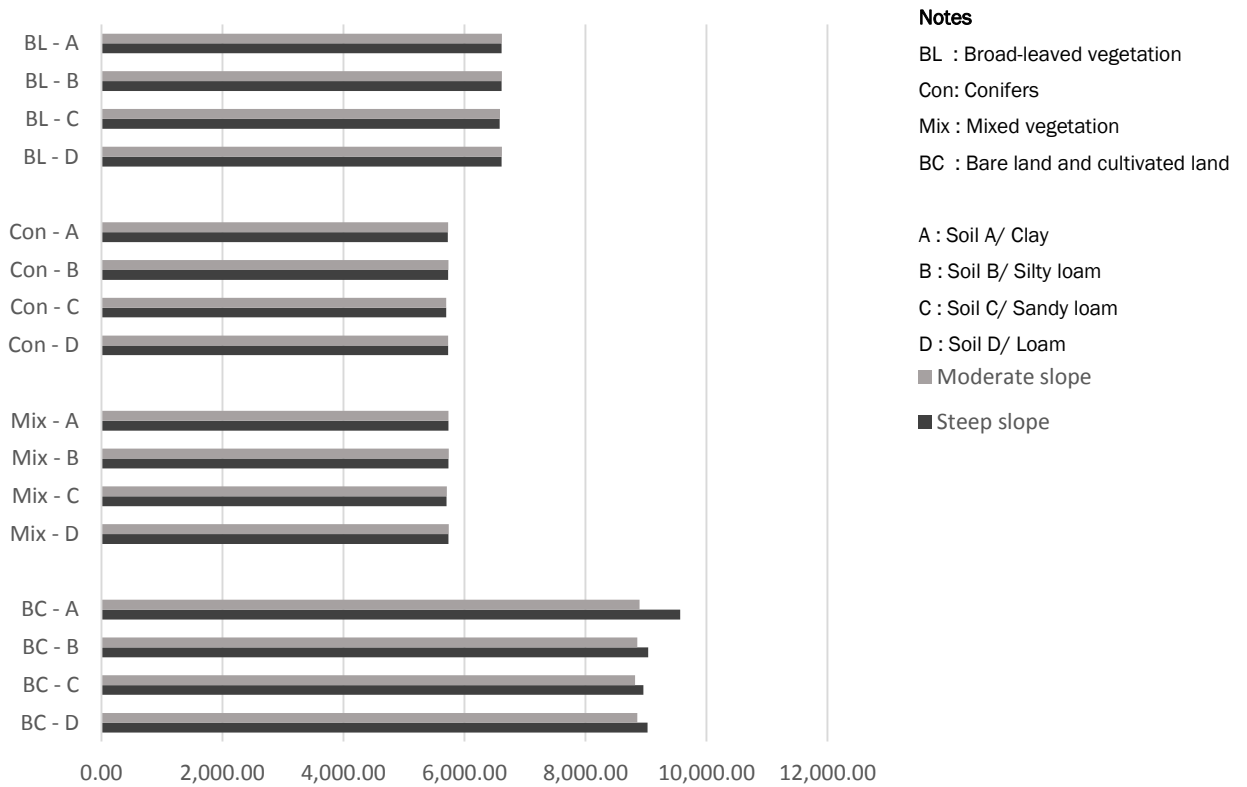


Figure 5-38 Accumulated overland boundary outflow of a hypothetical catchment with 32 combinations of different land cover, soil types, and slope gradients under low rainfall event (2008-2015) (5 mm/day)

In general, surface runoff could not be absorbed effectively on steep slopes in all scenarios during high precipitation (Figure 5-39). Overland outflow from four hypothetical catchments with soil A is higher than the outflow from other scenarios. It was also found that conifers on soil A, B, and D, and mixed vegetation on soil C generate the lowest volume of surface runoff on both slope gradients under heavy rainfall (146,003 - 235,694 mm).

Overall, these results indicate that **land cover, soil types, and slope gradients are the influential variables in flood regulation, particularly during heavy rainfall.** The effects of each variable in flood regulation are further discussed in the following chapter, which underlies the development of proposed landscape planning in the two upper water catchment areas.

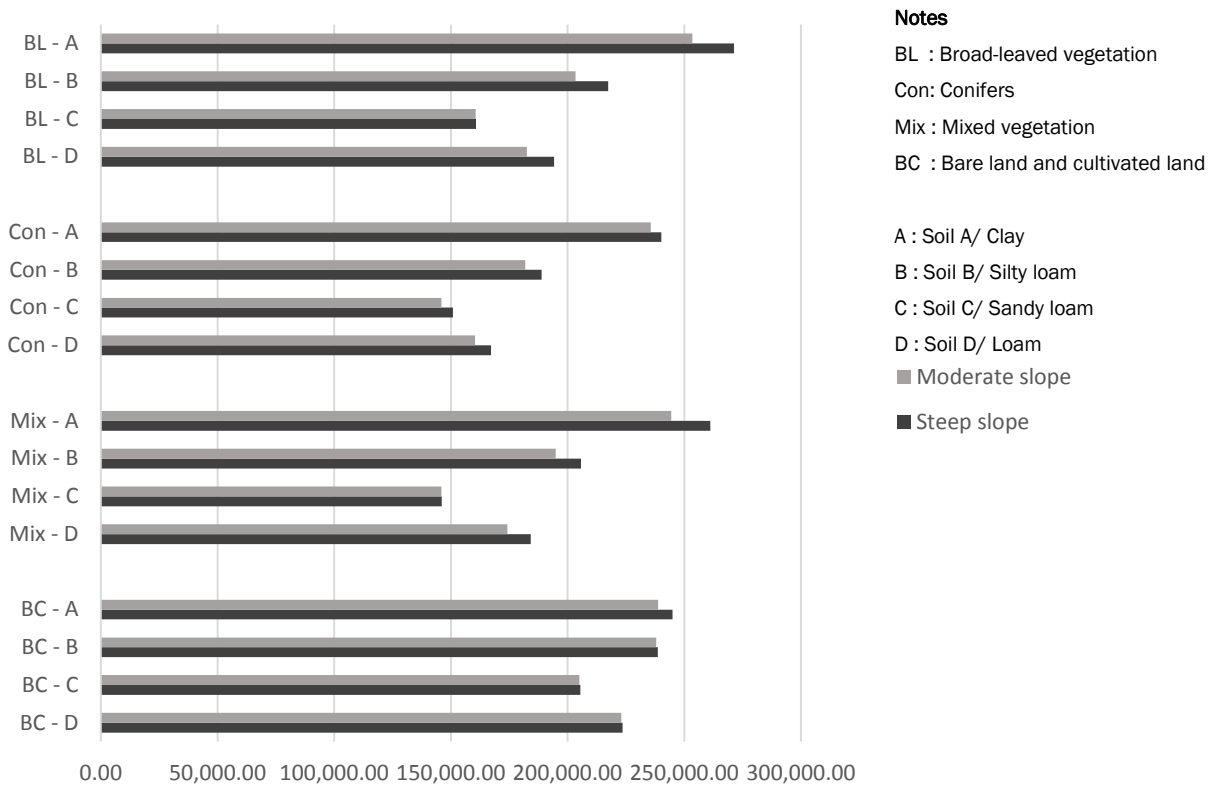


Figure 5-39 Accumulated overland boundary outflow of a hypothetical catchment with 32 combinations of different land cover, soil types, and slope gradients under high rainfall event (2008-2015) (100 mm/day)

## 5.5 Summary of Chapter 5

- (1) The modelling outcomes from 64 hypothetical catchments show that the overland flow is not only affected by the plant characteristics, but also by the rainfall trend, slope and soil conditions.
- (2) The increasing trend of Ci Kapundung River discharge in 2001-2017 was influenced by the land cover change. The declining trend of Ci Sangkuy River discharge in the same period was caused by the increasing percentage of forest cover and the decreasing precipitation rates.
- (3) The composition and distribution of land cover in each case study areas affect the river discharge and overland flow.

## Chapter 6 Discussion

The first part of this chapter reviews the challenges and the works to improve the accuracy of land cover maps, the land change model and the hydrologic model. The subsequent three subchapters present arguments regarding the results from the analyses to address the three research questions.

### 6.1 Accuracy of land cover maps, land change, and hydrologic models

#### 6.1.1 Challenges in developing highly accurate land cover maps

Five sources of uncertainty in the accuracy assessment of land cover maps have been identified in this study (e.g. sampling design, image processing, ground or reference data, the spatial distribution of error, and mixed pixels). The sources of uncertainty and the assumptions made during the land cover map development process are described as follows:

##### (1) Sampling design

In this study, transect walk was chosen as the method to conduct the field surveys, because of the limited access in the case study areas, especially in the forests and areas with steep slopes. Consequently, the sampling points could not be distributed evenly on the site. This problem caused pixels in the imagery might be classified incorrectly, affecting the image accuracy, especially in the forest classification. Therefore, maps from Perhutani were used to select samples of segments representing different forest types during the image classification process. It is assumed that the forest types were not changed in 2000-2017. However, when the forests were changed into other types of land cover (e.g. developed areas or agriculture), these changes were identified by referring the SPOT pan-sharpened infrared satellite imagery and the ESRI's base maps with higher resolution.

##### (2) Image processing

Image pre-processing for the SPOT and Landsat imagery was conducted using the *i.atcorr* plugin in GRASS GIS for the atmospheric correction (AC), and the SCS+C equation for topographic correction (TC) procedure. The TC model was manually developed using the ModelBuilder tool in ArcGIS based on the SCS+C equations (Soenen, Peddle, & Coburn, 2005). Thus there is a possibility to have uncertainties in the image processing because of this manual process. Nevertheless, the abstraction of geographical information (data modelling) could not be done with perfect accuracy because of its complexity process (Zhang & Goodchild, 2002).

The image pre-processing in this study was only conducted using one selected method for each image correction procedure. It is argued that different AC and TC methods applied can provide

distinct outcomes from the image classification process. The applications of other AC and TC and their effects on image accuracy have been covered in other studies (e.g. Vanonckelen et al. 2013; Sola et al. 2016), and are not the scope of this thesis.

In the image classification process, different pieces of software might give different results depending on the way they were set up. An example of the result from the image classification process of the same area using two GIS programs is further reviewed in the next part of this subchapter. Another challenge in the development of land cover maps is the clouds and cloud shadows which are often found in the satellite imagery of tropical regions. This issue has been solved in the last iteration of the map development process. Constant cloud coverage becomes a potential problem when classifying vegetation in these areas (Toure et al., 2018; Helmer et al., 2012).

#### (4) Ground or reference data

The high resolution of satellite imagery in the ESRI base maps was used as a reference dataset during the accuracy assessments of land cover maps. ESRI provides satellite imagery for base maps in ArcGIS from various resources. The satellite imagery for the two case study areas is WorldView 3 from DigitalGlobe taken in 2015. However, it is vital to identify the uncertainty factor in the accuracy assessment process. There is a possibility to have an error in the satellite imagery with higher resolution as reference data for validation of image classification (Foody 2002). This imperfect ground reference dataset increases the inaccuracy of maps (Foody 2010).

The pan-sharpened infrared SPOT images with a spatial resolution of 1.5m were also used to assess the accuracy for land cover maps. The images are clear enough to visually differentiate the main land cover types, such as developed areas, bare land and cultivated land, plantations, and water bodies. However, it is still difficult to differentiate the three types of forest (i.e. conifers, broad-leaved woodland, and mixed woodland). Therefore, the forest maps from Perhutani were also used in the assessment process.

#### (5) The spatial distribution of error

The error of land cover classification is mostly found in the boundary of classes because of mixed pixels, which is also addressed by Foody (2002). In this study, the error also occurred in the land cover classes next to clouds and/or cloud shadows. In the SPOT imagery, although the pixels showing clouds and cloud shadows have been delineated and masked out before the image classification process was conducted, many mixed pixels contain brightness from clouds/cloud shadows and the land cover next to them (Figure 6-1). As a result, these mixed pixels could not be masked out when the original values of thresholds for NIR and Blue bands for cloud masking

(Candra, Kustiyo, & Ismaya, 2014) were used. Therefore, the pixels were manually delineated and masked out in ArcGIS. Otherwise, those pixels would be assigned as other land cover classes with higher reflectance value, such as developed areas, as seen in the area inside the orange circle in Figure 6-1.

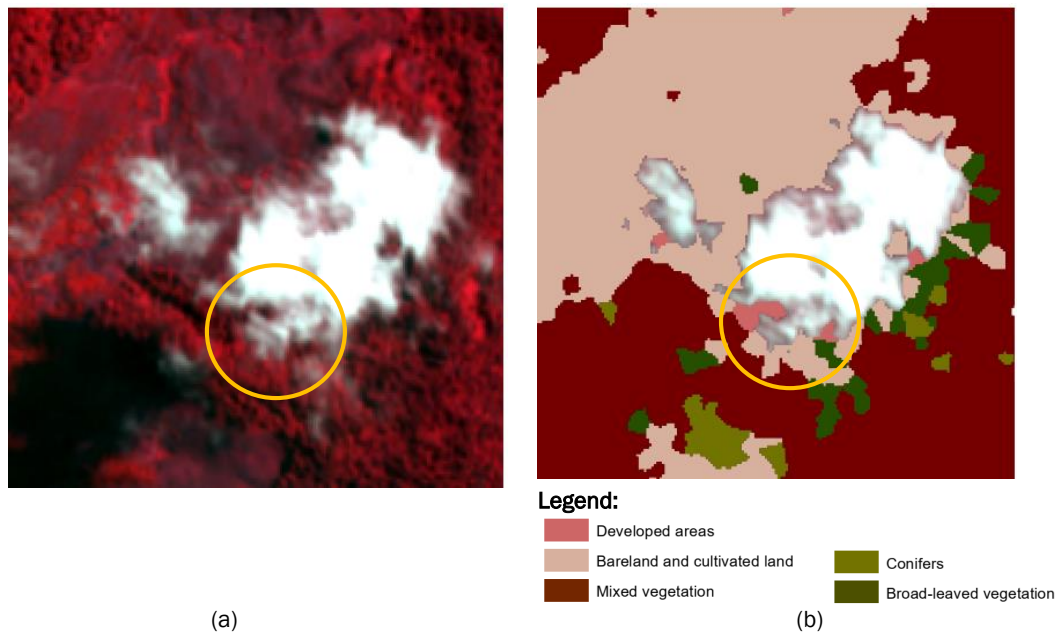


Figure 6-1 (a) Infrared image of the forest in Ci Kapundung watershed; (b) Distribution of error surrounding clouds (orange circle) (Source: SPOT imager from © AIRBUS DS 2015)

#### (6) Mixed pixels

Two types of satellite imagery with different spatial resolutions were used in the second iteration of the land cover map development process in this study. Although SPOT 6 imagery has a 6-m resolution and is higher than the resolution for Landsat imagery (30m), mixed pixels can still be found in the SPOT imagery. An example can be seen in pixels showing small roads next to agriculture. These pixels contain brightness of impervious areas (in this study, they belong to a land cover type called 'developed areas'), and the 'bare land and cultivated land', which were often be classified as one object during the image segmentation process. The procedures to solve this problem are discussed in the second section of this subchapter.

The problem of mixed pixels was also found in the Landsat imagery when there might be two or more land cover types are shown in one pixel. Therefore, the way the pixels were classified causes uncertainty. NDVI analyses were performed as part of the backdating process to classify the vegetation and non-vegetation objects in the 2000 Landsat imagery. The problem of mixed pixels in the Landsat imagery is illustrated in Figure 6-2. Although the NDVI analysis was not conducted for classifying the land cover in 2015, Figure 6-2 was created to show how pixels near the cultivated areas in the imagery could not be identified as developed areas due to the resolution of Landsat image. It can be seen from the pan-sharpened infrared image from SPOT

6 imagery that many pixels of Landsat imagery were not included in the 'developed area' class. This result could be affected by the lower resolution of Landsat images (30m). Pixels surrounding the identified developed areas are mixed pixels, containing the reflectance values of both developed areas and other land cover types. In this study, the thresholds for NDVI to identify the developed areas in Landsat images were determined only to cover the non-mixed pixels. Therefore, the mixed pixels surrounding the developed areas were identified as the other dominant land cover types next to developed areas.

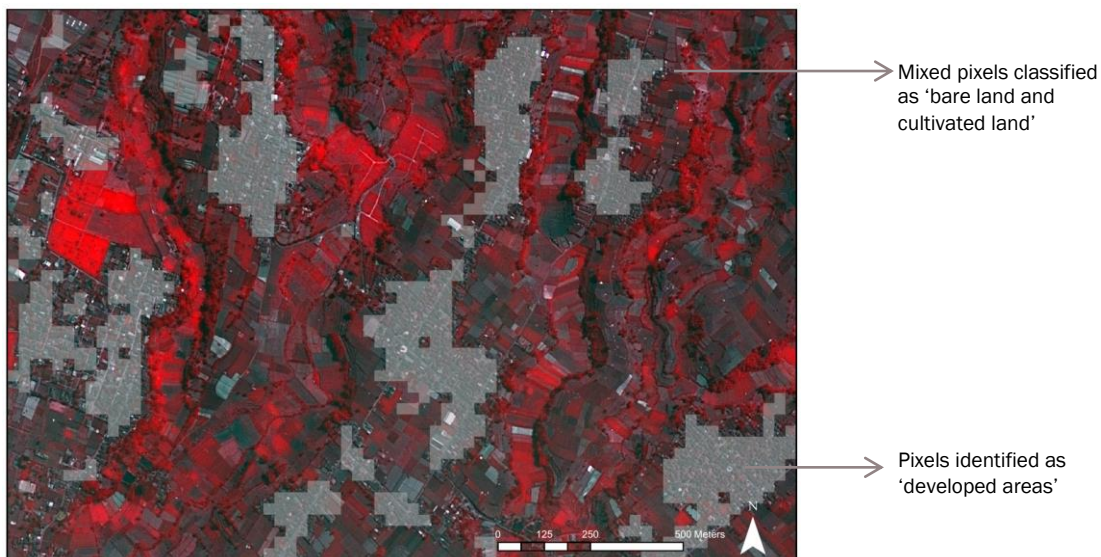


Figure 6-2. White pixels identified as developed areas in the 2015 Landsat imagery of the first case study area (Source: NDVI analysis using Landsat imagery from EROS USGS. Background image from © Airbus DS (2015))

It is argued that the uncertainty factors above have affected the classification accuracies for all generated land cover maps. The percentages of built-up areas in each case study were predicted based on the estimation of population number in 2017 (Subchapter 5.3) and the area required per-person, as part of a validation process for the 2017 land cover maps. It is expected that the coverages of built-up area based on the estimated population number in the first and the second case study areas in 2017 are approximately 15.88 km<sup>2</sup> (15.34% of total area) and 19.99 km<sup>2</sup> (9.75% of total area) respectively. However, the actual coverages derived from the 2017 generated maps are 19.82% for the Ci Kapundung watershed, and 16.14% for the Ci Sangkuy watershed.

The discrepancies of percentages of developed areas calculated based on the estimated population number and from the 2017 maps might be caused by the mixed pixels. There is a possibility that mixed pixels in each image were classified as different types of land cover, depending on which segments were chosen as training data during the image classification procedure.

Another factor which may partially affect the results is the application of the backdating and updating method in this study. The development of 2017 maps relied on the 2015 maps.



Therefore, any errors in the 2015 maps would be reflected in the generated 2017 maps. For example, it is assumed that the developed areas in 2015 would not change into other land cover types in 2017<sup>37</sup>. Thus, built-up areas in the c.2017 maps were assigned based on this assumption and the built-up areas identified in the individual 2017 maps. However, not all pixels classified as developed areas in 2015 are representing the actual developed areas, as suggested by the outcomes from the accuracy assessments.

### 6.1.2 Improving classification accuracy and consistency of multi-temporal land cover maps

#### (1) The land cover classification process

At the beginning of the land cover map development process of the first case study area using ArcGIS, pixels identified as water bodies had not been masked out before the image classification process was conducted. Therefore, the parts of the image identified as forests were classified as water bodies. This outcome could be caused by high moisture in the forests. Thus the pixels were mistakenly classified as water bodies. This classification problem was solved by excluding pixels identified as water bodies in the subsequent image classification processes by applying water masks to the images.

The problem of mixed pixels was found during the image classification of small size or thin objects, such as road lines near bare land or forests. In the object segmentation process in SAGA GIS, the pixels identified as road lines, which should be classified as developed areas, were often grouped with pixels next to them (e.g. bare land and cultivated land and forests). The problem occurred because the width of road lines is smaller than the spatial resolution of SPOT 6 images, which were used in the classification process (i.e. one pixel of a SPOT 6 image with 6 metres of spatial resolution can contain brightnesses from two or more land cover types). Therefore, the shapefiles of road networks in the case study areas retrieved from OpenStreetMap were used to mask out the road lines before the classification process was conducted.

During the third iteration of the land cover classification process, NDVI was used to classify vegetation and non-vegetation in the 2000 Landsat imagery, which could increase the computational speed. A specific threshold of NDVI has been assigned in each map. Due to a similar range of reflectance values, the non-vegetation class may contain both developed areas and bare land. Pixels identified as a non-vegetation class in the first level of classification were

---

<sup>37</sup> The backdating and updating method was used in the last iterations of land cover map generation process because of its efficiency and its capability to solve the problem found during the first iteration of land change modelling. In the LCM 1 of the first case study area, the coverages of all land cover types were changed significantly during the simulation period (2013-2015). Based on the land outcome from land change analysis, each land cover class gained and lost the total coverage of more than 4 km<sup>2</sup>. This result suggested that many mixed pixels were classified inaccurately.

put together with the 'cultivated land' sub-class, into the 'bare land and cultivated land' class at the second level of process (Chapter 4).

## (2) Image classification accuracies

Two initial image classification processes had been conducted using the object-based image classification in ArcGIS and SAGA GIS before the last iteration of the classification process was performed. The aim of these two preliminary studies is to test different approaches to conduct the image classification, in order to get higher accuracy of classification. It is important to have a relatively high accuracy of land cover maps, because it affects the accuracy of land change models, as suggested by Zubair & Ji (2015).

In the first preliminary study, only two forest types were classified (e.g. conifers and mixed forest<sup>38</sup>). Therefore, there are only five and six types of land cover in the first and second case study areas, respectively<sup>39</sup>. A modified sun-canopy-sensor correction (SCS+C) as topographic correction method (Soenen, Peddle, & Coburn, 2005) was applied to the satellite images of the Ci Kapundung watershed and half area of the Ci Sangkuy watershed (2015). The image classification process was conducted in ArcGIS. In this preliminary study, no atmospheric correction was applied to the imagery. This analysis was performed only to test the applicability of SCS+C as the selected topographic correction method in this study. The results showed that the correction method could improve the overall accuracies of image classification for the first and the second case study areas from 74.25% to 77% and from 80.44% to 87.58% respectively (Rani et al., 2017).

The second preliminary study was conducted using the 2015 imagery of the first case study area. The SCS+C topographic correction was applied to the imagery. No atmospheric correction was performed. In this study, the object-based image classification tool from SAGA GIS was used, instead of ArcGIS, and three forest types were classified during the process (i.e. conifers, broad-leaved plants, and mixed plants). The overall accuracy for the classified image for Ci Kapundung watershed is 87.40% with Kappa statistics of 0.83, and it is higher than the previous result of classification using ArcGIS (77%). These preliminary studies show that different parameters chosen in each type of GIS software affect the accuracy results<sup>40</sup>. Therefore, based on this result, the object-based image classification in SAGA was used in the final works on developing the land cover maps.

---

<sup>38</sup> The forests in the two case study areas were classified into two different types (i.e. conifers and non-conifers). The term mixed plants used in this initial study refers to the plants which are not solely composed of conifers, although in reality, mixed plants consist of both conifers and broad-leaved plants.

<sup>39</sup> The number of land cover classes is different with the actual land cover types identified in this PhD research, because only two types of forest were classified during this preliminary study. The five types of land cover in the first case study area are the developed areas, agriculture, conifers, mixed forest, and water bodies, whereas the six types of land cover in the second case study area are the developed areas, agriculture, tea plantations, conifers, mixed forest, and water bodies.

<sup>40</sup> The overall accuracy for the image classification of the second case study area has also been assessed in the second preliminary study. However, the result cannot be compared with the one generated from the first preliminary work (Rani et al., 2017), because they have different delineation of area.

### (3) Multitemporal land cover maps

Multitemporal land cover maps (i.e. maps developed from SPOT and Landsat satellite images) were used in this research as one of the input datasets for the second iteration of land change and hydrologic simulations (LCM 2 and MIKE SHE 2). The image classification process of the first case study area was conducted for each satellite image individually at the beginning of this research. For example, the development of the 2015 land cover map was performed without relating the process with the result from the 2013 land cover map. As a consequence, the maps of 2013, 2015, and 2017 show apparent land cover change within two years (Figure 5-6).

It is argued in this research that the apparent land change, which occurred between 2013-2015 and 2015-2017 in the two case study areas can be caused by many factors, such as the contaminated images<sup>41</sup> which affect to the misclassification, and the exogenous factors (e.g. socio-economic and climatic factors). The possibilities to have misclassification in each land cover map in this study stem from the missing data of land cover underneath the clouds. Clouds block all radiation reflected from the Earth's surfaces (Lu, 2007 *cited in* Liu et al. 2011) and the altered reflectance values of objects by cloud shadows. The overall accuracies of all land cover maps developed using SPOT 6 imagery show relatively high percentages (Table 6-1). However, only parts of images, which are free from clouds and cloud shadows, were included in the accuracy assessment. The pixels with missing data, then, were classified using the information on land cover in the previous year (i.e. the land cover in 2013 maps were used to fill in the missing data in the 2015 maps), because the images retrieved in different dates in the same year are not available.

The updating and backdating method (Linke et al., 2009) was implemented in this study in the last iteration of the land cover map development process. In the redevelopment of maps from SPOT 6 imagery, pixels with missing data were also classified based on the information on land cover in the previous year. SPOT images were purchased from Airbus, with a limited number of images that can be chosen due to the constant cloud coverage. Among all SPOT images taken in 2013, 2015, and 2017 for the two case study areas, the 2015 images have the least percentages of cloud coverage (i.e. 1.12% and 0% for the first and the second case study areas respectively). This constraint affected the selection of land cover maps to be used as base maps.

Table 6-1 The overall accuracies of individual land cover maps generated from SPOT 6 imagery

Images	Ci Kapundung watershed
2013	78,64%
2015	87.40%
2017	86.40%

<sup>41</sup> Clouds and cloud shadows in a satellite image can alter the actual reflectance values of pixels, thus leads to the misinterpretation and misclassification.

In this study, the distribution of land cover types in 2015 was used as a benchmark for the development of land cover maps in 2000 (backdating process) and 2017 (updating process). It is assumed that the types of forest with old trees did not change in 17 years (2000-2017). However, there is a possibility that the areas identified as bare land and cultivated land and/or developed areas in 2015 and 2017 were still covered by trees in 2000. In this case, it is assumed that the plants outside the forests are broad-leaved plants, whereas the vegetation inside the forests can be classified based on the forest map from Perhutani.

The land change analysis for the first case study area in LCM 2 shows that there are lower gains and losses of one vegetation type to another in 2000-2015, compared with the previous analysis using the individual 2013 and 2015 land cover maps in LCM 1. The validation of 2017 projected land cover map in LCM 2 shows higher accuracy in comparison to the result from LCM 1, suggesting that the backdating and updating method can improve the quality of land cover maps.

### 6.1.3 Uncertainty factors in the land change analysis

A preliminary land change simulation has been conducted using the 2013, 2015, and 2017 land cover maps of the first case study area (LCM 1). The study used the transition probabilities of land cover in 2013-2015 to predict the future land cover composition and distribution in 2017 and 2030 under different scenarios. Results from the validation using the actual 2017 land cover map suggested that the transition of land cover change from 2013-2015 and 2015-2017 is not stationary, which is indicated by the low accuracy in the validation result (i.e. 60.52%).

The land change analysis from 2013 to 2015 (LCM 1) shows high percentages of gains and losses of each land cover type in the first case study area. For example, the coverage of developed areas has increased by more than 4 km<sup>2</sup> within two years, but it was also altered to other land cover classes of approximately 4 km<sup>2</sup> (Figure 5-6). The contributors to the net change in developed areas are bare land and cultivated land class (approximately 0.62 km<sup>2</sup>) and the three types of vegetation (approximately 0.20 km<sup>2</sup>). This result indicated how fluctuate the land change identified in the model is. One of the base maps used in LCM 1 has an accuracy of 87.40% (the 2015 map), which can be considered as high according to the criteria given by Thomlinson et al. (1999 cited in Foody, 2002)<sup>42</sup>. However, the 2013 map has an accuracy of 78.64% (Table 6-1). There is still a possibility that the mixed pixels influenced the image classification; the same land cover type in 2013 and 2015 might be classified into two different classes.

---

<sup>42</sup> The minimum accuracy required for the image classification is 85% for an overall accuracy and no less than 70% for each class (Foody, 2002).

Changes in natural and socioeconomic processes are the examples of endogenous and exogenous variables which can alter the transition probability of land cover (Boerner et al. 1996; van Vliet et al., 2016). This suggests that the Markov model is not stationary. Other factors which can influence the validation result are the uncertainty in input data and model parameters (Brown et al., 2014; Verburg, Tabeau, & Hatna, 2013), and the short time scale (2013-2015) for the land change simulation, thus there is not enough training data that the LCM can learn from. Therefore, the subsequent land change modelling (LCM 2) was conducted using a longer simulation period (2000-2015).

The estimation of population number in 2017 and the area required per-person in each case study area (Subchapter 5.3) was also used to validate the outcomes from land change simulations (LCM 2). The LCM 2 results for the first case study area shows that approximately 18.70 km<sup>2</sup> or 18.09% of the total area is predicted to be built in 2017 under the Status-Quo scenario<sup>43</sup>. The percentage is higher than the expected coverage of the built-up area in the same year (i.e. 15.34%). It seems possible that this result is influenced by the high discrepancy of percentages of developed areas in 2000 and 2015 (i.e. 4.92% and 14.90% respectively). Therefore, due to the stationary nature of the Markov model to project the future land cover compositions, the model predicted more built-up areas in the simulated 2017 map than it has been expected.

A similar outcome was also achieved from LCM 2 for the second case study area. Only 9.75% of the total area is expected to be built in 2017. However, the output from land change modelling under the Status Quo scenario shows 10.57% would be built in the same year<sup>44</sup>.

Land cover change is a complex process characterised with uncertainty. Thus any land change models could not yield accurate results (van Vliet et al., 2016). “Geographical systems, despite being governed by largely deterministic processes, have open, undetermined futures” (White & Engelen, 2000). There is also a need to have a further interpretation of how the land cover would change. For example, the change from bare land to the tea plantations and vice-versa in the second case study area, as indicated in the table of transition probability. There might be a planting cycle that caused the land change identified by the model, although, in reality, the land-use (as tea plantations) remains unchanged.

This study only explored the use of one land change model (i.e. the LCM module of Terrset) to project the future land cover of the two case study areas. Different results might be achieved when using other land change models, and it is not covered in this research. A comparative

---

<sup>43&40</sup> This result was retrieved from the LCM simulation based on the transition probability maps generated from the MLP process using only three demographic-economic drivers (e.g. likelihood to change, distance from disturbance, and population density).

study of different land change models has been conducted by Mas *et al.* (2014). The study suggested that although the construction of LCM is easier and faster than other CA-Markov models, such as CA\_MARKOV from Terrset/IDRISI, CLUE, and DINAMICA, the modification of model behaviour in the LCM is difficult.

It should be noted that the CA-Markov model has its limitations, compared with the other types of land change models. The two assumptions are incorporated in the model; the same factors that influenced the land change in the past would cause the land change in the future, and no human decision is integrated into the model (Ghosh *et al.* 2017). Therefore, the outputs from land change modelling in this study should be interpreted according to the two limitations. It is assumed that there are no other endogenous and exogenous factors in the land change modelling during the period of simulation (2016-2030), which influence the land change other than the factors that have been identified before (2000-2015). The land cover transition probabilities, which were modelled in the LCM are stationary, although, in reality, the transitions are non-stationary (Boerner *et al.*, 1996).

The future land change was projected based on the transition probabilities, which were derived from the historical land change in both case study areas (2000-2015), and the states of surrounding cells at one time. No human decision can affect the land change. However, the LCM module from Terrset provides an option to include constraints and incentives to specific areas in the model, which can be used to investigate the effects of policies on land change (Eastman 2016). In this research, a set of constraint maps has been developed based on the future development scenarios to project the composition and distribution of land cover types in the two upper water catchment areas.

Different combinations of land change drivers were used to model the potential transition maps in LCM 2. Three drivers within the demographic-economic group (e.g. likelihood to change, distance from disturbance, and population density) were selected to be included in the final iteration of the MLP process. It is argued that different drivers used in the MLP process produce different suitability maps. It should also be noted that the projected 2017 and 2030 maps presented in Chapter 5 are only the plausible options from the suitability maps and not the definite land cover maps in the respective years.

Due to the multi-resolutions of SPOT and Landsat images, the c.2000 and 2015 land cover maps have a different number of pixels. Therefore, there is a possibility of one forest type to change to another type during the simulation time (less than 0.0034), as suggested in the transition probability matrices (Table 5-14, Table 5-16, Table 5-19, and Table 5-21). The map projection process in Terrset is also arguably affecting the results. This process was conducted to set the map projection and the number pixels in columns and rows so that the 2000 and 2015 maps can be compared and analysed in LCM.

#### 6.1.4 Approaches for improving land change simulations

The initial land change simulation for the first case study area had been done under different development scenarios (LCM 1) before LCM 2 were conducted. In LCM 1, weighting factors were applied to the transition probabilities, which varied in different scenarios, and different constraint maps were used in each scenario. The transition probabilities and constraint maps had been used to simulate 2017 land cover, in which the result was validated using the actual 2017 map. The findings indicated that the future land cover under the different scenarios in 2030 have relatively the same composition of land cover when no weighting factors applied, but have a different spatial arrangement (Rani et al., 2018). It also showed that the Markov model in the LCM affected only the composition and not the spatial arrangement of land cover.

MLP generates different transition probabilities in each run in LCM 1. In the initial simulations, MLP was run thirteen times, and the transition probabilities were generated based on the run with the highest accuracy among all MLP results (52.86%). Different results from MLP procedures might be caused by random variations which imply the uncertainty in the land-change process. Thus, different outcomes could be generated every run, and high accuracy from the LCM might be achieved by chance (Brown et al. 2005; van Vliet et al. 2016).

The low accuracy of modelling validation in LCM 1 for the first case study area was resolved by expanding the time period for calibration in the land change modelling in LCM 2 into 15 years (i.e. 2000-2015). The accuracy of the projected 2017 map for the first case study area could be improved from 60.52% in LCM 1 to 81.76% in LCM 2. It shows that the simulation period, the base maps, and the land change driver variables used in the modelling affected the modelling outcomes and accuracy. Although there is no accuracy assessment for the 2000 map, there is a slight improvement on the accuracy of the 2015 map of the first case study area (i.e. from 87.40% to 87.42%).

A procedure to determine the number of hidden nodes in MLP from Wang (1994) was used in LCM 2. It is proven that the method could generate almost the same MLP accuracy level for modelling the first case study area as when applying the Kolmogorov's theorem (Hecht-Nielsen, 1987), but with less simulation time.

The transition probability from the land change analysis (2000-2015) and the suitability maps resulted from the MLP was used to project the 2017 and 2030 land cover in both case study areas. The 2000 maps have been generated from SPOT and Landsat imagery using the backdating method, in which the issues from this process has been addressed in section 6.1.2. Therefore, it should be noted that the base maps might not represent the actual condition in 2000.

The outcomes from the land change modelling show how stationary the CA-Markov model is. The LCM 2 model suggested that more areas allocated for cultivated land are needed in the future due to the massive change from broad-leaved trees to bare land and cultivated land in

the first case study area that have been identified in 2000-2015. However, the land change could not be accommodated unless another type of land cover was assigned to change.

#### 6.1.5 Factors influencing the uncertainty in hydrologic models

The factors influencing the uncertainties in the hydrologic modelling are presented as follows.

##### (1) Input data for MIKE SHE

The list of input data for MIKE SHE has been mentioned in the first section of Subchapter 4.4. Among all input datasets used in the models, rainfall and river discharges are the only datasets which were measured directly in the two upper catchment areas by the Indonesian governmental agency. However, there might be errors in the input data, and this could influence the accuracy in the calibration process (Refsgaard & Storm, 1996).

In MIKE SHE, land cover maps were used as base maps to develop maps with values of Leaf Area Index (LAI) and Manning's  $M$ . Nevertheless, the land cover distributions, as shown in the land cover maps, are subject to uncertainty. The values of LAI were estimated based on the allometric equations, which were developed by various studies conducted in different regions in Indonesia and other tropical countries. The main limitation of this method is that the LAI values retrieved from the literature can be different from the actual LAI values in the two case study areas because the previous studies were conducted in different sites, using tree species in different ages (Deblonde, Penner, & Royer, 1994). There is a limited number of studies on the LAI of tropical rain forests due to their complexity in forest structure compared with forests in sub-tropical regions (Mcwilliam et al., 1993).

No evapotranspiration rate data is available to be directly used in the MIKE SHE models. So, the values were calculated using the Penman-Monteith equation, which requires the maximum and minimum temperature on the sites. However, the historical temperature data on the sites is also not available. Thus the daily temperature data from Bandung City (2000-2015) had been used and corrected to estimate the temperature in each case study area before the reference evapotranspiration was computed.

Hydrus 1D and the calculation made in the UZ (unsaturated zone) Soil Property module in MIKE SHE were utilised to estimate the soil parameters. Although the soil map of Bandung Basin provides reliable information on the soil distribution and the composition of sand, silt, and clay for each soil type, no data regarding other soil parameters are available (e.g. moisture content and saturated hydraulic conductivity). The estimated soil parameters might be different depending on the formula chosen for the estimation. For example, soil hydraulic conductivity can be calculated in MIKE SHE using two different equations; Van Genuchten and Campbell. Each equation has variables which differ from the other equation. This study used the Van



Genuchten formula to compute the hydraulic conductivity because it is widely used in hydrologic modelling (Danish Hydraulic Institute, 2017b).

## (2) Model parameterisation

In this study, the model parameters which could not be retrieved from the field surveys and governmental offices in Indonesia (e.g. soil properties and reference evapotranspiration) were derived directly from literature or were estimated using software and allometric equations. Therefore, there might be a possibility of incorrect parameters were used in the model because of miscalculation. The parameters could not be validated because there is no such data taken directly from the field. For example, reference evapotranspiration ( $ET_0$ ) was estimated for the whole area of the two sites. However, the values may vary depending on the altitudes and land cover types.

A trial-and-error procedure was used in the calibration process, implying little certainty in the model input. However, the trial-and-error using manual calibration is the most widely used among all calibration procedures and is recommended for complicated hydrologic models (Refsgaard & Storm, 1996).

## (3) Approaches in MIKE SHE modelling

MIKE Hydro River from DHI can be an option to be coupled with the MIKE SHE model because MIKE Hydro can explicitly simulate the river flow. The module also provides an option to include the information on available dams and other river structures on site. However, MIKE model is a fully distributed hydrologic model, which relies heavily on the measured field data. In the case of MIKE SHE model in this study, the input data, such as evapotranspiration, vegetation and soil properties, can be estimated and retrieved from the literature review. On the other hand, MIKE Hydro River requires various data related to the boundary conditions of each river branch, wave approximation module, and data for the runoff-rainfall model (Danish Hydraulic Institute, 2017c). Such data for the two case study areas are not available, and could not be generated from the secondary data. Therefore, only MIKE SHE model was used in this study without a link to MIKE Hydro River. Thus, it is important to note that the results from the MIKE SHE model were generated from the limited datasets, and no dams and other river structures were included in the modelling. Due to the limitations of MIKE SHE model, P Flux and Q Flux ( $m^3/s/m$ ) were simulated and used to calculate the river discharges ( $m^3/s$ ) in each watershed.

Different methods are offered in the MIKE SHE model to simulate evapotranspiration, overland flow and unsaturated flow. All options use different approaches and equations to model the flow. For example, MIKE SHE includes three options to calculate unsaturated flow; the full Richards

equation, a gravity flow procedure, and a simple 2-Layer water balance (Danish Hydraulic Institute, 2017b).

The simple 2-Layer water balance was used in MIKE SHE 1 and at the beginning of MIKE SHE 2. The method was selected because it does not require high computational capacity. However, there was an issue with the outcomes from the water balance analysis in MIKE SHE 2. The problem was prominent, especially when interpreting the results from the sixteen additional scenarios to assess the combination of land cover and soil types that can potentially reduce surface runoff (Appendix E). The canopy storage was estimated differently for four scenarios with the same land cover but different soil types. This result was retrieved given the same vegetation parameters assigned in the MIKE SHE model. The issue was solved by changing the method to compute the unsaturated flow to Richards equation. Due to the limited soil data, all parts of the area were assumed to have only one soil layer in the unsaturated zone, although the spatial distribution varies.

In this study, rainfall trend in 2008-2015 was also used in MIKE SHE to calibrate and validate the model and to assess the effect of future land cover change in each site in 2030 based on scenarios. A potential improvement for the model development is to integrate the future rainfall trend into hydrologic modelling. Available methods to project the future rainfall include the use of the Global Climate Models (GCMs) (e.g. Wilby et al. 1999 *cited in* Chang & Franczyk, 2008), time series analysis (e.g. Wang et al. 2013), and ANFIS/ Adaptive Neuro-Fuzzy Inference System (e.g. Tjasyono & Gernowo 2008).

#### 6.1.6 Improvement of the hydrologic model performance

The performance of the uncalibrated 120-m models was assessed at the beginning of MIKE SHE 2 modelling. The result suggests that the model parameters need to be adjusted during the calibration process. In this study, the judgement on model performance mainly only relies on the output from the Root Mean Square Error (RMSE) analysis.

The results from the model performance analysis suggest that the simulated discharges, particularly in the Ci Sangkuy watershed, could not be projected correctly, which can be seen from the high RMSE (14.55). As seen from Figure 5-36, the observed discharges in 2008-mid 2011 were significantly higher than the simulated discharges during calibration in the same period. One possible reason for this is the unsaturated condition of the soil in the model. The portion of rainfall that is not intercepted by the vegetation canopy will reach the soil surface and generate surface runoff or infiltrate to the unsaturated zone. Therefore, more time is required for the soil to be fully saturated until overland flow is generated on the catchments and flowing to the river.

MIKE SHE provides an option to set up an additional model (i.e. the HotStart model) that can accurately simulate the river discharges and water balance at the beginning of the actual simulations. The land cover map before 2015 (e.g. map in 2000) can be included in the additional model. Thus, the model begins with relatively saturated soil at the beginning of the actual simulation (2008). It is expected that the model can predict the simulated river discharges with higher accuracy. However, this option is not feasible to be performed in this study because of the incomplete precipitation data before 2008.

The performance of the model was slightly improved during the calibration process. The adjustment of model parameters, such as the vegetation and soil properties, is essential to increase the accuracy of the calibrated models. At the beginning of this study, soil parameters were estimated only based on the compositions of clay, silt, and sand (Table 4-12 and Table 4-13) using Hydrus 1D software. The results from Hydrus 1D (e.g. moisture content and hydraulic conductivity) were used to compute the other soil parameters in the MIKE Zero UZ soil properties model (e.g. water content at field capacity and wilting point).

The outcomes from the sixteen additional simulations of the first case study area indicate that the vegetated catchments with clayey soil generate the least accumulated volume of surface runoff (2008-2015) compared with other types of soil. Although the soil was unsaturated (fully dried) at the beginning of the simulations, the graph of the time-varying overland outflow from the catchment shows that clayey soil keeps generating a lower outflow over time (Appendix E). This result is on the contrary to the conclusion made by Nassif & Wilson (1975) who argued that different slope gradients with impermeable soil have low infiltration capacity. Therefore, the initial soil parameters in MIKE SHE model in this study were corrected by assigning the bulk density into the calculation of soil parameters in Hydrus 1D<sup>45</sup>. The bulk density for each soil type in the case study areas was estimated using the guidelines from Ad-hoc-AG-Boden (2005, as cited in FAO, 2006).

As has been described in the previous section, there was also an issue with the model that predicted different canopy storage for the same vegetation (Appendix E). This issue was solved after changing the method for modelling the unsaturated flow from the 2-Layer water balance into the Richards equation. The vegetation analysis was then conducted again with more scenarios involved; 64 hypothetical scenarios with the combinations of four land cover, four soil types, two slope gradient classes, and two uniform precipitation rates. The decision to include more variables into the simulation process was made after examining the results from the previous sixteen simulations. The initial modelling outcomes show that cultivated land could reduce more surface runoff than the forests when the actual precipitation and slope gradients of the first case study area were used in the model. It is argued that the model of Ci Kapundung watershed is complex; it receives accumulated precipitation of 0 to 181 mm/day during the

---

<sup>45</sup> The soil parameters used in the final MIKE SHE model are presented in Appendix A.

simulation period, and it has slopes ranging from 0 to 65°. This information implies that precipitation and slope gradients, the two variables which were not involved in the previous simulations, have a significant influence on the overland outflow.

## 6.2 Land cover alteration and flood regulating service

This sub-chapter discusses the research findings related to the first research question; “How does the land cover alteration in Ci Kapundung and Ci Sangkuy upper water catchment areas affect flood regulation in Bandung Basin?”.

Results from the 5-year Moving Average analyses suggested that the annual river discharge of Ci Tarum showed an increasing trend in 2001-2017 ( $y = 2.3665x - 4673.9$ ). The trend of Ci Kapundung River discharge also increased in 2001-2017 ( $y = 0.2107x + 419.27$ ). On the other hand, the Ci Sangkuy River discharges tend to decrease in the same period ( $y = -0.3329x + 680.4$ ). This subchapter discusses the trend of Ci Tarum River discharge and how the rainfall variability in the Bandung Basin might affect the trend. Then, the examination of the impact of land cover change to the provision of flood regulation service in the two case study areas (Research Question 1) is presented.

### 6.2.1 Rainfall variability

The variability of Thiessen-weighted precipitation in Bandung Basin and the variability of annual precipitation in the case study areas were analysed to see their correlation with the global climate variations (e.g. sea surface temperatures over the tropical Pacific Ocean). Although the trend of Ci Tarum discharges can be assessed using data from 2001-2017, the precipitation data for Bandung Basin is only available for 2008-2016.

The trend of Thiessen-weighted precipitation and the annual average precipitation rate in the Bandung Basin is illustrated in Figure 6-3. There is a high possibility that the rainfall variability was affected by ENSO (El Niño-Southern Oscillation). SST (sea surface temperature) anomaly data from NOAA (National Oceanic and Atmospheric Administration)<sup>46</sup> shows that La Niña events occurred in 2010-2011 (strong La Niña), 2011-2012 (moderate La Niña), and 2008-2009 (weak La Niña). On the other hand, El Niño happened in 2015-2016 (very strong El Niño), 2009-2010 (moderate El Niño), and 2014-2015 (weak El Niño) (Golden Gate Weather Services, 2019). It can be argued that the strong La Nina event in 2010 had an impact on the high annual discharge (237.95 m<sup>3</sup>/s) of Ci Tarum River. In February and March 2010, floods occurred in the basin with the peak discharge at the Nanjung water station of over a 10-year return period (JICA,

---

<sup>46</sup> NOAA uses the Oceanic Niño Index (ONI) to identify El Niño and La Niña events. The strength levels of El Niño and La Niña include Weak level (with a 0.5 to 0.9 SST anomaly), Moderate level (1.0 to 1.4 SST), Strong level (1.5 to 1.9), and Very Strong (more than 2.0). The list of Weak, Moderate, Strong, and Very Strong El Niño and La Niña events was retrieved from Golden Gate Weather Services (2019) at <https://ggweather.com/enso/oni.htm>

2010)<sup>47</sup>. JICA (2010) reported that the total inundated area during the flood event in 2010 was 91.8 km<sup>2</sup>, and was bigger than the flooded area in 1986 (71 km<sup>2</sup>).

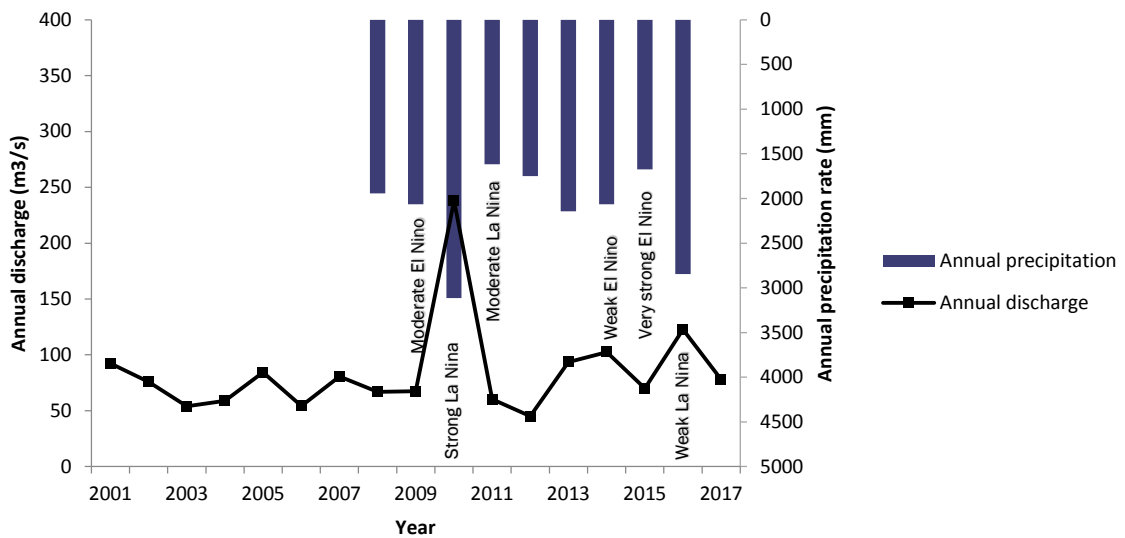


Figure 6-3 The annual trend of Ci Tarum River discharges and the precipitation in Bandung Basin

A further assessment of the Thiessen-weighted precipitation trend in the Ci Kapundung and Ci Sangkuy upper catchment areas (Figure 6-4) indicates that the annual precipitation rates in the areas increased during the La Niña events. In 2010, six stations in the two case study areas recorded high precipitation rates of more than 3,000 mm/year (strong La Niña). A weak La Niña in 2016 also caused the annual rainfall in both watersheds increased. A very strong El Niño occurred in 2015 and affected the low precipitation rates in the two case study areas.

Precipitation rates in the two case study areas in 2004-2017 also varied with the location and altitudes. Mountainous areas at higher latitude receive high precipitation than the other parts of watersheds (Whitten, Afiff, & Soeriaatmadja, 1996), showing the orographic effect. One of the mechanisms of air mass lifting in the formation of precipitation is orographic lifting. A mountain range causes an air mass to rise and pass the top of the mountain (Chow, Maidment, & Mays, 1988). In this study, Thiessen polygons in both case study areas have been generated based on the locations of weather stations in the Bandung Basin and the surrounding area. The highest volume of rainfall was recorded by Margahayu and Cibereum weather stations, which are located at the highest points of the first and second case study areas respectively.

<sup>47</sup> According to JICA (2010), the capacity of Ci Tarum River in 2010 was able to accommodate the 5-year return period (510 m<sup>2</sup>/s). However, the peak discharge during the 2010 flood was over the 10-year return period. Thus, the basin was heavily flooded. The estimated 5-year return period mentioned in this subchapter (510 m<sup>2</sup>/s) was calculated by JICA, and is different from the estimation of flood discharge provided in the third section of Subchapter 5.2. (i.e. 374.81 m<sup>3</sup>/s).

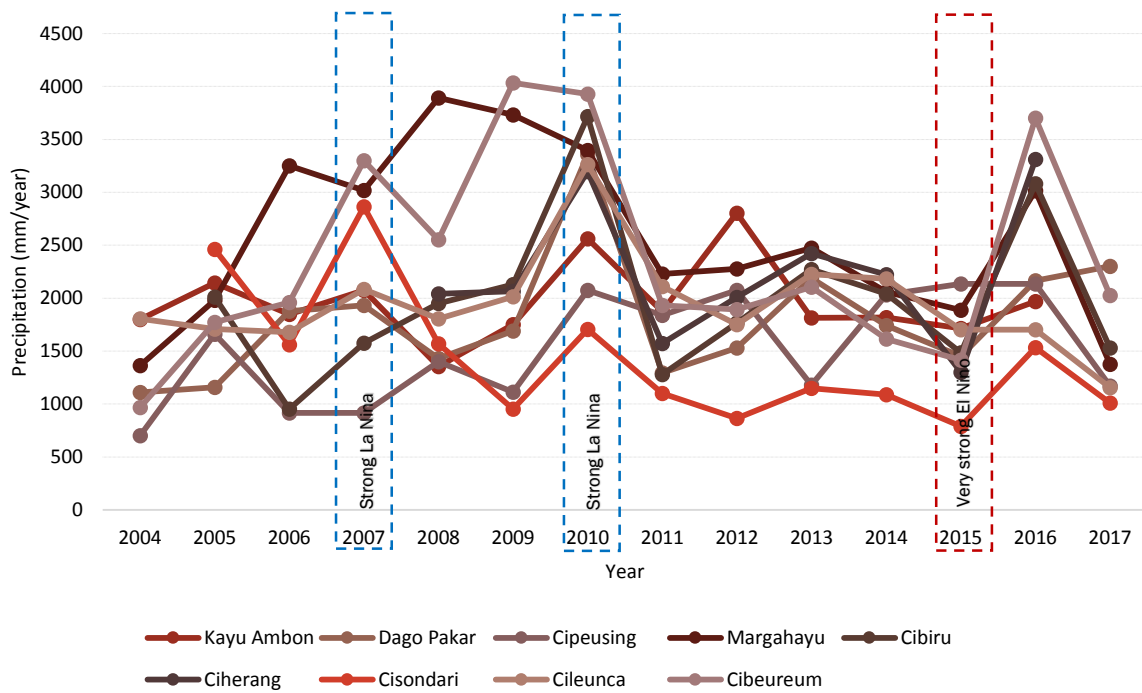


Figure 6-4. Annual precipitation rates recorded by nine weather stations in the two case study areas and the indication of strong La Nina and very strong El Niño events (Source: NOAA 2018 and author's analysis on precipitation data from PSDA 2017)

In this study, the direct surface runoff from precipitation in the Bandung Basin was assessed to see the effects of rainfall variability in the Ci Tarum river discharges. Regression models between the direct runoff (DROp) and the rainfall accumulation in Bandung Basin (2008-2015) were developed to assess the effects of rainfall variability in the river discharges. From the analysis, it can be concluded that the direct surface runoff in the basin is related to the accumulation of rainfall from the first day of rainfall event ( $R_0$ ) until the fourth consecutive days ( $R_4$ ) ( $R^2 = 0.337$ ). This result is similar with the previous research done by Dasanto et al. (2014) who assessed the effective rainfall which caused the flooding in Bandung Basin using Ci Tarum discharge data for 2000-2009 and the record of flood events in the region.

The moving average (MA) analysis was conducted to model the historical precipitation trends to assess the factors that affected the flood regulation. **Results from the 5-year MA analyses of average precipitation rates in the Ci Kapundung upper water catchment area show that the precipitation rate in the area declined in 2008-2016 ( $y = -0.0592x + 6.8075$ ). Rainfall rate in the Ci Sangkuy upper water catchment area (2008-2016) also decreased ( $y = -0.2412x + 6.3675$ ).**

### 6.2.2 Impact of land cover alteration on flood regulation in Bandung Basin

Based on the result from the initial assessment of case study areas as indicators of water catchments presented in Subchapter 3.2, it is argued that the alteration of land cover in the two sites influences the flood regulation in Bandung Basin. Runoff coefficients in the Ci Sangkuy water catchment area have the highest rate to change in 2008-2016 compared with the other catchment in the basin. On the other hand, the upper part of Ci Kapundung catchment has a positive linear trend in the same period. Therefore, the impact of land cover change in the two case study areas to the flood regulation in the basin was examined to address the first research question.

Land change analysis using the land cover maps in 2000, 2015, and 2017 suggested that the coverages of developed areas in both sites have increased. However, the trends of land change for bare land and cultivated land and forest cover in the two upper catchments were different.

In the case of Ci Kapundung upper water catchment area, an incline regression line from the Moving Average (MA) analysis was derived from the trend of river discharge in 2001-2017. The flood regulation in the first case study area was more likely affected by the land cover alteration in the area compared with weather conditions. The results from the MA for Thiessen-weighted average rainfall indicates a decreasing trend of precipitation rates ( $y = -0.0592x + 6.8075$ ). All five stations inside and surrounding the site recorded the increasing trend of precipitation rates, except for the Margahayu station. There was a rapid land cover change in the first case study area in 2000-2017. The total coverage of developed areas and bare land and cultivated land in the area in 2000 was 4.93%, and it increased to 19.83% in 2017. The area of bare land and cultivated land also increased from 31.66% to 36.88% within 17 years. In contrast, the forest cover has decreased from 63.41% to 43.30% during the same period. Therefore, it can be concluded **that the increasing trend of river discharges was mostly influenced by the land cover changes in the Ci Kapundung upper water catchment area.**

In the Ci Sangkuy upper water catchment area, there was a declining trend of river discharges throughout 2001-2017. A possible explanation for this might be related to the higher percentage of forest coverage in 2015 (43.30%) compared with the coverage in 2000 (39.27%), although the percentage decreased in 2017 (39.76%). Forest maps from Perhutani show that parts of the forests in the upper catchment were planted in the late 1990s to 2000s. Therefore, these areas appear to have more bare land than tree canopies in 2000. Within 2001-2017, the total built-up area increased from 3.37% to 16.14%. Another plausible reason for the tendency of river discharge to decrease over time is the declining trend of precipitation rates in the area, as described in the previous section. This finding raises a possibility that **the precipitation trend and the increasing forest coverage in the area had an impact on the decreasing trend of river discharges ( $y = -0.3329x + 680.4$ ), despite the increasing percentages of developed areas at the same time on the site.**

### 6.3 Effective scenarios of landscape structure to support flood regulation

This sub-chapter discusses the outcomes from assessments related to the second research question; “What are the most effective scenarios of landscape structure for the two upper water catchment areas which can benefit flood regulation?”. Three development scenarios were applied in the second iteration of land change modelling (LCM 2) in this study. The outcomes from the modelling were used as the input data for the MIKE SHE 2 model to project the flow metric responses across the different scenario.

#### 6.3.1 Driving forces and the rates of land cover changes

There were six land change drivers included in the LCM 2 of both case study areas (e.g. likelihood to change, distance from existing disturbance, population density, elevation, slopes, and distance from streams). Many studies have suggested that other variables can also affect the land change process, such as Gross Domestic Product (GDP) (Ju et al., 2016) and social data (Overmars & Verburg, 2005). However, the variables used in this study are limited to six because of two limitations. Firstly, there is no available road network map in 2000 could be retrieved at the time the analysis was conducted. Thus, a map showing the ‘distance from roads’ variable could not be generated in LCM 2<sup>48</sup>. This condition is in contrast with the LCM 1 process, where the same variable could be included in the MLP procedure. In LCM 1, the road network in 2013 could be retrieved from OpenStreetMap. Secondly, the spatial social data for creating the land change driver maps is limited, especially in the developing countries (Herold, Goldstein, & Clarke, 2003).

This study found that **‘likelihood to change’ is the most influential driver variable of land change in the two case study areas (2000-2015)**. The variable has Cramer’s V values of 0.5675 and 0.4680 for the first and second case study area, respectively. On the other hand, the ‘distance from stream’ is the least significant factor of land alteration during the same period. The variable in the modelling of the first and second case study areas have low Cramer’s V values of 0.0663 and 0.0909, respectively. This finding suggests that new development on both sites were more affected by the location of existing built-up areas rather than the other driving factors. The development of riparian areas still occurred during the simulation period (2000-2015).

Markov modelling within the coupled CA-Markov model simulates the future land change based on the historical trend of change (Brown et al., 2014). The 2000 and 2015 land cover maps of both watersheds had been used in the LCM 2 modelling to project the land cover in 2017, which later were validated using the actual 2017 maps. The model assumes that the land change is stationary. Thus it employs the information regarding the historical rate of change (2000-2015) to predict the 2017 land cover composition. However, in reality, the transition is not stationary

---

<sup>48</sup> This ‘distance from road’ variable used in the land change modelling was mapped based on the road network map in earlier simulation time. In LCM 2, the earlier time is 2000.



(Baker 1989). As a consequence, there are discrepancies between the land cover compositions in the predicted and actual 2017 maps.

The results from the land change modelling confirm that **the nature of land cover alteration in the two case study areas is non-stationary**. In the second land change simulation (LCM 2) of the first case study area, the percentage of developed areas in 2017 (18.09%) is predicted lower than the actual composition in the same year (19.82%). On the other hand, the predicted and actual percentages of built-up areas in the second case study area in 2017 are 10.57% and 16.14% respectively. It is argued that there are exogenous and endogenous factors that caused this discrepancy. These factors could not be assessed in the CA-Markov model and were not included in the simulations.

The transition probability matrices of the two case study areas (2000-2015) suggested that the likelihood of bare land and cultivated land to be converted to developed areas in Ci Kapundung watershed in 2017 (0.0872) is higher than the probability in Ci Sangkuy watershed (0.0336). This finding can explain as to why the rate of change is different in each watershed. The estimation of land cover composition shows that the coverage of developed areas in the first and second case study areas in 2000-2017 increased by 14.89% and 12.77% respectively, indicating the different level of land change on the two sites.

**No differences were found in the percentages of area for each land cover in the projected 2030 maps in the three scenarios of both case study areas** (Table 5-17 and Table 5-22). This outcome is likely to be related to the same transition probability matrix (2000-2015) used to compute the future land cover in the three scenarios. Therefore, **only the spatial arrangement of the future land cover in is different**, unless if the probability of land cover change in the Markov matrix is altered.

### 6.3.2 The comparison of results from MIKE SHE 2

This section discusses the outcomes from MIKE SHE 2 to predict the Ci Kapundung and Ci Sangkuy river discharges and water balance based on the three future development scenarios<sup>49</sup>. Only one base map derived from the 2015 land cover map was used to generate the LAI and surface roughness maps of each case study area, although the model runs from 1/1/2008 00:00:00 to 1/1/2016 00:00:00. No land cover maps at the beginning of the simulation (i.e. 2008) were included in this study. Only the trends of precipitation, reference evapotranspiration and the vegetation parameters related to plant growth (e.g. root depth and LAI) were adjusted in the models. As a result, lower river discharges were predicted at the beginning of simulations.

---

<sup>49</sup> The results from MIKE SHE 1 are not discussed in this section because the modelling was conducted only using the first case study area. Thus, the results could not be compared with the hydrologic simulations for the second case study area.

It is argued that the MIKE SHE modelling begins with dry soil conditions. Thus, the infiltration rates were high at the beginning of simulations.

Another boundary for the simulations conducted in this study is that there was no future rainfall trend (2016-2030) included in MIKE SHE. Therefore, the results from MIKE SHE 2 should be interpreted based on these circumstances.

#### (1) Projected river discharges

The evaluation of MIKE SHE model to project the river discharges was conducted by referring to the estimated flood discharges (see the third section in Subchapter 5.2). If the projected discharges are below the estimated flood discharges, then, it can be concluded that the proposed scenario(s) can support the flood regulation by reducing surface runoff flowing to the rivers. However, it is worth noting that flood discharges can be computed using a different method and the time span of data. Japan International Cooperation Agency (JICA) (2010) used the rational formula to calculate the Design discharge (2007) for Ci Tarum Rivers and its tributaries in the Bandung Basin, based on the rainfall pattern in 1986 (Figure 6-5). According to the proposed plan, the river discharges during the 5-year return period flood ( $Q_5$ ) and the 20-year return period flood ( $Q_{20}$ ) at the Nanjung station<sup>50</sup> are 510 m<sup>3</sup>/s and 630 m<sup>3</sup>/s respectively. As seen in Figure 6-5, the proposed design discharges for Ci Tarum River and its branches are different depending on the location and the river width. For example, the  $Q_5$  and  $Q_{20}$  for the Ci Tarum River near Dayeuh Kolot (a village which is often inundated during flood events in the basin) are 390 m<sup>3</sup>/s and 490 m<sup>3</sup>/s respectively.

In this study, the  $Q_5$  of Ci Tarum River was estimated at 374.81 m<sup>3</sup>/s, or slightly lower than the  $Q_5$  in Dayeuh Kolot. On the other hand, the flood discharge was calculated at 187.4 m<sup>3</sup>/s – 195.4 m<sup>3</sup>/s. The flood discharge calculation in this research relied heavily on DEM (Digital Elevation Model). There is a possibility that the DEM used might not represent the actual depth of the river because of its resolution and the river sedimentation that can affect the elevation showed on each DEM pixel. Therefore, the estimated flood discharges are lower than the  $Q_5$ . However, the estimation was still referred to when evaluating the MIKE SHE model. The purpose of this study is to assess if the proposed scenarios of landscape structure in both case study areas can support the flood regulation anytime in the future, not only during the 5-year return period flood.

---

<sup>50</sup> Nanjung station is the water station where the Ci Tarum River discharge data is collected from.



## (2) Water balance from hypothetical catchments

This study has demonstrated how different combinations of vegetation, soil types, slope gradients, and rainfall trends in 64 hypothetical catchments influence the overland flow (see 5.4.2). In general, the model projected a higher overland flow generated from cultivated land in the four soil types on moderate and steep slopes under low-intensity rainfall (Figure 5-38). This result might be related to lower evapotranspiration that the cultivated land has, compared with conifers, broad-leaved and mixed vegetation.

In accordance with the previous study from Nassif & Wilson (1975), MIKE SHE model in this research predicted a higher volume of overland flow on clay soil, particularly under the heavy rainfall (100 m/day), in contrast to other soil types. The volume is even higher in areas with steeper slopes. Nassif & Wilson (1975) concluded from their study using a rainfall simulation that slopes with fine clay soil have a lower infiltration rate than the slopes with standard soil under a similar rainfall intensity. It is argued from the study that water infiltration and surface runoff are also influenced by the rainfall intensity, catchment slopes, and land cover. Bare land with a standard soil type (permeability of 0.13 – 0.54 m/day) on a slope up to 16% and grassland with the same soil type on a slope up to 24% have a substantial effect on the surface runoff compared with the similar land cover and soil conditions in more flat slopes.

## (3) Landscape physical attributes that influence the flood regulation

Results from the water balance analysis vary with different future development scenarios in each case study area despite the similar composition of each land cover. It is argued that **the land cover distributions on specific soil types and slope gradients affected the river discharges and water balance (2008-2015) in the two case study areas.**

The compositions of each land cover on the flat-moderate slopes ( $\leq 15\%$ ) and steep slopes ( $>15\%$ ) in 2015 (existing condition) and 2030 (three scenarios) were estimated in this research<sup>51</sup>. The slope analysis for the three scenarios of Ci Kapundung and Ci Sangkuy upper water catchment areas shows that **although the land cover compositions are similar in each scenario, their distributions on the two slope conditions vary** (Figure 6-6 and Figure 6-7). For example, it is expected that 25.38% of the total area of Ci Kapundung watershed in 2030 will be built as developed areas in the three scenarios. However, most of the developed areas in the Ecological design-based scenario (scenario 3) will be built in the relatively flat and moderate slopes or 19.40% of the total area. This percentage is higher than those in the first and second scenarios (16.89% and 16.11% respectively).

---

<sup>51</sup> The approximate threshold for classifying the slope gradients for analysing the landscape physical attributes in this research was adopted from the study from Nassif & Wilson (1975).

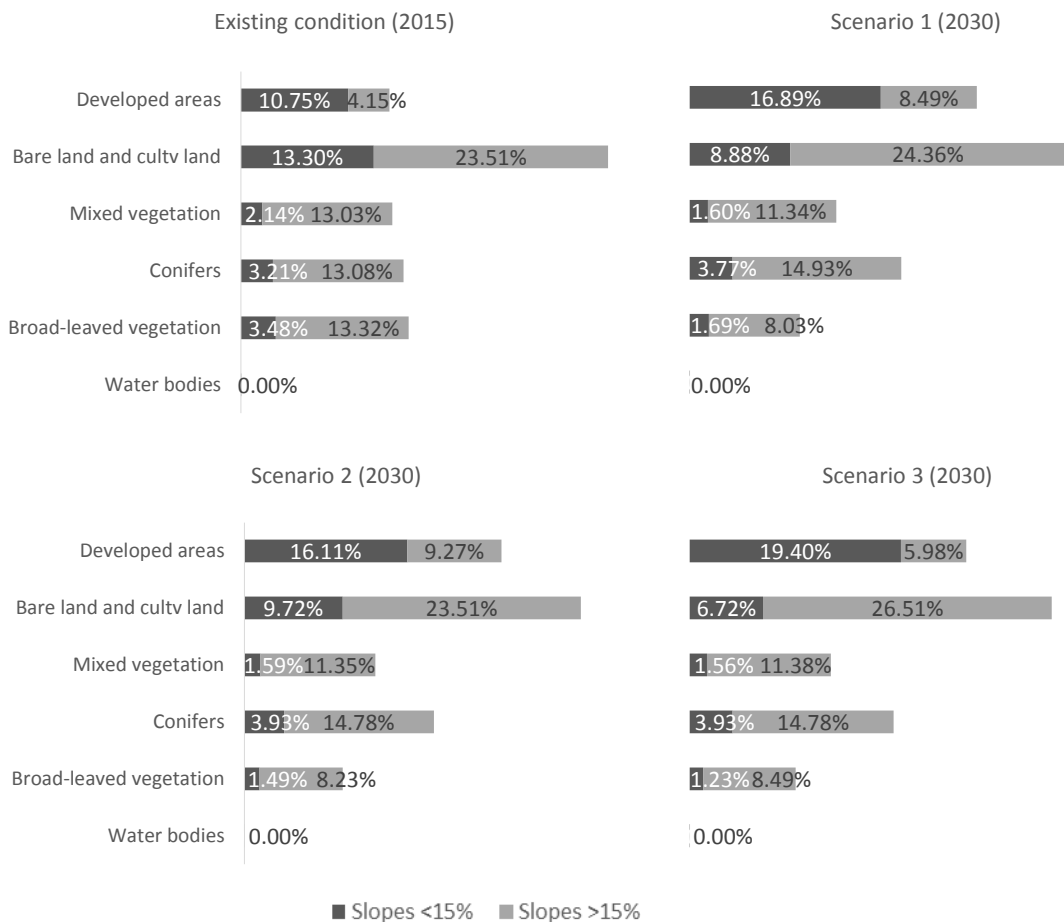
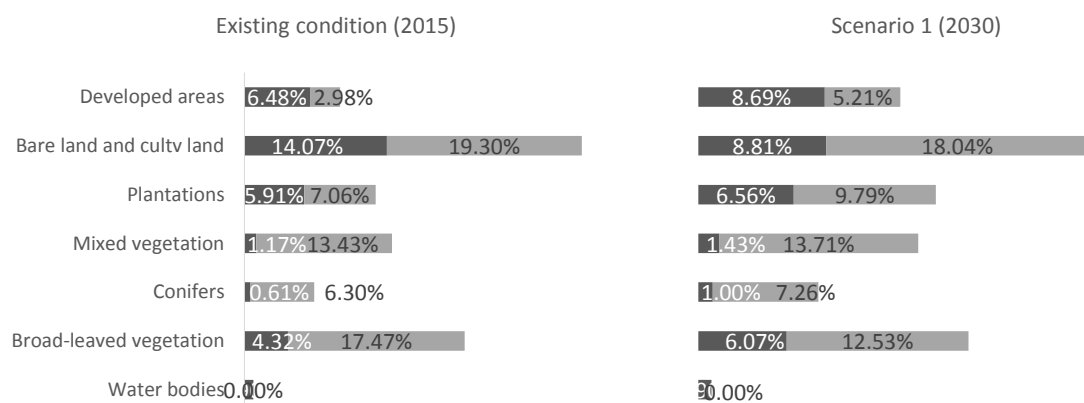


Figure 6-6 Land cover compositions of Ci Kapundung upper water catchment area on flat-moderate and steep slopes

On the other hand, 13.91% of the total area of Ci Sangkuy watershed is projected to be built in 2030 in the three scenarios (Figure 6-7). Less impervious areas will be built on the steep slopes in the third scenario (4.13%), compared with the other two scenarios. In contrast to scenario 1 and 2, scenario 3 has more coverages of conifers, broad-leaved, and mixed vegetation on the steep slopes (33.46%). **The discrepancy of land cover compositions on the two slope conditions is due to the different constraint maps assigned in each scenario.**



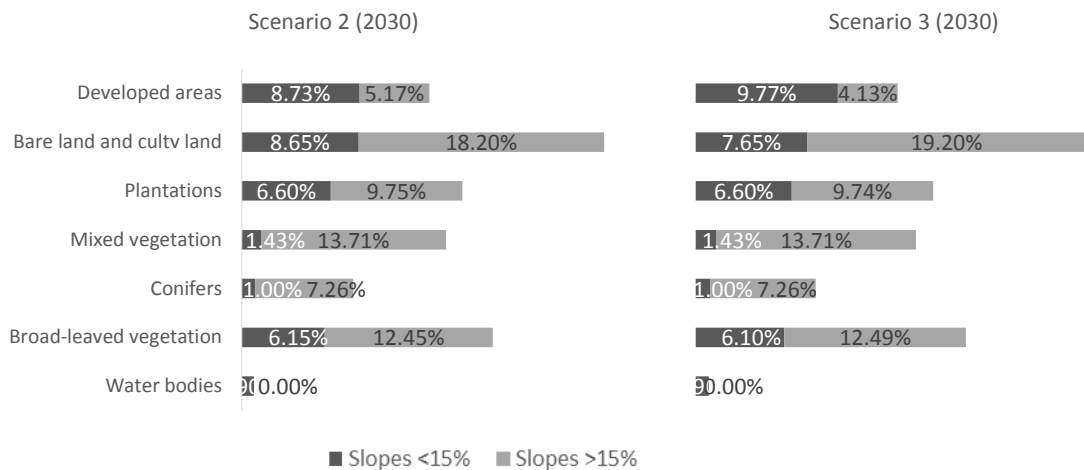


Figure 6-7 Land cover compositions of Ci Sangkuy upper water catchment area on flat-moderate and steep slopes

The soil distributions on the flat-moderate (<15%) and moderate-steep (>15%) slopes in both case study areas also vary in the existing condition and each future scenario (Figure 6-8 and Figure 6-9). It can be seen that most parts of the two case study areas are located on steep slopes; 67.10% of total Ci Kapundung catchment area, and 66.64% of total Ci Sangkuy catchment area.

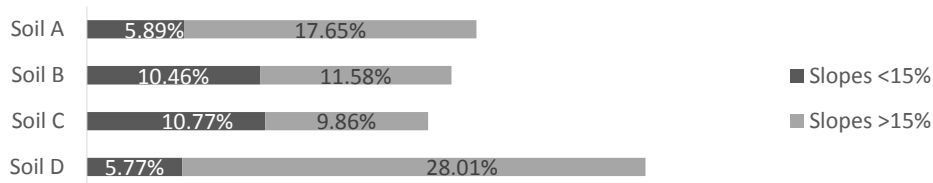


Figure 6-8 Soil compositions in the Ci Kapundung upper water catchment area on flat-moderate and steep slopes

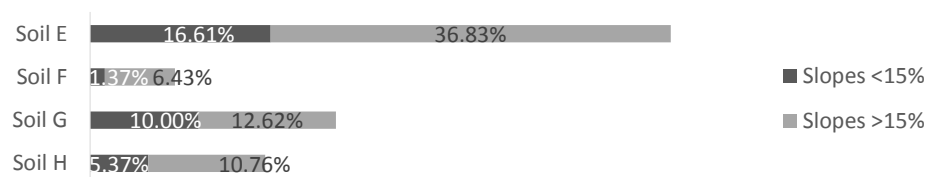


Figure 6-9 Soil compositions in the Ci Sangkuy upper water catchment area on flat-moderate and steep slopes

The soil types in the Ci Kapundung and Ci Sangkuy upper water catchment areas have different soil properties, including hydraulic conductivity, which is related to the soil permeability. A study conducted by Archer et al. (2013) showed that soil hydraulic conductivity is influenced by land cover types. Archer et al. (2013) employed sample points which are located in the area with the

same parent material. The study concluded that forests have higher field saturated hydraulic conductivities than grassland cover. However, there might be a case where the soil hydraulic conductivity ( $K_s$ ) in grassland and woodland is similar due to the higher gravel in the grassland. There is a continuous supply of organic material which develops as the organic horizon on the soil in the forest. But, the soil composition and organic colloids might have an effect on the soil permeability. Lower  $K_s$  in conifers can be caused by the organic colloids produced by pine needles.

In this research, the soil hydraulic conductivities ( $K_s$ ) were estimated from the compositions of sand, silt, and clay of each soil type on the sites. The soil in the Ci Kapundung and Ci Sangkuy upper catchments was composed by different parent materials (e.g. alluvium, volcanic ridges, and volcanic plain). Only the dominant soil types were used to estimate the soil compositions. The soil classes were then reclassified from eight and fifteen groups in the first and second case study areas respectively, to four on each site to reduce the simulation time. Therefore, it should be noted that the  $K_s$  estimated from the soil compositions might not represent the spatial specific soil characteristics, as indicated by Archer et al. (2013). Soil properties, including  $K_s$ , had been determined before land cover types in each scenario (2030) were assigned. Thus, the effect of different tree species to  $K_s$  could not be assessed in this study.

Water balance analysis for the Ci Kapundung upper water catchment area shows that scenario 1, 2, and 3 have lower overland outflow (2,590.24 mm, 3,173.42 mm, and 2,415.17 mm respectively), compared with the simulation of the existing condition (4,624.89 mm). This is an unexpected result, given the three scenarios have less vegetated areas (41.37%) compared with the 2015 condition (48.27%). A further examination on the daily precipitation rates estimated in MIKE SHE shows that there is no single day with precipitation that exceeds 100 mm/day during the simulation period (2008-2015). Therefore, this outcome might be due to the lower percentage of areas covered with conifers in 2015 (16.30%) than in the three scenarios (18.70%). This argument is supported by the outcomes from the water balance analysis of hypothetical catchments. It is suggested that conifers can generate the least volume of overland outflow in comparison to cultivated land, broad-leaved and mixed vegetation under the low-intensity rainfall (5 mm/day).

The accumulated volume of surface runoff from the Ci Sangkuy upper water catchment area generated from the existing condition (134,450 mm) is higher than the overland outflow from scenario 1, 2, and 3. This result is similar to the condition in the first case study area. An important point to make is that a precipitation lapse rate of 100% was used in the calibrated Ci Sangkuy model in this study (see Appendix A). Thus, a very high value was estimated for the accumulated rainfall volume (mm) in the eight-year simulations (approximately seven times higher than the estimated total rainfall in the first case study area), to generate a closer predicted river discharges during the calibration process. There are more than 780 days from

the eight-year simulations that have precipitation of more than 100 mm/day. This has resulted in the high simulated overland flow flowing outside the catchment, particularly in the existing condition.

A possible reason of the lower volume of surface runoff in the three scenarios of Ci Sangkuy upper water catchment is because that more areas are predicted as conifers in the future (8.26%) than in the existing 2015 condition (6.91%). The outcomes from the water balance analysis of the hypothetical catchments indicate that conifers generate less surface runoff, not only under the low precipitation (5 mm/day), but also high precipitation (100 mm/day) on soil A, B, and D (clay, silt loam, and loam), which are similar to soil E, F, and H in the second case study area.

The bigger size of coniferous woodland in the second case study area in the future scenarios (8.26%) is due to its increasing composition from 4.78% in 2000 to 6.91% in 2015. The CA-Markov model uses the historical trends of change to predict future land cover composition. Therefore, the model predicted that there would be more areas with conifers in all future scenarios. Consequently, the MIKE SHE model projected a much lower accumulated overland flow in the three scenarios (less than 71,000 mm), in contrast with the surface runoff in the existing condition (134,450 mm).

### 6.3.3 Optimization of land cover distributions

The parameters for three physical landscape attributes (e.g. land cover, soil, and slope gradients), as the x-axis in the scenario projection in the Pareto-frontier analysis, were determined based on the outcomes from MIKE SHE modelling of the hypothetical catchments. The result suggests that catchments with conifers on all soil and slope conditions have less volume of surface runoff under a low uniform precipitation rate. However, this outcome is not significantly different from the overland outflow from mixed woodland.

In general, steeper slopes with all land cover types generate more overland flow during heavy rainfall. Conifers on clayey, silt loamy, and loamy soil (e.g. Soil A, B, D, E, F, and H) reduce the higher volume of surface runoff under such rainfall condition. On the other hand, mixed vegetation planted on sandy loam (e.g. Soil C and G) can positively influence the flood regulation. The reason for this is that sandy loam has a higher saturated hydraulic conductivity compared with other types of soil on the sites, resulting in less surface runoff because more water infiltrates to the soil layer.

After reviewing these outcomes, then, the initial analysis of Pareto optimization was conducted by determining the criteria to assess the flood regulation in each scenario. In this case, **the criteria for the x-axis on the scenario projection graph is the area with clayey soil covered by conifers and mixed vegetation.** The percentage of area that falls within such criteria was



estimated, and the overland flow from each scenario was mapped on the graph to evaluate the capacity of each scenario to support flood regulation in the two upper catchments.

(1) Ci Kapundung upper water catchment area

The criteria for the physical landscape attributes (e.g. slope gradients, land cover and soil types) on the scenario projection graph for the first case study area can be seen in Figure 6-10. The total coverage of areas with such criteria was calculated from the land cover maps (Figure 6-11). The percentage of an area within the criteria in the 2015 land cover map generated from the remote sensing data is 3.01%. This number is lower than the percentages in the three scenarios.

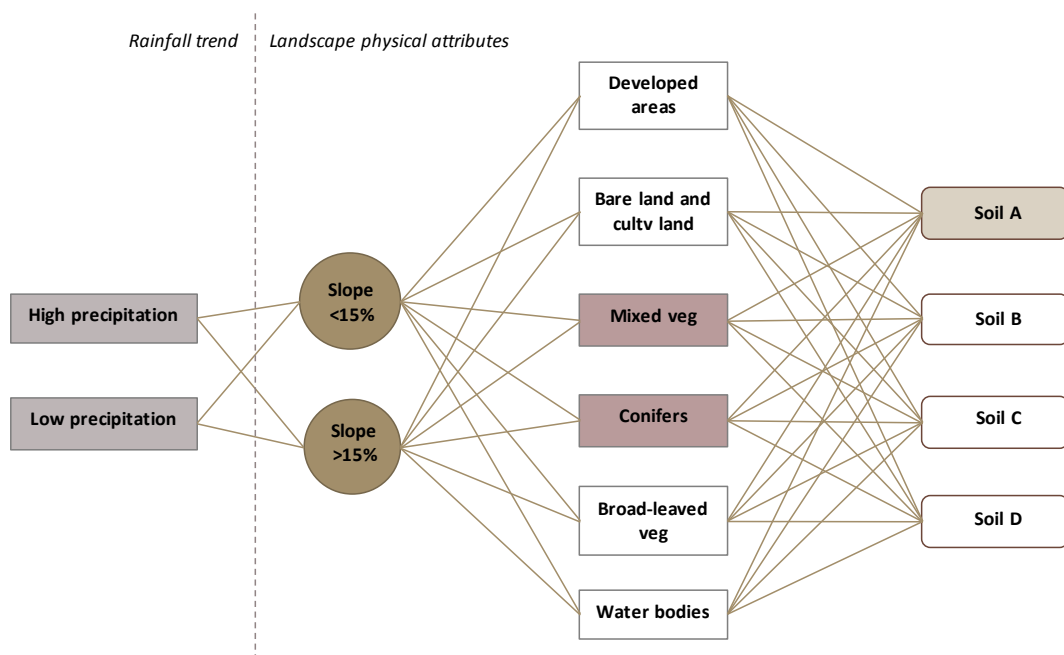


Figure 6-10 Rainfall and the physical attributes influencing the flood regulation in the Ci Kapundung upper water catchment area

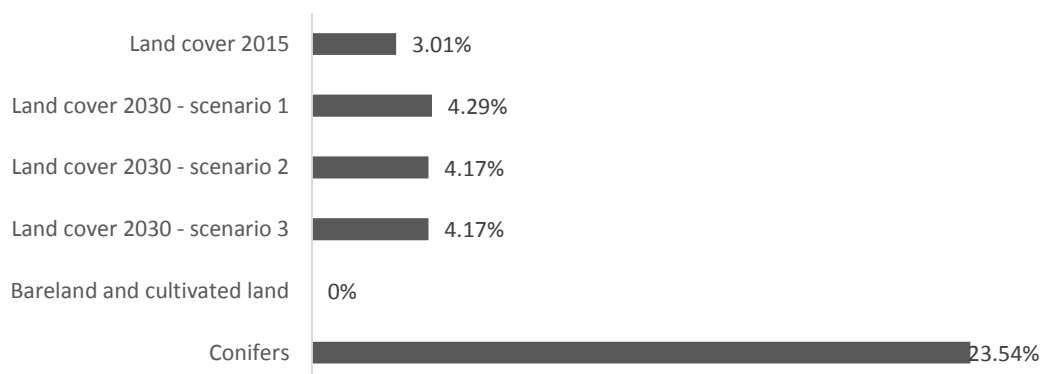


Figure 6-11 Total areas on flat-moderate slopes and are covered by vegetation in the Ci Kapundung upper water catchment area

Figure 6-12 shows the overland outflow simulated from the MIKE SHE model of the first case study area, based on the existing and the future conditions in each scenario. Two more scenarios with the uniform land cover of bare land and cultivated land (scenario A) and conifers (scenario B) have been added to the graph. It can be seen that scenario 1, 2, and 3 have lower overland outflow, compared with the conditions in 2015. This finding can be explained by the increasing coverage of areas covered with conifers and mixed vegetation on clayey soil from 3.01% in 2015 to more than 4.00% in 2030 in all future scenarios.

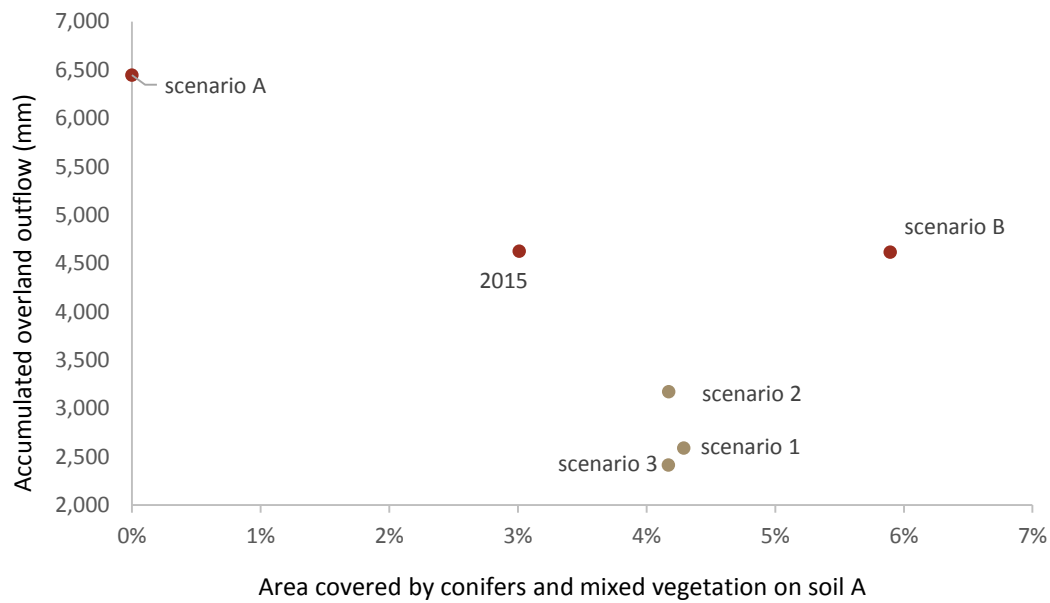


Figure 6-12 Scenario projection of overland flow in the Ci Kapundung upper water catchment area

(2) Ci Sangkuy upper water catchment area

The initial Pareto-frontier analysis for the second case study area was also focused on the areas covered with conifers and mixed vegetation on clayey soil (soil E and F) (Figure 6-13). The percentages of such areas in the existing and simulated land cover maps are shown in Figure 6-14.

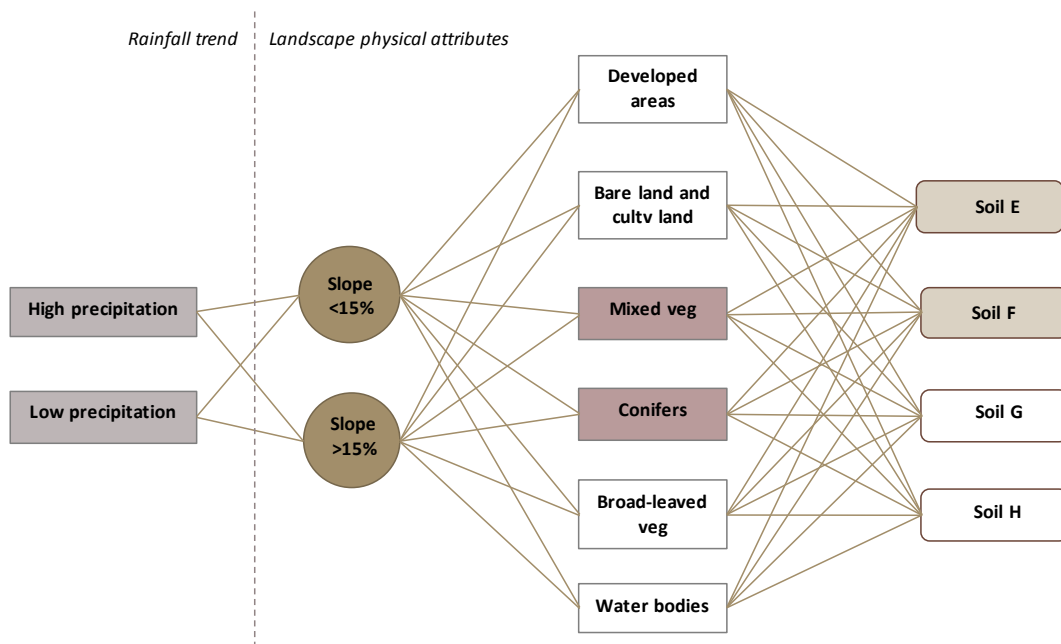


Figure 6-13 Rainfall and the physical attributes influencing the flood regulation in the Ci Sangkuy upper water catchment area

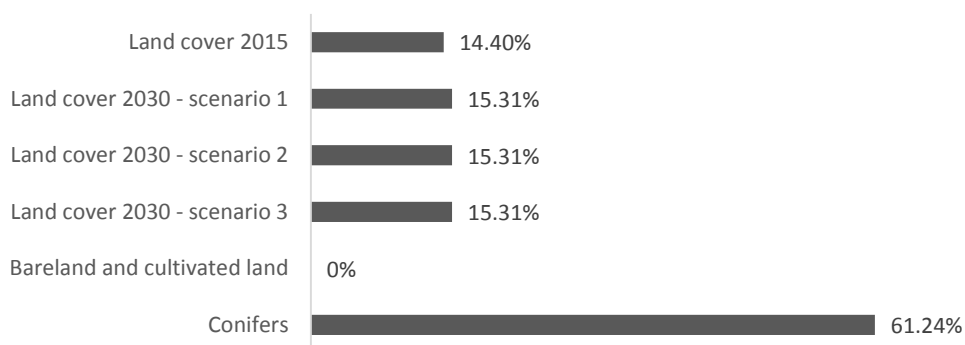


Figure 6-14 Total areas on flat-moderate slopes and are covered by vegetation in the Ci Sangkuy upper water catchment area

The projected overland outflow in the second case study area can be seen in Figure 6-15. There is no significant difference in the estimated overland outflow from the three future scenarios. This result is likely to be related to the composition of an area within the criteria that is similar for each scenario (15.31%). A lower overland flow in the existing conditions simulated using land cover in 2015 was estimated from the model (134,450 mm). The lower percentage of the vegetated area on soil E and F in the 2015 land cover map in comparison with the future scenarios could influence the outcome.

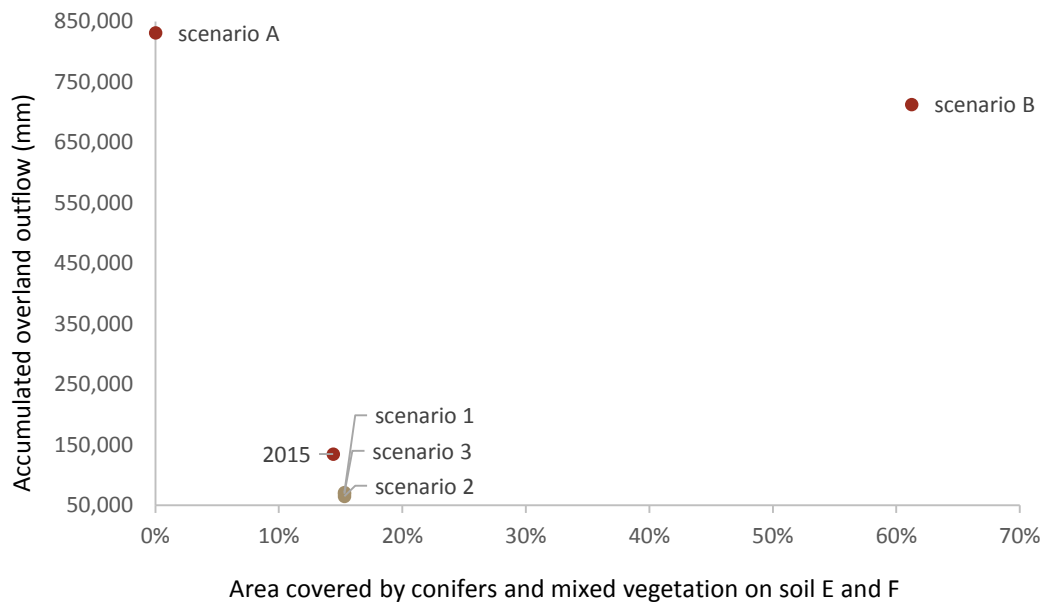


Figure 6-15 Scenario projection of overland flow in the Ci Sangkuy upper water catchment area

## 6.4 Characteristics of plants to improve flood regulation

The capacity of three vegetation types (e.g. conifers, broad-leaved vegetation, and mixed vegetation) to reduce surface runoff in two case study areas has been tested in MIKE SHE 1 and 2 to address the last research question; “Which types of vegetation can improve flood regulation in each upper water catchment area?”. Characteristics of plants related to the evapotranspiration in the modelling, including the canopy interception, are discussed in this subchapter.

### 6.4.1 Evapotranspiration

Evapotranspiration comprises of two processes by which water dissolve; evaporation from surfaces (e.g. ponded water, wet vegetation and soil) and transpiration from plants to the atmosphere (Allen et al., 1998). Evapotranspiration simulated in the MIKE SHE model includes the canopy interception, water flow to soil, water evaporation from canopy and soil, and transpiration from plant roots (Danish Hydraulic Institute, 2017b).

The model manual does not specify if bark interception is also included in the evapotranspiration modelling. A study from Herwitz (1984) shows that a tree bark can retain more than 50% of the total interception capacity of tropical tree species in the Curtain Fig forest, Australia (with a mean annual maximum of 132 mm/day) in the still-air conditions. The capacity increased to more than 80% during the turbulent air conditions. However, this result varies for different tree species in the tropical rainforest. In this study, both case study areas experienced a relatively high frequency of rainfall, particularly in the Ci Kapundung watershed where the rainfall recorded from the Cipeusing weather station exceeded 100 mm/day in 12 days during the simulation

time. Therefore, the interception capacity from bark might be significant, depending on the tree species.

The water balance analysis conducted in the second iteration of MIKE SHE modelling (2008-2015) shows that **the total evapotranspiration for the first case study area covered with conifers (13,264.50 mm or 1,658.06 mm/year) is higher than when broad-leaved vegetation was assigned (11,655.40 mm or 1,456.92 mm/year)<sup>52</sup>. The total evapotranspiration for the second case study area also shows a similar condition with that of the first case study area;** the catchment covered with conifers has higher evapotranspiration (13,195.40 mm or 1,649.42 mm/year) than the site with broad-leaved vegetation (11,412.60 mm or 1,426.57 mm/year). It is important to note that the total evapotranspiration estimated from the MIKE SHE model is the sum of evaporation from the canopy interception, evaporation from ponded water, vegetation root transpiration, and the evaporation from saturated zone.

The finding supports the conclusion made by Siswamartana et al. (2002) who reported that the evapotranspiration rate of *Pinus merkusii* in other study sites in Indonesia is higher than the values in other forests with broad-leaved vegetation, such as *Schima wallichii* and *Agathis* sp. Evapotranspiration rate of *Pinus merkusii* at a study site in Banyumas, Central Java, for example, was recorded at 1,002 – 1,253 mm/year or 29-67% of total rainfall (Soedjoko et al., 1998 cited in Siswamartana et al., 2002).

This finding also reflects the arguments from Swank & Douglass (1974), who stated that evapotranspiration of coniferous forests is higher than the broad-leaved forests in Coweeta, US. However, this conclusion is contrary to the work of other research conducted by Komatsu, Tanaka, & Kume (2007). The research concluded that evapotranspiration of conifers is relatively similar or lower than that of broad-leaved forests in Japan. It is argued that the evapotranspiration rates of broad-leaved and coniferous forests are affected by rainfall seasonality (Komatsu, Tanaka, & Kume, 2007).

In this research, the total evapotranspiration slightly varies in scenario 1, 2, and 3 in each case study area. The variation on the evapotranspiration can be caused by the distributions of vegetation on different soil types in the catchments, although the land cover compositions in each scenario are similar (refer to 5.1.2 for the land cover compositions). This argument is supported by the modelling outcomes from the iterative 64 simulations, which show that the evapotranspiration for vegetation on Soil A (clayey soil) is generally lower than the similar vegetation on other soil types.

Reference evapotranspiration (*ET<sub>o</sub>*) was used in MIKE SHE model to compute the crop reference evapotranspiration by multiplying the *ET<sub>o</sub>* with crop coefficient (Danish Hydraulic Institute, 2017b). It should be noted that *ET<sub>o</sub>* is the evapotranspiration from a reference surface where

---

<sup>52</sup> The assessment of water balance analysis of the catchments covered by broad-leaved vegetation is further elaborated in Appendix F.

water is abundant (Allen et al., 1998). Therefore, the model assumes that there is unlimited water during the simulations, but in reality, water is limited. Evapotranspiration fluctuates during the day depending on the climate.

In this study, the reference evapotranspiration ( $ET_o$ ) in each case study area was estimated from the corrected temperature data and the wind speed in Bandung City. The first and second case study areas are located at the altitudes between 760 to 2,206 m asl and 661 to 2,337 m asl respectively. Areas at the higher altitudes have a lower temperature than the area at the lower altitudes. However, the temperature to estimate the  $ET_o$  was assumed to be similar across the area. Therefore, the  $ET_o$  assigned in the models could not represent the actual data on the sites.

#### 6.4.2 Canopy interception

Interception of rainfall by canopy was modelled in MIKE SHE as part of the evapotranspiration simulations. This section discusses how the characteristics of the tree canopy have an effect on the outcomes from MIKE SHE modelling.

Results from MIKE SHE 1 suggest that the depth of overland flow at the two sample points in the first case study area with conifers as a single type of plant is lower than when the broad-leaved and mixed vegetation were assigned. **The plant capacity to intercept the rainfall is related to the canopy structure**, which can be characterized by many factors, such as maximum tree height, Branch Area Index (BAI), total Plant Area Index (PAI), and Leaf Area Index (LAI) (Parker, 1995). In general, conifers have a higher LAI (Leaf Area Index) compared with broad-leaved vegetation. Plants with a high LAI have a higher density of foliage (Ghazoul & Sheil, 2010) and a high interception loss (Zheng et al., 2018). According to Merriam (1960), an interception loss can be defined as the precipitation that is evaporated or absorbed into the plant.

Canopy structure in evergreen forests changes over the year due to the growing tree crowns. When the crowns are close to the adjacent tree canopies, the understory and shade-tolerant plants grow and create another vegetation layer. The canopy closure is one of the crown and canopy characteristics that influence rainfall retention and redistribution<sup>53</sup> (Parker, 1995).

An understory and ground layer (e.g. seedlings and herbaceous vegetation) were found under the canopy of broad-leaved trees and conifers in the case study areas. However, only the reflectance of tree crowns (overstory) can be captured by the satellite. Thus, the LAI of broad-leaved vegetation and conifers used in the model can only represent the LAI of overstory because the value was derived from the studies that estimated LAI from single trees without the understory (e.g. Das, 2014; Albaugh et al., 1998).

---

<sup>53</sup> Other crown and canopy characteristics include the tree species, branch, leaf shape and texture, bark surface and canopy height (Parker, 1995).

The LAI of mixed woodlands used in the MIKE SHE models was derived from the research conducted by Dietz et al. (2006) in a lower montane forest in Central Sulawesi, Indonesia (800 – 1,140 m asl). Based on the 2015 land cover maps, mixed vegetation in the Ci Kapundung and Ci Sangkuy upper water catchments is located in the areas at 1,137 – 2,201 m asl and 788 – 2,334 m asl respectively. It can be assumed that only the mixed woodlands on mountain slopes below about 1,200 m asl in the case study areas have the similar characteristics with the vegetation in the study by Dietz et al. (2006) because they grow at the similar altitudes. Whitemore (1984) and Grubb (1977) argued that trees at the higher altitude in the lower montane forest (1,200 – 1,800 m asl) are shorter (15 – 33 m) and less abundant. The upper montane forest (1,800 – 3,000 m asl) has a high occurrence of epiphytes and trees with microphyll leaves (as cited in Whitten, Afiff, & Soeriaatmadja, 1996). However, it should be noted that plant communities found in one mountain could be different from the other mountain because of the slope aspect and the age of soil (Whitten, Afiff, & Soeriaatmadja, 1996).

MIKE SHE 2 simulations showed that **conifers have a higher capacity to intercept rainfall than broad-leaved vegetation during the simulation period (2008-2015)**. This conclusion is supported by the findings from the simulated of canopy evaporation, throughfall, and canopy storage of conifers and broad-leaved vegetation in the two case study areas. **The accumulated canopy evaporation for the model with conifers as the uniform land cover** in the first case study area is 9,171.88 mm and **is higher than broad-leaved vegetation** (4,260.12 mm). A similar result was also achieved from the water balance analysis of the second case study area. The interception loss of conifers and broad-leaved vegetation in the area is 8,939.46 mm and 6,564.89 mm respectively (Appendix F).

An implication of this outcome is **the lower amount of throughfall for conifers compared with the values for broad-leaved vegetation**. Approximately 71% of total rainfall flows as throughfall in areas covered by conifers, whereas broad-leaved trees have more throughfall (86.60%) in the first case study area. In the second case study area, the estimated amount of water that passed through the conifer canopies is 96.28% of total rainfall and is slightly lower than that of broad-leaved vegetation (97.27%). These high percentages of throughfall can be explained by referring to the simulated total precipitation (2008-2015) in the area that is also high (240,866 mm) because the precipitation lapse rate was assigned on the MIKE SHE model. Throughfall is the source of water that flows as surface runoff or infiltrates to the soil layer. Plants with a higher volume of throughfall have less capacity to intercept rainfall, thus more water reaches the ground.

Conifers have higher accumulated canopy storage than broad-leaved plants in the two watersheds. MIKE SHE simulates the canopy interception process by estimating the interception storage, which varies with different vegetation types. Interception storage will be filled with

precipitation before stem flow occurs. The estimated canopy storage depends on LAI and the interception coefficient assigned in the model (Danish Hydraulic Institute, 2017b).

This result reflects a study in the Walat Mt. research forest, West Java, Indonesia in 1999-2001 (Mulyana 2002 cited in Siswamartana et al., 2002). The study concluded that *Pinus merkusii* has a higher interception loss (15.7%) compared with broad-leaved trees (e.g. *Agathis loranthifolia*) (14.7%). Pine has a high interception stemflow (0.07-12.33 mm/month) and throughfall (1.53-45.83 mm/month). Therefore, *Pinus merkusii*<sup>54</sup> is recommended to be planted in the areas with high precipitation (>2000 mm/year). They should be planted along with other trees, which have a lower capacity to evaporate, such as *Schima wallihii* and *Agathis* sp., in the area 1500-2000 mm/year. Otherwise, the tree species can cause drought in the area.

#### 6.4.3 Implication of the findings to the proposed landscape planning for the two case study areas

Water movement in a catchment is a complex process which is affected by various factors. Evapotranspiration, for example, is modelled in MIKE SHE based on the canopy interception, water infiltration to the soil, water evaporation from soil and transpiration from plant roots, and water infiltration to the saturated zone. Plant characteristics that influence the process include canopy structure, which determines the interception loss, and root density, as one of the factors that affect the vegetation transpiration<sup>55</sup> (Danish Hydraulic Institute, 2017b).

Each vegetation type has a uniform root depth that was assigned in the MIKE SHE model regardless the soil types where the plants are located. The logarithmic relations between root depth and evapotranspiration employed in MIKE SHE indicate that plants with shallow roots are estimated to have higher rates of transpiration from the upper soil layer because a larger proportion of roots are located in this zone, compared with the deep-root plants (Danish Hydraulic Institute, 2017b).

Root growth is affected by physical soil conditions (Bengough et al., 2006). Soil parameters (e.g. moisture content at field capacity and wilting point) were included in the estimation on actual transpiration in MIKE SHE (Danish Hydraulic Institute, 2017b). In this study, the soil moisture was computed based on the compositions of clay, sand, and silt, and the estimated bulk density. Therefore, there is a high possibility that the same type of vegetation on the sites have different rates of transpiration, thus affecting the total evapotranspiration.

All the findings and discussions regarding plant characteristics were considered during the development of constraint maps for the Backcasting scenario of the two catchments (refer to Chapter 7). Based on the outcomes from the MIKE SHE modelling, it can be concluded that the

---

<sup>54</sup> *Pinus merkusii* Jung et de Vriese is the common Pine species in Java that was widely planted in 1970s (Siswamartana et al., 2002).

<sup>55</sup> Other factors that influence the vegetation transpiration include the LAI and soil moisture.



model predicted high canopy evaporation and low volume of throughfall when a high number of Leaf Area Index (LAI) was assigned. This means that conifers have a higher capacity to reduce the portion of rainfall reaching to the ground from the canopy because it has a higher value of LAI, which characterises the canopy interception, compared with broad-leaved and mixed vegetation. Although the LAI of conifers in both case study areas varies depending on the estimated age of sample trees, the values can be as high as 14.98 in the 37-year-old forests in the first case study area.

In this study, there are only two sub-classes of broad-leaved vegetation in each watershed (e.g. trees located inside and outside the protected areas). The sub-classes were mainly determined by observing the dominant trees during the field surveys. Therefore, the vegetation parameters assigned for the two sub-classes in MIKE SHE model are the generalization of plant characteristics from the diverse broad-leaved tree species on the sites. An improvement in the future hydrologic modelling may include the identification and classification of trees on the site in more detail.

Water balance analysis for the hypothetical catchments demonstrates that one vegetation type has a distinct capacity to reduce surface runoff on different soil, particularly during heavy rainfall (100 mm/day). This finding indicates the importance of considering the evaluation of soil properties and the soil distributions on the sites during the landscape planning process. In this study, the outcomes from the water balance analysis were used as one of the indications to develop the guidelines for developing constraint maps for land change modelling. It is important to note that the outcomes from the analysis are not site-specific. However, although the analysis was performed under uniform precipitation and reference evapotranspiration rates, the model used the existing soil and vegetation properties on the sites. Therefore, the outcomes should be interpreted based on these conditions.

## **6.5 Summary of Chapter 6**

- (1) Land cover maps and the results from the land change and hydrologic modelling were influenced by the uncertainty factors in each step of analysis (e.g. map accuracy and model parameters). Selected approaches were performed to improve the accuracy of land cover maps and modelling.
- (2) The case study areas have different levels of land change (2000-2015). The likelihood of land cover to change is the most influential driver of land change in both watersheds.
- (3) The scenario projection graphs have been presented to show the capacity of each scenario of landscape structure (e.g. the distribution of land cover on different soil types) to support flood regulation in the watersheds. The results show how any alteration of landscapes can affect the provision of flood regulation.

## Chapter 7 Planning recommendation

Chapter 7 presents the Backcasting scenario for the landscape structure of Ci Kapundung and Ci Sangkuy upper water catchment areas. The scenario was generated based on the results from MIKE SHE 2 modelling and the initial phase of Pareto-frontier analysis for the first three scenarios of landscape planning for the sites.

This last scenario was developed to propose optimal solutions to landscape planning in the two case study areas. In this case, the planning outcome is to support flood regulation in the catchments while accommodating the needs of areas for settlements and agricultural areas for inhabitants in the future. No assessment on other types of ecosystem services in the catchment areas has been conducted and integrated into the development of landscape planning in this study.

### 7.1 Land change modelling of Backcasting scenario (LCM 3)

The outcomes from MIKE SHE 2 suggest that a new development guideline should be added when developing the constraint maps for scenario 4. The proposed planning guideline include:

- (1) Replantation of conifers in the existing bare land located above 1,500 m asl outside the protected areas. This planning guideline was developed based on the premise that the mountain slopes above 1,500 m asl receive higher precipitation rates compared to the adjacent lowlands (Whitten, Afiff, & Soeriaatmadja, 1996). Another reason is that conifers have high evapotranspiration rates. Thus, it is recommended to plant conifers along with the existing broad-leaved vegetation to avoid drought in the area (Siswamartana et al., 2002).
- (2) Replantation of mixed vegetation in the existing bare land located below 1,500 m asl, especially on the slopes with clayey soil.
- (3) Cultivated areas on relatively flat to moderate slopes (<15%) to reduce surface runoff. This plan is proposed in addition to the existing constraint map for agriculture in Scenario 3.

#### 7.1.1 Landscape planning for the Ci Kapundung upper water catchment area

Figure 7-1 shows the new constraint maps for the first case study area (scenario 4). Constraint maps showing the areas restricted to the new development of settlements and agriculture in scenario 3 were still be used in scenario 4. Mixed vegetation is proposed to be planted in the areas below 1,500 m asl, which also include the existing Perhutani forest. However, this guideline does not apply to the protected area due to the restriction to change the landscape by law. On the other hand, bare land inside the forest is planted with conifers. Conifers have high

canopy interception, which can reduce the throughfall. Thus it is expected that less surface runoff is generated from the area. Mixing conifers with the existing vegetation in the forest would also reduce the possibility of drought in the catchment.

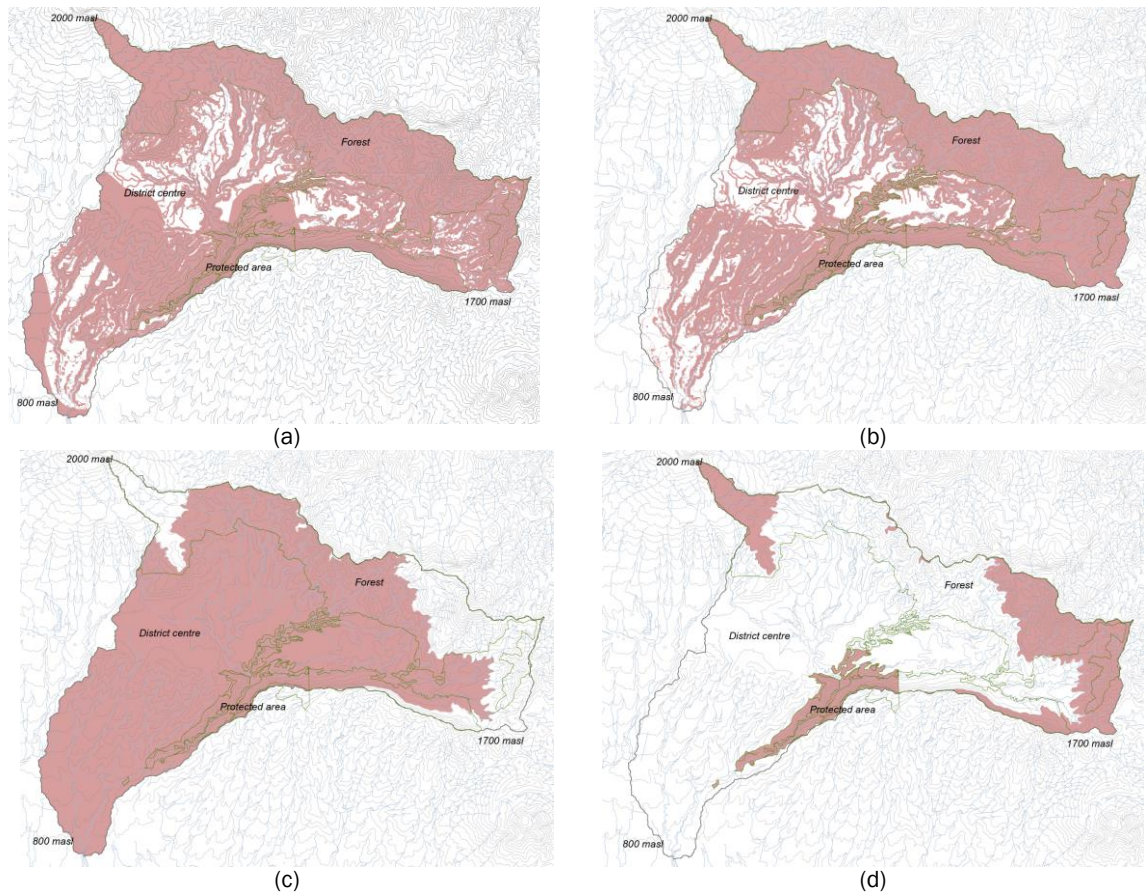


Figure 7-1 Constraints maps which delineate: (a-b) areas restricted to the new development of settlements and agriculture; (c-d) outside the area to be planted with conifers and mixed vegetation

The probability of bare land and cultivated land to change into mixed vegetation was added to the list of transition probability that was computed by MLP in LCM 2. A new Markov matrix to simulate the land cover maps of the first case study area is shown in Table 7-1. Weighting factors were applied to alter the probability of land cover change based on the proposed landscape planning guideline. No alteration to the original probability of land cover to be changed to developed areas, because one of the aims for backcasting scenario is to propose landscape planning that not only can reduce surface runoff, but also accommodate the needs for settlements.

Table 7-1 The altered Markov matrix to simulate the 2030 land cover map of the first study area

	Developed areas	Bare land cultv. land	Mixed veg.	Conifers	Broad-leaved veg.
Developed areas	0.9325	0.0561	0.0000	0.0000	0.0000
Bare land & cultv. land	0.2572	0.5513	0.1415	0.0500	0.0000
Mixed veg.	0.0061	0.1481	0.8458	0.0000	0.0000
Conifers	0.0070	0.0475	0.0000	0.9455	0.0000
Broad-leaved veg.	0.0607	0.4482	0.0070	0.0000	0.4911

The outcome from LCM 3 for the backcasting scenario of Ci Kapundung upper water catchment area is illustrated in Figure 7-2. More riparian areas in the catchment are covered by mixed vegetation, as a result of assigning related constraint maps in the model.

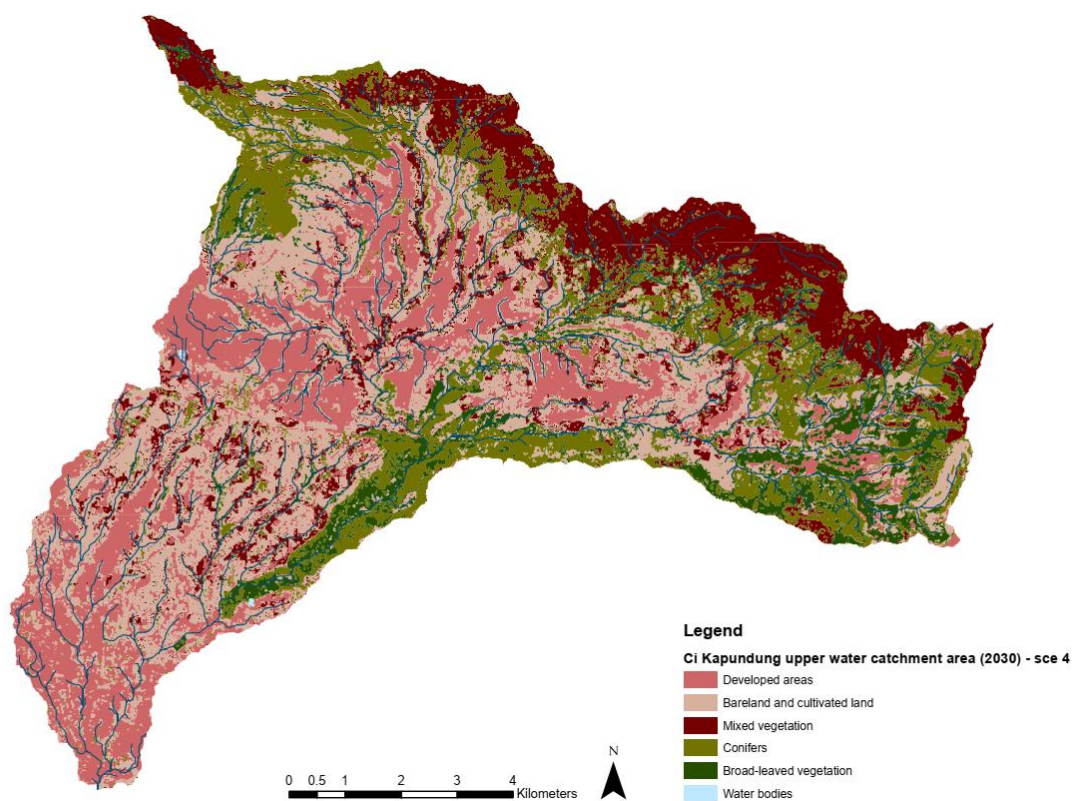


Figure 7-2 The projected 2030 land cover map of the first case study area based on scenario 4

The implication of the altered Markov matrix used in the land change modelling can also be seen in the land cover compositions (Table 7-2). There is a change in the coverage of mixed vegetation, from 12.94% in scenario 1, 2, and 3, to 18.16% in scenario 4. The land cover map in scenario 4 has lower percentages of broad-leaved vegetation (8.25%) and bare land and cultivated land (30.09%) in comparison to the first three scenarios.

Table 7-2 Land cover composition in the Ci Kapundung upper water catchment area in scenario 4 compared to the other scenarios

Land cover types	Predicted land cover composition in 2030			
	Scenario 1	Scenario 2	Scenario 3	Scenario 4
Developed areas	25.38%	25.38%	25.38%	25.38%
Bare land and cultivated land	33.23%	33.23%	33.23%	30.09%
Mixed vegetation	12.94%	12.94%	12.94%	18.16%
Conifers	18.71%	18.70%	18.70%	18.10%
Broad-leaved vegetation	9.72%	9.72%	9.72%	8.25%
Water bodies	0.02%	0.02%	0.02%	0.02%

The lower proportions of broad-leaved vegetation and bare land in scenario 4, compared with the condition in scenario 1, 2, and 3, could be associated with the transition probability of land cover assigned in the Markov matrix (Table 7-1). There is a higher possibility for bare land in the lowland areas in 2015 to change into mixed vegetation, as a response to the proposed planning guideline for scenario 4. However, the land cover transition from broad-leaved vegetation to bare land was also computed in the CA-Markov model. As has been discussed earlier, the Markov model in the integrated CA-Markov works based on the historical trend of land cover change in the area. In this case, the transition from broad-leaved vegetation to bare land has been identified from the two historical land cover maps (e.g. 2000 and 2015 maps) that were used to compute the transition probability of land cover change. Therefore, the model will assign a portion of broad-leaved woodland in the catchment (2015) to be altered into bare land and cultivated land (0.4482). At the same time, the model also changes another part of bare land and cultivated land into mixed vegetation (0.1415).

#### 7.1.2 Landscape planning for the Ci Sangkuy upper water catchment area

Constraint maps to project the 2030 land cover maps of Ci Sangkuy upper water catchment area based on the backcasting scenario is shown in Figure 7-3. The approach to developing the constraint maps for the first case study area was also applied in the land change modelling of the second case study area. The orographic effect influences the precipitation rates in the area. Thus mountainous area may receive a higher rate of precipitation compared to the other parts of the watershed. Conifers and mixed vegetation were proposed to be planted in the existing bare land depending on the altitudes.

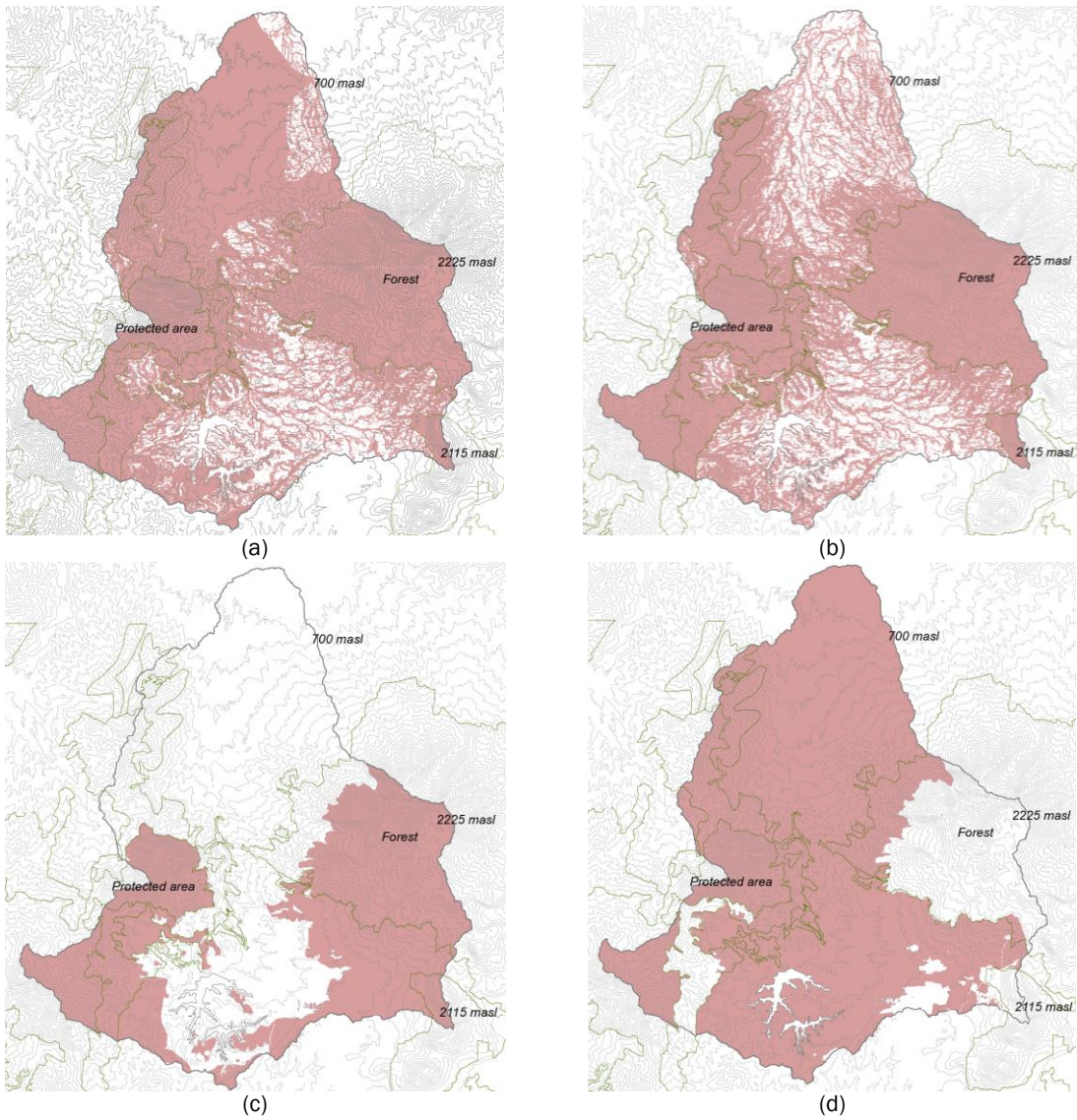


Figure 7-3 Constraints maps which delineate areas restricted to the new development of settlements and agriculture (a-b) and areas to be planted with broad-leaved trees and conifers (c-d) in scenario 4

The Markov matrix used to simulate the 2030 land cover maps in the first three scenarios was altered to project the land cover in the fourth scenario. The new Markov matrix is shown in Table 7-3. A higher probability of bare land to change into mixed vegetation was assigned from 0.0163 in the original Markov matrix to 0.2934, to increase the coverage of mixed vegetation in the lowland.

Table 7-3 The altered Markov matrix to simulate the 2030 land cover map of the second study area

	Developed areas	Bare land cultiv. land	Plantations	Mixed veg.	Conifers	Broad-leaved veg.
Developed areas	0.9996	0.0004	0.0000	0.0000	0.0000	0.0000
Bare land and cultiv.	0.1005	0.5056	0.0500	0.2934	0.0405	0.0100
Plantations	0.0158	0.1583	0.7679	0.0386	0.0194	0.0000
Mixed veg.	0.0000	0.0000	0.0000	1.0000	0.0000	0.0000
Conifers	0.0000	0.0000	0.0000	0.0000	1.0000	0.0000
Broad-leaved veg.	0.0504	0.3637	0.0848	0.0000	0.0000	0.5011

The land cover map from the last land change modelling (LCM 3) for the second case study area, which was simulated based on the backcasting scenario is presented in Figure 7-4. More areas on the catchment are covered with mixed vegetation, compared with the conditions in scenario 1, 2, and 3.

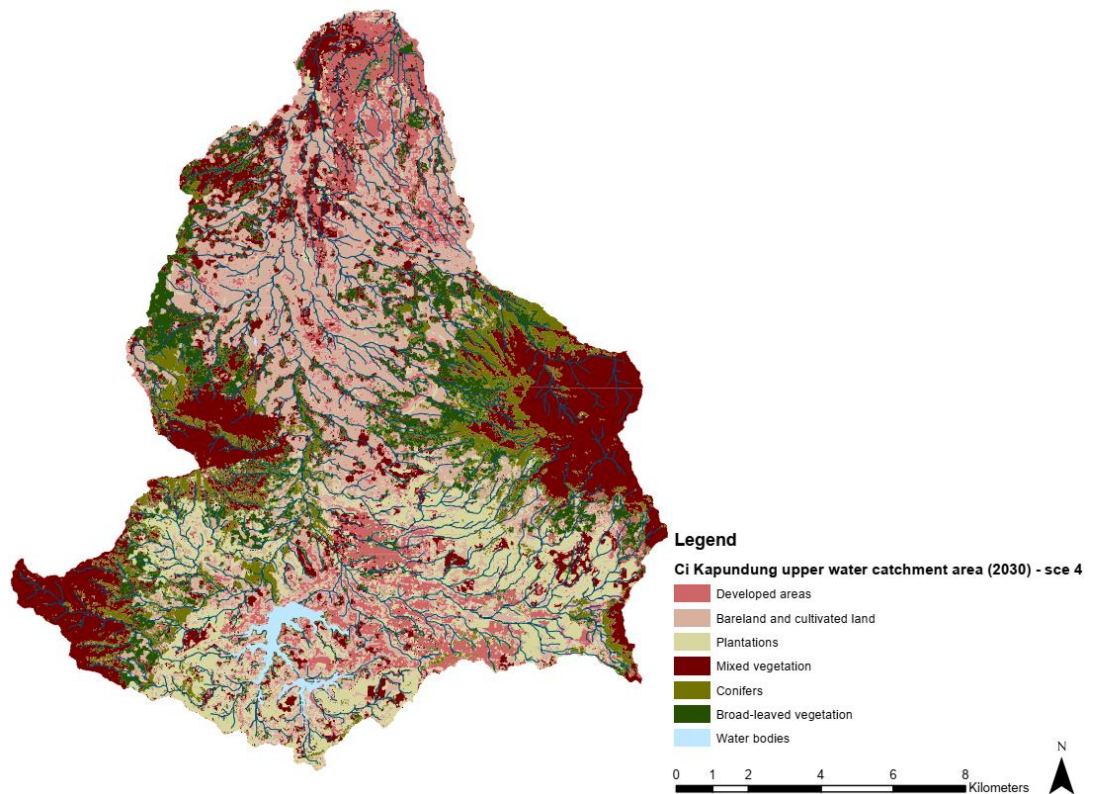


Figure 7-4 The projected 2030 land cover map of the second case study area based on scenario 4

Similar to the finding in the previous land change modelling for the first case study area, the alteration of transition probability from particular land cover types in the second case study area also affects their compositions in the watershed (Table 7-4). The composition of mixed vegetation increases from 15.14% in the first three scenarios to 24.39% in scenario 4. Less probability for land change to broad-leaved vegetation (Table 7-3) has influenced the decreasing

composition of broad-leaved vegetation in the area from 18.60% in scenario 1, 2, and 3, to 11.25% in scenario 4.

Table 7-4 Land cover composition in the Ci Sangkuy upper water catchment area in scenario 4 compared to the other scenarios

Land cover types	Predicted land cover composition in 2030			
	Scenario 1	Scenario 2	Scenario 3	Scenario 4
Developed areas	13.91%	13.91%	13.91%	13.91%
Bare land and cultivated land	26.85%	26.85%	26.85%	26.85%
Plantations	16.35%	16.35%	16.35%	14.44%
Mixed vegetation	15.14%	15.14%	15.14%	24.39%
Conifers	8.26%	8.26%	8.26%	8.26%
Broad-leaved vegetation	18.60%	18.60%	18.60%	11.25%
Water bodies	0.90%	0.90%	0.90%	0.90%

Developed areas and cultivated land have similar compositions with the same land cover in the previous scenarios. This is due to the same probabilities assigned in the initial Markov matrix from the two land cover types which were still used in scenario 4. However, there is also no change in the percentage of area covered with conifers in scenario 4, compared with the other three scenarios, despite different transition probability from other land cover types to conifers assigned in the Markov matrix. A possible explanation for this issue is that the alteration of all types of land cover in the case study area occurs at the same time.

## 7.2 Implication of landscape planning to flood regulation (MIKE SHE 3)

MIKE SHE 3 was conducted using the output from land change modelling based on the backcasting scenario (LCM 3) to assess the capacity of each case study area to reducing surface runoff. It was expected that the maximum discharges from the two catchments in the fourth scenario (2008-2015) would not exceed the estimated flood discharges. Based on the estimation, the flood discharges for the Ci Kapundung and Ci Sangkuy Rivers are 14.3 m<sup>3</sup>/s and 96 m<sup>3</sup>/s respectively.

### 7.2.1 Simulated river discharges and water balance in the Ci Kapundung upper water catchment area (MIKE SHE 3)

The projected Ci Kapundung River discharges from the backcasting scenario are illustrated in Figure 7-5. The estimated peak discharge is 16.90 m<sup>3</sup>/s, which is lower than the highest river magnitude recorded from the site (20.60 m<sup>3</sup>/s) and in the three future scenarios. However, the number is still higher than the estimated flood discharge (14.3 m<sup>3</sup>/s). It means that the projected river discharge from Ci Kapundung watershed might still give an influence to the occurrence of floods in Bandung Basin if the river discharges from other catchments exceed 173.1 m<sup>3</sup>/s (refer to 5.2.3).



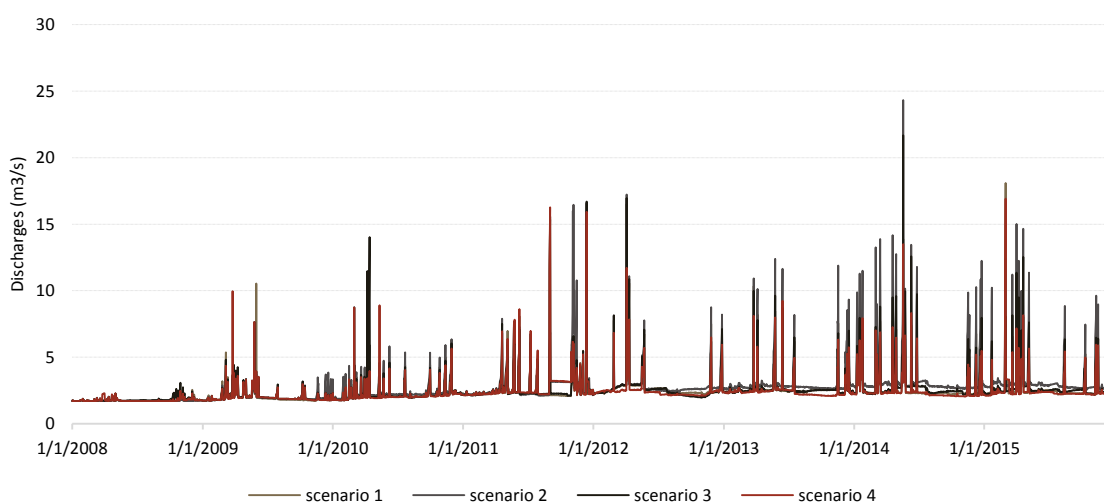


Figure 7-5 Simulated discharges (2008-2015) in the Ci Kapundung upper water catchment area

The result from the water balance analysis from the MIKE SHE model suggests that the accumulated overland flow is 2,740.02 mm, or is still higher than the total outflow from scenario 1 and 3 (Table 7-5). It was expected that a higher composition of mixed vegetation in the catchment could reduce the accumulated surface runoff within the simulation period. This argument was developed based on the results from the previous MIKE SHE 2 modelling of scenario 1, 2, and 3 and from the hypothetical catchments (refer to 6.3.3). Therefore, it is argued that the higher accumulated overland outflow can also be caused by the changes of compositions from other land cover types.

Table 7-5 Simulated water balance of Ci Kapundung upper water catchment area (2008-2015) (mm)

	Scenario 1	Scenario 2	Scenario 3	Scenario 4
Precipitation	-31,791.50	-31,791.50	-31,791.50	-31,791.50
Canopy storage ch	0.17	0.17	0.18	0.18
Evapotranspiration	10,913.80	10,801.90	10,772.80	11,083.80
OL storage change	838.69	882.10	803.19	827.89
OL boundary outflow	2,590.24	3,173.42	2,415.17	2,740.02
Subsurface storage ch	119.58	120.11	119.14	119.45
Total error	-17,329.10	-16,813.90	-17,681.10	-17,020.20

### 7.2.2 Simulated river discharges and water balance in the Ci Sangkuy upper water catchment area (MIKE SHE 3)

Figure 7-6 shows the simulated Ci Sangkuy River discharges from scenario 4 and the comparison with the discharges from other scenarios. The projected peak discharge from the backcasting scenario is 26.94 m<sup>3</sup>/s, which is still higher than the maximum river magnitudes in

scenario 2 and 3. However, the number is much lower than the highest recorded discharge from the river gauge on the site in 2008-2015 (96.6 m<sup>3</sup>/s), and the estimated flood discharge (96 m<sup>3</sup>/s).

The possible reasons for this significant discrepancy in the projection of river discharges are described as follows. It is highly likely that the model used for projecting the river discharges in each catchment is not fully calibrated. There is uncertainty in the model. Thus any output from the model should be interpreted with caution.

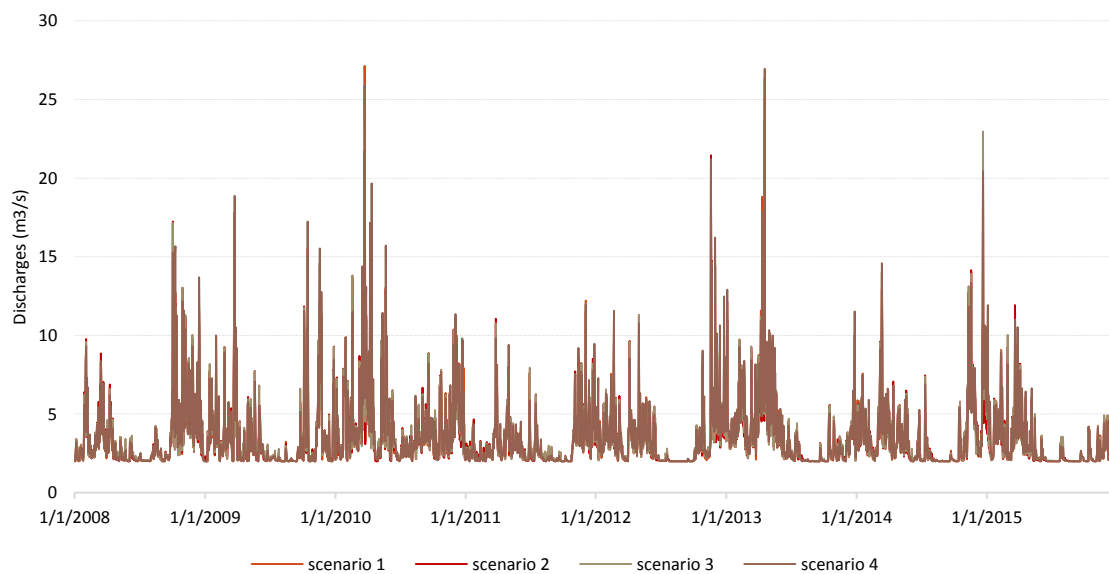


Figure 7-6 Simulated discharges (2008-2015) in the Ci Sangkuy upper water catchment area (scenario 4)

The result from water balance analysis reveals that more accumulated overland outflow is projected in scenario 4 than the outflow from the three scenarios. The proposed guidelines for landscape planning in the area have been applied in the last iteration of land change modelling (LCM 3) for the area. However, the outcomes from water balance analysis suggest that a high volume of overland outflow is generated from the catchment<sup>56</sup>. Therefore, further research should be undertaken to investigate potential variables that affected the results.

<sup>56</sup> A high rate of precipitation lapse has been applied into the model during the calibration process of MIKE SHE model for the second case study area (refer to Appendix A).

Table 7-6 Simulated water balance of Ci Sangkuy upper water catchment area (2008-2015) (mm)

	Scenario 1	Scenario 2	Scenario 3	Scenario 4
Precipitation	-240,866.00	-240,866.00	-240,866.00	-240,866.00
Canopy storage ch	2.55	2.85	2.52	2.52
Evapotranspiration	11,130.30	11,778.20	11,097.80	11,200.00
OL storage change	1,898.55	3,311.83	1,838.20	2,307.77
OL boundary outflow	70,933.10	64,554.60	69,187.20	75,302.40
Subsurface storage ch	19.66	21.12	19.56	20.10
Total error	-156,882.00	-161,197.00	-158,721.00	-152,033.00

### 7.3 Summary of Chapter 7

- (1) Backcasting scenarios were proposed to support the provision of flood regulation service in the two case study areas. The scenarios were developed based on the results from the previous MIKE SHE modelling using the first three scenarios and the hypothetical catchments.
- (2) The MIKE SHE modelling outcomes indicate that the Backcasting scenario can reduce the peak discharge of Ci Kapundung River. The second scenario of the land cover composition and distribution in the Ci Sangkuy watershed has the lowest peak discharge compared with the other scenarios.
- (3) It was expected that the plantation of conifers in the uplands and mixed vegetation in the lowlands, and the restriction for cultivated land on the steep slopes could lower the peak discharges in the two case study areas. However, the results from MIKE SHE 3 for the second case study could not provide the best outcome. The actual MIKE SHE models are highly complicated compared with the hypothetical catchments, and the hydrologic modelling was conducted with limitations.

## Chapter 8 Conclusions and outlook

This chapter draws the conclusions of research based on the results and discussion provided in the preceding chapters. Research novelty, main empirical and methodological findings, and research outlook are presented in this chapter.

### 8.1 Research novelty

This research aimed to examine potential landscape structure scenarios of Ci Kapundung and Ci Sangkuy upper water catchment areas in Bandung Basin, Indonesia. The novelty of this research can be seen from the four gaps of study that were addressed in this thesis. The first research gap is related to the land change model chosen. The coupled Cellular Automata (CA) and Markov model was used to model the future land change in the two watersheds, where more than 40% of the total areas were still covered by forest in 2015. According to Ghosh et al. (2017), **although the CA-Markov models have been applied to predict urban growth in many studies, the applications of the model to simulate changes in forest cover have rarely been explored (Gap 1).**

Different scenarios of landscape structure in the case study areas to support the streamflow regimes were evaluated using hydrology modelling. This approach was taken to investigate the research gap mentioned by Wu et al. (2015). In their paper, Wu et al. (2015) argued that **there are only a few studies that had assessed the development scenarios to support the streamflow regimes (Gap 2).**

At least fifteen studies have been conducted to investigate the impact of land-use changes on runoff generation process in Indonesia. However, **none of these studies assessed particular types of vegetation, including the composition and spatial distribution, to reduce surface runoff in catchment areas (Gap 3).** This research demonstrated how the distribution of vegetation in both case study areas influences flood regulation. The research findings arguably contribute to filling in the third research gap.

This research project responds to a call for a study to assess how the rate of ecosystem services changes with different landscape settings and scales (Jones et al. 2012). This thesis addresses **the ongoing needs of comparative studies using case study areas with the different biophysical environment when integrating the land change and hydrologic models (Gap 4).**

## 8.2 Main empirical findings

The empirical findings from this study can be described to answer the research questions as follows.

- (1) Research question 1: How does the land cover alteration in Ci Kapundung and Ci Sangkuy upper water catchment areas affect flood regulation in Bandung Basin?

The final generated land cover maps of Ci Kapundung and Ci Sangkuy upper water catchment areas in 2000, 2015, and 2017 indicate that the coverage of developed areas has increased in both watersheds. Further analysis on land cover alteration concluded that **the two case study areas experienced a different level of land change. Land cover alteration in both sites (2000-2015) was more influenced by the likelihood of land cover to change than the other identified driver variables** (e.g. the distance from existing disturbance, population density, elevation, slopes, and the distance from streams).

The output from the moving average (MA) analysis suggests that the increasing trend of annual Ci Kapundung River discharge (2001-2017) was influenced by the land cover change in the upper water catchment. The trend of Thiessen-weighted average rainfall shows a decreasing linear regression, indicating that the precipitation factor may not have a significant influence on the trend of Ci Kapundung river discharge.

A declining trend of Ci Sangkuy River discharge in the second case study area (2001-2017) may be caused by the increasing percentage of forest cover from 39.27% in 2000 to 43.30% in 2015 due to the reforestation program, although the forest cover decreased in 2017 to 39.76%. The decreasing precipitation rates are argued to be the other factor that affected the trend of river discharge.

**These findings suggest that land change is a significant factor that affected flood regulation in both case study areas.** This problem is due to the increasing demands for new settlements and agricultural land in the areas. Therefore, planning guidelines to address the issue and to mitigate the flooding issue are required.

- (2) Research question 2: What are the most effective scenarios of landscape structure for the two upper water catchment areas which can benefit flood regulation?

Results from the iterative MIKE SHE modelling confirm that **the compositions and distributions of land cover affect the flood regulation (e.g. river discharges and overland flow) in the Ci Kapundung and Ci Sangkuy upper water catchment areas.** This study concludes that the proposed landscape structure for the Ci Kapundung upper water catchment area in the scenario 4 (Backcasting scenario) has the lowest peak discharge under the weather conditions in 2008-2015 (16.90 m<sup>3</sup>/s), compared with the other scenarios. However, the simulated total overland

outflow from the catchment under the fourth scenario is still higher than the outflow from scenario 1 and 3. On the other hand, scenario 2 (existing policy-based scenario) provides is the most effective landscape planning for the Ci Sangkuy upper water catchment area to support flood regulation, by reducing the peak discharge and the accumulated surface runoff during the simulation period (2008-2015).

Constraint maps for scenario 4 were generated based on the feedback from the MIKE SHE 2 modelling outcomes, which comprise of the results from the iterative simulations on 64 hypothetical catchments. It was expected that the replantation of conifers in the uplands and mixed trees in the lowlands, and the restriction for cultivated land on the steep slopes could lower the peak discharges in the two case study areas. However, the hydrologic models used in this study were developed with limitations.

Uncertainty factors in the development of land cover maps using remote sensing data, the land change modelling, and the model parameterisation have an influence on the MIKE SHE model to accurately simulate the river discharges and water balance in each scenario. Therefore it is important to identify and mitigate the source of uncertainty in every stage of the analysis process.

(3) Research question 3: Which types of vegetation can improve flood regulation in each upper water catchment area?

The capacity of vegetation to reducing surface runoff in the case study areas is not only related to the plant characteristics (e.g. canopy interception and root transpiration), but also to the rainfall trends and the physical landscape attributes (e.g. slope gradients and soil types). The findings from the water balance analyses of the hypothetical catchments indicate that **conifers on moderate and steep slopes with the four types of soils can effectively reduce overland outflow under low precipitation** (5 mm/day). This is due to the higher canopy interception and evapotranspiration from conifers compared to the other vegetation types.

The second part of the vegetation analysis reveals that the simulated overland outflow differs significantly in the 64 scenarios during heavy rainfall. In general, more overland outflow is generated from the steep slopes and clayey soil. This study has found that conifers on clay, silt loam, and loam soil, and mixed vegetation on sandy loam soil have the lowest volume of overland outflow. **The findings provide insights into the development of landscape planning guidelines for the Ci Kapundung and Ci Sangkuy upper water catchment areas** in response to the needs for a flood mitigation plan in the Bandung Basin.

### 8.3 Main methodological findings

This research provides **a framework to conduct a similar topic of research using case studies with data gaps**. In this case, decision tree diagrams are presented in this thesis to show a range of possible methods to develop land cover maps using remote sensing data and to conduct the land change and hydrologic modelling with limitations and boundaries.

Data gaps in satellite imagery caused by a persistent cloud cover in the case study areas were mitigated by applying the backdating and updating method when developing the land cover maps (Linke et al., 2009). It is found that the method could improve the quality of the maps, which then were used in the second iteration of land change modelling to project the 2017 maps. The validation for the simulated land cover map (2017) for the first case study area was conducted using the 2017 map generated from the remote sensing data. The validation result shows that the model accuracy increased from 60.52% (before applying the method) to 81.76% (after applying the method) (Rani, Lange, Schroth, et al., 2019). This indicates **the applicability of the backdating and updating method to mitigate data gaps in satellite imagery**.

This study also shows that **heterogeneous data sources can be integrated into land change modelling** (Brown et al., 2014). The data includes the spatial demographic datasets, remotely sensed data, and the digital elevation model (DEM). Limited studies related to vegetation and soil in the case study areas have prompted **the estimation of missing data for the hydrologic modelling** using allometric equations and a software program (Hydrus1D).

### 8.4 Research outlook

This thesis demonstrates how land change and hydrologic modelling can be used by researchers and practitioners to quantify the implications of landscape planning in a water catchment area to flood regulation. Further studies can be conducted to minimize the uncertainty variables in the development of land cover maps and the simulations of land change and flood risk in a catchment area. There is a potential to include more land change drivers in the land change modelling (LCM), providing more information for the MLP neural network to model the transition probability maps. Therefore, it is crucial to mitigate the problem regarding the limited spatial social data, especially when conducting similar research in developing countries.

A future rainfall trend analysis and the simulation of saturated flow can be incorporated in the hydrologic model. On-site measurement can be done to collect the data that could not be retrieved in this study, such as evapotranspiration and Leaf Area Index (LAI). Another site survey can also be conducted to identify the sources of discharges for each tributary. This would provide a possibility to integrate particular modules of MIKE software to explicitly simulate river discharges from catchments (e.g. MIKE Hydro and MIKE 11).

It is vital to note that the planning recommendation for the two case study areas was proposed only to support the flood regulating service. A further study can be conducted to include multiple ecosystem services in the analysis to provide a more comprehensive planning recommendation in the catchment areas. Social systems (e.g. human intervention in ecosystems) can be integrated into the analysis, and the assessment on the implication of the work for the actual landscape can be performed.



## References

- Abson, D. J., von Wehrden, H., Baumgärtner, S., Fischer, J., Hanspach, J., Härdtle, W., Heinrichs, H., Klein, A. M., Lang, D. J., Martens, P. & Walmsley, D. (2014). Ecosystem Services as a Boundary Object for Sustainability. *Ecological Economics*, 103, 29–37. Retrieved from <http://linkinghub.elsevier.com/retrieve/pii/S0921800914001219>
- Adhikari, S. & Southworth, J. (2012). Simulating Forest Cover Changes of Bannerghatta National Park Based on a CA-Markov Model: A Remote Sensing Approach. *Remote Sensing*, 4(10), 3215–3243.
- Adrionita. (2011). Analisis Debit Sungai Dengan Model SWAT Pada Berbagai Penggunaan Lahan Di DAS Citarum Hulu Jawa Barat [Analysis of River Discharge by SWAT Model on Several Landuse at Upper Citarum Watershed, West Java].
- Ahmad, A. G., Siregar, C. A., Siregar, U. J. & Arifin, H. S. (2014). Biomassa Tusam (Pinus Merkusii Jungh et De Vriese Tapanuli Strain) Pada Sebaran Alami Di Sumatera Utara [Biomass Estimation of Pinus Merkusii Jungh et de Vriese Tapanuli Strain at Its Natural Distribution in North Sumatra]. *Indonesian Forest Rehabilitation Journal*, 2(2), 123–144.
- Akbar AS, M., Saleh, B., Nurdin, N. & Sofian, I. (2015). Cellular Automata-Markov Model of Vegetation Cover Changes on a Small Island Spermonde Archipelago, Indonesia, in: Lagmay, A. M. (Ed.), *36th Asian Conference on Remote Sensing 2015 (ACRS 2015)*. Quezon City. Retrieved from <https://www.scopus.com/inward/record.uri?eid=2-s2.0-84964066336&partnerID=40&md5=e79bace20317314865ae3cf1e03549e4>
- Albaugh, T. J., Allen, H. L., Dougherty, P. M., Kress, L. W. & King, J. S. (1998). Leaf Area and Above- and Belowground Growth Responses of Loblolly Pine to Nutrient and Water Additions. *Forest Science*, 44(2), 317–328.
- Aldrian, E. & Susanto, R. D. (2003). Identification of Three Dominant Rainfall Regions within Indonesia and Their Relationship to Sea Surface Temperature. *International Journal of Climatology*, 23(12), 1435–1452.
- Allen, R. G., Pereira, L. S., Raes, D. & Smith, M. (1998). *Crop Evapotranspiration: Guidelines for Computing Crop Requirements*. Retrieved from <http://www.kimberly.uidaho.edu/water/fao56/fao56.pdf>
- Amatya, D. M., Sun, G., Rossi, C. G., Ssegane, H. S., Nettles, J. E. & Panda, S. (2013). Forests, Land Use Change, and Water.
- de Araujo Barbosa, C. C., Atkinson, P. M. & Dearing, J. A. (2015). Remote Sensing of Ecosystem Services: A Systematic Review. *Ecological Indicators*, 52, 430–443. Retrieved from <http://linkinghub.elsevier.com/retrieve/pii/S1470160X15000084>
- Archer, N. A. L., Bonell, M., Coles, N., MacDonald, A. M., Auton, C. A. & Stevenson, R. (2013). Soil Characteristics and Landcover Relationships on Soil Hydraulic Conductivity at a Hillslope Scale: A View towards Local Flood Management. *Journal of Hydrology*, 497, 208–222. Retrieved from <http://dx.doi.org/10.1016/j.jhydrol.2013.05.043>
- Baker, W. L. (1989). A Review of Models of Landscape Change. *Landscape Ecology*, 2(2), 111–133.
- Basuki, T. M. (2015). Leaf Area Index Derived from Hemispherical Photograph and Its Correlation with Above-Ground Forest Biomass. *Indonesian Journal of Forestry Research*, 2(1), 31–41.
- Beckers, J., Smerdon, B. & Wilson, M. (2009). *Review of Hydrologic Models for Forest Management and Climate Change Applications in British Columbia and Alberta*. Retrieved from [www.forrex.org/publications/forrexseries/fs25.pdf](http://www.forrex.org/publications/forrexseries/fs25.pdf)
- Beets, P. N., Reutebuch, S., Kimberley, M. O., Oliver, G. R., Pearce, S. H. & McGaughey, R. J.

- (2011). Leaf Area Index, Biomass Carbon and Growth Rate of Radiata Pine Genetic Types and Relationships with LiDAR. *Forests*, 2(3), 637–659.
- Bengough, A. G., Bransby, M. F., Hans, J., McKenna, S. J., Roberts, T. J. & Valentine, T. A. (2006). Root Responses to Soil Physical Conditions; Growth Dynamics from Field to Cell. *Journal of Experimental Botany*, 57(2), 437–447.
- Bennett, E. M. et al. (2015). Linking Biodiversity, Ecosystem Services, and Human Well-Being: Three Challenges for Designing Research for Sustainability. *Current Opinion in Environmental Sustainability*, 14, 76–85. Retrieved from <http://www.sciencedirect.com/science/article/pii/S1877343515000366>
- Beven, K., Lamb, R., Leedal, D. & Hunter, N. (2015). Communicating Uncertainty in Flood Inundation Mapping: A Case Study. *International Journal of River Basin Management*, 13(3), 285–295.
- Boer, R., Dasanto, B. D., Perdinan & Marthinus, D. (2012). Hydrologic Balance of Citarum Watershed under Current and Future Climate, in: Filho, W. L. (Ed.), *Climate Change and the Sustainable Use of Water Resources*. Springer Berlin Heidelberg. Retrieved from <http://link.springer.com/10.1007/978-3-642-22266-5>
- Boerner, R. E. J., DeMers, M. N., Simpson, J. W., Artigas, F. J., Silva, A. & Berns, L. A. (1996). Markov Models of Inertia and Dynamism on Two Contiguous Ohio Landscapes. *Geographical Analysis*, 28(1).
- Bolte, J. & Vache, K. (2012). *Envisioning Puget Sound Alternative Futures - PSNERP Final Report*.
- Bréda, N. J. J. (2003). Ground-Based Measurements of Leaf Area Index: A Review of Methods, Instruments and Current Controversies. *Journal of Experimental Botany*, 54(392), 2403–2417.
- Brown, D. G., Band, L. E., Green, K. O., Irwin, E. G., Jain, A., Lambin, E. F., Pontius, R. G., Seto, K. C., Turner, B. L. & Verburg, P. H. (2014). *Advancing Land Change Modeling: Opportunities and Research Requirements*. Washington, U.S.A: The National Academies Press.
- Brunner, S. H., Huber, R. & Grêt-Regamey, A. (2016). A Backcasting Approach for Matching Regional Ecosystem Services Supply and Demand. *Environmental Modelling and Software*, 75, 439–458.
- Börjeson, L., Höjer, M., Dreborg, K.-H., Ekvall, T. & Finnveden, G. (2006). Scenario Types and Techniques: Towards a User's Guide. *Futures*, 38, 723–739.
- Candra, D. S., Kustiyo & Ismaya, H. (2014). Cloud Masking Data Spot-6 Dengan Menggunakan Pendekatan Nilai Reflektansi Dan Geometri [Cloud Masking for Spot-6 Data Using Reflectance and Geometry Approach], in: *Seminar Nasional Penginderaan Jauh 2014*, (pp. 189–197).
- Chapman, J. B. & Wynne, R. H. (2011). *Introduction to Remote Sensing*. The Guilford Press.
- Chander, G., Markham, B. L. & Helder, D. L. (2009). Summary of Current Radiometric Calibration Coefficients for Landsat MSS, TM, ETM+, and EO-1 ALI Sensors. *Remote Sensing of Environment*, 113(5), 893–903. Retrieved from <http://dx.doi.org/10.1016/j.rse.2009.01.007>
- Chang, H. & Franczyk, J. (2008). Climate Change, Land-Use Change, and Floods: Toward an Integrated Assessment. *Geography Compass*, 2(5), 1549–1579.
- Chaudhary, S., McGregor, A., Houston, D. & Chettri, N. (2015). The Evolution of Ecosystem Services: A Time Series and Discourse-Centered Analysis. *Environmental Science & Policy*, 54, 25–34. Retrieved from <http://linkinghub.elsevier.com/retrieve/pii/S1462901115001239>
- Chen, J. M. & Black, T. A. (1992). Defining Leaf Area Index for Non-flat Leaves. *Plant, Cell and Environment*, 15(4), 421–429.

- Chen, Y.-Y. & Li, M.-H. (2016). Quantifying Rainfall Interception Loss of a Subtropical Broadleaved Forest in Central Taiwan. *Water (Switzerland)*, 8(14), 1–19.
- Chow, V. Te, Maidment, D. R. & Mays, L. W. (1988). *Applied Hydrology*. McGraw-Hill International Editions.
- Clark, W. A. V. (1965). Markov Chain Analysis in Geography: An Application to the Movement of Rental Housing Areas. *Annals of the Association of American Geographers*, 55(2), 351–359.
- Clarke, K. C. (2014). Cellular Automata and Agent-Based Models, in: *Handbook of Regional Science*, (pp. 1217–1231). Retrieved from <http://link.springer.com/10.1007/978-3-642-23430-9>
- Congalton, R. G. (1991). A Review of Assessing the Accuracy of Classifications of Remotely Sensed Data. *Remote Sensing of Environment*, 37(1), 35–46.
- Crosetto, M., Moreno Ruiz, J. A. & Crippa, B. (2001). Uncertainty Propagation in Models Driven by Remotely Sensed Data. *Remote Sensing of Environment*, 76(3), 373–385.
- Dang, A. N. & Kawasaki, A. (2016). A Review of Methodological Integration in Land-Use Change Models. *International Journal of Agricultural and Environmental Information Systems*, 7(2), 1–25. Retrieved from <http://services.igi-global.com/resolvedoi/resolve.aspx?doi=10.4018/IJAEIS.2016040101>
- Danish Hydraulic Institute. (2017a). *MIKE SHE Volume 1: User Guide*.
- Danish Hydraulic Institute. (2017b). *MIKE SHE Volume 2: Reference Guide*.
- Danish Hydraulic Institute. (2017c). *MIKE HYDRO River*.
- Darul, A., Irawan, D. E., Trilaksono, N. J., Pratama, A. & Fitria, U. R. (2016). Conceptual Model of Groundwater and River Water Interactions in Cikapundung Riverbank, Bandung, West Java. *IOP Conference Series: Earth and Environmental Science*, 29. Retrieved from <http://stacks.iop.org/1755-1315/29/i=1/a=012026?key=crossref.2fc5499350447190c74e4ff2558cf135>
- Das, N. (2014). Allometric Modeling for Leaf Area and Leaf Biomass Estimation of Swietenia Mahagoni in North-Eastern Region of Bangladesh. *Journal of Forest and Environmental Science*, 30(4), 351–361. Retrieved from <https://www.hindawi.com/archive/2014/486478/>
- Dasanto, B. D., Boer, R., Pramudya, B. & Suharnoto, Y. (2014). Simple Method for Assessing Spread of Flood Prone Areas under Historical and Future Rainfall in the Upper Citarum Watershed. *EnvironmentAsia*, 7(2), 79–86.
- Deblonde, G., Penner, M. & Royer, A. (1994). Measuring Leaf Area Index with the Li-Cor LAI-2000 in Pine Stands. *Ecology*, 75(5), 1507–1511.
- Dietz, J., Hölscher, D., Leuschner, C. & Hendrayanto. (2006). Rainfall Partitioning in Relation to Forest Structure in Differently Managed Montane Forest Stands in Central Sulawesi, Indonesia. *Forest Ecology and Management*, 237(1–3), 170–178.
- Dimitriou, E., Moussoulis, E., Stamati, F. & Nikolaidis, N. (2009). Modelling Hydrological Characteristics of Mediterranean Temporary Ponds and Potential Impacts from Climate Change. *Hydrobiologia*, 634(1), 195–208.
- Djaenuddin, D., Basumi, Hardiwigeno, S., Subagyo, H., Sukardi, M., Ismangun, Ds, M., Suharta, N., Hakim, L., Widagdo, Dai, J., Suwandi, V., Bachri, S. & Jordens, E. R. (1994). *Kesesuaian Lahan Untuk Tanaman Pertanian Dan Tanaman Kehutanan [Land Suitability for Agricultural and Silvicultural Plants]*. Bogor.
- Djaenuddin, D. (2004). Some Specific Soil Characteristics of Andisols as Series Differentiae: A Case Study of Cikajang and Cikole Regions, West Java. *Jurnal Tanah dan Lingkungan*, 6(1),

14-21.

- Eastman, J. R. (2006). *Guide to GIS and Image Processing*. Worcester: Clark University.
- Eastman, J. R. (2016). *TerrSet: Geospatial Monitoring and Modeling System - Tutorial*.
- Ediriweera, S., Pathirana, S., Danaher, T., Nichols, D. & Moffiet, T. (2013). Evaluation of Different Topographic Corrections for Landsat TM Data by Prediction of Foliage Projective Cover (FPC) in Topographically Complex Landscapes. *Remote Sensing*, 5(12), 6767–6789.
- Eraso, N. R., Armenteras-Pascual, D. & Alumbrosos, J. R. (2013). Land Use and Land Cover Change in the Colombian Andes: Dynamics and Future Scenarios. *Journal of Land Use Science*, 8(2), 154–174. Retrieved from <http://www.tandfonline.com/doi/abs/10.1080/1747423X.2011.650228>
- ESRI. (2016). Hydrologic Toolset: Fill. Retrieved December 3, 2018, from <http://desktop.arcgis.com/en/arcmap/10.3/tools/spatial-analyst-toolbox/fill.htm>
- FAO. (2006). *Guidelines for Soil Description*. Rome: Food and Agriculture Organization of The United Nations.
- Feng, Y. & Liu, Y. (2016). Scenario Prediction of Emerging Coastal City Using CA Modeling under Different Environmental Conditions: A Case Study of Lingang New City, China. *Environmental Monitoring and Assessment*, 188:540. Retrieved from <http://dx.doi.org/10.1007/s10661-016-5558-y>
- Fisher, P. F., Comber, A. J. & Wadsworth, R. (2005). Land Use and Land Cover: Contradiction or Complement, in: Fisher, P. (Ed.), *Re-Presenting GIS*. Wiley.
- Foody, G. M. (1992). On the Compensation for Chance Agreement in Image Classification Accuracy Assessment. *Photogrammetric Engineering and Remote Sensing*, 58(10), 1459–1460.
- Foody, G. M. (2002). Status of Land Cover Classification Accuracy Assessment. *Remote Sensing of Environment*, 80, 185–201.
- Forman, R. T. T. (1995). *Land Mosaic: The Ecology of Landscape and Regions*. Cambridge: Cambridge University Press.
- Forman, R. T. T. & Godron, M. (1986). *Landscape Ecology*. New York: John Wiley and Sons Ltd.
- Fu, X., Wang, X. & Yang, Y. J. (2018). Deriving Suitability Factors for CA-Markov Land Use Simulation Model Based on Local Historical Data. *Journal of Environmental Management*, 206, 10–19.
- Gallant, S. I. (1993). *Neural Network Learning and Expert Systems*. Cambridge, Massachusetts: The MIT Press.
- Gao, Y. & Mas, J. F. (2008). A Comparison of the Performance of Pixel-Based and Object-Based Classifications over Images with Various Spatial Resolutions. *Online Journal of Earth Sciences*, 2(8701), 27–35. Retrieved from <http://docsdrive.com/pdfs/medwelljournals/ojesci/2008/27-35.pdf>
- Ghazoul, J. & Sheil, D. (2010). *Tropical Rain Forest Ecology, Diversity, and Conservation*. New York: Oxford University Press Inc.
- Ghosh, P., Mukhopadhyay, A., Chanda, A., Mondal, P., Akhand, A., Mukherjee, S., Nayak, S. K., Ghosh, S., Mitra, D., Ghosh, T. & Hazra, S. (2017). Application of Cellular Automata and Markov-Chain Model in Geospatial Environmental Modeling- A Review. *Remote Sensing Applications: Society and Environment*, 5, 64–77. Retrieved from <http://linkinghub.elsevier.com/retrieve/pii/S2352938516300258>
- Gidey, E., Dikinya, O., Sebego, R., Segosebe, E. & Zenebe, A. (2017). Cellular Automata and Markov Chain (CA\_Markov) Model-Based Predictions of Future Land Use and Land Cover

- Scenarios (2015–2033) in Raya, Northern Ethiopia. *Modeling Earth Systems and Environment*, 3(4), 1245–1262. Retrieved from <http://link.springer.com/10.1007/s40808-017-0397-6>
- Gigante, V., Iacobellis, V., Manfreda, S., Milella, P. & Portoghese, I. (2009). Influences of Leaf Area Index Estimations on Water Balance Modeling in a Mediterranean Semi-Arid Basin. *Natural Hazards and Earth System Sciences*, 9(3), 979–991.
- Golden Gate Weather Services. (2019). El Niño and La Niña Years and Intensities. Retrieved July 24, 2019, from <https://ggweather.com/enso/oni.htm>
- Gong, J., Liu, Y. & Chen, W. (2012). Optimal Land Use Allocation of Urban Fringe in Guangzhou. *Journal of Geographical Sciences*, 22(1), 179–191.
- Gorantiwar, S. D., Krishnamoorthy, Y. V. N., Pandit, D. S., Joshi, A. K. & Das, S. (2015). Climate Change Modelling, Planning and Policy for Agriculture, in: Singh, K. A., Dagar, C. J., Arunachalam, A., R. G., and Shelat, N. K. (Eds.), (pp. 199–217). New Delhi: Springer India. Retrieved from [http://dx.doi.org/10.1007/978-81-322-2157-9\\_20](http://dx.doi.org/10.1007/978-81-322-2157-9_20)
- Guzy, M. R., Smith, C. L., Bolte, J. P., Hulse, D. W. & Gregory, S. V. (2008). Policy Research Using Agent-Based Modeling to Assess Future Impacts of Urban Expansion into Farmlands and Forests. *Ecology and Society*, 13(1).
- Hamdy, O., Zhao, S., Osman, T., Salheen, M. A. & Eid, Y. Y. (2016). Applying a Hybrid Model of Markov Chain and Logistic Regression to Identify Future Urban Sprawl in Abouelreesh, Aswan: A Case Study. *Geosciences*, 6(43), 1–17. Retrieved from <http://www.mdpi.com/2076-3263/6/4/43>
- Haryanto, E. T., Herwanto, T. & Kendaro, D. R. (2007). Perubahan Bentuk Penggunaan Lahan Dan Implikasinya Terhadap Koefisien Air Larian DAS Citarum Hulu Jawa-Barat [Land-Use Change and the Implication to Runoff Coefficient in the Upper Citarum Catchment West Java]. *Jurnal Bionatura*, 9(1), 1–15.
- Haslauer, E., Biberacher, M. & Blaschke, T. (2016). A Spatially Explicit Backcasting Approach for Sustainable Land-Use Planning. *Journal of Environmental Planning and Management*, 59(5), 866–890. Retrieved from <http://www.tandfonline.com/doi/abs/10.1080/09640568.2015.1044652>
- Hay, G. J. & Castilla, G. (2006). Object-Based Image Analysis: Strengths, Weaknesses, Opportunities and Threats (SWOT). *The International Archives of the Photogrammetry, Remote Sensing and Spatial Information Sciences*.
- Hecht-Nielsen, R. (1987). Kolmogorov's Mapping Neural Network Existence Theorem, in: *Proceedings of the International Conference on Neural Networks, III*, (pp. 11–14). New York: IEEE Press.
- Helmer, E. H., Ruzycski, T. S., Benner, J., Voggesser, S. M., Scobie, B. P., Park, C., Fanning, D. W. & Ramnarine, S. (2012). Detailed Maps of Tropical Forest Types Are within Reach: Forest Tree Communities for Trinidad and Tobago Mapped with Multiseason Landsat and Multiseason Fine-Resolution Imagery. *Forest Ecology and Management*, 279, 147–166. Retrieved from <http://dx.doi.org/10.1016/j.foreco.2012.05.016>
- Herold, M., Goldstein, N. C. & Clarke, K. C. (2003). The Spatiotemporal Form of Urban Growth: Measurement, Analysis and Modeling. *Remote Sensing of Environment*, 86, 286–302.
- Hidayat, Y., Murti Laksono, K., Wahjunie, E. D. & Panuju, D. R. (2013). Pencirian Debit Aliran Sungai Citarum Hulu [The Characteristics of River Discharge of Citarum Hulu]. *Jurnal Ilmu Pertanian Indonesia (JIPI)*, 18(2), 109–114.
- Hosoi, F. & Omasa, K. (2009). Estimating Vertical Leaf Area Density Profiles of Tree Canopies Using Three-Dimensional Portable LIDAR Imaging. *Laser Scanning 2009*, 152–157. Retrieved from <http://park.itc.u-tokyo.ac.jp/joho/Omasa/462.pdf>

- House, A. R., Thompson, J. R. & Acreman, M. C. (2016). Projecting Impacts of Climate Change on Hydrological Conditions and Biotic Responses in a Chalk Valley Riparian Wetland. *Journal of Hydrology*, 534, 178–192. Retrieved from <http://linkinghub.elsevier.com/retrieve/pii/S0022169416000172>
- Hulse, D., Branscomb, A., Enright, C. & Bolte, J. (2009). Anticipating Floodplain Trajectories: A Comparison of Two Alternative Futures Approaches. *Landscape Ecology*, 24(8), 1067–1090.
- Hümam, M., Schüler, G., Müller, C., Schneider, R., Johst, M. & Caspari, T. (2011). Identification of Runoff Processes – The Impact of Different Forest Types and Soil Properties on Runoff Formation and Floods. *Journal of Hydrology*, 409(3–4), 637–649. Retrieved from <http://linkinghub.elsevier.com/retrieve/pii/S0022169411006329>
- Ichwan, M. (2009). Perencanaan Lanskap Bumi Perkemahan Ranca Upas Berdasarkan Pendekatan Daya Dukung Ekologi [Landscape Planning of Ranca Upas Camping Ground Based on Ecological Carrying Capacity Approach].
- Irish, R. R. (2000). Landsat 7 Automatic Cloud Cover Assessment, in: Shen, S. S. and Descour, M. R. (Eds.), *Algorithms for Multispectral, Hyperspectral, and Ultraspectral Imagery VI*, (pp. 1–8).
- Irish, R. R., Barker, J. L., Goward, S. N. & Arvidson, T. (2006). Characterization of the Landsat-7 ETM+ Automated Cloud-Cover Assessment (ACCA) Algorithm. *Photogrammetric Engineering and Remote Sensing*, 72(10), 1179–1188.
- Jafari, M., Majedi, H., Monavari, S. M., Alesheikh, A. A. & Zarkesh, M. K. (2016). Dynamic Simulation of Urban Expansion through a CA-Markov Model Case Study: Hyrcanian Region, Gilan, Iran. *European Journal of Remote Sensing*, 49, 513–529. Retrieved from <http://www.aitjournal.com/articleView.aspx?ID=1000>
- JICA. (2010). *The Preparatory Survey for Upper Citarum Basin Tributaries Flood Management Project in Indonesia*.
- John Monteith & Unsworth, M. H. (1973). *Principles of Environmental Physics*. Oxford: Butterworth-Heinemann.
- Jones, K. B., Zurlini, G., Kienast, F., Petrosillo, I., Edwards, T., Wade, T. G., Li, B. & Zaccarelli, N. (2013). Informing Landscape Planning and Design for Sustaining Ecosystem Services from Existing Spatial Patterns and Knowledge. *Landscape Ecology*, 28(6), 1175–1192.
- Ju, H., Zhang, Z., Zuo, L., Wang, J., Zhang, S., Wang, X. & Zhao, X. (2016). Driving Forces and Their Interactions of Built-up Land Expansion Based on the Geographical Detector – a Case Study of Beijing, China. *International Journal of Geographical Information Science*, 30(11), 2188–2207. Retrieved from <http://dx.doi.org/10.1080/13658816.2016.1165228>
- Kalyanapu, A. J., Burian, S. J. & McPherson, T. N. (2009). Effect of Land Use-Based Surface Roughness on Hydrologic Model Output. *Journal of Spatial Hydrology*, 9(2), 51–71. Retrieved from <http://spatialhydrology.net/index.php/JOSH/article/view/84>
- Kangas, A., Korhonen, K. T., Packalen, T. & Vauhkonen, J. (2018). Sources and Types of Uncertainties in the Information on Forest-Related Ecosystem Services. *Forest Ecology and Management*, 427, 7–16. Retrieved from <https://doi.org/10.1016/j.foreco.2018.05.056>
- Karim, S. (2014). Strategi Penanggulangan Sedimen Di Sub-DAS Citanduy Hulu Provinsi Jawa Barat Dengan Menggunakan Model SWAT [Sediment Mitigation Strategy in Sub-DAS Upstream of Citanduy West Java Province Using SWAT Model]. *Bogor Institute of Agriculture*.
- Keilholz, P., Disse, M. & Halik, Ü. (2015). Effects of Land Use and Climate Change on Groundwater and Ecosystems at the Middle Reaches of the Tarim River Using the MIKE SHE Integrated Hydrological Model. *Water (Switzerland)*, 7(6), 3040–3056.

- Keshtkar, H. & Voigt, W. (2016). A Spatiotemporal Analysis of Landscape Change Using an Integrated Markov Chain and Cellular Automata Models. *Modeling Earth Systems and Environment*, 2(10).
- Komatsu, H., Tanaka, N. & Kume, T. (2007). Do Coniferous Forests Evaporate More Water than Broad-Leaved Forests in Japan? *Journal of Hydrology*, 336(3–4), 361–375.
- Konôpka, B., Pajtík, J., Marušák, R., Bošela, M. & Lukac, M. (2016). Specific Leaf Area and Leaf Area Index in Developing Stands of *Fagus Sylvatica* L. and *Picea Abies* Karst. *Forest Ecology and Management*, 364, 52–59.
- Kouwen, N. & Fathi-Moghadam, M. (2000). Friction Factors for Coniferous Trees along Rivers. *Journal of Hydraulic Engineering*, 126(10), 732–740.
- Kusratmoko, E., Albertus, S. D. Y. & Supriatna. (2017). Modelling Land Use/Cover Changes with Markov- Cellular Automata in Komerling Watershed, South Sumatera. *IOP Conference Series: Earth and Environmental Science*, 54, 1–8.
- Lasco, R. D. & Boer, R. (2006). *An Integrated Assessment of Climate Change Impacts, Adaptations and Vulnerability in Watershed Areas and Communities in Southeast Asia*. Washington.
- Li, X. & Yeh, A. G.-O. (2000). Modelling Sustainable Urban Development by the Integration of Constrained Cellular Automata and GIS. *International Journal of Geographical Information Science*, 14(2), 131–152.
- Li, X. & Yeh, A. G.-O. (2002). Neural-Network-Based Cellular Automata for Simulating Multiple Land Use Changes Using GIS. *International Journal of Geographical Information Science*, 16(4), 323–343.
- Lillesand, T., Kiefer, R. W. & Chipman, J. (2008). *Remote Sensing and Image Interpretation*. United States of America: John Wiley & Sons.
- Linke, J., McDermid, G. J., Pape, A. D., McLane, A. J., Laskin, D. N., Hall-Beyer, M. & Franklin, S. E. (2009). The Influence of Patch-Delineation Mismatches on Multi-Temporal Landscape Pattern Analysis. *Landscape Ecology*, 24(2), 157–170.
- Liu, C., Hu, J., Lin, Y., Wu, S. & Huang, W. (2011). Haze Detection, Perfection and Removal for High Spatial Resolution Satellite Imagery. *International Journal of Remote Sensing*, 32(23), 8685–8697. Retrieved from <http://dx.doi.org/10.1080/01431161.2010.547884>
- Liu, G., Du, S., Peng, S. & Wang, G. (2014). Rainfall Interception in Two Contrasting Forest Types in the Mount Gongga Area of Eastern Tibet, China. *Hydrology, Current Research*, 4(4), 1–6.
- Liu, Y. & Feng, Y. (2016). Simulating the Impact of Economic and Environmental Strategies on Future Urban Growth Scenarios in Ningbo, China. *Sustainability*, 8(10). Retrieved from <http://www.mdpi.com/2071-1050/8/10/1045>
- Lu, D. & Weng, Q. (2007). A Survey of Image Classification Methods and Techniques for Improving Classification Performance. *International Journal of Remote Sensing*, 28(5), 823–870.
- Ma, L., He, C., Bian, H. & Sheng, L. (2016). MIKE SHE Modeling of Ecohydrological Processes: Merits, Applications, and Challenges. *Ecological Engineering*, 96, 137–149. Retrieved from <http://dx.doi.org/10.1016/j.ecoleng.2016.01.008>
- Malhado, A. C. M., Costa, M. H., de Lima, F. Z., Portilho, K. C. & Figueiredo, D. N. (2009). Seasonal Leaf Dynamics in an Amazonian Tropical Forest. *Forest Ecology and Management*, 258(7), 1161–1165.
- Maria, R. (2008). Hidrogeologi Dan Potensi Resapan Airtanah Sub Das Cikapundung Bagian Tengah [Hydrogeology and the Potential Groundwater Infiltration at the Centre of Cikapundung Sub-Catchment]. *Jurnal Riset Geologi dan Pertambangan*, 18(2), 21–30.

- Marko, K., Zulkarnain, F. & Kusratmoko, E. (2016a). Coupling of Markov Chains and Cellular Automata Spatial Models to Predict Land Cover Changes (Case Study: Upper Ci Leungsi Catchment Area). *IOP Conference Series: Earth and Environmental Science*, 47(1).
- Marko, K., Zulkarnain, F. & Kusratmoko, E. (2016b). Coupling of Markov Chains and Cellular Automata Spatial Models to Predict Land Cover Changes (Case Study: Upper Ci Leungsi Catchment Area). *IOP Conference Series: Earth and Environmental Science*, 47(012032), 1–10.
- Martínez-López, J., Carreño, M. F., Palazón-Ferrando, J. A., Martínez-Fernández, J. & Esteve, M. A. (2014). Remote Sensing of Plant Communities as a Tool for Assessing the Condition of Semiarid Mediterranean Saline Wetlands in Agricultural Catchments. *International Journal of Applied Earth Observation and Geoinformation*, 26, 193–204. Retrieved January 25, 2018, from <https://www.sciencedirect.com/science/article/pii/S0303243413000858>
- Mas, J.-F., Kolb, M., Paegelow, M., Olmedo, M. T. C. & Houet, T. (2014). Inductive Pattern-Based Land Use/Cover Change Models: A Comparison of Four Software Packages. *Environmental Modelling and Software*, 51, 94–111. Retrieved from <http://dx.doi.org/10.1016/j.envsoft.2013.09.010>
- Mason, E. G., Diepstraten, M., Pinjuv, G. L. & Lasserre, J.-P. (2012). Comparison of Direct and Indirect Leaf Area Index Measurements of *Pinus Radiata* D. Don. *Agricultural and Forest Meteorology*, 166–167, 113–119. Retrieved from <file://www.sciencedirect.com/science/article/pii/S0168192312002122>
- McWilliam, A.-L. C., Roberts, J. M., Cabral, O. M. R., Leitao, M. V. B. R., De Costa, A. C. L., Maitelli, G. T., Zamparoni, C. A. G. P., Cabral, M. R., Leitao, M. V. B. R., Maitelli, G. T. & Zamparoni, C. A. G. P. (1993). Leaf Area Index and Above-Ground Biomass of Terra Firme Rain Forest and Adjacent Clearings in Amazonia. *Source: Functional Ecology Functional Ecology Functional Ecology*, 7(7), 310–317.
- Megahed, Y., Cabral, P., Silva, J. & Caetano, M. (2015). Land Cover Mapping Analysis and Urban Growth Modelling Using Remote Sensing Techniques in Greater Cairo Region—Egypt. *ISPRS International Journal of Geo-Information*, 4(3), 1750–1769. Retrieved from <http://www.mdpi.com/2220-9964/4/3/1750/>
- Merriam, R. A. (1960). A Note on the Interception Loss Equation. *Journal of Geophysical Research*, 65(11), 3850–3851.
- Millennium Ecosystem Assessment. (2005). *Ecosystems and Human Well Being: Synthesis*. Washington: Island Press.
- Miller, H. J. (2009). Geocomputation, in: Fotheringham, A. S. and Rogerson, P. A. (Eds.), *The SAGE Handbook of Spatial Analysis*, (pp. 398–418).
- Mishra, V. N., Rai, P. K. & Mohan, K. (2014). Prediction of Land Use Changes Based on Land Change Modeler (LCM) Using Remote Sensing: A Case Study of Muzaffarpur (Bihar), India. *Journal of the Geographical Institute 'Jovan Cvijic', SASA*, 64(1), 111–127. Retrieved from <http://www.doiserbia.nb.rs/Article.aspx?ID=0350-75991401111M>
- Moreira, E. P. & Valeriano, M. M. (2014). Application and Evaluation of Topographic Correction Methods to Improve Land Cover Mapping Using Object-Based Classification. *International Journal of Applied Earth Observation and Geoinformation*, 32(1), 208–217. Retrieved from <http://dx.doi.org/10.1016/j.jag.2014.04.006>
- Morris, D. A. & Johnson, A. I. (1967). *Summary of Hydrologic and Physical Properties of Rock and Soil Materials, as Analyzed by the Hydrologic Laboratory of the U.S. Geological Survey, 1948-1960*.
- Moussoulis, E., Zacharias, I. & Nikolaidis, N. P. (2016). Combined Hydrological, Rainfall-Runoff, Hydraulic and Sediment Transport Modeling in Upper Acheloos River Catchment. *Desalination and Water Treatment*, 57(25), 11540–11549. Retrieved from <http://www.tandfonline.com/doi/abs/10.1080/19443994.2015.1102769?journalCode>



=tdwt20

- Mujiono, Indra, T. L., Harmantyo, D., Rukmana, I. P. & Nadia, Z. (2017). Simulation of Land Use Change and Effect on Potential Deforestation Using Markov Chain - Cellular Automata, in: *AIP Conference Proceedings*, (pp. 1–8). American Institute of Physics. Retrieved from <http://aip.scitation.org/doi/abs/10.1063/1.4991281>
- Mulianta, I. & Hariadi, Y. (2004). *Urban Area Development in Stochastic Cellular Automata*. University Library of Munich, Germany.
- Munguia, M. de O., Harmsworth, G., Young, R. & Dymond, J. (2009). The Use of an Agent-Based Model to Represent Māori Cultural Values. , (July), 2849–2855.
- Nagendra, H. (2001). Review Article - Using Remote Sensing to Assess Biodiversity. *International Journal of Remote Sensing*, 22(12), 2377–2400.
- Nassif, S. H. & Wilson, E. M. (1975). The Influence of Slope and Rain Intensity on Runoff and Infiltration. *Hydrological Sciences Bulletin*, 20(4), 539–553.
- National Aeronautics and Space Administration (NASA). (2015). Earth Atmosphere Model. Retrieved July 15, 2019, from <https://www.grc.nasa.gov/WWW/k-12/airplane/atmosmet.html>
- La Notte, A., D’Amato, D., Mäkinen, H., Paracchini, M. L., Liqueste, C., Egoh, B., Geneletti, D. & Crossman, N. D. (2017). Ecosystem Services Classification: A Systems Ecology Perspective of the Cascade Framework. *Ecological Indicators*, 74, 392–402.
- Nurliana, L. & Widodo, L. E. (2009). Potensi Imbuhan Dan Imbuhan Airtanah Cekungan Airtanah Bandung [Infiltration Potential and Groundwater Infiltration in Bandung Basin]. *JTM*, XVI(4), 261–268.
- Nurmiaty, Baja, S. & Arif, S. (2014). GIS-Based Modelling of Land Use Dynamics Using Cellular Automata and Markov Chain. *Journal of Environment and Earth Science*, 4(4), 61–66. Retrieved from <http://iiste.org/Journals/index.php/JEES/article/view/11192>
- Overmars, K. P. & Verburg, P. H. (2005). Analysis of Land Use Drivers at the Watershed and Household Level: Linking Two Paradigms at the Philippine Forest Fringe. *International Journal of Geographical Information Science*, 19(2), 125–152.
- Park, A. & Cameron, J. L. (2008). The Influence of Canopy Traits on Throughfall and Stemflow in Five Tropical Trees Growing in a Panamanian Plantation. *Forest Ecology and Management*, 255(5–6), 1915–1925.
- Parker, D. C., Manson, S. M., Janssen, M. A., Hoffmann, M. J. & Deadman, P. (2003). Multi-Agent Systems for the Simulation of Land-Use and Land-Cover Change: A Review. *Annals of the Association of American Geographers*, 93(2), 314–337.
- Parker, G. G. (1995). Structure and Microclimate of Forest Canopies, in: Lowman, M. D. and Nadkarni, N. M. (Eds.), *Forest Canopies*, (pp. 73–106). California: Academic Press, Inc.
- Peterson, G. D., Cumming, G. S. & Carpenter, S. R. (2003). Scenario Planning: A Tool for Conservation in an Uncertain World. *Conservation Biology*, 17(2), 358–366.
- Poff, N. L., Allan, J. D., Bain, M. B., Karr, J. R., Presteggaard, K. L., Richter, B. D., Sparks, R. E. & Stromberg, J. C. (1997). The Natural Flow Regime: A Paradigm for River Conservation and Restoration. *BioScience*, 47(11), 769–784.
- Pradiko, H., Arwin, Soewondo, P. & Suryadi, Y. (2015). The Change of Hydrological Regime in Upper Cikapundung Watershed, West Java Indonesia. *Procedia Engineering*, 125, 229–235. Retrieved from <http://dx.doi.org/10.1016/j.proeng.2015.11.033>
- Putri, D. R. (2016). Analisis Hidrologi Menggunakan Model SWAT Di Sub DAS Ciwidey Kabupaten Bandung [Hydrological Analysis Using SWAT Model in Sub DAS Ciwidey, Bandung].

- Qalbi, H. B., Faqih, A. & Hidayat, R. (2017). Future Rainfall Variability in Indonesia under Different ENSO and IOD Composites Based on Decadal Predictions of CMIP5 Datasets. *IOP Conference Series: Earth and Environmental Science*, 54.
- Rahmaniar, I. & Kamil, I. M. (2015). Remediation of Cu in the Contaminated Soil by Using Equisetum Debile (Horsetail). *Journal of Engineering and Technological Sciences*, 47(2), 126–136. Retrieved from <http://journals.itb.ac.id/index.php/jets/article/view/1438>
- Rajan, D. (2007). Understanding the Drivers Affecting Land Use Change in Ecuador: An Application of the Land Change Modeler Software. *University of Edinburgh, Edinburgh*. Retrieved from [http://crg.ee.uct.ac.za/~aka/aka\\_thesis.pdf](http://crg.ee.uct.ac.za/~aka/aka_thesis.pdf)
- Ramirez-Garcia, J., Almendros, P. & Quemada, M. (2012). Ground Cover and Leaf Area Index Relationship in a Grass, Legume and Crucifer Crop. *Plant, Soil and Environment*, 58(8), 385–390.
- Rani, M. S., Lange, E., Cameron, R. & Schroth, O. (2018). Future Development Scenarios for Adaptation to Climate Change in the Ci Kapundung Upper Water Catchment Area, Bandung Basin, Indonesia. *JoDLA – Journal of Digital Landscape Architecture*, 3, 23–33.
- Rani, M. S., Lange, E., Cameron, R. & Schroth, O. (2019). An Interactive Landscape Planning Process for Sustaining Flood Regulation in the Ci Kapundung Upper Water Catchment Area, Bandung Basin, Indonesia. *JoDLA – Journal of Digital Landscape Architecture*, 4, 33–41.
- Rani, M. S., Lange, E., Schroth, O. & Cameron, R. (2019). Mitigating Uncertainties in Land Change Modelling of Ci Kapundung Upper Water Catchment Area, Java Island, Indonesia. *under review*.
- Rani, M. S., Schroth, O., Cameron, R. & Lange, E. (2017). The Effect of Topographic Correction on SPOT6 Land Cover Classification in Water Catchment Areas in Bandung Basin, Indonesia
- Refsgaard, J. C. (1997). Parameterisation, Calibration and Validation of Distributed Hydrological Models. *Journal of Hydrology*, 198, 69–97.
- Refsgaard, J. C., Sonnenborg, T. O., Butts, M. B., Christensen, J. H., Christensen, S., Drews, M., Jensen, K. H., Jørgensen, F., Jørgensen, L. F., Larsen, M. A. D., Rasmussen, S. H., Seaby, L. P., Seifert, D. & Vilhelmsen, T. N. (2016). Climate Change Impacts on Groundwater Hydrology – Where Are the Main Uncertainties and Can They Be Reduced? *Hydrological Sciences Journal*, 61(13), 2312–2324. Retrieved from <http://www.tandfonline.com/doi/full/10.1080/02626667.2015.1131899>
- Refsgaard, J. C. & Storm, B. (1996). Construction, Calibration and Validation of Hydrological Models, in: M. B., A. and Refsgaard, J. C. (Eds.), *Distributed Hydrological Modelling*, (pp. 41–54). Netherlands: Kluwer Academic Publishers. Retrieved from <http://link.springer.com/10.1007/978-94-009-0257-2>
- Robinson, J. B. (1982). Energy Backcasting: A Proposed Method of Policy Analysis. *Energy Policy*, 10(4), 337–344.
- Robinson, J., Burch, S., Talwar, S., O’Shea, M. & Walsh, M. (2011). Envisioning Sustainability: Recent Progress in the Use of Participatory Backcasting Approaches for Sustainability Research. *Technological Forecasting and Social Change*, 78(5), 756–768. Retrieved from <http://dx.doi.org/10.1016/j.techfore.2010.12.006>
- Rosenberg, M., Syrbe, R.-U., Vowinckel, J. & Walz, U. (2014). Scenario Methodology for Modelling of Future Landscape Developments as Basis for Assessing Ecosystem Services. *Official Journal of the International Association for Landscape Ecology (IALE)*, 33(April), 1–20.
- Rossmann, L. A. & Huber, W. C. (2016). Storm Water Management Model Reference Manual Volume I – Hydrology (Revised). *U.S. Environmental Protection Agency*, (January). Retrieved from [www2.epa.gov/water-research](http://www2.epa.gov/water-research)

- Rotmans, J. (1998). Methods for IA: The Challenges and Opportunities Ahead. *Environmental Modeling and Assessment*, 3, 155–179.
- Roy, S. & Mistri, B. (2013). Estimation of Peak Flood Discharge for an Ungauged River: A Case Study of the Kunur River, West Bengal. *Geography Journal*, 2013.
- Rykiel, E. J. (1996). Testing Ecological Models: The Meaning of Validation. *Ecological Modelling*, 90, 229–244.
- Sahoo, G. B., Ray, C. & de Carlo, E. H. (2006). Calibration and Validation of a Physically Distributed Hydrological Model, MIKE SHE, to Predict Streamflow at High Frequency in a Flashy Mountainous Hawaii Stream. *Journal of Hydrology*, 327, 94–109.
- Sajikumar, N. & Remya, R. S. (2015). Impact of Land Cover and Land Use Change on Runoff Characteristics. *Journal of Environmental Management*, 161, 460–468. Retrieved from <http://linkinghub.elsevier.com/retrieve/pii/S0301479714006203>
- Seppelt, R., Lautenbach, S. & Volk, M. (2013). Identifying Trade-Offs between Ecosystem Services, Land Use, and Biodiversity: A Plea for Combining Scenario Analysis and Optimization on Different Spatial Scales. *Current Opinion in Environmental Sustainability*, 5(5), 458–463. Retrieved from <http://dx.doi.org/10.1016/j.cosust.2013.05.002>
- Setiawan, H. W. & Sabana, S. (2015). Priangan Dalam Kehidupan Franz Wilhelm Junghuhn [Priangan in the Life of Franz Wilhelm Junghuhn]. *Jurnal Kajian Sejarah & Pendidikan Sejarah*, 3(1), 31–56.
- Singh, R. & Kundu, D. K. (2010). Physico-Chemical and Hydraulic Characteristics of Soils of Major Sub-Groups of Eastern India. *Journal of the Indian Society of Soil Science*, 58(3), 267–278.
- Siregar, C. A. (2007). Biomass Estimation and Soil Carbon Conservation of Pinus Merkusii Jungh et de Vriese Plantation in Cianjen, West Java. *Jurnal Penelitian Hutan dan Konservasi Alam*, 4(3), 251–266.
- Siregar, C. A. & Heriyanto, N. M. (2010). Accumulation of Carbon Biomass Under Secondary Forest Scenario in Maribaya, Bogor, West Java. *Jurnal Penelitian Hutan dan Konservasi Alam*, 7(3), 215–226.
- Siregar, S. A. (1990). Bandung: The Architecture of a City in Development, Urban Analysis of a Regional Capital as a Contribution to the Present Debate on Indonesian Urbanity and Architectural Identity.
- Siswamartana, S., Utomo, W. H., Soedjoko, S. A., Priyono, C. N. S., Mulyana, N. M., Rusdiana, O. & Irfan Budi Pramono. (2002). *Hutan Pinus Dan Hasil Air* (C. N. S. Priyono, Ed.).
- Soenen, S. A., Peddle, D. R. & Coburn, C. A. (2005). SCS+C: A Modified Sun-Canopy-Sensor Topographic Correction in Forested Terrain. *IEEE Transactions on Geoscience and Remote Sensing*, 43(9), 2148–2159.
- Sohel, M. S. I., Mukul, S. A. & Burkhard, B. (2015). Landscape's Capacities to Supply Ecosystem Services in Bangladesh: A Mapping Assessment for Lawachara National Park. *Ecosystem Services*, 12, 128–135. Retrieved from <https://www.sciencedirect.com/science/article/abs/pii/S2212041614001545>
- Soil Survey Staff. (1999). *Soil Taxonomy: A Basic System of Soil Classification for Making and Interpreting Soil Surveys*.
- Sola, I., González-Audícana, M. & Álvarez-Mozos, J. (2016). Multi-Criteria Evaluation of Topographic Correction Methods. *Remote Sensing of Environment*, 184, 247–262. Retrieved from <http://dx.doi.org/10.1016/j.rse.2016.07.002>
- Stape, J. L., Binkley, D. & Ryan, M. G. (2004). Eucalyptus Production and the Supply, Use and Efficiency of Use of Water, Light and Nitrogen across a Geographic Gradient in Brazil. *Forest Ecology and Management*, 193(1–2), 17–31.

- van Steenis, C. G. G. J. & Schippers-Lammerste, A. F. (1965). *Concise Plant-Geography of Java*.
- Steinitz, C. (2012). *A Framework for Geodesign*. California: Esri Press.
- Stuecker, M. F., Timmermann, A., Jin, F.-F., Chikamoto, Y., Zhang, W., Wittenberg, A. T., Widiasih, E. & Zhao, S. (2017). Revisiting ENSO/Indian Ocean Dipole Phase Relationships. *Geophysical Research Letters*, 44(5), 2481–2492.
- Stürck, J., Poortinga, A. & Verburg, P. H. (2014). Mapping Ecosystem Services: The Supply and Demand of Flood Regulation Services in Europe. *Ecological Indicators*, 38, 198–211. Retrieved from <http://linkinghub.elsevier.com/retrieve/pii/S1470160X13004287>
- Subarna, D. (2015). Strategi Konservasi Pengelolaan Daerah Aliran Sungai Berbasis Variabilitas Iklim Di DAS Cisangkuy Citarum Hulu [Conservation Strategy of River Area Management Based on Climatic Variability in DAS Upstream of Cisangkuy Citarum].
- Susilo, B. (2011). Modeling Spatial Integration Probabilistic Markov Chain and Cellular Automata for the Study of Land Use Changes Regional Scale in DIY Yogyakarta. *Jurnal Geografi GEA*, 11(2), 163–178.
- Swank, W. T. & Douglass, J. E. (1974). Streamflow Greatly Reduced by Converting Deciduous Hardwood Stands to Pine. *Science*, 185(4154), 857–859.
- Tanton, T. W. (1979). Some Factors Limiting Yields of Tea (*Camellia Sinesis*). *Expl Agric.*, 15(2), 187–191.
- Tárník, A. & Igaz, D. (2017). Validation of Hydrus 1D Model in Selected Catchment of Slovakia. *Acta Horticulturae et Regiotechnicae*, 20(1), 24–27. Retrieved from <http://www.degruyter.com/view/j/ahr.2017.20.issue-1/ahr-2017-0006/ahr-2017-0006.xml>
- Teillet, P. M., Guindon, B. & Goodenough, D. G. (1982). On the Slope-Aspect Correction of Multispectral Scanner Data. *Canadian Journal of Remote Sensing*, 8(2), 84–106.
- Thompson, J. R., Sørensen, H. R., Gavin, H. & Refsgaard, A. (2004). Application of the Coupled MIKE SHE / MIKE 11 Modelling System to a Lowland Wet Grassland in Southeast England. *Journal of Hydrology*, 293, 151–179.
- Tjasyono H. K., B. & Gernowo, R. (2008). Curah Hujan Ekstrim Di Area Monsun Basin Bandung [Extreme Precipitation Rates in the Monsoon Region of Bandung Basin]. *Jurnal Meteorologi dan Geofisika*, 9(2), 1–7.
- Tjasyono H. K., B., Gernowo, R., Woro B. H., S. & Ina, J. (2008). The Character of Rainfall in the Indonesian Monsoon. *International Symposium on Equatorial Monsoon System*.
- Tommi. (2011). Pengaruh Perubahan Penggunaan Lahan Terhadap Karakteristik Hidrologi DAS Citarum Hulu.
- Toure, S. I., Stow, D. A., Shih, H., Weeks, J. & Lopez-Carr, D. (2018). Land Cover and Land Use Change Analysis Using Multi-Spatial Resolution Data and Object-Based Image Analysis. *Remote Sensing of Environment*, 210, 259–268. Retrieved from <https://doi.org/10.1016/j.rse.2018.03.023>
- Turner, M. G. (1989). Landscape Ecology: The Effect of Pattern on Process. *Annual Review of Ecology and Systematics*, 20, 171–197.
- Turner, M. G., Donato, D. C. & Romme, W. H. (2013). Consequences of Spatial Heterogeneity for Ecosystem Services in Changing Forest Landscapes: Priorities for Future Research. *Landscape Ecol*, 28(6), 1081–1097. Retrieved from <http://link.springer.com/10.1007/s10980-012-9741-4>
- Turner, M. G., Gardner, R. H. & O’Niell, R. V. (2001). *Landscape Ecology in Theory and Practice Pattern and Process*. New York: Springer-Verlag.

- USGS. (2018). Landsat Surface Reflectance Data Products. Retrieved December 14, 2018, from <https://landsat.usgs.gov/landsat-surface-reflectance-data-products>
- Vanonckelen, S., Lhermitte, S. & Van Rompaey, A. (2013). The Effect of Atmospheric and Topographic Correction Methods on Land Cover Classification Accuracy. *International Journal of Applied Earth Observation and Geoinformation*, 24(1), 9–21. Retrieved from <http://dx.doi.org/10.1016/j.jag.2013.02.003>
- Venkatraman, K. & Ashwath, N. (2016). Canopy Rainfall Intercepted by Nineteen Tree Species Grown on a Phytocapped Landfill. *International Journal of Waste Resources*, 6(1). Retrieved from <https://www.omicsonline.com/open-access/canopy-rainfall-intercepted-by-nineteen-tree-species-grown-on-aphytocapped-landfill-2252-5211-1000202.php?aid=69954>
- Verburg, P. H., Schot, P. P., Dijst, M. J. & Veldkamp, A. (2004). Land Use Change Modelling: Current Practice and Research Priorities. *GeoJournal*, 61(4), 309–324.
- Verburg, P. H., Tabeau, A. & Hatna, E. (2013). Assessing Spatial Uncertainties of Land Allocation Using a Scenario Approach and Sensitivity Analysis: A Study for Land Use in Europe. *Journal of Environmental Management*, 127, S132–S144. Retrieved from <http://dx.doi.org/10.1016/j.jenvman.2012.08.038>
- Verstegen, J. A., Jonker, J. G. G., Karssenbergh, D., van der Hilst, F., de Jong, S. M. & Faaij, A. P. C. (2017). How a Pareto Frontier Complements Scenario Projections in Land Use Change Impact Assessment. *Environmental Modelling & Software*, 97, 287–302.
- van Vliet, J., Bregt, A. K., Brown, D. G., van Delden, H., Heckbert, S. & Verburg, P. H. (2016). A Review of Current Calibration and Validation Practices in Land-Change Modeling. *Environmental Modelling and Software*, 82, 174–182. Retrieved from <http://dx.doi.org/10.1016/j.envsoft.2016.04.017>
- van der Voorn, T., Pahl-Wostl, C. & Quist, J. (2012). Combining Backcasting and Adaptive Management for Climate Adaptation in Coastal Regions: A Methodology and a South African Case Study. *Futures*, 44(4), 346–364. Retrieved from <http://dx.doi.org/10.1016/j.futures.2011.11.003>
- Wahdani, D. K. (2011). Perkiraan Debit Sungai Dan Sedimentasi Dengan Model MWSWAT Di Sub-DAS Citarum Hulu, Provinsi Jawa Barat [River Discharge and Sedimentation Estimation Using SWAT Model].
- Waldick, R., Bizikova, L., Bolte, J., MacDonald, D., Zaytseva, A., Lindsay, K., White, D., Gasser, P. Y., Mitchell, S., Vache, K., Hamalainen, S. & Swanson, D. (2015). *Mainstreaming Climate Change: Integrated Landscape Assessment, Decision-Support Process & Tool Kit*.
- Walker, D. J. & Kenkel, N. C. (2000). The Adaptive Geometry of Boreal Conifers. *Community Ecology*, 1(1), 13–23.
- Walz, U. (2011). Landscape Structure, Landscape Metrics and Biodiversity. *Living Rev. Landscape Res.*, 5(3).
- Wang, F. (1994). The Use of Artificial Neural Networks in a Geographical Information System for Agricultural Land-Suitability Assessment. *Environment and Planning A: Economy and Space*, 26, 265–284.
- Wang, S., Feng, J. & Liu, G. (2013). Application of Seasonal Time Series Model in the Precipitation Forecast. *Mathematical and Computer Modelling*, 58(3–4), 677–683. Retrieved from <http://dx.doi.org/10.1016/j.mcm.2011.10.034>
- Wassahua, Z. (2010). The Use of Markov Cellular Automata Technique for Predicting Forest Cover Change in Rokan Hulu, Riau Province, Indonesia.
- Wen, W. (2008). Wetland Change Prediction Using Markov Cellular Automata Model in Lore Lindu National Park Central Sulawesi Province, Indonesia.

- Wen, Y., Chen, F., Liu, S., Liang, H., Yuan, C. & Zhu, H. (2009). Relationship between Species Diversity and Biomass of Eucalyptus Plantation in Guangxi, South China. *Frontiers of Forestry in China*, 4(2), 146–152.
- White, R. & Engelen, G. (2000). High-Resolution Integrated Modelling of the Spatial Dynamics of Urban and Regional Systems. *Computers, Environment and Urban Systems*, 24, 383–400.
- Whitten, T., Afiff, S. & Soeriaatmadja, R. E. (1996). *The Ecology of Java and Bali*. Hongkong: Periplus Editions.
- Wiryanan, B. (2017). *Hydrodynamic Modelling for Flood Reduction and Climate Resilient Infrastructure Development Pathways in Jakarta*. Jakarta.
- Woodcock, C. E. & Strahler, A. H. (1987). The Factor of Scale in Remote Sensing. *Remote Sensing of Environment*, 21, 311–332.
- Wu, H., Bolte, J. P., Hulse, D. & Johnson, B. R. (2015). A Scenario-Based Approach to Integrating Flow-Ecology Research with Watershed Development Planning. *Landscape and Urban Planning*, 144, 74–89. Retrieved from <http://linkinghub.elsevier.com/retrieve/pii/S016920461500167X>
- Xia, Y., Liu, D., Liu, Y., He, J. & Hong, X. (2014). Alternative Zoning Scenarios for Regional Sustainable Land Use Controls in China: A Knowledge-Based Multiobjective Optimisation Model. *International Journal of Environmental Research and Public Health*, 11(9), 8839–8866.
- Xiao, Q., McPherson, E. G., Ustin, S. L. & Grismer, M. E. (2000). A New Approach to Modeling Tree Rainfall Interception. *Journal of Geophysical Research*, 105(D23), 29173–29188.
- Xiaoke, Z., Chao, M., Haifeng, H. & Fangfang, L. (2009). Radiometric Correction Based on Multi-Temporal SPOT Satellite Images. *IEEE*.
- Yulianto, F., Prasasti, I., Pasaribu, J. M., Fitriana, H. L., Zylshal, Haryani, N. S. & Sofan, P. (2016). The Dynamics of Land Use / Land Cover Change Modeling and Their Implication for the Flood Damage Assessment in the Tondano Watershed, North Sulawesi, Indonesia. *Modeling Earth Systems and Environment*, 2(47). Retrieved from <http://link.springer.com/10.1007/s40808-016-0100-3>
- Zabrett, K. & Sraj, M. (2015). Rainfall Interception by Deciduous and Coniferous Trees in an Urban Area. *Geophysical Research Abstracts*, 17.
- Zhang, J. & Goodchild, M. (2002). *Uncertainty in Geographical Information* (P. Fisher and J. Raper, Eds.). London: Taylor & Francis.
- Zhang, Z., Wang, S., Sun, G., McNulty, S. G., Zhang, H., Li, J., Zhang, M., Klaghofer, E. & Strauss, P. (2008). Evaluation of the MIKE SHE Model for Application in the Loess Plateau, China. *Journal Of The American Water Resources Association*, 44(5), 1108–1120.
- Zheng, J., Fan, J., Zhang, F., Yan, S. & Xiang, Y. (2018). Rainfall Partitioning into Throughfall, Stemflow and Interception Loss by Maize Canopy on the Semi-Arid Loess Plateau of China. *Agricultural Water Management*, 195, 25–36. Retrieved from <http://dx.doi.org/10.1016/j.agwat.2017.09.013>
- Zhu, X. (2016). *GIS for Environmental Applications*. New York: Routledge.

## Appendix

### A. Calibrated parameters for MIKE SHE 2 models

The calibrated MIKE SHE parameters for the Ci Kapundung and Ci Sangkuy models are presented in Table A-1 and Table A-2, respectively. Only parameters that were altered for the final simulations are shown in the following tables. Other parameters stated in Subchapter 4.4 were still used in the calibrated models.

Table A-1 Calibrated parameters for Ci Kapundung model

Parameter	Calibrated value
<b>Climate</b> (Precipitation lapse rate)	5%
<b>Vegetation</b>	
(Evapotranspiration)	Canopy interception 1 mm
(Bareland-cultivated land properties)	LAI ini/ LAI mid/ LAI end 800/ 800/ 0 mm Kc ini/ Kc mid/ Kc end 0/ 1.15/ 0.65
<b>Overland flow</b> (Detention storage)	Water bodies Other areas 2-3 m 0 m
<b>Unsaturated zone</b>	
(Soil A)	Residual moisture content (Qr) Saturated moisture content (Qs) Alpha n Saturated hydraulic conductivity 0.0737 0.3091 0.0234 1.1540 8.33e-8 m/s
(Soil B)	Residual moisture content (Qr) Saturated moisture content (Qs) Alpha n Saturated hydraulic conductivity 0.0600 0.4043 0.0050 1.6839 3.02e-6 m/s
(Soil C)	Residual moisture content (Qr) Saturated moisture content (Qs) Alpha n Saturated hydraulic conductivity 0.0710 0.7090 0.0338 1.3108 1.96e-05 m/s
(Soil D)	Residual moisture content (Qr) Saturated moisture content (Qs) Alpha n Saturated hydraulic conductivity 0.0699 0.4343 0.0062 1.6228 2.47e-06

Table A-2 Calibrated parameters for Ci Sangkuy model

Parameter		Calibrated value
<b>Climate</b> (Precipitation lapse rate)		100%
<b>Vegetation</b> (Evapotranspiration)	Canopy interception	1 mm
(Bareland-cultivated land properties)	LAI ini/ LAI mid/ LAI end	0/ 1/ 2.09
	Root ini/ Root mid/ Root end	800/ 800/ 0 mm
	Kc ini/ Kc mid/ Kc end	0/ 1.15/ 0.65
<b>Overland flow</b> (Detention storage)	Water bodies	2-3 m
	Other areas	0 m
<b>Unsaturated zone</b>		
(Soil E)	Residual moisture content (Qr)	0.0776
	Saturated moisture content (Qs)	0.3138
	Alpha	0.0221
	n	1.1557
	Saturated hydraulic conductivity	8.80e-8 m/s
(Soil F)	Residual moisture content (Qr)	0.0790
	Saturated moisture content (Qs)	0.3531
	Alpha	0.0212
	n	1.1800
	Saturated hydraulic conductivity	2.22e-7 m/s
(Soil G)	Residual moisture content (Qr)	0.0130
	Saturated moisture content (Qs)	0.7067
	Alpha	0.0229
	n	1.3438
	Saturated hydraulic conductivity	2.97e-5 m/s
(Soil H)	Residual moisture content (Qr)	0.0801
	Saturated moisture content (Qs)	0.4648
	Alpha	0.0101
	n	1.5015
	Saturated hydraulic conductivity	2.61e-6 m/s



## B. Land cover maps for the Ci Kapundung and Ci Sangkuy watersheds (first iteration)

Appendix B presents the result from the accuracy assessment for the first iteration of land cover map development for the first case study area and the southern part of the second case study area. The complete description of this process was presented as a conference paper (Rani et al., 2017). In the first iterative land cover map development process, there are four land cover classes in the Ci Kapundung watershed (e.g. developed areas, bare land and cultivated land, conifers, and mixed vegetation). On the other hand, there are five land cover classes in the Ci Sangkuy watershed (e.g. developed areas, bare land and cultivated land, plantations, conifers, and mixed vegetation).

The classification accuracy for the uncorrected and corrected maps of Ci Kapundung upper water catchment area (2015) can be seen in Table B-1 and Table B-2, respectively. In this assessment, the uncorrected map refers to the land cover map developed from satellite imagery where no atmospheric and topographic correction procedures were applied. On the other hand, the corrected map is the land cover map developed from satellite imagery where the topographic correction (i.e. SCS+S) was applied into.

Table B-1 Confusion matrix for the 2015 uncorrected land cover map of the Ci Kapundung watershed (first iteration)

Classified image	Reference dataset				Total	User Acc. (%)
	Dev.	Bare land cultivated land	Conifers	Mixed vegetation		
Developed areas	49	11	0	1	61	80.33
Bare land and cult land	15	156	2	12	185	84.32
Conifers	0	15	38	29	82	46.34
Mixed vegetation	0	15	29	129	173	74.57
Total	64	197	69	171	501	0.00
Producer Accuracy (%)	76.56	79.19	55.07	75.44	0.00	77.00
<b>Overall Accuracy: 74.25%</b>						
Kappa statistic: 0.63						

The uncorrected and corrected land cover maps for the first case study area have overall accuracies of 74.25% and 77% respectively. 'Conifers' has the lowest user and producer accuracy in both maps. 'Developed areas' and 'bare land and cultivated land' are the two classes that have higher percentages of user and producer accuracy compared to other land cover classes. This result implies the difficulty to differ the two forest types (e.g. conifers and mixed vegetation) on the satellite images.

The confusion matrices showing the accuracy for the uncorrected and corrected land cover maps of the South Ci Sangkuy watershed are given in Table B-3 and Table B-4, respectively. The overall accuracies for the two maps are 80.44% and 87.58%. 'Mixed vegetation' has the least

percentages of user and producer accuracy (i.e. 25%-37.50%), indicating that the land cover type was often mistakenly classified as the other land cover types.

Table B-2 Confusion matrix for the 2015 corrected land cover map of the Ci Kapundung watershed (first iteration)

Classified image	Reference dataset					User Acc. (%)
	Dev.	Bare land cultivated land	Conifers	Mixed vegetation	Total	
Developed areas	46	12	0	0	58	79.31
Bare land and cult land	9	162	7	7	185	87.57
Conifers	0	12	48	28	88	54.55
Mixed vegetation	1	20	19	129	169	76.33
Total	56	206	74	164	500	0.00
Producer Accuracy (%)	82.14	78.64	64.86	78.66	0.00	77.00
<b>Overall Accuracy: 77%</b>						
Kappa statistic: 0.67						

Table B-3 Confusion matrix for the 2015 uncorrected land cover map of the South Ci Sangkuy watershed (first iteration)

Classified image	Reference dataset					User Acc. (%)	
	Dev.	Plantations	Bare land cultivated land	Conifers	Mixed vegetation		Total
Developed areas	22	0	0	11	0	33	66.67
Plantations	1	74	2	19	2	98	75.51
Bare land and cult land	0	2	152	24	5	183	83.06
Conifers	6	9	10	152	0	177	85.88
Mixed vegetation	0	0	6	1	3	10	30.00
Total	29	85	170	207	10	501	0.00
Producer Accuracy (%)	75.86	87.06	89.41	73.43	30.00	0.00	80.44
<b>Overall Accuracy: 80.44</b>							
Kappa statistic: 0.72							

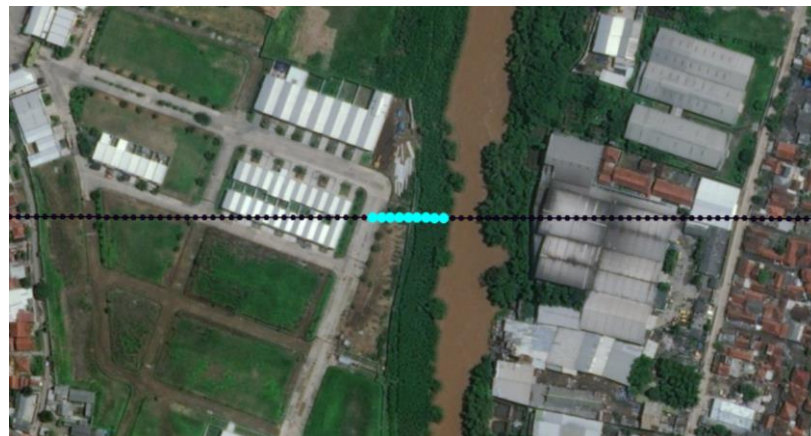
Table B-4 Confusion matrix for the 2015 corrected land cover map of the Ci South Sangkuy watershed (first iteration)

Classified image	Reference dataset					User Acc. (%)	
	Dev.	Plantations	Bare land cultivated land	Conifers	Mixed vegetation		Total
Developed areas	24	1	1	4	0	30	80.00
Plantations	0	92	6	14	1	113	81.42
Bare land and cult land	0	2	171	2	4	179	95.53
Conifers	4	11	3	147	0	165	89.09
Mixed vegetation	0	0	9	0	3	12	25.00
Total	28	106	190	167	8	499	0.00
Producer Accuracy (%)	85.71	86.79	90.00	88.02	37.50	0.00	87.58
<b>Overall Accuracy: 87.58</b>							
Kappa statistic: 0.82							

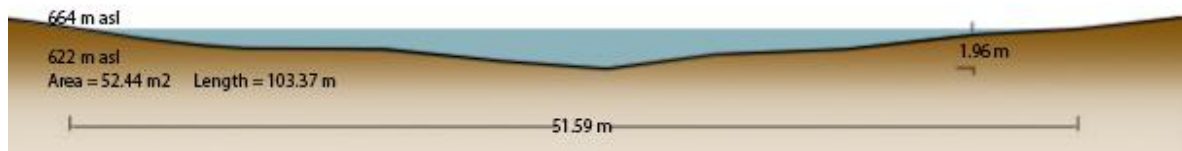
### C. The flood discharge ( $Q_{bkf}$ ) of Ci Tarum River

The flood discharge of Ci Tarum River was estimated as part of the assessment to determine the discharges of Ci Kapundung and Ci Sangkuy Rivers that have high possibility to affect the occurrence of floods in Bandung Basin. At the beginning of the analysis, two sections were drawn across the Ci Tarum River (Figure C-1). Then, the hydraulic radius ( $R$ ) was calculated based on the cross-sectional area ( $A$ ) and wetted perimeter ( $wp$ ). The discharge at bankfull was estimated by multiplying the bankfull width with the water velocity and the bankfull depth. The estimations of flood discharge at the two sections are described as follows.

#### (1) Section A-A' of Ci Tarum River



(a)



(b)

Figure C-1 (a-b). Section A-A' of Ci Tarum River (662.039 – 664.00 m asl); Sources for background image: ESRI, HERE, DeLorme, Intermap, increment P Corp., GEBCO, USGS, FAO, NPS, NRCAN, GeoBase, IGN, Kadaster NL, Ordnance Survey, Esri Japan, METI, Esri China (Hong Kong), swisstopo, MapmyIndia, OpenStreetMap, GIS User Community

Cross-sectional area ( $A$ ) = 54.45 m<sup>2</sup>

Wetted perimeter ( $wp$ ) = 103.37 m

Hydraulic radius ( $R$ ) =  $A/wp$ . Thus,  $R = 0.527$  m or 1.729 ft

The velocity ( $u_{bkf}$ ) can be estimated using the information on the hydraulic radius ( $R$ ) and the slope of the water surface ( $S$ ), and the Manning resistance coefficient ( $n$ ) as:

$$u_{bkf} = \frac{1.49 R^{2/3} S^{1/2}}{n}$$

$$u_{bkf} = \frac{1.49 \cdot 1.729^{2/3} \cdot 0.02^{1/2}}{0.05} = 6.08 \text{ ft/sec}$$

where bankfull width ( $w_{bkf}$ ) is 51.59 m or 169.25853 ft, and bankfull depth ( $d_{bkf}$ ) is 1.96 m or 6.430446 ft. Therefore, the discharge at bankfull or when the channel is at the full capacity can be calculated as:

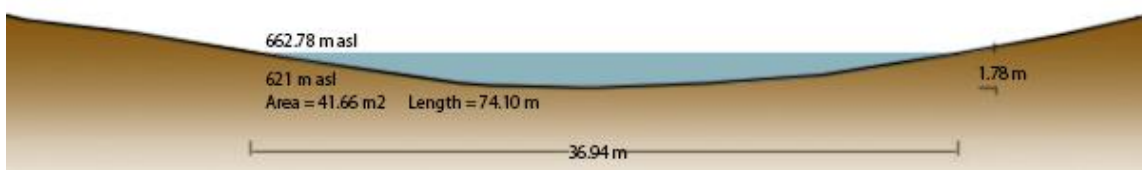
$$Q_{bkf} = w_{bkf} \times u_{bkf} \times d_{bkf}$$

$$Q_{bkf} = 169.25853 \text{ ft} \times 6.08 \frac{\text{ft}}{\text{sec}} \times 6.430446 \text{ ft} = 6,617.52 \text{ ft}^3/\text{sec} \text{ or } 187.387298659 \text{ m}^3/\text{sec}$$

(2) Section B-B' of Ci Tarum River



(a)



(b)

Figure C-2 (a-b). Section B-B' of Ci Tarum River (661.00 – 662.7827 m asl); Sources for background image: ESRI, HERE, DeLorme, Intermap, increment P Corp., GEBCO, USGS, FAO, NPS, NRCAN, GeoBase, IGN, Kadaster NL, Ordnance Survey, Esri Japan, METI, Esri China (Hong Kong), swisstopo, MapmyIndia, OpenStreetMap, GIS User Community

**Section B-B'**

Cross-sectional area (A) = 41.6624 m<sup>2</sup>

Wetted perimeter (wp) = 74.1045 m

Hydraulic radius (R) = A/wp. Thus, R = 0.562 m or 1.84 ft

The velocity ( $u_{bkf}$ ) can be estimated using the information on the hydraulic radius (R) and the slope of the water surface (S), and the Manning resistance coefficient (n) as:

$$u_{bkf} = \frac{1.49 R^{2/3} S^{1/2}}{n}$$

$$u_{bkf} = \frac{1.49 \cdot 1.84^{2/3} \cdot 0.02^{1/2}}{0.05} = 6.34 \text{ ft/sec}$$

where bankfull width ( $w_{bkf}$ ) is 51.59 m or 169.25853 ft, and bankfull depth ( $d_{bkf}$ ) is 1.96 m or 6.430446 ft. Therefore, the discharge at bankfull or when the channel is at the full capacity can be calculated as:

$$Q_{bkf} = w_{bkf} \times u_{bkf} \times d_{bkf}$$

$$Q_{bkf} = 169.25853 \text{ ft} \times 6.34 \frac{\text{ft}}{\text{sec}} \times 6.430446 \text{ ft} = 6,900.5 \text{ ft}^3/\text{sec} \text{ or } 195.4 \text{ m}^3/\text{sec}$$

## D. Baseflow of Ci Kapundung and Ci Sangkuy Rivers

Baseflow of Ci Kapundung and Ci Sangkuy Rivers (2008-2015) were calculated using the river discharge data as part of the estimation of discharges from the MIKE SHE modelling. Baseflow was defined from a flow duration curve following Dasanto *et al.* (2014). It is assumed that baseflow has a probability of exceeding the flow by 90%. The results from the assessment are presented as follows.

### (1) Baseflow of Ci Kapundung River

The streamflow data (2008-2015) was ranked by the magnitude and the percentages that each discharge to exceed a certain level were calculated and mapped (Table D-1 and Figure D-1). The result shows that the baseflow of Ci Kapundung River is 1.71 m<sup>3</sup>/s.

Table D-1 Samples of the Ci Kapundung streamflow data and the rank within the period of 2008-2015; Source for the streamflow data: PSDA (Water Resource Management in West Java province).

Date	Streamflow (m <sup>3</sup> /s)	Rank	Percent Exceeded
14/12/2012	20.6	1	0.034211427
19/12/2012	16.5	2	0.068422853
10/11/2011	15.6	3	0.10263428
16/01/2012	14.7	4	0.136845706
10/12/2012	14.7	5	0.171057133
20/12/2012	14.7	6	0.20526856
7/12/2015	14.5	7	0.239479986
9/12/2015	14.3	8	0.273691413
28/12/2013	13.7	9	0.30790284
23/12/2014	13.5	10	0.342114266
...	...	...	...
17/11/2010	1.71	2629	89.94184057
21/11/2010	1.71	2630	89.976052
22/11/2010	1.71	2631	90.01026343
27/11/2010	1.71	2632	90.04447485
29/11/2010	1.71	2633	90.07868628
...	...	...	...
5/12/2010	0.98	2913	99.65788573
7/12/2010	0.98	2914	99.69209716
8/12/2010	0.98	2915	99.72630859
12/12/2010	0.98	2916	99.76052001
21/12/2010	0.98	2917	99.79473144
22/12/2010	0.98	2918	99.82894287
23/12/2010	0.98	2919	99.86315429
27/12/2010	0.98	2920	99.89736572
7/11/2009	0.8	2921	99.93157715
8/11/2009	0.68	2922	99.96578857
MAX VALUE	20.6	2922	100
MIN VALUE	0.68		0
COUNT	2922		

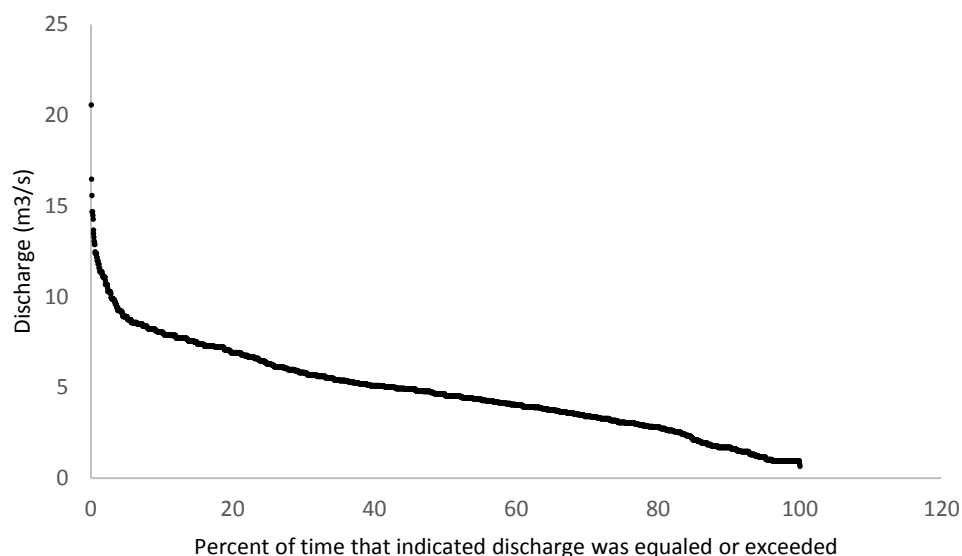


Figure D-1 Flow duration curve for the Ci Kapundung River (2008-2015)

(2) Baseflow of Ci Sangkuy River

The baseflow of Ci Sangkuy River (2008-2015) was also estimated using a similar method when calculating the baseflow for the Ci Kapundung River. The samples of streamflow data and the flow duration curve are given in Figure D-2 and Table D-2, respectively. From the estimation, it can be concluded that the baseflow for the Ci Sangkuy River (2008-2015) is 2 m<sup>3</sup>/s.

Table D-2 Samples of the Ci Sangkuy streamflow data and the rank within the period of 2008-2015; Source for the streamflow data: PSDA (Water Resource Management in West Java province).

Date	Streamflow (m <sup>3</sup> /s)	Rank	Percent Exceeded
18/02/2010	96.6	1	0.034211427
20/03/2010	96	2	0.068422853
19/02/2010	91.5	3	0.10263428
05/12/2010	90.4	4	0.136845706
16/03/2008	87.7	5	0.171057133
15/02/2010	82.4	6	0.20526856
08/12/2010	82.4	7	0.239479986
09/12/2010	80.3	8	0.273691413
03/12/2010	79.8	9	0.30790284
16/02/2010	75.3	10	0.342114266
...	...	...	...
11/09/2013	2	2629	89.94184057
20/09/2013	2	2630	89.976052
29/09/2013	2	2631	90.01026343
13/10/2013	2	2632	90.04447485
17/10/2013	2	2633	90.07868628
...	...	...	...
01/11/2014	1.01	2913	99.65788573
03/11/2013	1	2914	99.69209716

Date	Streamflow (m <sup>3</sup> /s)	Rank	Percent Exceeded
20/08/2013	0.9	2915	99.72630859
26/09/2013	0.9	2916	99.76052001
22/08/2013	0.88	2917	99.79473144
24/08/2013	0.88	2918	99.82894287
27/09/2013	0.88	2919	99.86315429
05/07/2011	0.84	2920	99.89736572
07/07/2011	0.84	2921	99.93157715
23/10/2011	0.84	2922	99.96578857
MAX VALUE	96.6	2922	100
MIN VALUE	0.84		0
COUNT	2922		

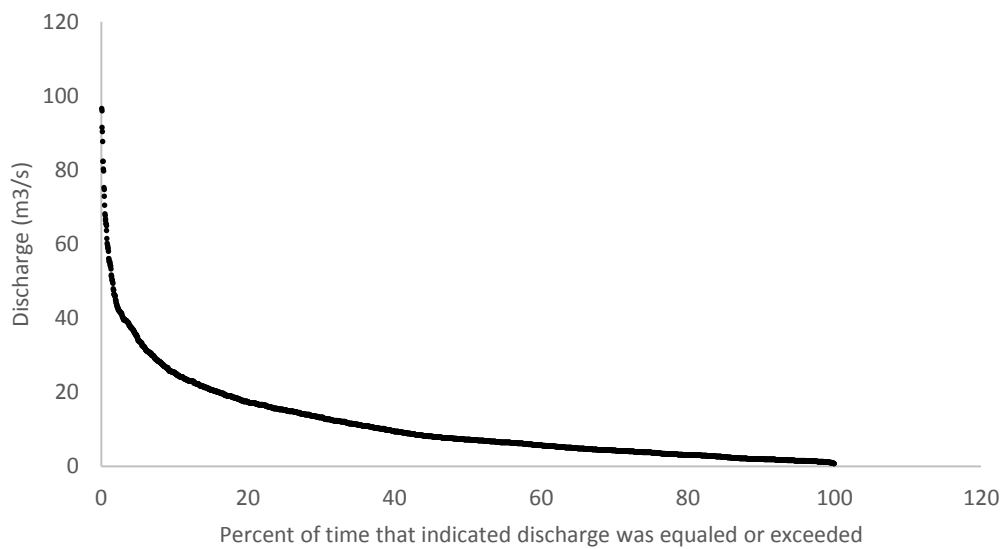


Figure D-2 Flow duration curve for the Ci Sangkuy River (2008-2015)



## E. Vegetation analysis

The initial vegetation analysis was conducted by simulating the water balance from sixteen combinations of four land cover and four soil types in the first case study area. The results from the analysis can be seen in Table E-1. The calculation was conducted from the MIKE SHE 2 model that used the Richards equation for modelling the unsaturated flow and the calibrated parameters in Table A-1, without applying the precipitation correction rate. The OL boundary inflow is 0 for all scenarios. Refer to Subchapter 4.4 for the categorisations of soil types.

Table E-1 Initial results from water balance analysis for the Ci Kapundung upper water catchment area (mm) (2008-2015)

Scenarios	Precipitation	Canopy interception	Evapotranspiration	OL storage change	OL boundary outflow	Sub-surface storage change	Total error
BL-Soil A	-19,168.10	0.0322	12,558.80	961.35	2,809.71	72.27	-2,765.93
BL-Soil B	-19,168.10	0.0258	12,668.70	1,072.79	8,296.30	57.10	2,926.85
BL-Soil C	-19,168.10	0.0550	12,725.80	1,016.51	13,015.20	84.34	7,673.78
BL-Soil D	-19,168.10	0.0337	12,535.50	977.90	2,898.43	62.56	-2,693.64
Con-Soil A	-19,168.10	0.2248	13,416.60	753.13	733.12	66.05	-4,198.98
Con-Soil B	-19,168.10	0.2267	13,485.90	794.29	1,294.08	50.04	-3,543.53
Con-Soil C	-19,168.10	1.2914	13,606.10	878.60	2,188.85	80.10	-2,413.16
Con-Soil D	-19,168.10	1.2327	13,611.90	949.01	2,525.33	58.93	-2,021.76
Mix-Soil A	-19,168.10	-0.0003	13,542.50	927.62	2,449.63	69.84	-2,178.43
Mix-Soil B	-19,168.10	0.1401	13,511.60	1,044.14	3,877.48	54.08	-680.62
Mix-Soil C	-19,168.10	0.1364	13,771.60	1,044.97	5,314.45	83.30	1,046.38
Mix-Soil D	-19,168.10	0.0029	13,524.40	1,040.02	3,022.77	61.50	-1,519.44
BC-Soil A	-19,168.10	0.0001	12,759.00	767.16	705.24	59.40	-4,877.13
BC-Soil B	-19,168.10	0.0188	12,802.90	769.64	666.13	40.95	-4,888.50
BC-Soil C	-19,168.10	0.0002	12,909.30	789.78	1,466.64	79.34	-3,914.08
BC-Soil D	-19,168.10	0.0003	12,739.10	748.26	600.03	45.00	-5,035.77

Notes: BL (Broad-leaved vegetation), Con (Conifers), Mix (Mixed vegetation), BC (Bareland and cultivated land)

A detailed examination was done to assess the fluctuation of overland outflow on the Ci Kapundung upper catchment covered by one vegetation type (broad-leaved plants). The outcome (Figure E-1) shows that Scenario BL-C (broad-leaved vegetation on Soil C) generates the highest volume of runoff despite a high percentage of sand (72.05%) compared with the other three scenarios. Figure E-1 also illustrates how dry the soil was at the beginning of the simulation, which is indicated by the low outflow values on the graph.

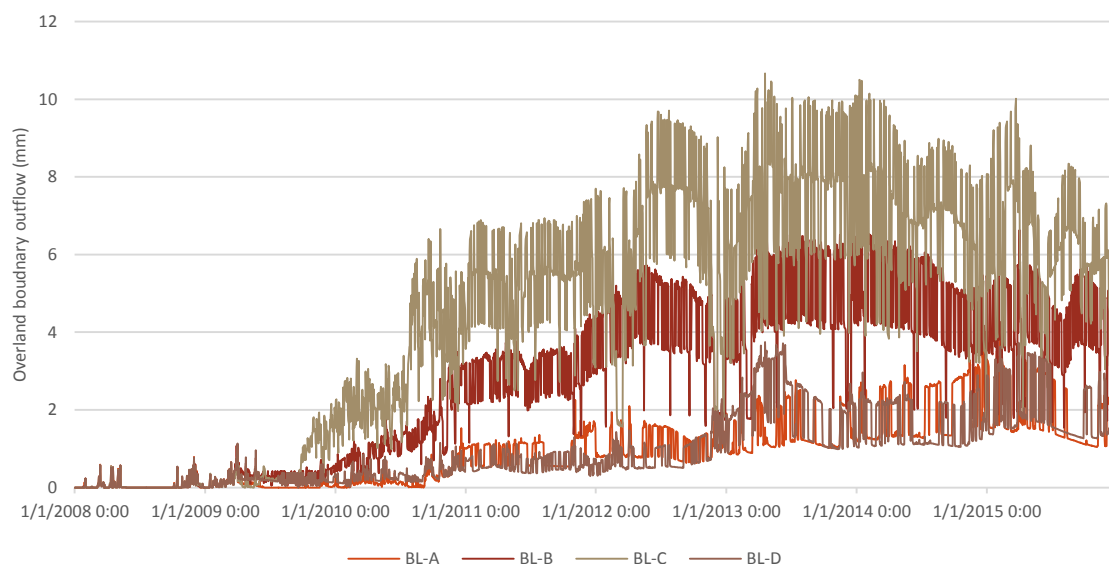


Figure E-1 Simulated overland outflow from Ci Kapundung catchment covered by broad-leaved vegetation with soil A, B, C, and D

The final results from water balance analysis for the hypothetical catchment are presented in Table E-2.

Table E-2 Final results from the water balance analysis for the Ci Kapundung upper water catchment area (mm) (2008-2015)

Scenarios	Precipitation	Canopy interception	Evapotranspiration	OL storage change	OL boundary outflow	Sub-surface storage change	Total error
L-S1-BL-A	-14,605.00	1.00	7,886.92	0.74	6,617.21	118.58	19.05
L-S1-BL-B	-14,605.00	1.00	7,886.92	0.74	6,619.85	115.88	19.00
L-S1-BL-C	-14,605.00	1.00	7,886.92	0.74	6,586.16	149.14	18.57
L-S1-BL-D	-14,605.00	1.00	7,886.92	0.74	6,618.17	117.49	18.92
L-S1-C-A	-14,605.00	11.98	8,763.00	0.33	5,730.86	118.57	19.56
L-S1-C-B	-14,605.00	11.98	8,763.00	0.33	5,733.35	115.87	19.35
L-S1-C-C	-14,605.00	11.98	8,763.00	0.33	5,699.80	149.14	19.06
L-S1-C-D	-14,605.00	11.98	8,763.00	0.33	5,731.68	117.48	19.28
L-S1-M-A	-14,605.00	3.20	8,763.00	0.76	5,738.50	118.57	19.13
L-S1-M-B	-14,605.00	3.20	8,763.00	0.76	5,741.17	115.88	19.11
L-S1-M-C	-14,605.00	3.20	8,763.00	0.76	5,707.39	149.14	18.58
L-S1-M-D	-14,605.00	3.20	8,763.00	0.76	5,739.63	117.48	19.18
L-S1-BC-A	-14,605.00	0.00	5,605.19	0.20	8,896.01	118.56	14.97
L-S1-BC-B	-14,605.00	0.00	5,646.97	0.20	8,857.50	115.87	15.54
L-S1-BC-C	-14,605.00	0.00	5,652.85	0.20	8,818.54	149.13	15.72
L-S1-BC-D	-14,605.00	0.00	5,647.02	0.20	8,855.92	117.47	15.62
L-S2-BL-A	-14,605.00	1.00	7,886.92	0.28	6,612.21	114.90	10.21
L-S2-BL-B	-14,605.00	1.00	7,886.92	0.28	6,614.67	112.50	10.28

Scenarios	Precipitation	Canopy interception	Evapotranspiration	OL storage change	OL boundary outflow	Sub-surface storage change	Total error
L-S2-BL-C	-14,605.00	1.00	7,886.92	0.28	6,583.96	142.09	9.15
L-S2-BL-D	-14,605.00	1.00	7,886.92	0.28	6,613.12	113.93	10.15
L-S2-C-A	-14,605.00	11.98	8,763.00	0.12	5,727.48	113.67	11.12
L-S2-C-B	-14,605.00	11.98	8,763.00	0.12	5,729.91	111.28	11.15
L-S2-C-C	-14,605.00	11.98	8,763.00	0.12	5,698.67	140.86	9.50
L-S2-C-D	-14,605.00	11.98	8,763.00	0.12	5,728.40	112.70	11.08
L-S2-M-A	-14,605.00	3.20	8,763.00	0.28	5,735.25	113.67	10.39
L-S2-M-B	-14,605.00	3.20	8,763.00	0.28	5,737.67	111.28	10.42
L-S2-M-C	-14,605.00	3.20	8,763.00	0.28	5,706.75	140.86	9.07
L-S2-M-D	-14,605.00	3.20	8,763.00	0.28	5,736.01	112.70	10.18
L-S2-BC-A	-14,605.00	0.00	4,958.42	0.10	9,564.55	116.02	34.09
L-S2-BC-B	-14,605.00	0.00	5,485.61	0.08	9,037.48	114.85	33.04
L-S2-BC-C	-14,605.00	0.00	5,539.71	0.08	8,955.39	145.28	35.44
L-S2-BC-D	-14,605.00	0.00	5,494.55	0.08	9,027.06	116.26	32.94
H-S1-BL-A	-292,100	0.00	38,458	6.86	253,536	107.48	12.52
H-S1-BL-B	-292,100	0.00	88,560	5.99	203,471	116.61	59.80
H-S1-BL-C	-292,100	0.00	131,402	5.13	160,574	149.71	35.23
H-S1-BL-D	-292,100	0.00	109,549	5.61	182,507	118.14	68.54
H-S1-C-A	-292,100	0.00	60,968	3.28	235,694	107.48	4,680.40
H-S1-C-B	-292,100	0.00	110,776	2.71	181,847	116.50	644.18
H-S1-C-C	-292,100	0.00	146,001	2.35	146,003	149.63	63.46
H-S1-C-D	-292,100	0.00	131,851	2.50	160,359	118.03	233.15
H-S1-M-A	-292,100	0.00	47,596	7.49	244,399	107.48	10.68
H-S1-M-B	-292,100	0.00	97,142	6.52	194,890	116.58	59.32
H-S1-M-C	-292,100	0.00	146,007	5.40	145,971	149.66	33.11
H-S1-M-D	-292,100	0.00	117,893	6.08	174,156	118.11	71.72
H-S1-BC-A	-292,100	0.00	60,869	2.93	238,875	119.33	7,765.85
H-S1-BC-B	-292,100	0.00	61,803	2.97	237,950	116.64	7,773.20
H-S1-BC-C	-292,100	0.00	93,399	1.64	205,013	149.56	6,463.55
H-S1-BC-D	-292,100	0.00	76,200	2.65	223,016	118.17	7,237.65
H-S2-BL-A	-292,100	0.00	28,208	3.35	271,280	106.27	7,488.88
H-S2-BL-B	-292,100	0.00	78,999	2.72	217,430	116.61	4,437.50
H-S2-BL-C	-292,100	0.00	131,401	2.18	160,713	149.68	160.72
H-S2-BL-D	-292,100	0.00	100,423	2.48	194,241	118.14	2,684.47
H-S2-C-A	-292,100	0.00	59,809	2.88	240,166	106.27	7,990.88
H-S2-C-B	-292,100	0.00	109,373	2.23	188,861	116.50	6,256.70
H-S2-C-C	-292,100	0.00	146,000	1.75	150,843	149.63	4,908.80
H-S2-C-D	-292,100	0.00	130,279	1.96	167,233	118.03	5,535.68
H-S2-M-A	-292,100	0.00	35,550	3.36	261,158	106.27	4,719.10
H-S2-M-B	-292,100	0.00	86,436	2.85	205,797	116.58	253.38
H-S2-M-C	-292,100	0.00	146,009	2.29	146,025	149.63	75.08

Scenarios	Precipitation	Canopy interception	Evapotranspiration	OL storage change	OL boundary outflow	Sub-surface storage change	Total error
H-S2-M-D	-292,100	0.00	107,889	2.66	184,261	118.11	170.21
H-S2-BC-A	-292,100	0.00	55,302	2.86	244,969	116.73	8,290.53
H-S2-BC-B	-292,100	0.00	61,316	2.76	238,672	116.64	8,007.19
H-S2-BC-C	-292,100	0.00	93,306	1.51	205,474	149.56	6,831.20
H-S2-BC-D	-292,100	0.00	75,866	2.48	223,609	118.17	7,495.65

Notes: L (Low precipitation), H (High precipitation), S1 (Slope <15%), S2 (Slope >15%), BL (Broad-leaved vegetation), Con (Conifers), Mix (Mixed vegetation), BC (Bareland and cultivated land)

## F. Additional water balance analysis

Water balance analyses were also conducted using the MIKE SHE model with broad-leaved vegetation as the single land cover in the first and second case study areas. The aim of this assessment is mainly to identify the characteristics of broad-leaved vegetation (e.g. total evapotranspiration, canopy evaporation, and throughfall). Table F-1 and Table F-2 present the results from water balance analysis for catchments covered by conifers and broad-leaved vegetation.

Table F-1 Accumulated water balance of Ci Kapundung upper water catchment area with a uniform land cover type (2008-2015) (mm)

	<b>Conifers</b>	<b>Broad-leaved vegetation</b>
Precipitation	-31,791.50	-31,791.50
Canopy storage change	2.65	0.08
Evapotranspiration	13,264.50	1,649.00
OL storage change	1,041.51	1,161.11
OL boundary outflow	4,616.01	7,923.42
Subsurface storage change	120.34	123.99
Throughfall	22,617.00	
Canopy evaporation	9,171.88	
Total error	-12,746.60	-10,933.90

Table F-2 Accumulated water balance of Ci Sangkuy upper water catchment area with a uniform land cover type (2008-2015) (mm)

	<b>Conifers</b>	<b>Broad-leaved vegetation</b>
Precipitation	-240,866.00	-240,866.00
Canopy storage change	8.27	3.14
Evapotranspiration	13,195.40	11,412.60
OL storage change	17,510.80	3,027.00
OL boundary outflow	713,180.00	151,514.00
Subsurface storage change	38.69	21.87
Throughfall	231,922.00	234,303.00
Canopy evaporation	8,939.46	6,564.89
Total error	503,068.00	-74,887.30